RE-ORDER NO. 62-711

Final Rough Draft *(Report)*
9 July - 9 September 1962

INVESTIGATION OF THERMIONIC ENERGY CONVERSION

Prepared for

Jet Propulsion Laboratory
4800 Oak Grove Drive
Pasadena, California

Contract No. 950188

EOS Report 2210 Final

(NASA contract NAS 7-100)

10 September 1962

Prepared by

A.O. Jensen

A.O. Jensen and H.R. Moore
Principal Investigators

OTS PRICE

XEROX $ 2.00 FS
MICROFILM $ 2.00 mf.

Approved by

J. Neustein

J. Neustein, Manager
Advanced Power Systems Division.

2904001

ELECTRO-OPTICAL SYSTEMS, INC. - PASADENA, CALIFORNIA

CONTENTS

CONTENTS (contd)

CONTENTS (contd)

1. HIGH TEMPERATURE CERAMIC MATERIALS

1.1 Introduction

Ceramic materials are applicable to thermionic diodes in several distinct areas such as seals, radiative coatings, and electrical insulative coatings. Many different forms and kinds of refractory materials are available and it is highly probable that more than one material would be suitable for any particular application. Furthermore, the state-of-the-art in ceramic materials is rapidly developing and new materials may solve current compatibility, corrosion, expansion and other problems in the near future.

The following sections summarize the current state of knowledge concerning refractory ceramic oxides useful in thermionic diodes. Many commercial refractories are multiphase and usually contain an appreciable fraction of a glassy constituent which aids in the densification process. Oxide glasses and refractory oxide compositions containing a glass or low melting liquid as one constituent can be used only to moderate temperatures and will not be considered in this discussion. Another class of refractories excluded from discussion are those ceramics that contain a large proportion of spinel, periclase, fosterite phases, and silica, which are subject to severe cesium vapor corrosion and offer no significant advantages over the more pure forms of ceramic oxides discussed in this chapter.

Additional material on the use of ceramics in a vacuum tight seal structure will be included in the chapter on ceramic-metal seals, including the geometrical and thermal expansion requirements for good seal structure.

1.1.1 Ceramic Material Application in a Thermionic Diode

The possible applications of ceramics in a thermionic diode structure are outlined in Figure 1-1 and are described as follows:

1. The electrical insulator between the collector and emitter structures is a vacuum-tight ceramic seal similar in many respects to seals used in electronic vacuum tubes except that the ceramic material will be exposed to cesium vapor corrosion and may operate normally at a higher temperature than is encountered in electron tubes. The ceramic material is brazed in a vacuum-tight fashion to the emitter and collector structure.

2. The external portion of the ceramic seal, which is used as a stress reliever for the internal portion of the ceramic seal, may be used as an electrical insulator for attachment of the thermionic diode to a generator structure.

3. A ceramic separator used to maintain a given distance between the emitter and collector.

4. A ceramic coating or sheath on the emitter structure used as an electrical insulator and to separate the diode from other diodes and/or generator structure.

5. A high emissivity coating for the radiator structure.

1.1.2 Desirable Ceramic Material Properties

Many properties must be considered in the selection of ceramic materials for the applications outlined in Figure 1-1. The vacuum-tight seal structure, offers perhaps, the most problems to date, due to cesium vapor corrosion of the ceramic and ceramic-to-metal seal, the necessity for matching almost exactly the thermal expansion characteristics of the refractory metal diode components, and the requirement of high resistance to thermal shock. The properties of interest for the ceramic seal structure are listed below:

1. Impervious to leakage

2. Ability to form vacuum-tight ceramic-to-metal seal

3. Mechanically strong
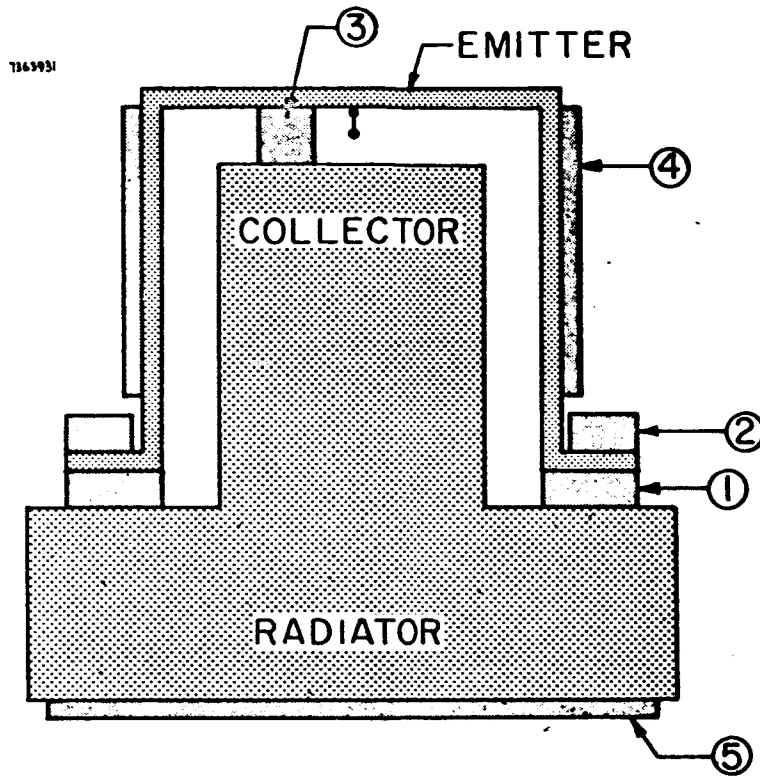
① Electrical insulator between collector and emitter - vacuum tight ceramic seal.

② "External" portion of ceramic seal.

③ Separator between emitter and collector.

④ Electrical insulating coating or sheath on emitter structure.

⑤ High emissivity radiator coating.

FIG. 1-1 POSSIBLE APPLICATION OF CERAMICS TO THERMIONIC DIODES

4. Resistant to cesium vapor corrosion

5. Nonreactive with adjacent metals

6. Low vapor pressure

7. Highly resistant to thermal shock, both cooling and heating

8. High thermal conductivity

9. Low electrical conductivity

10. Low creep rates at temperatures and stresses encountered during normal operation

11. Thermal expansion characteristics which match adjacent metal structures

12. Low impurity content

13. Ability to be outgassed

14. Available in the structures of interest at relatively low cost

Most of the properties listed above are applicable towards other ceramic structures of the thermionic diode. The other possible internal ceramic structure, the collector to emitter separator (Number 3 in Figure 1-1) must have all the above properties (at higher temperatures) with the exception that low thermal conductivity is desirable and a different type of thermal expansion matching may be required.

The external ceramics used for electrical insulation and radiative coatings may be applied by flame spraying or other processes. The properties of the coating may be significantly different from the bulk specimen, and should be carefully examined.

Safety is an additional factor in some materials; for example, beryllium oxide may, under high temperature conditions, produce toxic beryllium vapor.

1.1.3 Initial Material Selection and Availability

High refractoriness is possessed by a rather large group of oxides, but of these, perhaps less than a dozen may be selected on a basis of utility at very high temperatures.

Current practice in the ceramic electron tube industry relies almost exclusively upon fosterite-titanium, zircon-zirconium, and alumina-columbium or alumina-tantalum for matching ceramic-metal seals. When tube designs require the use of other metals, alumina is called upon to serve as a ceramic member even though the expansion mismatch may be great.

The oxides of use may be divided into two general groups: the single oxides, which contain only one metallic element, and complex oxides, which contain two or more different metallic elements whose oxides may exist together either as compounds or solid solutions. The compound oxides generally are identified by more specific terms than merely oxides, and of importance among refractory compound oxides are aluminates, chromites, phosphates, silicates, titanates, and zirconates. Of these, aluminates and chromites having formula $RO \cdot R_2O_3$ are called spinels. Modern refractories are made of both the single and complex oxides, but refractories that withstand the highest temperature consist primarily of the single oxides.

The ceramic field traditionally has associated itself with the concept of plasticity, which was imparted by clays, and with silicate chemistry. In the postwar period, however, rapid progress was made in ceramic bodies that possessed no silica or clay in their structure. These new refractories are processed at high temperatures, even up to fusion. The pure dense particles form a skeleton that is resistant to shrinkage at high temperatures. The particles are bonded, in most cases, by fine particles of the same pure material, and the mixtures are compacted and fired at high temperatures, usually above $1600^{o}C$. In firing, these materials do not form glassy bonds, but center or recrystallize at solid reactions. These materials frequently are called pure oxide heavy refractories. It is chiefly with this type of refractory that the present chapter is concerned.

A variety of ceramic and intermetallic materials that have to date not found permanent application is available but need more extensive study; these include the borides, berylides, carbides, nitrides, and silicides. An excellent review of the state-of-the-art of these materials is given in Ref. 6. In complete data, limited availability, and various physical limitations exclude these materials from consideration in this discussion. The future commercial status for each of these materials can be summarized with the expression: "potential applications are being explored."

1.2 Comparison of Ceramic Properties

Investigators to date have confined their attention almost exclusively to determining the properties of the single oxides, Al_2O_3, BeO, MgO, ZrO_2, and ThO_2. Al_2O_3 has received the most attention. Among the mixed oxides, refractory silicates, aluminates, titanates, niobates, zirconates, and phosphates have been investigated. A comprehensive summary of the accumulated data on the thermal and electrical properties (through 1957) of refractory single and mixed oxides is available in Ref. 1; Ref. 2 is an excellent and thorough accumulation of the available data (through 1960) on mechanical properties of oxide materials and provides additional reference material on thermal and electrical properties. References 1 through 9 contain worthwhile comparisons of ceramic materials. Test results obtained from various sources are difficult to compare because microstructure, porosity, chemical composition, and other conditions and properties are generally not well defined. Only in rare cases is such complete information available. Nevertheless, a fairly accurate picture of thermal, electrical, mechanical, and other properties of oxide ceramics emerges.

The characteristics of oxide refractories depend not only on chemical composition but to a large extent on the physical structure as well. Most favorable characteristics for many purposes are obtained in single crystals or dense, single phase crystalline solids. Materials

in this form will be the major consideration in the present review, since in this state we obtain the maximum chemical inertness, the best high temperature strength, and the best thermal conductivity. For application as separators and thermal insulators, however, it may be desirable to have a more porous or coarse physical structure, as discussed later.

The constituents of a ceramic structure generally comprise:
1. Crystals
2. A glassy phase
3. Pores, holes or voids made up of closed pores that are vacuum-tight, or interconnecting (open) pores that are not vacuum tight.

Until recently, ceramics were universally sintered, using a little glassy phase. For example, a 99 percent alumina body consisted of single crystals of α-alumina (99 percent by weight) with the remainder being SiO_2, CaO and MgO. An alumina structure, in general, is easier to make if the percentage of glass forming constituents added to the finely ground alumina is increased. Ninety-four percent alumina bodies comprise α-alumina, SiO_2, MgO, CaO, Fe_2O_3 and traces of other elements. These form a liquid phase at maturing temperatures and assist the sintering process. On cooling, the phase diagrams indicate that the primary phase is α-Al_2O_3 with secondary crystallization of mullite ($3Al_2O_3 \cdot SiO_2$) anorthite ($CaO \cdot Al_2O_3 \cdot 2SiO_2$) (which form a eutectic at $1550^{\circ}C$) plus smaller amounts of spinel (MgO, $FeO - Al_2O_3$) and other trace compounds which can lower the melting point to $1400^{\circ}C$. The cooling of the 94 percent alumina bodies is too rapid to allow significant crystallization to proceed, resulting in a glassy matrix surrounding the alumina crystals.

1.2.1 Property Summary

In Table 1-I are collected a variety of data from Kingery (Ref. 3) that are typical of oxide refractories as normally prepared sintered products of nominally high purity characterized by

TABLE 1-I   PROPERT

	Composition	Porosity (Vol. %)	Fusion Temp. (°C)	Max Normal Use Temp. (°C)	Density, Bulk(b), True(t), (gm/cc)	Specific Heat Capacity (cal/gm/°C) 20-1000°C
Sapphire crystal	99.9 Al_2O_3	0	2030	1950	3.97(t)	0.26
Sintered alumina	99.8 Al_2O_3	3-7	2030	1900	3.97(t)	0.26
Sintered beryllia	99.8 BeO	3-7	2570	1900	3.03(t)	0.50
Sintered calcia	99.8 CaO	5-10	2600	2000	3.32(t)	0.23
Chrome-alumina cermet (Haynes-Stellite LT-1)	77 Cr, 23 Al_2O_3	2	1850	1300	5.9(b)	0.16
Sintered magnesia	99.8 MgO	3-7	2800	1900	3.58(t)	0.25
Sintered mullite	72 Al_2O_3 28 SiO_2	3-10	1800	1750	3.03(t)	0.25
Sintered forsterite	99.5 Mg_2SiO_4	4-12	1885	1750	3.22(t)	0.23
Sintered spinel	99.8 $MgAl_2O_4$	3-10	2135	1850	3.58(t)	0.25
Sintered titania	99.5 TiO_2	3-7	1840	1600	4.24(t)	0.20
Sintered thoria	99.8 ThO_2	3-7	3050	2500	10.50(t)	0.06
Sintered yttria	99.8 Y_2O_3	2-5	2410	2000	4.50(t)	0.13
Sintered urania	99.8 UO_2	3-10	2800	2200	10.96(t)	0.06
Sintered stabilized zirconia	92 ZrO_2, 4 HfO_2, 4 CaO	3-10	2550	2200	5.6(t)	0.14
Sintered zircon	99.5 $ZrSiO_4$	5-15	2420	1800	4.7(t)	0.16
Silica glass	99.8 SiO_2	0	1710	1100	2.20(t)	0.18
Mullite porcelain	70 Al_2O_3, 27 SiO_2, 3 MO + M_2O	2-10	1750	1400	2.8(b)	0.25
High alumina porcelain	90-95 Al_2O_3, 4-7 SiO_2 1-4 MO + M_2O	2-5	1800	1500	3.75(b)	0.26

Linear Expansion (10^{-6} in/ in/^{o}C) 20-1000°C	Thermal Conductivity (cal sec^{-1} ^{o}C^{-1} cm^{-2} cm.)		Modulus of Rupture (MR) or Tensile Strength (TS) (psi)		Modulus of Elasticity 10^{6} psi	Thermal Stress Resistance
	at 100°C	at 1000°C	at 20°C	at 1000°C		
8.6	0.072	0.019	40,000-150,000(MR)	30,000-100,000(MR)	55	Very good
8.6	0.069	0.014	30,000(MR)	22,000(MR)	53	Good
8.9	0.500	0.046	20,000(MR)	10,000(MR)	45	Excellent
13.0	0.033	0.017	---	---	---	Fair-poor
8.9	0.08	0.05	45,000(MR)	20,000(MR)	37.5	Excellent
13.5	0.082	0.016	14,000(MR)	12,000(MR)	30.5	Fair-poor
5.3	0.013	0.008	12,000(MR)	7,000(MR)	21	Good
10.6	0.010	0.005	10,000(MR)	---	---	Fair-poor
8.8	0.033	0.013	12,300(MR)	11,000(MR)	34.5	Fair
8.7	0.015	0.008	8,000(MR)	6,000(MR)	---	Fair-poor
9.0	0.022	0.007	12,000(MR)	7,000(MR)	21	Fair-poor
9.3	(0.02)	---	---	---	---	Fair-poor
10.0	0.020	0.007	12,000(MR)	18,000(MR)	25	Fair-poor
10.0	0.005	0.005	20,000(MR)	15,000(MR)	22	Fair-good
4.2	0.015	0.008	12,000(MR)	6,000(MR)	30	Good
0.5	0.004	0.012	15,500(MR)	---	10.5	Excellent
5.5	0.007	0.006	10,000(MR)	6,000(MR)	10	Good
7.8	0.05	0.015	50,000(MR)	---	53	Very good

a porosity of approximately 5 percent. These values are typical, rather than an indication of the optimum that can be obtained by present techniques. They are not representative of the wide variety of results that can be obtained by what sometimes seem minor variations in composition, fabrication methods, or resulting microstructures. Nevertheless, they indicate the range usually obtained and some useful conclusions can be drawn.

As tabulated, the best thermal stress resistance can be obtained from sapphire crystal, sintered alumina, sintered beryllia, a zircon structure, and several high alumina content ceramic materials containing silica. Structures containing a large amount of silica are eliminated from further discussion due to poor compatibility with cesium vapor. Therefore, on the basis of thermal stress resistance alumina and beryllia bodies appear best. Sapphire crystal seal structures are difficult to fabricate due to the directionality of thermal expansion; i.e., expansion along one axis of the crystal is very low while expansion along the second axis is comparable to poly-crystalline alumina. The cermet material mentioned in Table 1-I has not been used successfully in fabricating ceramic-metal seals and will not be discussed further.

Table 1-II is a summary of data from several manufacturers' catalogs regarding oxide materials of interest. While much data are missing, it is evident from the various alumina ceramics that the amount of SiO_2 and other "auxiliary" constituents has a strong effect on material properties.

Table 1-II is only a representative sample and is not intended to serve as a complete catalog of manufacturers' products.

1.2.2 Compatibility with Cesium

Very little experimental data is available regarding the compatibility of ceramic oxide materials with cesium gas. Some data were recently made available by Slivka (Ref. 41) which demonstrate the suitability of certain ceramic oxides with cesium.

Corrosion may take place by several fairly common mechanisms. One is a relatively uniform solution attack on the solid surface by the gaseous corrodant. Another common method of attack is direct alloying, the interaction between liquid and solid to form surface films or typical diffusion layers of intermetallic compounds and solid solutions as shown in Fig. 1-2. These may form a loosely adherent scale or, if held tightly, may serve as a barrier to slow down additional diffusion.

Selective reaction of the alkali vapor with minor constituents of the solid may result in intergranular penetration or in the depletion of a dissolved component of the solid. Selective grain-boundary attack can drastically alter the physical properties of a material without appreciably changing its weight or appearance. This type of attack is often accelerated by the application of stress to the solid during exposure to the alkali vapor. (See Fig. 1-3)

Another type of attack results from corrosion by comtaminants rather than by the alkali vapor itself. Such contaminants may include oxygen, nitrogen or alkali vapors other than cesium, which may result from inadequate outgassing procedures, comtaminants in the cesium reservoir or other factors.

Experimental data to date do not differentiate between the above types of corrosion. Static methods of testing, as indicated in Fig. 1-4, have been generally used; i.e., samples are weighed before and after exposure and the results are reported or are converted to equivalent changes in thickness. (See Fig. 1-5) This method is widely used in the study of corrosion in aqueous and atmospheric environments. It is well suited to evaluation of corrosion provided that the corrosion is known to involve uniform removal of material from the solid surface. It is also useful where uniform buildup of an adherent coating by diffusion penetration and reaction occurs. But if the corrosion is intergranular, if a nonadherent-diffusion-reaction
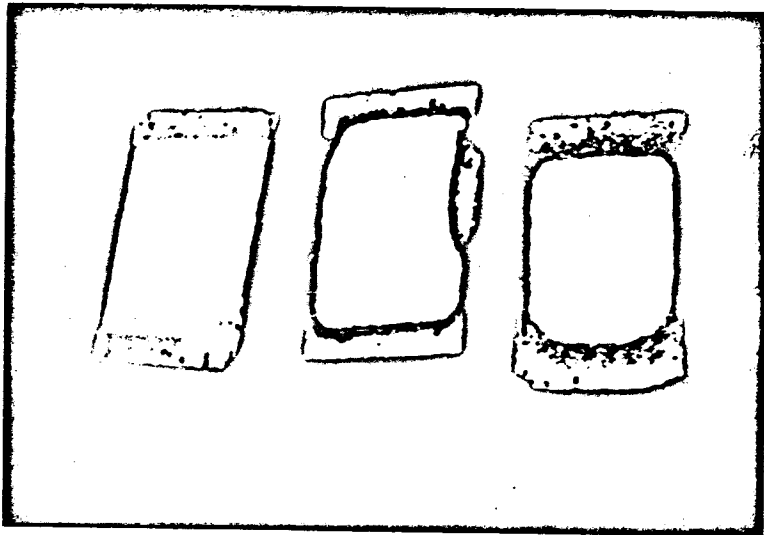
FIG. 1-2

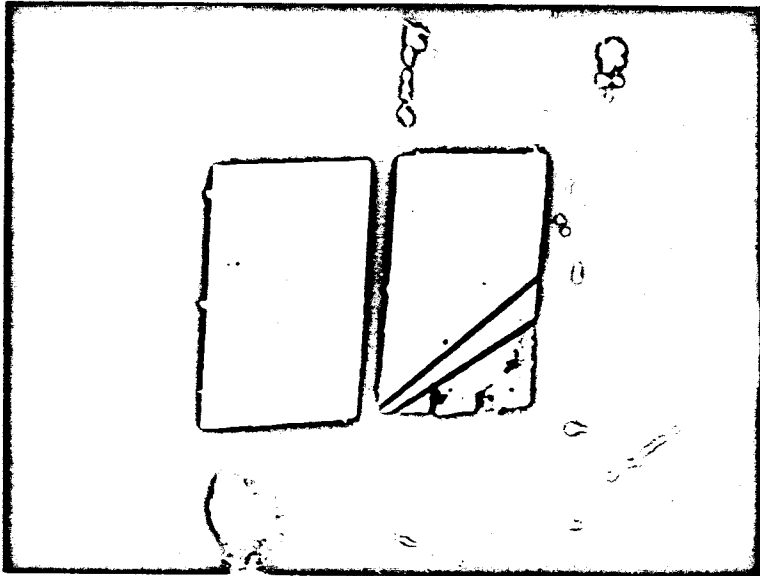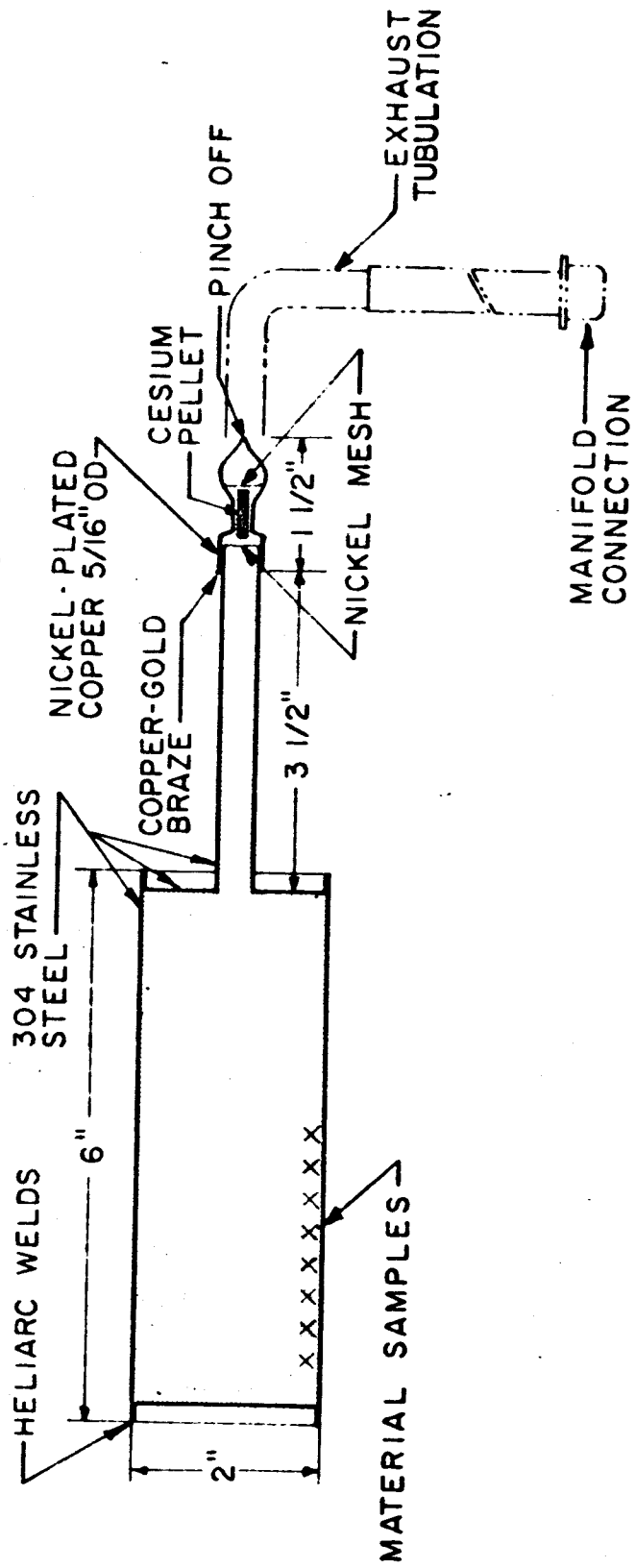EXAMPLE OF CESIUM ATTACK ALONG SEAL
BOUNDARY.

FIG. 1-3

CESIUM CORROSION OF CONVERTER SEAL
DEMONSTRATING PREFERENTIAL ATTACK
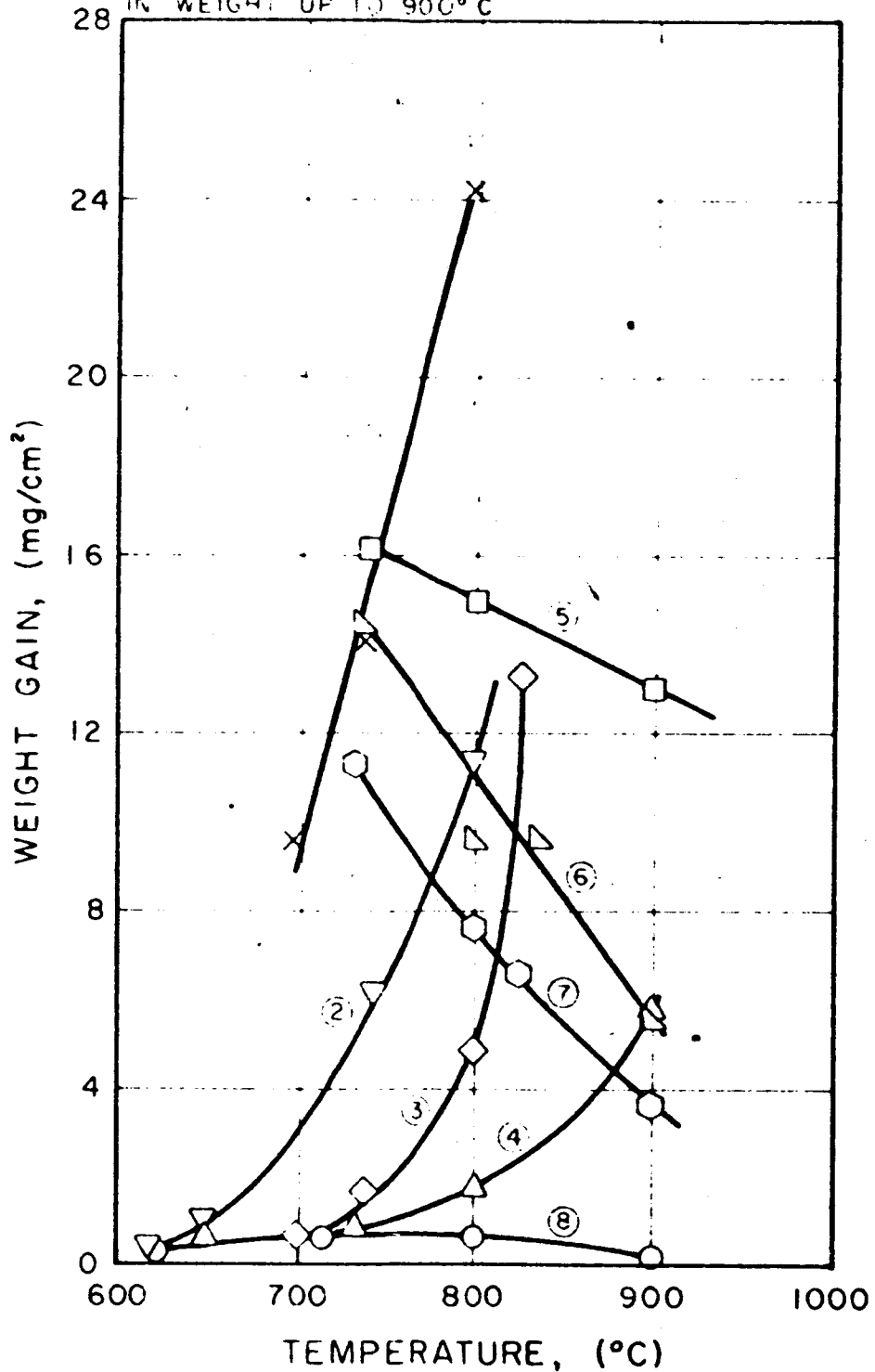IN STRESS CONCENTRATED AREAS.

FIG. 12   WEIGHT GAIN OF CERAMIC MATERIALS FROM CESIUM CORROSION

product results, or if difficulty is encountered in cleaning the solid sample, weight-change data may be meaningless or even misleading.

Results of liquid-metal testing procedures are frequently reported as corrosion rates, i.e., weight change or linear penetration per unit of time. These data must be properly qualified to avoid misleading conclusions. In most liquid-metal testing procedures, the ratio of container surface to volume of liquid is relatively large; therefore, the concentration tends to approach saturation quite rapidly and the corrosion rate is not constant. If diffusion coatings are formed, the corrosion rates will also decrease with time and build up of the coating. To regard the total attack over an extended period as an average rate can thus result in serious misinterpretation.

Microscopic examination of metallographically prepared cross-sections is, perhaps, the best single tool for the general study of cesium corrosion attack since differentiation can be made between intergranular penetration, a formation of diffusion layers, and the actual removal of materials as a function of depth of penetration (see Fig. 1-6) or thickness of material buildup or removal. Metallographic examination is presently being used in several research programs directed toward corrosion evaluation in relation to ion engine and thermionic diode programs (Ref. 13, 14, and 15). Figure 1-7 illustrates a typical cross section of cesium corrosion on a ceramic material.

Several ceramic oxide materials have been subjected to static testing in sodium with a view to their possible use as valve seats, bearings, and insulators. Beryllia, zirconia, magnesia, alumina, molybdenum disilicide, and numerous metal-ceramics, which are thermodynamically stable to sodium, resist sodium attack if they are sufficiently dense, but are penetrated and disintegrated if porous. The temperature of the test, the character of the ceramic binder, and such factors as particle size and firing temperature also influence the attack. High density material produced by hot pressing or fusion may be susceptible to spalling rather than penetration attack. Table

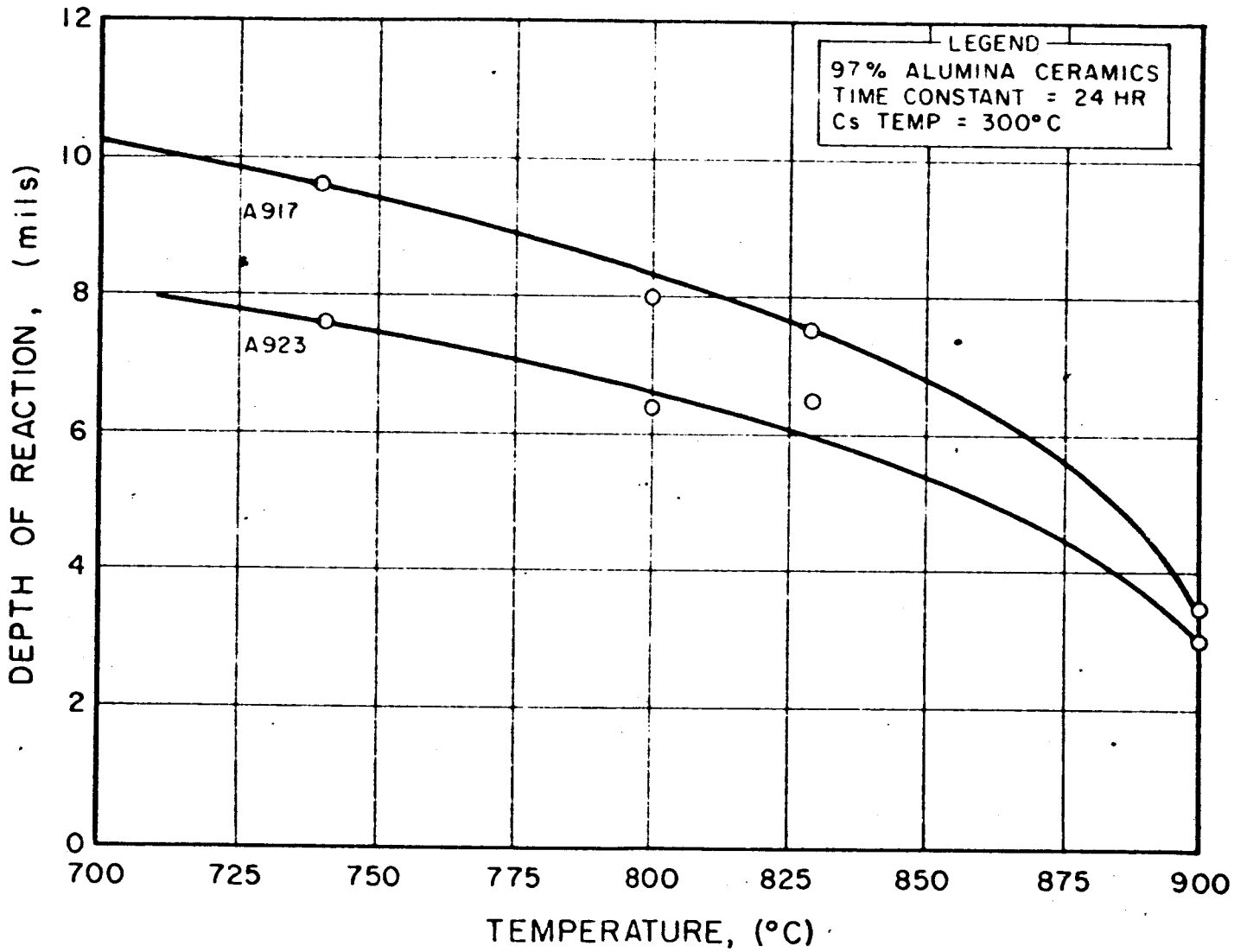97% ALUMINA CERAMICS
TIME CONSTANT = 24 HR
Cs TEMP = 300°C

FIG. 1-7

CESIUM ATTACK ON TYPICAL CERAMIC.

1-III shows the results of selected static tests on a number of ceramic materials investigated at Knolles Atomic Power Laboratory using aged and filtered sodium. Table 1-IV shows the relative resistance of materials to liquid Na, NaK, and K as a function of temperature according to static corrosion tests conducted at Argonee National Laboratories. The effect of impurities in the molten alkali metal is unknown and could result in increased corrosion. Oxygen and other contaminants in a liquid sodium test are likely to result in severe attack of ceramic materials. Burger (Ref. 19) indicates that pure alumina, magnesium, titania, zirconia, etc., are unaffected by exposure to sodium. The difficulties which arise in sodium are primarily mechanical in nature. Many of these ceramic bodies are not 100 percent dense,with the result that when they are exposed to sodium they soak it up; then subsequent thermal cycling produces cracking. Many of the binders, especially silicates, react with sodium. The dense, fired, pure oxides perform most satisfactorily.

Wagner and Coriell (Ref. 11) exposed several dielectrics under controlled conditions to cesium gas at sample temperatures ranging from $1200^{\circ}C$ to $1475^{\circ}C$ and pressures of 20 and 110 mm Hg. Once the cesium pressure had been established, a sample was heated to the desired temperature. The results of the test can be summarized as follows:

1. The only specimen that appeared to be totally unaffected by the test was a fused alumina sample.

2. All sintered samples appeared discolored at the conclusion of the test. The discoloration appeared to be less dependent on purity than on porosity.

3. The extent of the reactions that caused the discoloration was so slight that no evidence of reaction could be found by use of x ray, metallographic, or polarizing microscope techniques.

TABLE 1-III

RESISTANCE OF SELECTED CERAMICS TO ATTACK BY AGED

AND FILTERED SODIUM (REF. 17)

MOLE COMPOSITIONS	CORROSION RATE mg/cm^2 month		ABSORPTION %
	500°C	750°C	
Artificial Periclase Crystal	-0.4	-0.25	
BeO	0.14		
Stabilized ZrO_2	2.7		
$1BeO:1Al_2O_3$	0.0003		0.18
$1MgO:4ZrO_2$	-0.091	-14.6	0.01
$1MgO:8BeO:1Al_2O_3$	-0.44	-1.6	0.03
$76BeO:4Al_2O_3:20ZrO_2(+2Wt\%CaO)$	-0.64	0.54	0.01
$3MgO:90BeO:1ZrO_2$	-0.68	0.96	0.03

TABLE 1-IV

CORROSION RESISTANCE RATINGS TO Na AND NaK (REF. 16)

DEGREES CENTIGRADE

| | 100 | 200 | 300 | 400 | 500 | 600 | 700 | 800 |

AL$_2$O$_3$

Be O

Mg O

PYREX, VYCOR & OTHER GLASSES

GOOD, < I mil/year

LIMITED, < I—IO mil/year

UNKNOWN

954
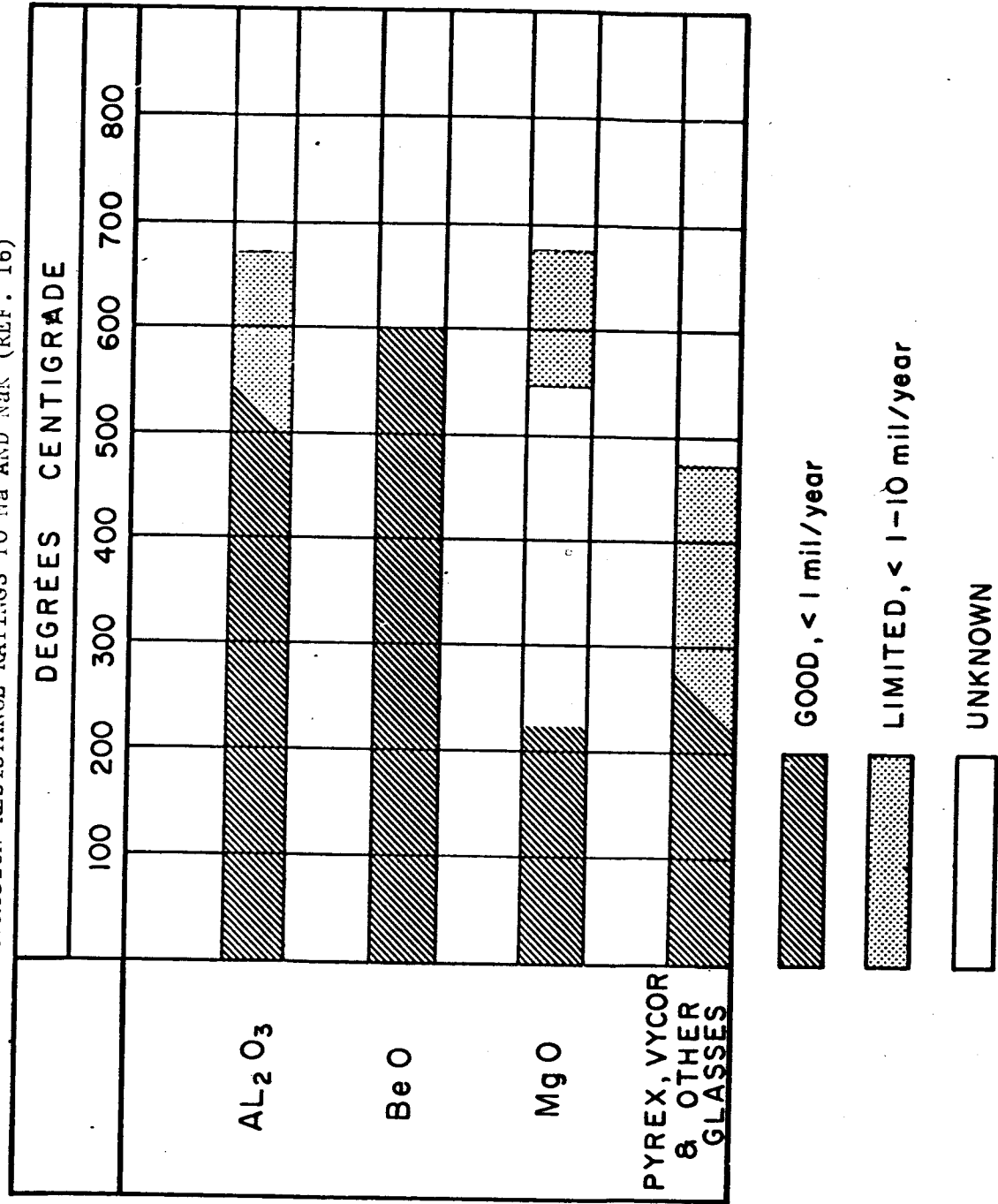
4. It was concluded that cesium probably reacted with the impurities of the parent material but could only be observed when the surface areas available for reaction were relatively large.

5. The only material that showed evidence of reaction was the niobium carbide specimen in which the surface was pitted at the conclusion of the experiment.

Reed (Ref. 18) reports the results of corrosion experiments utilizing liquid sodium in a range 800 to 1500°C using alumina, zirconia, and other materials, The results are tabulated in Table 1-V. Morganite sintered alumina bodies (6 percent porosity) disintegrated into small black grains, whereas synthetic sapphire alumina remained clear and was little affected. This difference is probably due to the higher purity and lower porosity of the sapphire specimen. Synthetic spinel was dissolved completely. Some corrosion was evident for single crystal sodium carbide. The affect of specimen porosity and/or purity is again evident from the effect on magnesia. Sintered magnesia (12 percent porosity) also turned black and swelled. in sodium whereas the single crystal material remained clear and showed practically no weight change. Sintered zirconia (23 percent porosity) also turned black and swelled. Cast molybdenum disilicide and sintered thoria showed essentially no corrosion in sodium.

Burger, et al (Ref. 19) investigated the effects of cesium vapor attack on a 95 percent Al_2O_3 body (GE2548), by measurement of the leakage resistance across the ceramic as a function of cesium vapor temperature, ceramic temperature, voltage, and time of exposure. While insufficient data were collected to provide definite rates of attack, some observations are of interest. Figure 1-8 illustrates the typical effect of time and ceramic temperature on leakage resistance. For all cesium temperatures there exists a certain ceramic temperature for which the leakage resistance is a maximum. This

TABLE 1-V

STATIC CORROSION OF REFRACTORIES IN SODIUM (REF. 18)

Refractories	Results	Na Temp. (°C)	Time (hr)	Specimen Weight Change (%)	Appearance
Spinel (MgO 3.5 Al$_2$O$_3$), synthetic	Completely dissolved	925	168	-100.0	Disappeared
Alumina, Al$_2$O$_3$ (Morganite triangle RR, 6% porosity)	Corrosion severe	940	168		Disintegrated into many small black grains
Alumina, Al$_2$O$_3$ (synthetic sapphire)	Very little corrosion compared w/Morganite	900	168	-1.0	Remained clear
Magnesia, MgO (LM-160 35, 12% porosity)	Some corrosion evident	940	168	+1.2	Turned black; swelled
Magnesia, MgO (single crystal)	Practically no corrosion	925	168	-0.02	Remained clear
Zirconia (Norton LZO-169B-35, 23% porosity, CaO stabilized)	Appreciable corrosion; specimen shattered	890	168	+3.7	Turned black; swelled
Molybdenum, disilicide (cast material)	Apparently little corrosion	900	168	No data	Bright
Thoria (Norton LT 10A 35)	Practically no corrosion	925	168	-0.06	No change

$$\frac{1}{R_L} = \frac{1}{R_A} + \frac{1}{R_S}$$

$t_3 > t_2 > t_1$

Predominate resistance at low temperature is R_a, due to surface absorbtion of Cs on ceramic.

Predominate resistance at high temperature is R_S, due to chemical reaction between ceramic and Cs.

Time = t_1

t_2

t_3

R_L, LEAKAGE RESISTANCE IN KILO-OHMS AT 700 VOLTS
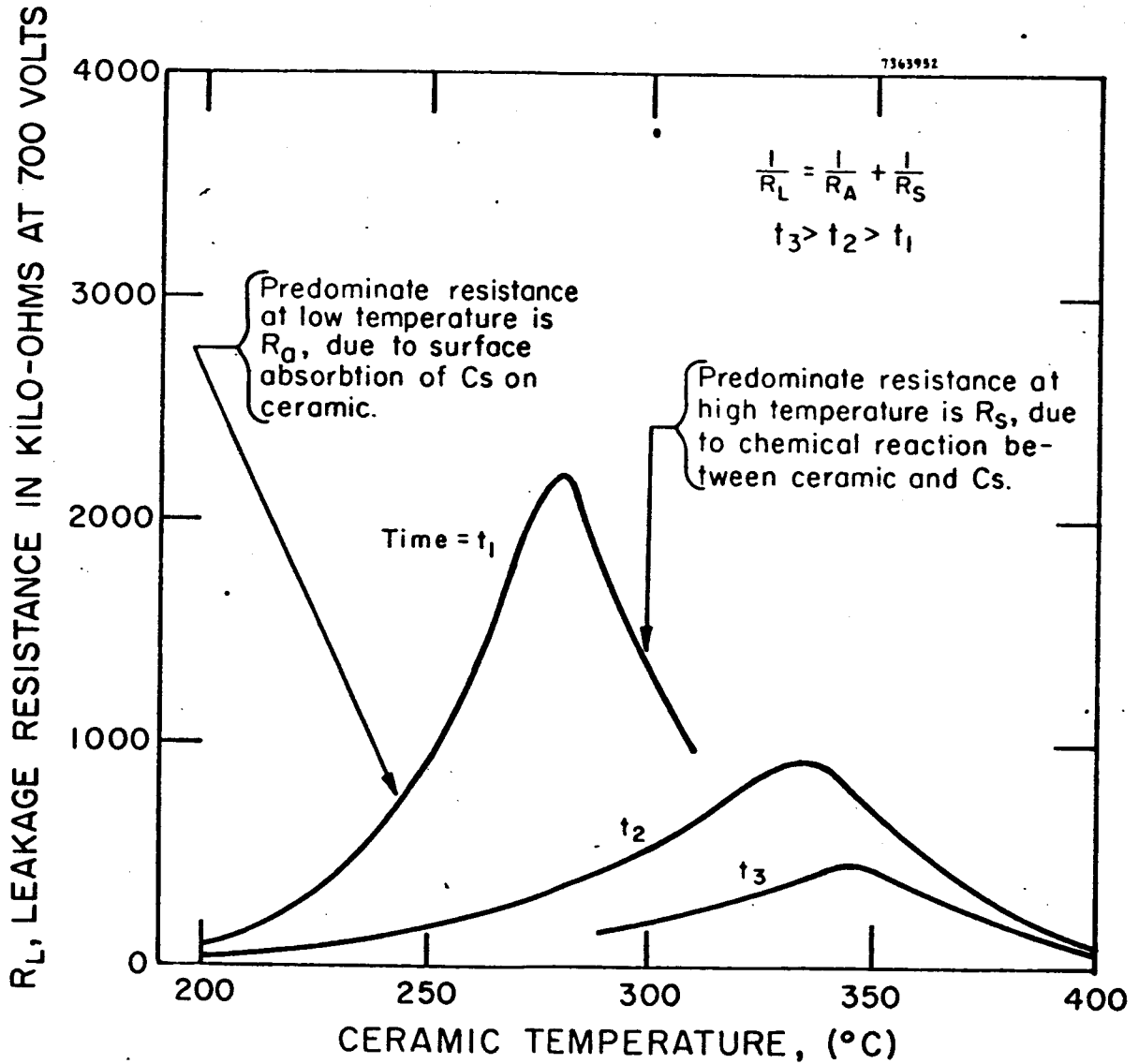
CERAMIC TEMPERATURE, (°C)

FIG. 1-8   TYPICAL EFFECT OF CESIUM ATTACK ON CERAMIC MATERIALS FROM BURGER (REF. 19)

The most stable of any group of compounds are those with the largest negative free energy of formation from the elements. The most stable oxides are: CaO, Y_2O_3, La_2O_3 and ThO_2. In practice, calcium oxide is disadvantageous to use since it hydrates rapidly in air. However, it can be manufactured as dense products and maintained for long times in a completely dry atmosphere. Lanthamum oxide shows rapid hydration and also exhibits a polymorphic conversion that makes fabrication difficult. Yttria and thoria are the most stable oxide refractories suitable for general use. The high cost of yttria has limited its general use although it has satisfactory properties. As a result, thoria, in spite of its moderately high cost and slight radioactivity, is the most widely suitable material in cases where maximum chemical stability is required.

Refractory oxides can react with the atmosphere, with one another, or with adjacent materials. In general, the oxides are stable up to their melting points in dry air and oxidizing atmospheres. In reducing atmospheres and atmospheres containing carbon and sulphur, reactions may occur.

For operation in fuel fired converters under atmospheric conditions, all refractory oxides of interest would need protection of some type.

Oxide materials are generally stable in contact with carbides and refractory metals, but at sufficiently high temperatures all react. Some reaction temperatures between refractory oxides and metals involving gross changes are collected in Table 1-VI (Ref. 3). Some data regarding the extend of reaction between metals and oxides at 1800°C are given in Table 1-VII (Ref. 3).

The behavior of tungsten, molybdenum, and tantalum at high temperatures in combination with some refractory oxide materials is shown in Table 1-VIII, which indicates the threshold temperature levels beyond which reaction may constitute a materials problem. It should be noted that even thoria begins to react with tungsten when

TABLE 1-VI

REACTION TEMPERATURES FOR REFRACTORY COMBINATIONS IN VACUO (REF. 3)

	W	Mo	C	Al_2O_3	BeO	MgO	SiO_2	ThO_2	ZrO_2
W	----	2300	1500	>2000	2100	2000	1600	2300	2100
Mo	2300	----	1600	2000	1900	1800	1500	2200	2150
C	1500	1600	----	1800	2300	1800	1400	1950	1800

TABLE 1-VII

DEGREE OF REACTION BETWEEN METALS AND OXIDES AT 1800°C (REF.3)

Metal	Oxide					
	Al_2O_3	BeO	MgO	ThO_2	TiO_2	ZrO_2
Mo	N	N	N	N	N	N
Ni	N	N	N	N	N	N
Cb	N	P, C, NPh	N, P	N, P, C	N, C	N, P
Ti	P, SC	P, SC	P, SC, NPh	N, P	SC	P, SC
Zr	P, SC	P	SC	N, P	SC	N, P
Be	P, SC	N, P	P, SC	N, P	C	N, P
Si	P, NPh	P, C	NPh	P, C	----	NPh

N	No physical alteration of interface.
P	Penetration along grain boundaries and alteration of oxide.
C	Corrosion of oxide observed.
SC	Severe corrosion of oxide.
NPh	New phase formed at interface.

TABLE 1-VIII

STABILITY OF HIGH-TEMPERATURE HEATING-ELEMENT MATERIALS TOWARDS OXIDES AND FURNACE PARTS (REF. 29)

MATERIAL	MOLYBDENUM	TUNGSTEN	TANTALUM
Graphite	Strong carbide formation beyond 1200 C	Strong carbide formation beyond 1400 C	Strong carbide formation beyond 1000 C
Al_2O_3	Up to 1900 C	Up to 1900 C	Up to 1900 C
BeO	Up to 1900 C[a]	Up to 2000 C[a]	Up to 1600 C
MgO	Up to 1800 C[a]	Up to 2000 C[a] (strong magnesia evaporation)	Up to 1800 C
ZrO_2	Up to 1900 C[a] (strong molybdenum evaporation)	Up to 1600 C[a]	Up to 1600 C
ThO_2	Up to 1900 C[a]	Up to 2200 C[a]	Up to 1900 C
Firebrick	Up to about 1200 C	Up to about 1200 C	Up to about 1200 C
Magnetic Brick	Up to about 1600 C	Up to about 1600 C	Up to about 1500 C

(a) In vacuum of 10^{-4} mm Hg: under protective gas about 100 to 200 C lower temperatures.

maximum resistance will decrease significantly with increasing cesium temperatures and with increasing time.

Burger postulated that the principal phenomena responsible for the leakage resistance characteristics were cesium absorption on the ceramic surface and the creation of a layer of new semiconductor materials due to chemical reaction. The peaked curve resulted from a combination of these two effects, surface absorption being the dominant mechanism at lower ceramic temperatures and the effects of the semiconductor layer being dominant at higher ceramic temperatures. At low ceramic temperatures where a large amount of cesium is retained on the ceramic surface, the experimental resistance curves indicated absorption behavior i. e., decreasing resistance as the amount of absorbed cesium becomes less at higher ceramic temperatures. The experimental leakage behavior at high temperatures correlated with typical semiconductor action; i.e., as ceramic temperature increases bulk resistance decreases.

1.2.3 Compatibility with Refractory Metals

The stability of refractory oxides in contact with different metals cannot be predicted with accuracy since the amount of reaction of attack that occurs depends upon physical factors as well as thermodynamic properties. It often is possible, therefore, to use materials that thermodynamically are not stable, in contact with each other at high temperatures. For general stability with metals at very high temperatures, Kingery (Ref. 3) lists some of the most refractory of the oxides in the following order of decreasing reactivity; thoria, beryllia, zirconia, alumina, and magnesia. This order by no means holds for all metals and is completely changed for contact with some nonmetallic materials. Thoria, beryllia, and zirconia, however, not only have high chemical inertness but also have relatively low vapor pressures at high temperatures, and they may be used in many applications, particularly under vacuum, where other refractories fail.

the temperature exceeds about 2200°C. Therefore, where a reasonably long service life is demanded at temperatures higher than this, tungsten must be used in such a manner that surfaces above 2200°C are contact free.

Table 1-IX shows some Russian data (Ref. 27) regarding the reaction of oxides with refractory metals.

1.2.4 Vapor Pressure

At very high temperatures the vapor pressure so some of the refractory oxides become appreciable and may limit their usefulness. Comparative data regarding volatization, as indicated by weight losses of the samples during firing, are given below (Ref. 3).

Thoria   - 2800°C

Zirconia - 2300°C

Beryllia - 2100°C

Magnesia - 1600°C

Equations relating the vapor pressure as a function of temperature for refractory oxides can be derived from the known free energies of formation. However, the theoretical calculations can differ considerably from reality due to the effects of chemical reactions with specimen containers and the difficulty of identifying quantitatively and qualitatively, the chemical species that exist in the vapor phase. In general, very complex molecules exist in the metal oxide systems, which may be of minor importance under reducing or neutral conditions, but which may minor consequence under oxidizing conditions.

Figure 1-9 shows the measured values of the vapor pressure of several refractory oxides. As indicated, most of the oxides of interest can be used in ceramic seal structures where temperatures of operation are expected to be less than 1000°K.

1.2.5 Mechanical Properties

The main variables that have been found to effect results of material strength and creep characteristics are temperature,

TABLE 1-IX

THE REACTION OF CERTAIN OXIDES WITH REFRACTORY METALS (UNDER VACUUM)   (REF. 27)

Contacted Material	Duration of Reaction Hours	Temperature, °C					
		1600	1700	1800	1900	2000	2100
Beryllium Oxide							
Niobium	0.5	N	N	N	N	-	-
	1.0	N	W	S	S	-	-
Molybdenum	0.5	N	N*	N	N	-	-
	1.0	N	W	W	W	-	-
Tungsten	0.5	N	N	-	S	-	-
	1.0	N	N	S	S	-	-
Magnesium Oxide							
Niobium	0.5	N	N	N	N	N	-
	1.0	N	N	N	N	W	-
	5.0	N	N	N	W	S	-
Molybdenum	0.5	N	N	N	N	N	-
	1.0	N	N	N	N	N	-
	5.0	N	N	N	N	N	-
Tungsten	0.5	N	N	N	N	N	N
	1.0	N	N	N	N	N	N
	5.0	N	N	N	N	N	N
Zirconium Dioxide (+CaO)							
Niobium	0.5	N	N	N	N	N	N
	1.0	N	N	N	N	N	S
	5.0	N	N	N	N	W	W
Molyb...	0.5	N	N	N	N	N	-
	1.0	N	N	N	N	N	-
	5.0	N	N	N	N	N	-
Tungsten	0.5	N	N	N	N	N	-
	1.0	N	N	N	N	W	-
	5.0	N	N	N	W	W	-

These symbols were used: N - no reaction; W - weak reaction; S - strong reaction.
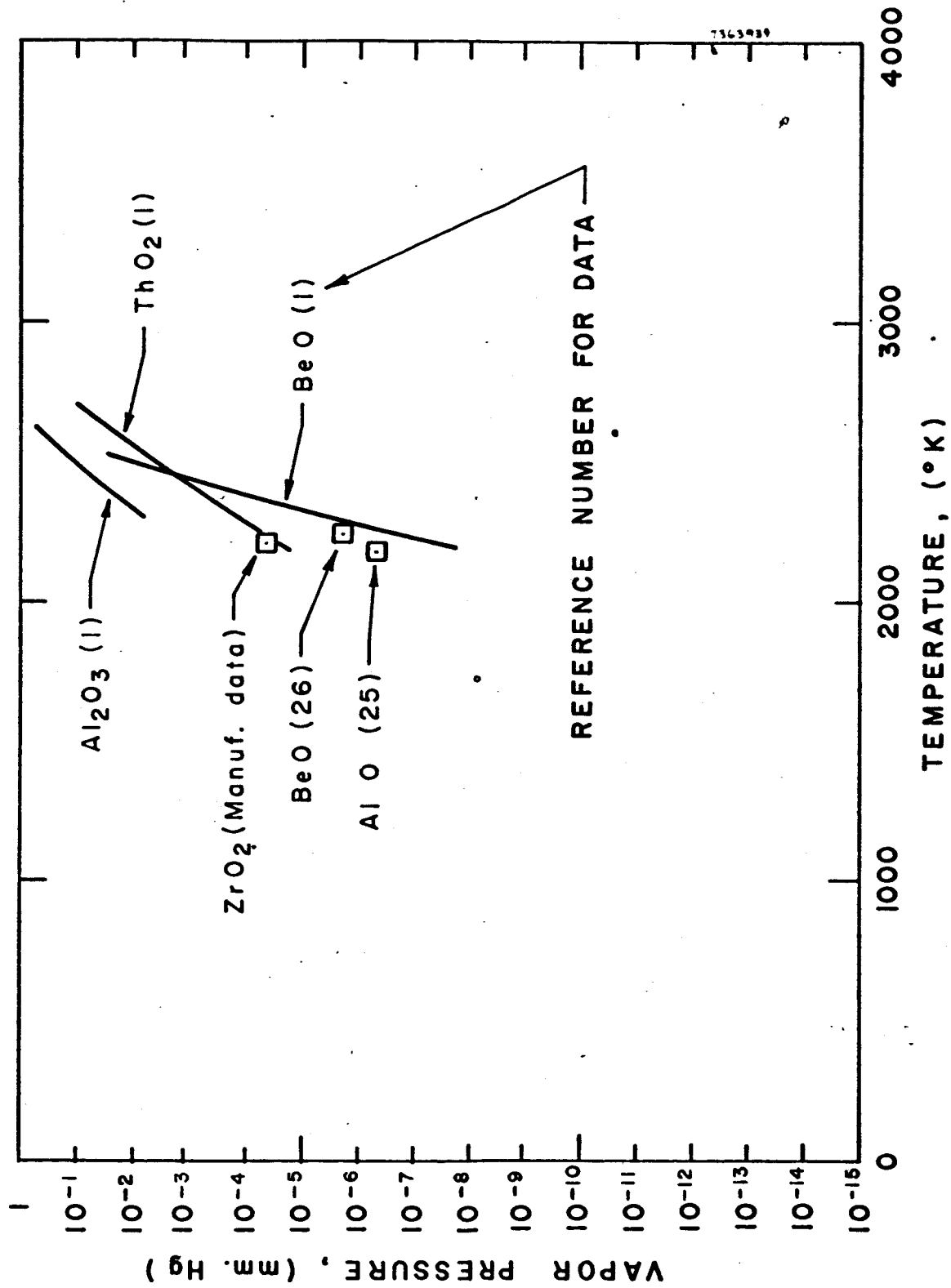
FIG. 1 - 9 MEASURED VAPOR PRESSURES OF REFRACTORY OXIDES

stress, strain rate, environment, sample composition (including porosity) and sample microstructure. Comparison between different experimenters is sometimes difficult due to failure to report all of these variables. Comparative data for tensile, shear, and compressive strength is given in Tables 1-X, 1-XI, and 1-XII (see Ref. 5) for a number of nominally pure oxide materials as a function of temperature.

Figure 1-10 illustrates the tensile strength of several oxides (Ref. 3) as a function of temperature and illustrates the sharpness of the break in the curve of tensile strength that is characteristic of these materials. This sharp decrease in the high temperature short term strength of polycrystalline oxides corresponds to the temperature at which the nature of the fracture changes from intragranular at the lower temperatures to intergranular grain boundary fracture at the higher temperatures. Measurements of Figure 1-10 are all for samples of nominal purity corresponding to better than 99 percent of the oxide that is a major phase. However, they all contain a certain fraction of impurity that is probably concentrated along grain boundaries. The effect of this impurity concentration in lowering the temperature at which grain boundary deformation and fraction occur is not known. Comparison between Figure 1-10, Table 1-X, and other available data indicates the same trends and conclusions; e.g., Al_2O_3 exhibits the highest material strengths for the ceramic oxides of interest.

In the same way that the short time strength at elevated temperatures indicates failure by grain boundary cracking, deformation of polycrystalline oxides in long time tests corresponds to grain boundary creep as the major process taking place. There is a large temperature dependence for the process, and the rate of deformation is strongly dependent on grain size and the details of composition that effect the structure of the boundary material. Tables 1-XIII and 1-XIV summarize the available creep data for ceramic materials of interest from various literature sources. Insufficient data are available to draw general curves.

TABLE 1-X

TENSILE STRENGTH OF SOME REFRACTORY OXIDES, psi (REF. 5)

Temperature, °C	Al_2O_2*	BeO*	MgO[†] (11% porosity)	ZrO_2[†] (4% porosity)	$MgO \cdot Al_2O_3$	$ZrO_2 \cdot SiO_2$[‡]
20	37,700	-	14,000	20,000	19,200	-
200	-	-	14,200	16,800	-	-
300	33,600	-	-	-	-	-
400	-	-	15,200	17,500	-	-
500	-	11,100	-	-	-	-
550	-	-	-	-	13,700	-
600	-	-	-	17,600	-	-
800	34,200	-	16,000	16,000	-	-
900	-	7,000	-	-	10,800	-
1000	-	-	11,500	14,800	-	-
1050	33,900	-	-	-	-	8,700
1100	-	-	10,000	13,500	-	-
1130	31,400	-	-	-	-	-
1140	-	2,000	-	-	-	-
1160	-	-	-	-	6,100	-
1200	18,500	-	8,000	12,100	-	3,600
1300	6,400 §	600	6,000	10,200 §	1,100	-
1400	4,300	-	-	-	-	-
1460	1,500	-	-	-	-	-

* Circular rods pulled in tension. Rods of small diameters gave higher specific strengths than rods of large diameters.

[†] Rectangular rods made by slip casting. ZrO_2 stabilized with 4% CaO. Tensile strengths determined by transverse loading.

[‡] Specimens hot-pressed, machined, and pulled in tension.

§ Calculated tensile strengths of 11,000 psi for Al_2O_2 and 20,000 psi for ZrO_2 from torsion measurements at 1300°C.

TABLE 1-XI

STRENGTH UNDER SHEAR BY TORSION OF SOME

REFRACTORY OXIDES, psi (REF. 5)

Temperature, $^{\circ}$C	Al_2O_2* (nonporous)	MgO* (12% porosity)	ThO_2† (1.7% porosity)	$MgO-Al_2O_3$* (5% porosity)
25-30	29,400	12,100	-	9,400
200	-	-	-	9,300
400	-	-	-	9,100
500	29,300	8,500	-	-
600	-	-	-	8,700
800	-	-	-	8,200
1000	23,600	7,700	-	7,500
1100	19,800	-	3,500	-
1200	13,200	-	-	6,400
1300	11,400	5,700	1,200	5,300
1400	6,500	-	-	-
1500	3,350	-	-	-

* Slip-cast specimens.

† Hydrostatically pressed specimens.

TABLE 1-XII

COMPRESSIVE STRENGTH OF SOME REFRACTORY OXIDES, psi (REF. 5)

Temperature, °C	Al_2O_3	BeO	ThO_2	ZrO_2	$MgO \cdot Al_2O_3$
20	427,000	114,000	214,000	300,000	270,000
400	214,000	-	156,000	-	-
500	-	71,000	-	228,000	199,000
600	199,000	-	85,000	-	-
800	185,000	64,000	71,000	-	171,000
1000	128,000	35,500	51,000	171,000	-
1100	85,000	-	-	-	85,500
1200	71,000	28,500	28,500	114,000	71,000
1400	35,600	24,000	5,700	18,500	21,400
1500	14,000	17,000	1,500	2,800	-
1600	7,000	7,000	-	-	8,500

NOTE: Samples were powder-pressed cubes about 6 mm square. The ZrO_2 was stabilized with MgO. Cylindrical shapes yielded values 15-20% higher. Bodies were fired at 1900°C.
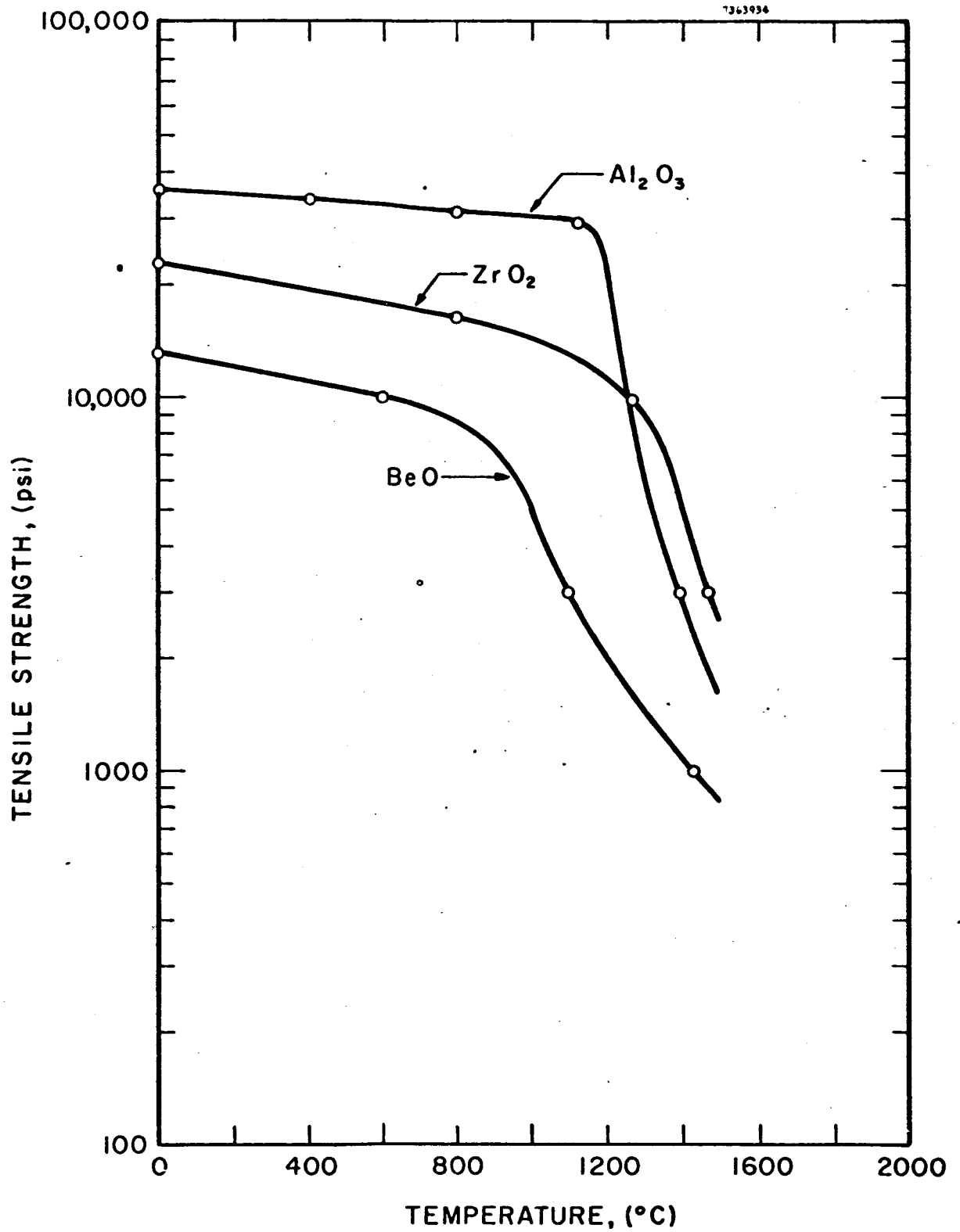
FIG. 1-10   EFFECT TEMPERATURE ON THE SHORT TIME STRENGTH OF
             SEVERAL OXIDE MATERIALS, AFTER KINGERY (REF. 3)

TABLE 1-XIII

LINEAR CREEP STRENGTH CERAMIC OXIDES (TENSION)

Material (Polycrystalline)	Stress, psi	Temperature $^\circ$C	Creep Rate (in/in hr)	References (see below)
Al_2O_3 - Sintered (7% perosity)	600	20	1.5×10^{-6}	(a)
Al_2O_3	50	1500	6×10^{-4}	(b)
Al_2O_3	50	1600	2×10^{-3} .	(b)
Al_2O_3	50	1700	6×10^{-3}	(b)
Al_2O_3	327	1462	6×10^{-1} (Fractured in 6 min. at 2.3% elongation)	(c)
Al_2O_3	278	1467	3×10^{-2} (after 40 minutes)	(c)
MgO	50	1400	4×10^{-2}	(b)
MgO	50	1300	9×10^{-5}	(b)
Cast MgO	1200	1100	0.7×10^{-6}	(d)
Hydrostatically Pressed MgO	1200	1100	0.15×10^{-6}	(d)
ThO_2	1200	1100	2.06×10^{-6}	(d)
BeO	108	1650	3.3×10^{-5}	(e)
BeO	108	1700	7.7×10^{-5}	(e)
BeO	108	1744	1.47×10^{-4}	(e)
BeO	54	1550	9.5×10^{-6}	(e)
BeO	108	1550	2.0×10^{-5}	(e)
BeO	216	1550	4.0×10^{-5}	(e)

Reference (a)   Coble, R. L. and Kingery, W. D., "Effect of Porosity on Physical Properties of Sintered Alumina," J. Am. Ceram. Soc., Vol. 39, 1956.

   (b)   Kingery, W. D., "Oxides for High Temperature Applications," "High Temperature Technology, 1959 Symposium."

TABLE 1-XIII (Cont.)

(c) Chang, Roger, "Creep and Anelastic Studies of Al_2O_3," U. S. Atomic Energy Comm. Research and Development Report, NAA-SR-2770, Atomics International, Sept. 1958.

(d) Wygant, F., "Elastic and Flow Properties of Dense, Pure Oxide Refractories," J. Am. Ceram. Soc., 39 (12), 1951.

(e) Chang, R., "Creep of Polyerystalline BeO at High Temperatures and Low Stresses," U. S. Atomic Energy Comm. R and D Rept., NAA-SR-2458, May 1, 1958.

TABLE 1-XIV

RELATIVE TORSIONAL CREEP FOR SEVERAL OXIDES (REF. A-3)

Oxide	Creep Rate at $1300^{\circ}C$, 1800 psi*
Al_2O_3, sapphire crystal	0.01×10^{-5} in/in/hr
Al_2O_3, polycrystalline	0.13×10^{-5}
BeO, polycrystalline	(30×10^{-5})
MgO, polycrystalline, slip cast	33×10^{-5}
MgO, polycrystalline, hydrostatically pressed	3.3×10^{-5}
$MgAl_2O_4$, polycrystalline (2-5 μ grain size)	26.3×10^{-5}
$MgAl_2O_4$, polycrystalline (1-3 mm. grain size)	0.1×10^{-5}
ThO_2, polycrystalline	(100×10^{-5})
UO_2, polycrystalline	(18×10^{-5})
ZrO_2, polycrystalline, stabilized	3×10^{-5}
$ZrSiO_4$, polycrystalline (Containing SiO_2 glass?)	$(10,000 \times 10^{-5})$

*Values in parentheses are extrapolated.

The difference between polycrystalline and single crystal deformation is illustrated for Al_2O_3 in Table 1-XIV. In the same way, data for spinel indicates the large effect of crystallite size for a single phase polycrystalline material; in this case, the creep rate for a 2-5 micron grain size sample was found to be 263 times that for a 1-3 millimeter grain size sample of the same composition. Unfortunately, there are few descriptions of grain sizes, detailed microstructures, and grain boundary composition reported in the literature.

A small amount of porosity will have a particularly large affect on the deformation of polycrystalline oxides. Kingery has shown (Ref. 3) that the presence of 10 volume percent porosity (which is common in sintered oxides refractories) decreases the creep strength by an order of magnitude. Because of the combined and large affects of grain size and porosity, Kingery estimates that most of the creep strength data and literature for polycrystalline oxides is lower by at least an order of magnitude than the optimum values that could be achieved. He predicts that, for materials such as aluminum oxides that have strongly crystallographic deformation with only one active slip plane, it is probable that completely dense polycrystalline material of high purity would have greater deformation resistance than a random orientation of single line crystals. This prediction is borne out by the strength data of Table 1-II, which shows that 100 percent dense alumina (GE Lucalox and National Beryllia Alox) exhibits tensile strengths almost double that of 99 percent alumina bodies.

1.2.6 Thermal Properties and Thermal Shock Resistance

The thermal properties of main interest for thermionic diode application are the thermal expansion coefficient, conductivity, stress resistance and emissivity. These properties for the refractory oxides of interest are presented in Figures 1-11 through 1-14. The curves represent a selection of best or average values from extensive compliations of data presented in Ref. 1.
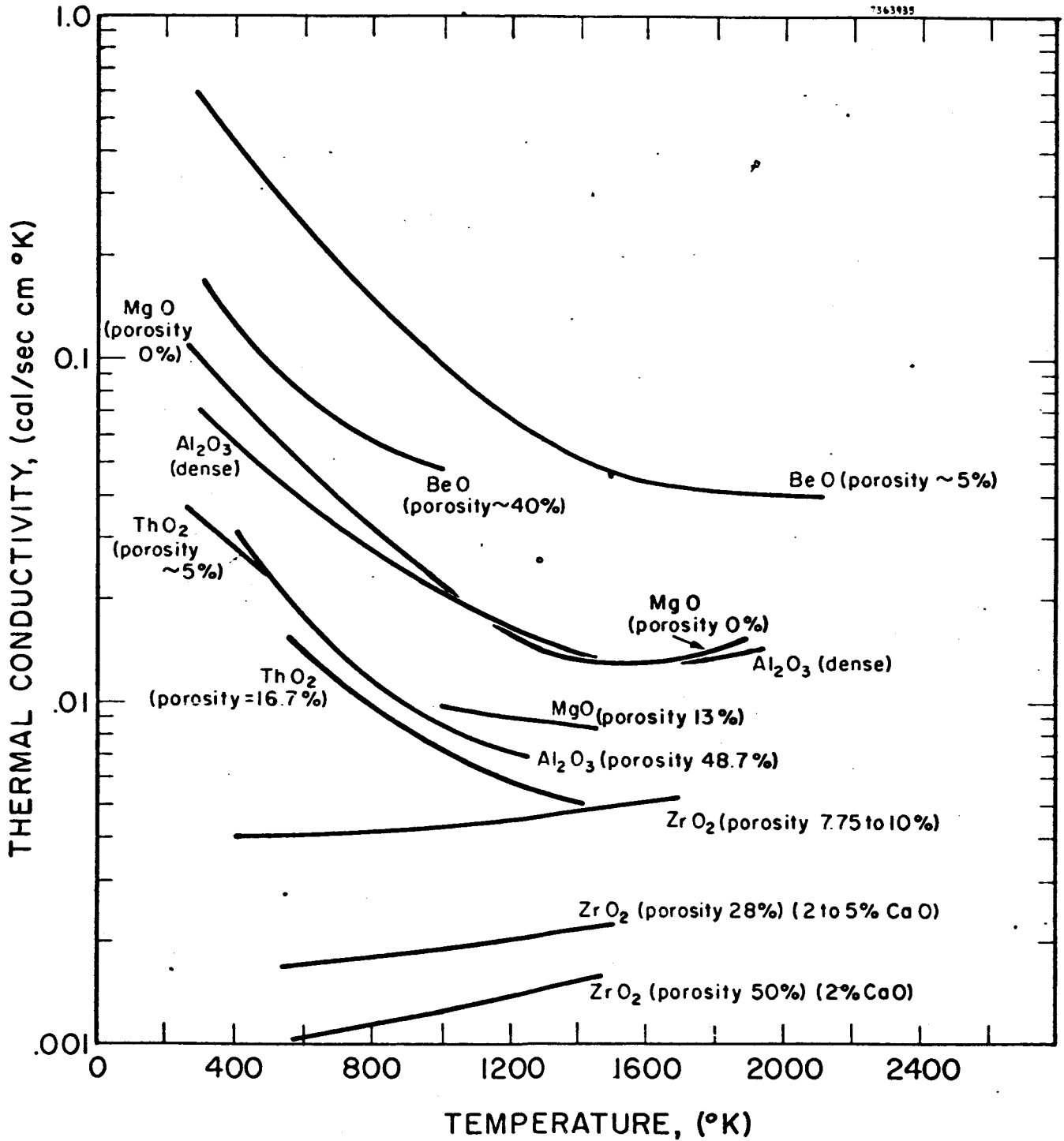
FIG. 1-11 THERMAL CONDUCTIVITY OF POLYCRYSTALLINE CERAMIC MATERIALS (REF. 1)
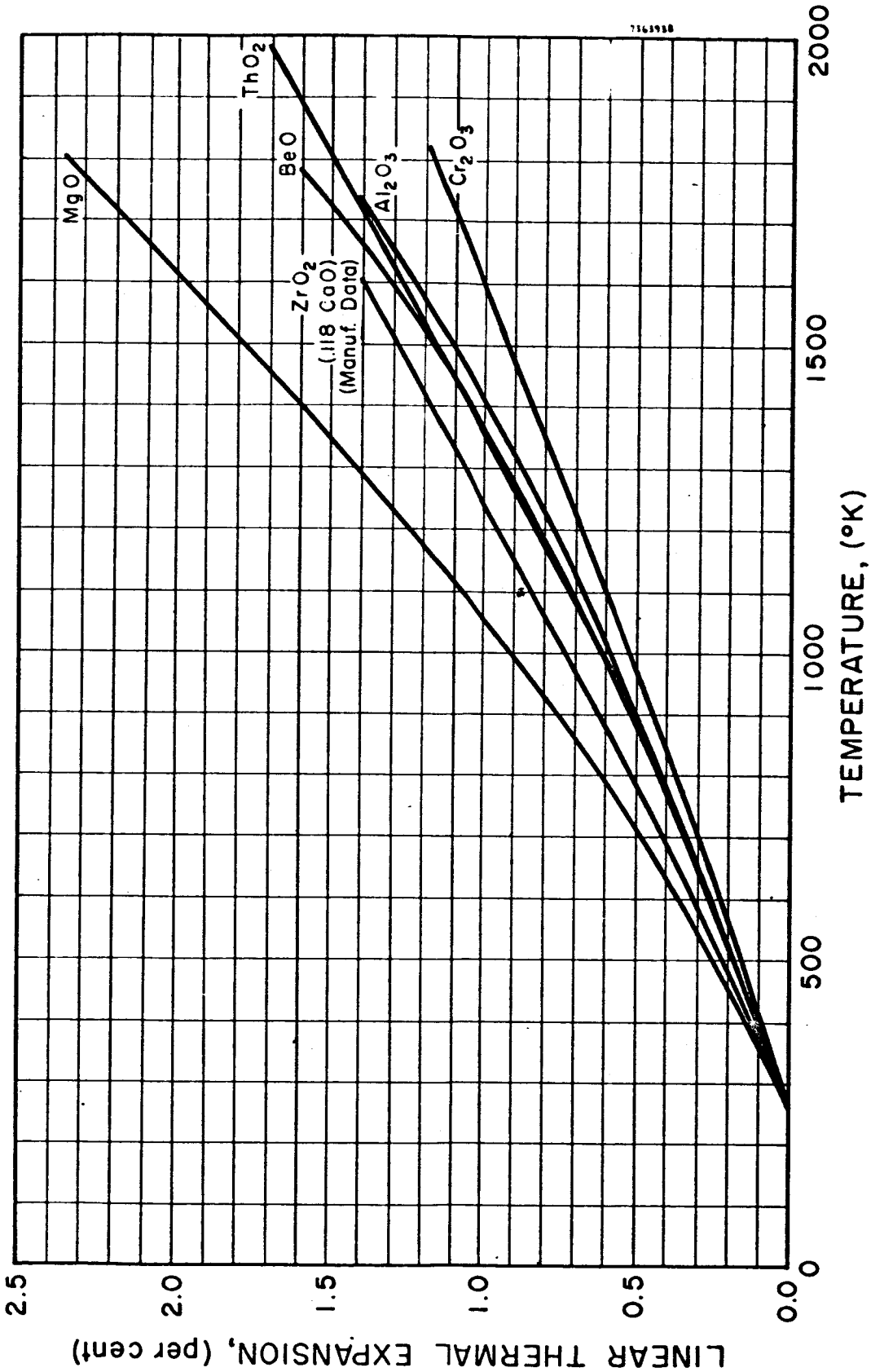
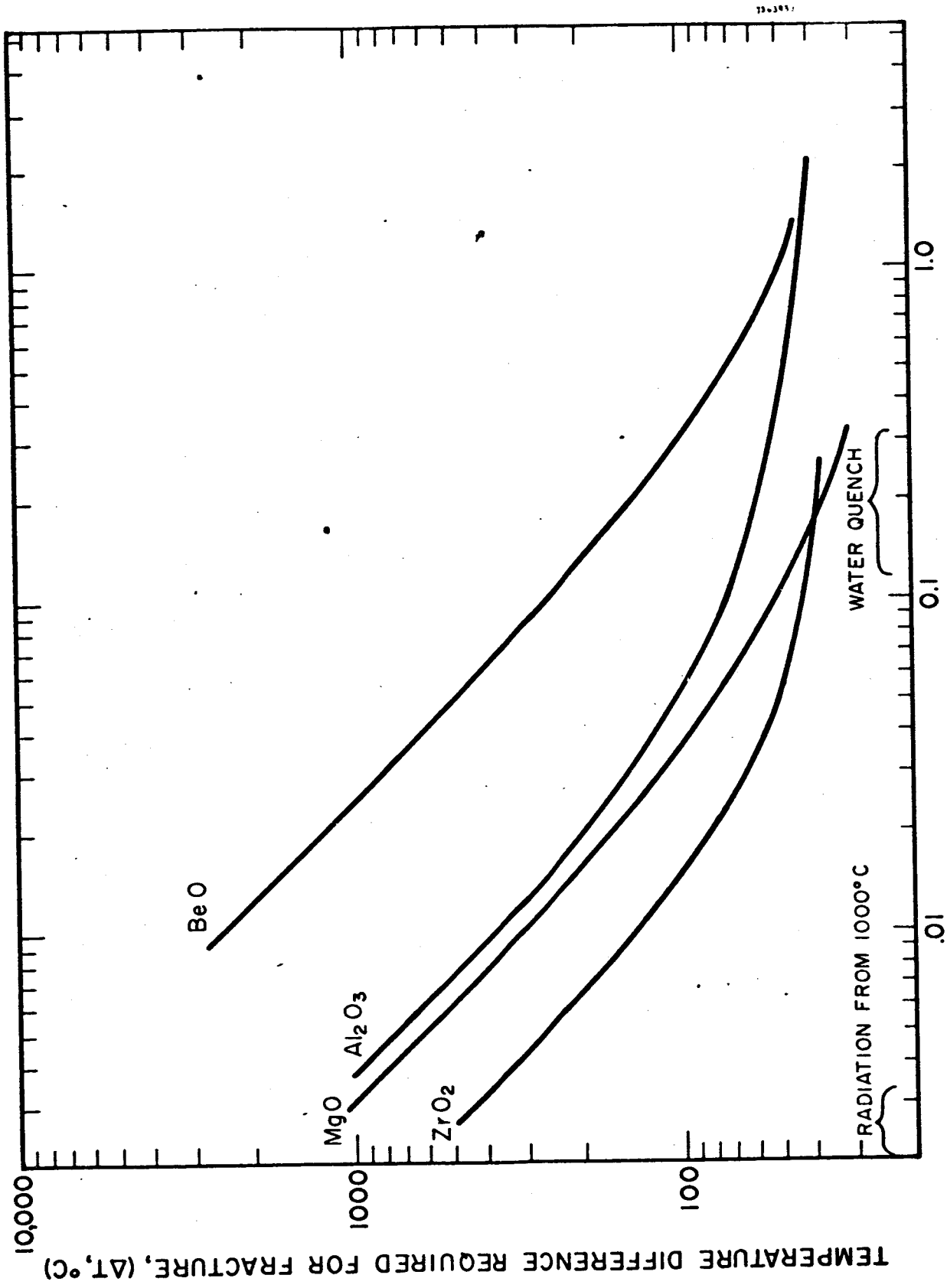FIG. 1-12 LINEAR THERMAL EXPANSION OF CERAMIC OXIDES (REF. 1)

FIG. 1-13 THERMAL RESISTANCE OF A NUMBER OF OXIDES, AFTER KINGERY (REF. 3)
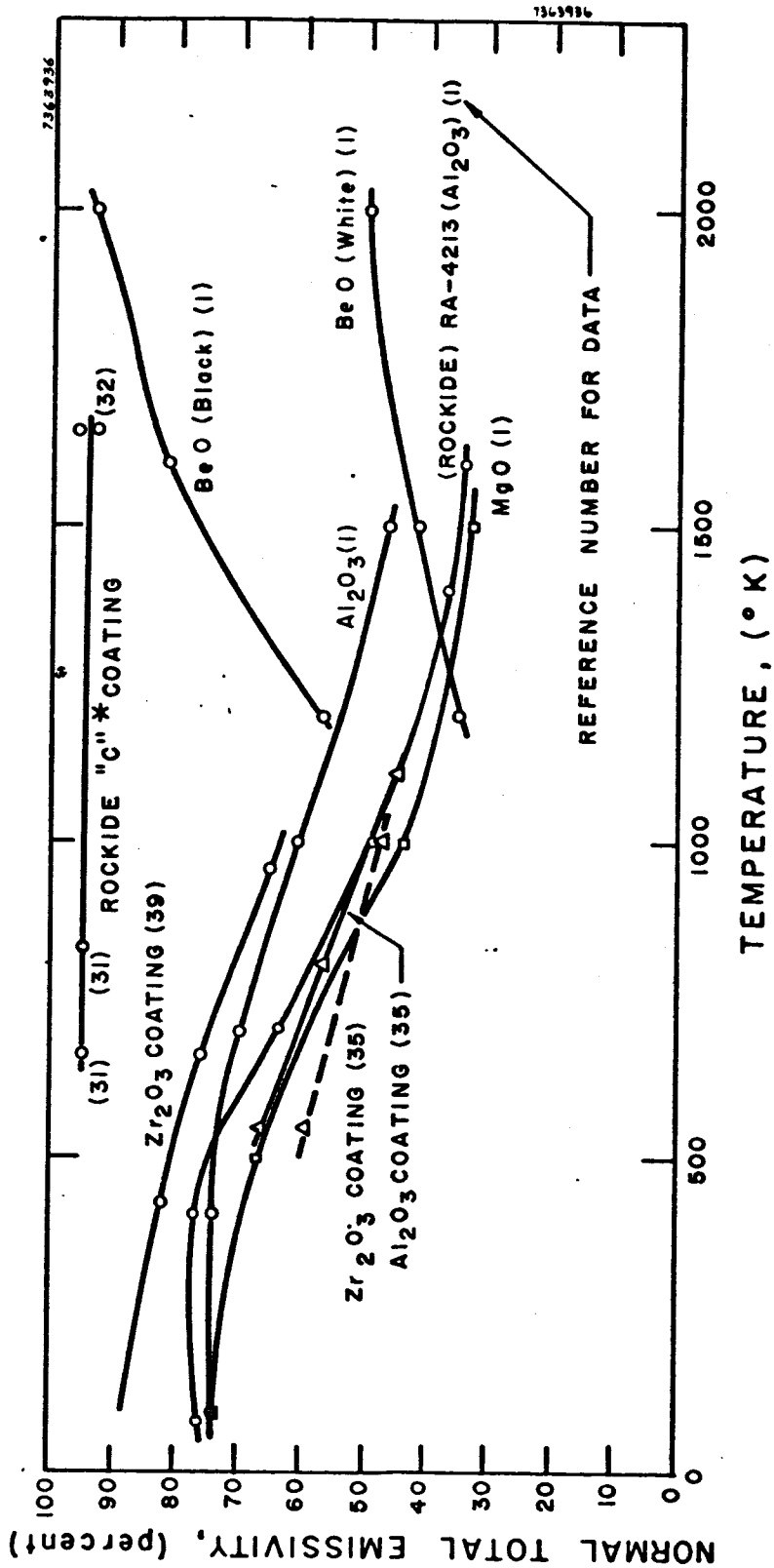
7363933

FIG. 1-14 TOTAL NORMAL EMISSIVITY OF CERAMIC MATERIALS

The expansion coefficient, as shown in Table 1-II, will tend to decrease when increasing amounts of silica are used which can absorb considerable energy without increasing the specific volume. The thermal conductivity is a strong function of porosity as illustrated in Figure 1-11. As illustrated in Table 1-II, the thermal conductivity also depends greatly on the details of composition and structure. In particular, solid solutions have a substantially decreased thermal conductivity. Therefore, a small amount of impurities can cause a substantial decrease in conductivity.

Thermal stresses which result in fracture of ceramic materials arise as a result of differential expansion tendencies of different parts of a structure caused by different changes in temperature relative to some average value. These may be particularly harmful in oxides during cooling when the surface has a lower than average temperature and surface tensile stresses result. The magnitude of these stresses depends on the dtails of the thermal treatment and the thermal-mechanical properties of the material. These relationships are complex (see Refs. 1 and 5). In general, the thermal stress resistance determining the temperature difference between initial conditions and final conditions that can be withstood without failure is proportional to a shape factor times a material stress resistance factor as given below.

$$\Delta T_f = \frac{(ts)(1-\mu)}{E\alpha} \cdot S \qquad \text{rapid rate of cooling}$$

$$\Delta T_f = \frac{k(ts)(1-\mu)}{E\alpha} \cdot S \qquad \text{slow rate of cooling}$$

where

ts = tensile strength

μ = Poisson's ratio

E = elastic modulus

k = thermal conductivity

α = expansion coefficient

s = shape factor

The relationship between the maximum temperature difference required for surface stresses equal to the tensile strength for different sample sizes and conditions was calculated by Kingery and is shown in Figure 1-13. As indicated there, the relative utility of different kinds of materials changes with the conditions of heat transfer. All of the values can be substantially raised if data corresponding to the optimum strength values that can be obtained are used. The thermal shock resistance shown in Figure 1-13 corresponds to the initiation of fracture at a surface. In practice it is found that cracks initiated at the surface in porous bodies or in polyphase ceramics are frequently not transferred from the highly stressed area in the surface into the interior. Consequently, while surface checking may occur, complete fracture and spalling of pieces from the body does not take place. For this reason samples with moderate porosity frequently are described as having superior thermal spalling resistance. Cracks initiate but do not propagate; consequently, the thermal stress cracks are not observed unless they are very carefully searched out. In general, the thermal shock resistance is most satisfactory for high conductivity ceramics such as beryllium oxide, aluminum oxide and, perhaps, magnesium oxide. For materials of lower thermal conductivity, such as zerconia and thoria, resistance to thermal stresses is less satisfactory.

Figure 1-14 shows some curves of measured data for normal thermal emissivity of ceramic bodies and coatings. Emissivity will be strongly effected by porosity, the nature of the sintering and coating process, and other factors.

In recent years it has become possible to coat metallic structures with thin layers of refractory oxides by flame spraying and other techniques. Commercially available coatings include alumina, stabilized zerconia, thoria, magnesia, chromic oxide, several types of silicates, and mixtures of refractory oxides. For safety reasons, beryllia has not yet been commercially applied.

2210-Final

The material properties of the flame spray coatings
are changed somewhat. Porosities on the order of 7 to 15 percent can
be expected, and, at least in the case of zirconia, some changes
in crystal structure can result.

1.2.7 Electrical Properties

The two electrical properties of most interest to
thermionic diode application are the electrical resistivity of the
material and the dielectric breakdown strength. A summary of the
experimental data regarding electrical resistivity of the ceramic
oxides of interest is presented in Ref. 11 and is shown in Figure 1-15.
The curves refer is dense samples with low porosity; however, the exact
nature of the material is generally not specified. As shown, alumina
and beryllia exhibit high resistivity at all temperatures of interest.
Some care must be used in selecting zirconia, thoria, and chromic
oxide for structural bodies and for coatings.

Very little data have been accumulated on the dielectric
strength of ceramic materials. Dielectric strength, i.e., the voltage
at which electrical breakdown will occur through a sample slab of a
given thickness is generally dependent on temperature, specimen thick-
ness and the vacuum environment. From observation of the scattered
data in Table 1-XV it appears that dielectric breakdown may be a
strong function of the glassy constituents of the ceramic body.

Since the output voltage of the thermionic diode is
in the range of a few volts, the chances of dielectric breakdown across
the seal structure are remote. However, it may be desirable to use
ceramic coatings on the exterior of the diode for thermal or electrical
insulation. During testing with electron bombardment heater, up to
several kilovolts may exist as a potential across these coatings and
dielectric breakdown must be considered as a source of potential trouble.
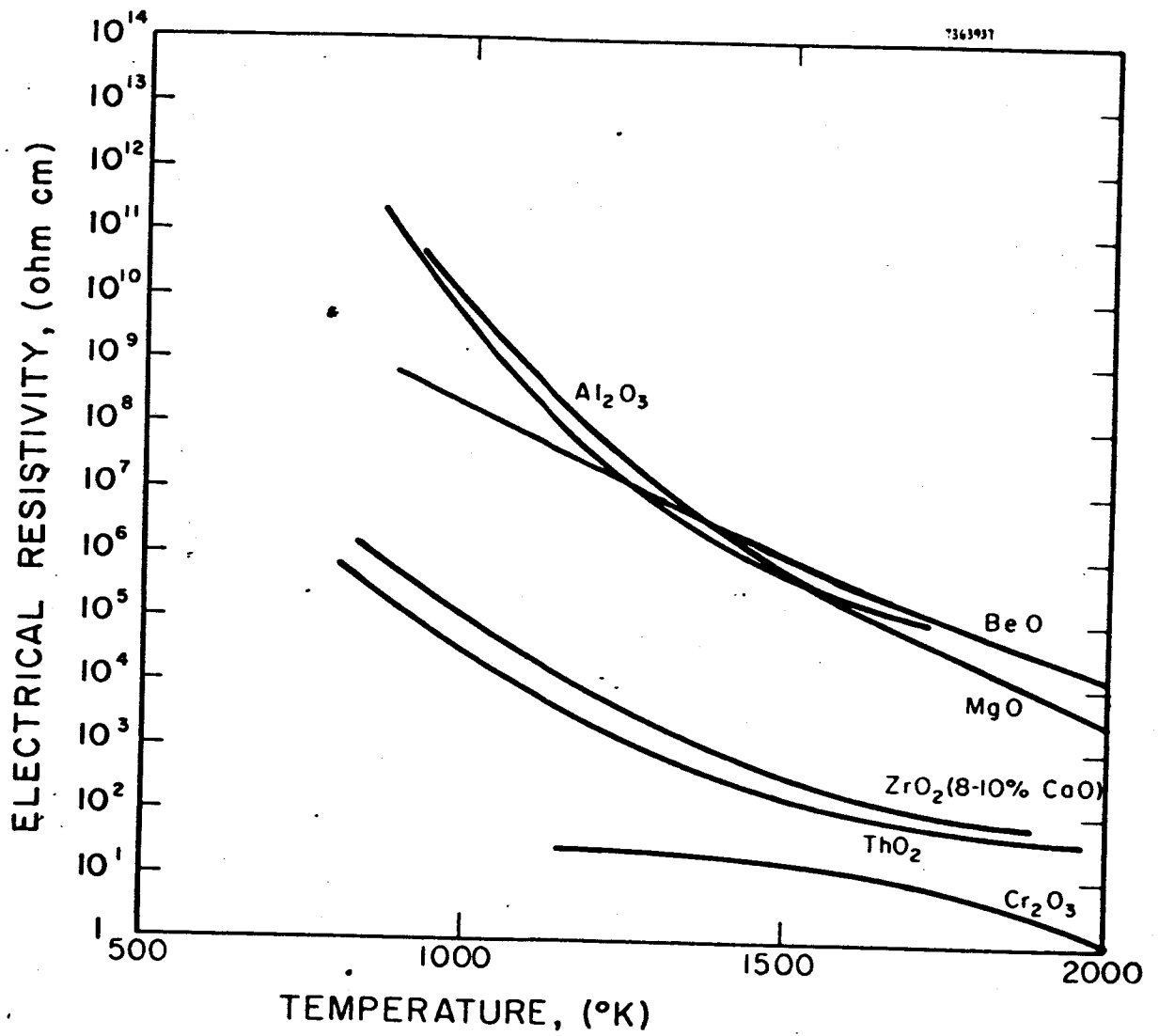
FIG. 1-15   ELECTRICAL RESISTIVITY OF CERAMIC MATERIALS (REF. 1)

TABLE 1-XV

DIELECTRIC BREAKDOWN OF MATERIALS

Material	Purity %	Sample Thickness in.	Temperature °C	Breakdown Strength volts/mil	Note
Al_2O_3	-	0.200	1200	4.0	Ref. 9
MgO	-	0.200	1200	4.0	Ref. 9
BeO	-	0.200	1000	4.0	Ref. 9
ZrO_2	-	0.200	780	4.0	Ref. 9
Al_2O_3	99.9+	-	20	1700	Mfg. data G.E.
Al_2O_3	94	-	20	225	Mfg. - Frenchtown
Al_2O_3	99	0.25	20	220-240	Mfg. - Coors
		0.125	20	330	Mfg. - Coors
Al_2O_3	96	0.25	20	220-240	Mfg. - Coors
		0.125	20	340	Mfg. - Coors
BeO	99.5	0.030	20	200	Mfg. - Brush Bery.
BeO	98.5	0.030	20	300	Mfg. - Brush Bery.
BeO	96	0.25	20	238	Mfg. - Coors
		0.125	20	339	Mfg. - Coors

REFERENCES

The following references summarize the material on hand at EOS that was used in preparation of the chapter on High Temperature Ceramic Materials. Many of these references are summary-type articles which represent collections of data from more specific types of literature. References 1 through 8 summarize the general state-of-the-art in ceramic materials and contain about 80 or 90 percent of the available data of interest, including most of the pertinent specific references.

REFERENCES

1. Goldsmith, Waterman, Hirschhorn, Handbook of Thermophysical Properties of Solid Materials, MacMillan, 1960.

2. Smiley, W. D., et al, Mechanical Property Survey of Refractory Nonmetallic Crystalline Materials and Intermetallic Compounds, Stanford Research Institute, WADC Technical Report 59-448, January 1960.

3. Kingery, W. D., Oxides for High Temperature Application, Proceedings of an International Symposium on High Temperature Technology, McGraw-Hill Book Company, October 1959.

4. Kingery, W. D., Property Measurement at High Temperatures, John Wiley and Sons, Inc., New York, 1959.

5. Campbell, I. E., Editor, High Temperature Technology, John Wiley and Sons, Inc., New York, 1956.

6. Latva, I. D., Ceramics and Intermetallics, part of Materials Symposium, ASD Technical Report 61-322, 13-15 September 1961.

7. OTS PB 161194, DMIC Memo 44, Refractory Materials, Defense Metals Information Center, Battelle Memorial Institute, Columbus, Ohio, February 26, 1960.

8. Kohl, W. H., chapter on Ceramics in Materials and Techniques for Electron Tubes, Reinhold Publishers, 1960.

9. Knoll, M., Materials and Process of Electron Devices, Springer-Verlag, 1959.

10. Collins, J. F., Stability of Ceramic Materials in Liquid Sodium at Temperatures up to $2000^{\circ}F$, Fairchild Engine and Airplane Corp., Report IC-51-1-58, January 23, 1951.

11. Wagner, P., and Coriell, S., On the High-Temperature Compatability of Cesium Gas with Sonce Dielectrics, Review of Scientific Instruments, Vol. 30, No. 10, October 1959.

12. Brotherton, et al, Properties and Handling Procedures for Rubidium and Cesium Metals, AIME National Meeting, St. Louis, February 28 - March 2, 1961.

13. Hughes Research Laboratory, Design, Fabrication and Testing of a Cesium Ion Rocket Engine, NAS 5-517, QPR No. 2, February 1961.

14. Hughes Research Laboratory, Design, Fabrication and Testing of a Cesium Ion Rocket Engine, NAS 5-517, QPR No. 3, May 1961.

15. Kuskevics, Cesium Properties and Interactions with Surface Ion Emitters, General Electric Report No. R61FPD455, September 12, 1961.

16. Liquid Metals Handbook, NAVEXOS P-733 (Rev.), June 1952.

17. McCreight, L. R., Static Sodium Corrosion Test of Ceramic Materials, KAPL, Memo-LRM-2, July 6, 1951.

18. Reed, E. L., Stability of Refractories in Liquid Metals, J. of the Amer. Ceram. Soc., Vol. 37, No. 3.

19. Burger, E. E., and J. H. Westbrook, Characteristics of Cesium Electron Tubes, General Electric Research Laboratory, RL-430, August 30, 1950.

20. Wachtman, J. B., and Maxwell, L. H., Factors Controlling Resistance to Deformation and Mechanical Failure in Polycrystalline (Glass-free) Ceramics, PB Report 131623, U.S. Govt. Rsch. Report 29(5)274, 1958.

21. Dorn, J. E., Editor, Mechanical Behavior of Materials at Elevated Temperatures, McGraw-Hill, 1961.

22. Folweiler, R. C., Creep Behavior of Pore-Free Polycrystalline Aluminum Oxide, J. of Applied Physics, Vol. 32, No. 5, May 1961.

23. Dushman, and Lafferty, Scientific Foundations of Vacuum Technique, John Wiley and Sons, Inc., New York, 1962.

24. Kelly, K. K., Contributions to the Data on Theoretical Metallurgy; The Free Energies of Vaporization and Vapor Pressures of Inorganic Substances, U.S. Bur. Mines Bul. 383, 15, 1935.

25. Navias, L., and Sears, G. W., Evaporation of Aluminum Oxide, J. of Applied Physics.

26. Pollock, B. D., Saul, A. M., Milne, T. A., The Vaporization of Beryllium Oxide, NAA-SR-3727, 1960.

27. Samsonov, G. V., Yasinskaya, G. A., Shiller, E. A., The Reaction of Certain Oxides and Carbides with Refractory Metals at High Temperatures, AD 265808.

28. Bergeron, C. G., Tennery, V. J., Freidberg, A. L., Reaction Studies of Ceramic-Coated Tungsten, J. of the Amer. Ceram. Soc., Vol. 44, No. 4.

29. Barth, V. D., Rengstoroff, G. W. P., Oxidation of Tungsten, DMIC Report No. 155, July 17, 1961.

30. Klein, J. D., Radiation Heat Transfer To and From Ceramic Coatings on Metals, Ceramic Bulletin, Vol. 40, No. 6, 1961.

31. Blair, G. R., Determination of Spectral Emissivity of Ceramic Bodies at Elevated Temperatures, J. of the Amer. Ceram. Soc., Vol. 43, No. 4, April 1960.

32. Allen, R. D., Spectral and Total Emissivities of Rokide C on Molybdenum Above $1800^{o}F$, J. of Amer. Ceram. Soc., Vol. 40, No. 7, 1961.

33. Wade, W. R., Slemp, W. S., Measurements of Total Emittance of Several Refractory Oxides, Cermets, and Ceramics for Temperatures from $600^{o}F$ to $2000^{o}F$, NASA TN D-998, March 1962.

34. Wood, W. D., Deem, H. W., Lucks, C. F., The Emittance of Coated Materials Suitable for Elevated-Temperature Use, OTS PB 171622, DMIC Memo 103, May 4, 1961.

35. Coatings for the Protection of Refractory Metals from Oxidation, DMIC Memo 162, November 24, 1961.

36. Levenstein, M. A., Properties of Plasma Sprayed Materials, WADD Technical Report 60-654, January 1961.

37. Klopp, W. D., Review of Recent Developments on Oxidation-Resistant Coatings for Refractory Metals, DMIC Memo 120, July 31, 1961.

38. Florio, J. V., Dielectric Properties of Alumina at High Temperatures, J. of the Amer. Ceram. Soc., Vol 43, No. 5.

39. Pappis, J. Kingery, W. D., Electrical Properties of Single-Crystal and Polycrystalline Alumina at High Temperatures, J. of the Amer. Ceram. Soc., Vol. 44, No. 9.

40. Kingery, W. D., J. of Amer. Ceram. Soc., 38, 3, 1955.

41. Slivka, J. M., Thermionic Power Conference, 1962, Colorado Springs

2. MATERIALS

2.1 Emission Properties of Emitter and Collector Materials, and In Particular Various Refractory Substrates

Thermionic emission from cesium films on tungsten was given early theoretical and experimental treatment by a number of investigators (Refs. 1 - 4). The majority of experimental work was involved with low orders of cesium arrival rates, low emitter temperatures, and a narrow selection of emitter materials. On the other hand, the theoretical contributions were somewhat complete and have sustained only minor corrections and few further significant contributions to date. The impetus for most of these early investigations was research knowledge in itself (e.g., the formulation of general theories for evaporation, condensation, and absorption).

At present, advanced power requirements for space flight have involved thermionic emission from cesiated surfaces as an agent for direct conversion of heat into useable electric energy. These applications generally require long life and high emission densities. The research areas have accordingly been directed towards higher cesium arrival rates, higher emitter temperatures, and the thermionic performance of a wide selection of cesiated refractory materials.

This section is devoted to a presentation and discussion of the thermionic emission data presently available for various cesiated refractory substrates. Thermionic theory, as it applies to the emission from cesiated surfaces, is also briefly reviewed. Where applicable, the text is directed to the problems of design and operation of practical converter devices. The data presented on thermionic emission from cesiated substrates applies equally well to thermionic converter emitters or collectors.

The predicted electron emission from a cesium layer on tungsten follows from a model first proposed by Langmuir (Ref. 1). There have since been reinterpretations, revisions, and additions to this work (Refs. 5 - 7) but it still stands today as the primary source of acceptable theory and experiment

for adsorption and emission phenomena pertaining to cesiated surfaces. This model asserts that the energy difference between the work function of tungsten (4.62 volts) and the ionization potential of cesium (3.88 volts) favors the transfer of a valence electron from the cesium atom to the tungsten. The cesium, now a positively charged ion, forms a dipole with its electrostatic image in the tungsten. By considering this dipole layer as a parallel plate condenser, a potential energy of the dipole layer derives as:

$$V_s = 2\pi M \epsilon \text{ (e.s.u.)} \qquad\qquad \text{Eq. (1)}$$

where

M is the dipole moment of the positive ion and its negative image

ϵ is the surface concentration of cesium ions as a percentage of the total available surface

V can more appropriately be regarded as the change in work function or the contact potential because it is the change in energy required to remove an electron from the substrate material covered by an adsorbed layer of cesium.

The ratio of electron emission from a cesiated tungsten surface to the bare tungsten surface in thermodynamic equilibrium is given as:

$$\upsilon_e/\upsilon_w = e^{Ve/kT} \qquad\qquad \text{Eq. (2)}$$

where:

υ_e is the electron emission from the cesiated tungsten surface

υ_w is the electron emission from bare tungsten surface

V is the contact potential between bare tungsten and the cesiated tungsten

T is the surface temperature in $^{\circ}K$

Since the emission, υ_w, is known from vacuum emission experiments, the emission from cesiated surfaces, υ_e, may be computed. In practice, it is found that the contact potential does not increase as predicted beyond a surface coverage of approximately 47 percent of the bare surface. Instead, repulsive short range forces between adions causes the contact potential to decrease

as the coverage increases beyond 67 percent.

This phenomenon gives rise to a maximum electron emission at that coverage. At higher coverages the emission decreases. When the electron emission as a function of emitted temperature is plotted in the proper fashion one obtains the familiar Langmuir "S" curve. Because the cesium arrival rate and the emitter temperature define a certain emitter coverage, θ, each "S" curve is associated with a particular arrival rate and an entire family of curves may be generated with different arrival rates as a parameter as indicated in Fig. 2-1.

Langmuir summed up the behavior of such adsorbed films on surfaces in his surface phase postulate, "All the properties of an adsorbed film on an underlying surface of given composition are uniquely determined by θ and T."

2.1.1 Survey of Existing Thermionic Data

In this section the currently available data for emission from cesiated surfaces is reviewed. Figure 2-2 references the data and includes a summary of remarks that identify the appropriate experimental areas. Figures 2-3 through 2-7 are a compendium of recent thermionic data displayed on Langmuir plots with lines of constant work function ($A = 120$ amps/cm^{2}K^2) for reference.

2.1.2 Measurement Evaluation

There appear to be six areas pertaining to measurement of electron emission from cesiated substrates where extreme care concerning experimental technique and interpretation is required. The six areas are enumerated and discussed as follows:

1. Zero-field emission measurements
2. Emitter temperature measurement
3. Cesium arrival rate
4. Emission area and electrode geometry
5. Emitter heating method
6. Material preparation
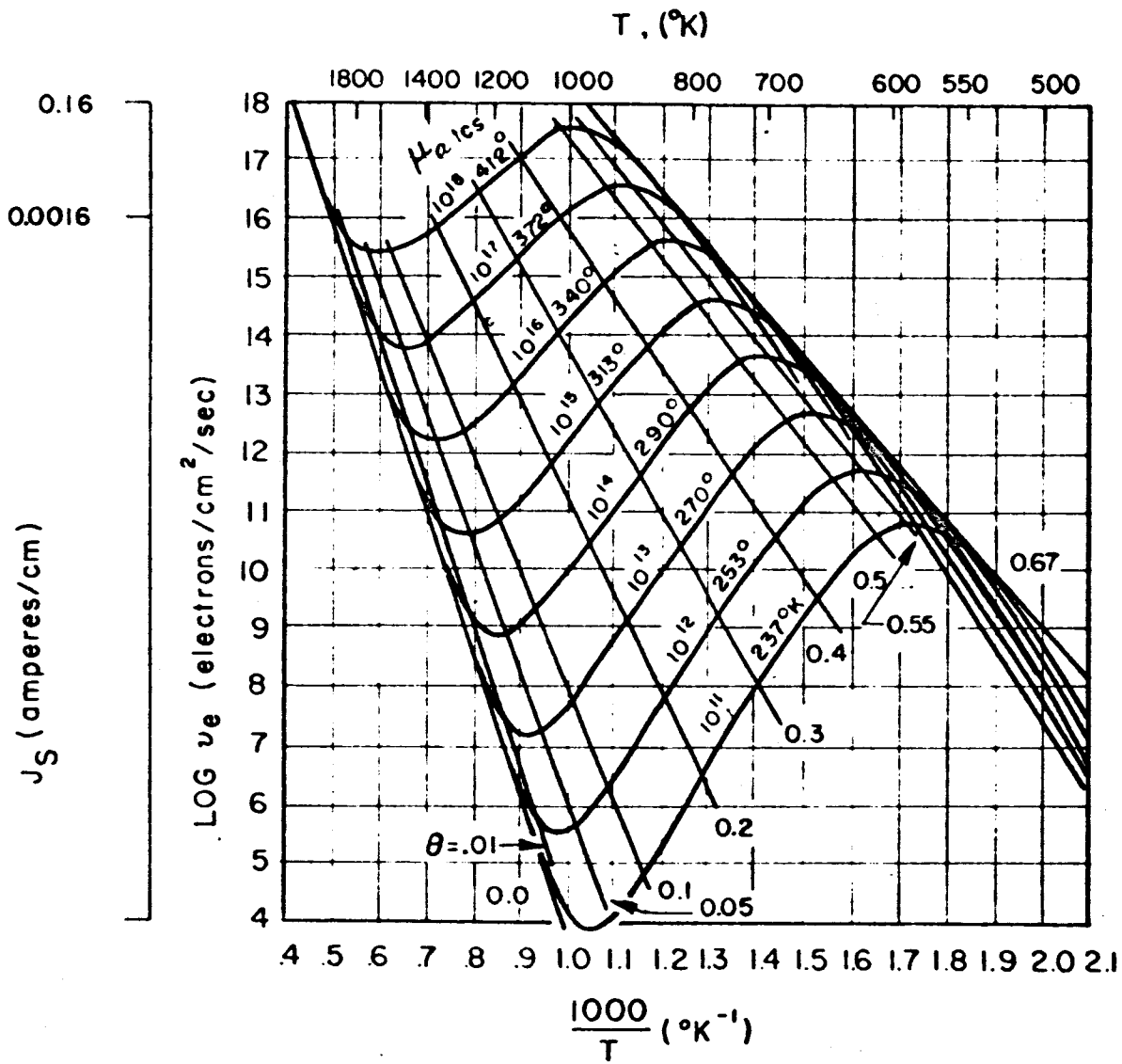
FIGURE 2-1   FIELD-FREE ELECTRON EMISSION (CALCULATED) FROM A
TUNGSTEN FILAMENT IN EQUILIBRIUM WITH Cs VAPOR AT
FILAMENT TEMPERATURE T

MATERIAL	AUTHORS	REFERENCE	CS RESERVOIR
W, TA, Re, Ir	GUST, W.H.	UCRL 6809 REV. I	NO INFORMATION
MO	RASOR, N.S.	ARS SPACE POWER SYSTEMS CONFERENCE 1960	NO INFORMATION
MO	AAMODT, R.E.	1962 THERMIONIC POWER CONVERSION CONFERENCE	NO INFORMATION
TA, MO	THERMO-ELECTRON ENGINEERING CORPORATION	TEE-4015-I	EXTREMELY LONG TRANS-FER TUBE FROM RESERVOIR TO ELECTRODES.
TA, MO, W Re	HOUSTON, J.M.	BULL. AM. PHYS. SOC. SERIES II, NO. 6 1961 P. 358.	ENTIRE DISCHARGE TUBE EMMERSED IN ISOTHERMAL BATH
TA, MO, W	FIRLE, T.E.	GA-2511	LONG TRANSFER TUBE FROM RESERVOIR TO HOT ZONE.
TA	CAMPBELL, A.E.	THESIS (SAN DIEGO STATE COLLEGE); UNPUBLISHED	ENTIRE DIODE IN ISOTHER-MAL BATH. I.E. NO TRANS-FER TUBE.
TA	WILSON, V.C.	1962 THERMIONIC POWER CONVERSION CONFERENCE.	LONG TRANSFER TUBE FROM RESERVOIR TO ELECTRODES.
MO	JENSEN, A.O.	PROCEEDINGS OF THE 15 TH ANNUAL POWER SOURCES CONFERENCE	SHORT TRANSFER TUBE FROM RESERVOIR
TA	WESTINGHOUSE	ASD TECHNICAL REPORT 61-281	NO INFORMATION

FIG 2.2 (A)

ZERO FIELD EMISSION MEASUREMENT	MATERIAL FORM	REMARKS TEMPERATURE MEASUREMENT
SWEEP TRANSFORMER	WIRE FILAMENTS	OPTICAL PYROMETER MEASUREMENTS OF EMITTER TEMPERATURES
X-Y PLOTTER	NO INFORMATION	NO INFORMATION
100 μ SEC PULSES SYNCHRONIZED WITH NULL PORTION OF HEATING CYCLE	LONG WIRE	OPTICAL PYROMETER ABOVE 1000 °K. RESISTIVITY MEASUREMENTS BELOW 1000 °K
POINT BY POINT I-V PLOT. MANUAL SWITCHING OF LOAD.	NO INFORMATION	EMITTER TEMPERATURE MEASUREMENT BY PYRO FROM HOHLRAUM.
POINT BY POINT I-V PLOT.	WIRE FILAMENTS	OPTICAL PYROMETER CALIBRATION OF RESISTIVITY OF FILAMENTS.
SWEEP TRANSFORMER 60 CYCLE. LEAKAGE CURRENTS PREDOMINATE BELOW 2×10^{-3} amps/cm^2	Ta & Mo EMITTERS OF SEAMLESS TUBING. W EMITTER SOLID ROD.	EMITTER TEMPERATURE DETERMINED BY T/C. CALIBRATED BY PYRO TO HOHLRAUM.
SWEEP TRANSFORMER & POINT BY POINT. CHILD'S PLOTS FOR ZERO FIELD EMISSION.	Ta (ELECTRON BEAM MELT) BAR STOCK.	EMITTER TEMPERATURE DETERMINED BY T/C. CALIBRATED BY PYRO TO HOHLRAUM.
NOT GIVEN	NOT GIVEN	NOT GIVEN
SWEEP TRANSFORMER 60 CYCLE AND POINT BY POINT I-V PLOT	MOLY FLAT STOCK	EMITTER TEMPERATURE DETERMINED BY T/C AND PYRO.
SWEEP TRANSFORMER 60 CYCLE	FLAT STRIP FROM SHEET STOCK.	EMITTER TEMPERATURE MEASURED WITH PYROMETER THRU SAPPHIRE WINDOW.

FIG. 2.2 (B)

EMITTER HEATING	MATERIAL PREPARATION	EMISSION AREA AND ELECTRODE GEOMETRY
DIRECT HEATING	EXTENSIVE OUTGAS OF ALL PARTS IN FINAL ASSEMBLY	CYLINDRICAL GEOMETRY GUARD RINGED GLASS ENVELOPE. EMISSION AREA NOT GIVEN.
NO INFORMATION	NO INFORMATION	CYLINDRICAL GEOMETRY
DIRECT HEATING	EXTENSIVE OUTGAS $\sim 10^{-9}$ mm Hg AT SEAL OFF.	CYLINDRICAL GEOMETRY, GUARD RING
INDIRECT BY ELECTRON BOMBARDMENT POSSIBLE TEMPERATURE GRADIENT ON SURFACE.	LONG OUTGAS. ASSEMBLY BAKEOUT WITH VAC ION Ta GETTER.	4.25 cm^2 PLANE PARALLEL GEOMETRY. VARIABLE SPACING; NON POSITIVE. NO GUARD RING.
DIRECT HEATING	EXTENSIVE OUTGAS AND "FLASHING". SEAL OFF AT 10^{-8} mm Hg	$\sim .05$cm^2. FILAMENTS INSERTED IN Cs DISCHARGE TUBE.
RADIATION HEATING FROM FURNACE TO COLLECTOR, THEN RERADIATED TO EMITTER	NOT GIVEN	6.6 cm^2. CYLINDRICAL GEOMETRY. ELECTRODE SPACING OF 4 mm. NOT CONCENTRIC.
INDIRECT BY ELECTRON BOMBARDMENT SMALL TEMPERATURE GRADIENT ON SURFACE.	EXTENSIVE OUTGAS AND FINAL ASSEMBLY BAKEOUT. Ta GETTER. VAC ION EXHAUST.	2 CM^2. PLANE PARALLEL. VARIABLE SPACING; NON POSITIVE GUARD RING.
INDIRECT HEATED BY ELECTRON BOMBARDMENT.	NOT GIVEN	10.7 cm^2 AREA OF EMITTER. CYLINDRICAL GEOMETRY. POSITIVE SPACING.
INDIRECT BY ELECTRON BOMBARDMENT.	NOT GIVEN	4.2 cm^2 PLANE PARALLEL.
DIRECT HEATING	NO INFORMATION	$.406$ cm^2 PLANE PARALLEL VARIABLE SPACING; NON POSITIVE NO GUARD RING.

FIG. 2-2(C) SUMMARY OF DATA AND REMARKS CONCERNING EMISSION FROM CESIATED SURFACES.

Figure Z-3 (A)

Top axis: 2500, 2000, 1667

Y-axis: $J_s \left(\dfrac{amperes}{cm^2} \right)$, 10^1, 10^0, 10^{-1}, 10^{-2}, 10^{-3}

Curve labels: 5.0 ev, 4.5, 4.0, 3.5, 3.0, 2.7, 2.5

X-axis: .3, .4, .5, .6

2210 - FINAL

FIG. 2-3 (B)

ELECTRON EMISSION FROM CS ON MO
- ● Cs = 99-101°C AAMODT
- ◇ Cs = 200°C HOUSTON
- ⊡ Cs = 150°C HOUSTON
- △ Cs = 321-327°C TEECO
- ⊙ Cs = 303-309°C TEECO
- ✕ Cs = 276-278°C TEECO
- ⊖ Cs = 331-332°C TEECO
- ⬡ Cs = 264-266°C TEECO
- ◤ Cs = 275°C JENSEN
- ◆ Cs = 250°C JENSEN
- ◢ Cs = 285°C RASOR

1.5

1.1   1.2   1.3

FIG 2-3(C) ELECTRON EMISSION FROM Cs ON Mo

Top axis labels: 2500, 2000, 1667

Left axis: $J_s \left(\dfrac{\text{amperes}}{\text{cm}^2} \right)$

Vertical scale: 10^1, 10^0, 10^{-1}, 10^{-2}, 10^{-3}

Work function lines: 5.0 ev, 4.5, 4.0, 3.5, 3.0, 2.7, 2.5

Bottom axis: .3, 4, .5, .6

2210 - FINAL

7364733

FIG. 2-4(A1)

T_E (°K)

1429 1250 1111 100(

2.3 2.0 1.9 1.8 1.7 1.6

.7 .8 .9 1.0

$\dfrac{1000}{T_E}$ (°K^{-1})

FIG 2-4(B)

ELECTRON EMISSION FROM
Cs ON TA

☐ tcs = 200°C HOUSTON
◇ tcs = 150°C HOUSTON
△ tcs = 110°C FIRLE
⌂ tcs = 180°C FIRLE
✕ tcs = 140°C FIRLE
⬡ tcs = 250°C CAMPBELL
⬤ tcs = 95°C CAMPBELL
⊙ tcs = 304°C TEECO
◁ tcs = 344°C TEECO, WILSON
◇ tcs = 401°C TEECO
◑ tcs = 270°C GUST
▲ tcs = 230°C GUST
⌂ tcs = 322°C WILSON
▣ tcs = 293°C WESTINGHOUSE

FIG. 2-4(c) ELECTRON EMISSION FROM Cs ON Ta

FIG. 2-5(A)
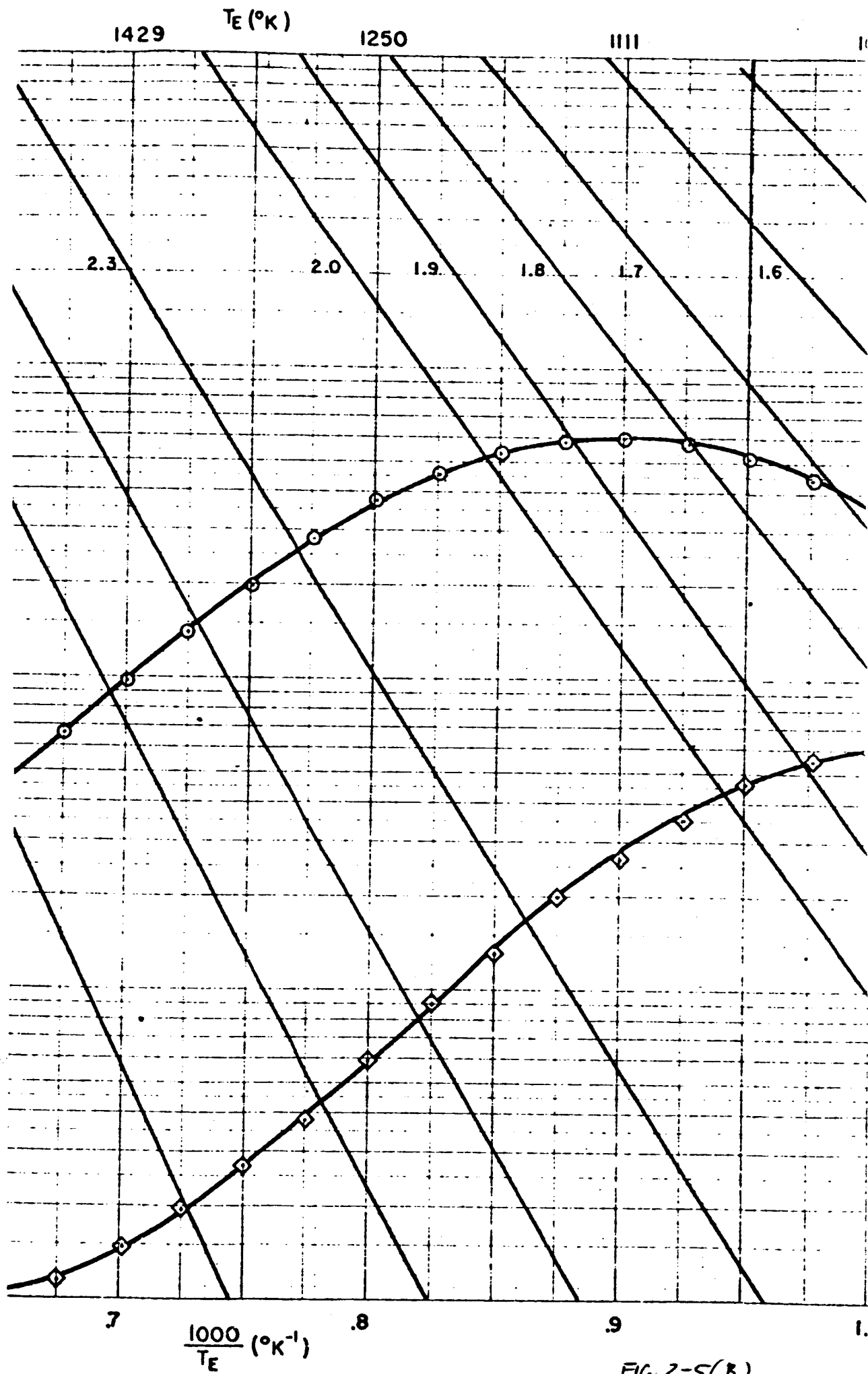
FIG 2-5(B)
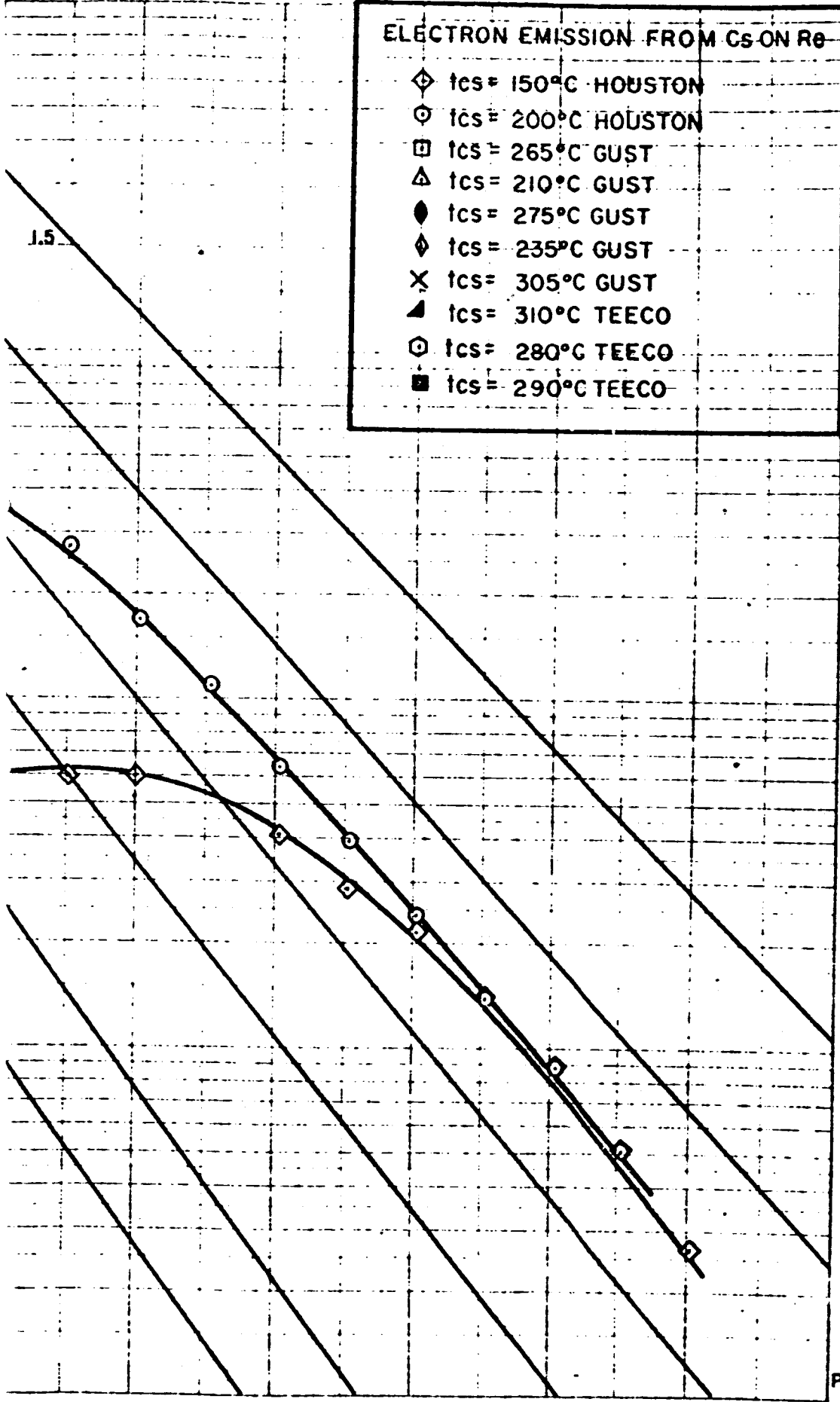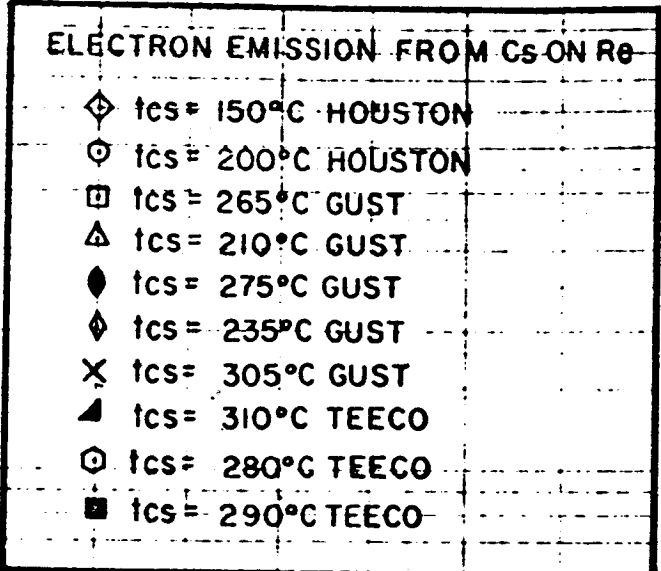
FIG. 2-5(C) ELECTRON EMISSION FROM Cs ON Re

FIG 2-6(A)

T_E (°K)

1429   1250   1111   100

3.   2.0   1.9   1.8   1.7   1.6   1.5

.7 $\frac{1000}{T_E}$ (°K^{-1})   .8   .9   1.0

FIG 7-16(B)

909
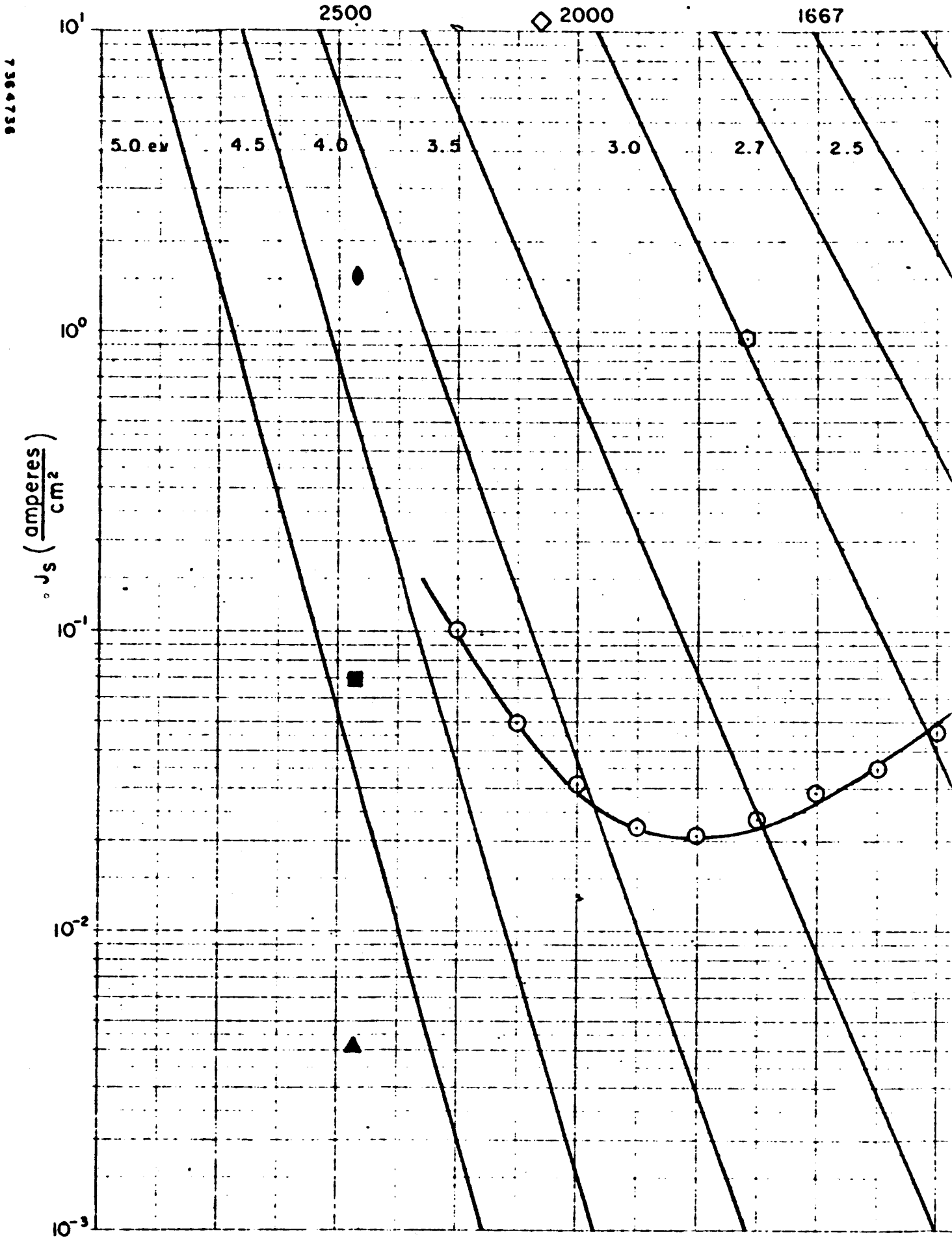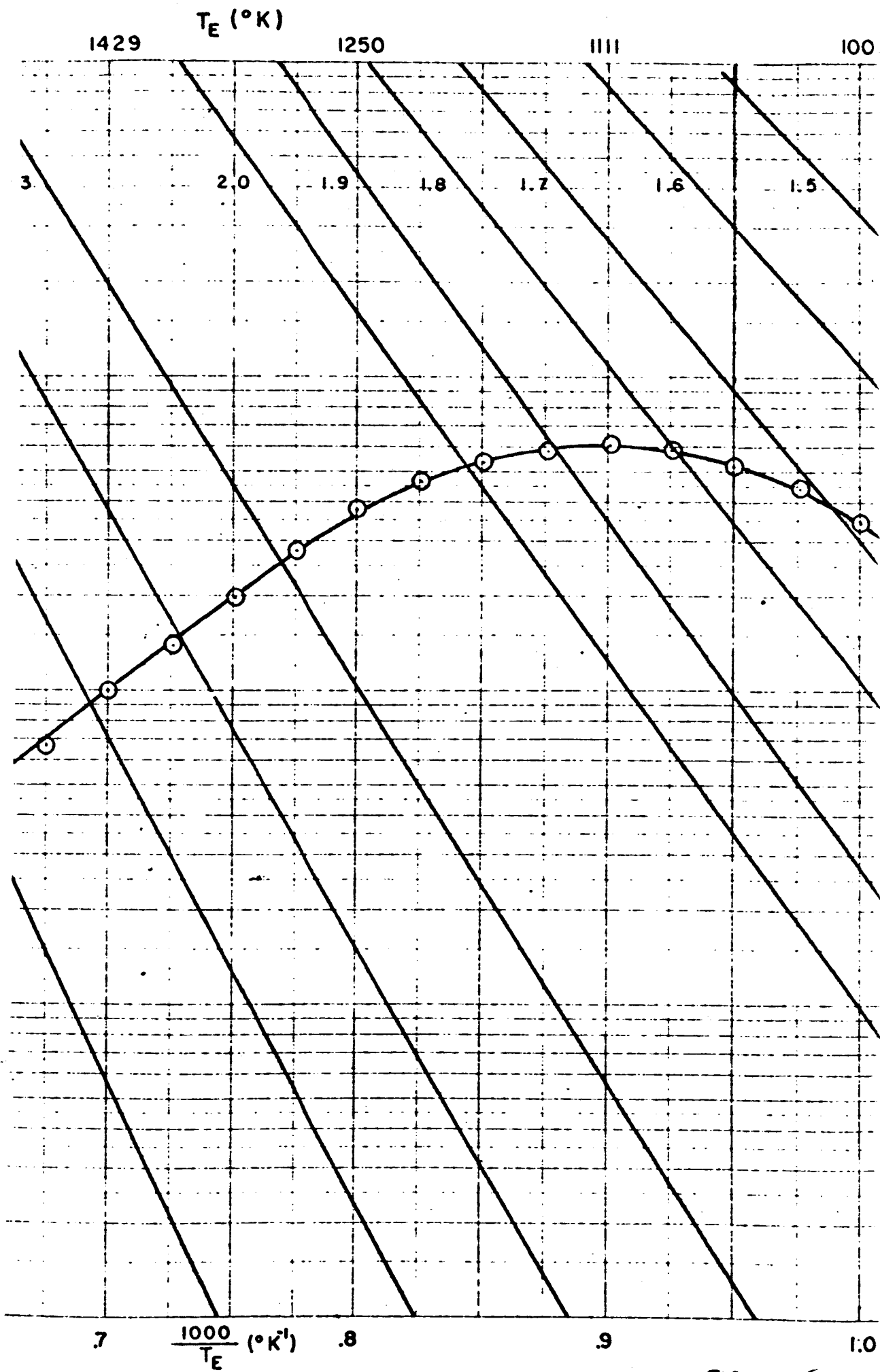
ELECTRON EMISSION FROM Cs ON Ir

⊙ tcs = 200°C (Re reference data by HOUSTON)
▲ tcs = 150° C GUST
▣ tcs = 185° C GUST
⬟ tcs = 240°C GUST
⬡ tcs = 257°C MARTIN
◆ tcs = 305°C MARTIN
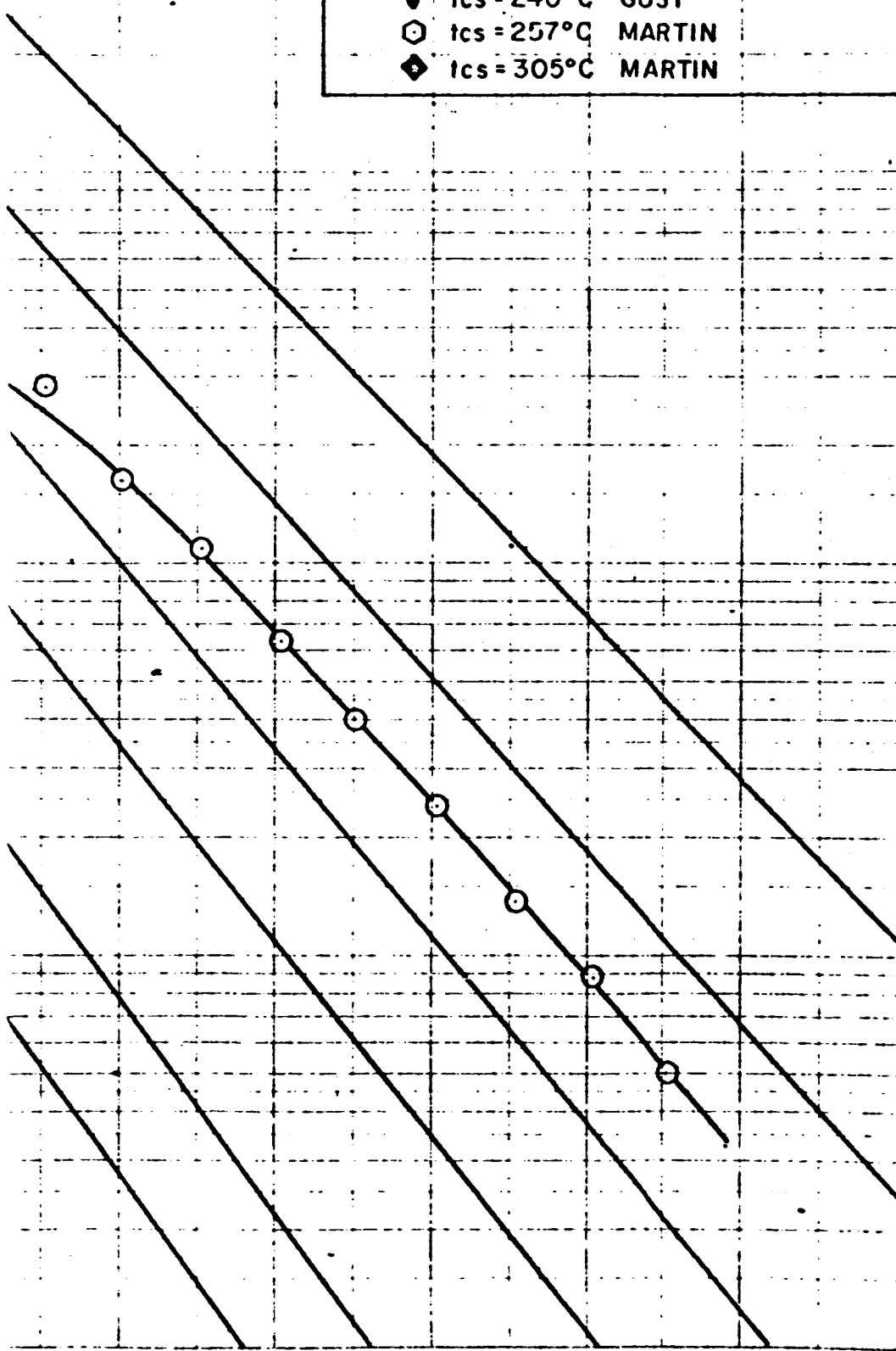
1.1   1.2   1.3

Pg. 2-9

FIG. 2-6(C) ELECTRON EMISSION FROM Cs ON Ir

Fig. 2-7 (A)

FIG 2-7(R)

ELECTRON EMISSION FROM
Cs ON W

◇	Tcs = 200°C	HOUSTON
⊙	Tcs = 150°C	HOUSTON
▢	Tcs = 100°C	HOUSTON
▲	Tcs = 190°C	GUST
✕	Tcs = 240°C	GUST
●	Tcs = 130°C	GUST
⬡	Tcs = 180°C	FIRLE
◺	Tcs = 120°C	FIRLE
◇	Tcs = 280°C	WILSON
▢	Tcs = 310°C	TEECO
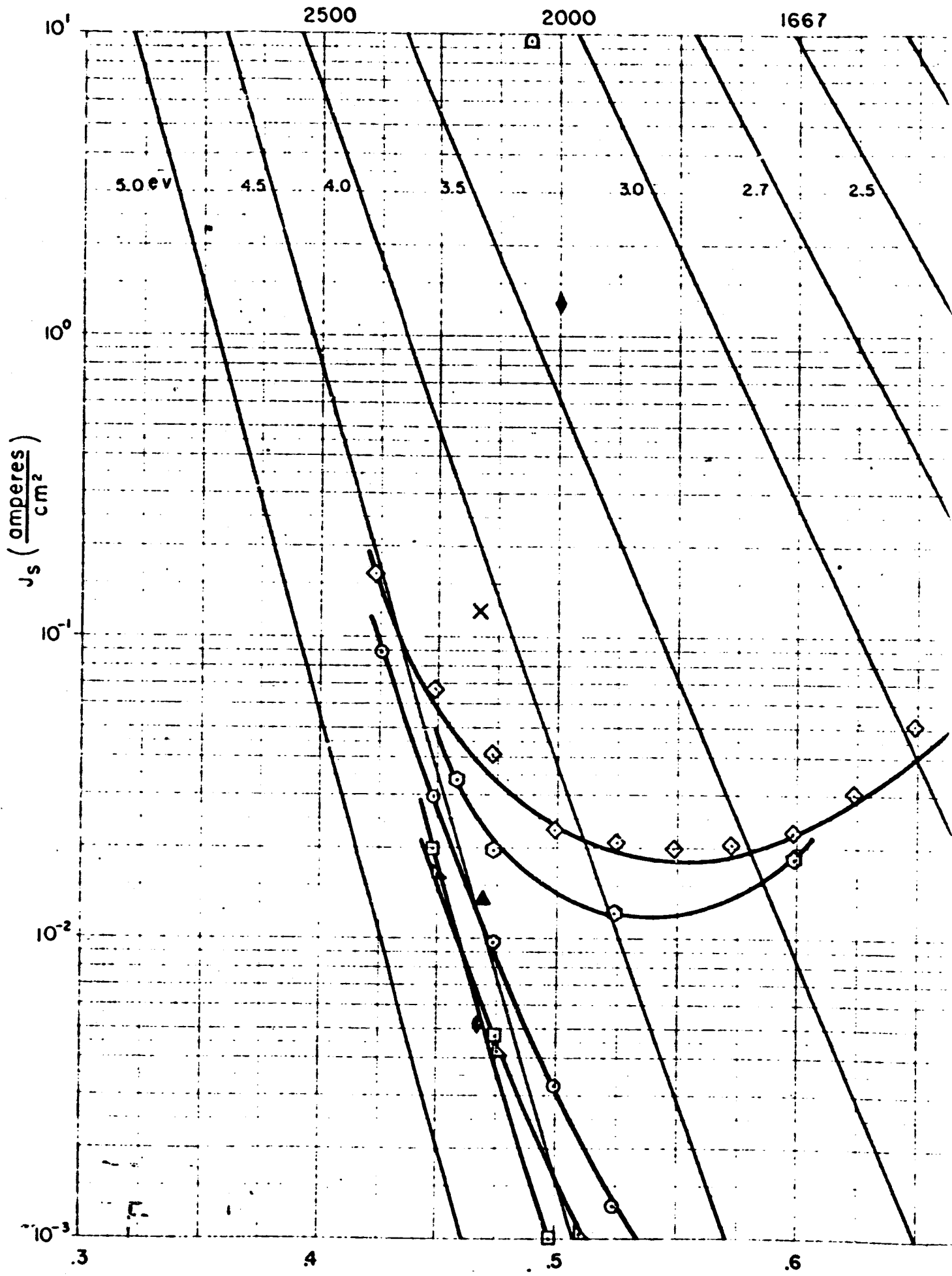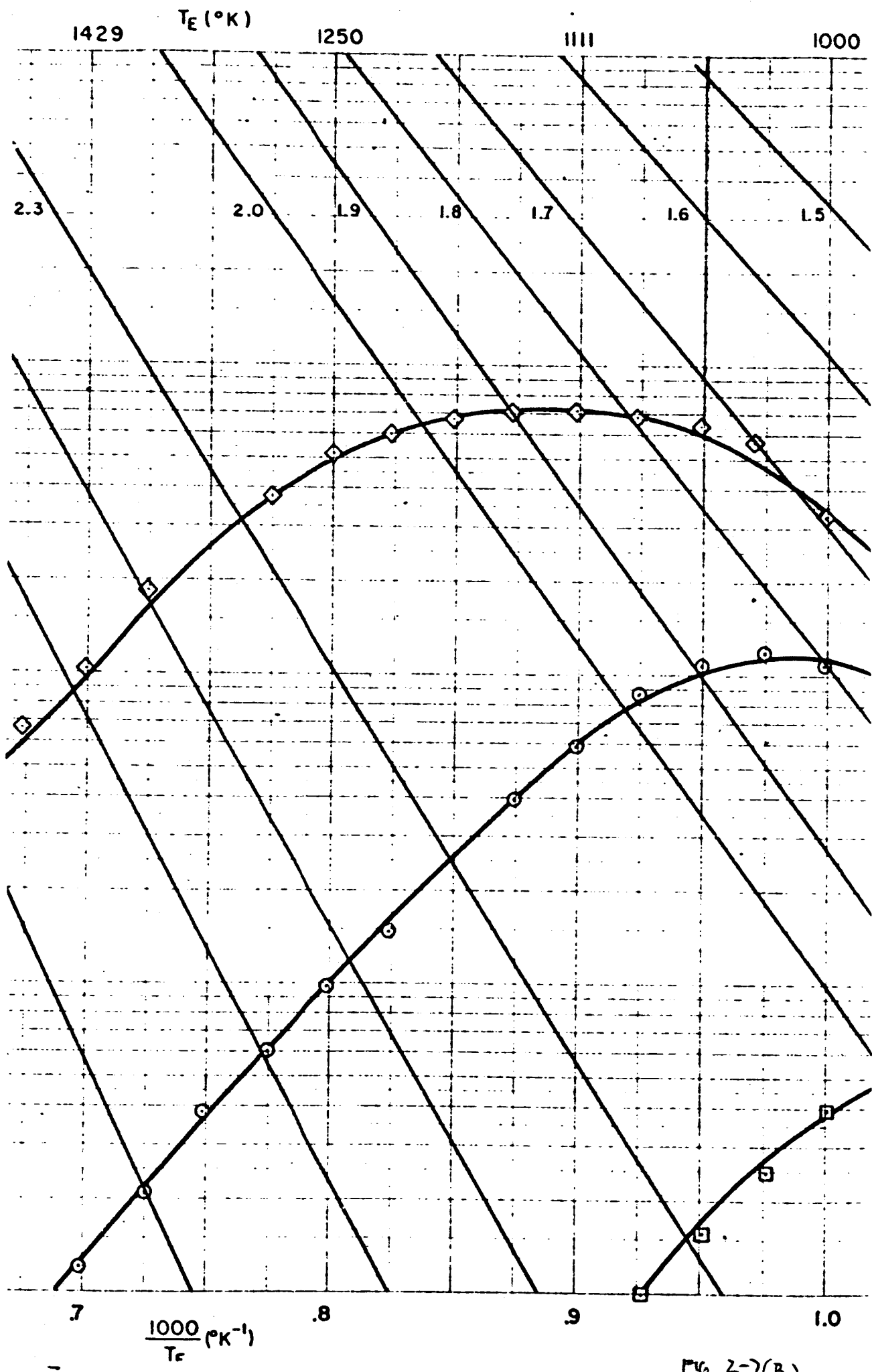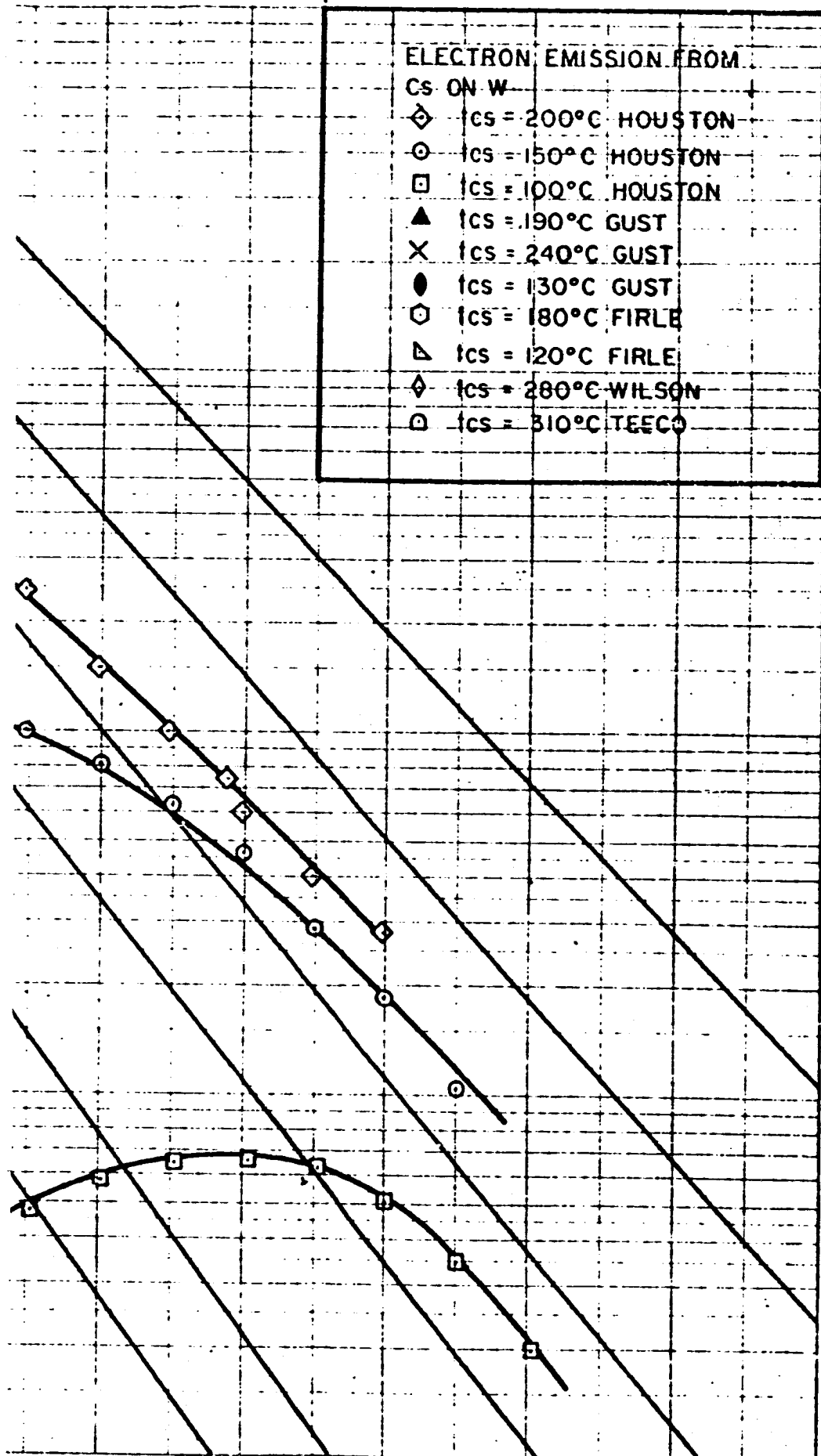
1.1

1.2

1.3

FIG. 2-7(C) ELECTRON EMISSION FROM Cs ON W

Pg. 2-10

2.1.2.1 Zero-Field Measurements

Since equation (2) is the result of a mathematical analysis which assumes thermodynamic equilibrium, experimental data to be compared with this theory must be extrapolated to zero-field conditions.

The data from practical thermionic converter devices is usually displayed as a volt-ampere curve in the power quadrant as shown in **Fig. 2-8** (after Thermo Electron Engineering Corporation). The break in the curve is identified with the departure from the electron space charge limited mode to the electron emission limited mode. This is to be taken as the zero-field electron emission. Some workers prefer to extrapolate the electron emission saturated mode to the zero voltage axis defining this value as zero-field current. Schottky-type effects in this region lead to zero-field emission values which may be a factor of two to four times larger than the values obtained from the break. Moreover, if the curve saturates poorly as in **Fig. 2-9** (after Westinghouse) there probably exists an ill defined emission area resulting from side wall emission. It should be remembered that emission current densities of 50 amperes per square centimeter can be obtained from many of the refractory metals for arrival rate of 10^{21} atoms/cm^2/sec and substrate temperatures near 1500°K. This indicates the need for carefully defined emission area.

Field free electron emission is difficult to obtain from plasma discharge tubes such as Houston's. In operation the emitter is run at a potential negative with respect to the plasma. Ions extracted from the plasma neutralize the electron space charge in the sheath permitting current flow. If the ion current exceeds the value necessary to neutralize the space charge, a field exists at the emitter and the measured current is in excess of zero-field. Figure 2-10 (after Houston) illustrates the disagreement between two separate probe measurements of zero-field emission under the same experimental conditions. The variance in data may well be attributed to affects other than interpreting the value of the zero-field electron emission from probe plots. Temperature profile on the probes, probe position relative to the discharge electrodes, or leakage currents
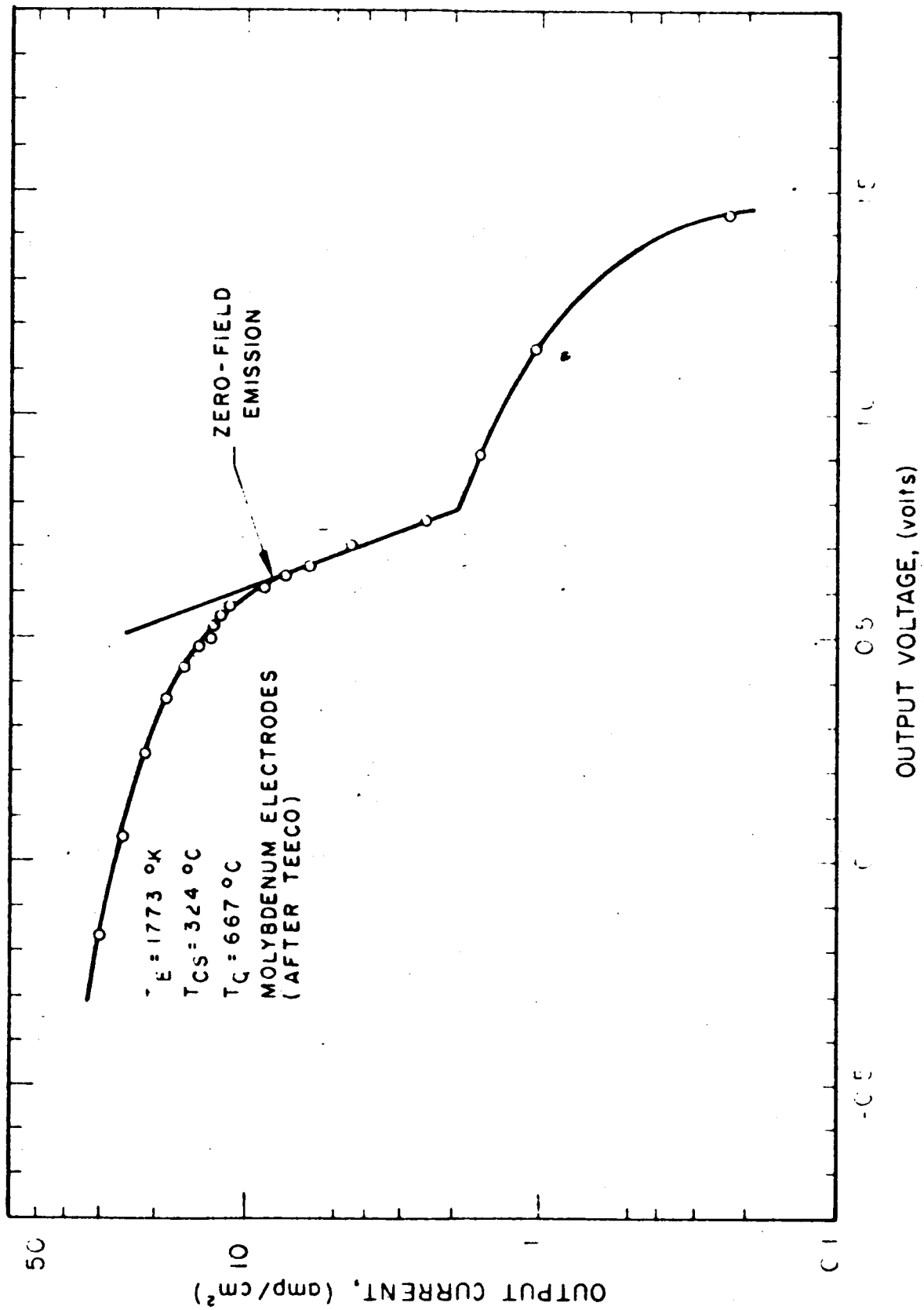
FIG. 2-8   VOLTAGE-AMPERE CHARACTERISTIC AFTER THERMO-ELECTRON ENGINEERING CORPORATION
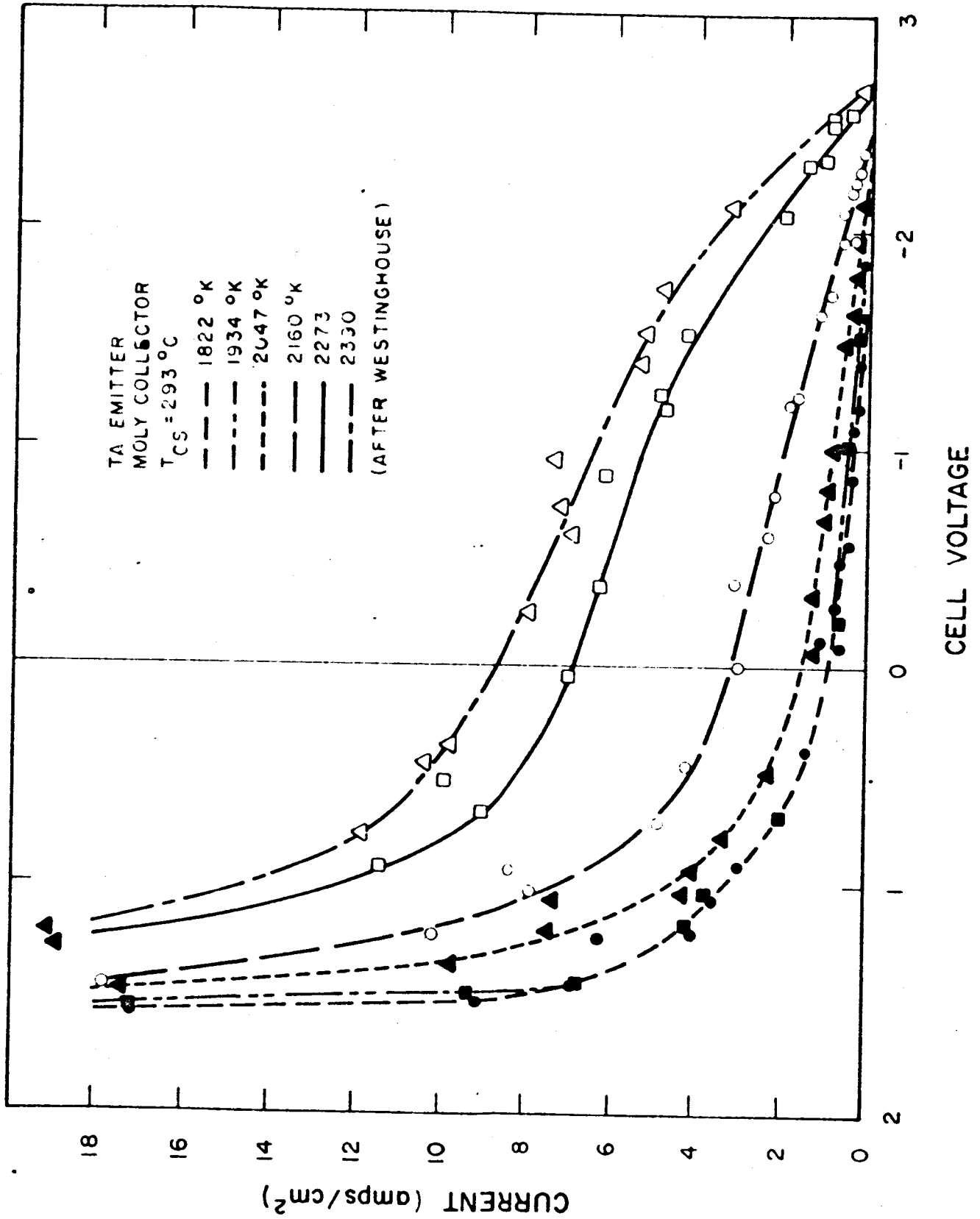
FIG. 2-9   VOLTAGE-AMPERE CHARACTERISTIC AFTER WESTINGHOUSE
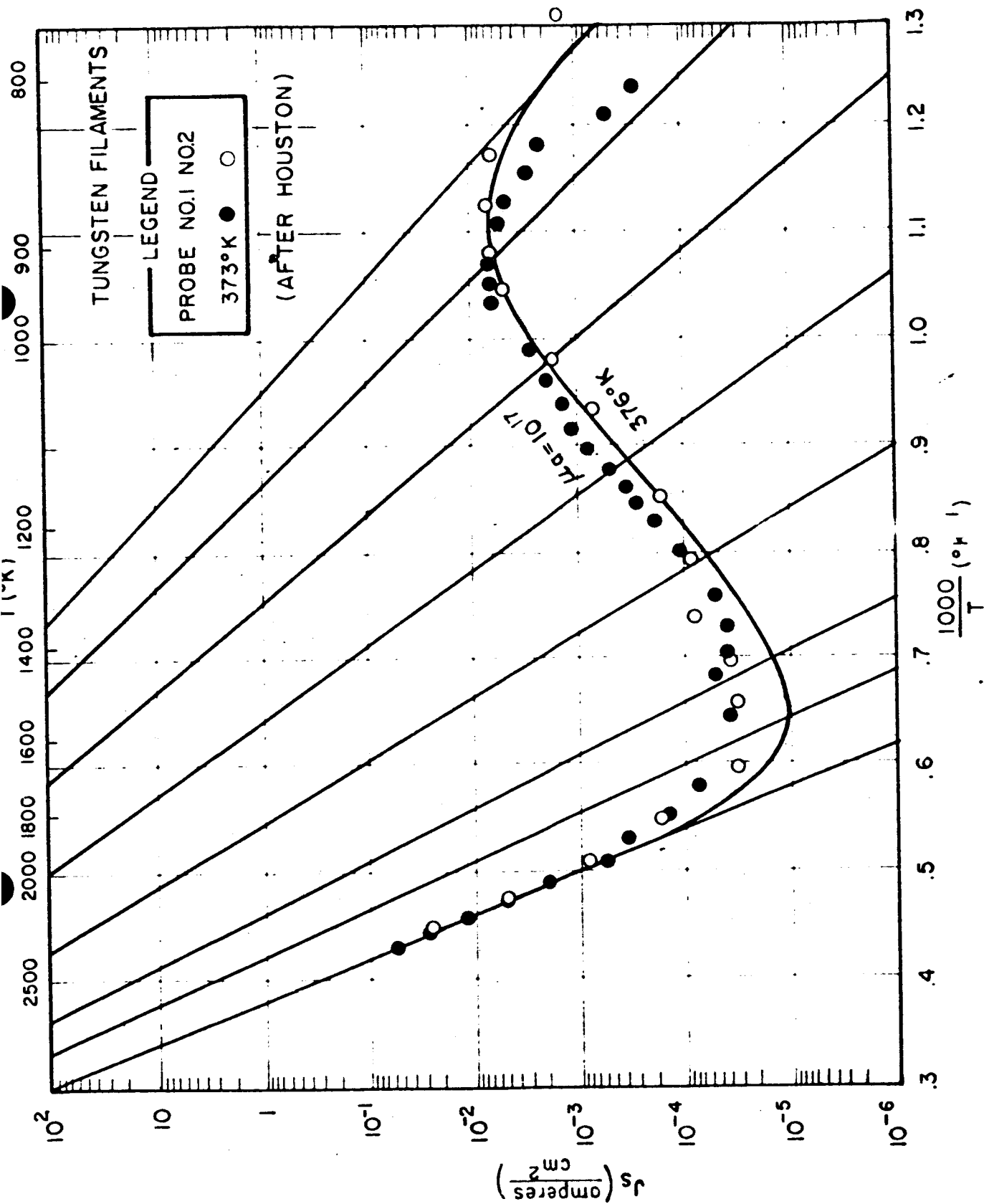
FIG. 2-10 FIELD-FREE EMISSION DATA AFTER HOUSTON

could be responsible in part. At any rate, it is unfortunate that this data is ill-defined since the work function determination of cesiated surfaces at low temperatures (1000°K) is of vital concern to the output of practical devices.

Consider a device whose collector is to be operated with a work function of 1.7 volts. In reality, if a collector work function of 1.4 volts can be achieved the converter may operate at a power level which is 30 percent to 80 percent greater than a converter with a 1.7 volt collector work function with no increase in input thermal energy.

An assortment of experimental apparatus falls outside the category of practical devices or discharge tubes. These have been generally constructed to conduct parametric studies of electrode spacing, arrival rate, and emitter materials. Occasional data may be analyzed for zero-field current as in Fig. 2-11 (after Campbell). A Child's plot of current versus applied voltage was examined for a break in the space charge limited region and found suitable to interpret as zero-field emission.

2.1.2.2 Temperature Measurements

The dependence of electron emission upon emitter temperature is obvious from Equation 2 presented in the theory. What is not too obvious and should be stated here is that the temperature of the emitter must be uniformly the same.

The most common means of measuring the emitter temperature of practical devices is with a micro-optical pyrometer. Since surface conditions resulting from grain growth, thermal etching, oxide formation, or machining exhibit greatly different spectral emissivities, brightness temperature readings are almost meaningless.

It is well known that the radiation emitted from a properly dimensioned hole is characteristic of unit emissivity, hence the brightness temperature of the hole is the true temperature of the body at that point. The proper hole depth to diameter ratio has been interpreted as being between 4 (Ref. 8a) and six to eight (Ref. 8). Jensen, Wilson, and Thermo Electron Engineering Corporation have employed this technique to obtain emitter temperatures.

Figure axes:
- Y-axis: $j(\text{amp}/\text{cm}^2)^{\frac{2}{3}} \times 10^{-1}$
- X-axis: APPLIED VOLTAGE (volts)

ZERO-FIELD EMISSION

$T_E = 1000\ °K$

$T_{CS} = 200\ °C$

TANTALUM EMITTER
COPPER COLLECTOR
(AFTER CAMPBELL)
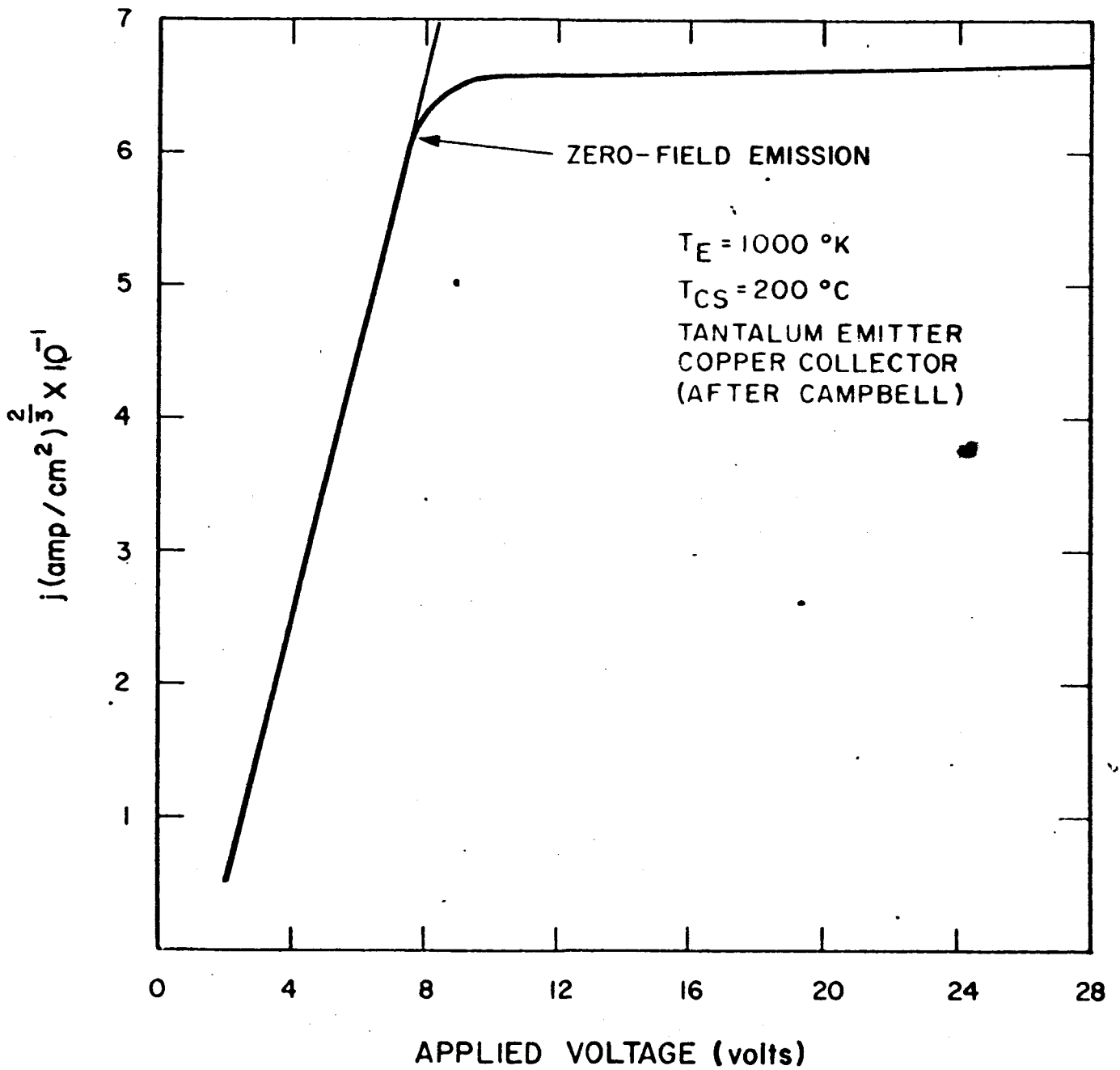
FIGURE 2-2   CHILD'S PLOT FOR CATHODE TEMPERATURE OF $1000°K$, Cs BATH TEMPERATURE $473°K$

Inevitably pyrometer measurements require corrections for transmission losses in glass, sapphire, or pyrex. Moreover, contaminating films from brazing and outgassing operations or obstructions from bell jar cages can reduce true temperature readings literally by hundreds of degrees. Finally, pyrometers themselves require periodic calibration by standard lamps to maintain desirable accuracy.

High temperature thermocouples can also be employed to measure emitter temperatures. To this end, commercially available tungsten-tungsten rhenium wire has become increasingly popular for the high temperature region ($1800^{o}C$). The couple must be calibrated for each application. Figure 2-12 (after Campbell) illustrates the necessity for thermocouple calibration.

Thermocouples are subject to a variety of limitations. Their millivolt response is extremely sensitive to impurities such as oxides, nitrides, and silicides. At high temperatures constituent materials such as rhenium and rhodium may undergo excessive diffusion, thus changing the thermo-electric properties of the couple.

Some workers employing filaments as emitters, have chosen to measure temperature indirectly by means of resistivity measurements on the filament. This scheme has inherent limitations.

1.   The resistance which is measured at the terminals is an average resistance for both the hot and cold portions of the filament. Only in those cases where the resistance of the hot portion is greater than the resistance of the cold portion by a factor of approximately 100 can these measurements be meaningful.

2.   The radiation shielding of the wire filament and the filament end supports must be designed in such a fashion that the temperature is constant over the major portion of the filament. This is a difficult feat particularly when a large electron emission density is being drawn from the central part of the filament.

3.   Grain growth which results from high temperature operation tends to change the resistivity, rendering initial calibration of little value.
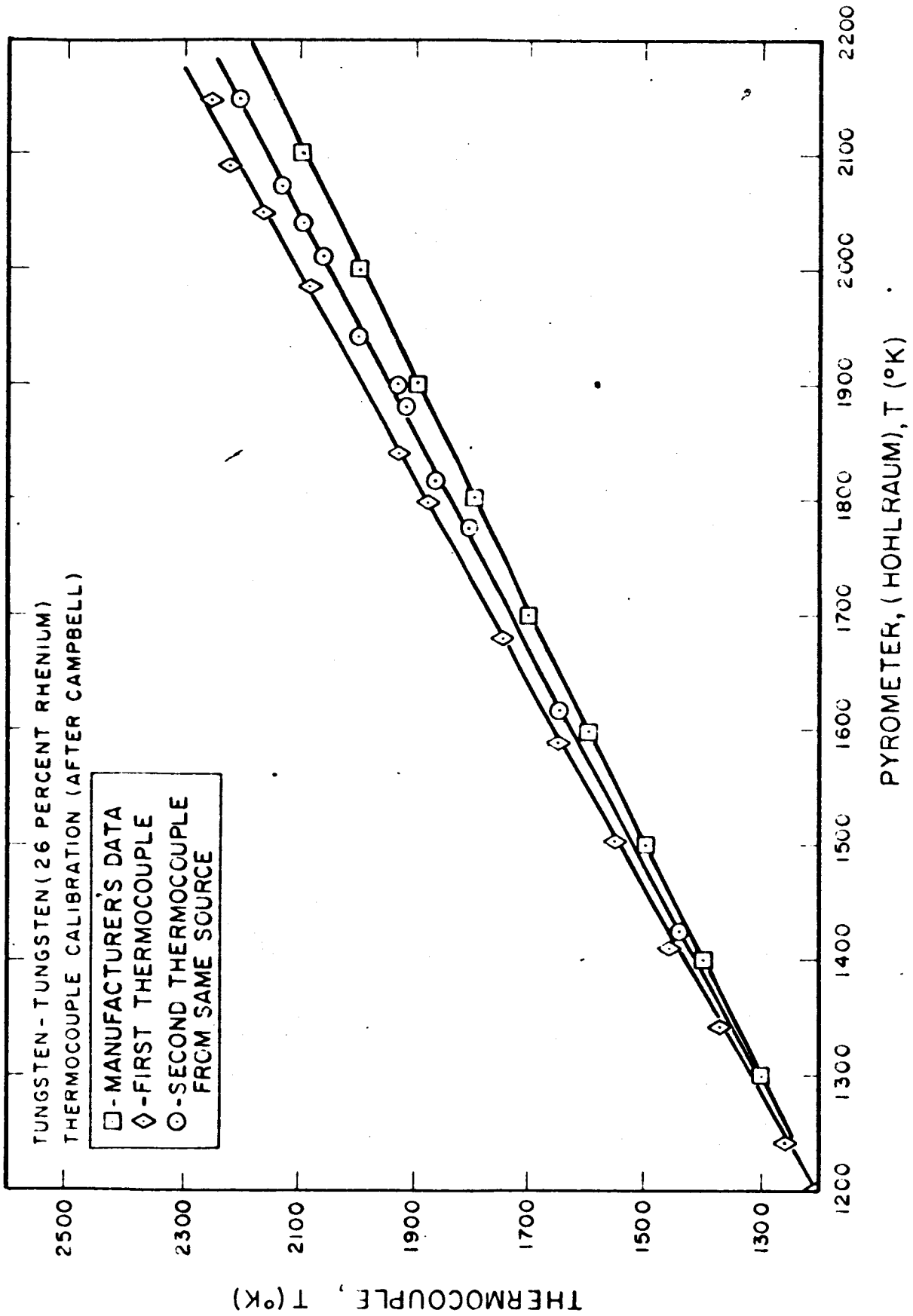
FIG. 2-12   TUNGSTEN - TUNGSTEN 26°/o RHENIUM THERMOCOUPLE CALIBRATION

4. Evaporation of emitter material as a result of life testing is certain to alter the resistivity.

2.1.2.3 Cesium Arrival Rate

Theoretical considerations have indicated that the emitter surface coverage and temperature determine the Langmuir "S" curve characteristic for a particular arrival rate of atoms. From kinetic theory considerations the cesium arrival rate, μa, is related to the cesium vapor pressure, p, and cesium reservoir temperature, T, by the formula:

$$\mu_a = p(2\pi mkT)^{-1/2} \tag{3}$$

A practical device is usually operated such that the electrode gap is much greater than the atom-atom mean free path for cesium. At a vapor pressure of 10 mm Hg the cesium atom collision frequency is so high that even spacings of .001 inches are large compared to the mean free path. Under such conditions the pressure is constant throughout the device and arrival rate corrections are necessary for temperature differences in the device geometry. Calculations show the corrected arrival rate to be higher by a factor of 1.5 to 2 times the rate computed from equation (3).

The construction of converter devices requires careful attention to the problem of cesium reservoir attachment. Long transfer tubes have been employed by a number of investigators (Wilson, and Thermo Electron Engineering Corporation). Analytic and experimental evidence indicate that temperature distributions may occur in long tube geometry, which establish in effect, a low temperature parasitic reservoir. Such parasitic reservoirs, which set the device vapor pressure, may lower the arrival rate by a factor of 8 to 10.

Other types of laboratory apparatus such as those operated by Aamodt, Gust, and Westinghouse, are immersed in mechanically stirred oil baths to ensure controlled arrival rates. Consequently, the envelope or encasement of this apparatus sets the arrival rate. Precision work requires envelopes of glass since metal is affected by emitter radiation at high temperatures resulting in areas of 10-20°C higher than the "isothermal" bath.

The geometry of these devices can be critical in determining the arrival rate. If the wall temperature is to govern the vapor pressure, then the mean free path of arriving cesium atoms must be greater than the electrode spacing. Low bath temperatures (100°C and below) guarantee long mean free paths with an arrival rate at the emitter set by the envelope temperature. Higher bath temperatures increase the frequency of atom-atom collision creating a temperature gradient in the vapor near the emitter. It is necessary to correct the arrival rate in such situations.

Discharge apparatus such as that employed by Houston require vapor pressure correction when the main discharge current is flowing. Shukhtin (Ref.9a) has measured the positive column vapor pressure under various degrees of current flow. His results indicate that the arrival rate present at the measuring probes may be seven times the value obtained from envelope temperatures.

2.1.2.4   Emitter Area and Electrode Geometry

Since the Langmuir "S" plot relates the zero field electron emission current density to the emitter temperature, it is of particular importance to properly define the emitting area since one measures only total current.

The most common means of isolating or defining the area of electron emission is the use of a guard ring. The collector is so situated that it collects the electron emission from an emitting area of constant temperature. The guard ring surrounds or is adjacent to the collector and operated at the same electrical potential. It is important to note that the guard ring and collector form an equipotential surface, hence, insuring that the electric field lines are perpendicular to the electrode under study. Figures 2-13 and 2-14 illustrate a guard ring geometry for plane parallel or cylindrical electrodes.

Practical devices are rarely fitted with guard rings and the measured current usually involves emission from side walls (Jensen and Thermo Electron Engineering Corporation).

A seemingly overlooked fact concerning the emitting area of the device is the discrepancy between the apparent and
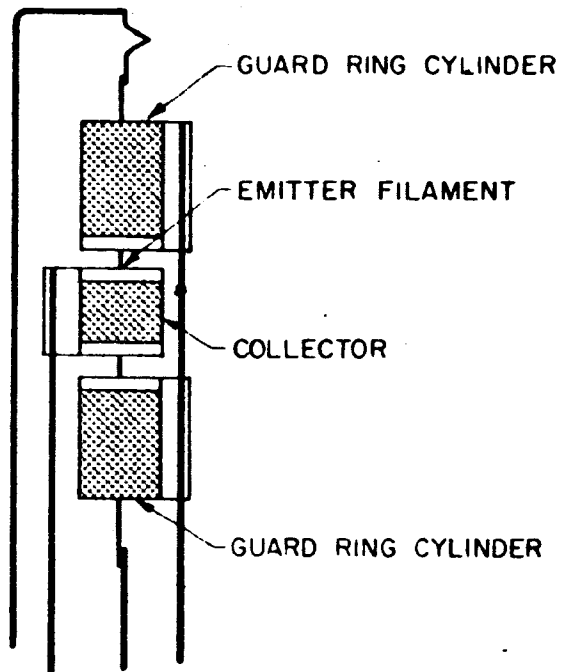
FIG. 2-13   CYLINDRICAL GUARD RING GEOMETRY
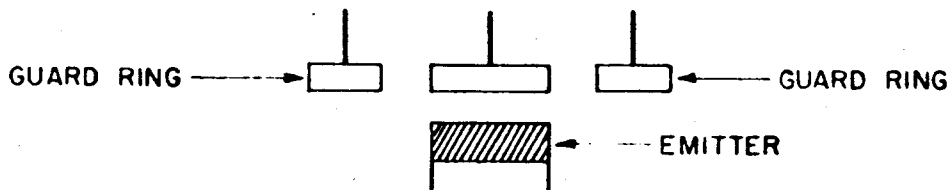
FIG. 2-14   PLANE PARALLEL GEOMETRY

true surface area. Langmuir (Ref. 2) considered this for a tungsten filament and it was established that the actual area was 1.3 times the apparent area.

There has been no extensive mention of this problem in the current literature. Emission densities are generally given as measured current divided by apparent area.

2.1.2.5   Emitter Heating

This discussion and the following two are three areas mentioned earlier that have resulted from the experience of investigators in thermionics and allied fields. These contributions are perhaps as valuable, if not more so, than those previously mentioned.

Consideration of the method of delivering heat energy to an emitter is often important for correct interpretation of the thermionic emission data. Indirect heating by electron bombardment is generally recognized as the most practical laboratory means for achieving high emitter temperatures; however, direct heating has also been used in some cases (Westinghouse and Gust). The two most common heating methods are presented and discussed below:

1.   Indirect heating by electron bombardment requires the proper assembly of an auxiliary electron emitter and a high voltage direct current power supply. The auxiliary emitter, generally tungsten wire, is hot wound to a shape compatible with the emitter geometry. A low voltage source of alternating current heats the auxiliary emitter to a temperature adequate for electron emission. The electrons from the auxiliary emitter are accelerated to the emitter under study by potentials of the order of one kilovolt. The energy released on impact with the emitter under study is sufficient to achieve temperatures up to the melting point of the substrate. If the auxiliary emitter is properly designed and located with respect to the emitter under study a uniform temperature can be achieved over the entire emitter sample.

2.   Direct or resistive heating is accomplished by the passage of current, usually pulsed direct current, through the emitter sample. The geometry is limited somewhat to emitters of wire or strap,

since the current requirements for the resistive heating of large cross sections is enormous. Coupled to this problem is the attachment of current carrying electrodes to the emitter. The contact resistance of attachment can almost equal that of the emitter resulting in I^2R losses and subsequent heating at undesirable points in the emitter circuit. For correct interpretation the diode current and voltage output should be measured in the interval between pulses for now the emitter is no longer a unipotential surface during the heating cycle. The presence of a voltage drop along a directly heated emitter can introduce effects which lead to erroneous conclusions when this method is used to study electron emission from a sample located in a cesium vapor environment.

Occasional use is made of indirect heating by radiation from hot filaments (Firle). Indirect filament heating is generally inefficient, depends heavily on material properties such as emissivity, and resistivity, and has quite limited application at temperatures above 1500°K.

2.1.2.6 Predominant Crystal Orientation and Material Preparation

Nothing in the thermionic emission theory infallibly predicts or accounts for the variation of emission from cesiated surfaces possesing different substrate crystal orientations. Therefore, the treatment of this topic is empirical and the resultant measurements are herein described.

Emission current densities of an order of magnitude difference have been observed by Webster (Ref. 9) from cesiated tantalum with different crystal surfaces exposed. The failure of many investigators to identify the gross nature of their emitter material (i.e., bar stock, sheet, arc cast ingot, etc.) indicates an unawareness of this problem. Polycrystalline material after recrystallization always presents predominant surface crystal orientations dependent not only upon the type of material and previous heat treatment history but also upon the fabrication procedures used in forming or working the original metal.

Langmuir and Taylor (Ref. 2) gained early insight into the necessity for extensive thermal aging to insure reproducible emission results. Presumably this aging treatment yielded 110 and 112 crystal surfaces on their tungsten wire sample. The bulk of their data is, therefore, single crystal data.

Hughes and Levinstein (Ref. 10) have employed aging and etching methods to grow and identify predominant crystal directions on tungsten wire. Vacuum emission measurements taken at a pressure of 5×10^{-10} mm Hg. yield an experimental field free work function of 5.25 electron volts which was independently checked by surface ionization measurements. Virtually no one has conducted post operation metallurgical examination to identify the predominant crystal orientation of the emission data. Hughes and Levinstein's results may be compared to a work function of 4.62 electron volts for tungsten wire without specified treatment or indicated crystal plane direction (Houston). Hence, his emission data in this report can only be associated with the form of the material as indicated in Fig. 2-2.

Material preparation such as extensive outgassing, gettering, hydrogen firing, and sputtering have reached converter development by way of the electron tube industry. The general rule of thumb for any device operation is to vacuum outgas the part substantially above the intended temperature level of operation. The literature is abundant with comments concerning the deleterious affects of gases, metal impurities, water vapor, etc. as it pertains to thermionic emission. Therefore, there are occasional procedures to be noted which appear to present a paradox. To cite two examples:

1. Oxide layers are removed from tungsten by "flashing" in vacuo to extremely high temperatures ($>1900°$K), wherein the adsorbed contaminants (i.e., oxides and nitrides) are evaporated from the surface. Without this treatment investigators are reporting emission data from a system similar to Cs-O-W, which has been examined earlier (Ref. 11).

2. To maintain a clean platinum surface after outgassing, it is necessary to bombard the sample with positive oxygen ions which are deposited in and below the surface. The oxygen forms a barrier to the diffusion of other body contaminants. The actual surface layer of oxygen is then removed by sputtering with rare gas positive ions. A similar treatment is employed for iron, however, nitrogen forms a better diffusion barrier than oxygen.

2.1.3 Recommendations

The lack of high arrival rate data (10^{20}-10^{21} atoms/ cm^2/sec) and definitive emission measurements precludes the specific recommendation for one emitter material. It would appear that all body-centered cubic high temperature materials are potential emitters for practical devices.

For high temperature applications (1800^{0}K or higher) tantalum or tungsten has suitable emission properties. Availability of data and material cost disfavors rhenium. For less stringent temperature requirements (1600°K or lower) molybdenum appears satisfactory.

REFERENCES

Section 2.1

1. I. Langmuir, J. Am. Chem. Soc. $\underline{54}$, 2798 (1932)

2. J. B. Taylor and I. Langmuir, Phys. Rev. $\underline{44}$, 423 (1933)

3. J. A. Becker, Trans. of the Am. Electrochemical Soc. $\underline{55}$, 154 (1929)

4. I. Langmuir and K. H. Kingdon, Phys. Rev. $\underline{34}$, 129 (1929)

5. J. H. deBoer and C. F. Veenemas, Physica 953 (1934)

6. L. P. Gyftopoulos and J. D. Levine, J. Appl. Phys. $\underline{33}$, 67 (1962)

7. N. S. Razor Nonr-3192(00), Nov.(1961)

8. F. G. Block, PIC-ELE-TI 209/1.1, Proceedings of the Third Government-Industry Thermionic Roundtable Discussion, Vol. II, page 9-1

8a. C. S. Williams, Applied Optics, 564 (1961)

9. H. F. Webster Research on Thermionic Converters, Contract AF 19(604)-5472, June 1961, page 47

9a. A. M. Shukhtin, Doklady Akad. Nauk, USSR, $\underline{82}$, 41, 1952 (in Russian)

10. F. L. Hughes, H. Levinstein and R. Kaplan, Phys. Rev. $\underline{113}$, 1023, (1959)

11. I. Langmuir and K. H. Kingdon, Phys. Rev. $\underline{24}$, 510 (1924)

2.2 Thermophysical Properties of Converter Materials

This section is a survey of the thermal and physical properties of metals that are pertinent to the range of temperatures, times, and stresses common to the operation of practical converter devices.

It is to be noted that in many instances these data are quite recent (Ref. 1) and are the results of one laboratory or investigator. However, where it is possible, ample data are given so that average values may be used with a degree of confidence.

The context is arranged to present with a minimum of discussion those materials and material properties of prime interest to converter technology. The sections are as follows:

1. Creep strength
2. Grain growth
3. Thermal expansion
4. Emissivity
5. Vapor pressure
6. Resistivity
7. Thermal conductivity and specific heat
8. Young's modulus

A variety of metals of interest to thermionic converter technology are reviewed and the section is concluded with specific recommendations on material selection for practical converter application.

2.2.1 Creep Strength

Creep may be defined as the plastic strain occurring from constant or nearly constant stress. The rate of creep in a specific material depends on the temperature, the imposed stress, and time. Possibly the most important design consideration for high temperature, long life thermionic devices, the creep strength of materials has been given only scant attention in converter literature.

It appears that the field of direct energy conversion has failed to profit fully from the pertinent literature of allied fields. An example of germaine, but neglected, information is the fact that the commercial turbine and turbojet industries have been designing devices and assemblies to operate at high temperatures under applied loads for three to ten years. Likewise, the electron tube industry and the electric bulb industry have designed and operated long life devices for years with much design emphasis on creep strength of materials at elevated temperatures.

Creep data for materials useful to thermionic converters are displayed on graphs which show limiting stress in 1000 psi as a function of creep rate in percent per hour with temperature as a parameter. A converter may, therefore, be properly designed mechanically if the pertinent loads or stresses, temperature, life requirements, and creep properties of available materials are taken into account. Where closed-spaced parts must maintain a specific clearance for a specified life at a given temperature, the loading stresses must be compensated through design to meet the creep requirement.

Tensile strength or yield point data, even at elevated temperature, is of little value in the design of a long life converter. For instance, the ultimate tensile strength of tantalum at 1000°C is 55,000 psi. However, for 100 hours operation at the same temperature for 0.5 percent creep, the limiting stress value from the creep strength diagram is 3,000 psi. Creep strength data for eight materials of interest to thermionic converter technology are shown in the following pages.
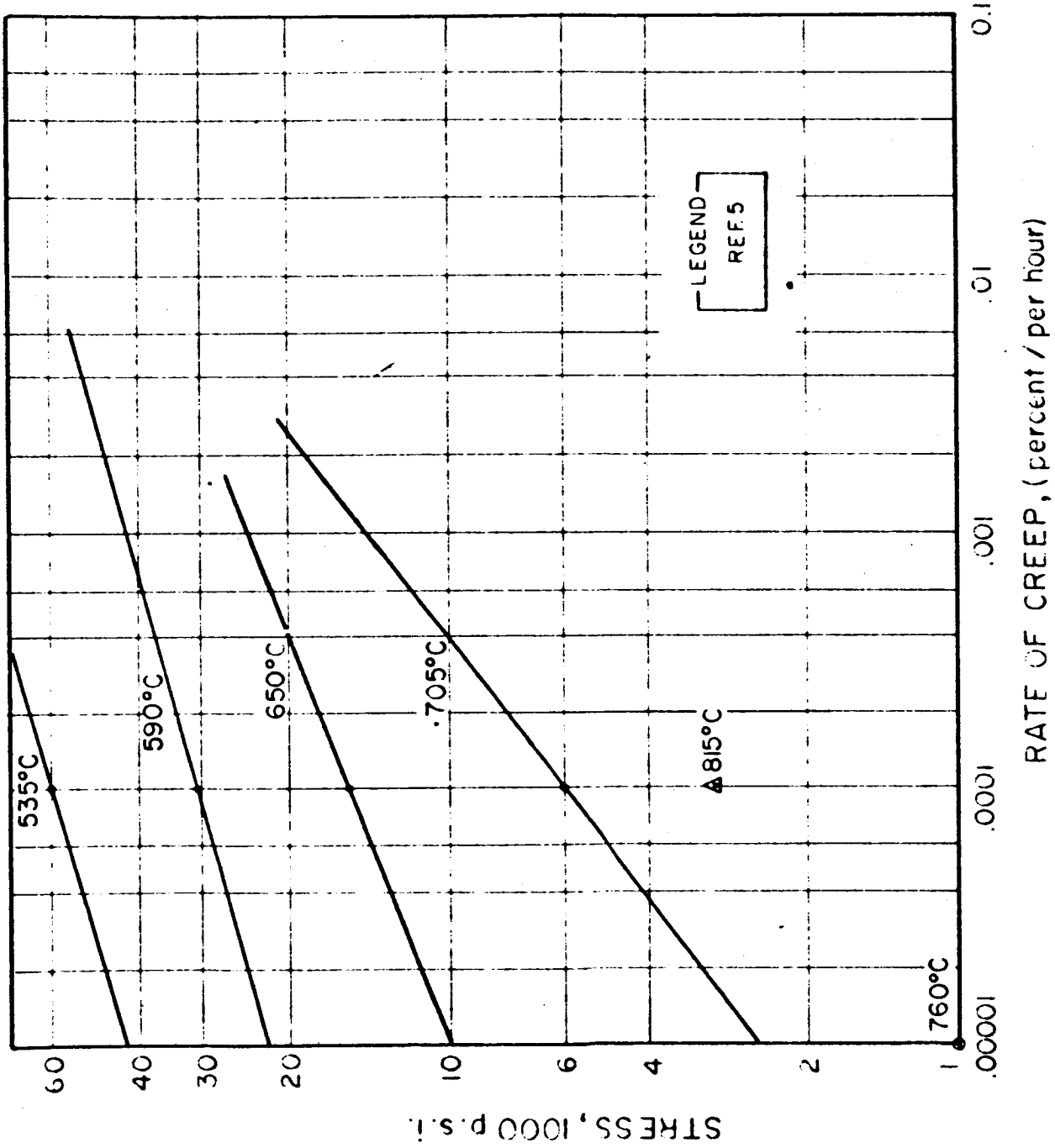
FIG. 2-15   CREEP STRENGTH OF S.S. 446

RATE OF CREEP, (percent / per hour)

STRESS, 1000 p.s.i.

LEGEND
○ REF.6

535°C
590°C
650°C
705°C
760°C
815°C
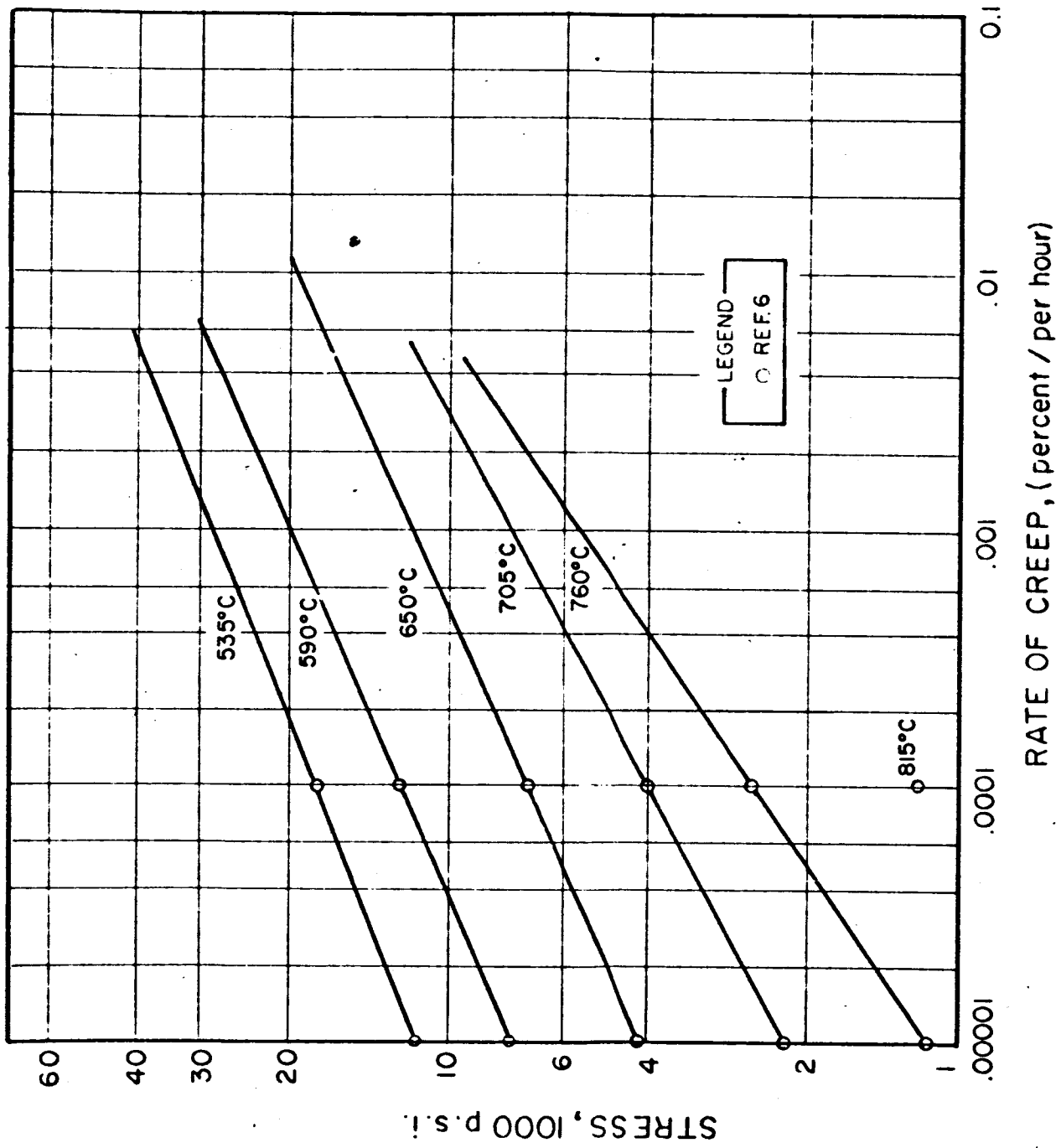
CREEP STRENGTH OF S.S. 304

FIG. 2-16

7364870
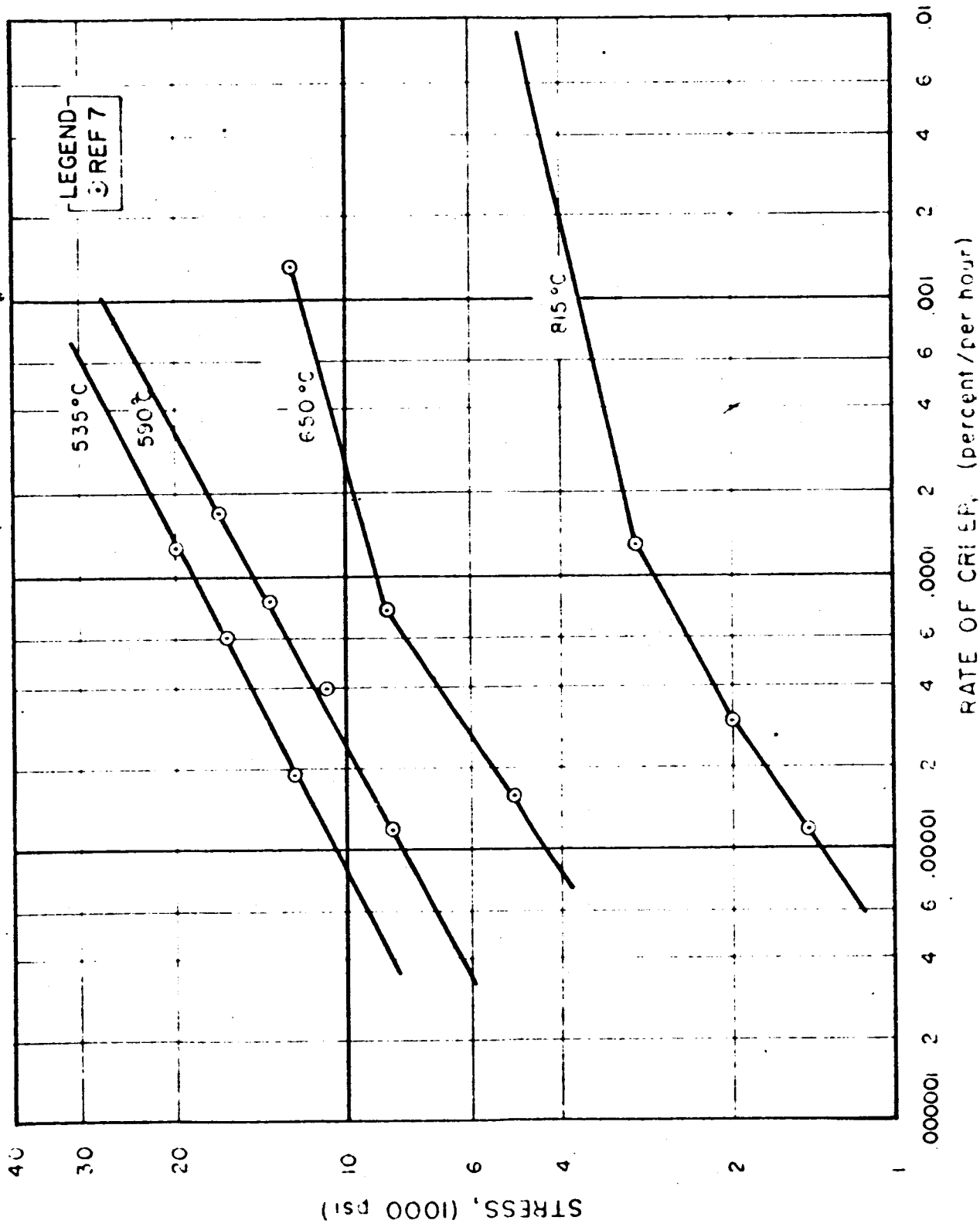
FIG. 2-17   CREEP STRENGTH OF S.S. 18-8
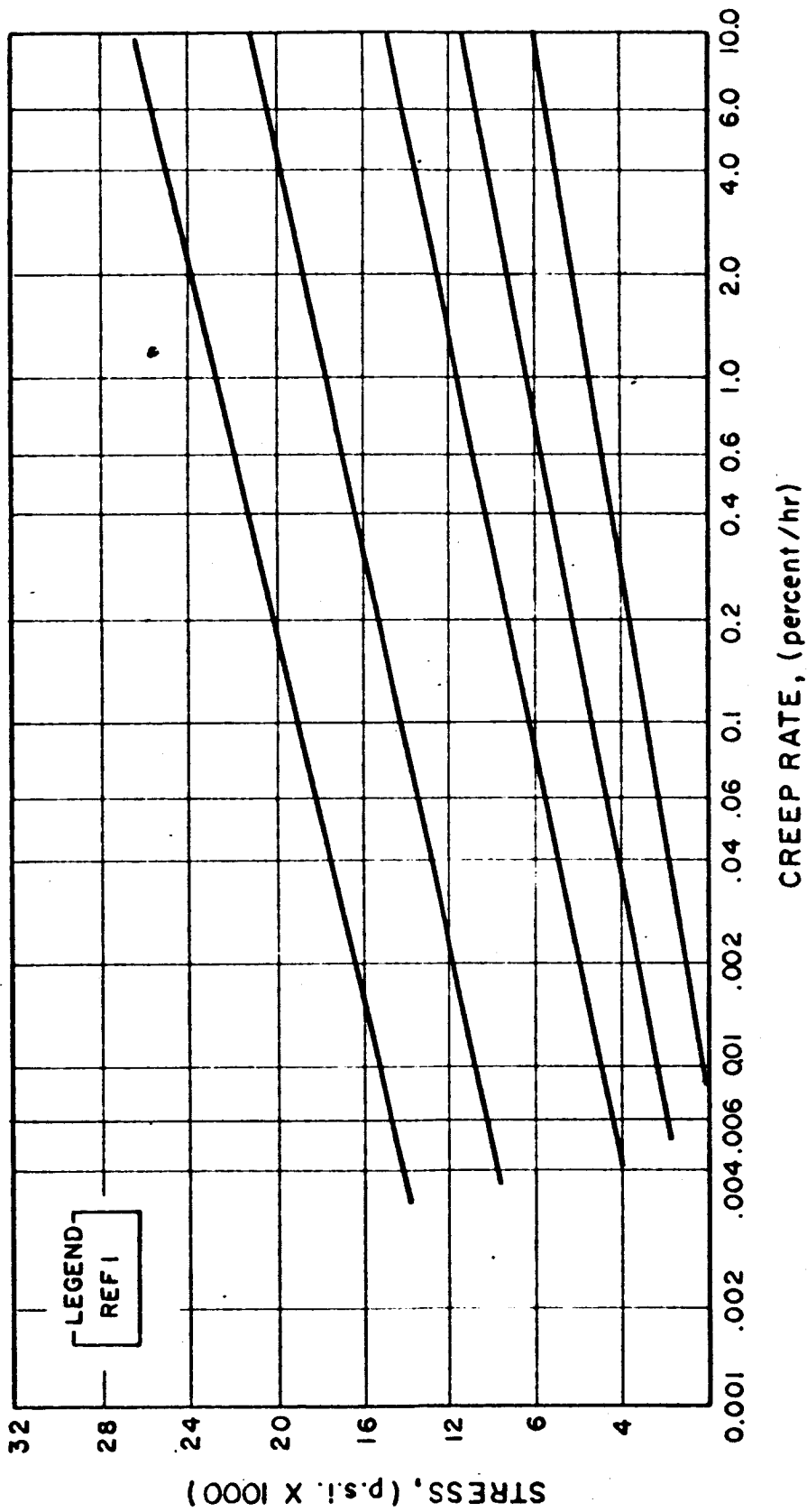
FIG. 2-18   CREEP STRENGTH OF NIOBIUM ALLOY (95Nb-5Va)
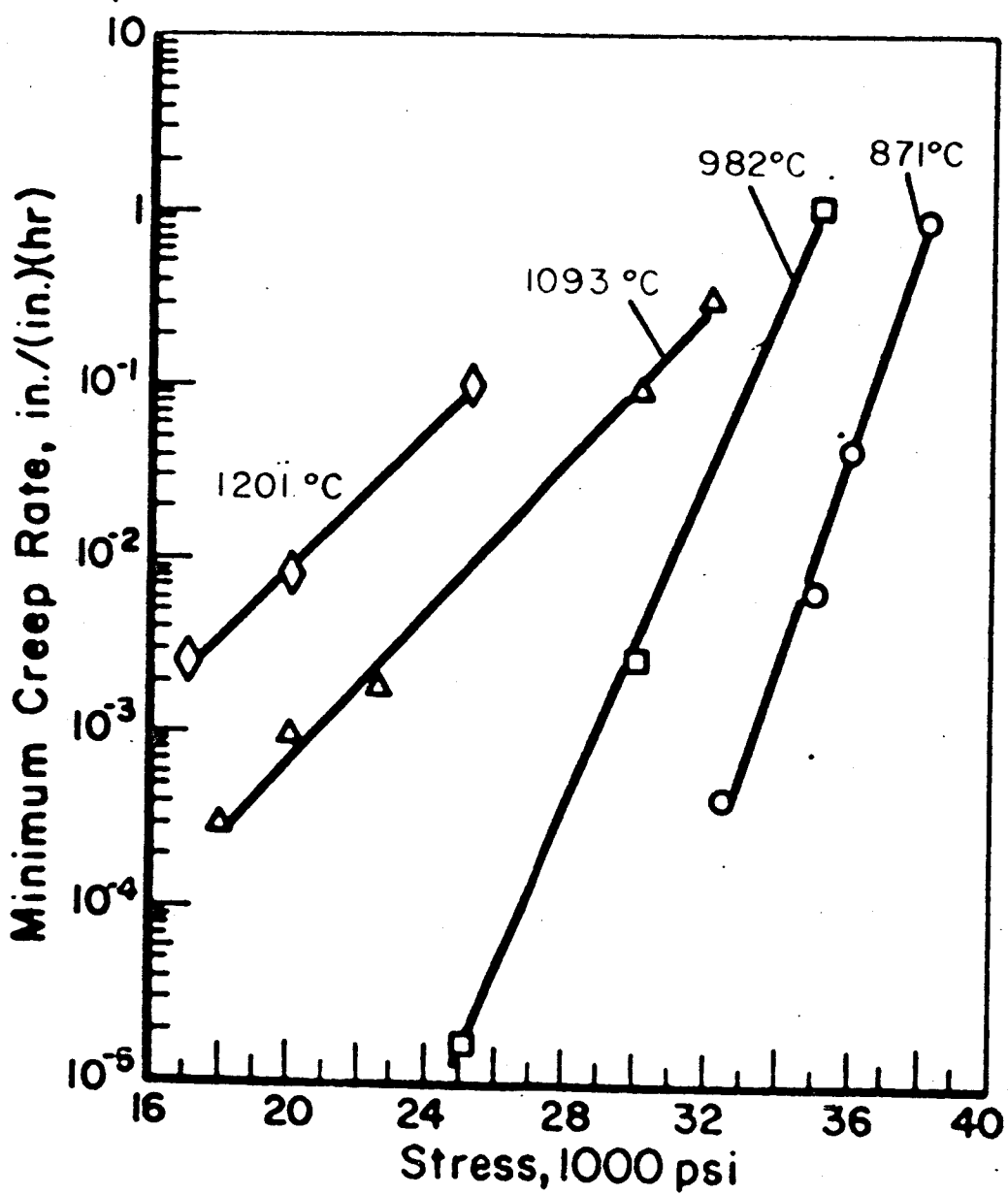
FIG. 2-19   MINIMUM CREEP RATE AS A FUNCTION OF STRESS FOR RECRYSTALLIZED TUNGSTEN

2.2.2 Grain Growth and Recrystallization

The recrystallization of cold worked metals at elevated temperatures is well documented in the literature (Ref. 2). Depending upon the temperature, time at temperature, and the amount of cold work reduction, new small crystals are formed along the grain boundaries and slip planes of the metal. Increasing the temperature results in a coalescence of crystals and a deterioration of mechanical properties.

It has been pointed out in a previous section (Processing of Emitter Materials) that all metals intended for use in a converter will probably be used in the recrystallized state resulting from prolonged vacuum outgassing. Consequently, design considerations for practical devices should be based on the physical and mechanical properties of recrystallized materials. There is often a considerable difference in creep strength between a cold worked material and the same material in a recrystallized condition. The use of hot strength data for cold worked material will usually tend to be too optimistic.

Examination of the recrystallization and grain growth diagrams of a material is often helpful in interpreting its thermionic emission phenomena and its mechanical strength behavior. It has been shown that recrystallization and grain growth in materials such as tungsten, molybdenum, tantalum and vanadium is often accompanied by processes of growth selectivity, in which a particular set of crystal faces in the surface of the material tends to grow at the expense of others present.

Recrystallization and grain growth diagrams for two materials of interest to the thermionic converter technology are shown in the following pages.
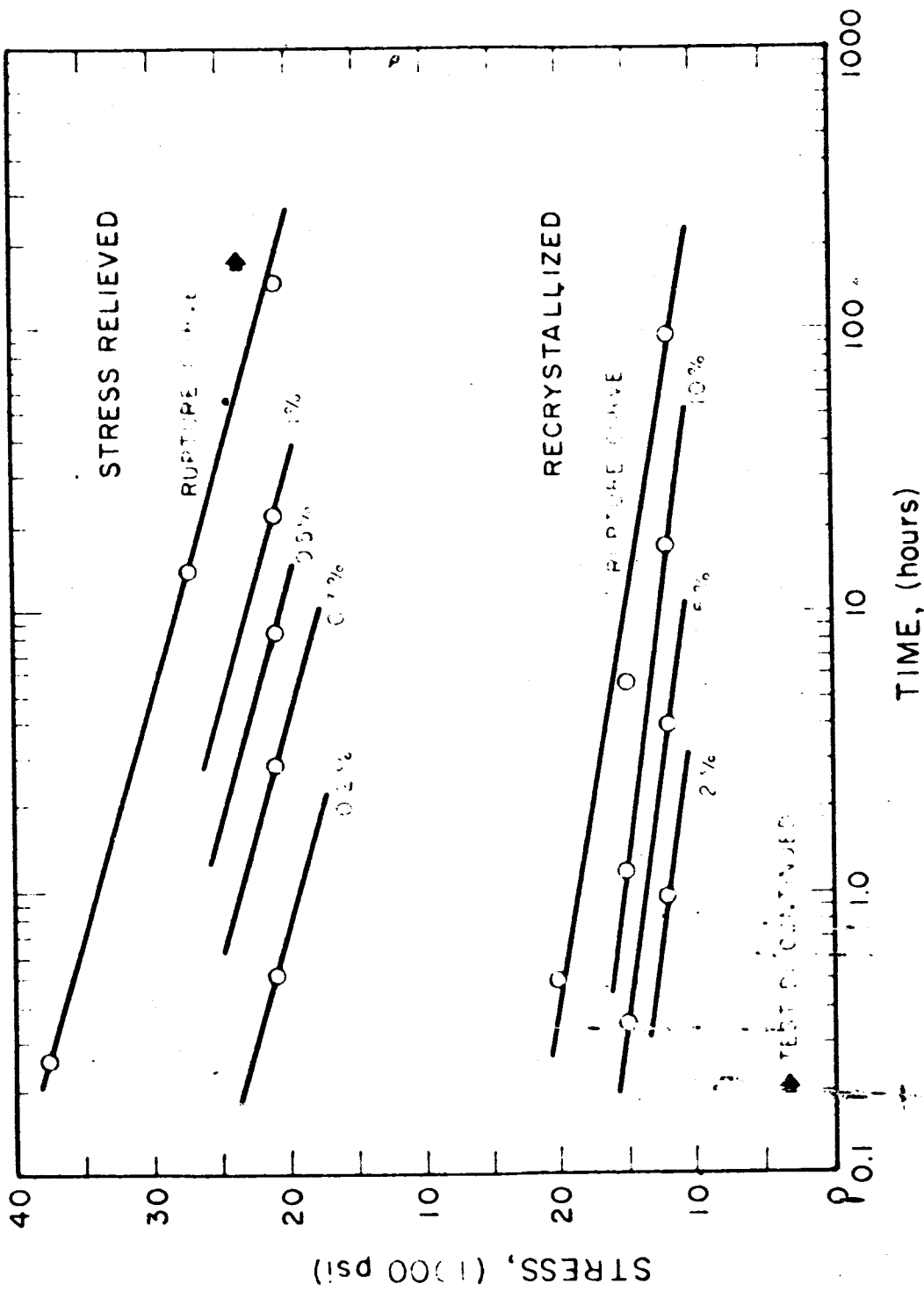
FIG. 2-20   DESIGN CURVES FOR ARC-CAST MOLYBDENUM AT 982°C
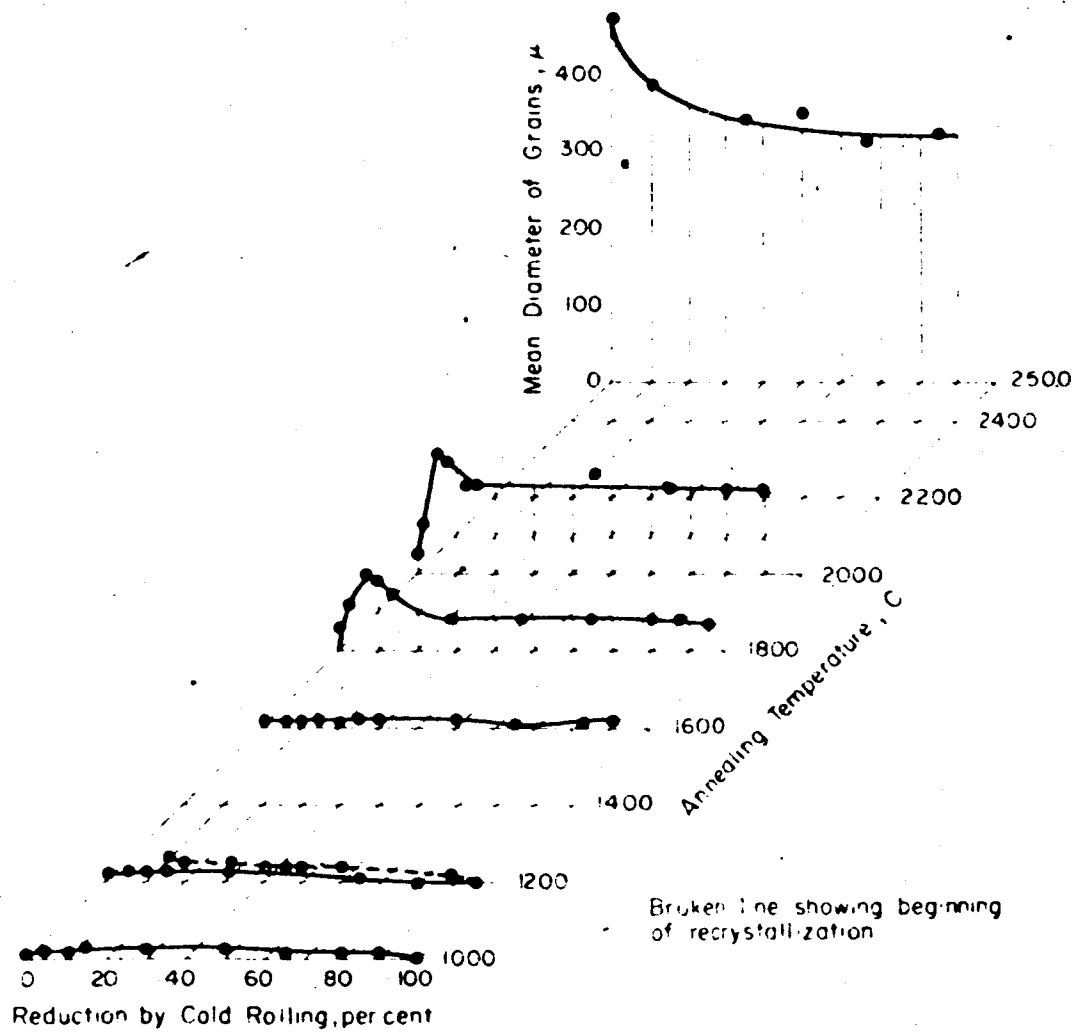
FIG. 2-21   DIAGRAM OF RECRYSTALLIZATION OF THE FIRST KIND FOR TANTALUM
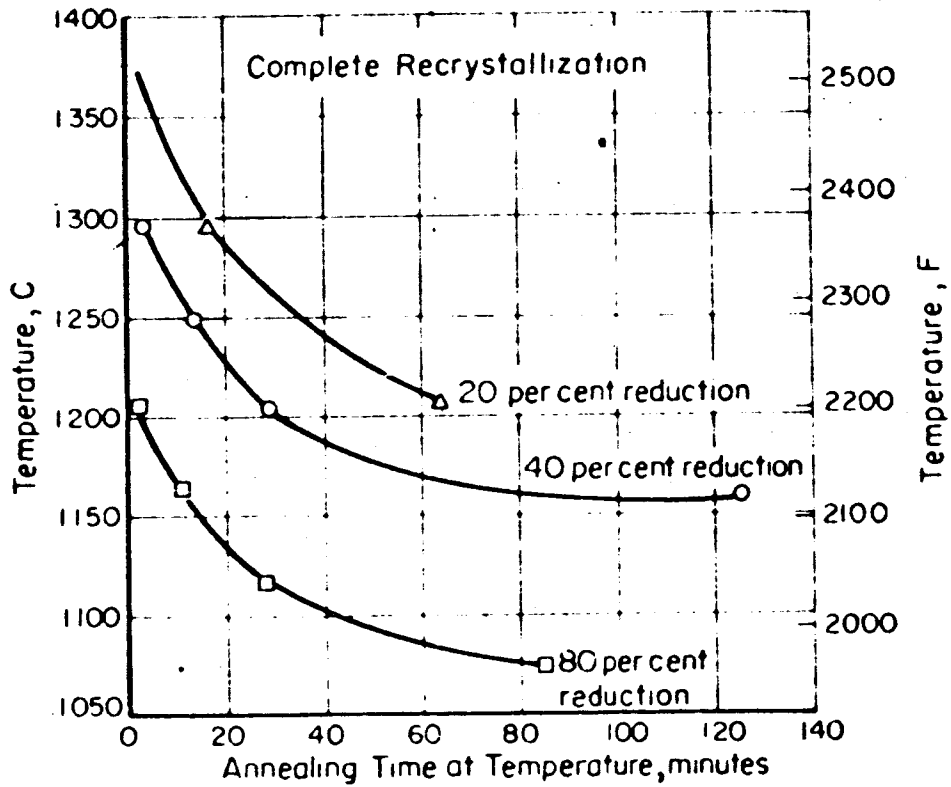
FIG. 2-22   EFFECT OF ANNEALING TIME AND REDUCTION ON THE
RECRYSTALLIZATION BEHAVIOR OF TANTALUM
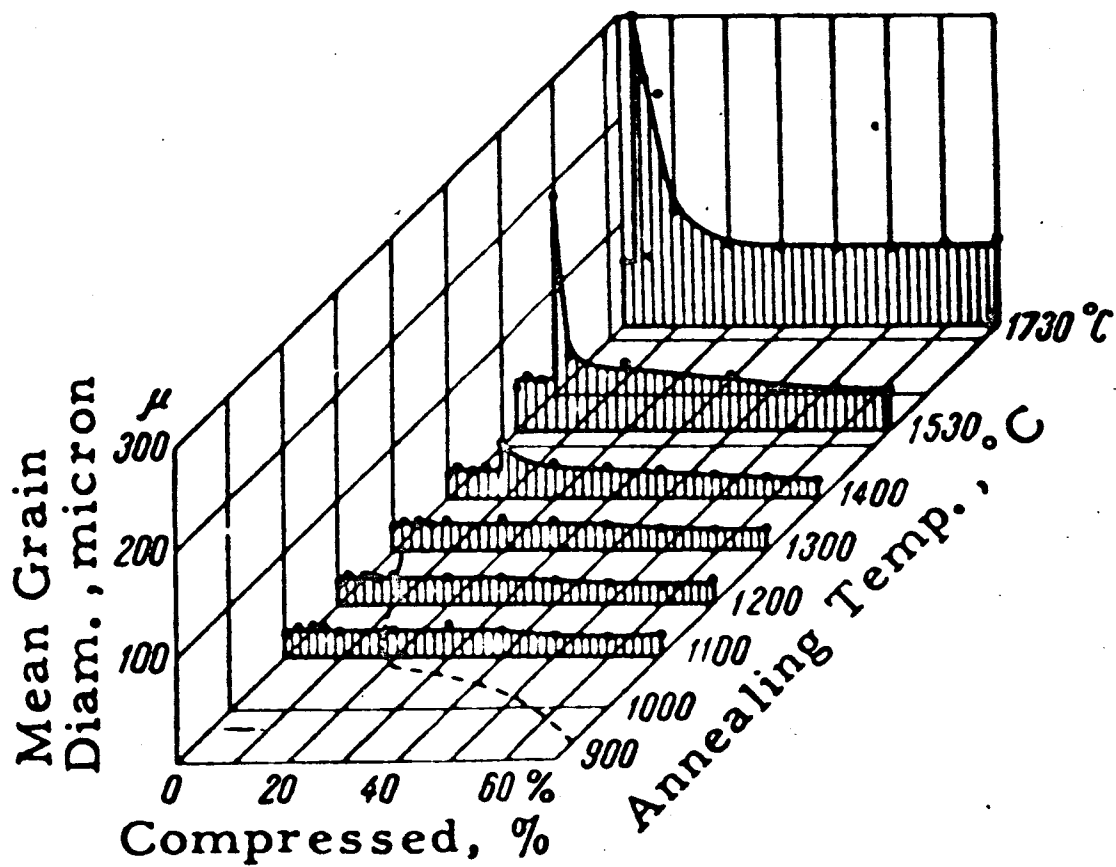
FIG. 2-23   DIAGRAM OF RECRYSTALLIZATION OF THE FIRST KIND, FOR MOLYBDENUM

2.2.3 Thermal Expansion

The linear expansion of heated materials is given over a moderate temperature range by the simple relation

$$\Delta l = l_o c (\Delta t)$$

Δl = the difference between the original length and final length

c = coefficient of linear expansion

$\Delta \tau$ = the difference between the original temperature and final temperature

Over a very wide temperature range, however, c does not remain constant, and generally becomes a function of temperature.

Thermal expansion or contraction data are very important for matching metals to ceramics in a manner such that thermal stresses in the seal area are maintained within tolerable limits. Some converter design have used the expansion properties of materials to provide interelectrode spacing. This technique is commented on in Section 3.

Pertinent thermal expension data for eleven materials follow.
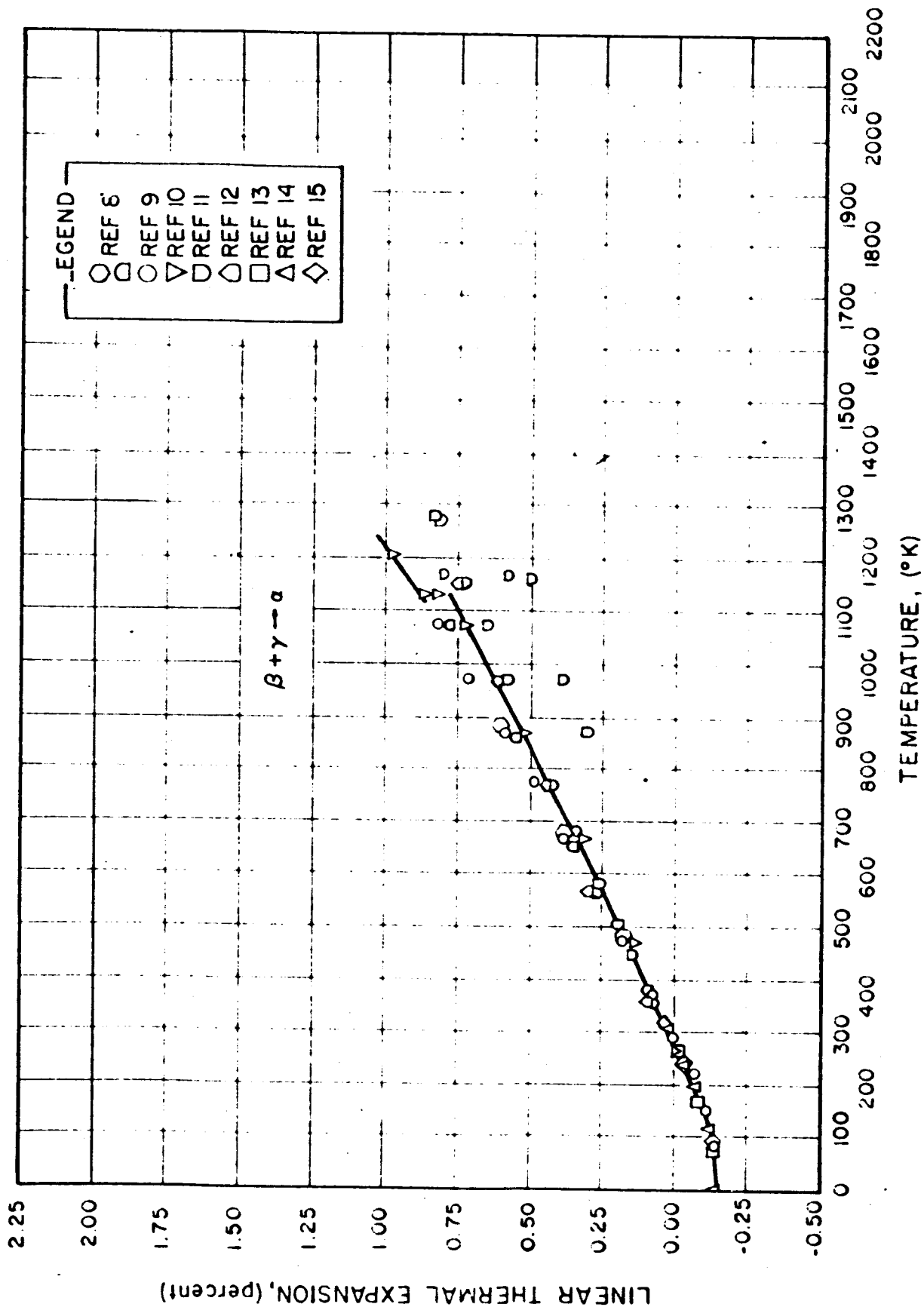
FIG. 2-24   LINEAR THERMAL EXPANSION - TITANIUM
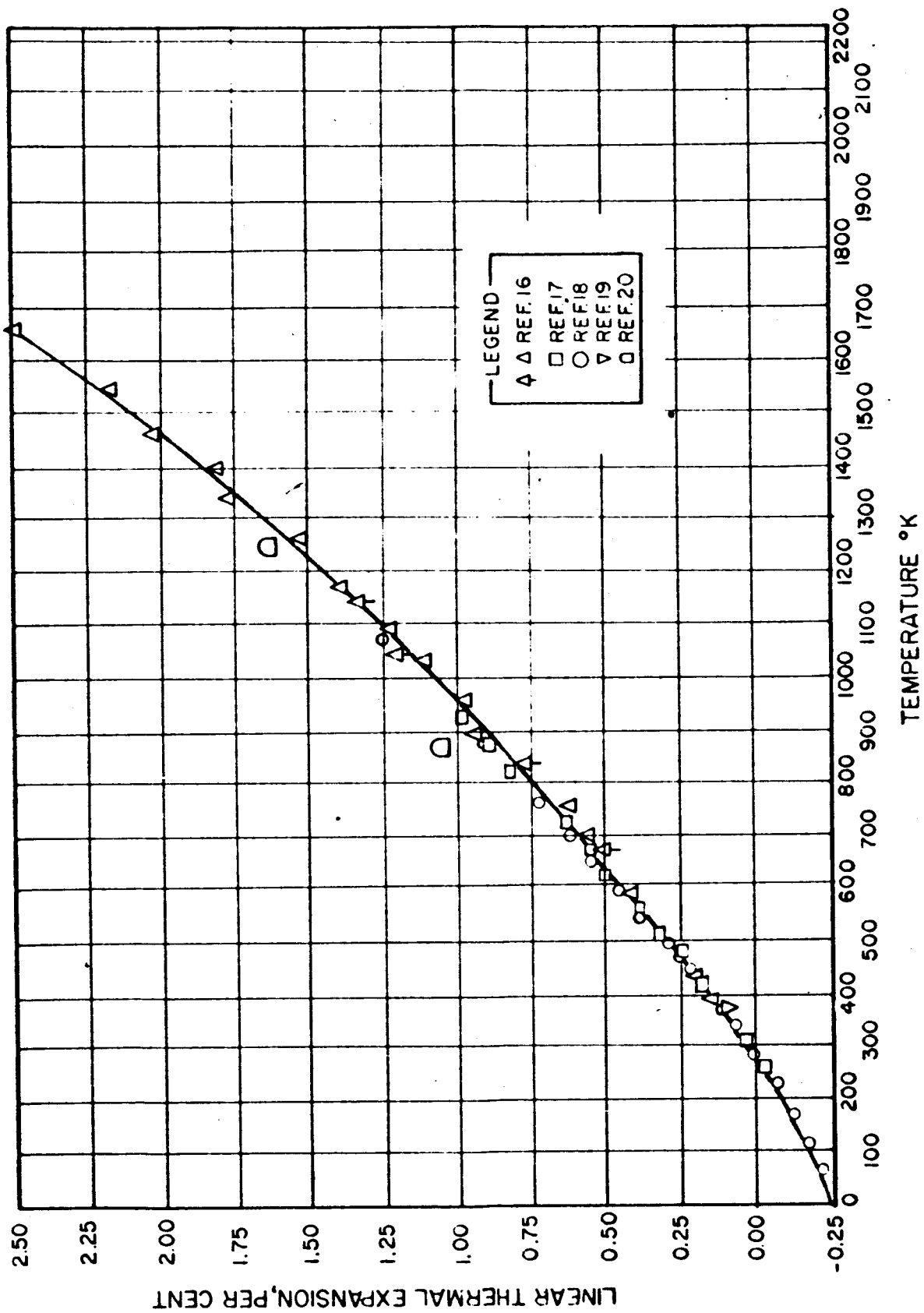
FIG. 2-25   LINEAR THERMAL EXPANSION - NICKEL

7364853
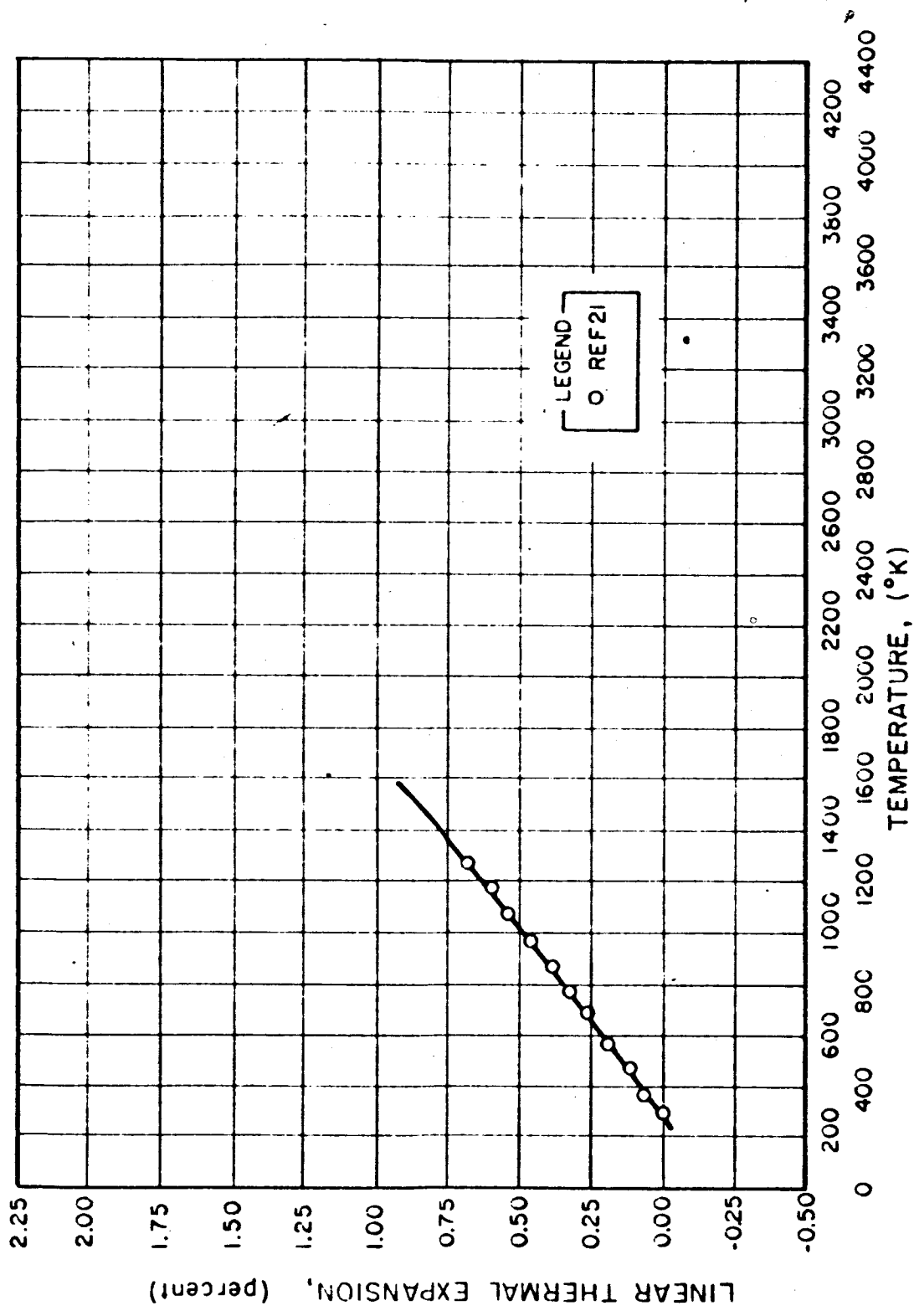
FIG. 2-26   LINEAR THERMAL EXPANSION - RHENIUM

7364841
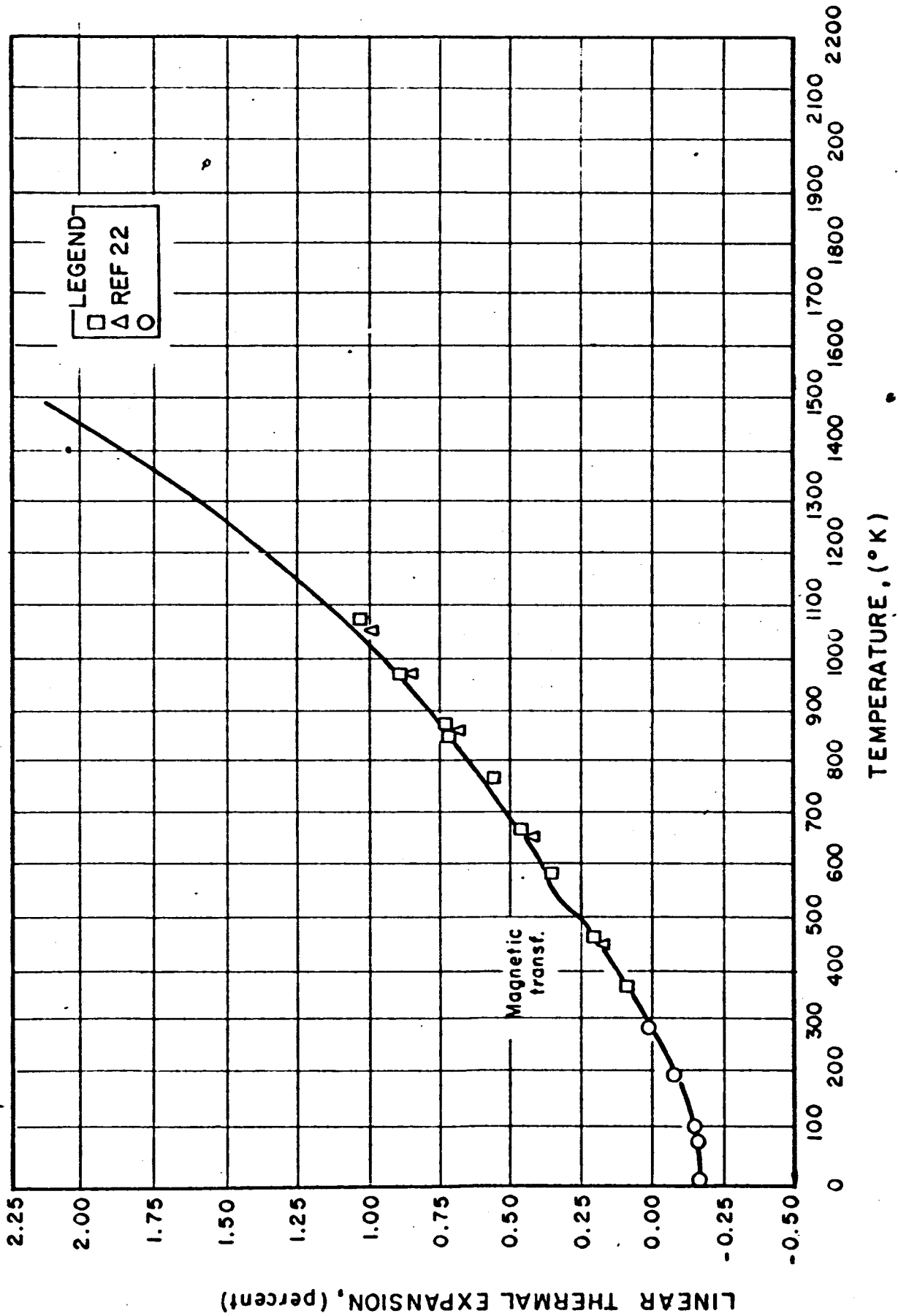
FIG. 2-27   LINEAR THERMAL EXPANSION - IRON + CHROMIUM

7364863
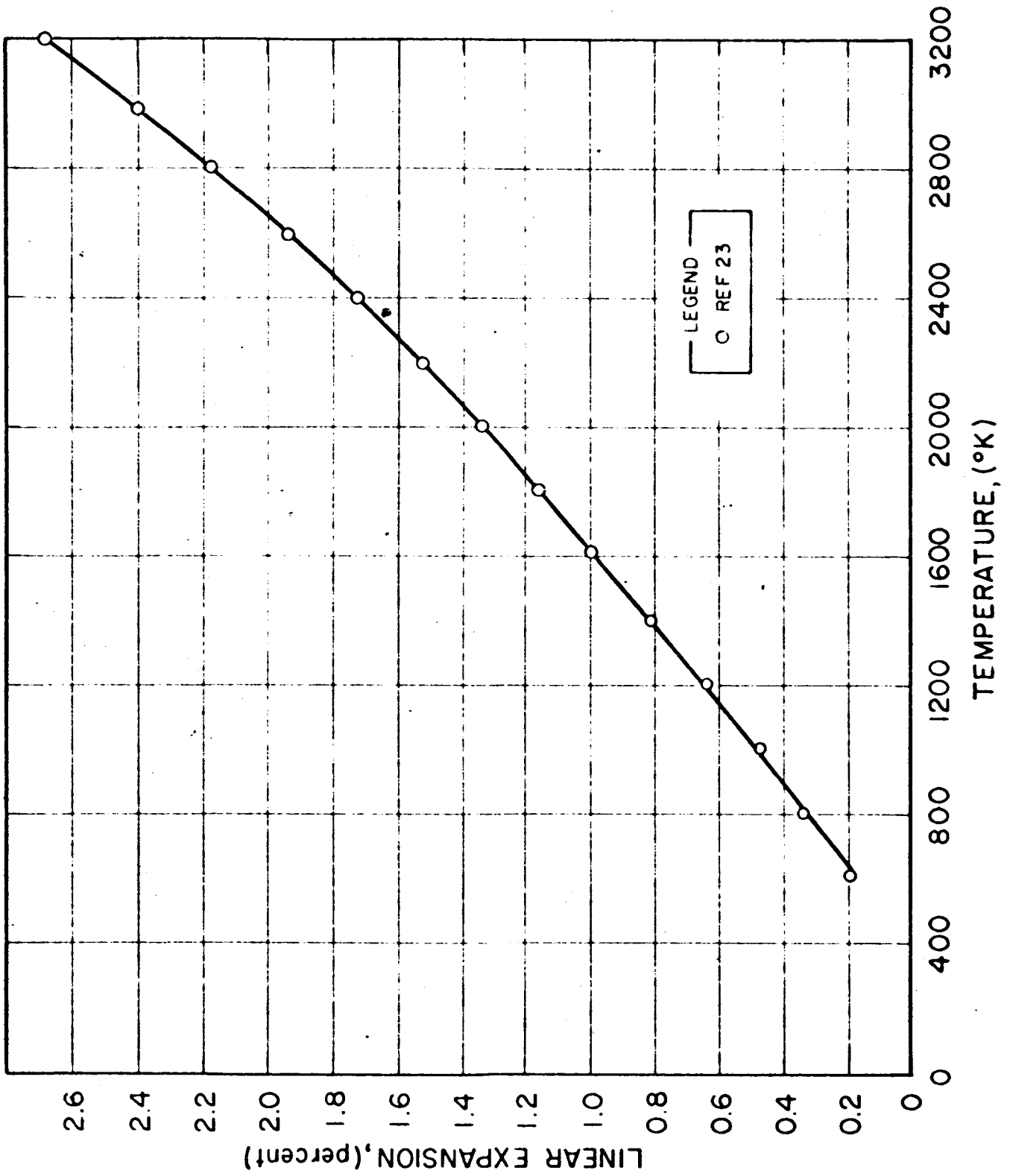
FIG. 2-28   LINEAR EXPANSION OF TANTALUM
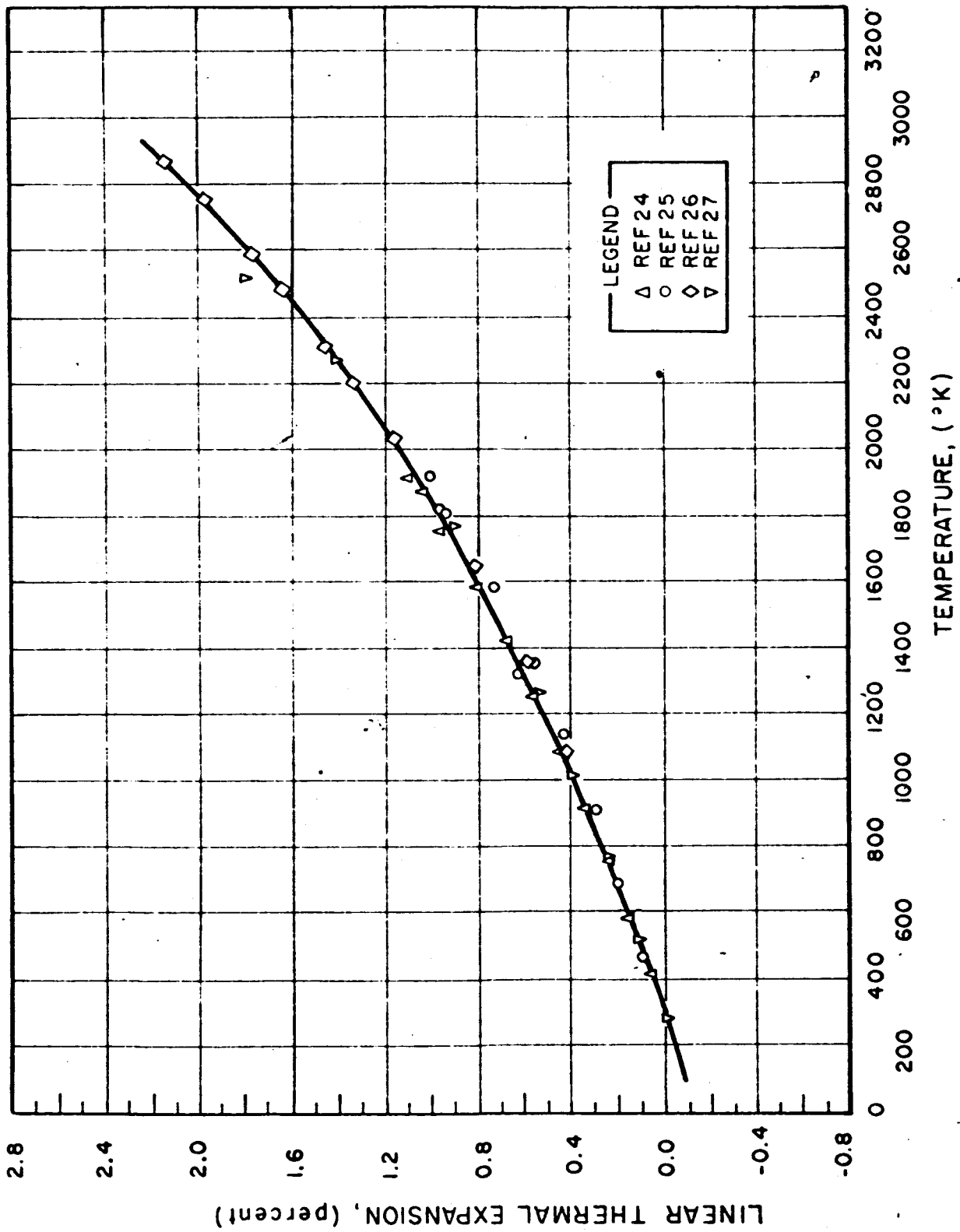
FIG. 2-29   LINEAR THERMAL EXPANSION - MOLYBDENUM
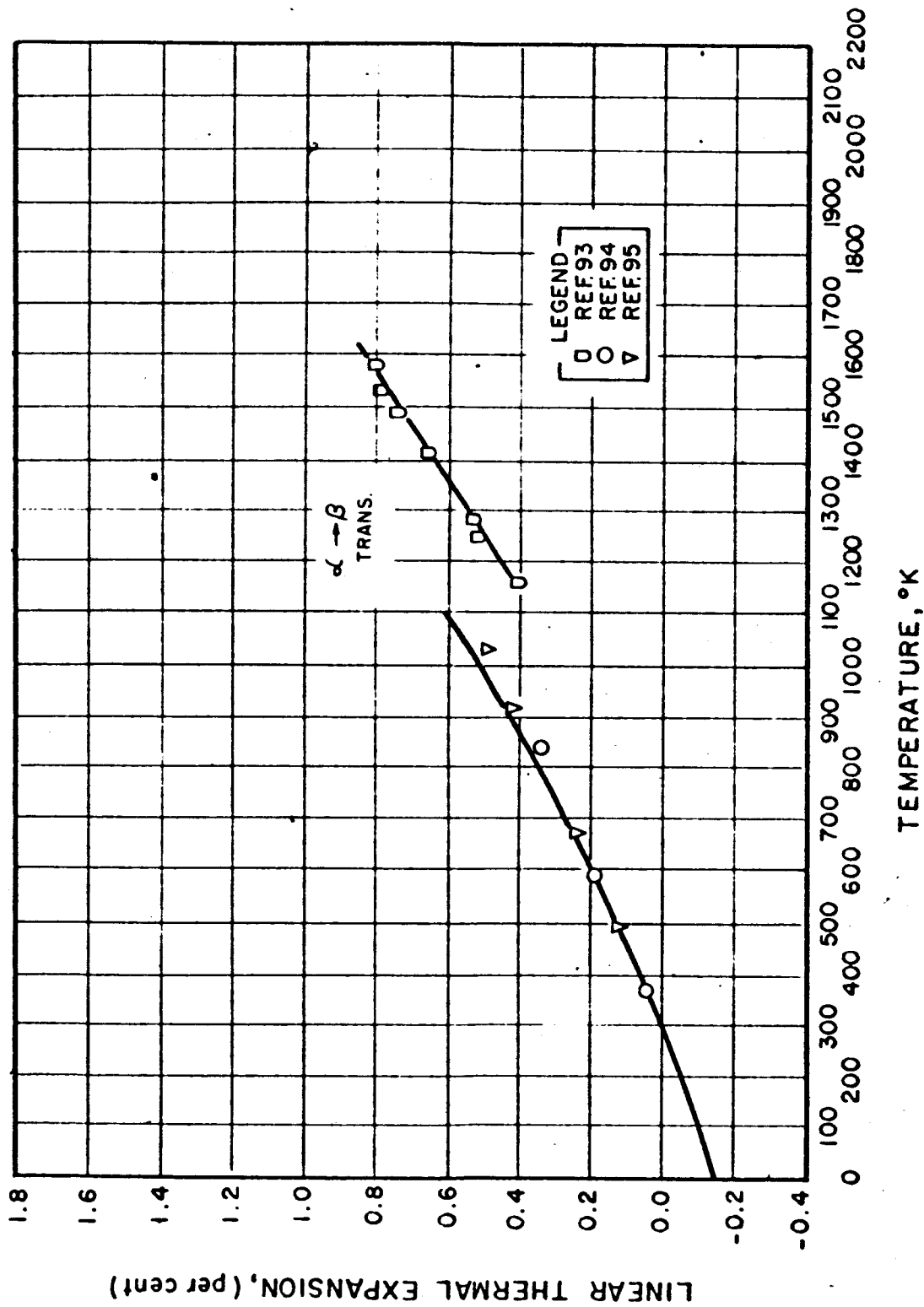
FIG. 2-30   LINEAR THERMAL EXPANSION - ZIRCONIUM
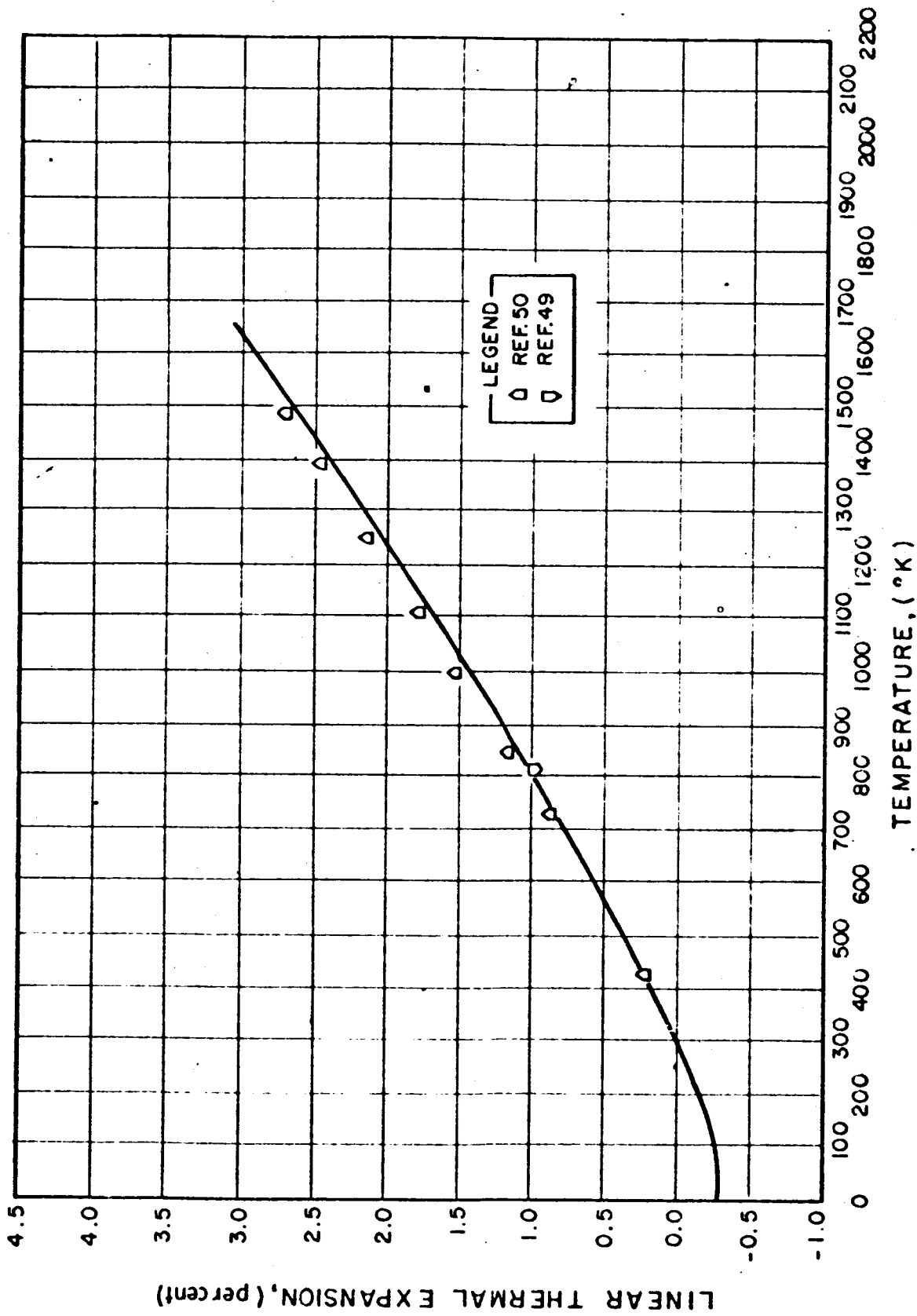
FIG. 2-31   LINEAR THERMAL EXPANSION - IRON: CHROMIUM + NICKEL + X (16-19%Cr; 7-16%Ni)

14839
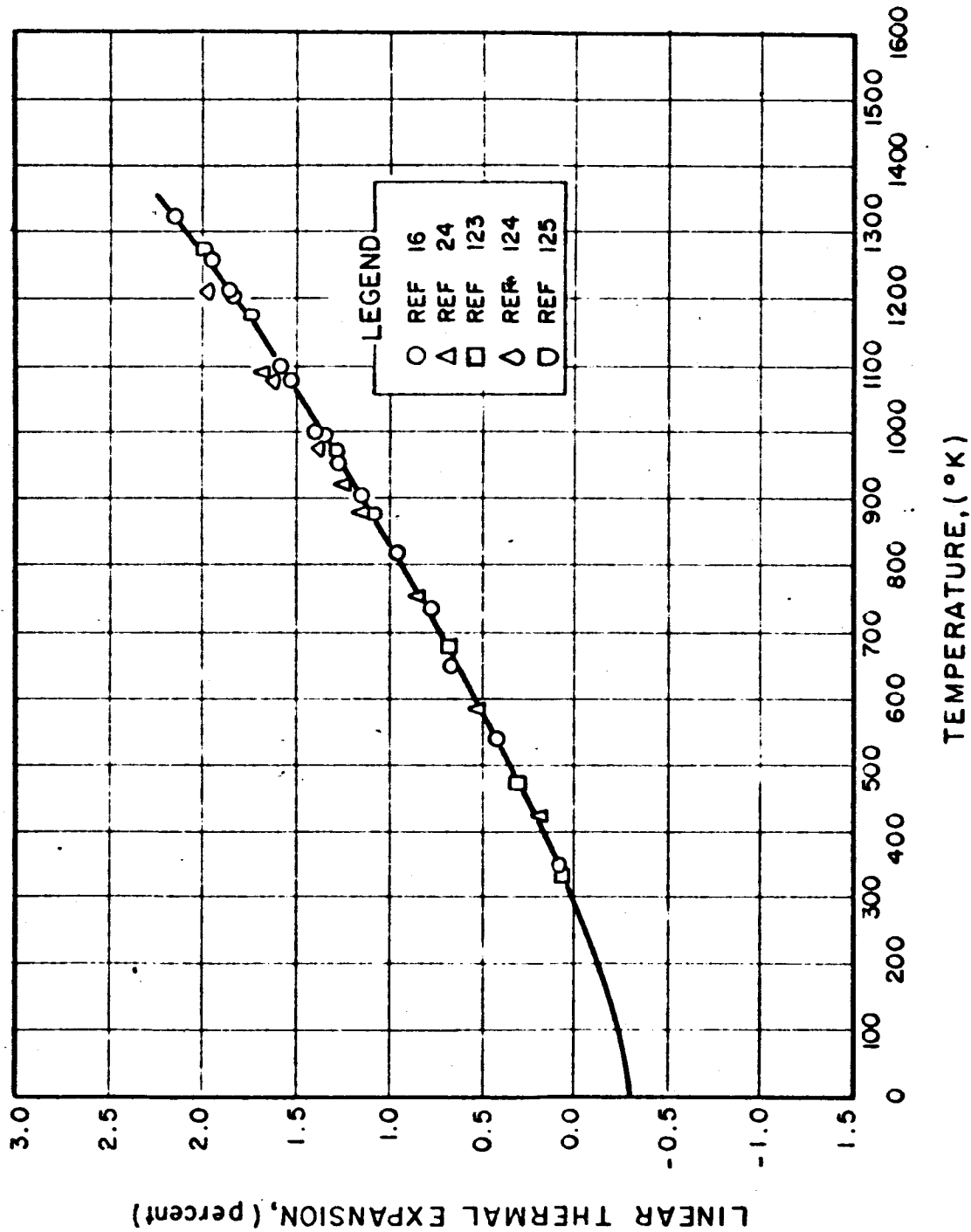
FIG. 2-32   LINEAR THERMAL EXPANSION - COPPER
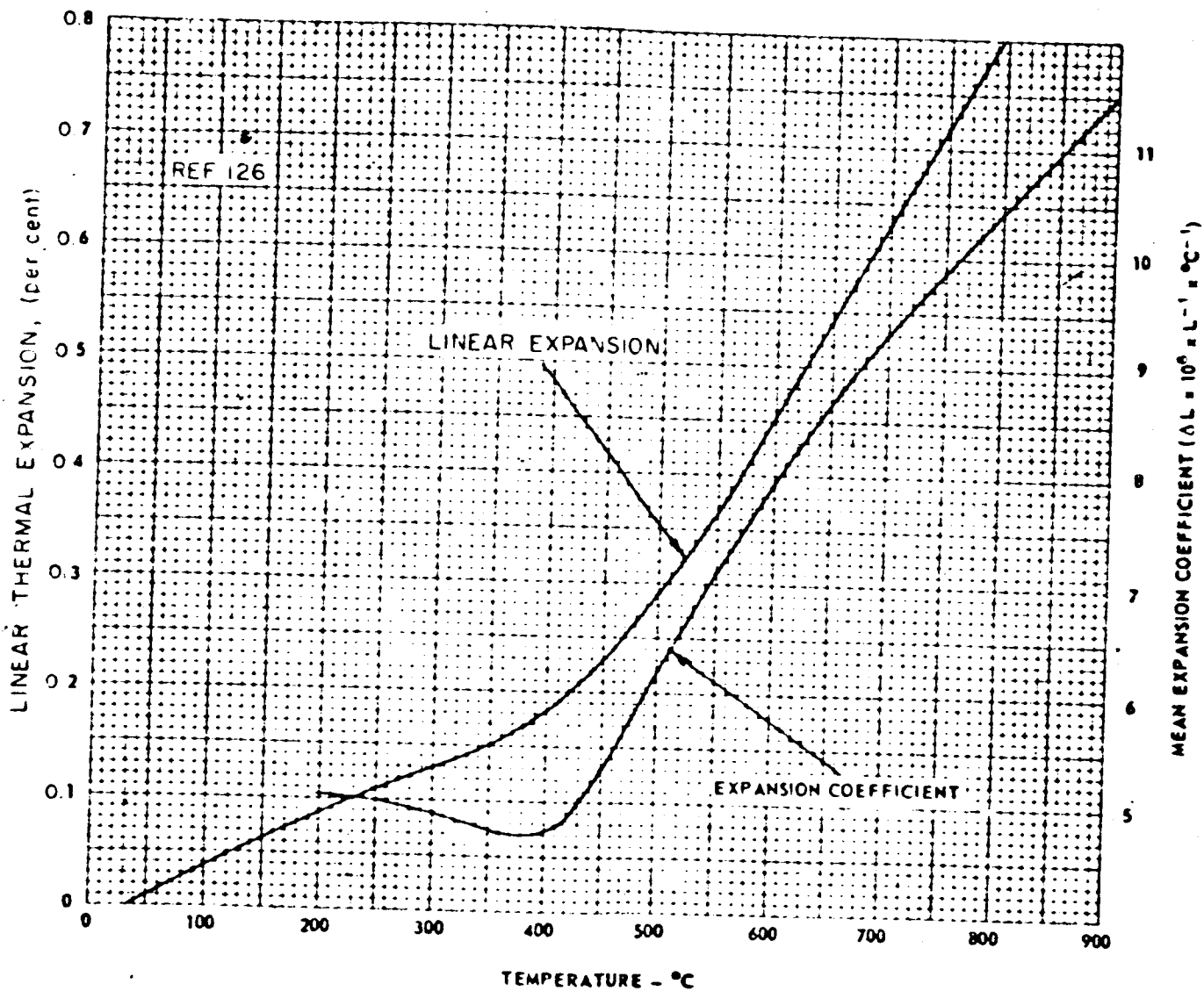
FIG. 2-33   LINEAR THERMAL EXPANSION AND COEFFICIENT OF EXPANSION FOR KOVAR
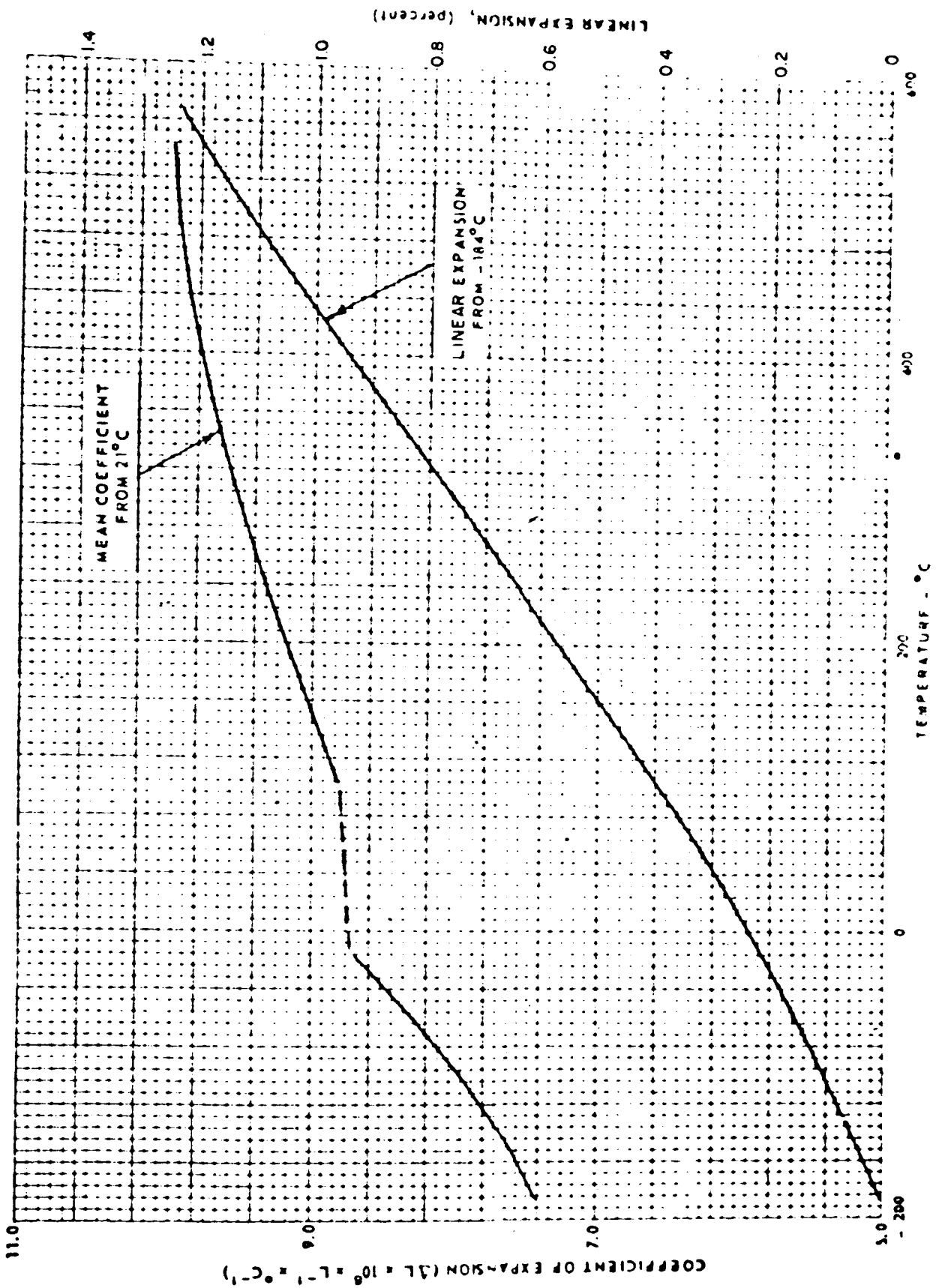
FIG. 2-34   LINEAR THERMAL EXPANSION AND MEAN COEFFICIENT OF EXPANSION FOR TYPE 304 STAINLESS STEEL

1942

2.2.4 Emissivity

Two types of emissivity data are included in this section. They are total (normal) emissivity and spectral (0.665μ) emissivity as a function of temperature.

The total emissivity is useful in converter design and operation for the calculation of heat losses resulting from radiation between emitter and collector and from emitter leads, reservoir tubulation, and envelopes.

The spectral emissivity of a material may be used to ascertain its temperature when the preferred means of observing a black body hole temperature is not possible. Caution must be exercised, however, since the spectral emissivity is a critical function of surface conditions. The values are reported for a wavelength of 0.665, since this corresponds to the optics of most common pyrometers.

Spectral and total emissivity data for a number of pertinent materials may be found in the following pages.
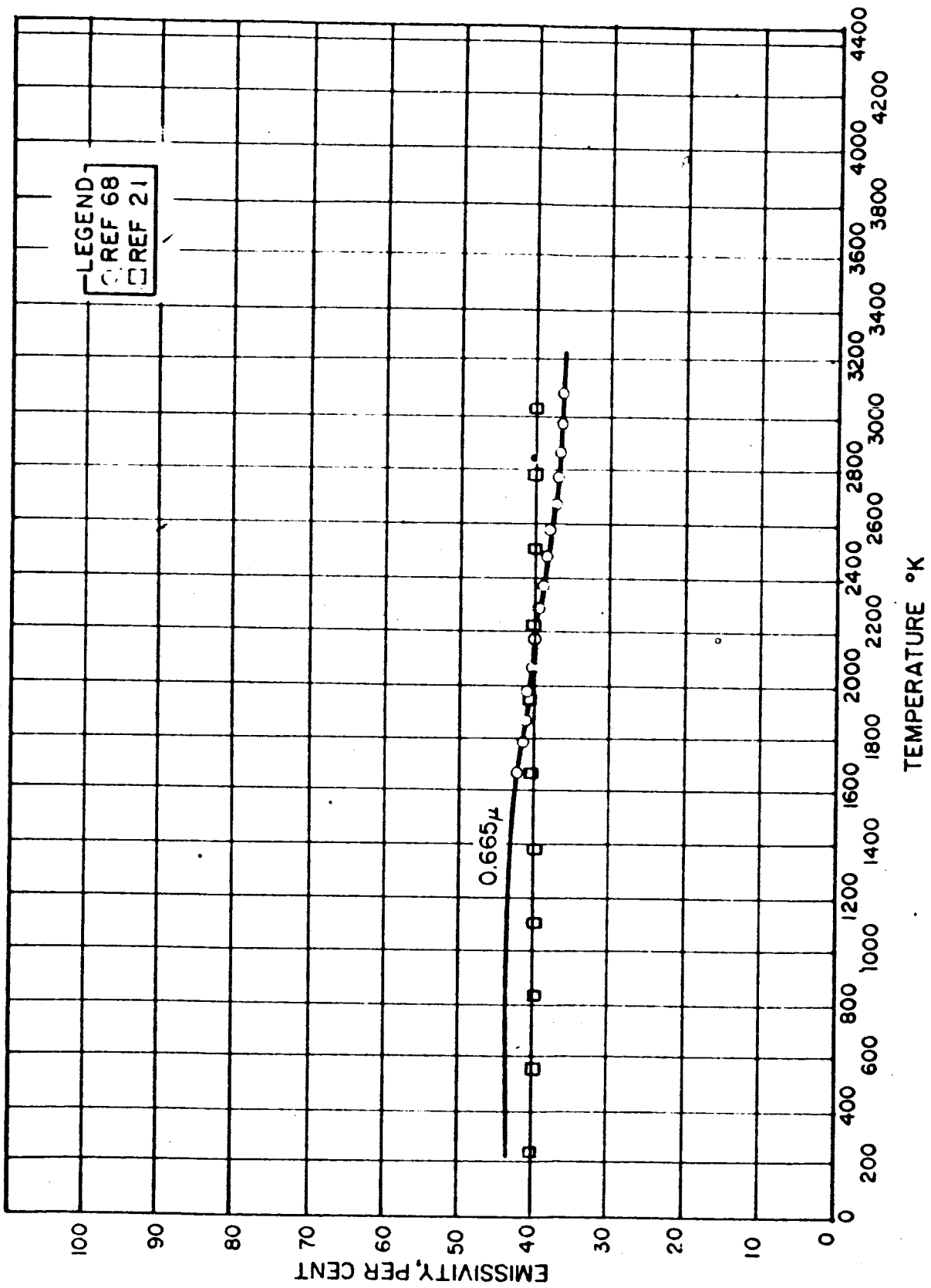
FIG. 2-35 · EMISSIVITY - RHENIUM
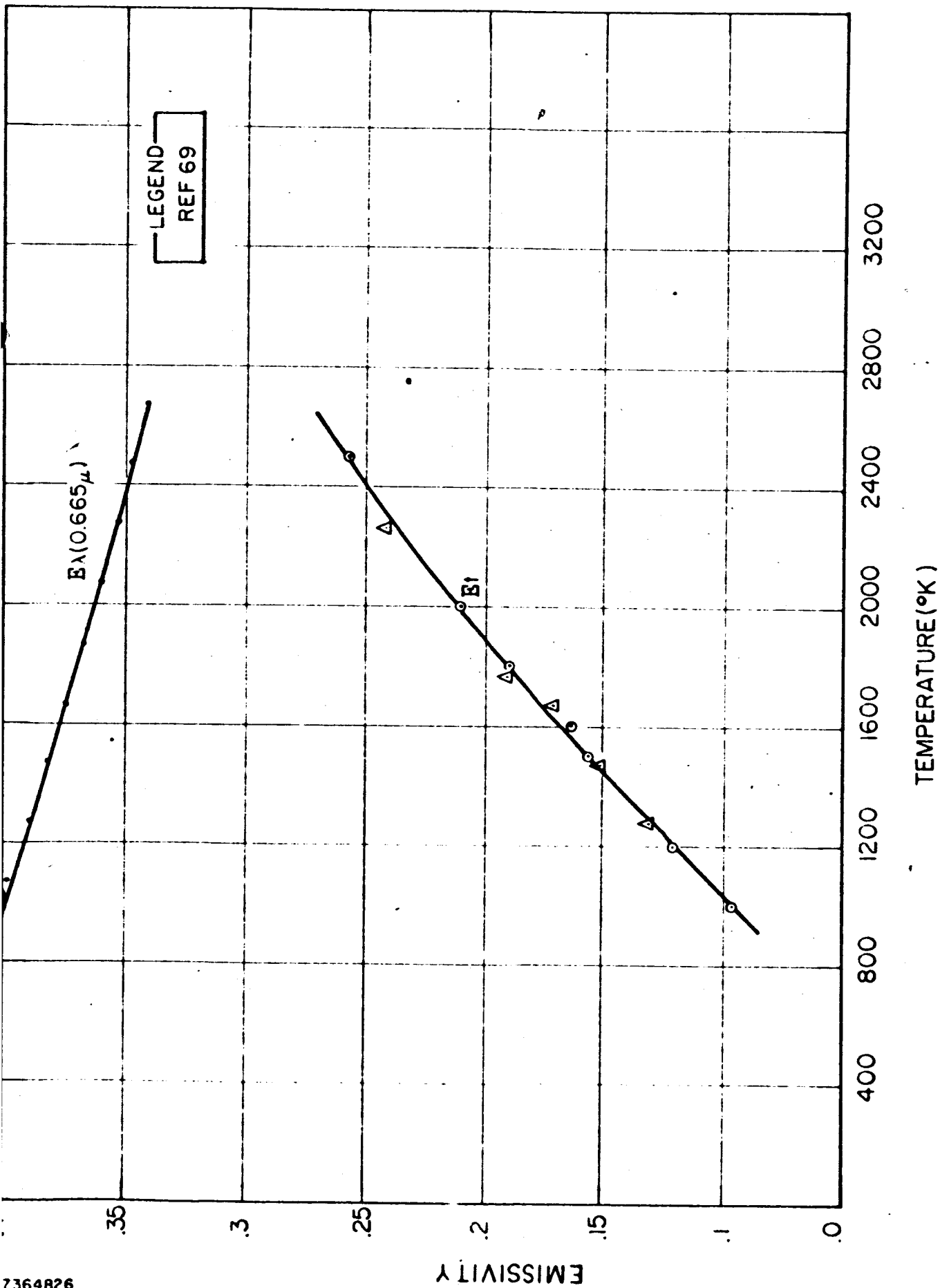
FIG. 2-36   EMISSIVITY OF MOLYBDENUM
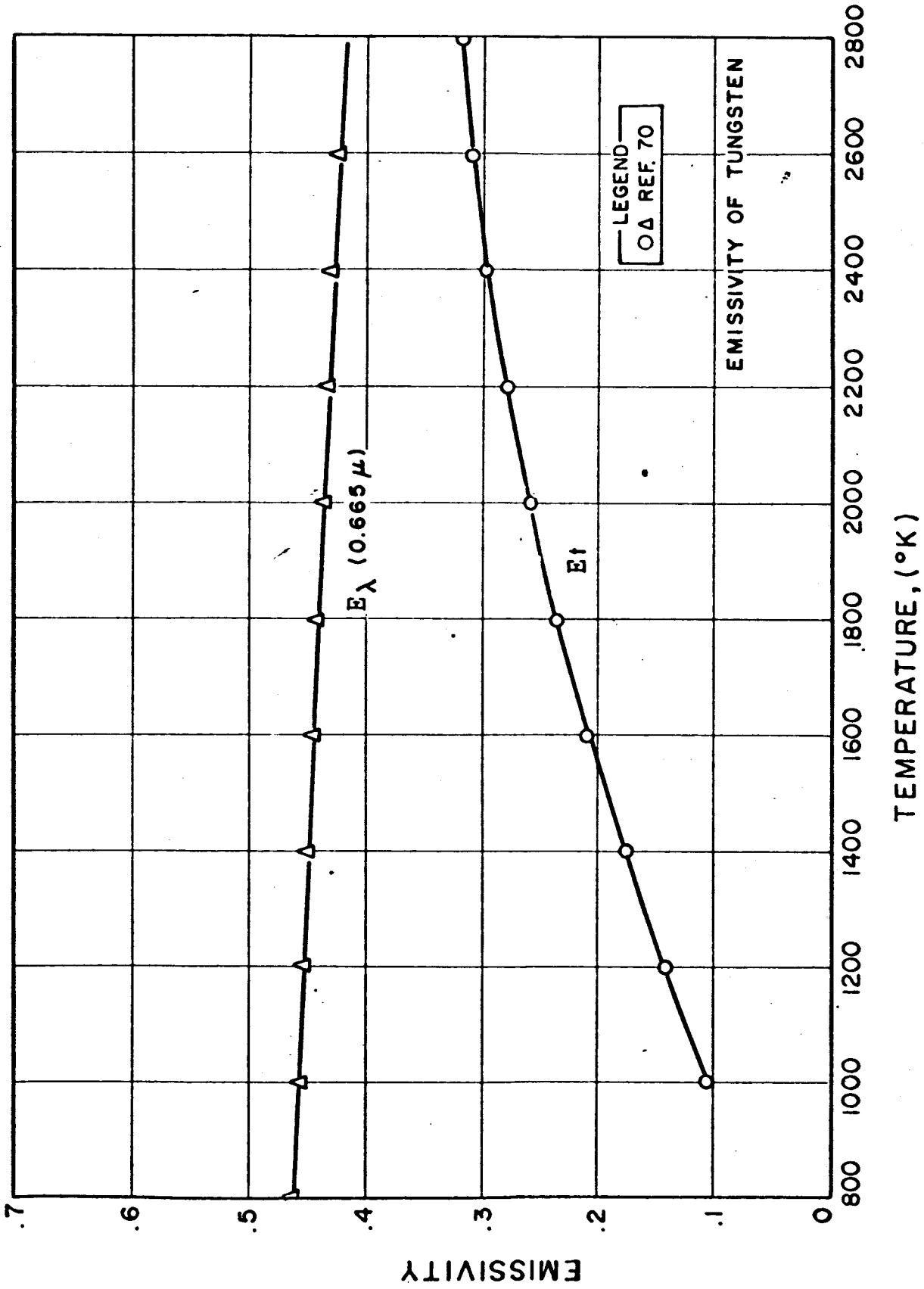
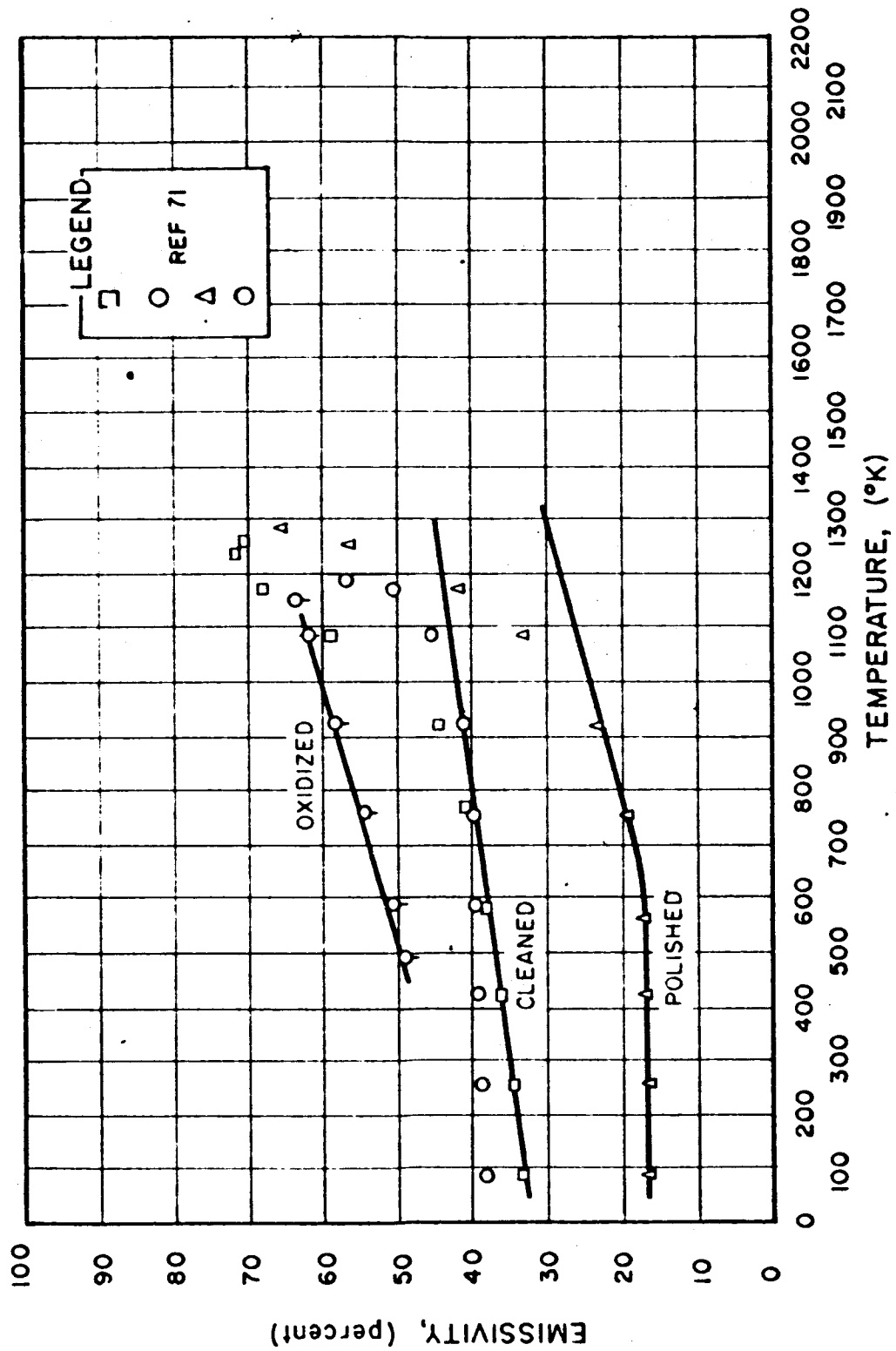FIG. 2-37   EMISSIVITY OF TUNGSTEN

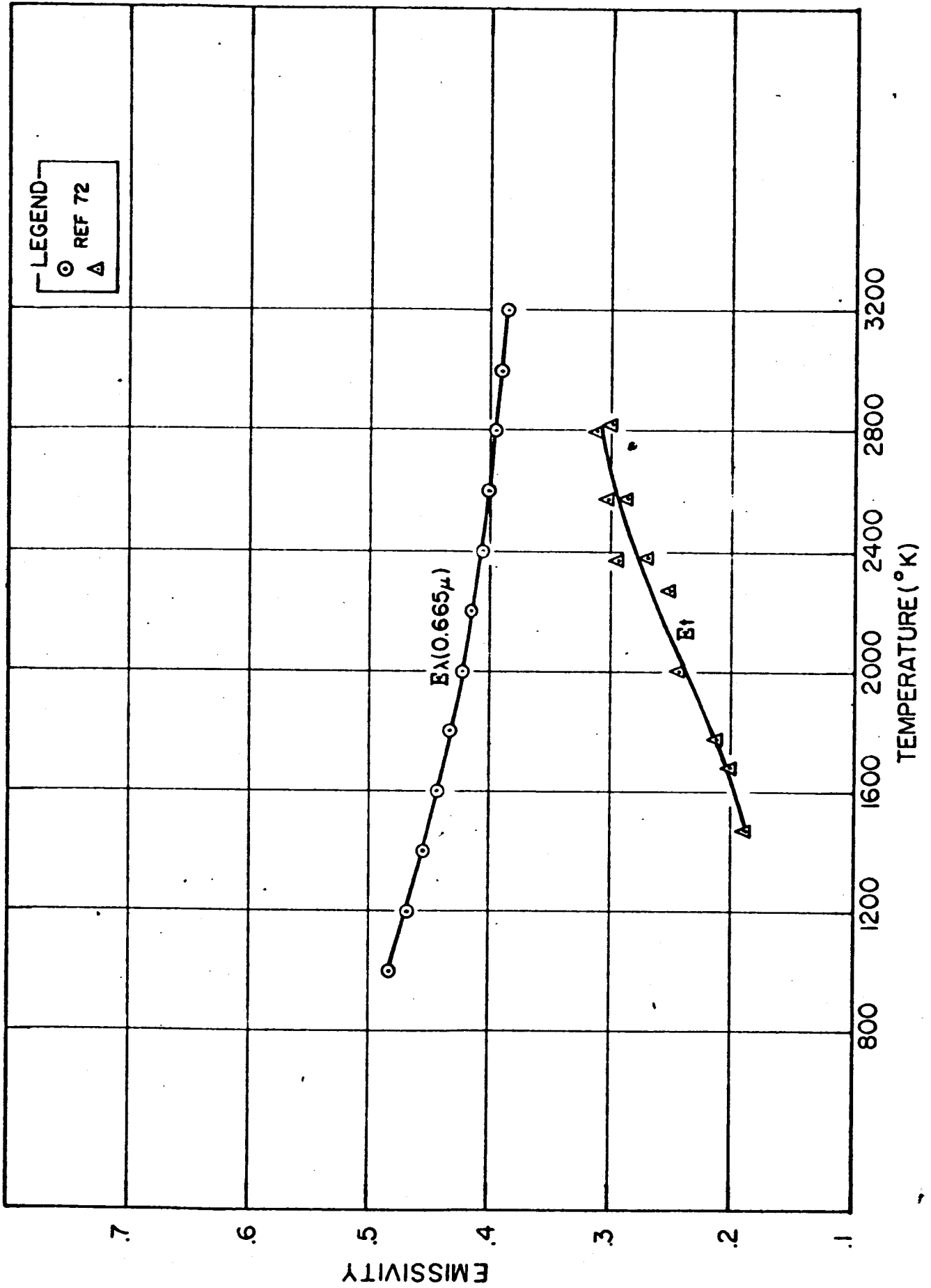FIG. 2-38   EMISSIVITY - IRON + CHROMIUM + NICKEL + X AISI 347

'364858

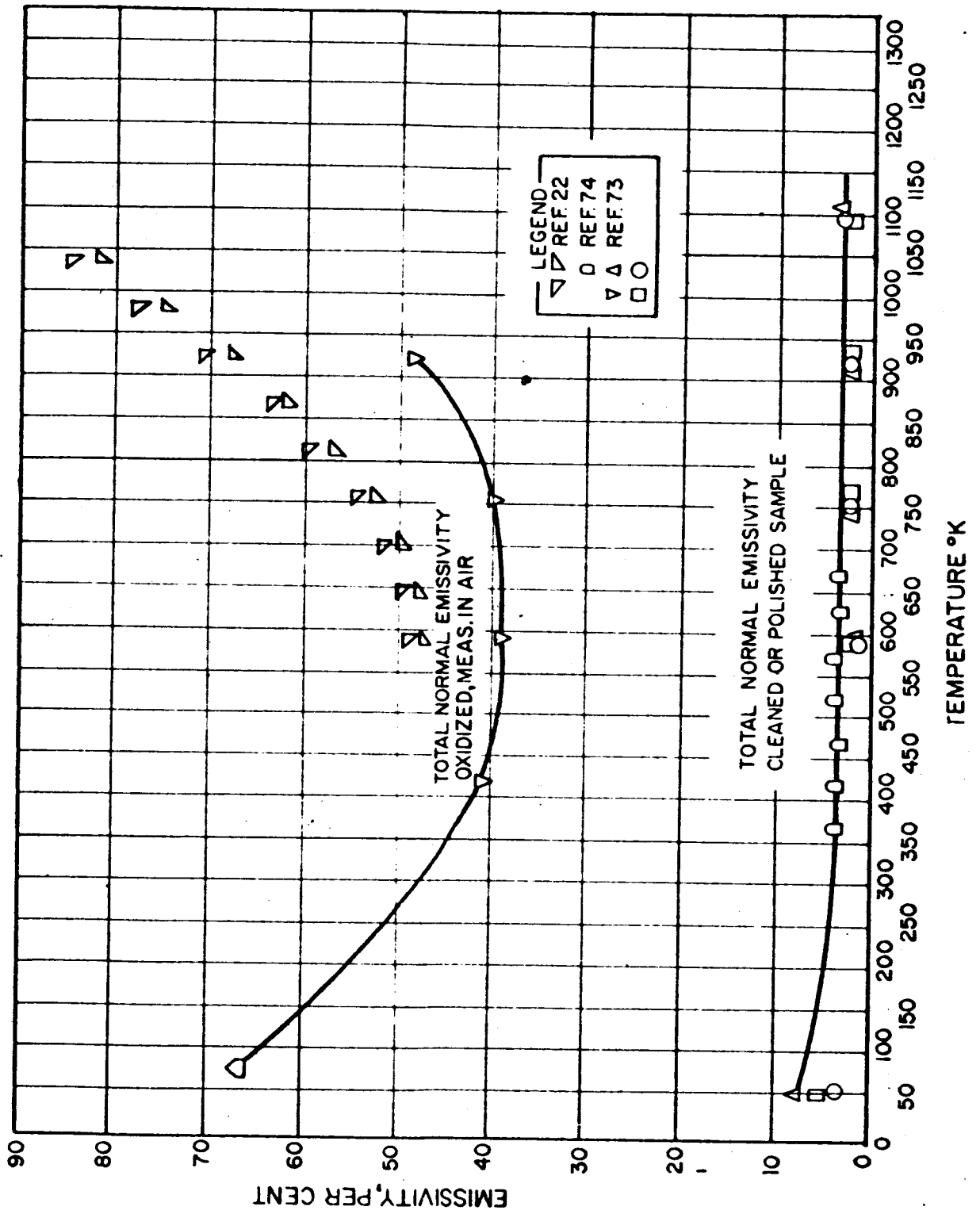FIG. 2-39 · - TOTAL AND SPECTRAL EMISSIVITY OF TANTALUM :
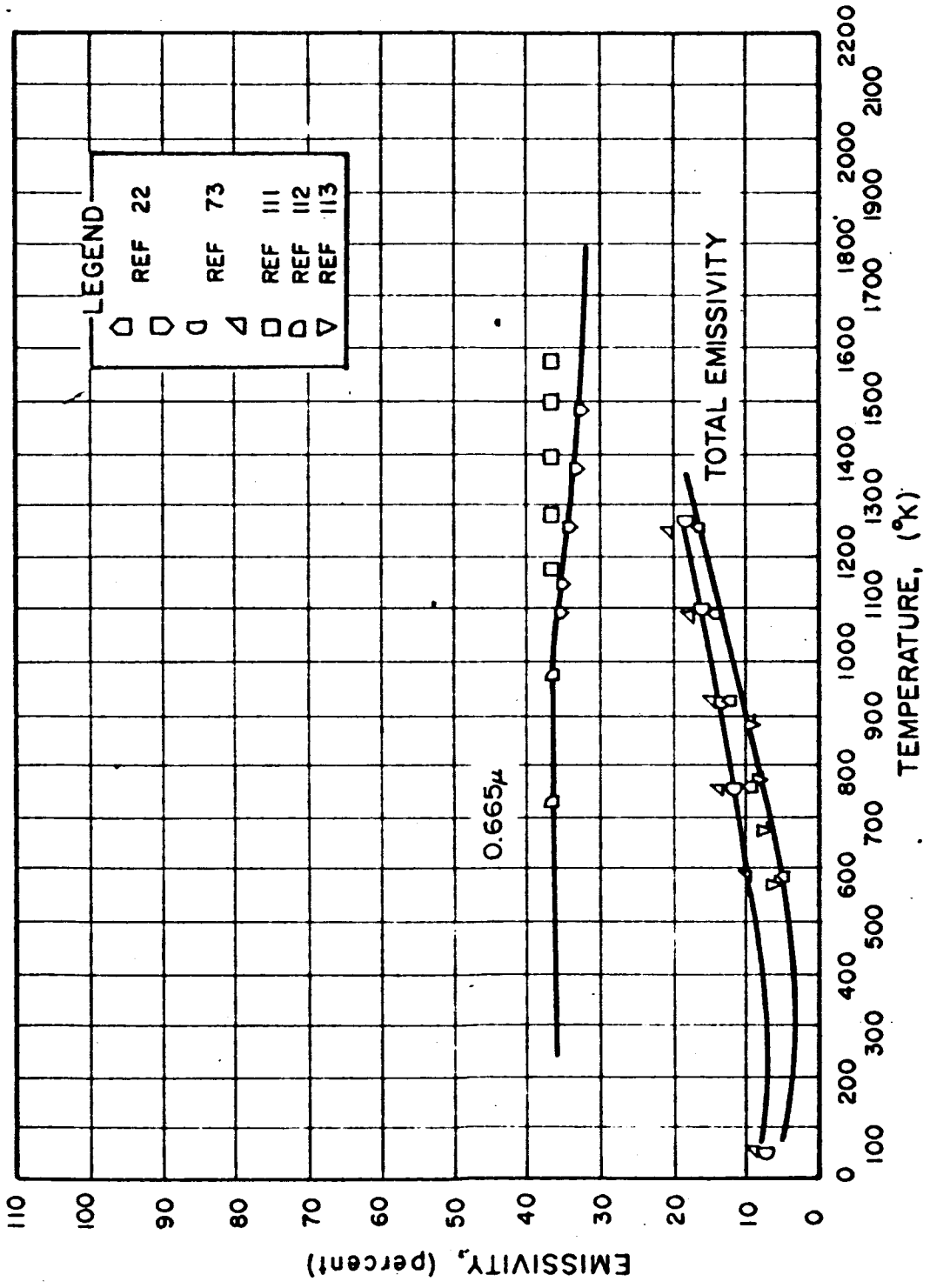
FIG. 2-40. EMISSIVITY - COPPER

FIG. 2-41   EMISSIVITY - NICKEL

2.2.5 Vapor Pressure

Converters have been constructed and operated wherein high vapor pressure materials were operated at impractically high temperatures resulting in harmful behaviour or imminent failure (Ref. 3).

Vapor pressure data is a necessity in the choice of braze materials for joining structures to be operated at high temperatures.

Critical to the long life operation of emitter materials is the consideration of surface weight loss derived from vapor pressure data. Figure 2-79 is a presentation of emitter material weight loss and surface depletion in $Å/cm^2/1000$ hr as a function of temperature. Weight loss considerations may well preclude, for example, the use of molybdenum emitters for high temperature ($1900°K$) application. The weight loss data has been presented in terms of $Å/cm^2/1000$ hr for emphasis. Only a few hundred angstrom layers of material need be evaporated in a low vacuum environment in order to produce a "black" deposit on a collecting surface. Such a deposit radically changes the total emissivity of the surface and may increase the combined emissivity of an emitter and collector combination by a factor of two to three. The evaporation of coatings in environments containing a few mm Hg of Argon has been used in the vidicon tube industry to produce fluffy dark coatings at coating thicknesses of less than 1000 Å.

The point to be made is that life time estimates for emitter materials have been made in the thermionic converter art where the assumption has been that one mil of material thickness could be lost before performance of a converter is degraded. It would appear that, practically speaking, the loss of even a few hundred Å layers of material is deleterious.
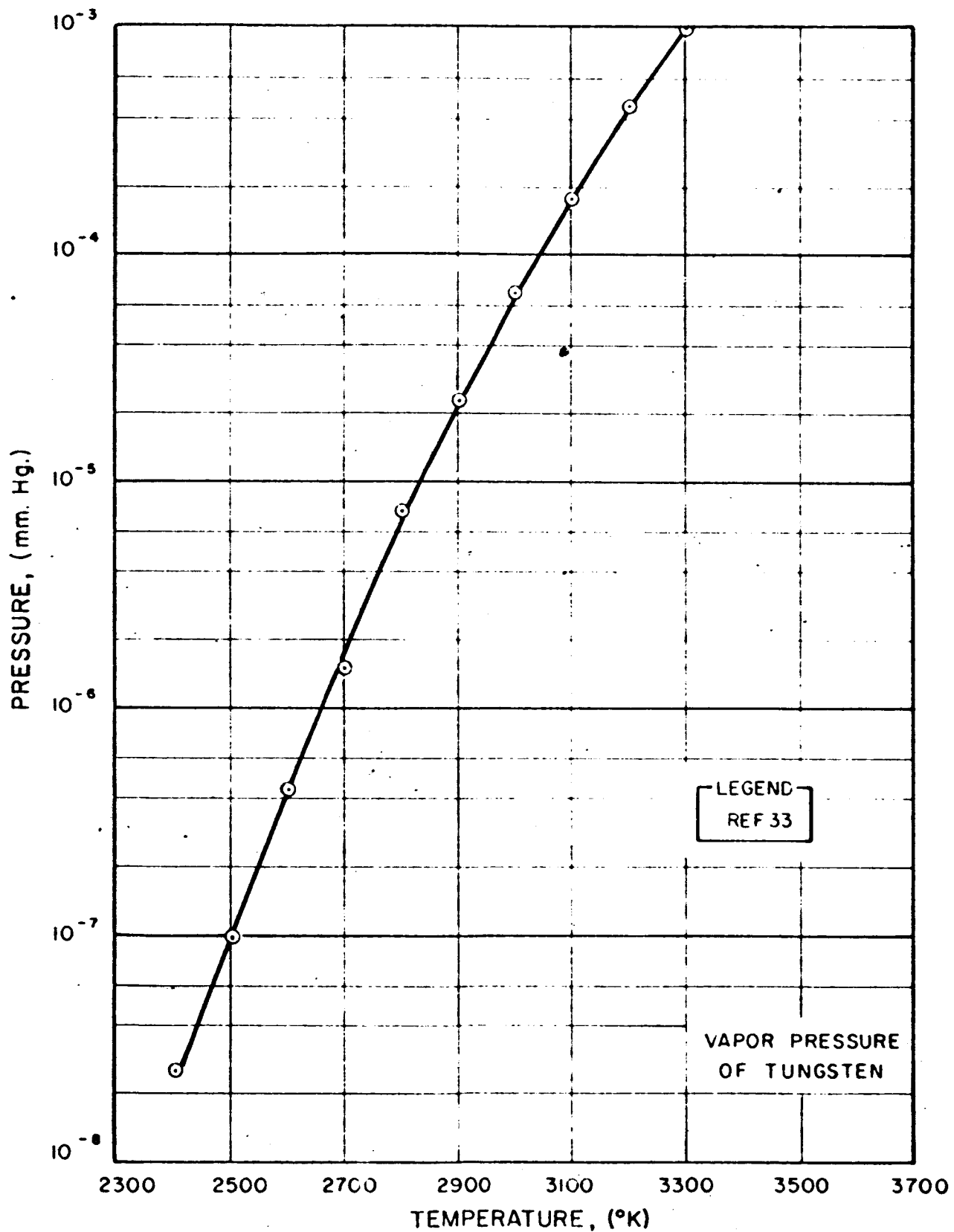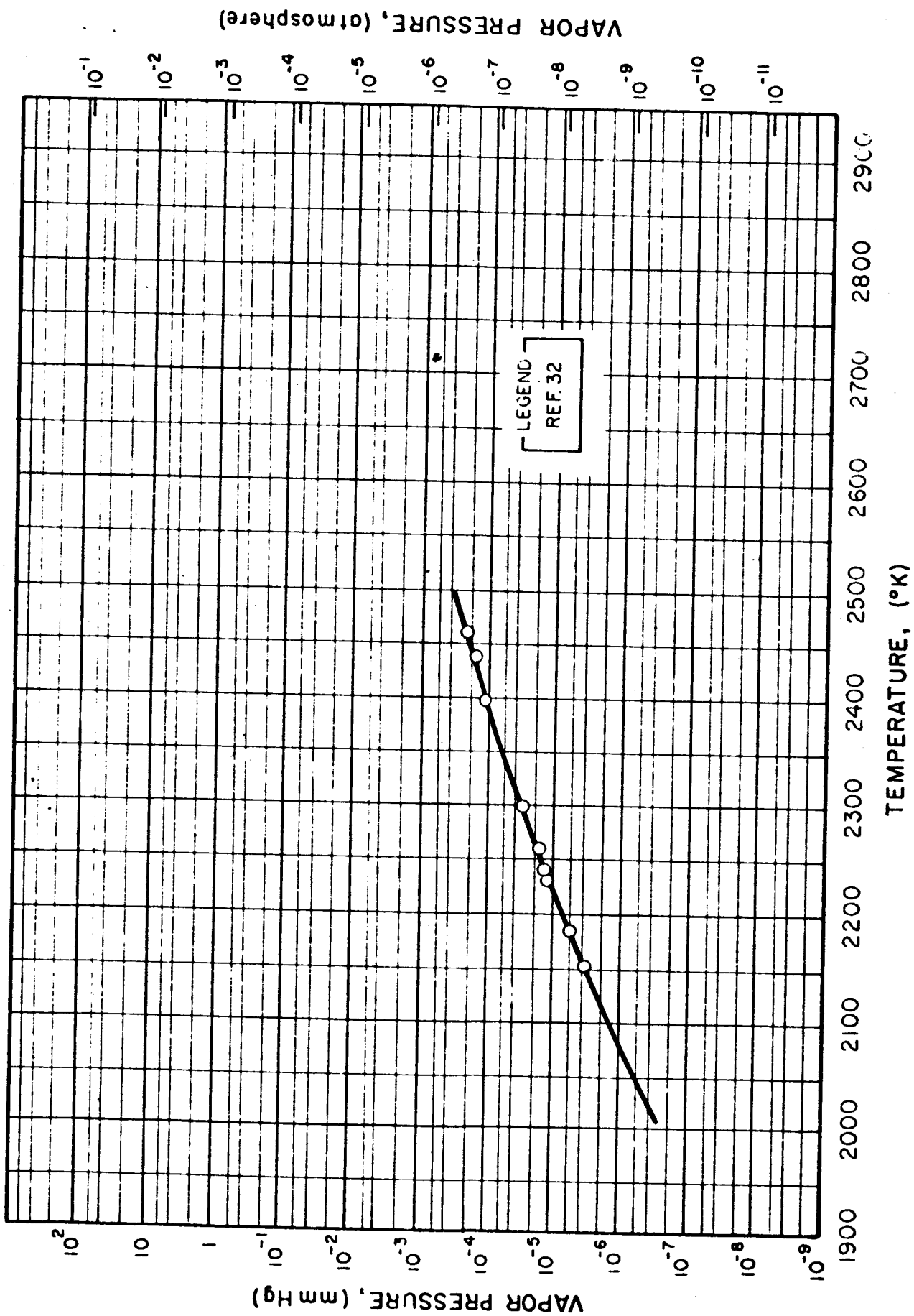
FIG. 2-42   VAPOR PRESSURE OF TUNGSTEN

FIG. 2-43   VAPOR PRESSURE – MOLYBDENUM
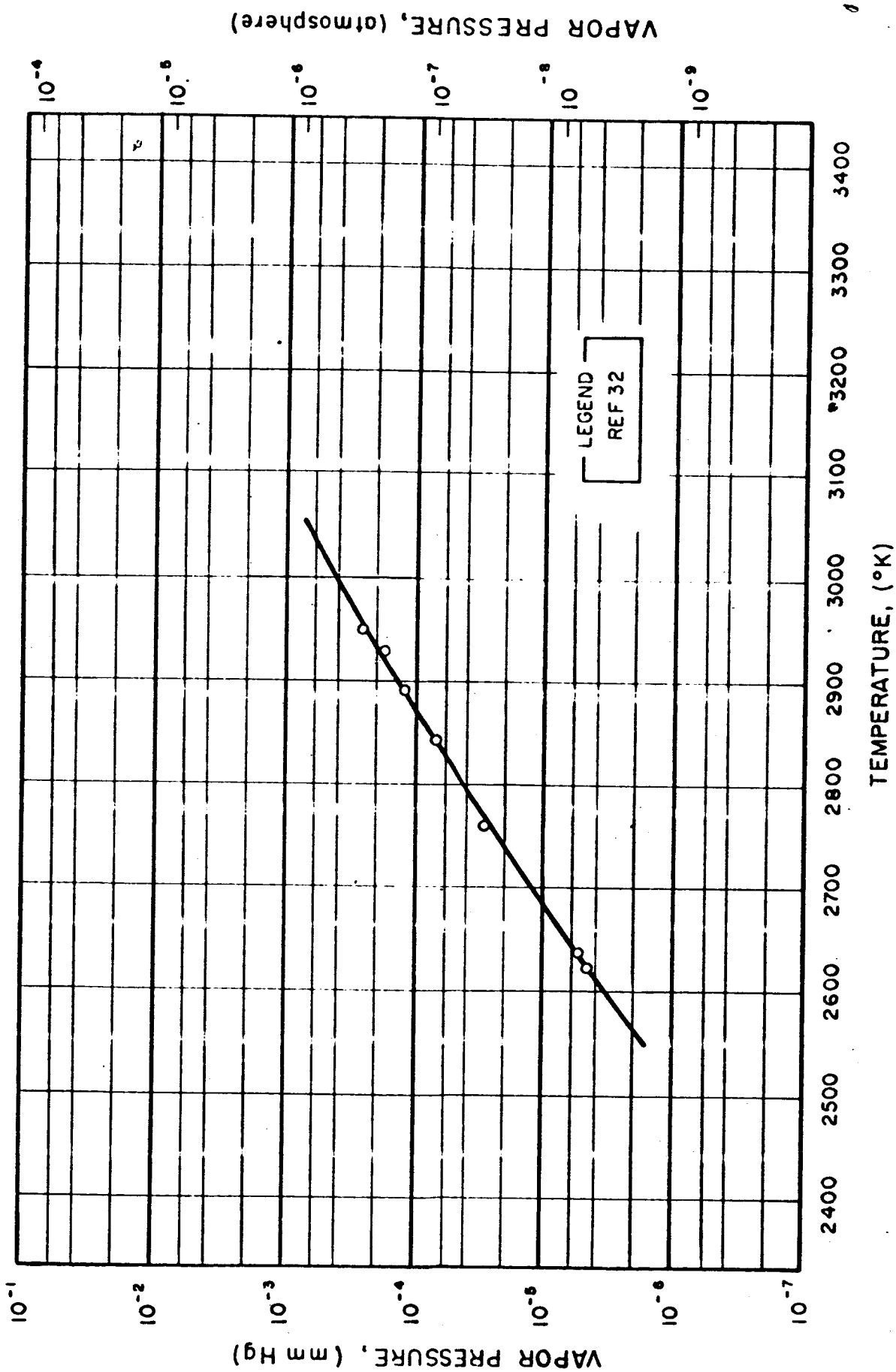
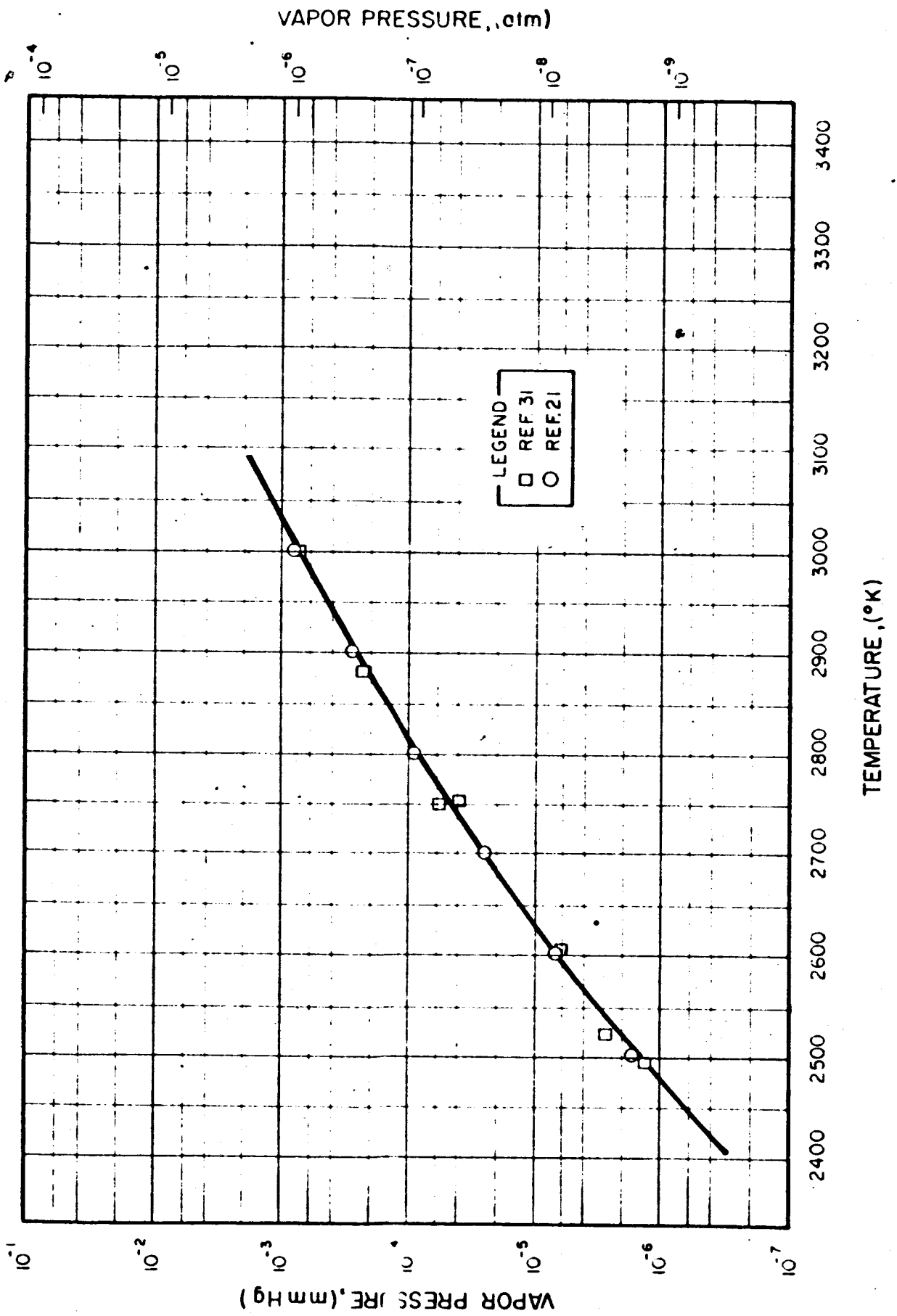4820

FIG. 2-44   VAPOR PRESSURE - TANTALUM
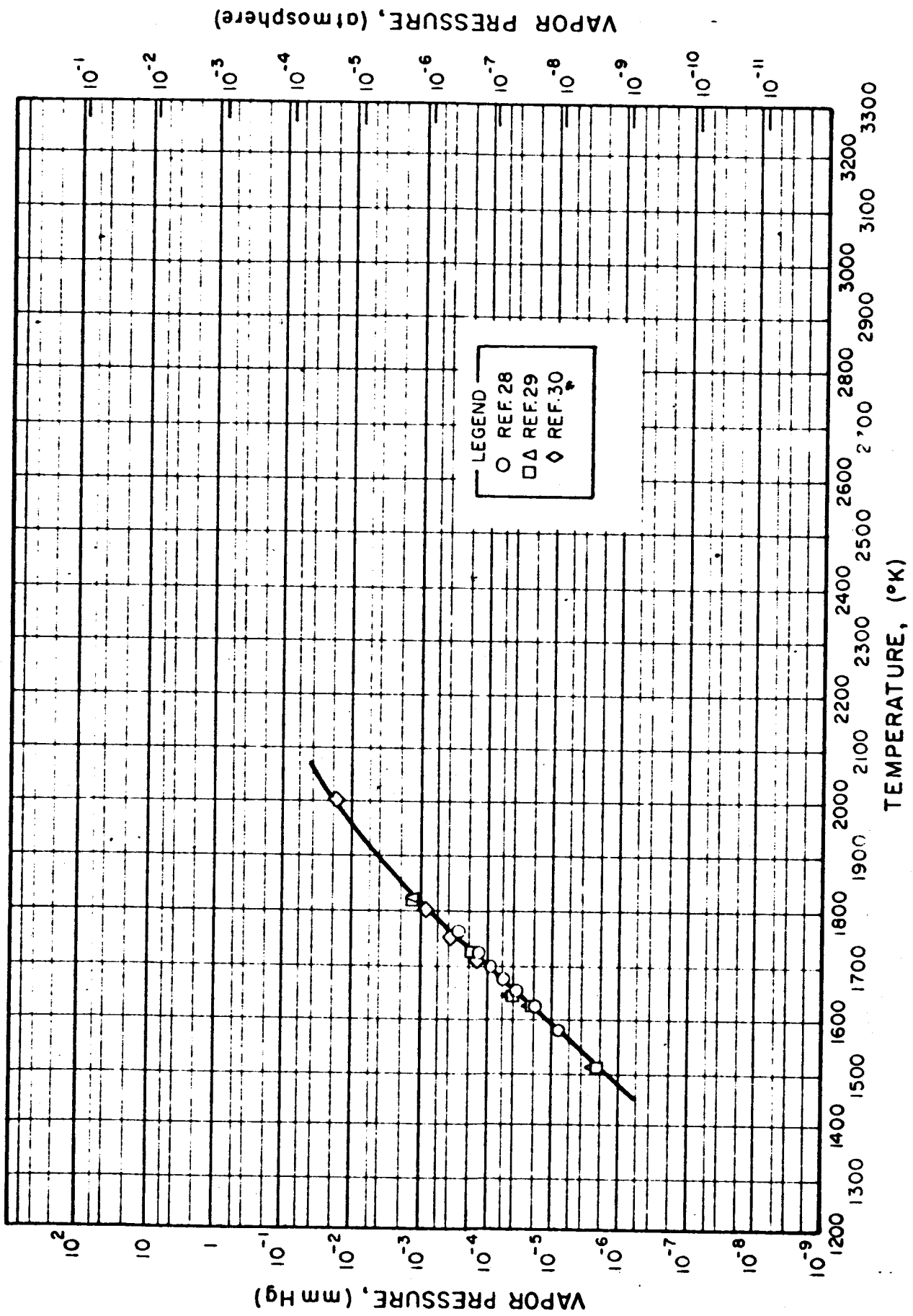
FIG. 2-45   VAPOR PRESSURE - RHENIUM

FIG. 2-46   VAPOR PRESSURE - TITANIUM

4813
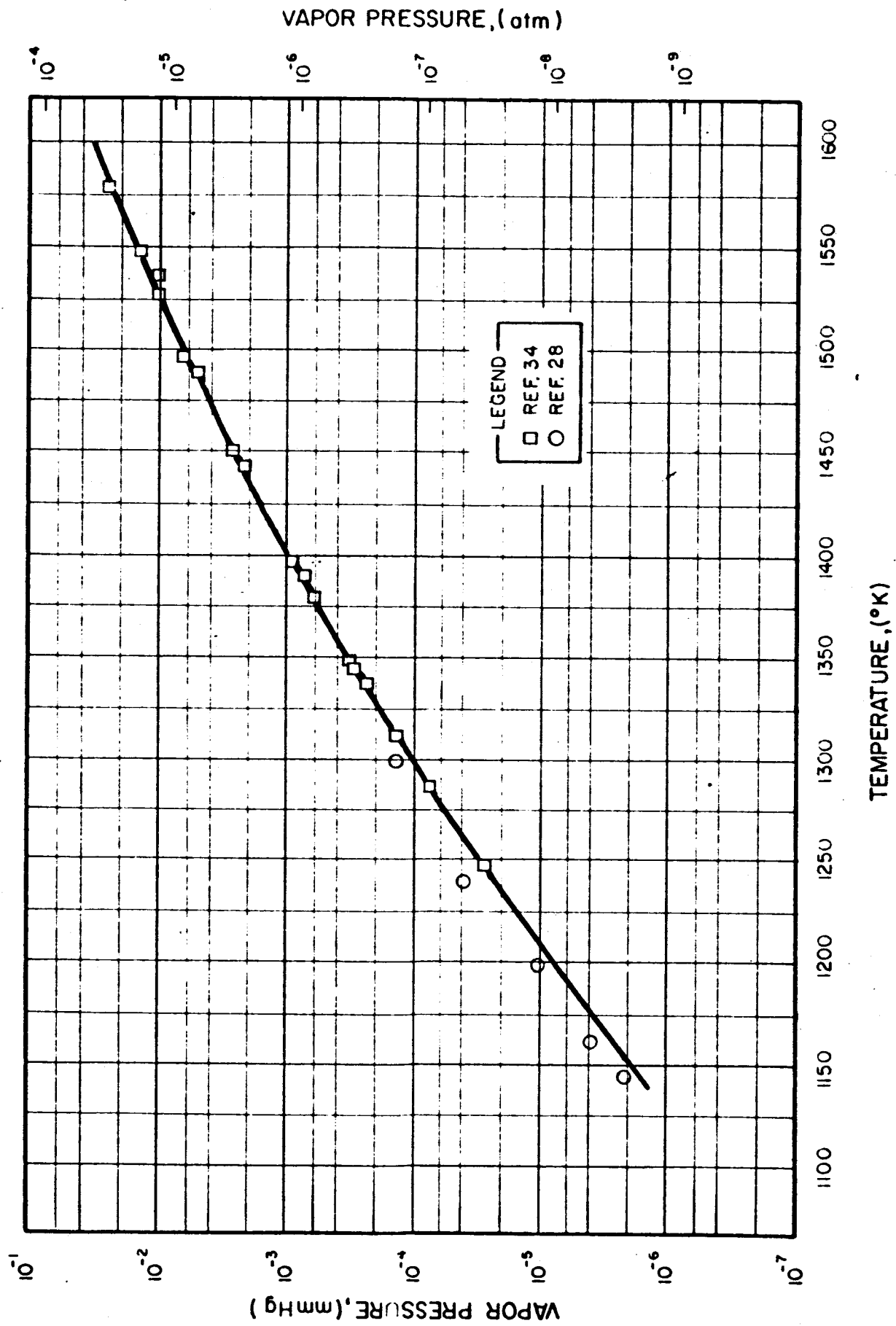
FIG. 2-47   VAPOR PRESSURE - COPPER
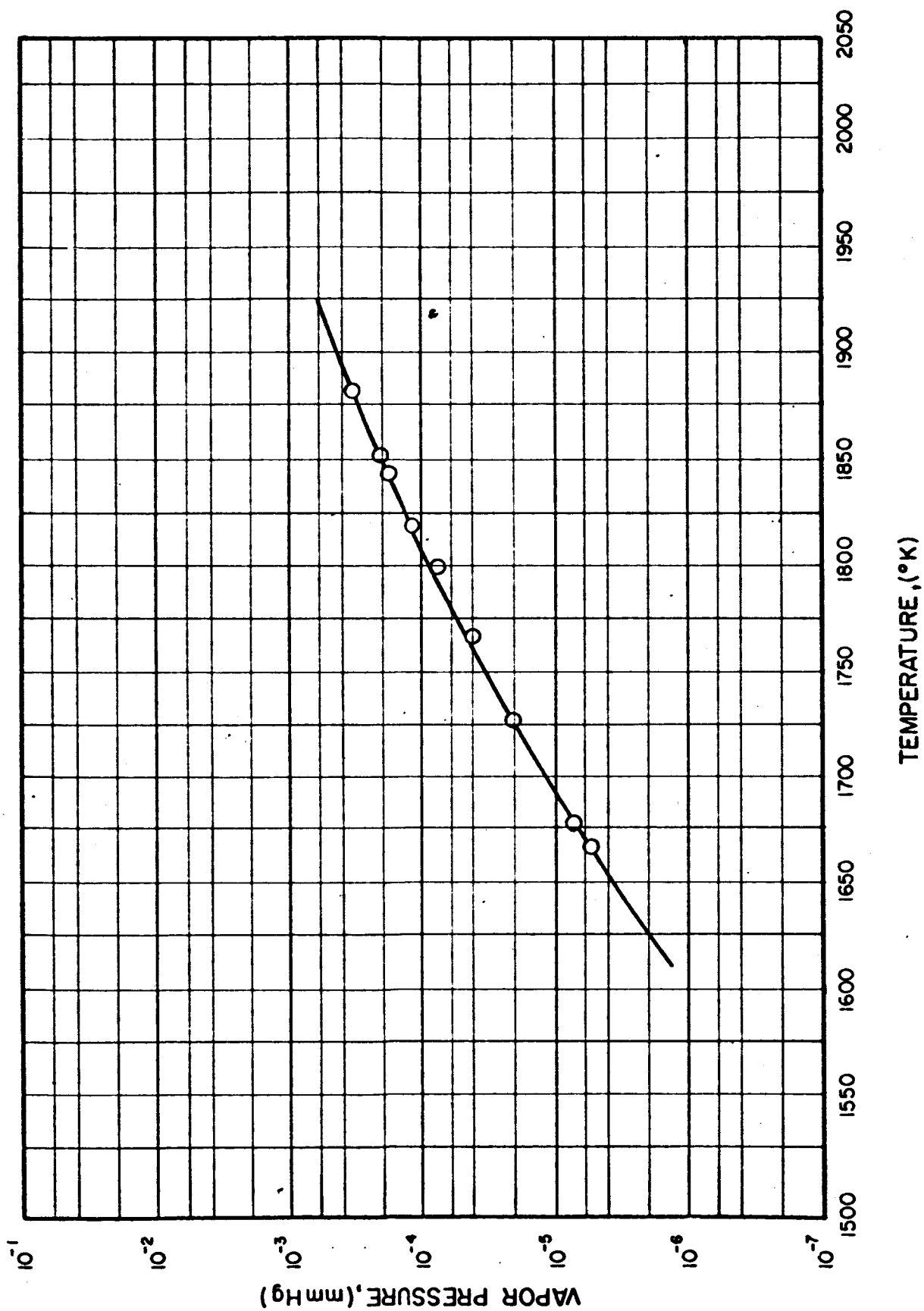
FIG. 2-48   VAPOR PRESSURE - VANDADIUM

VAPOR PRESSURE,(mmHg)

TEMPERATURE,(°K)
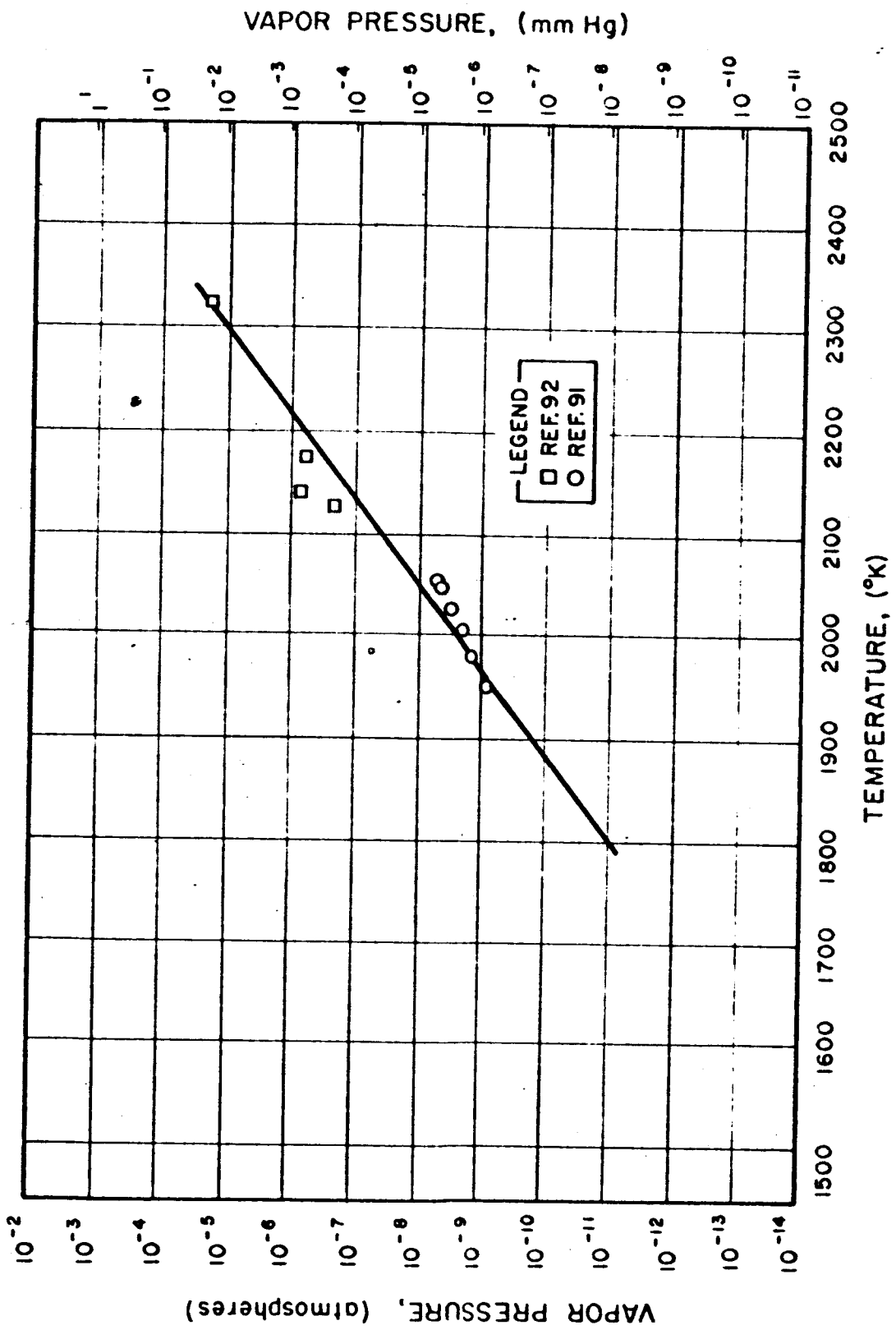
FIG. 2-49 VAPOR PRESSURE : ZIRCONIUM
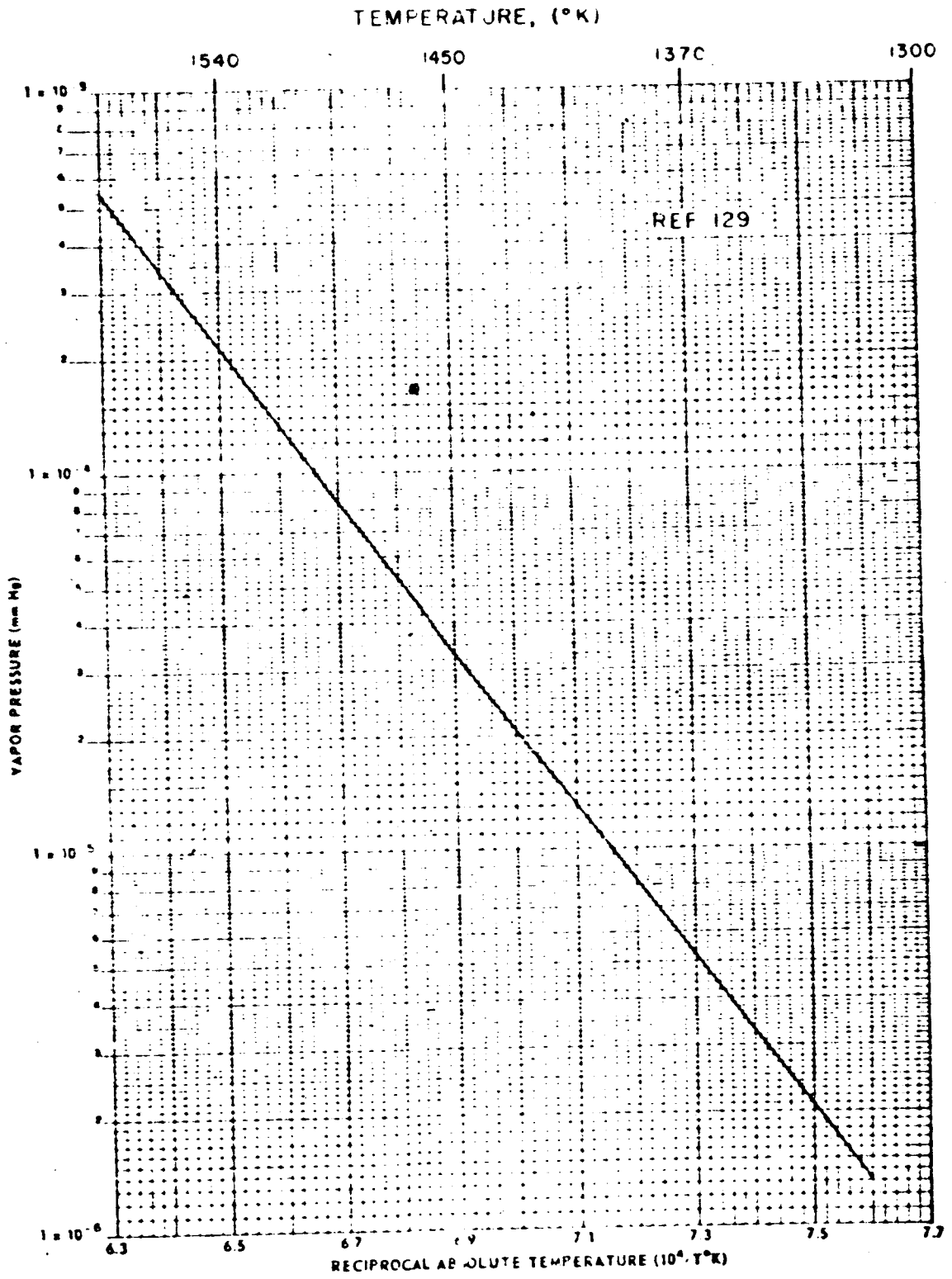
TEMPERATURE, (°K)

FIG. 2-50   VAPOR PRESSURE OF KOVAR

2210-Final

2-68

1564941
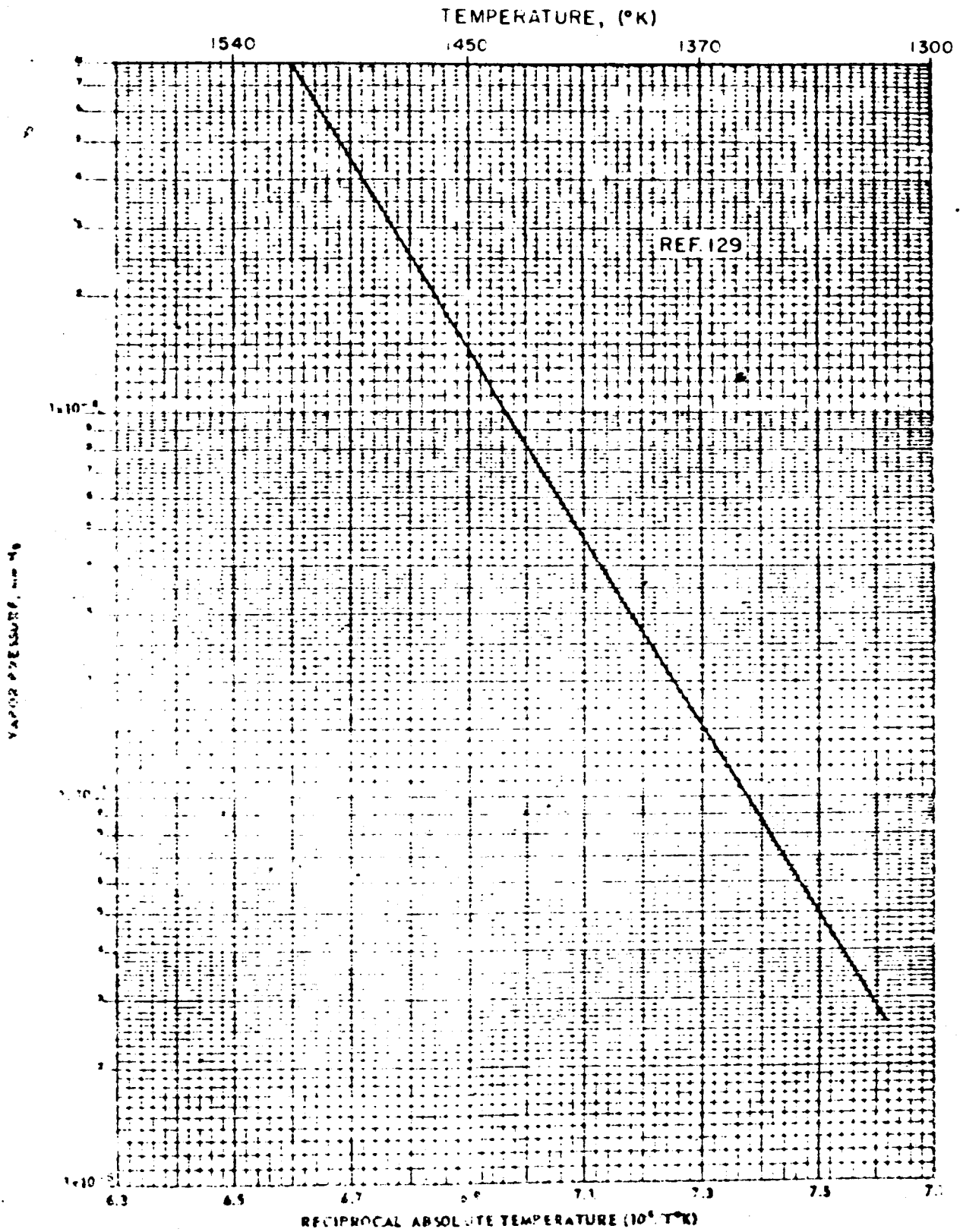
FIG. 2-51   VAPOR PRESSURE OF TYPE 304 STAINLESS STEEL

54944
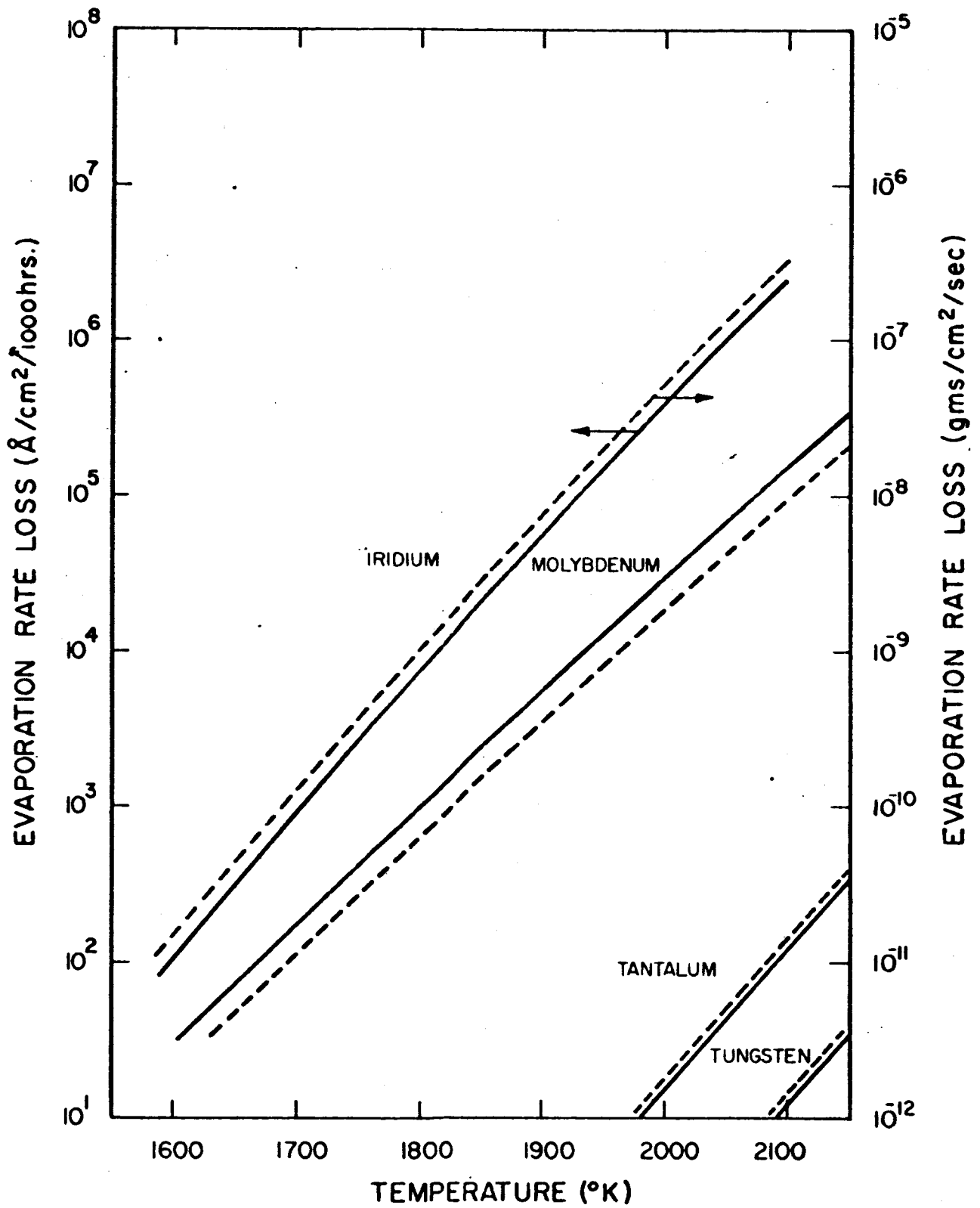
FIG. 2-52   EVAPORATION RATE LOSS FROM SELECTED EMITTER MATERIALS

2.2.6 Resistivity

The resistivity of materials as a function of temperature is a necessary consideration in the design of leads and envelopes. It is to be noted that some materials suffer a transition in the solid state that radically affect the resistive and mechanical properties of the material. Resistivity versus temperature data for a number of selected materials follow in the next few pages.

ELECTRIC RESISTIVITY, (ohm cm x 10⁶)

TEMPERATURE, (°K)

LEGEND

△ REF. 75	
◁ REF. 76	
◁ REF. 77	
△ REF. 78	
○ REF. 79	

MAGNETIC TRANSFER
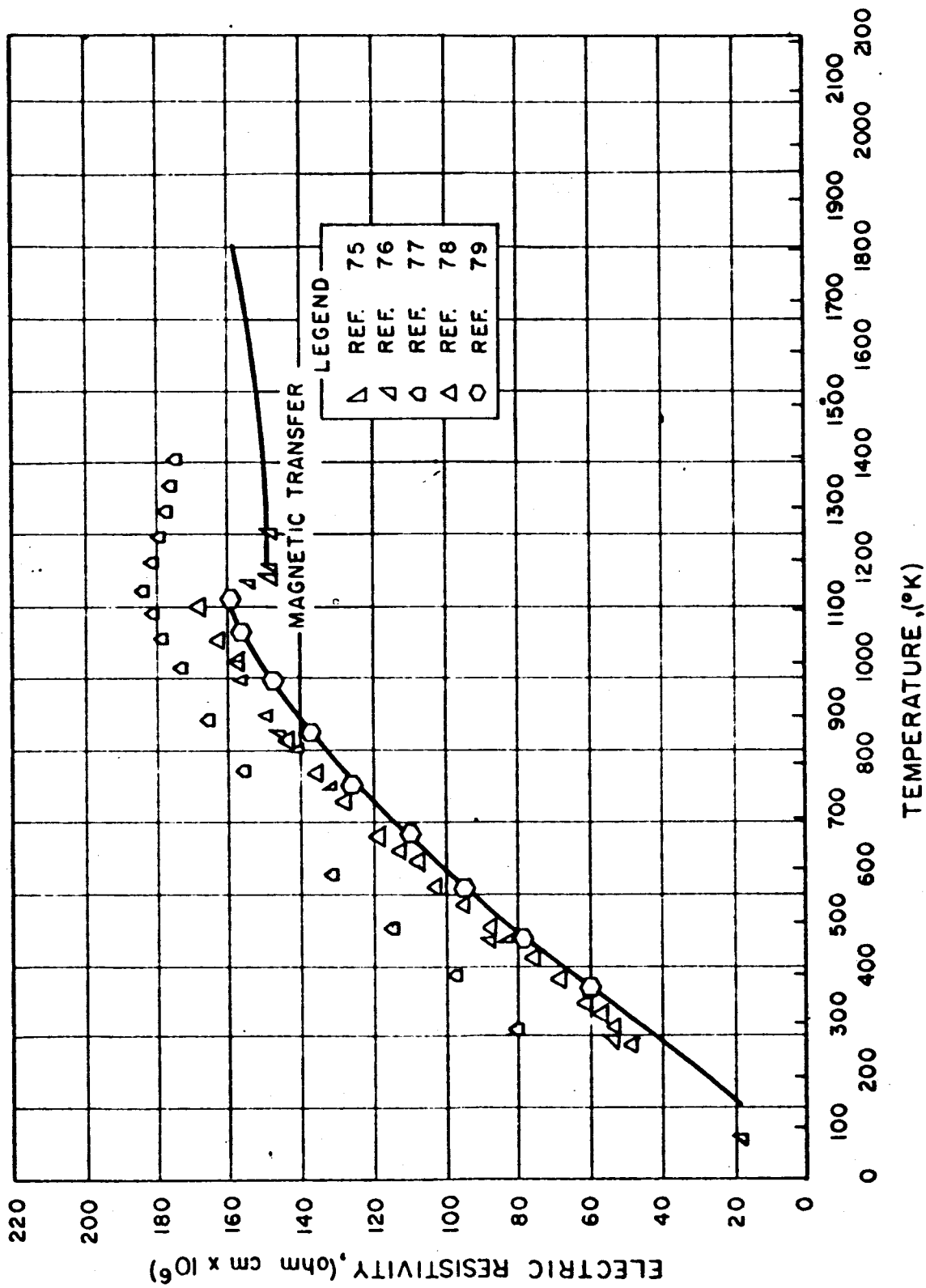
FIG. 2-53   ELECTRIC RESISTIVITY - TITANIUM

7364814

TEMPERATURE, (°K)

ELECTRIC RESISTIVITY, (ohm cm x 10⁶)

LEGEND
☐ REF 42
○ REF 80
△ REF 81
◇ REF 82
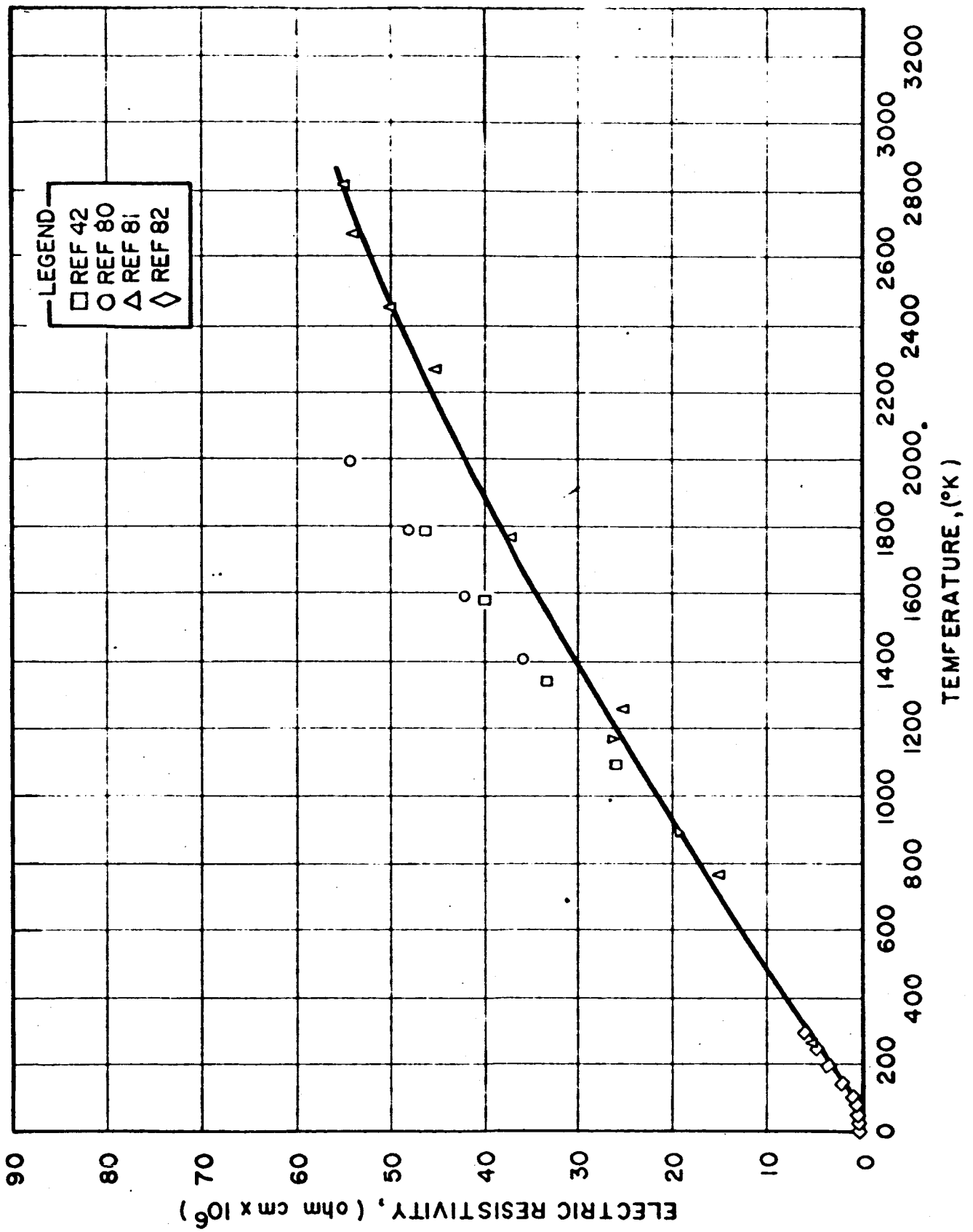
FIG. 2-54   ELECTRIC RESISTIVITY MOLYBDENUM
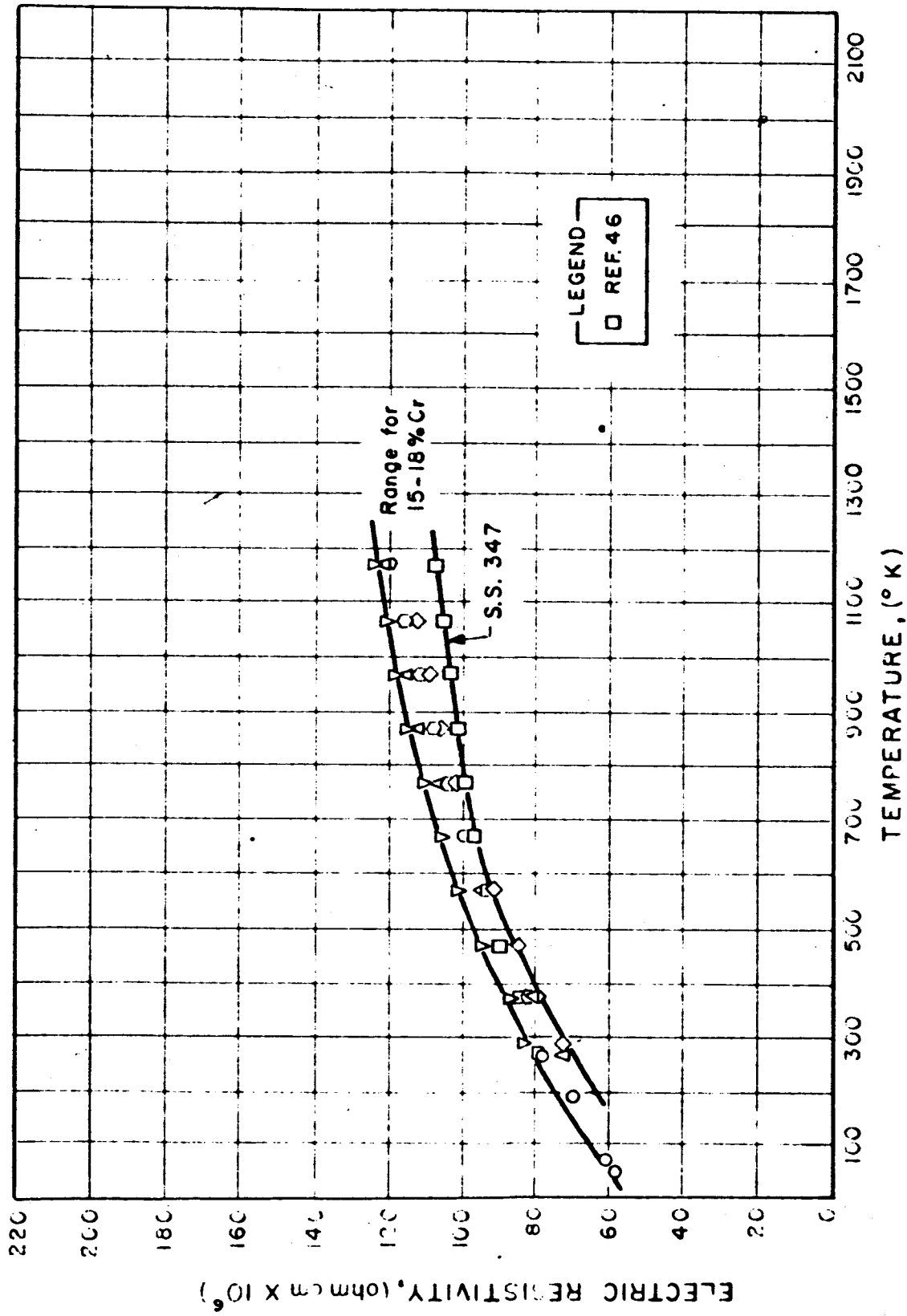
FIG. 2-55   ELECTRIC RESISTIVITY - IRON + CHROMIUM + NICKEL + X
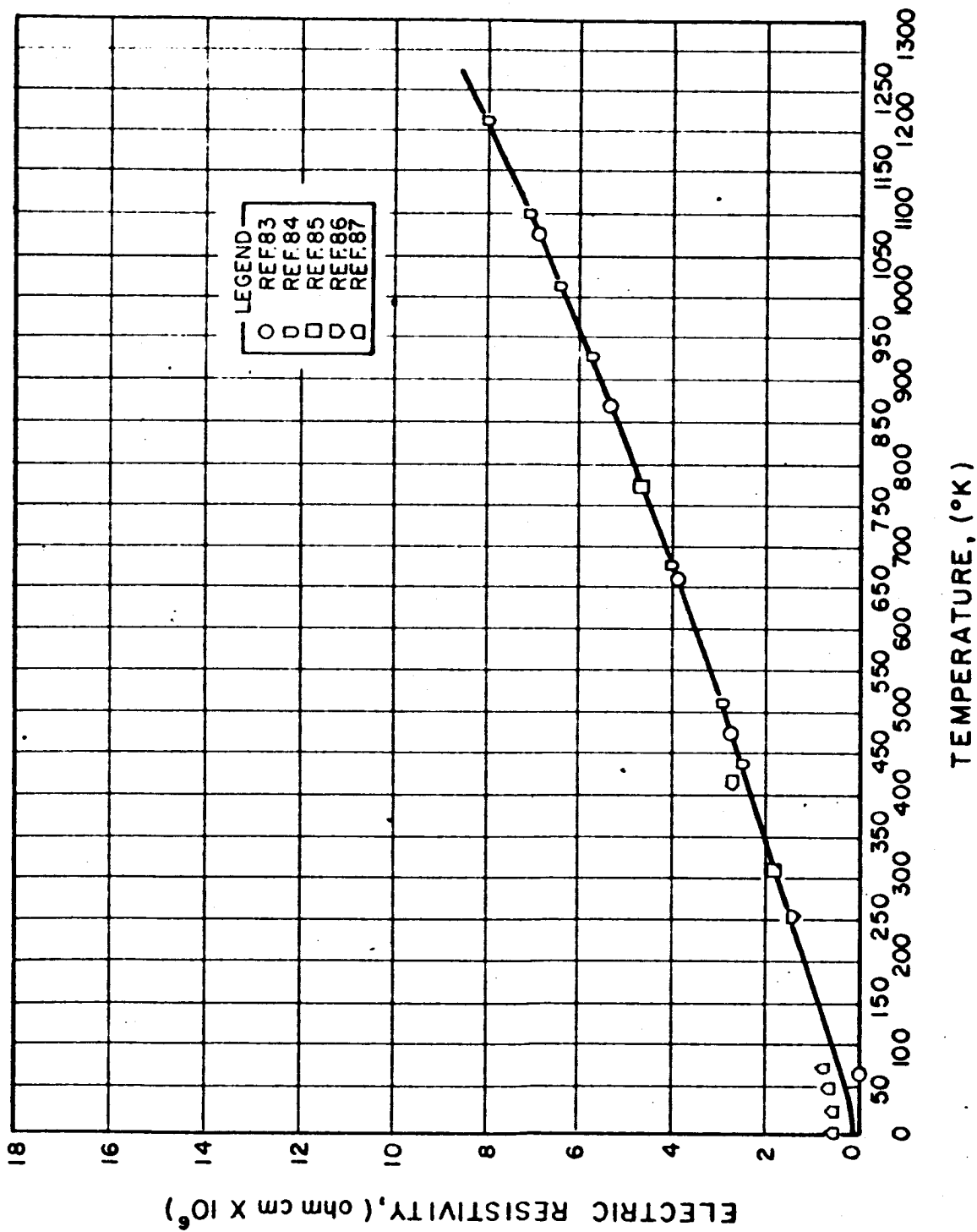
FIG. 2-56   ELECTRIC RESISTIVITY
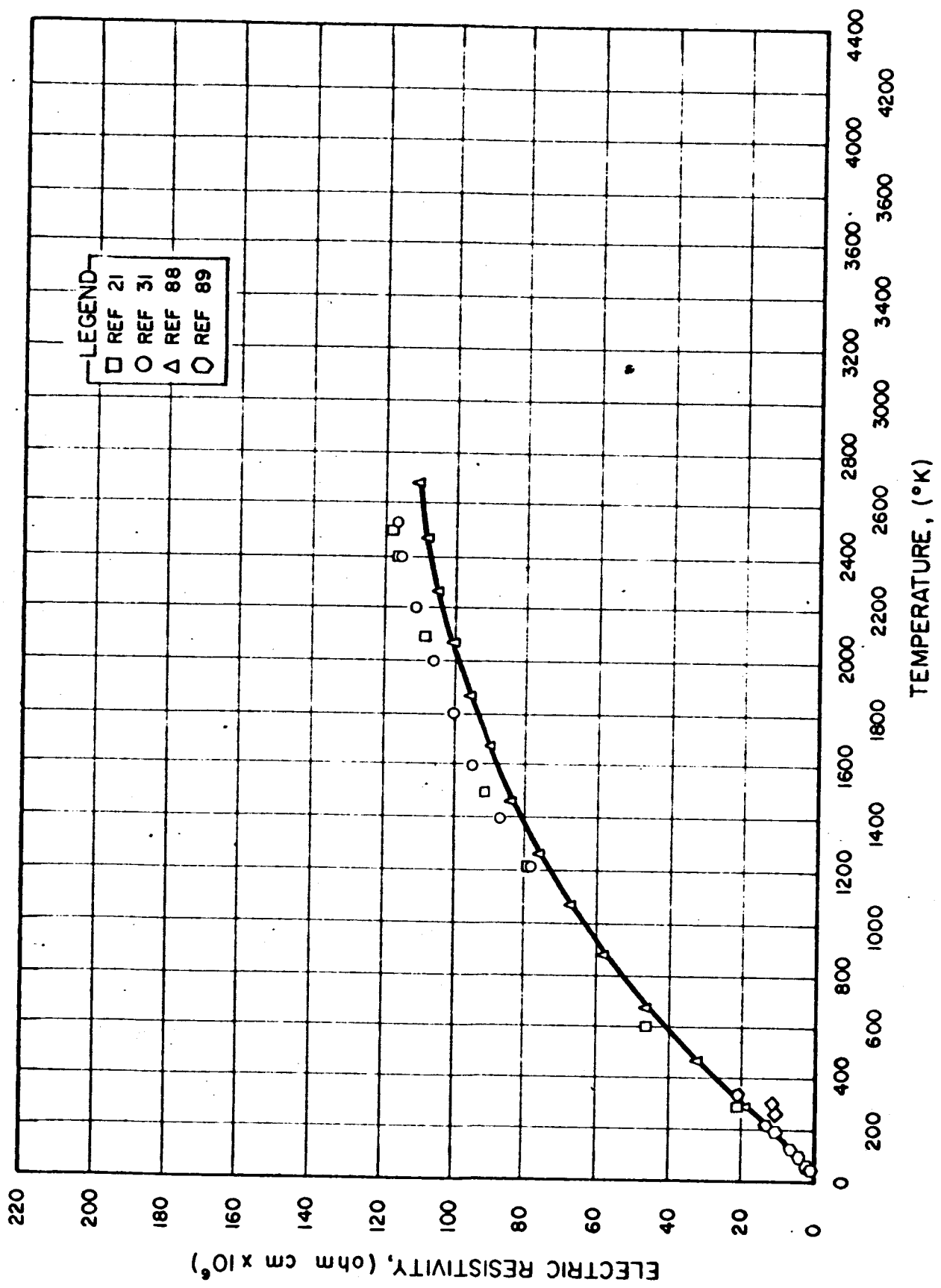
FIG. 2-57   ELECTRIC RESISTIVITY - RHENIUM
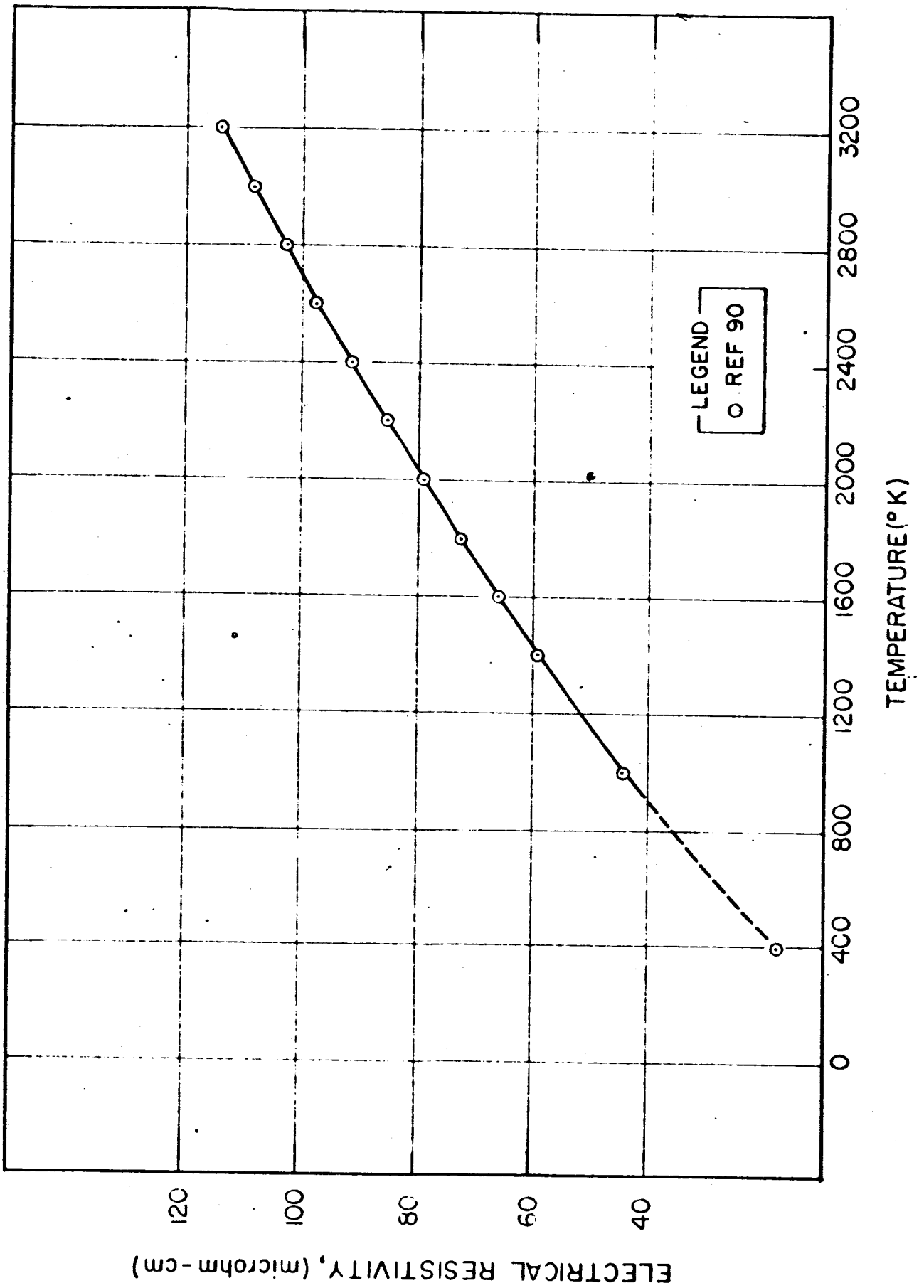
FIG. 2-58   ELECTRICAL RESISTIVITY OF TANTALUM

824

ELECTRIC RESISTIVITY - NICKEL
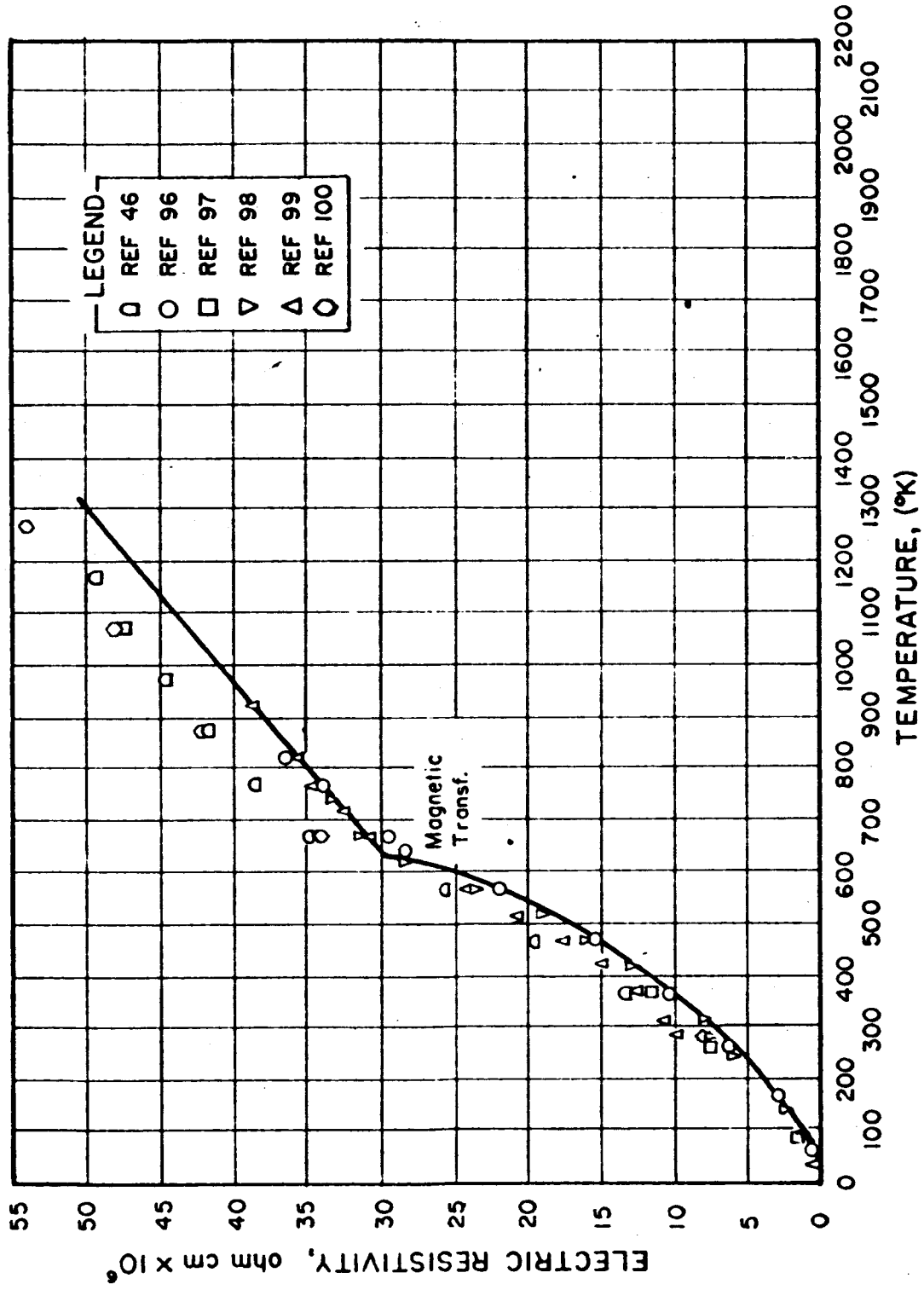
FIG. 2-59   ELECTRIC RESISTIVITY - NICKEL
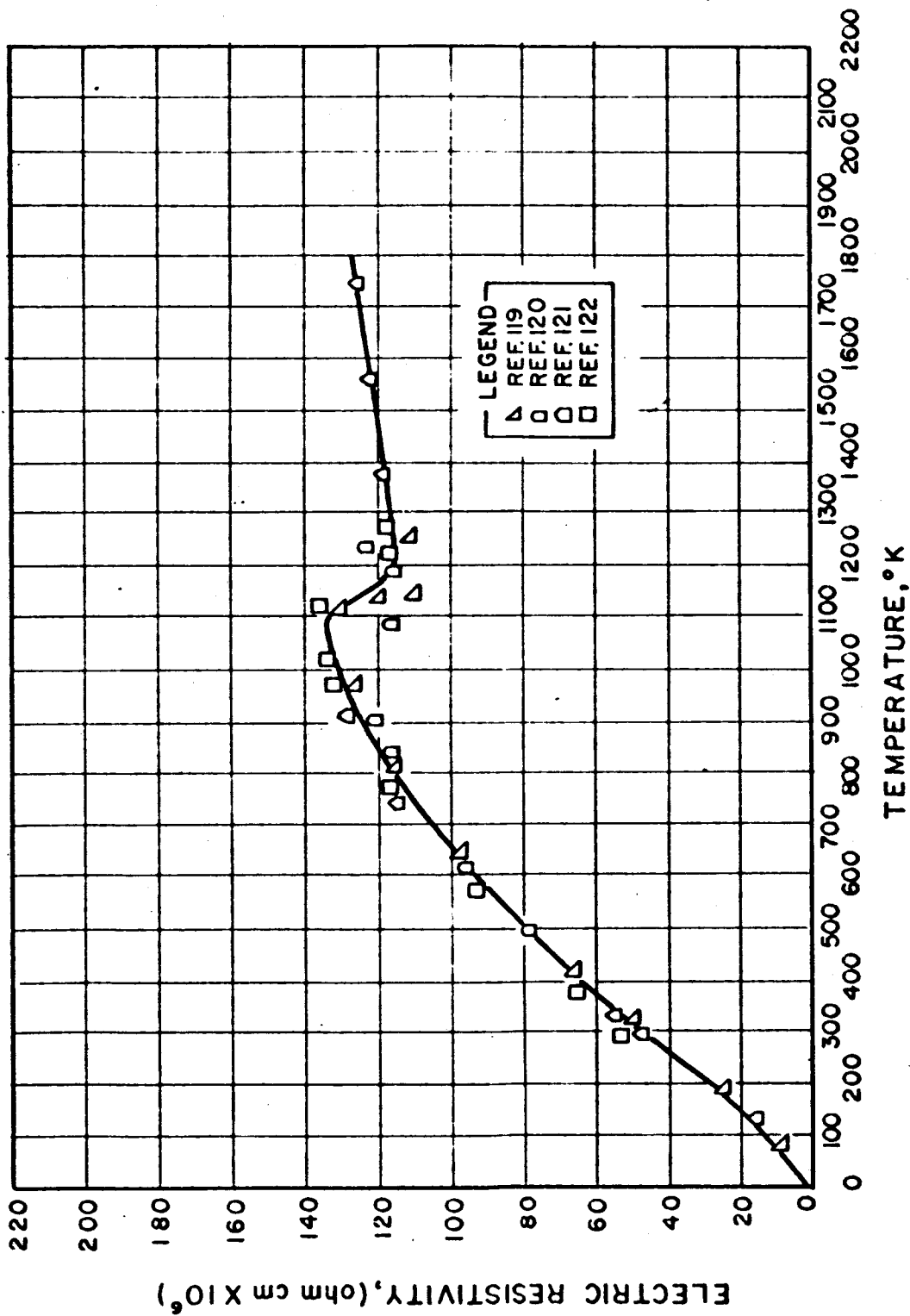
FIG. 2-60   ELECTRIC RESISTIVITY - ZIRCONIUM
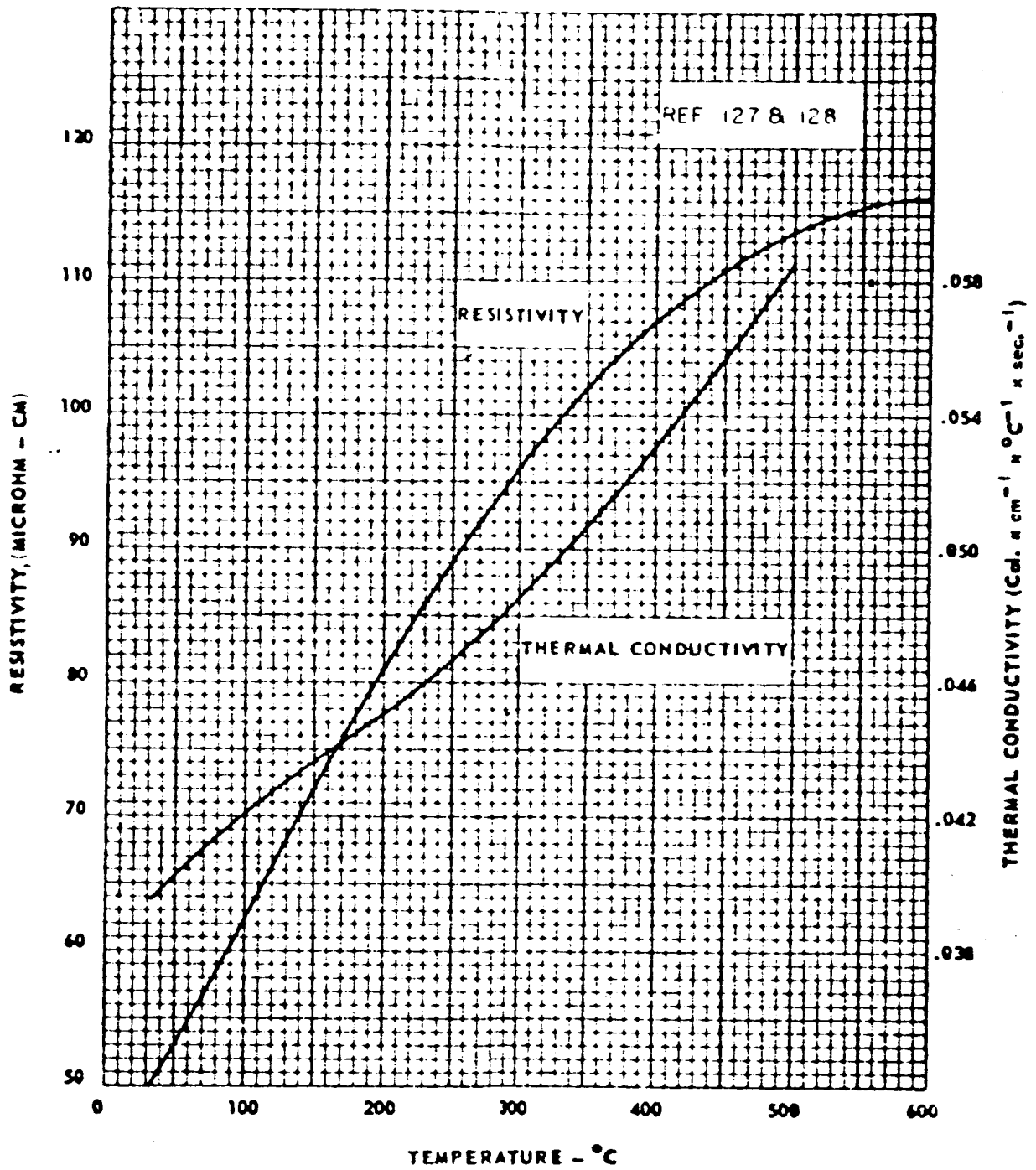
FIG. 2-61   ELECTRICAL RESISTIVITY AND THERMAL CONDUCTIVITY OF KOVAR

4940
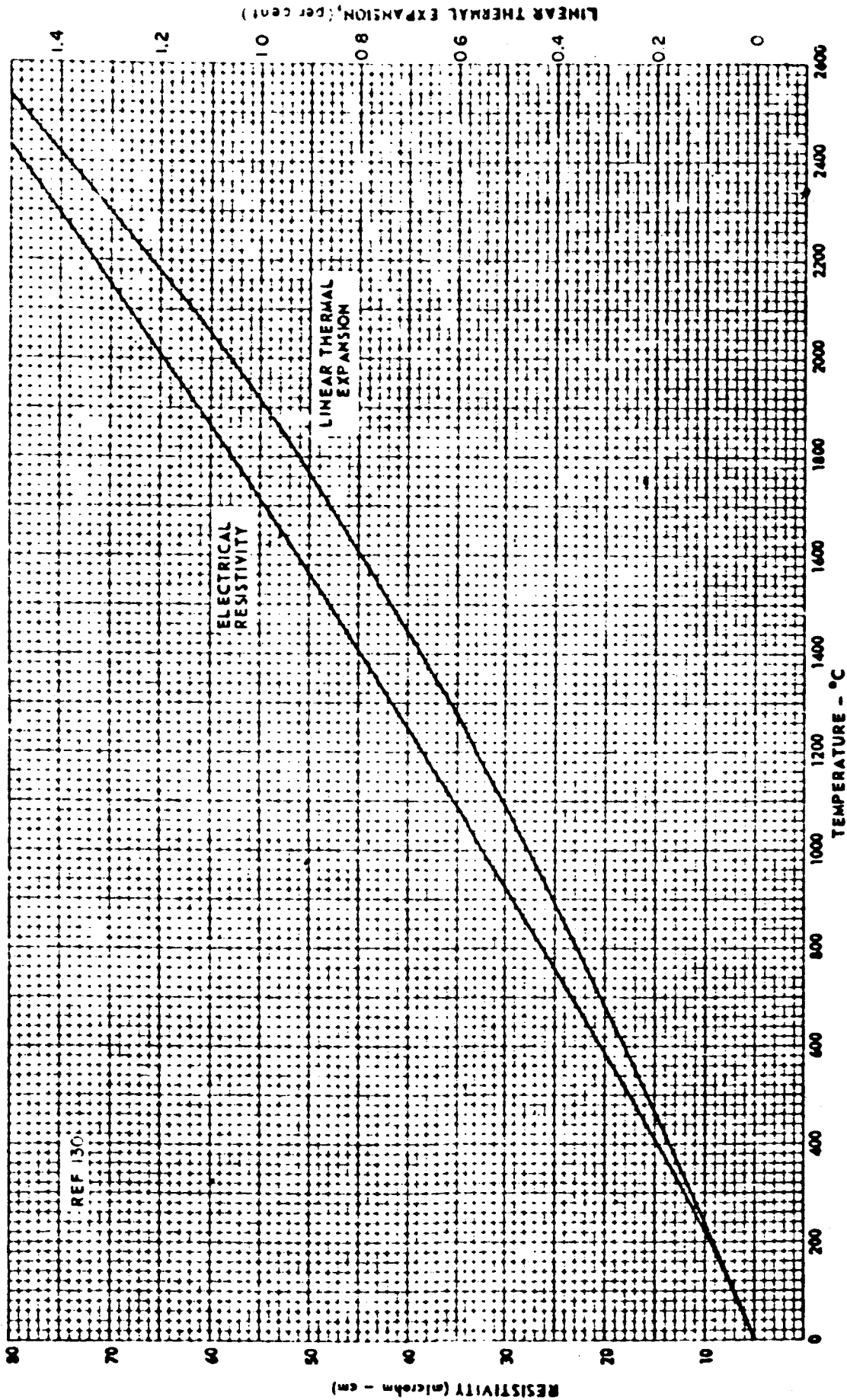
FIG. 2-62   ELECTRICAL RESISTIVITY AND LINEAR THERMAL EXPANSION OF TUNGSTEN
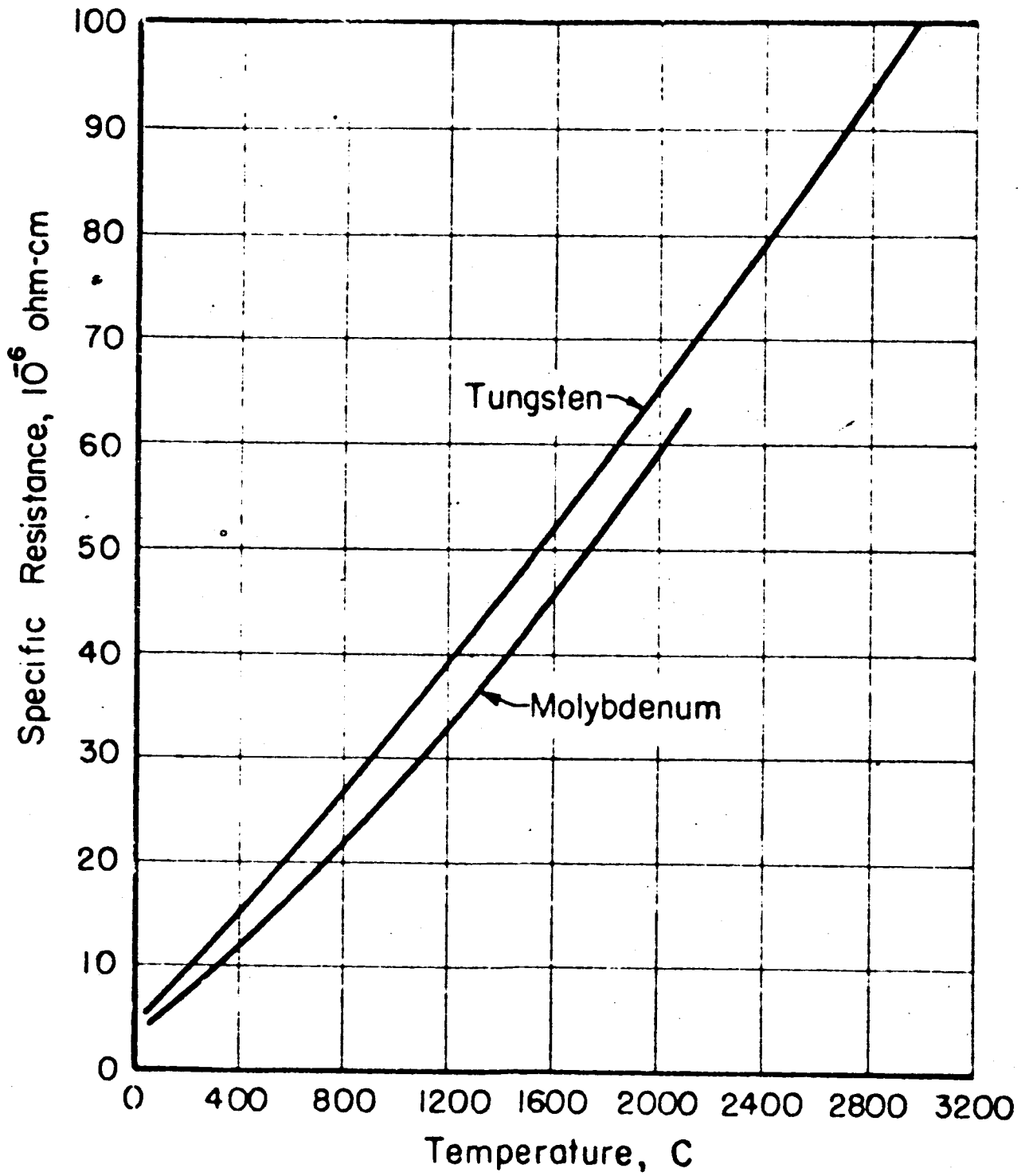
FIG. 2-63   SPECIFIC RESISTANCE OF TUNGSTEN AND MOLYBDENUM

938

2.2.7 Thermal Conductivity and Specific Heat

Thermal conductivity and specific heat are essential design data for heat transfer calculations involving the entire converter structure. This would include seals, reservoirs, envelopes, collectors, and leads. The heat transfer calculations usually require in addition resistivity data, for I^2R losses, and emissivity data for radiation losses, as previously mentioned.

The subject of heat transfer as applied to converter technology is given treatment in a separate chapter.

Representative thermal conductivity and specific heat data follow in the next few pages.
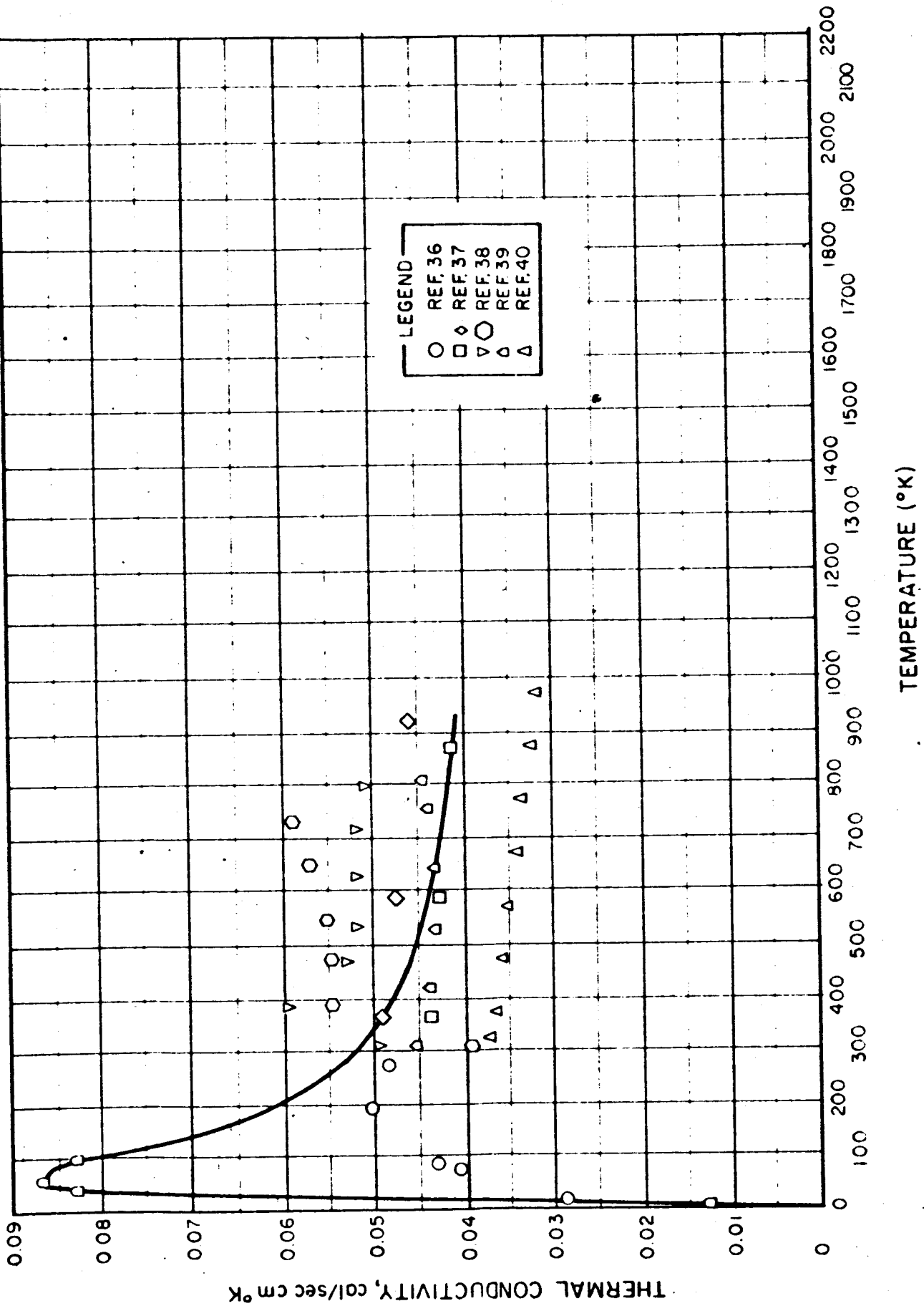
FIG. 2-64   THERMAL CONDUCTIVITY - TITANIUM
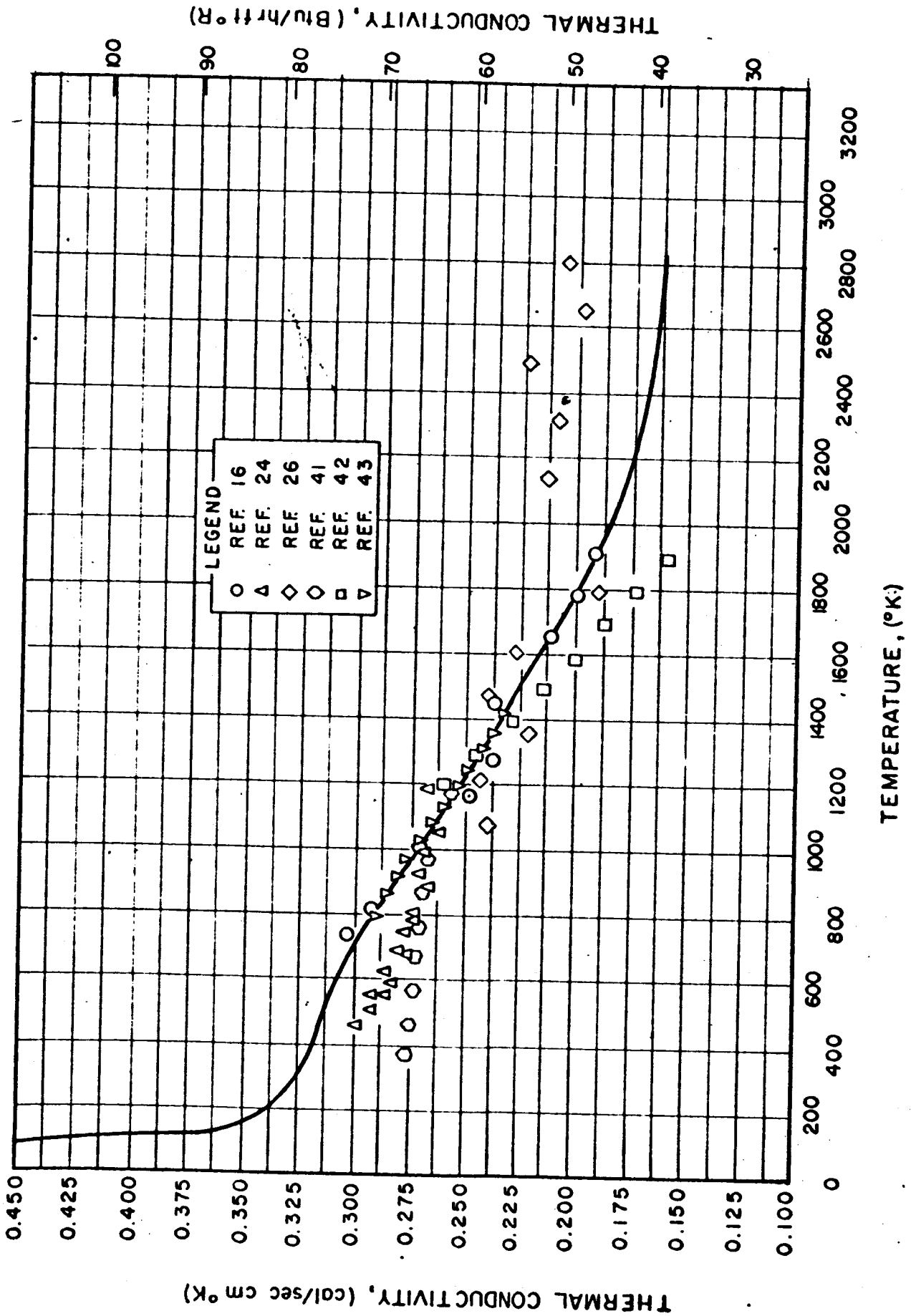
FIG. 2-65   THERMAL CONDUCTIVITY - MOLYBDENUM
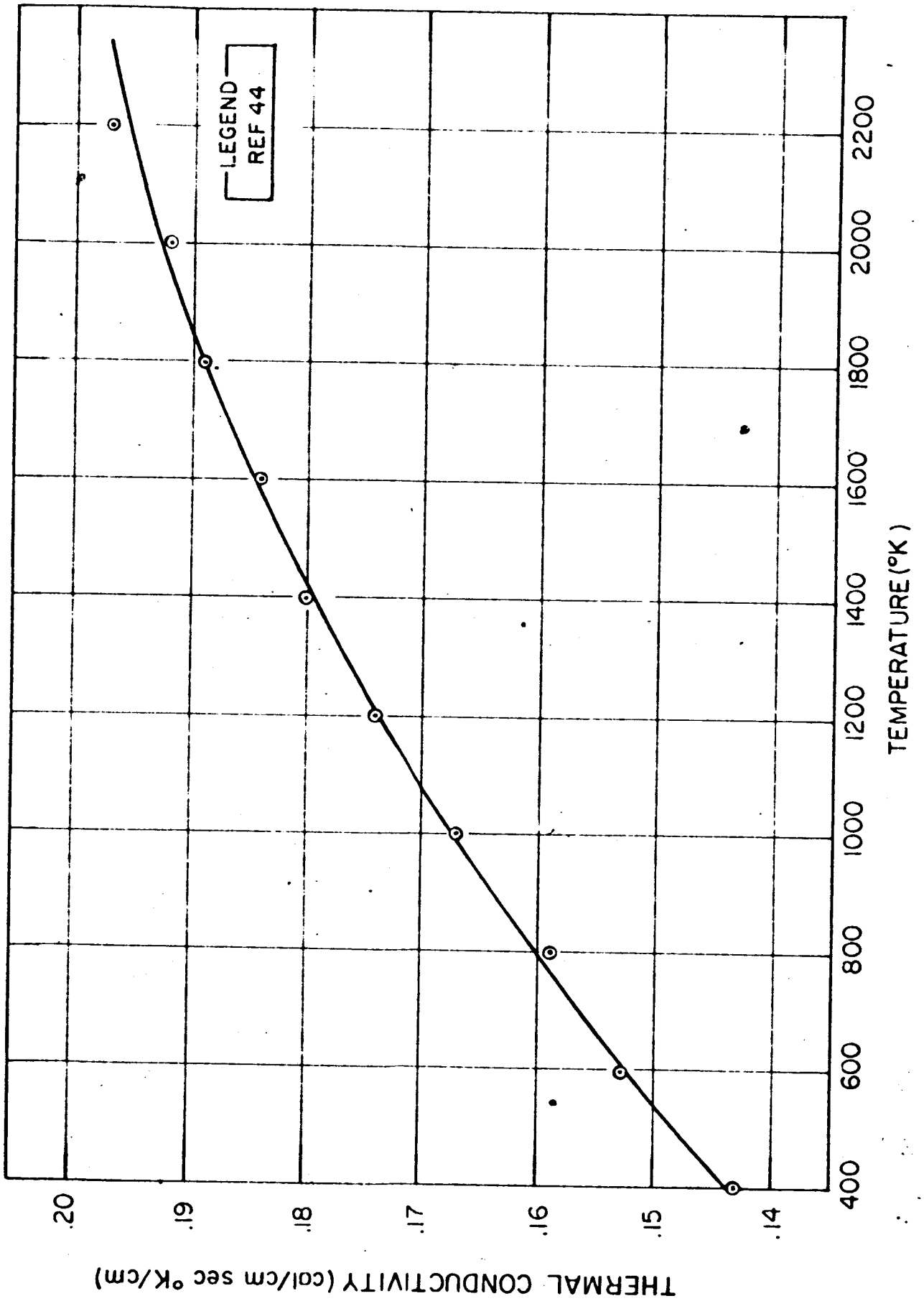
FIG. 2-66   THERMAL CONDUCTIVITY OF TANTALUM
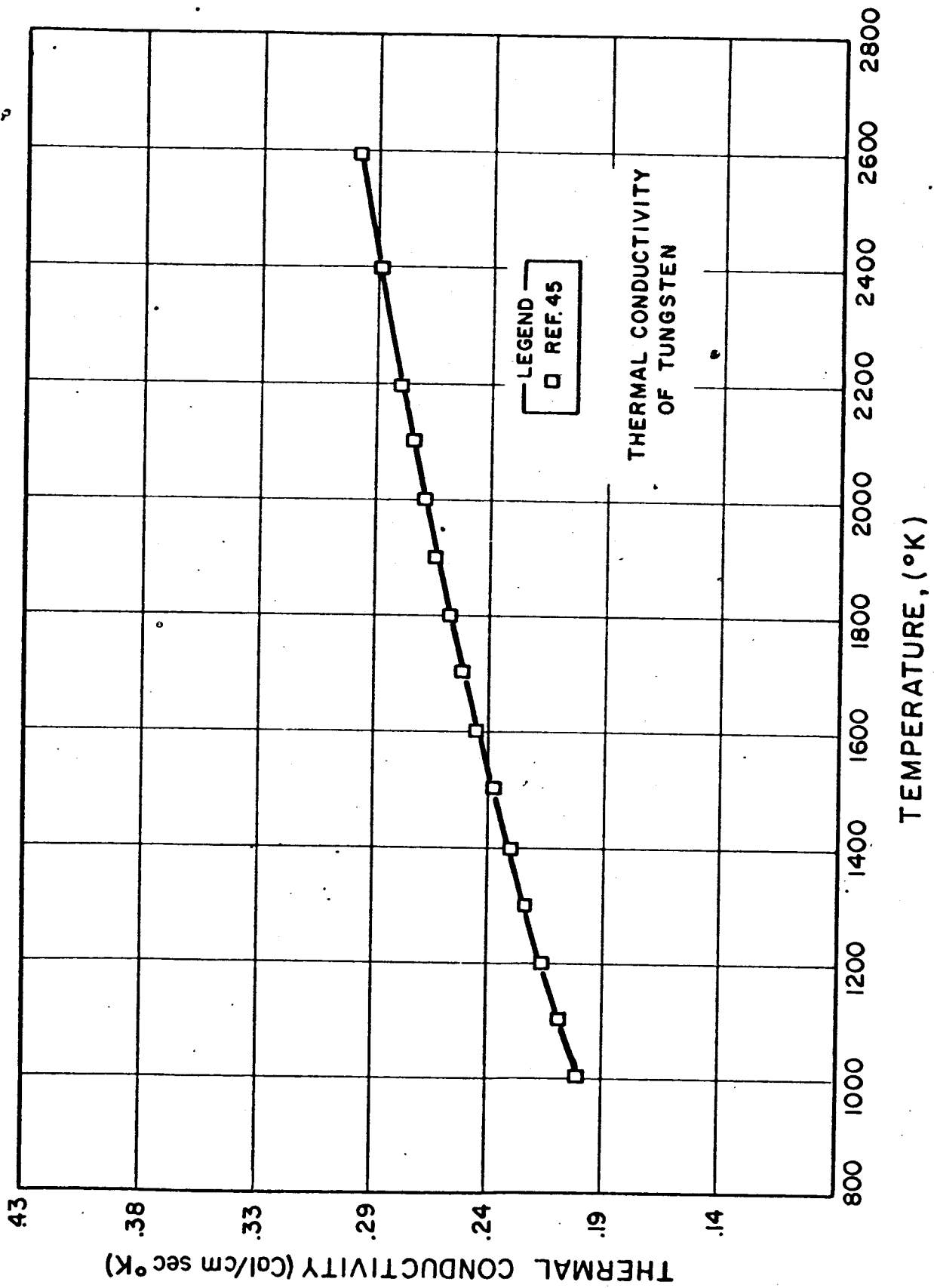
FIG. 2-67   THERMAL CONDUCTIVITY OF TUNGSTEN

4865
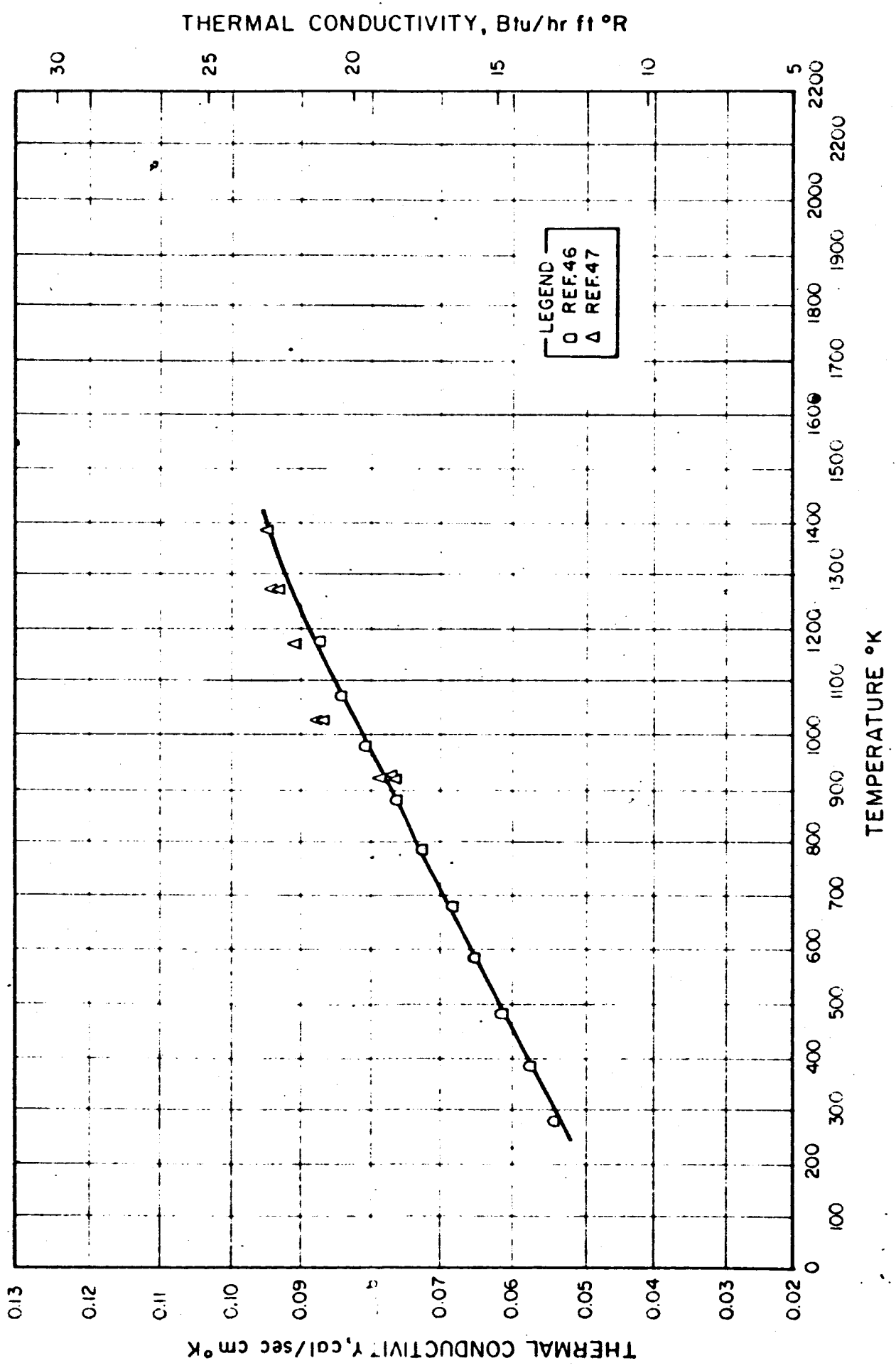
FIG. 2-68   THERMAL CONDUCTIVITY - IRON + CHROMIUM (446 STAINLESS STEEL)
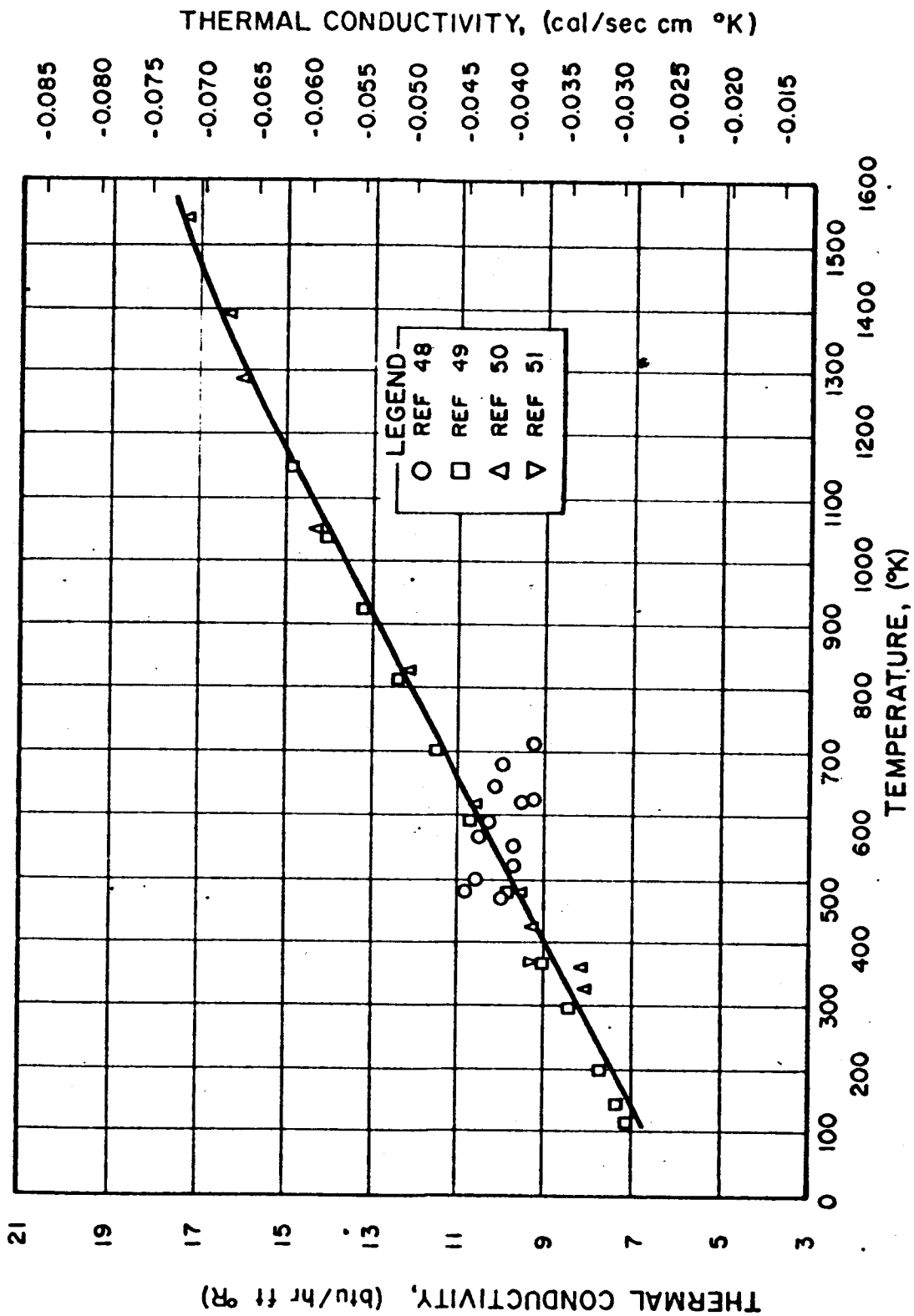
FIG. 2-69   THERMAL CONDUCTIVITY - IRON + CHROMIUM + NICKEL + X (AISI 347 STAINLESS STEEL)
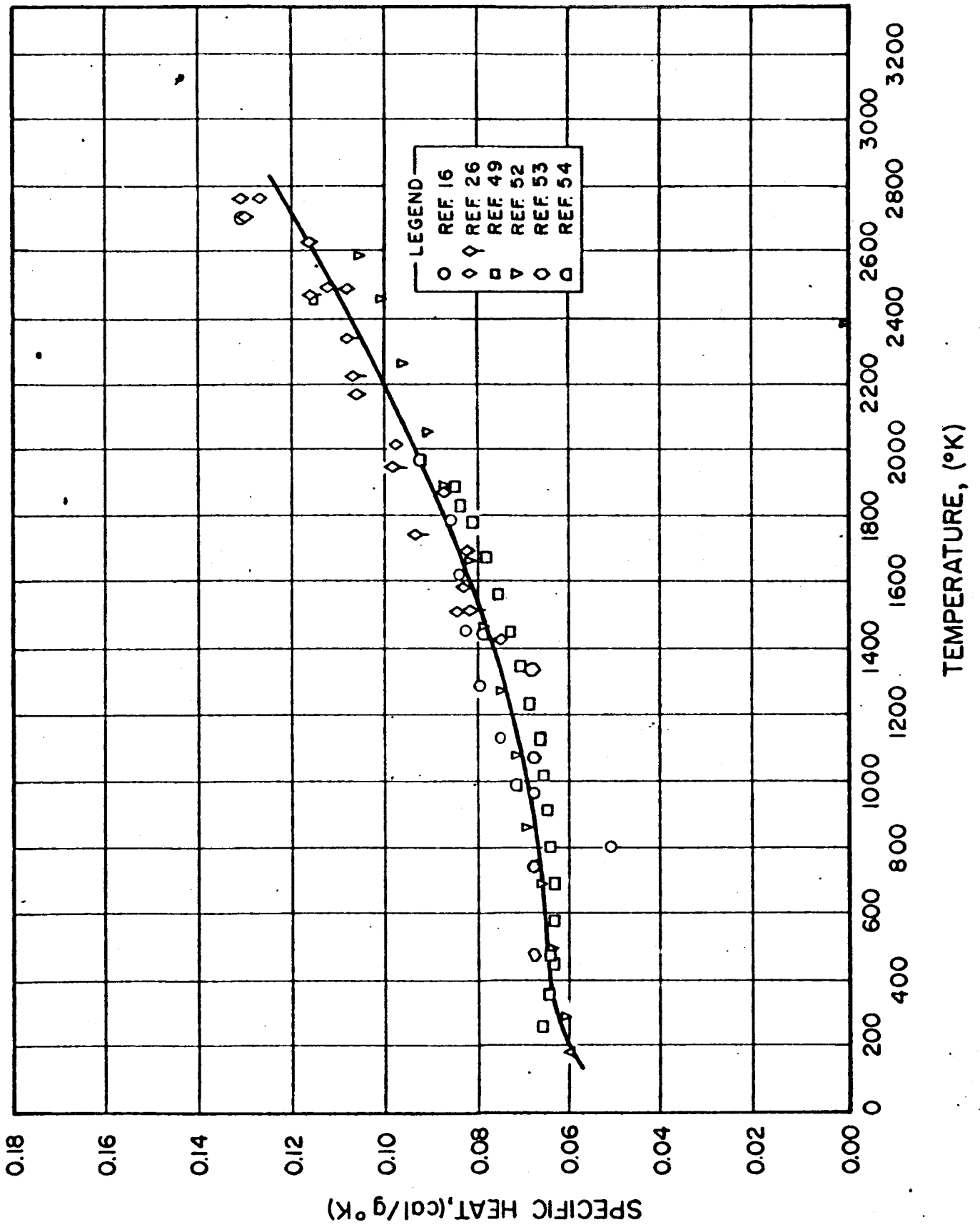
FIG. 2-70   SPECIFIC HEAT - MOLYBDENUM

4817
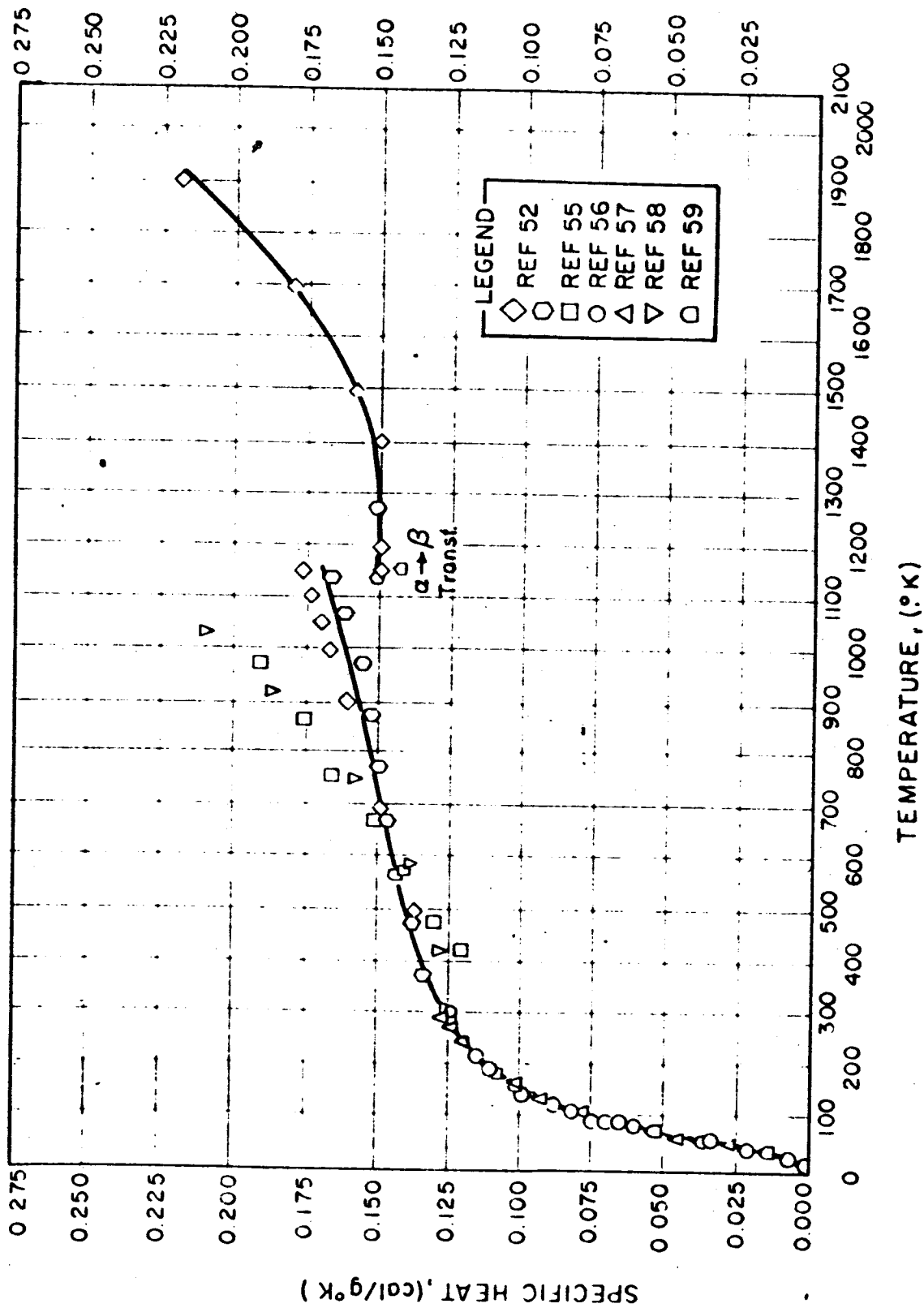
FIG. 2-71   SPECIFIC HEAT - TITANIUM
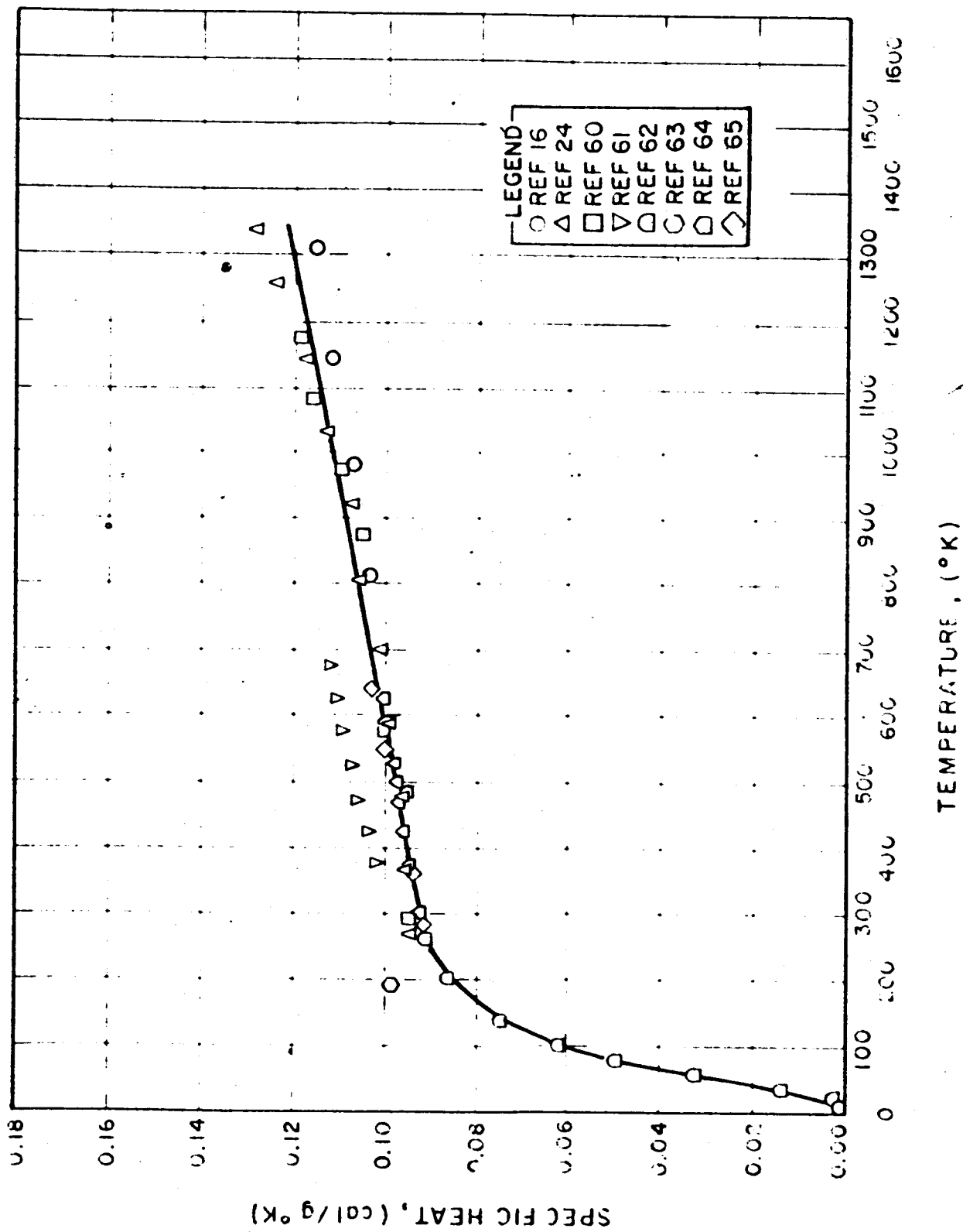
FIG. 2-72   SPECIFIC HEAT - COPPER
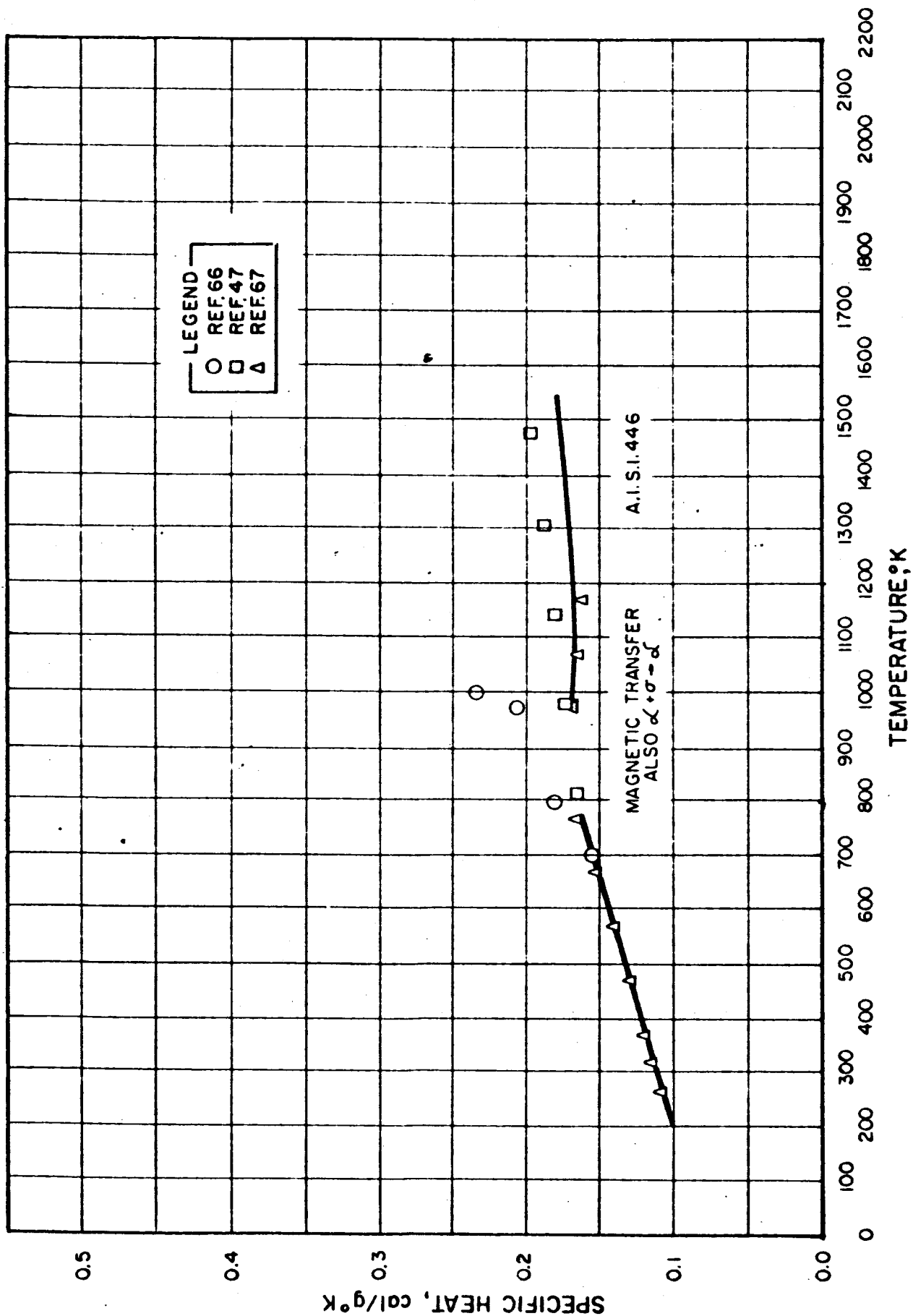
FIG. 2-73   SPECIFIC HEAT - IRON + CHROMIUM (14 - 27% Cr)
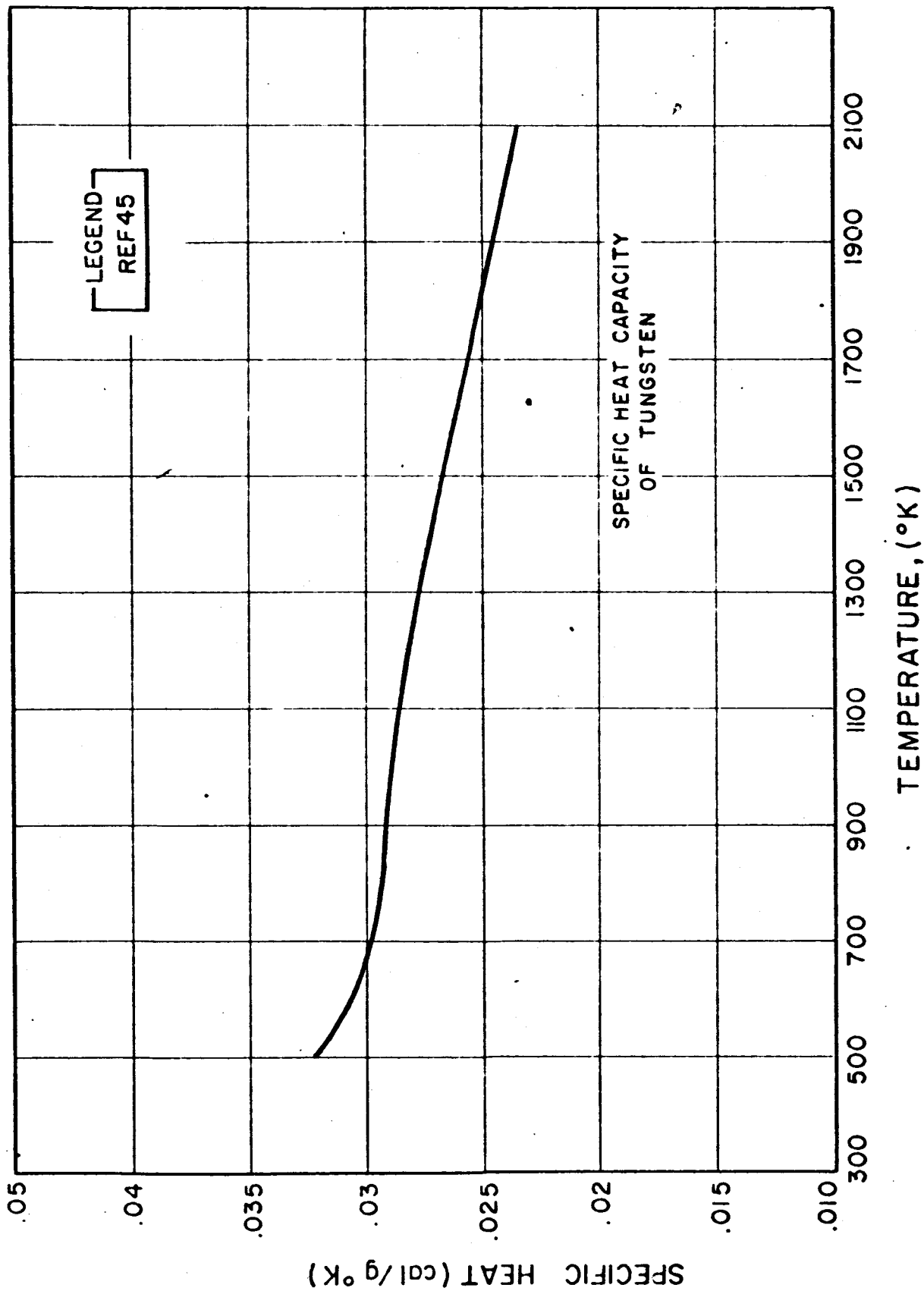
FIG. 2-74   SPECIFIC HEAT CAPACITY OF TUNGSTEN
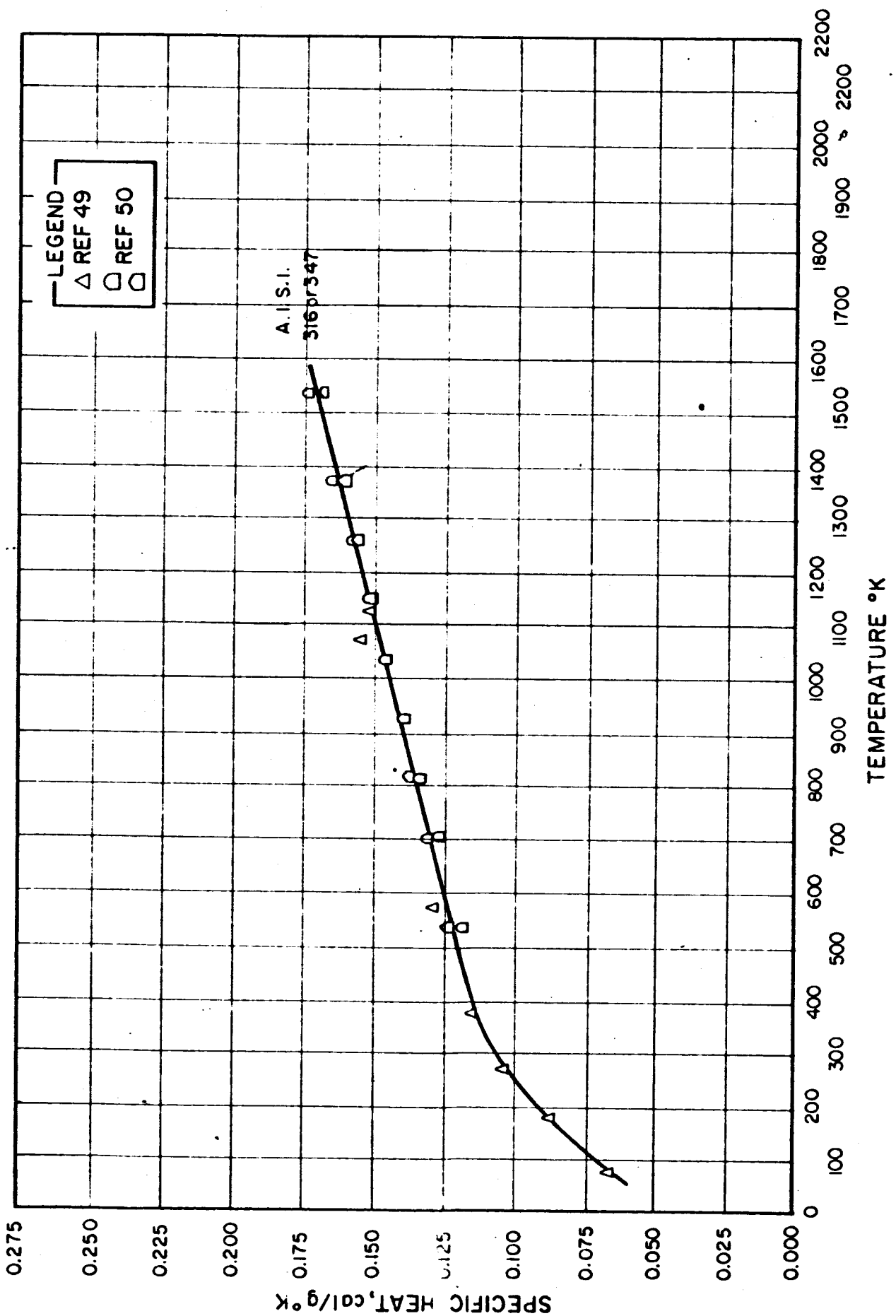
FIG. 2-75   SPECIFIC HEAT - IRON + CHROMIUM ÷ NICKEL + X

54857
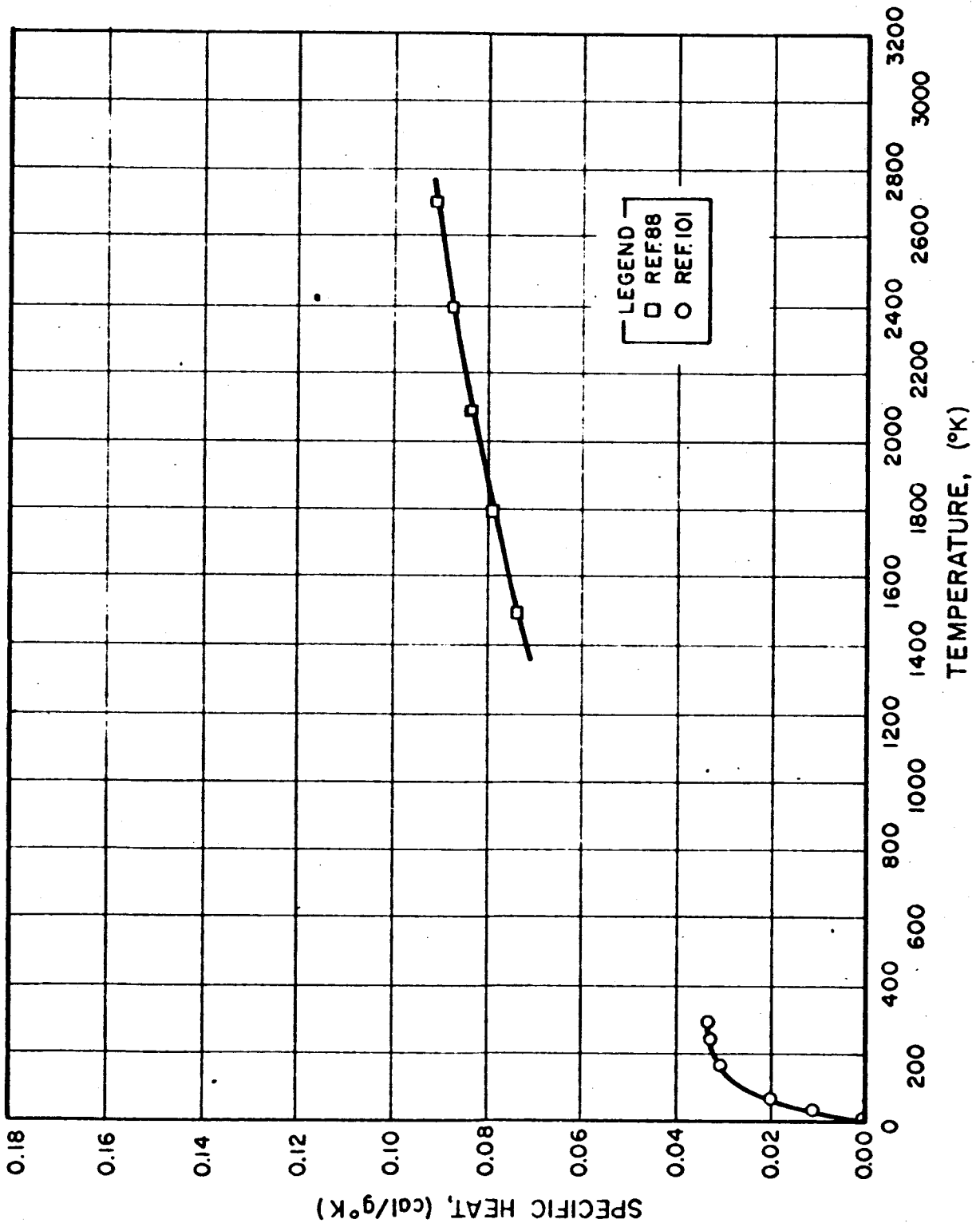
FIG. 2-76   SPECIFIC HEAT - RHENIUM
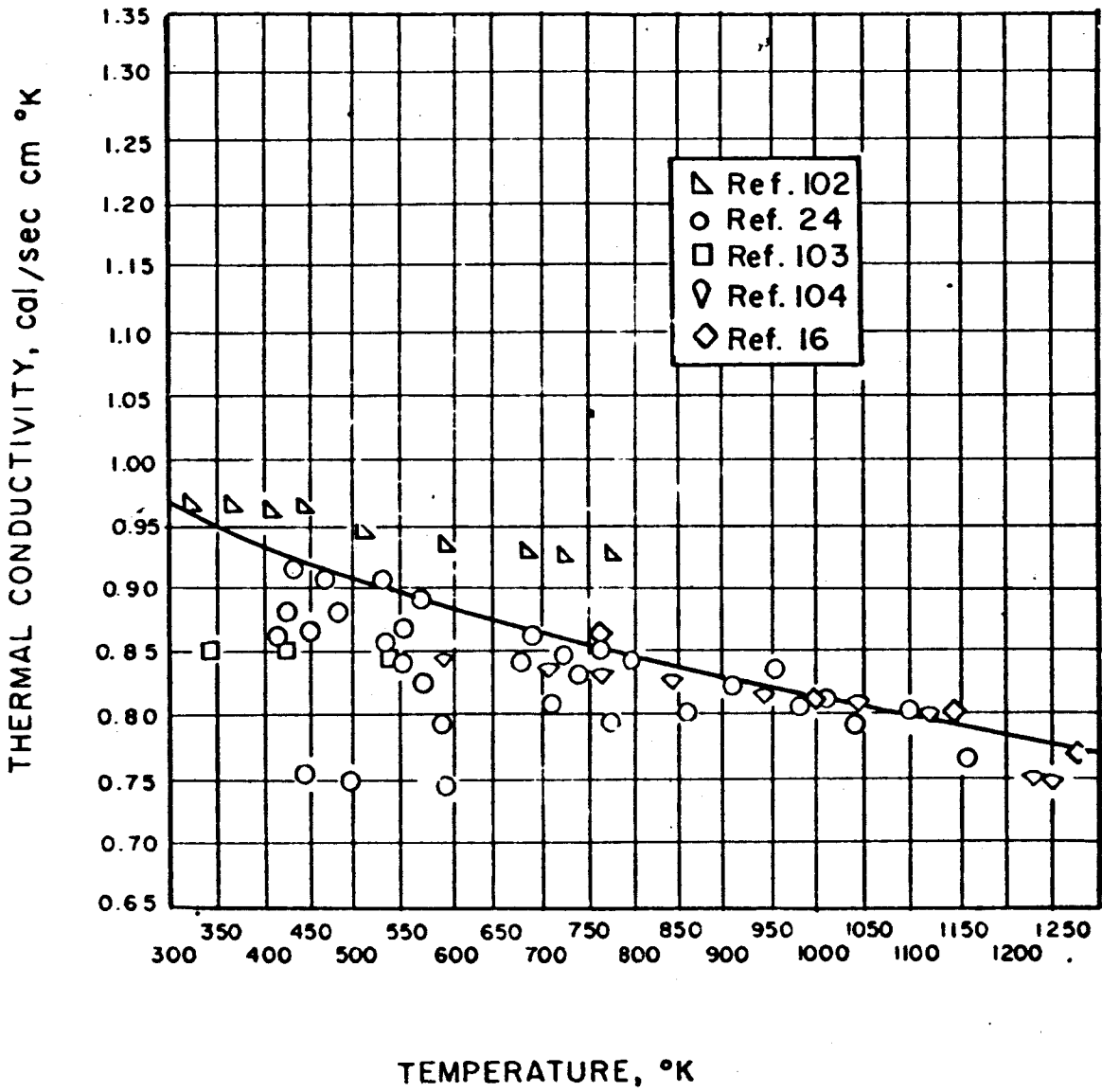
FIG. 2-7.7   THERMAL CONDUCTIVITY - COPPER
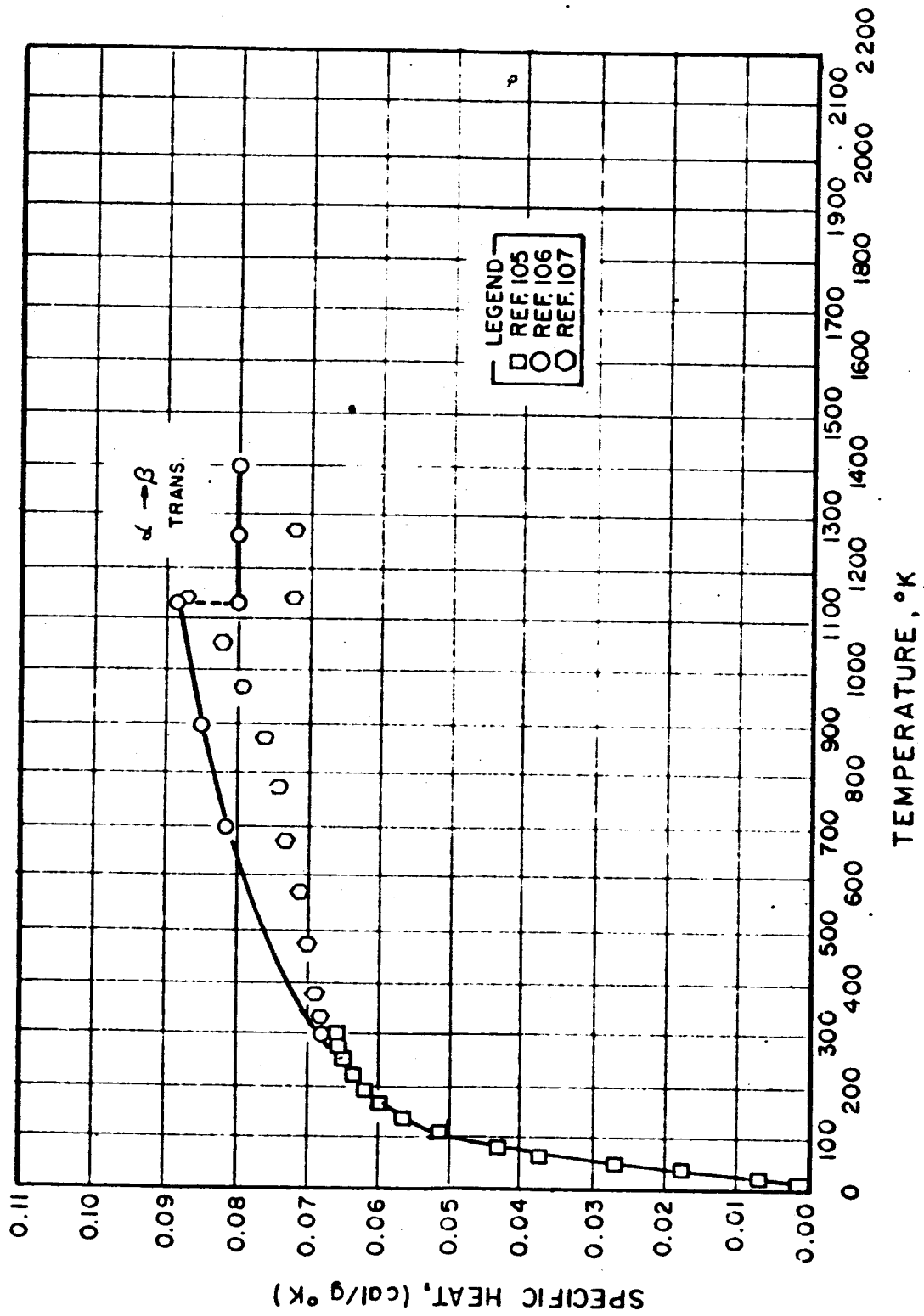
FIG. 2-78   SPECIFIC HEAT -- ZIRCONIUM
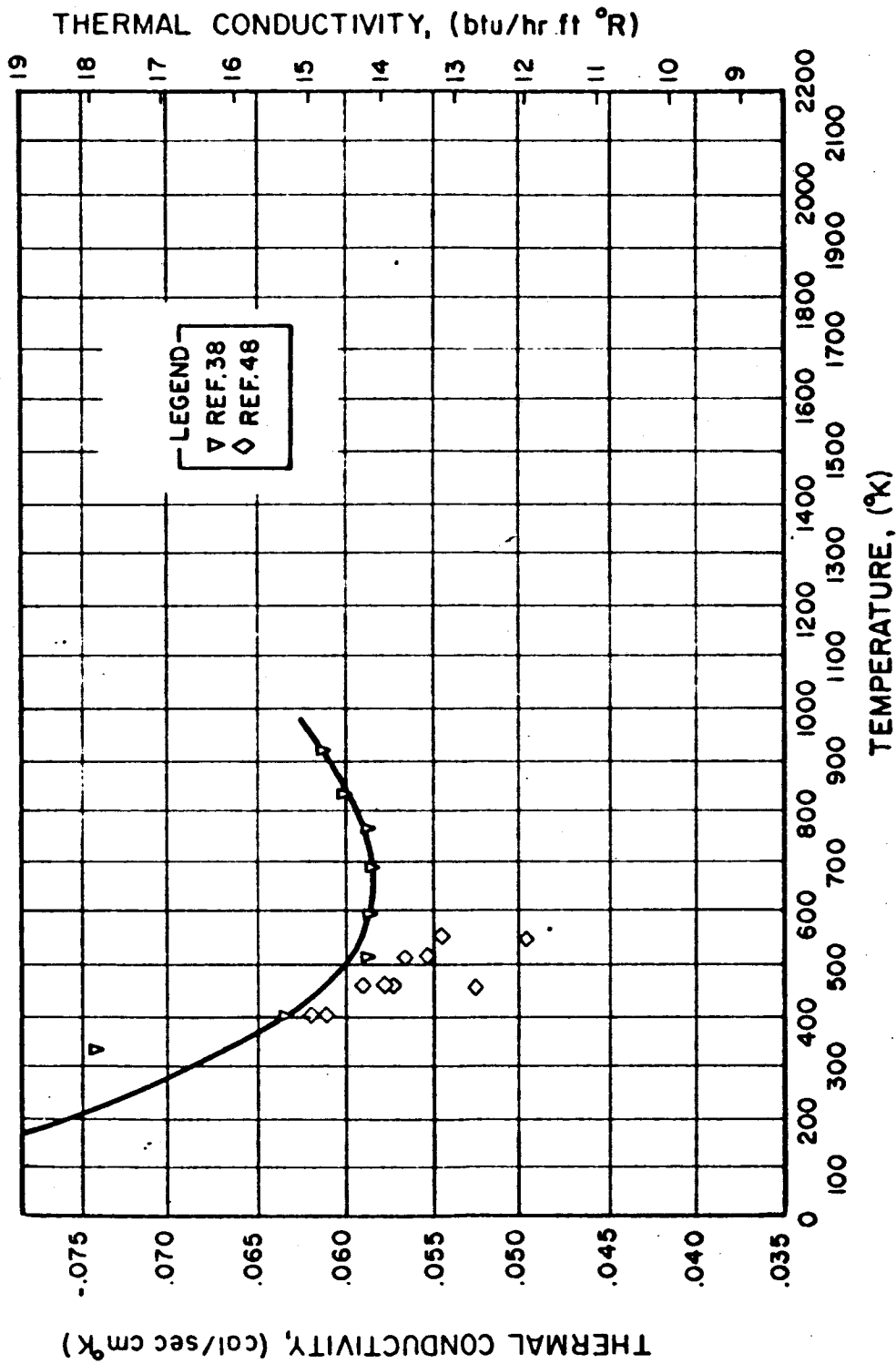
FIG. 2-79   THERMAL CONDUCTIVITY - ZIRCONIUM
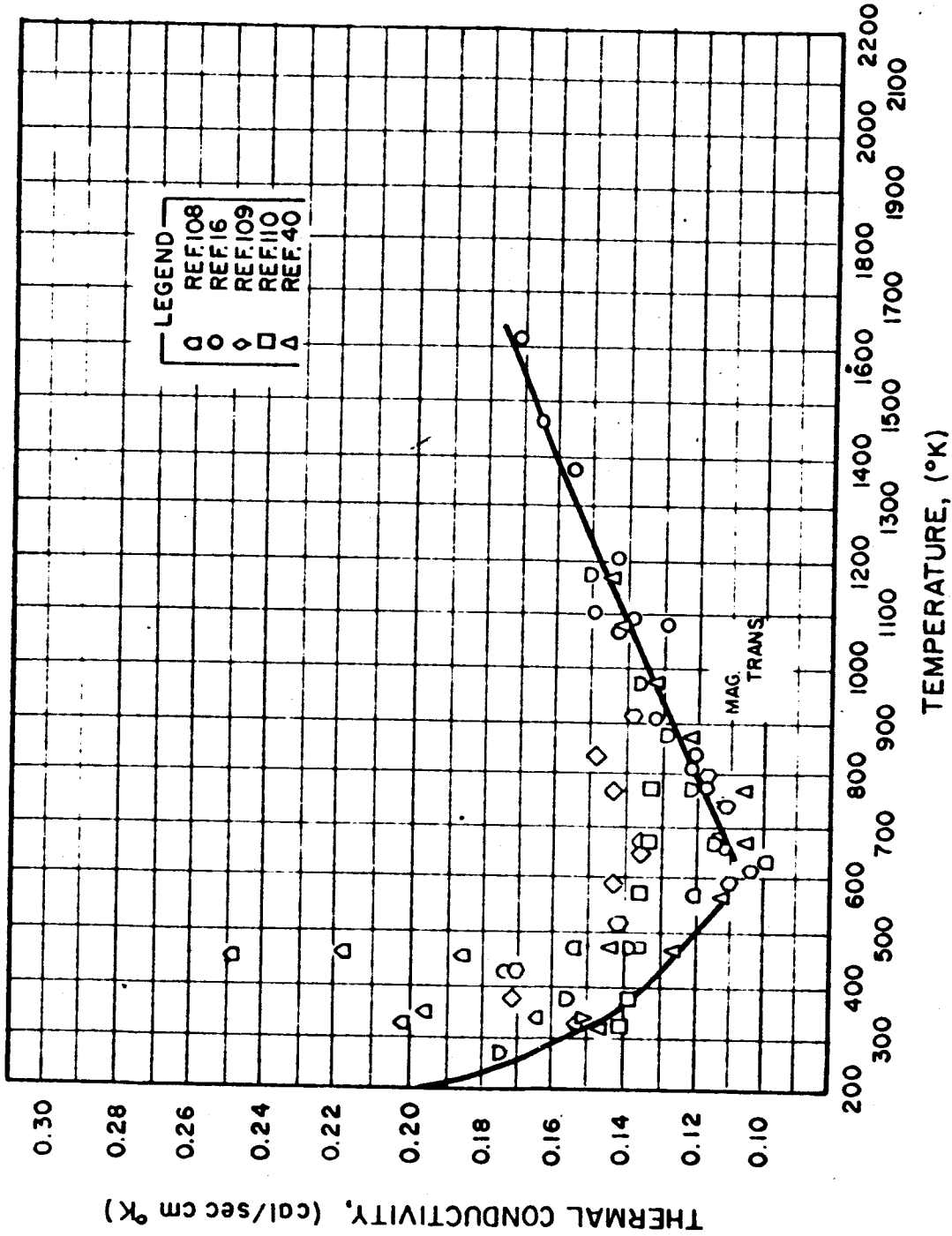
FIG. 2-80   THERMAL CONDUCTIVITY - NICKEL

7364851
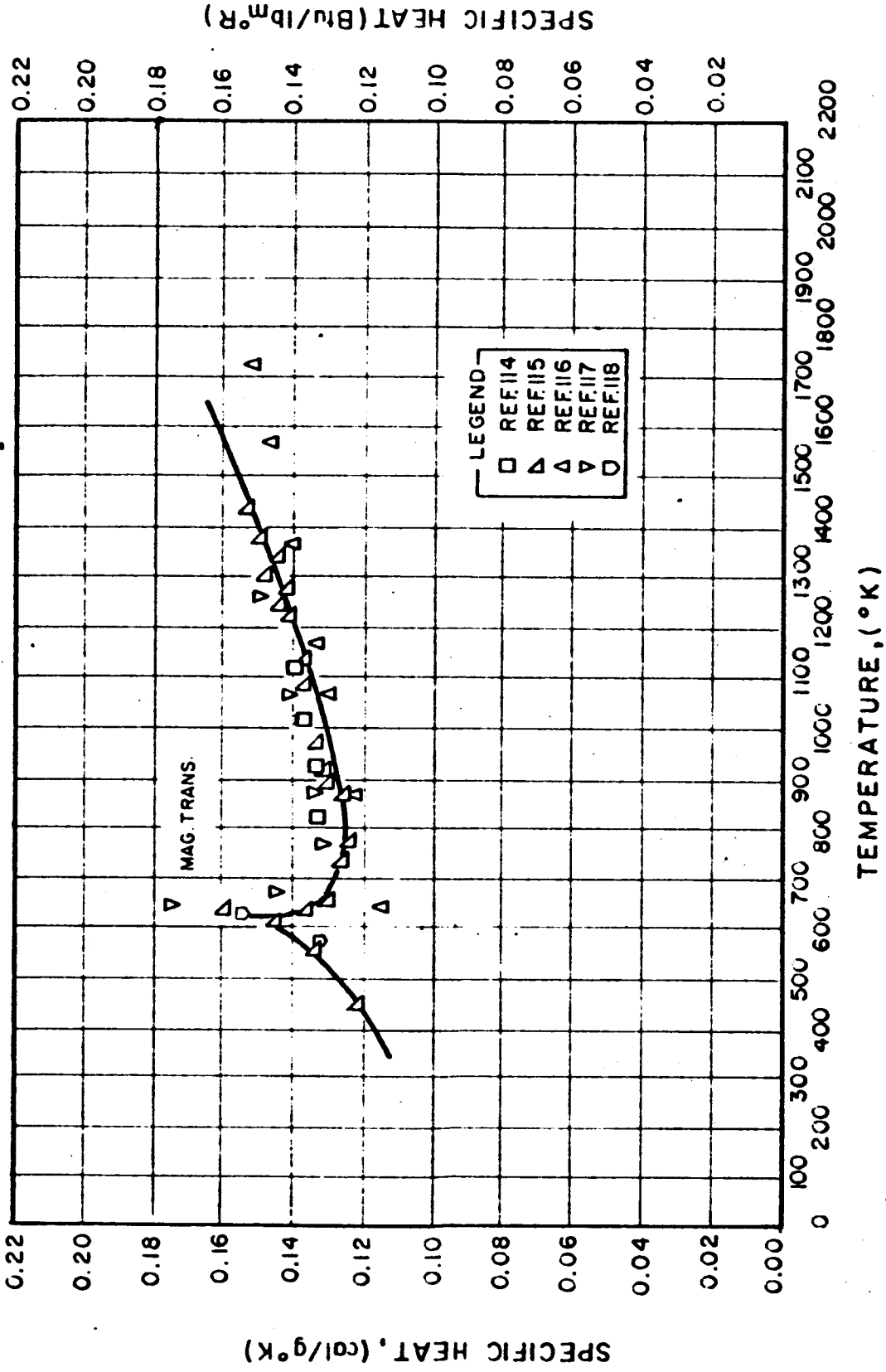
FIG. 2-81   SPECIFIC HEAT - NICKEL

7364850
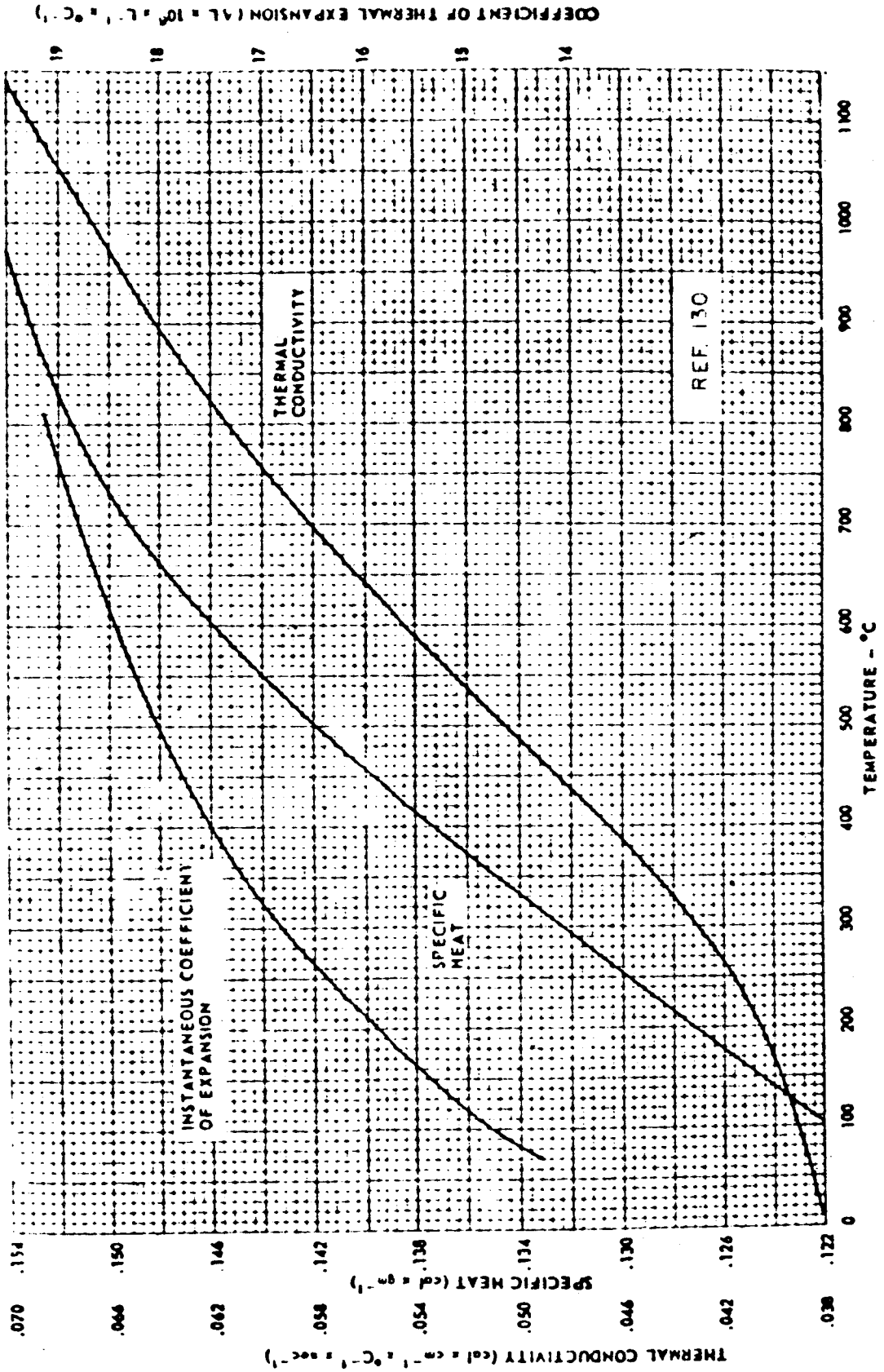
FIG. 2-82 SPECIFIC HEAT, THERMAL CONDUCTIVITY AND INSTANTANEOUS EXPANSION COEFFICIENT FOR TYPE 304 STAINLESS STEEL
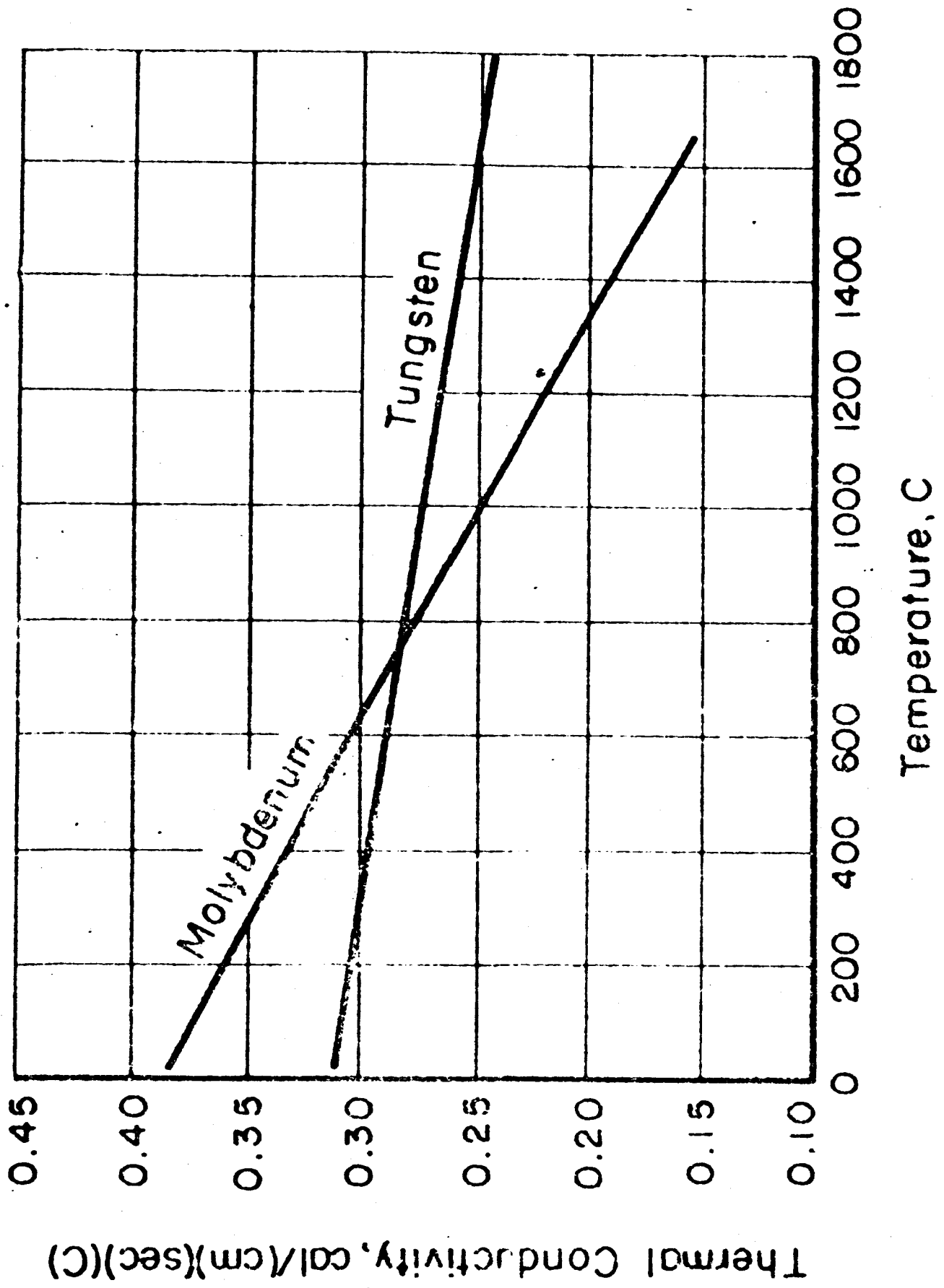
FIG. 2-8.3   THERMAL CONDUCTIVITY OF TUNGSTEN AND MOLYBDENUM
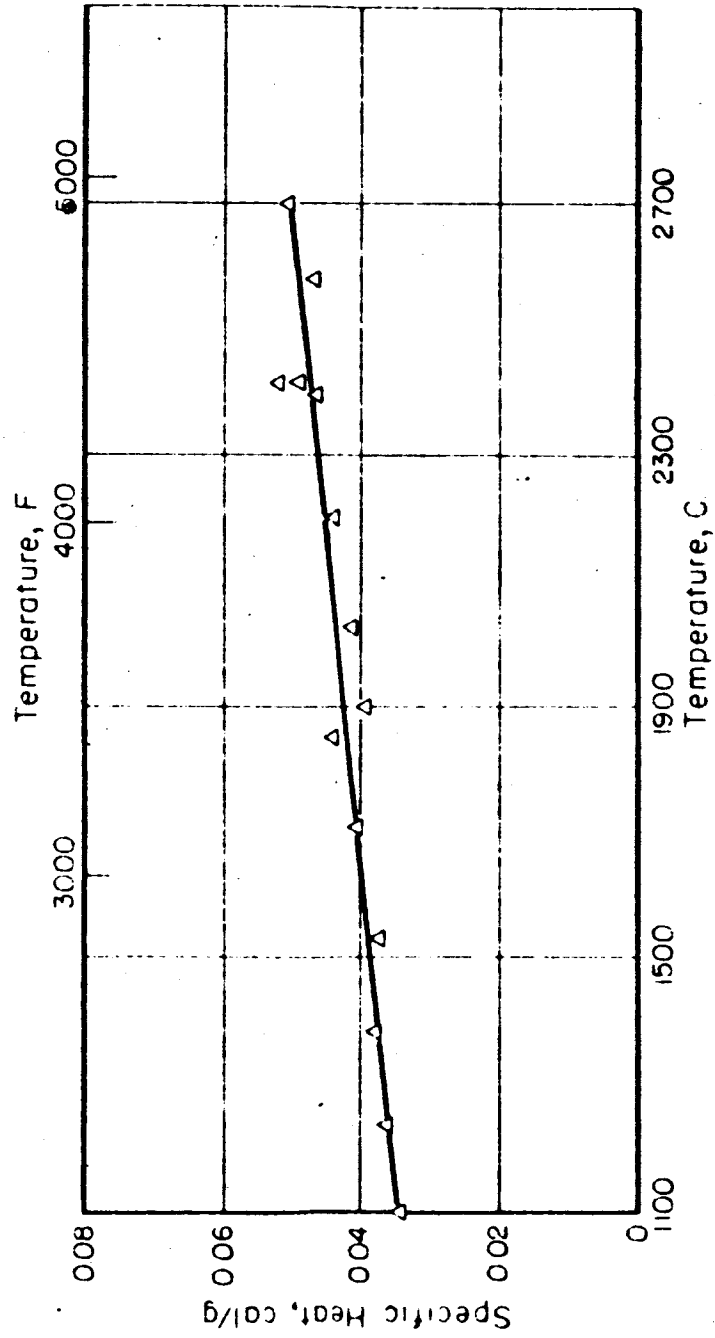
FIG. 2-84   SPECIFIC HEAT OF TANTALUM

2.2.8 Young's Modulus

Young's modulus is simply the constant of proportionality relating the elastic strain of a material to the applied stress. It is to be noted that Young's modulus is applicable to the region where strain is plastic, but additional empirical terms are required to fit the observed data (Ref. 4).

It was pointed out in Sec. 1 (Ceramics) that Young's modulus is a factor in the determination of the maximum cooling or heating rate for ceramic materials. Poisson's ratio is also required in this analysis but a lack of high temperature data precludes reporting this quantity in detail. Poisson's ratio is generally found to be in the region of .30 - .38 for most metals.
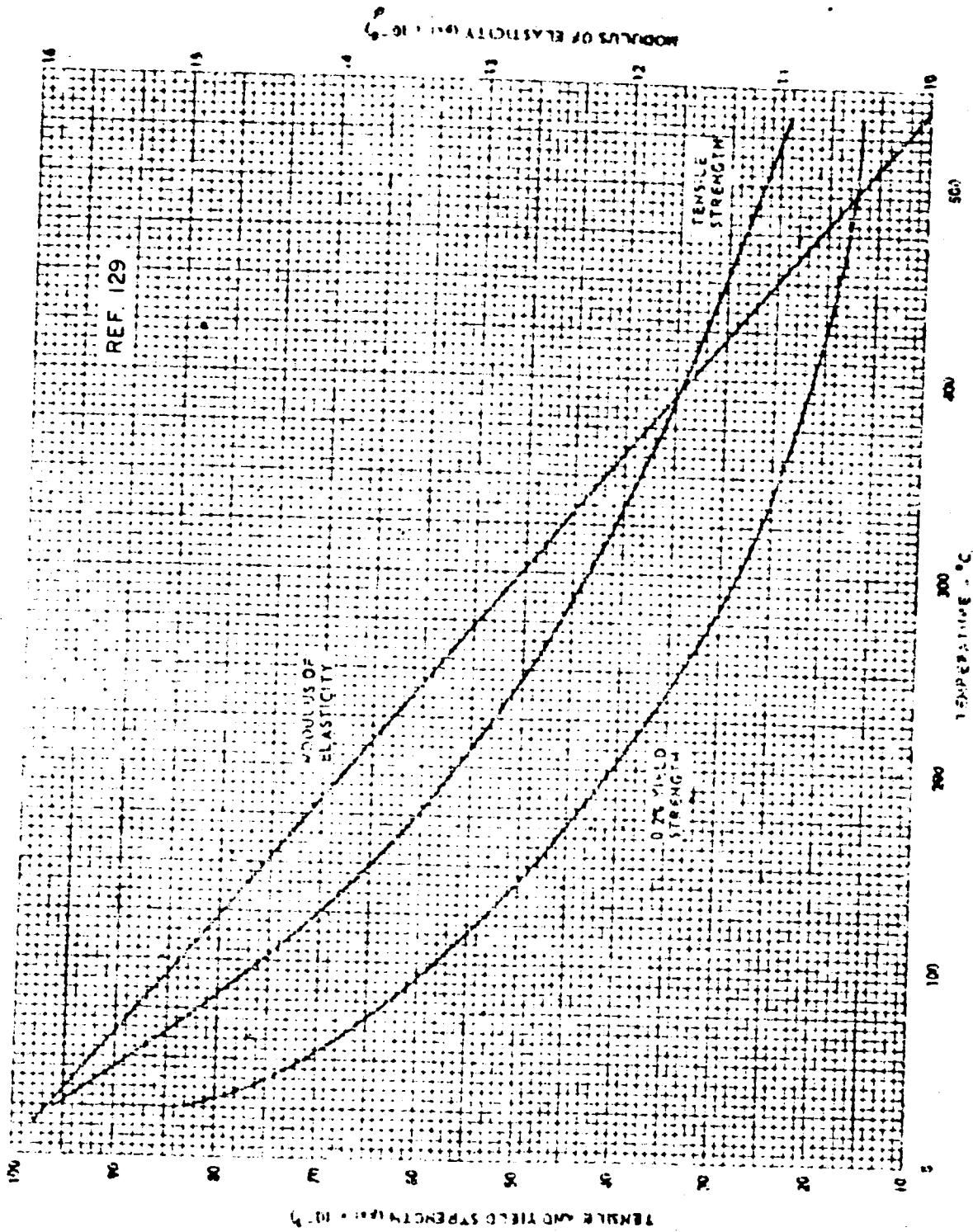
FIG. 2-85   MECHANICAL PROPERTIES OF TITANIUM

945
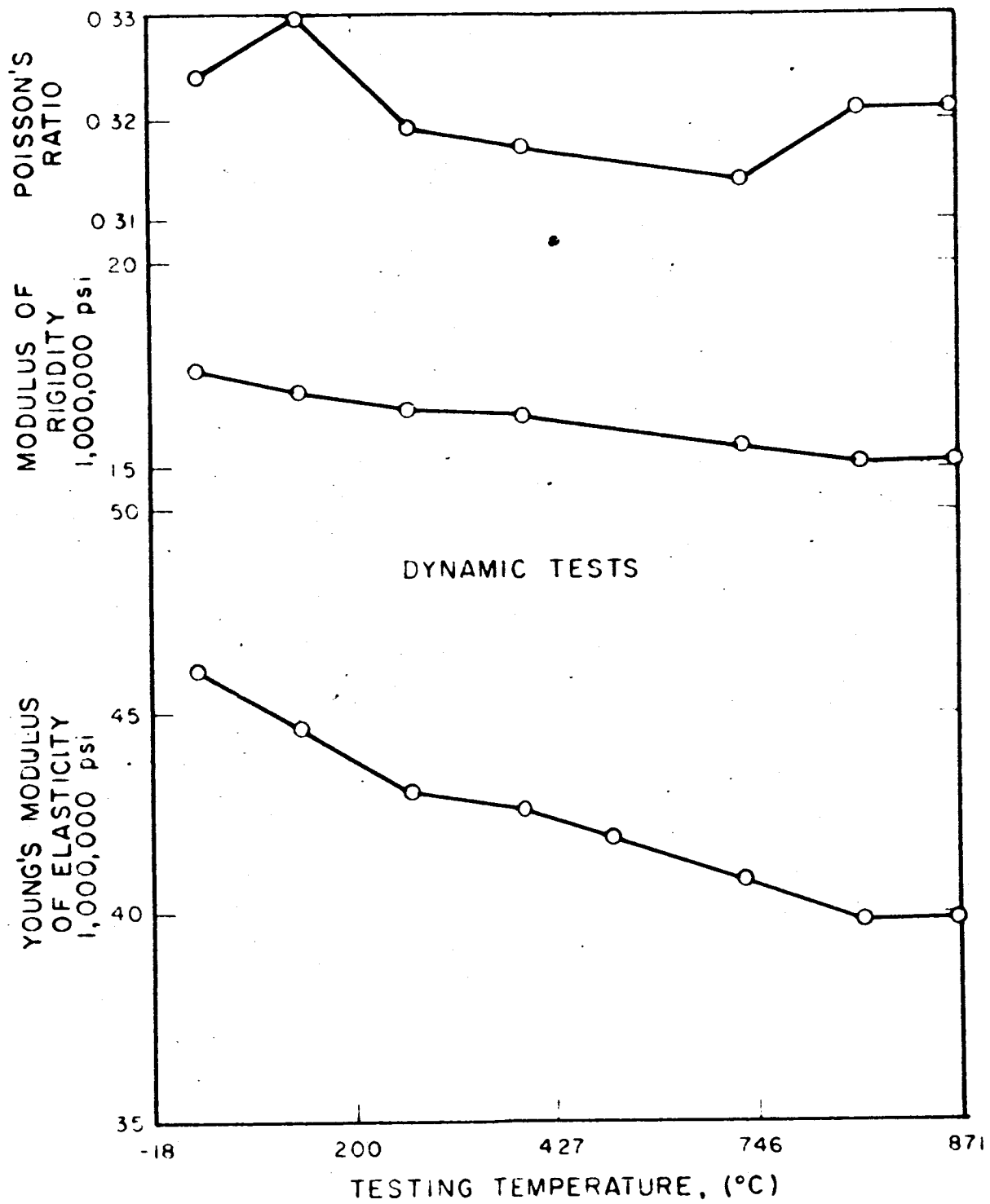
FIG. 2-86   YOUNG'S MODULUS AND POISSON'S RATION FOR MOLYBDENUM
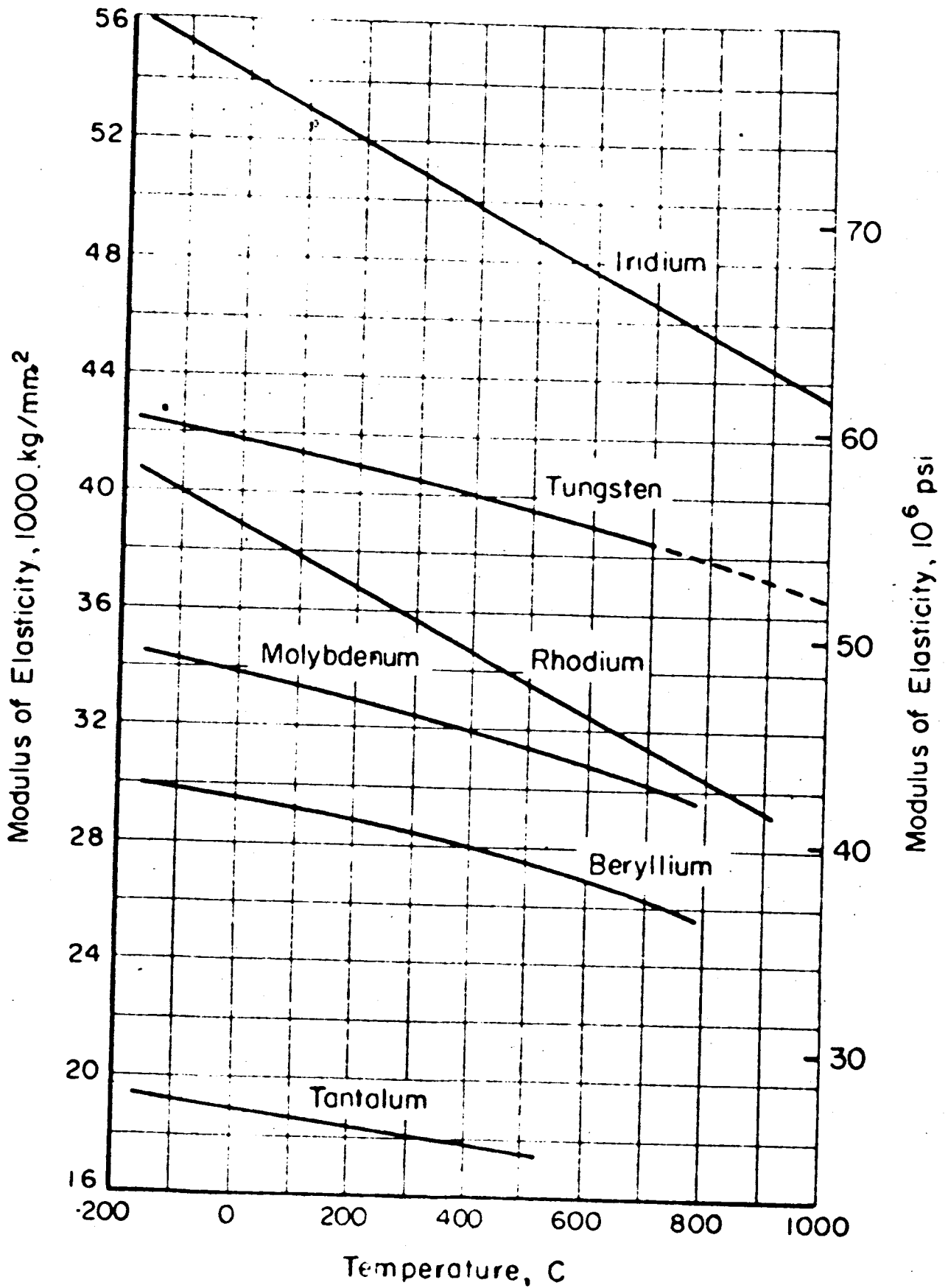
FIG. 2-87   TMEPERATURE DEPENDENCE OF THE ELASTIC MODULUS OF TUNGSTEN AND OTHER METALS
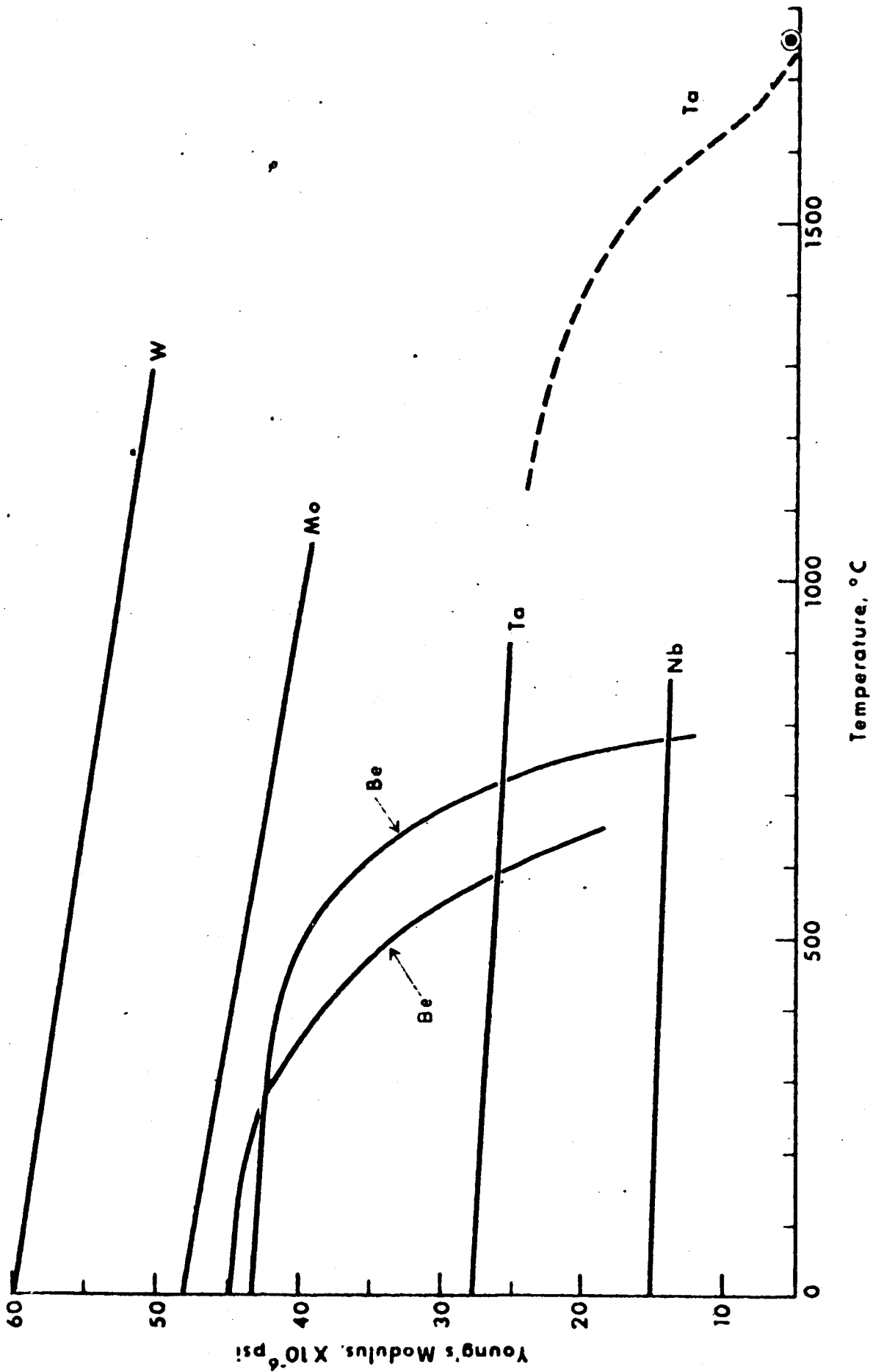
YOUNG'S ELASTICITY MODULUS, Ta, W, Mo, Nb, Be

FIG. 2-88

934
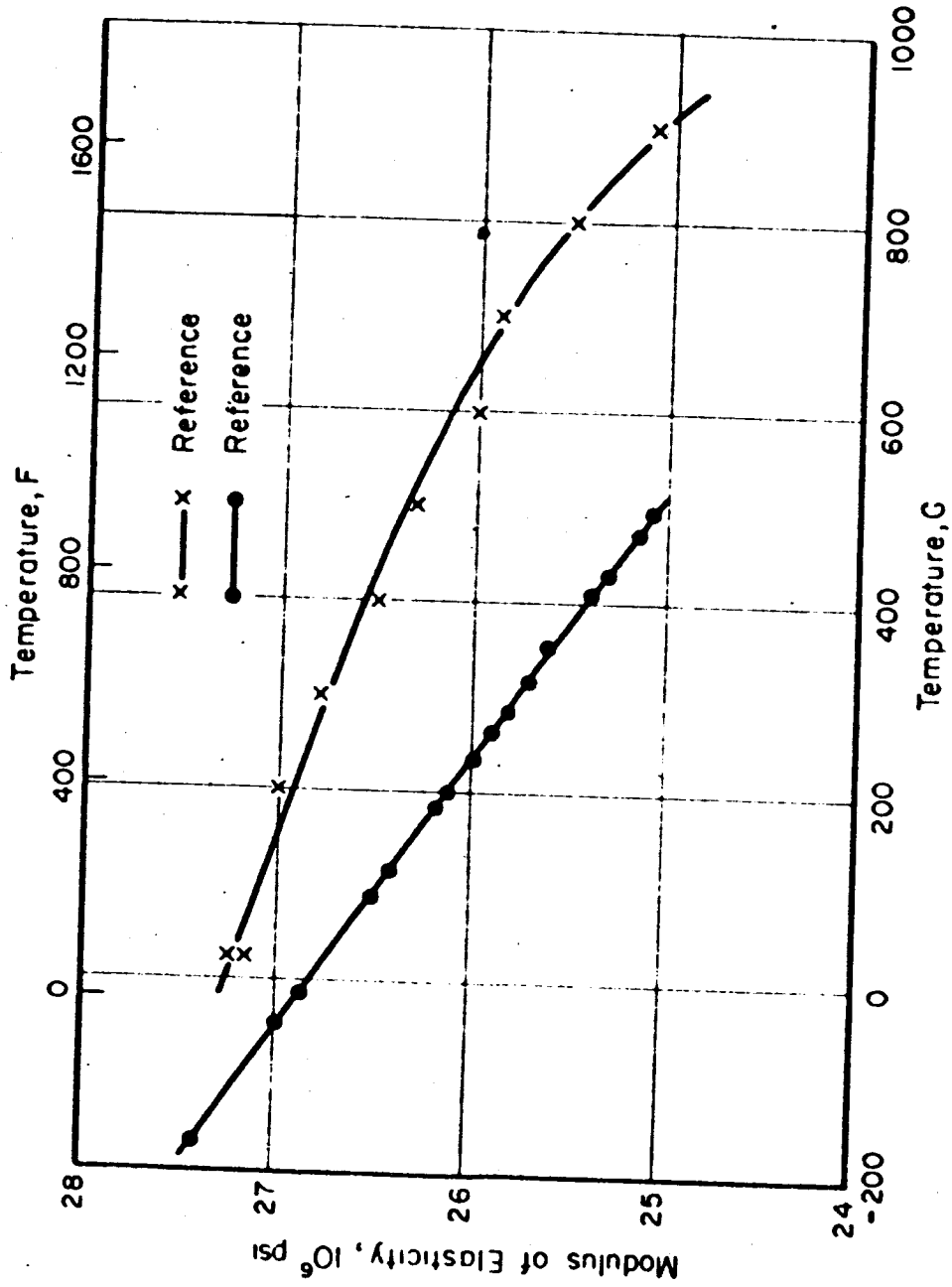
FIG. 2-89   EFFECT OF TEMPERATURE ON THE MODULUS OF ELASTICITY OF TANTALUM

2.2.9 Recommendations

Envelope materials should possess high creep strength, high thermal conductivity, low electrical resistivity, and low vapor pressure. Tantalum and tantalum-tungsten alloys are suitable materials choices. A separate chapter (Heat Transfer) discusses envelope and lead design more thoroughly.

Radiator materials should be chosen to effectively reject heat from a converter. Molybdenum probably best satisfies the requirement of strength at high rejection temperatures ($900^{\circ}C$ and higher). While copper has excellent thermal properties, it fails to meet the strength requirement.

Emitter materials were discussed previously from the standpoint of emission. In addition to the obvious requirements of low vapor pressure or weight loss, low total emissivity, and high conductivity (to limit temperature gradients at high heat flux), emitter materials ought to possess minimum creep rate for given stress and life requirements.

BIBLIOGRAPHY

Section 2.2

1. Special Technical Data, 52-363, Materials Manufacturing Division Westinghouse Electric Corporation, June 8, 1962

2. Knoll, M., Materials and Processes of Electron Devices, Springer-Verlag, Berlin, 1959

3. 1962 Thermionic Power Conference, Nuclear Thermionic Fuel Element Experiments, Vallecitos Atomic Laboratory, General Electric Company

4. Dorn, J. E., Mechanical Behavior of Materials at Elevated Temperatures, McGraw-Hill Book Company, New York, 1961

5. ASM Handbook (1948), p. 72

6. ASM Handbook (1948), p. 58

7. ASM Handbook (1955 Supplement), p. 179

8. Greiner, E. S. and Ellis, W. C., "Thermal and Electrical Properties of Ductile Titanium", Metal Technol. AIMME Tech. Publ. No. 2466, Vol. 15.

9. Hidnert, Peter, "Thermal Expansion of Titanium", J. Research Natl. Bur. Standards RP1520. Vol. 30 (2). pp 101-5

10. Bell, I. P., and Makin, S. M., "Fast Reactor -- Physical Properties of Materials of Construction, Review of Progress from Sept. 1, 1953 to April 1, 1954", (RDB(c)/TN-70). 17 p. (England)

11. Savitskii, E. M., Burhkanov, G. S., "Composition Diagrams of Titanium-Lanthanum and Titanium-Cerium Alloys", Zhur. Neorg. Khim. Vol. 2, pp. 2609-16 (USSR)

12. Petersen, V. C. and Huber, R. W., "The Titanium-Germanium System from 0 to 30 percent Germanium", U. S. Bur. of Mines Publ. BM-RI-5365, 23 p.

13. Altman, H. W., Rubin, T., and Johnston, H. L., "Coefficient of Thermal Expansion of Solids at Low Temperature. III. The Thermal Expansion of Pure Metals, with the Data for Aluminum, Nickel, Titanium and Zirconium", Cryogenic Lab., Ohio State U., Research Foundation, Tech. Rpt. No. TR264-27 (Contract W33-038-2c-14794). 11 p. AD-26 970.

14. Laquer, Henry, L., "Low-temperature Thermal Expansion of Various Materials", U.S. Atomic Energy Comm. AECD-3706. 58 p.

15. Erfling, Hanns-Dieter, "Studies of Thermal Expansion of Solids at Low Temperature. III. Calcium, Columbium, Thorium, Vanadium, Silicon, Titanium", Ann. Physik. Vol. 41, pp. 467-475. (Germany)

16. Fieldhouse, I. B., Hedge, J. C., et al., "Measurements of Thermal Properties", Armour Research Foundation, Chicago, Ill. WADC TR 55-495, pt. 1, Contract AF 33(616)-2903, 64 p.

17. Hugon, Lionel and Jaffray, Jean, "The Thermal Conductivity of Nickel above and below the Curie Point", Ann. Phys. Vol. 12 pp. 377-85 (French)

18. Nix, F. C., and MacNair, D., "Thermal-Expansion of Pure Metals: Copper, Gold, Aluminum, Nickel and Iron", Phys. Rev., Vol. 60. pp. 597-605.

19. Pupke, Gerhard, "Anisotropy of the Thermal Expansion of Iron-Nickel Alloys. I", Z. Physik Chem. Vol. 207, pp. 91-110 (Germany)

20. Bell, I. P., and Makin, S. M., "Fast Reactor -- Physical Properties of Materials of Construction, Review of Progress from Sept. 1, 1953 to April 1, 1954", (RDB(c)/TN-70). 17 p. (England)

21. Sims, C. T., Craighead, C. M. Jaffee, R., et al. "Investigation of Rhenium", WADC Technical Report No. 54-371. Contr. AF 33(616)-232, AD 48 279. 138 p.

22. Betz, H. T. and Olson, O. H., "Determination of Emissivity and Reflectivity Data on Structural Materials", WADC TR 56-222 Part II. Contract AF 33(616) 3002 Task 73603. 184 p.

23. H. R. Ogden, "Physical and Mechanical Properties of Tantalium," Battelle Memorial Institute, DMIC Memo. 32 (1959).

24. Lucks, C. F., and Deem, H. W., "Thermal Conductivities, Heat Capacities, and Linear Thermal Expansion of Five Materials", Battelle Memorial Inst., Columbus, Ohio, WADC Tech. Rpt. No. 55-406. 65 p.

25. Apblett, W. R. and Pellini, W. S., "A Recording Dilatometer for High Temperatures (Linear Expansion of Molybdenum, Tungsten, Inconel, and Vitallium)", Am. Soc. Metals Preprint. (2W). 15 p.

26. Rasor, N. S. and McClelland, J.D., "Thermal Properties of Materials -- Part I, Properties of Graphite, Molybdenum and Tantalum to Their Destruction Temperatures", WADC Tech. Rpt. 56-400, Pt. 1 (Contract AF 33(616) 2909). AD 118 144, 53 p.

27. Demarquay, Jean, "New Method of Studying the Expansion of Bodies at Elevated Temperatures", Compt. rend. Vol. 220(2). pp. 81-83 (France)

28. Edwards, James W. and Johnston, Herrick L., "Vapor Pressures of Inorganic Substances. XI, Titanium between 1587 and 1764 $^\circ$K and Copper between 1143 and 1292 $^\circ$K", J. Am. Chem. Soc., Vol. 75, pp. 2467-70.

29. Blocher, John and Campbell, I. E., "Vapor Pressure of Titanium", J. Am. Chem. Soc., Vol. 71, pp. 4040-2.

30. Redfield, T. A. and Hill, J. H., "Heat Capacity of Molybdenum", U.S. Atomic Energy Comm. Publ. ORNL-1087, 9 p.

31. Sims, C. T., Gideon, D. N., and others, "Investigation of Rhenium", Battelle Memorial Inst., Columbus, Ohio (Contr. AF33(616)232). 52 p. AD-100 581.

32. Edwards, James W., Johnston, Herrick, L., and Blackburn, Paul E., "Vapor Pressures of Inorganic Substances. VIII. Molybdenum between 2151 and 2462 $^\circ$K", J. Am. Chem. Soc., Vol. 74, pp. 1539-40

33. Knoll, M., Materials and Processes of Electron Devices, Springer-Verlag, Berlin (1959).

34. Hersh, Herbert, N., "Vapor Pressure of Copper", J. Am. Chem. Soc., Vol. 75, pp. 1529-31

35. Edwards, James W. and Johnston, Herrick L., "The Vapor Pressures of Inorganic Substances. VI. Vanadium between 1666°K and 1882°K", J. Am. Chem. Soc., Vol. 73, pp. 174-6

36. Rigney, C. J. and Bockstahler, L. I., "The Thermal Conductivity of Titanium between 20° and 273°K", Phys. Rev., Vol. 83. p. 220

37. Loewen, E. G., "Thermal Properties of Titanium Alloys and Selected Tool Materials", Trans. Am. Soc. Mech. Engr. Vol. 78, pp. 667-70.

38. Mikryukov, V. E., "Temperature Dependence of the Heat Conductivity and Electrical Resistance of Ti, Zr, and Zr Alloys", Vestnik Moskov Univ. Vol. 12(5). pp. 73-80 (USSR)

39. Deem, H. W., Wood, W. D. and Lucks, C. F., "The Relation between Electrical and Thermal Conductivities of Titanium Alloys", Trans. Met. Soc. AIME 212, pp. 520-3.

40. Silverman, L., "Thermal Conductivity Data Presented for Various Metals and Alloys up to 900°", J. Metals, Vol. 5, pp. 631-2.

41. Bell, I. P., and Makin, S. M., "Fast Reactor -- Physical Properties of Materials of Construction, Review of Progress from Sept. 1, 1953 to April 1, 1954", (RDB(c)/TN-70. 17 p. (England)

42. Osborn, Robert H., "Thermal Conductivities of Tungsten and Molybdenum at Incandescent Temperatures", J. Opt. Soc. Am., Vol. 31, pp. 428-32.

43. Mikol, Edward P., "The Thermal Conductivity of Molybdenum over the Temperature Range 1000 to 2100 °F", Reprint of Oak Ridge Natl. Lab. Rept. ORNL-1131, Tech. Rpt. No. 2, Engineering Experiment Station, College of Engineering, U. of Alabama, Cont. No. W-7405-eng-2b, 7 p.

44. Schmidt, F. F., "Tantalium and Tantalum Alloys," Battelle Memorial Institute, DMIC 133, (1960).

45. Barth, V. D., "Physical and Mechanical Properties of Tungsten and Tungsten Base Alloys," Battelle Memorial Institute, DMIC 127 (1960).

46. Hogan, C. L., and Sawyer, R. B., "The Thermal Conductivity of Metals at High Temperatures", J. Appl. Phys. Vol. 23, pp. 177-80

47. Fieldhouse, I. B., Hedge, J. C., et al., "Thermal Properties of High Temperature Materials", WADC Tech. Rpt. No. 57-487 (Contract AF 33(616)3701). AD 150 954, 79 p.

48. Vianney, L. R., "Thermal Conductivity of 347 Stainless Steel and Zirconium", DIC Project 6627, Feb. 15, 1951. AD 140 931. 6 p.

49. Lucks, C. F. and Deem, H. W., "Thermal Properties of Thirteen Metals", Am. Soc. Testing Materials, Spec. Tech. Publ. Vol. No. 227. 29 p.

50. Fieldhouse, I. B., Hedge, J. C., and Lang, J. L., "Measurements of Thermal Properties", WADC Tech. Rpt. 58-274, (Contract No. AF 33(616)-3701). AD-206 892, 79 p.

51. Smith, K. F., and Chiswik, H. H., "High Temperature Strength Zirconium and Titanium Base Alloys for Fuel Element Jacketing", U. S. AEC Publ. ANL 5339. 16 p.

52. Kothen, Charles W., "High-temperature Heat Contents of Molybdenum and Titanium and the Low-temperature Heat Capacities of Titanium", Univ. Microfilms (Ann Arbor, Mich.) Publ. No. 23697. 93 p.

53. Redfield, T. A. and Hill, J H. "Heat Capacity of Molybdenum", U. S. Atomic Energy Comm. Publ. ORNL-1087. 9 p.

54. Rasor, N. S. (Personal communication, D137, re: SPECIFIC HEAT -- TANTALUM) WADC TR 59-439.

55. Rea, Joseph Ambrose, "The Construction of a Furnace Calorimeter and the Evaluation of a Method of Thermal Analysis for Obtaining the Specific Heat of Solids at High Temperatures", Oklahoma A. and M. Coll., Stillwater, Master Thesis, 52 p.

56. Kothen, C. W. and Johnston, H. L., "Low-temperature Heat Capacities of Inorganic Solids. XVII. Heat Capacity of Titanium from 15 to 305 ^{o}K", J. Am. Chem. Soc. Vol. 75, pp. 3101-2.

57. Kelley, K. K., "Specific Heats at Low Temperatures of Ti and TiC", Ind. Eng. Chem. Vol. 36. pp 865-6.

58. Loewen, E. G., "Thermal Properties of Titanium Alloys and Selected Tool Materials", Trans. Am. Soc. Mech. Engrs. Vol. 78, pp. 667-70.

59. Friedberg, S. A. "Investigations of Thermal and Electrical Properties of Solids at Very Low Temperatures", U. S. AEC Publ. NP-5668. 73 p.

60. Forster, Fritz and Tschentke, G., "A Method for the Measurement of the Temperature Relationships of Electrical Resistivity and Specific Heat of Solid and Liquid Metals", Z. Metallkunde. Vol. 32 (6) pp. 191-5 (Germany)

61. Hirano, Kenichi, Maniwa, Hideyo, and Takagi, Yutaka, "Specific-heat Measurements on Quench-annealed Aluminum, Copper and a-phase Alloys of Copper", J. Phys. Soc. Vol. 10, pp. 909-10.

62. Giauque, W. F. and Meads, P. F., "The Heat Capacities and Entropies of Aluminum and Copper from 15 to 300 ^{o}K", J. Am. Chem. Soc. Vol. 63. pp. 1897-1901.

63. Boosz, H. J. "The Average Specific Heat of Hard Metals between Room Temperature and -190°", Metall. Vol. 11, pp 22-3 (Germany)

64. Suzuki, Taira., "The Release of Energy Associated with Crystal Restoration Process in Cold-Worked Polycrystalline Copper", Sci. Repts. Research Insts. Tohoku. Vol. Ser. A 1. pp. 193-201 (Japan)

65. Persoz, B., "New Method of Measuring the True Specific Heat of Metals at High Temperatures (Specific Heats of Platinum and Nickel)", Ann. Physique (xiii). Vol. 14. pp. 237-301. (France)

66. Stull, Daniel R. and McDonald, Richard A., "The Enthalpy and Heat Capacity of Magnesium and of Type 430 Stainless Steel from 700 to 1100°K", J. Am. Chem. Soc. Vol. 77, p. 5293

67. Douglas, T. B. and Dever, J. L., "Enthalpy and Specific Heat of Four Corrision-resistant Alloys (80:20 Nickel, Chromium, Stainless Steel and Monel) at High Temperatures", J. Research Nat. Bur. Stand. Vol. 54 (1). pp. 15-19.

68. Sims, Chester T., Craighead, Charles M., and Jaffee, Robert I., "Physical and Mechanical Properties of Rhenium", Trans. Amer. Inst. Min. Met. Eng. (in J. Metals, 1955, 7). Vol. 203 (1). pp. 168-79 (England)

69. Gubareff, G. G., Ko, S. Y. and McNall, P. E., "Review of the Thermal Radiation Property Values for Metals and Other Materials," Minneapolis-Honeywell Regulator Company, (1956).

70. Smithell, C. J., Tungsten, Chemical Publishing Company, (1953).

71. Wilkes, G. B., "Total Normal Emissivities and Solar Absorptivities of Materials", WADC Tech Rept. No. 54-42 (Contr. W33-)33-(ac)-20486). 94 p.

72. Malter, L. and Langmuir, D.B., "Resistance, Emissivities, and Melting Point of Tantalum", Phys. Rev., 55, p. 743

73. Betz, H. T., Olson, O. H., et al., "Determination of Emissivity and Reflectivity Data on Aircraft Structural Materials. Part I, Techniques for Measurement of Total Normal Emissivity and Reflectivity with Some Data on Copper and Nickel", WADC TR 56 222, Pt. I (Contr. AF 33(616)-3002, Task 73603). AD 110 485. 43 p.

74. Best, Geo., "Emissivity of Copper and Aluminum", J. Optical Soc. Am. Vol. 39. pp 1009-11.

75. Deegan, G. E., "Thermal and Electrical Properties of Graphite Irradiated at Temperatures from 100 to 425 °K", Atomic Energy Commission, NAA-SR-1716. 77 p.

76. Bostrom, W. A., "Electrical Resistance of Zirconium and Titanium", WAPD-T-176. (Contr. AT-11-1-GEN-14). 13 p.

77. Michels, Walter C. and Wilford, Sally, "The Physical Properties of Titanium. I. Emissivity and Resisitivity of the Commercial Metal", J. Appl. Phys. Vol 20, pp 1223-6.

78. Weiner, L., Chiotti, P., and Wilhelm, H. A., "Temperature Dependence of Electrical Resistivity of Metals", US AEC Publ. ISC-305. 82 p. AD-18042.

79. Ames, S. L., and McQuillan, A. D., "Effect of Addition Elements on the Electrical Resistivity of α-Titanium", Acta Met. Vol. 4, pp. 619-26.

80. Baldwin, G. J., Shilts, J. L., and Coomes, E. A. "Temperature Scale for Molybdenum", Notre Dame U., Ind., (Contract Nonr-162300). 18 p.

81. Glaser, Frank W., Arbiter, William, Ford, Michael J., and others, "Cemented Borides (an Appendixes I thru IV)", Summary Prog. Rept. USN Contr. No. N6-ONR-256. 146 p.

82. Legvold, S. and Spedding, F. H., "Magnetic and Electrical Properties of Gadolinium, Dysprosium, and Erbium Metals", Revs. Mod. Phys. Vol. 25. pp. 129-30.

83. Domenicali, Charles A., "Research in Thermoelectricity", Quarterly Progress Report (Contract DA 36-039-sc-15460) (Rept. No. P. 2292-4) AD-5400. 9 p.

84. Meechan, C. J. and Eggleston, R. R., "Formation Energies of Vacancies in Copper and Gold", Acta Met. Vol. 2. pp. 680-3.

85. Pawlek, Franz and Reichel, Karl, "The Effect of Impurities on the Electrical Conductivity of Copper. I. The Electrical Conductivity of Pure Copper, Its Maximum Value, and Its Variations with Impurities", Z. Metallkunde. Vol. 47. pp. 347-56 (Germany)

86. Los, G. J. "Resistance and Magneto-Resistance of Dilute Alloys of Copper and Gold with Nickel at Low Temperatures", Physica, Vol. 23. pp. 633-40 (Holland)

87. White, Guy K., and Woods, S. B., "Thermal and Electrical Conductivities of Solids at Low Temperatures", Can. J. Phys. Vol. 33, pp. 58-73 (Canada)

88. Sims, C. T., Craighead, C. M., et al., "Investigations of Rhenium", WADC-TR 54-371, suppl. 1, (Contr. AF 33(616) 232)PB 121653, AD 97301. 86 p.

89. White, G. K. and Woods, S. B., "Low-Temperature Resistivity of the Transition Elements: Cobalt, Tungsten, and Rhenium", Canad. J. Physics. Vol. 35, pp. 656-65 (Canada)

90. Malter, L. and Langmuir, D.B., "Resistance Emissivities, and Melting Point of Tantalum", Phys. Rev., 55, p. 743 (1939)

91. Skinner, G. B., Edwards, J. W., and Johnston, H. L., "Vapor Pressure of Inorganic Substances. V. Zirconium between 1949 and 2054 $^{\circ}$K", J. Am. Chem. Soc., Vol. 73. pp. 174-6

92. Chupka, W. A., Berkowitz, J. and Inghram, M. G., "Thermodynamics of the Zr-ZrO$_2$ System; The dissociation Energies of ZrO and ZrO$_2$", In cooperation with Argonne Natl. Lab., Lemont, Ill. Sponsored by OOR. AD 107 062. 12 p.

93. Skinner, G. B., and Johnston, H. L., "Thermal Expansion of Zirconium between 298°K and 1600°K", J. Chem. Phys. Vol. 21. pp. 1383-4.

94. Rentschler, Russel R., "Determination of Thermal Expansivity of Zirconium Hydride", Air Force Institute of Techn., Air University, Master's Thesis. 48 p.

95. Adenstedt, H. K., "Physical, Thermal, and Electrical Properties of Hafnium and High-purity Zirconium", Am. Soc. Metals Preprint. (1W). 19 p.

96. Domenicali, C. A. and Otter, F. A., "Thermoelectrical Resistivity of Dilute Alloys of Silicon in Copper, Nickel, and Iron", J. Appl. Phys. Vol. 26., pp. 377-80.

97. Broom, T., "The Effect of Temperature of Deformation on the Electrical Resistivity of Cold-Worked Metals and Alloys", Proc. Phys. Soc. Vol. 65B. pp. 871-81 (London)

98. Schindler, A. I., Smith, R. J., and Salkovitz, E. I., "The Electrical Resistivity of the Ni-Pd Alloy System between 300°K and 730°K", NRL Rept. No. 4974 AD 138 499. 6 p.

99. Hugon, Lionel and Jaffray, Jean, "The Thermal Conductivity of Nickel above and below the Curie Point", Ann. Phys. Vol. 12. pp. 377-85 (French)

100. Thomas, Han, "Resistance Alloys", Z. Physik. Vol. 129. pp. 219-32 (Germany)

101. Smith, Jr., Wm. T. and Oliver, G. D., "Thermodynamic Properties of Technetium and Rhenium Compounds. IV. Low Temperature Heat Capacity and Thermodynamics of Rhenium", J. Am. Chem. Soc. Vol. 75, pp. 5785-6.

102. Mikryukov, V. E., "Thermal and Electric Properties of Copper Alloys", Vestnik Moskov. Univ., Ser. Mat., Mekh., Astron., Fiz. i Khim., Vol. 11 (2). pp. 53-70 (USSR)

103. Goglia, M. J., Hawkins, G. A., and Deverall, J. E., "Determination of Thermal Conductivity of Copper and Deoxidized Copper-Iron Alloys, Apparatus and Technique", Analy. Chem. Vol. 24, pp. 493-6.

104. Mikryukov, V. E. and Rabotonov, S. N., "Thermal and Electrical Conductivities of Mono-and Poly-crystalline Substances from $100^{\circ}C$ to the Melting Point", Uchen. Zapiski Moskov Ordena Lenia Gosurdarst. Uni M. V. Lomonosova. Vol. 74. pp. 167-79 (USSR)

105. Skinner, Gordon B. and Johnston, Herrick L., "Low-Temperature Heat Capacities of Inorganic Solids. VIII. Heat Capacity of Zirconium from 14 to 300 $^{\circ}K$", J. Am. Chem. Soc. Vol. 73. pp. 4549-51.

106. Coughlin, J. P. and King. E. G., "High-temperature Heat Contents of Some Zirconium-containing Substances", J. Am. Chem. Soc. Vol. 72. pp. 2262-5.

107. Scott, J. L., "A Calorimeter Investigation of Zirconium, Titanium, and Zirconium Alloys from 60 to 960 $^{\circ}C$", ORNL-2328 Contr. No. W-7405-eng-26. AD 138 838. 122 p.

108. Bell, I. P. and McDonald, J. J., "Thermal Conductivity of Metals and Uranium Compounds -- A Review of Progress to Dec. 19, 1952", RDB(c)/TN-24. 10 p.

109. Moss, Marvin, "Apparatus for Measuring the Thermal Conductivity of Metals in Vacuum at High Temperatures", Rev. Sci. Instr. Vol. 26, pp. 276-80.

110. Francl, J. and Kingery, W. D., "Thermal Conductivity. IX. Experimental Investigation of Effect of Porosity on Thermal Conductivity", J. Am. Ceram. Soc. Vol. 37. pp. 99-107.

111. Powers, R. M. and Wilhelm, H. A., "The Titanium-Vanadium System", US AEC Publ. (ISC-228). 165 p. AD 18 838

112. Wahlin, H. B., Zenter, R. and Martin J., "The Spectral Emissivity of Iron-Nickel Alloys", J. Applied Phys. Vol. 23, pp. 107-8

113. Sully, A. H., Brandes, E. A., and Waterhouse, R. B., "Some Measurements of the Total Emissivity of Metals and Pure R fractory Oxides and the Variation of Emissivity with Temperature", Brit. J. Appl. Physics. Vol. 3 (3). pp. 97-101. (England)

114. Hagel, William C., Pound, Guy M., and Mehl, Robert F., "The Free-Energy Change of Austemite-Pearlite Transformations", Metals Research Lab., Carnegie Inst. of Tech., Pittsburgh, Pa. Contract DA 36-061-ORD-350, Project TB 2-0001 (534). 103 p. AD-39272

115. Krauss, Friedrich and Warncke, Heinz, "Specific Heat of Nickel between 180°-1160°C", Z. Metallkunde, Vol. 46, pp 61-69 (Germany)

116. Kubaschewski, Iswald, "Atomic Heats of Metals", Z. Metallkunde, Vol. 41, pp 445-451 (Germany)

117. Oelsen, Willy, Rieskamp, Karl Heinz and Oelsen, Olaf, "Thermodynamic Analysis" II. The Heat Capacity Curve of a Material from a Single Calorimetric Test", Arch. Eisenhiitenwesen, Vol. 26, pp 253-266 (Germany)

118. Masumoto Hakaru, Saito, Hideo and Takahaslu, Minoru, "The Anomaly of Specific Heat at High Temperatures in α-Phase Copper-Aluminum Alloys", Nippon-Kinzoku-Gakkai (J. Japan Inst. Metals) Vol. 18, pp 98-100 (Japan)

119. Edwards, J.W., Johnson, H.L., and Blackburn, P.E., "Vapor Pressure of Inorganic Substances. V. Tantalum between 2624°-2943°", Tch. Rept. No. 6 Ohio State Univ. Cryog. Lab. USAEC Publ. No. 1933, pp 15

120. Squire, C.F. and Kaufmann, R.R., "The Magnetic Susceptibility of Titanium and Zirconium", J. Chem. Phys. Vol. 9, pp 673-677

121. Edwards, J.W., Johnson, H.L., and Blackburn, P.E., "Vapor Pressure of Inorganic Substances. V. Tantalum between 2624°-2943°", Tch. Rept. No. 6 Ohio State Univ. Cryog. Lab. USAEC Publ. No. 1933, pp 15

122. Saller, H.A. and Dickerson, R.F., "Induction-Melted Zirconium and Zirconium Alloys", U.S. Atomic Energy Comm. BMI-908 pp 5-37 AD-29 367

123. Hidnert, P. and Krider, H.S., "Thermal Expansion of Some Copper Alloys", J. Research Nat. Bur. Stand. (Res. Paper No. 1838) Vol. 39 pp 419-421

124. Richards, J.W., "The Over-all Linear Expansion of Face-Centered Cubic Metals from Absolute Zero to their Melting Points", Univ. Microfilms (Ann Arbor, Mich.) Pub. No. 276, p 30

125. Esser, H. and Eusterbrock, H., "Investigation of the Thermal Expansion of Some Metals and Alloys with an Improved Dilatometer", Arch. Eisenhiitenwesen, Vol. 47, pp 519-526 (Germany)

126. "Kovar Alloy", Form #5134, The Carborundum Co., Refractories Division, Latrobe, Pa. (1958)

127. "Kovar Alloy", Form #5134, The Carborundum Co., Refractories Division, Latrobe, Pa. (1958)

128. "Thermal Conductivity of Kovar Alloy", File Ref. 100 EBS, The Carborundum Co.

129. Thornburg, D.L., Thall, E.S., and Brous, J., "A Manual of Materials for Microwave Tubes", WADD Technical Report 60-325, 1961

130. Smithells, C.J., "Metals Reference Book", Butterworth's Scientific Publications, London (1955)

2.3 Processing of Emitter Materials

Great care should be taken in ordering refractory materials for use in thermionic converters. The "electron tube grade" materials classification usually indicates the highest grade of commercially available material. At the insistence of the electron tube industry, the metals suppliers have developed more stringent standardization and processing methods for tube grade materials than for other commercial applications. It is fairly certain that material ordered to electron tube standards will be the same (within limits) on different orders. However, it must not be assumed that absolutely pure material is being purchased. As the table below indicates, even the highest purity materials generally available contain gases and low vapor pressure constituents that must be removed or at least reduced in quantity before they can be used in a thermionic converter.

Another factor which is often overlooked is the problem of impurities which may be introduced in a relatively pure material during a fabrication process. The process of sawing a piece from a bar of molybdenum can introduce iron impurities from the saw blade. The iron impurity content in a small piece of sawed molybdenum may be as high as 2 percent.

Lubricants and other contaminants introduced to the metals during machining and handling operations must be removed by a series of processes involving chemical cleaning and vacuum firing at high temperature.

Typical impurity content of several clean "as received" refractory metals is shown below. Electron beam and arc melted stock have substantially lower impurity levels than average melts, as is shown in Table 2-I for tantalum and molybdenum (Ref. 1).

The adverse effect of gaseous impurities on thermionic measurements has been known for some time (Ref. 2). Metallic impurities such as silicon, iron, and chromium are certain to evaporate from the emitter during converter operation, if not correctly processed.

TABLE 2-I

COMPARISON OF IMPURITY CONTENT FOR VARIOUS GRADES OF TANTALUM AND MOLYBDENUM

Tantalum		Arc Melted Tantalum		Molybdenum		Arc Melted Molybdenum	
Cb	.020%	Cb	.01 %	W	.01 %	Ir	.010%
Si	<.010%	Si	.03 %	Si	.03 %	Ni	.002%
H_2	.001%	H_2	.001%	Fe	.06 %	Si	.008%
N_2	.005%	N_2	.005%	Co	.01 %	O_2	.0015%
O_2	.020%	O_2	.015%	H_2	.001%	H_2	.0005%
C	.030%	C	.005%	N_2	.002%	N_2	.002%
Others Fe, Ni, Cr, Ti,Cu <.004% each		Others Fe, Ti, Al .005% each		O_2	.05 %	C	.04 %
				C	.03 %	Mo	99.9%
Ta	99.8% approx.	Ta	99.9%	Mo	99.8% approx.		

Recently, original impurity elements have been recovered from converter collectors during post-operation examination (Ref. 3). Their presence could well affect device efficiency by altering the collector emissivity.

The critical point in processing is control of the process. . Vacuum degassing requires a vacuum of 5×10^{-6} mm Hg or better, with a minimum of hydrocarbon residual background present. Hydrocarbon compounds have an extremely deleterious effect upon refractory materials such as tantalum. Figure 2-91 illustrates the formation and diffusion of tantalum carbide in an emitter structure as a result of vapor back stream from an improperly trapped oil diffusion pump.

Hydrogen firing where applicable is also a processing technique to consider. The hydrogen must have a minimum water vapor content in order to allow the reduction of surface oxides. Dew points of -70°C are not uncommon in the practice of hydrogen brazing and firing. Such low dew points may be achieved in a number of ways, among which is routing the hydrogen over hot zirconium chips or molten sodium.

Five promising emitter materials are listed below and discussed from a processing standpoint. The investigators in the materials processing field differ widely on technique (probably due to the wide variety of applications). Ballpark numbers will have to suffice at this time.

2..3.1 Tungsten

Some oxides of tungsten are tenacious even at temperatures as high as 1900°K. Most workers (Refs. 4 and 5) favor outgassing of tungsten at 2000°C and above. Knoll (Ref. 6) prescribes a "preoutgas" treatment of 1800°C for eight hours before final assembly. WADD report No. 60-325 page 185, recommends an outgas of 800°C - 1000°C for 10 to 30 minutes. This is substantially hower than any other source. Trappnel (Ref. 4) notes that silicon outgases efficiently from tungsten at 2130°C. In fact, of the common metal impurities found in tungsten, chromium has the highest melting point at about 1900°C.

Langmuir (Ref. 7) established that the temperature for thermal aging tungsten necessary to yield reproducible cesium adsorption

FIG. 2-90   EXAMPLES OF CARBIDE FORMATION IN TANTALUM

data was $2800^{\circ}K$. At this temperature the tungsten surface atoms are mobile, the dislocations are homogeneously distributed, and all impurities from the metallic matrix are removed.

For device applications a temperature of $2600^{\circ}K$ and a pressure of 1×10^{-6} mm Hg or better are recommended. The firing time should be on the order of 1 hour.

2.3.2 Molybdenum

The gases removed from molybdenum upon degassing are reported (Ref. 5) to contain 60 percent nigrogen, 15 to 36 percent CO, 3 to 65 percent CO_2, and a negligible amount of hydrogen. Some investigators have reported that the process of first hydrogen firing and then vacuum outgassing facilitates the removal of the oxide layers from molybdenum. It is recommended that molybdenum be vacuum outgassed at approximately $1900^{\circ}C$ at 1×10^{-6} mm Hg or better. The treatment should remove all gaseous and metal impurities in a matter of 20 minutes to one hour.

2.3.3 Tantalum

Tantalum has received a great deal of attention as a getter in vacuum tubes. It forms extremely stable oxides and nitrides, and absorbs hydrogen readily. It has been specifically inserted in some converters and operated at the proper temperatures to better evolve gases (Ref. 8). Gebhardt and Preisendanz (Ref. 9) have out-gassed tantalum at 2600° to $2800^{\circ}C$ at 5×10^{-6} mm Hg to remove all oxygen. They report that at 2200°-$2300^{\circ}C$ not quite all oxygen is removed. Hydrogen is effectively removed from tantalum by heating in vacuo at $1000^{\circ}C$. Hydrogen is known to embrittle tantalum and is used as a processing technique at high temperatures. For practical converter applications it is recommended that tantalum be outgassed at 2300° to $2400^{\circ}C$ at 1×10^{-6} mm Hg or lower for approximately one hour.

2.3.4 Rhenium

Rhenium, because of its cost and limited commercial availability, has been mentioned only briefly in the processing

literature. WADD report No. 60-325 recommends hydrogen firing and vacuum outgas at 2000°C or higher (Ref. 10).

No recommendations are made concerning this material.

2.3.5 Iridium

No recommendations are made concerning this material.

The bulk of the thermal-physical properties and processing techniques for iridium have yet to be developed.

2.3.6 General Remarks

Generally, a rule of thumb for processing converter materials is to outgas at temperatures at least 400° to 500°C higher than the highest intended temperature of operation. This is only approximate since, in the case of molybdenum, which is to be used for a collector, it would be preferable to vacuum outgas the material at about 1800°C for at least 20 minutes even though the collector temperature during operation might not exceed 900°C.

The time at temperature during the outgassing procedure is governed by at least two considerations. The first consideration involves the bulk diffusion time of impurities in the material. An emitter material which is to operate in a device for many thousands of hours may have to be outgassed for a considerably longer period than usual in order to allow sufficient time for the impurities in the bulk of the material to diffuse to the surface and evaporate.

The second consideration has to do with grain growth in converter materials. In some cases, too much of a good thing (very long time at very high temperature) during outgassing may actually be detrimental to satisfactory converter operation. The subject of the effect of grain growth on the electronic operation of a converter is only now being investigated.

The presence of oxygen and nitrogen in materials which are to be joined by welding inevitably leads to weld embrittlement in the fabricated assemblies. This subject is discussed more fully in the text concerning fabrication.

REFERENCES

Section 2.3

1. Haynes Stellite, Kawecki Chemical, and Climax Metals data sheets.

2. S. Dushman: Rev. Mod. Phys. $\underline{2}$ 381-476 (1930).

3. EOS 1850 Test - Final

4. B. M. W. Trapnell: Chemisorption, Butterworths Scientific Publications, London (1956).

5. F. J. Norton and A. L. Marshall: "The Degassing of Metals," Trans. Am. Inst. Mining Met. Engrs., $\underline{156}$ 351-371 (1944).

6. M. Knoll, Springer - Vertag, Berlin (1959).

7. J. B. Taylor and I. Langmuir, Phys. Rev. $\underline{44}$ (1933).

8. Thermal Electron Engineering Corporation, TEE-4015-1.

9. E. Gebhardt and H. Preisendanz, Z. Metallkunde $\underline{46}$, 560-568 (1955).

2.4 Fabrication of Converter Materials

This section deals with fabrication techniques that are applicable to the joining of high-temperature thermionic converter materials. For the usual case where the joints must be vacuum tight, there are four common techniques available to effect this joining of materials. Specifically, these techniques are:

1. Electron beam welding
2. Tungsten inert gas welding
3. Brazing
4. Vapor deposition

Each of these techniques will be discussed in the following pages with the emphasis being placed upon the elements of the technique, the major area of application of the technique to converter fabrication, and the advantages and disadvantages of each particular technique. It should be emphasized from the outset that there probably is no one particular technique which is _the_ correct technique for the joining of materials in a thermionic converter. Each technique has its specific areas of application and in many cases where a method of joining is inadequate in one region of a converter it may well be the most effective joining method for another region of the converter.

2.4.1 Electron Beam Welding

2.4.1.1 Elements of the Technique

In the most elemental sense the method of electron beam welding involves three components. These components are an electron gun, a vacuum environment of approximately 10^{-6} mm Hg, and the workpiece to be welded. In essence the electron gun furnishes a well focused electron beam of energy of the order of 25 kv to 150 kv. The workpiece serves as the anode or collector for the electron beam. Energy densities of approximately one megawatt per square centimeter can be achieved on the workpiece with such a scheme. These energy densities are sufficient to melt even the very high temperature refractory materials such as tungsten. Since the electron beam is very well defined, the energy

density is very high, and the dwell-time on a particular area of the joint is very small, welds can be achieved that have very small heat-affected zones. Minimization of the heat-affected zone in a weld usually leads to a much stronger weld joint.

The technique of electron beam welding is very effective when the joint possesses cylindrical symmetry, or is of a linear nature. There are a number of companies in the United States today that are developing techniques for the electron beam welding of refractory materials. Because the electron beam welding process is reasonably novel from a commercial viewpoint, the results achieved by job-shopping small precision parts to these companies is often disappointing. The vacuum welding environment used by many of these companies leaves a great deal to be desired. It is not unusual to find companies operating an electron beam welding apparatus in a vacuum chamber which is evacuated by an oil diffusion pump without a cold trap. In such situations refractory metals such as tantalum and tungsten develop carbide layers in the vicinity of the weld zone. The refractory carbides are almost impossible to remove in subsequent cleaning operations. In the event that vendors must be used to fabricate parts by the electron beam welding method, careful examination of the capabilities of the company doing the work is advisable.

2.4.1.2 Major Area of Application to Converter Fabrication

Considering the rather extensive apparatus and jigging required to make an electron beam weld, it is possible that the only joint which merits such a weld in a thermionic converter is the envelope-to-emitter joint. This is the only joint in a thermionic converter that operates at temperatures which are too high for usual brazing techniques. This joint may sustain an excessive heat-affected zone and loss of mechanical strength if fabricated by tungsten inert gas techniques. In a practical sense, there have not been enough vacuum tight, high temperature structures fabricated by the electron beam welding technique to fully assess its applicability to converter technology.

2.4.1.3 Advantages and Disadvantages of Electron Beam Welding

Perhaps the main advantage of electron beam welding is a result of the high vacuum environment which is required for the process. If properly done, this technique has the potential of introducing a minimum of contaminants to the weld joint. In addition, the joint should be capable of operation up to the melting temperature of the structural metals. The latter fact presents a distinct advantage over techniques such as brazing, in which a relatively low melting point braze alloy usually limits the maximum operating temperature for the joint. Other than cost and availability, the most serious disadvantage of electron beam welding is involved with control of the electron beam welder. It has been found in practice that perhaps the most important component of the electron beam welding apparatus is an experienced technician who knows how to operate the apparatus in a consistent manner. Even in the event that such a technician is available, much time and money is required to acquaint him with the idiosyncrasies of a specific design. In conclusion, it would appear that the process of electron beam welding has the potential of becoming a superior fabrication technique for thermionic converter application. At this time, however, the cost, availability, and control of such a welder prohibit widespread application of the technique to small one-of-a-kind development projects.

2.4.2 Tungsten Inert Gas Welding

2.4.2.1 Elements of the Technique

Tungsten inert gas welding has been used for many years in the electron tube industry for the joining of refractory metals. Essentially three elements are involved in this technique of joining:

1. An inert atmosphere, such as helium
2. The piece to be welded
3. A tungsten electrode

In operation an arc is struck between the tungsten electrode and the joint to be welded. The heat developed by

the arc is sufficient to melt one or both of the materials to be joined. The technique is relatively simple and has been in widespread use for production joining of stainless steels, molybdenum tubing, zircalloy, and other high temperature refractory metals.

In the welding of stainless steel by the tungsten inert gas method, a shielded arc may be used. The shielded arc depends upon the shielding effect of a stream of inert gas blowing on the weld area to prevent oxidation of the weld. While such a technique has been found satisfactory for stainless steels, it is not adequate for the refractory metals such as tantalum or tungsten. Inert arc welding of these refractory metals requires a drybox containing an appropriate inert gas atmosphere having very low levels of oxygen, nitrogen, and hydrogen impurities. Inert arc welds of refractory metals utilizing the latter technique have been found to be quite satisfactory.

2.4.2.2 Major Area of Application to Converter Fabrication

The process of tungsten inert arc welding can be used for joining in every area of a thermionic converter except the metal ceramic seal region. This method has been successfully used to join molybdenum to molybdenum, tantalum to molybdenum, and tantalum to tantalum, to mention a few specific cases. In no case, where a proper environment and jigging procedure has been used, has this method failed to produce successful joints. This method has been used to successfully join a tantalum envelope to a molybdenum emitter slug which was subsequently operated for many hundreds of hours in a cesium vapor environment without failure. The temperature of the tantalum-molybdenum joint was 1530°C during operation. It remains to be seen whether this technique will prove adequate for emitter to envelope joint temperatures in the region of 1700° to 1800°C. The technique has also been used to join the cesium reservoir to the collector structure and the metal seal flanges to the collector and emitter structures.

2.4.2.3 Advantages and Disadvantages of the Tungsten Inert Gas Welding Method

One of the major advantages of the tungsten inert arc welding method for the fabrication of thermionic converter substructures

is that the method is relatively cheap and easy to apply. The technique requires a small investment in a controlled atmosphere chamber and welding power supplies which is a fraction of that required for electron beam welding. The skill and training required for operation of the tungsten inert gas technique is also small in comparison to that required for electron beam welding.

There are two major disadvantages associated with the tungsten inert gas welding technique. The first concerns the environment in which the weld is made. Very great care must be exercised to assure the absence of oxygen, nitrogen, and hydrogen impurities in the inert atmosphere. In the past, many methods have been proposed for the gettering of a drybox to assure the absence of these impurities. Some methods involve the heating of titanium ribbons, running an arc on zirconium metal, the use of desiccants, and various other materials effective for the gettering of oxygen, hydrogen, and nitrogen.

Probably the most effective method for achieving a pure inert atmosphere has been the use of alkali metal getters. Essentially the method consists of exposing liquid alkali metals, such as sodium, potassium, or a sodium potassium alloy, to the chamber atmosphere after the chamber has been baked out, evacuated, and thoroughly flushed with gas. When such a chamber is sealed for one or two days, it is usually found that the chamber atmosphere contains almost no oxygen, nitrogen, or hydrogen due to the gettering action of the liquid alkali metal.

Inert arc welds made in such an environment are clean and exhibit no oxidation or nitriding of the weld zone. Once the proper atmosphere has been established in the drybox with the technique, it becomes quite simple to make a continuous series of welds of high quality by introducing the parts through an evacuated airlock.

The second major disadvantage of the inert arc welding method involves grain growth in the weld zone of the joined materials. Because the area of heat application in this method cannot

be as carefully controlled as with the electron beam welding technique, a large region in the vicinity of the weld zone is brought to a temperature very close to the melting point of the participating materials. The high temperatures promote large grain growth in the weld region. Failure of inert arc welded joints at the joint during high temperature tensile tests is often attributed to this grain growth. It should be pointed out, however, that the occurrence of grain growth in the inert arc welding method need not necessarily be a limitation in the application of this technique to converter technology. The high operational temperatures which most converter components experience during life has a tendency to promote grain growth that is as large as that in the heat-affected zone in an inert arc weld.

2.4.3 Brazing

2.4.3.1 Elements of the Technique

Metals-joining by the process of brazing has received much attention in a number of industries for well over fifty years. Of all the methods of metals-joining which have been mentioned in this section, the process of brazing is in the most widespread use and has been most widely studied. In the elementary case, brazing reduces to a process of bonding two structural materials together with a metal brazing alloy that has a lower melting point than either of the structural members.

In this section discussion concerns only those brazes and braze materials that can operate for long periods at temperatures in excess of $600^{\circ}C$. This dispenses with all low melting point, high vapor pressure, soft solders such as tin-lead compounds, etc.

The brazing process reduces in its most elemental sense to the following:

1. The materials to be joined
2. A suitable braze material
3. An appropriate source of heat
4. A proper atmosphere

The discussion here will be limited to the brazing of fractory metal parts and to those brazes which are compatible with cesium vapor, which removes from consideration all braze alloys containing noble metals or compounds containing silica. Within this framework the brazing atmosphere is also specified, being limited to those atmospheres that do not react with refractory materials. In essence, the atmosphere may be pure noble gas, high vacuum (on the order of 10^{-6} mm Hg), or hydrogen where applicable.

Appropriate temperature on the joint to be brazed is most commonly achieved by radiofrequency induction heating, or by resistance heating. In the case of radiofrequency induction heating, induced currents in the workpiece may heat the joint directly, or induced currents may heat a susceptor can surrounding the workpiece, which heats the joint indirectly by radiation. The latter method is preferred because the workpiece is located in an isothermal oven.

The resistance heating method consists of surrounding the workpiece with a high temperature refractory metal heater which is shielded so that the workpiece is enclosed in an isothermal oven. The resistance heating method allows very careful control of brazing temperature and yields highly reproducible results.

The major disadvantage of the resistance heating method is that each different joint design which is to be brazed must have its own properly sized oven. The radiofrequency induction method, on the other hand, offers a very flexible heating unit for all conceivable sizes and shapes of work. It tends to require, however, much care in controlling temperature to achieve reproducible results.

One essential component of the brazing technique is an appropriate braze material. There are, however, techniques well known in the electron tube industry that require no braze alloy or only one braze shim of a pure metal. The technique is known as active alloy brazing or eutectic brazing. Two metals which are to be joined are placed in contact and brought to an appropriate temperature. The appropriate temperature is dictated by the temperature at which a low melting point eutectic is formed between the two materials to be joined.

One example of the method is the joining of rhenium to tungsten. Rhenium melts at approximately 3180°C; tungsten melts at approximately 3300°C. Yet when these materials are placed in contact and brought to a temperature of approximately 2800°C, a eutectic mixture between tungsten and rhenium is formed at points of contact and the mixture suffices to bond the materials. A phase diagram for the rhenium-tungsten system is shown in Fig. 2-91. In Figs. 2-92 through 2-96 are shown the phase diagrams for various nickel-refractory metal systems. It is of interest to note that several of the diagrams, such as the nickel-titanium, the nickel-niobium, and the nickel-zirconium phase diagrams, are useful not only in the metals-joining area but also in the metal-to-ceramic seal joining area. The eutectic mixtures formed in systems containing an active metal, such as zirconium, titanium, or niobium, are very active, and readily promote wetting of the structural members by reduction of oxides on the surface. This entire area of eutectic brazing as applied to practical electron devices was pioneered by J. E. Beggs of the General Electric Company.

Several other phase diagrams of interest are shown in Figs. 2-97 through 2-100. One interesting feature of the eutectic brazing method is that the braze is made at a temperature considerably below the melting point of any of the constituents of the system. This feature leads to brazes which are clean and do not tend to contaminate other regions of a device with evaporated braze material, as is the case when pure copper is used as a braze material.

2.4.3.2 Major Area of Application to Converter Fabrication

Except for eutectic brazing involving systems such as the rhenium-tungsten system shown in Fig. 2-91, brazing is not recommended for the emitter end of a thermionic converter. This is because the formation of alloys and eutectics between structural members involves diffusion of one material into the other. In the practical operation of a thermionic converter, such a high temperature braze
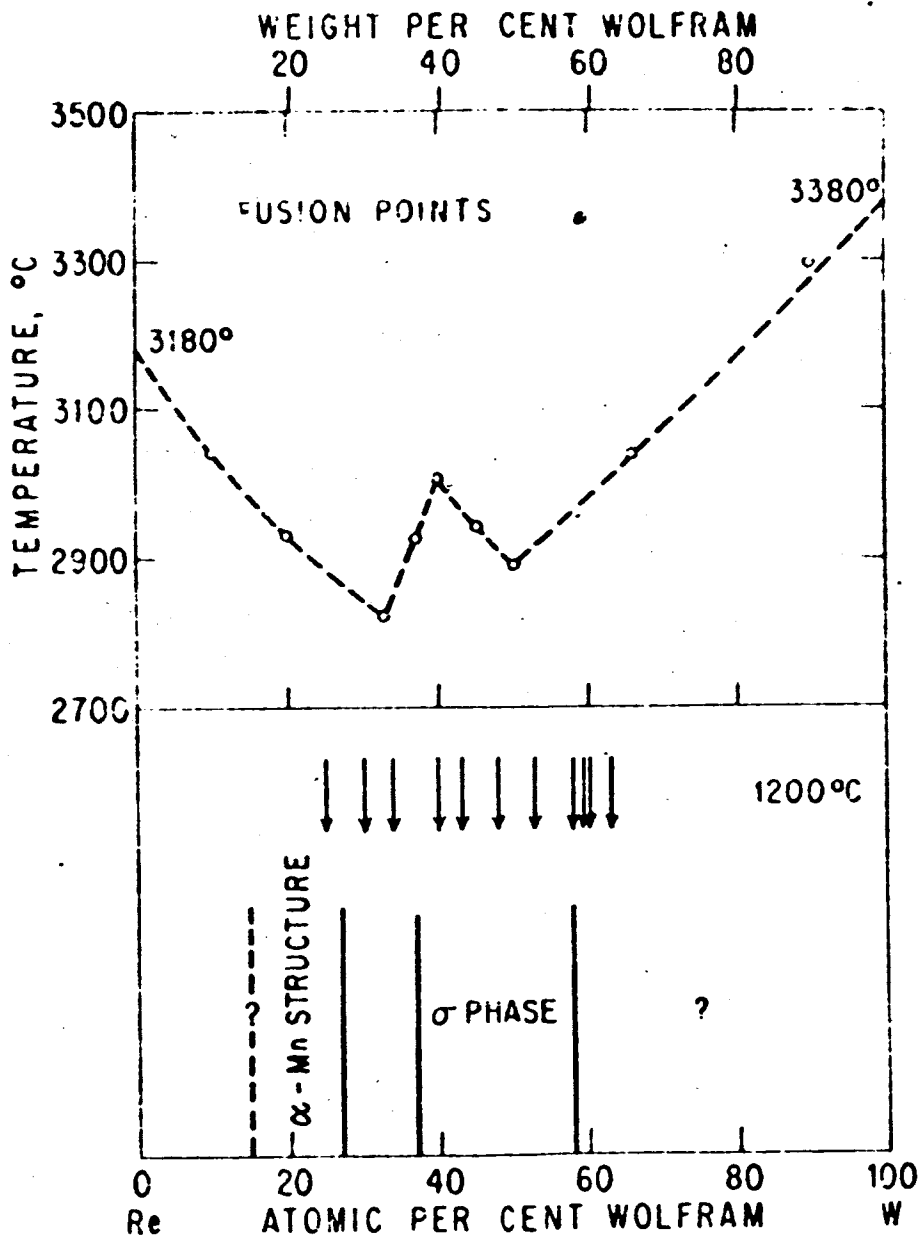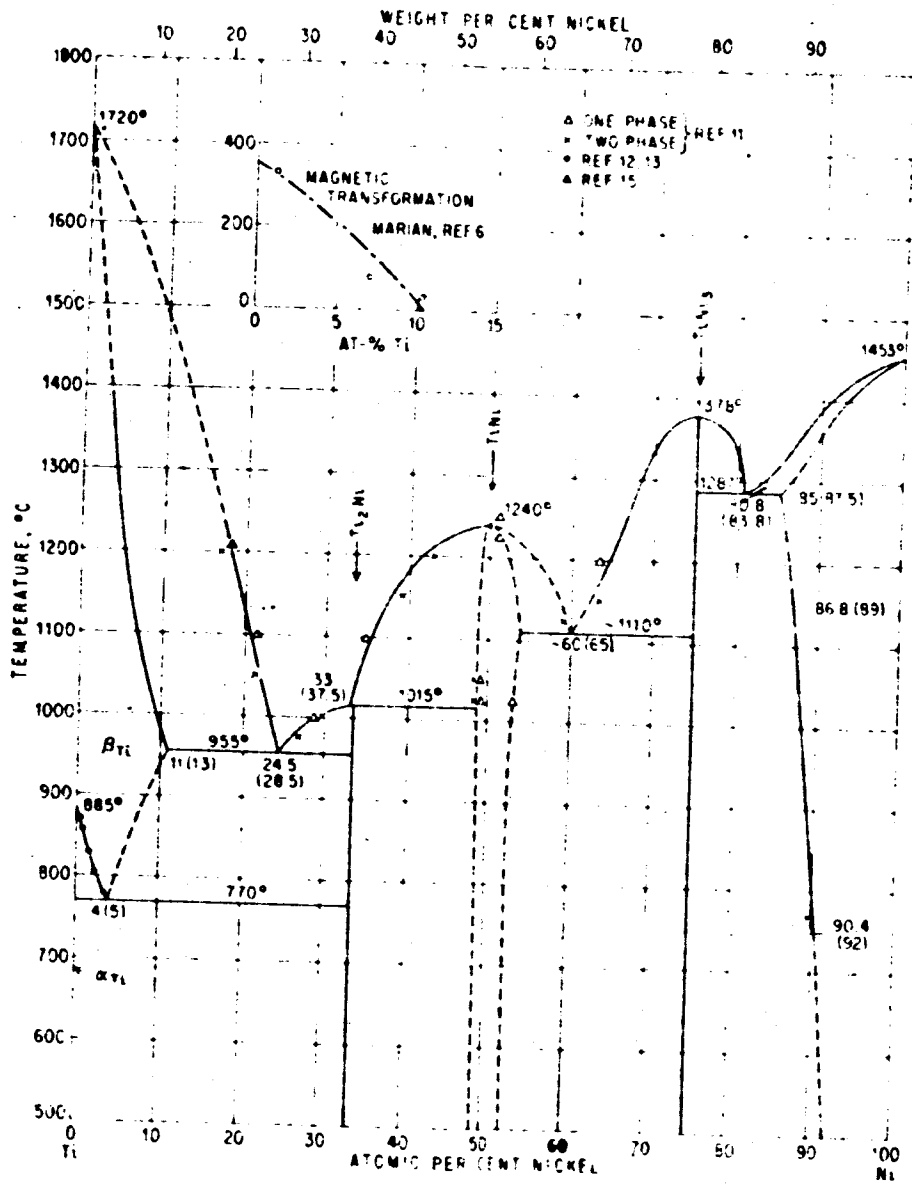
FIG. 2-91. Re-W PHASE DIAGRAM

FIG. 2-92 .   Ni-Ti PHASE DIAGRAM
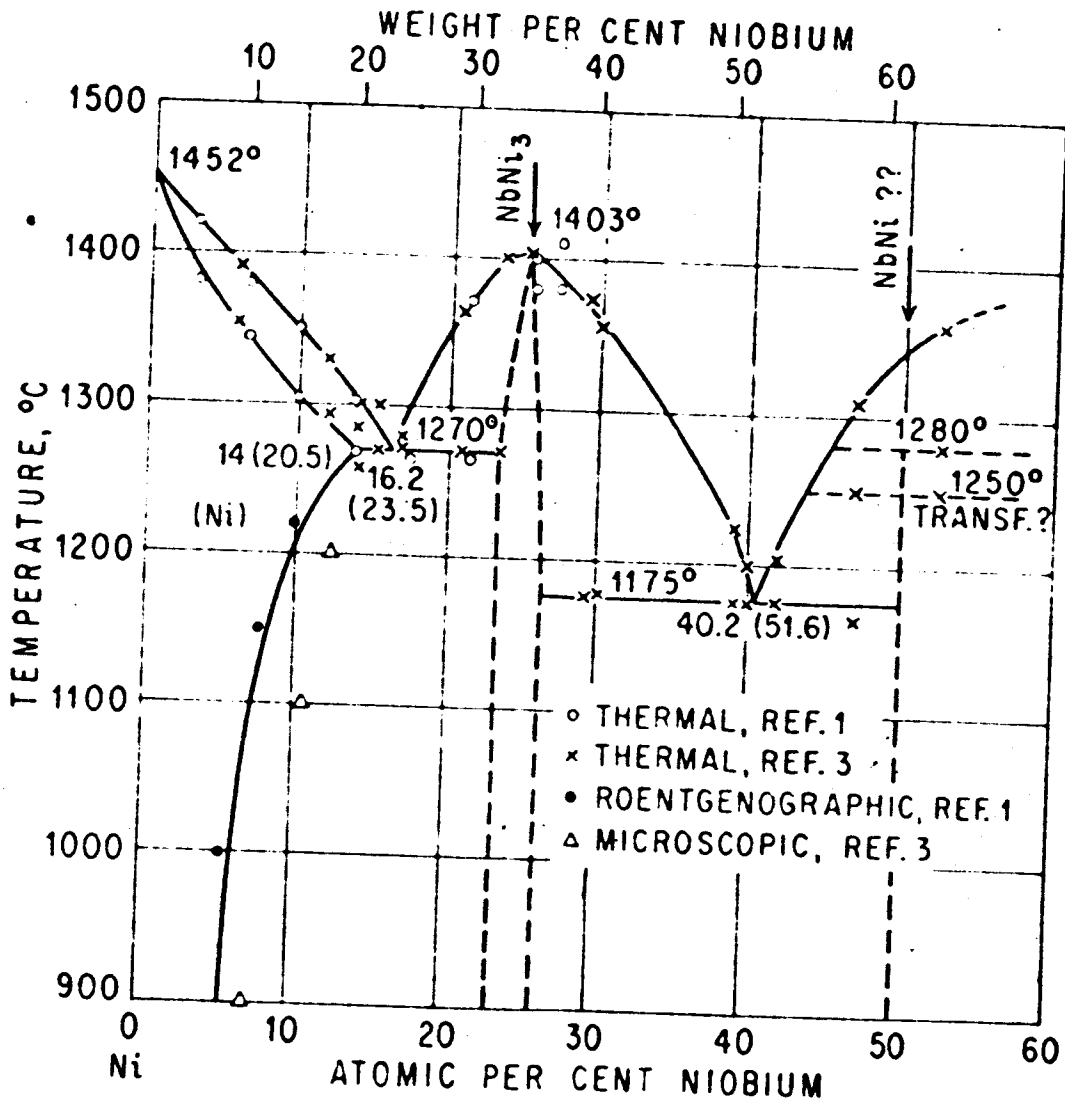
FIG. 2-93   Nb-Ni PHASE DIAGRAM
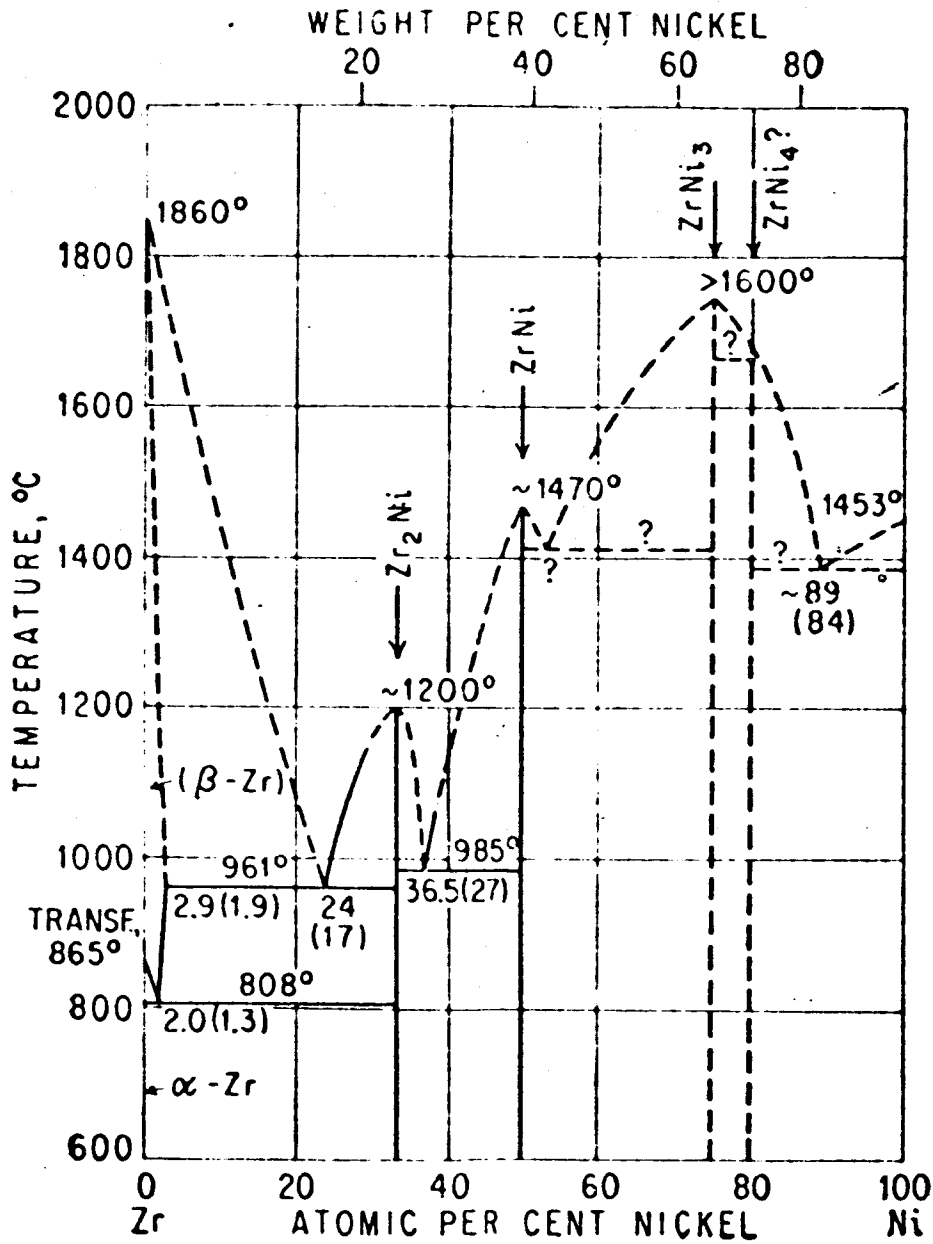
FIG. 2-94   Ni-Zr PHASE DIAGRAM
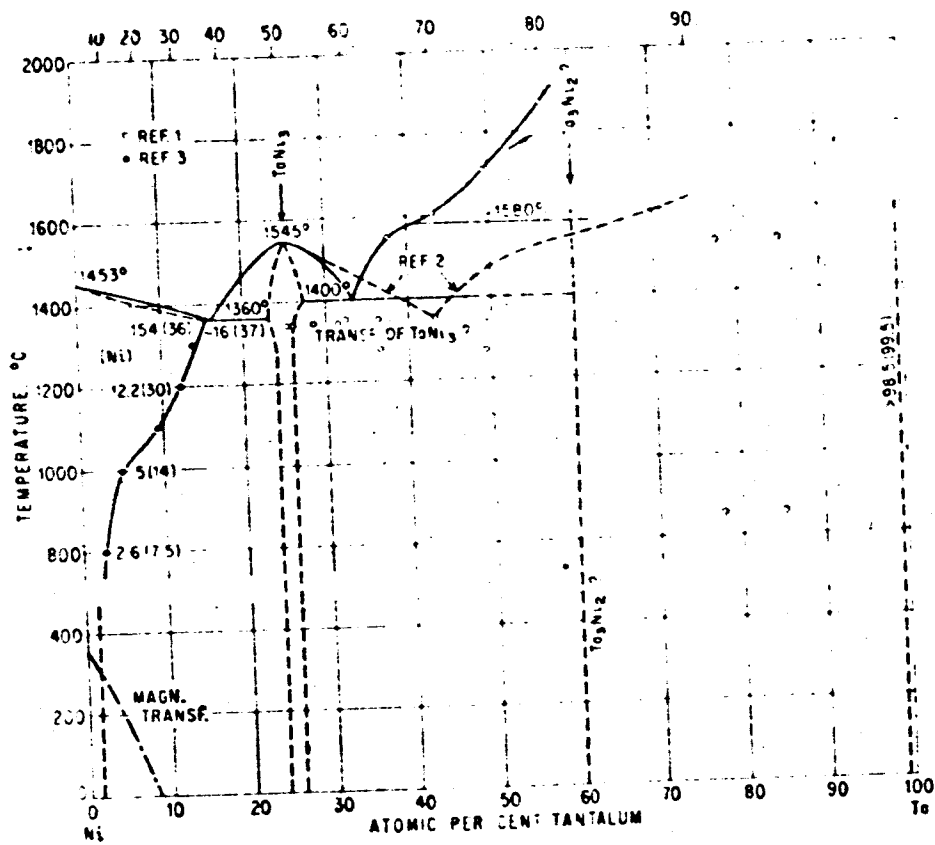
FIG. 2-95   Ni-Ta PHASE DIAGRAM
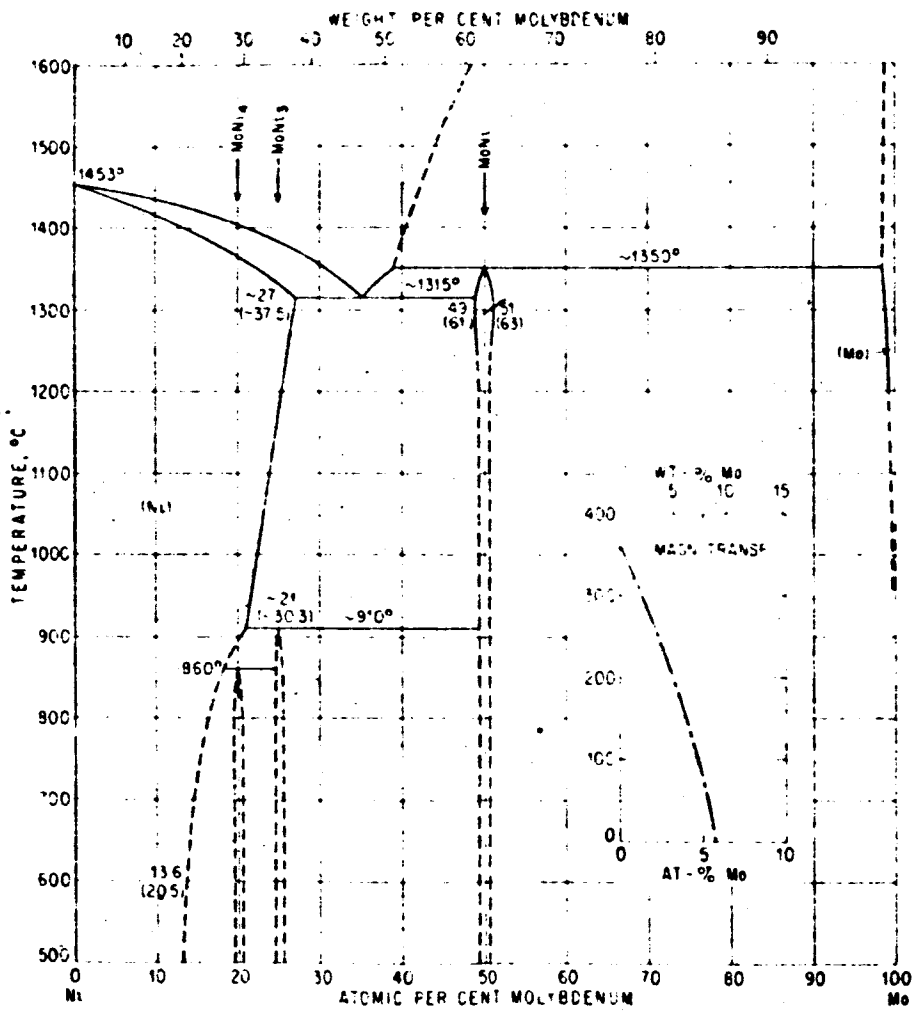
FIG. 2-96   Mo-Ni PHASE DIAGRAM
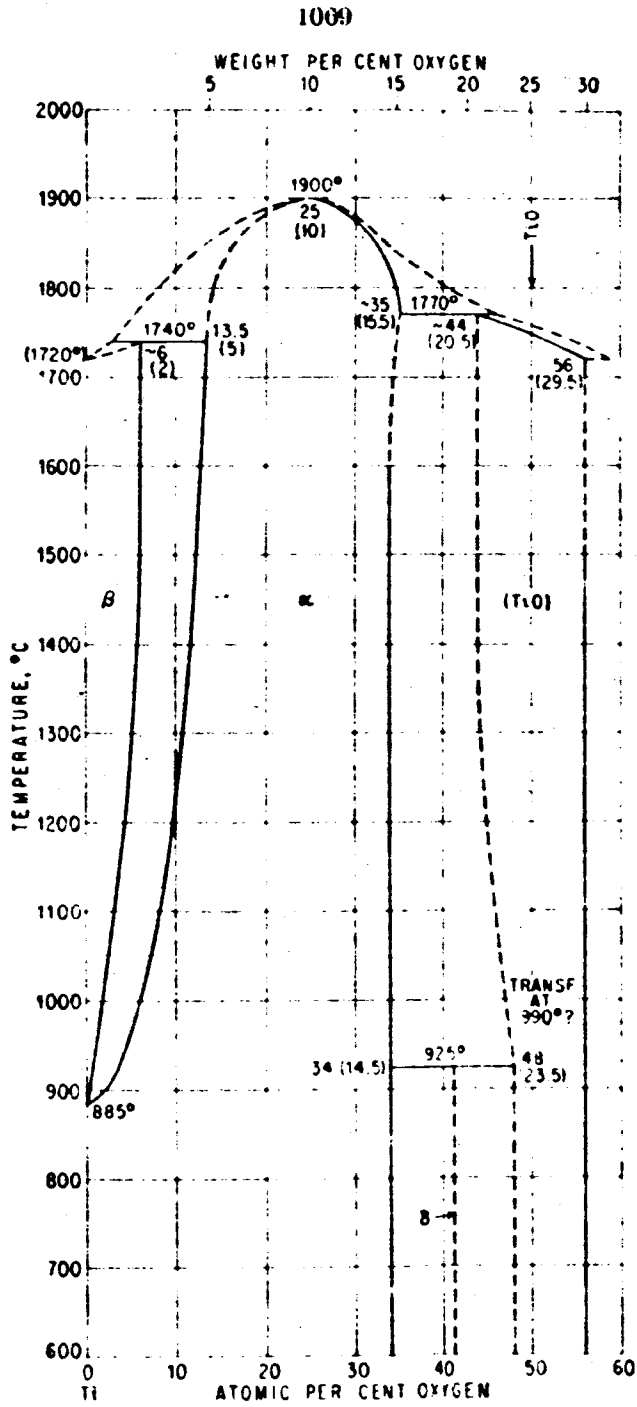
FIG. 2-97   Cu-Ti PHASE DIAGRAM
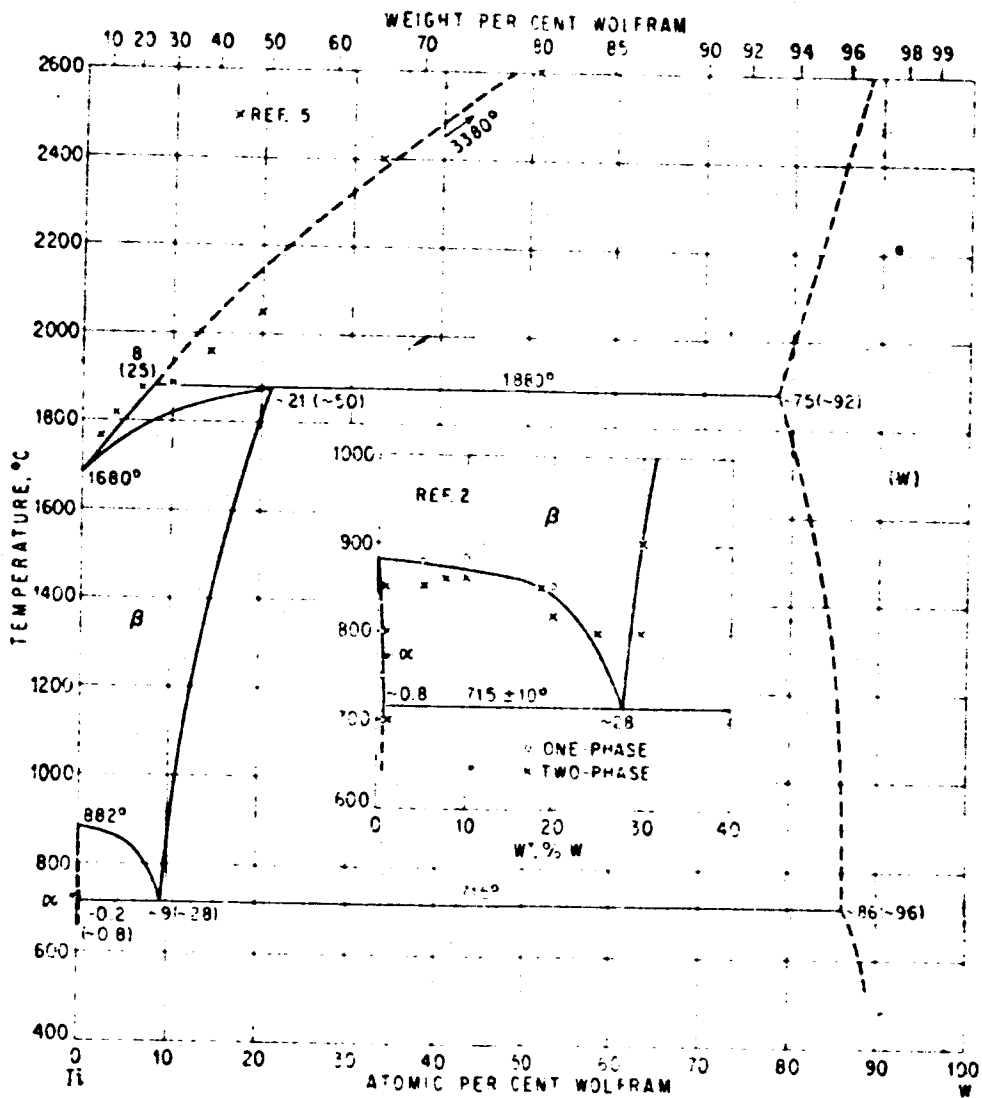
FIG. 2-98   Ti-W PHASE DIAGRAM
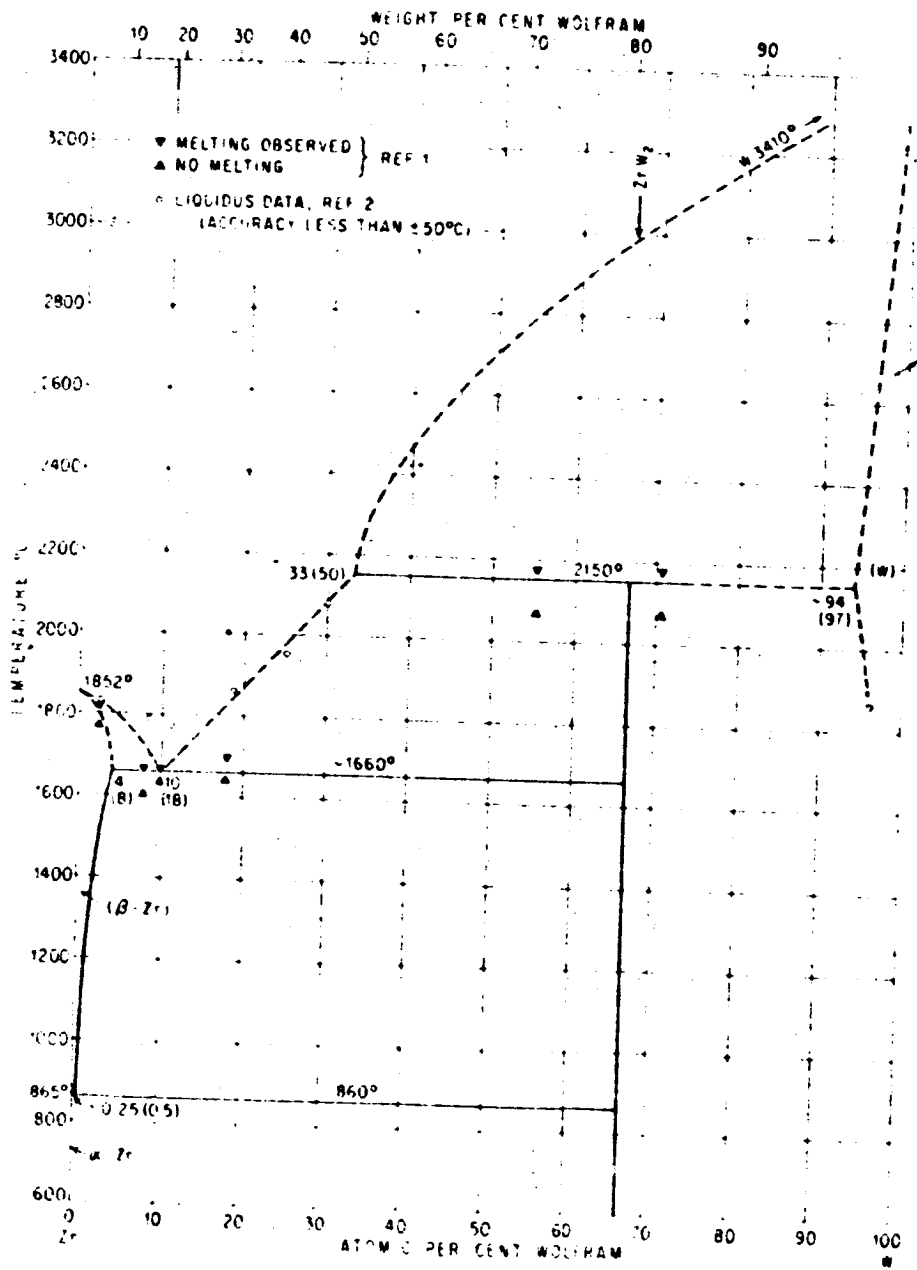
FIG. 2-99   W-Zr PHASE DIAGRAM
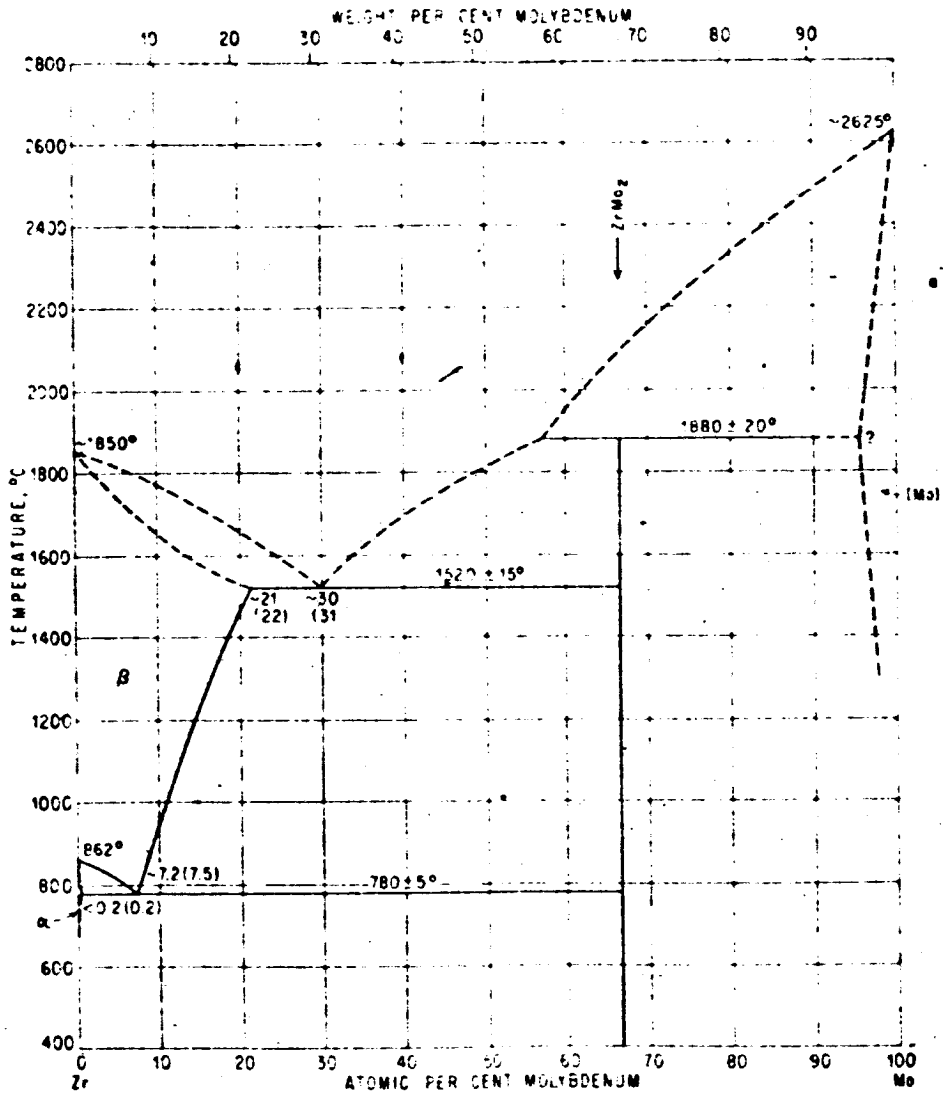
FIG. 2-100   Mo-Zr PHASE DIAGRAM

joint usually experiences embrittlement and/or diffusion of braze material from the braze zone. In general this leads to cracks or vacuum leaks and poor thermal impedance of the joint. The latter point dictates against brazes being used in a high temperature heatflow path.

The major area of application for brazing in the thermionic converter technology is in the collector region, the cesium reservoir system, and in the metal-to-ceramic seal area. These are areas where the operating temperatures do not exceed approximately $1000^{o}C$ to $1200^{o}C$. Even at these temperatures, material combinations and braze materials which have a tendency to diffuse must be excluded. A case in point is the system of nickel and tantalum, the phase diagram for which is shown in Fig. 2-95. Although the lowest melting point in the nickel-tantalum system is approximately $1360^{o}C$, there are a number of references in the electron tube literature to the rapid diffusion of nickel in tantalum at temperatures as low as $600^{o}C$. The net result of such diffusion is that the tantalum tends to become embrittled, and is subsequently subject to cracking along grain boundaries when subjected to thermal stresses. The same general considerations also hold for the molybdenum-nickel system shown in Fig. 2-96. In addition, molybdenum-nickel alloys tend to be very brittle and have expansion coefficients which are significantly different from both pure molybdenum and nickel.

2.4.3.3 Advantages and Disadvantages of Brazing

The main advantage of brazing in joining thermionic converter materials is that the method is well established, is reasonably simple, and can be made highly reproducible if proper care is taken. The main disadvantages of the method are the care required in the jigging of parts to be joined and the environment in which the braze is made.

When brazes are to be made to materials such as tantalum, niobium, and titanium, the partial pressure of oxygen in the brazing environment must be kept at a minimum. Figures 2-101 and
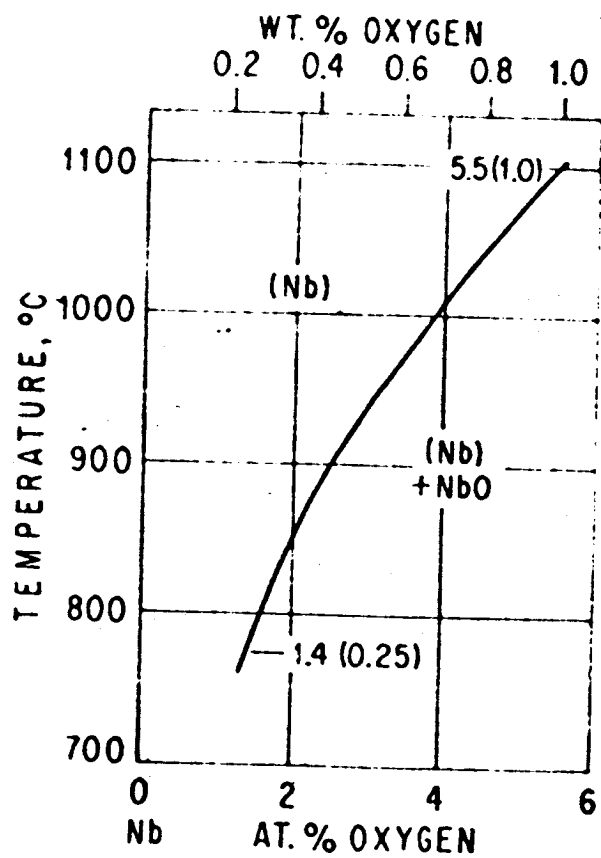
FIG. 2-101.   Nb-O PHASE DIAGRAM

2-102 show the phase diagrams for the niobium-oxygen and the titanium-oxygen systems, respectively. A small percentage of oxygen in these materials tends to produce embrittlement and outgassing during continued high temperature operation. Very large background pressures of oxygen, of course, lead to severe oxidation and almost catastrophic destruction of these materials.

A somewhat different case exists for the systems of tantalum and hydrogen, and titanium and hydrogen. The phase diagrams for these two systems are shown in Figs. 2-103 and 2-104. It will be noted that these materials are very active getters or can absorb large amounts of hydrogen in the temperature range from $500^{\circ}C$ to $1000^{\circ}C$. A practical use is made of this behavior in devices such as the hydrogen thyratron where a controllable hydrogen reservoir is made by enclosing titanium hydride, tantalum hydride, or zirconium hydride within a heater structure. Therefore the active refractory materials such as titanium, tantalum, zirconium and niobium should never be processed in a hydrogen environment if they are to be used subsequently in a high vacuum enclosure.

That other atmospheric gases, such as nitrogen, may be a problem is illustrated in Fig. 2-105, which shows the phase diagram for the nitrogen-titanium system. In general it might be pointed out that the nitrides of the refractory materials are usually much more stable than the oxides or the hydrides.

Perhaps the most critical part of the brazing procedure pertains to the question of time and temperature. During the brazing cycle, if the joint is not held at the braze temperature for a sufficient time to allow braze materials to diffuse and wet the surface, an unsound joint can result. On the other hand, if the joint is held too long at the brazing temperature, excessive diffusion of braze materials occurs, excessive evaporation of the braze material takes place, and structural members may be severely embrittled by the penetration of brazing alloy along the grain boundaries. The net result is
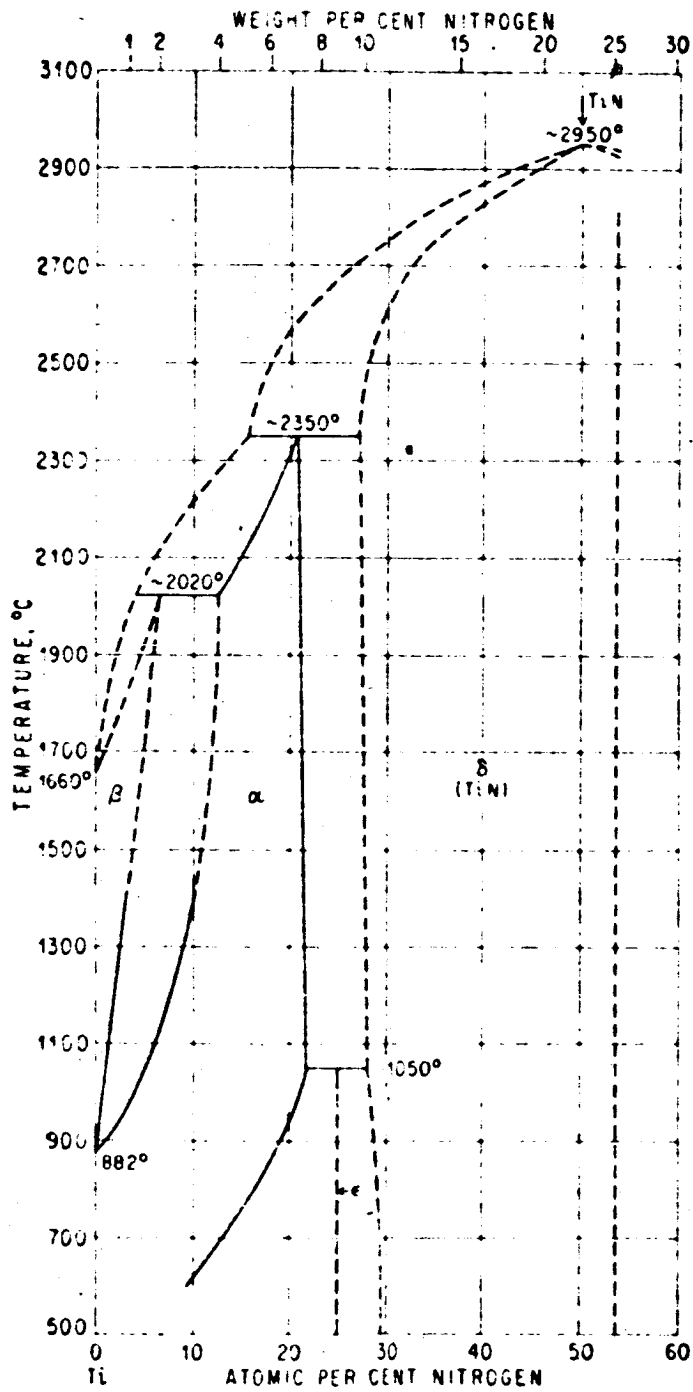
FIG. 2-102   O-Ti PHASE DIAGRAM
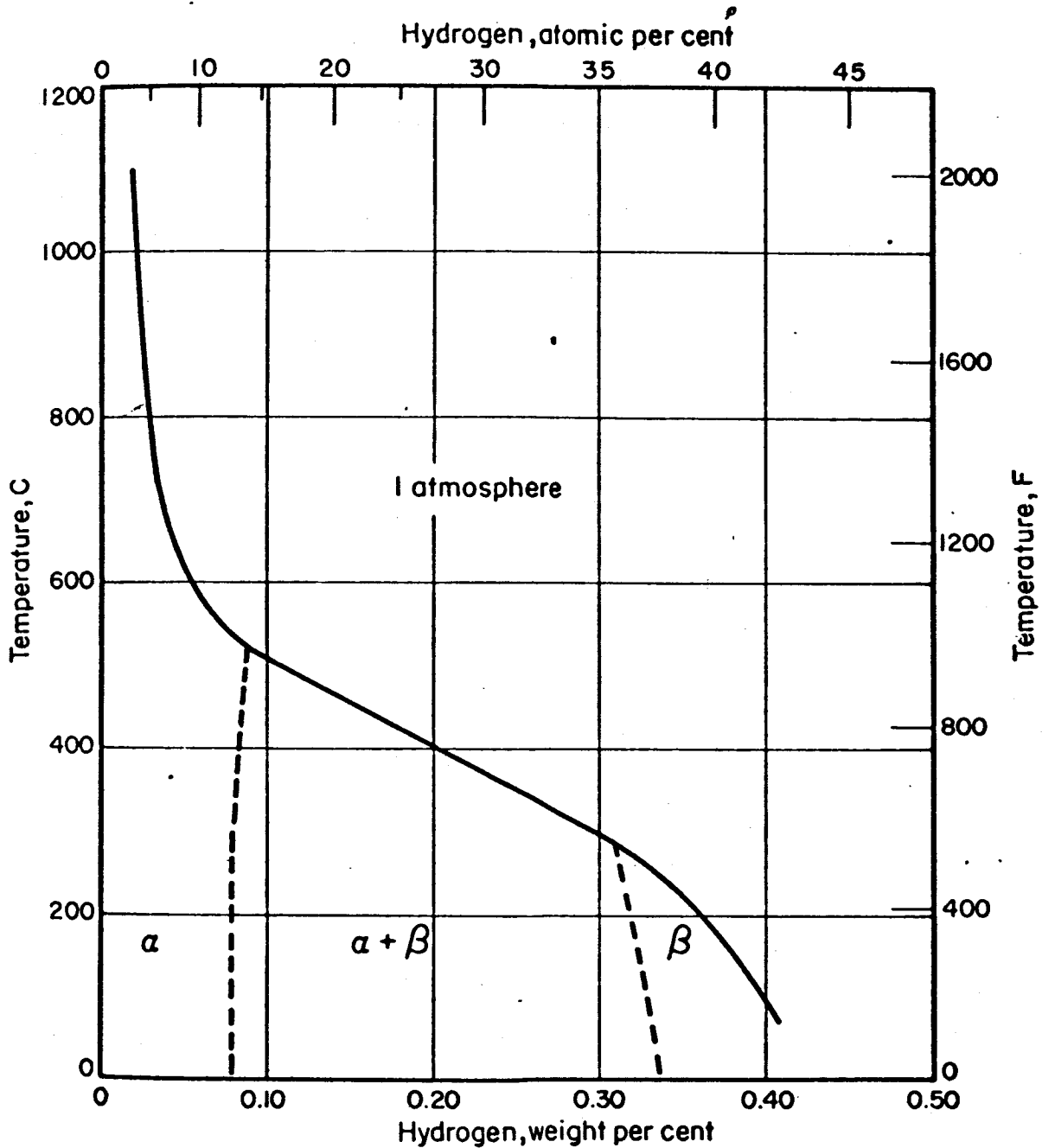
FIG. 2-103   CONSTITUTION DIAGRAM FOR THE SYSTEM TANTALUM-HYDROGEN
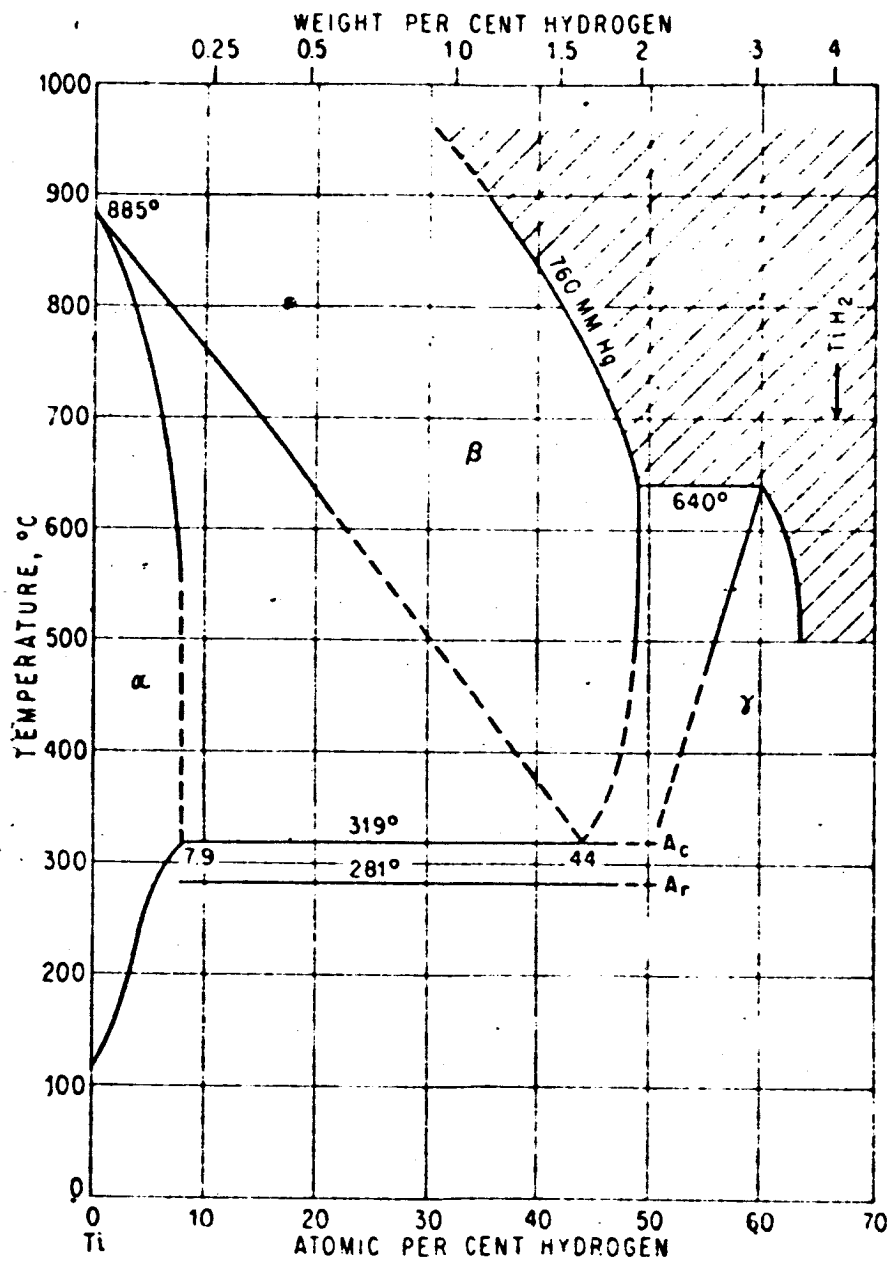
FIG. 2-104   H-Ti PHASE DIAGRAM
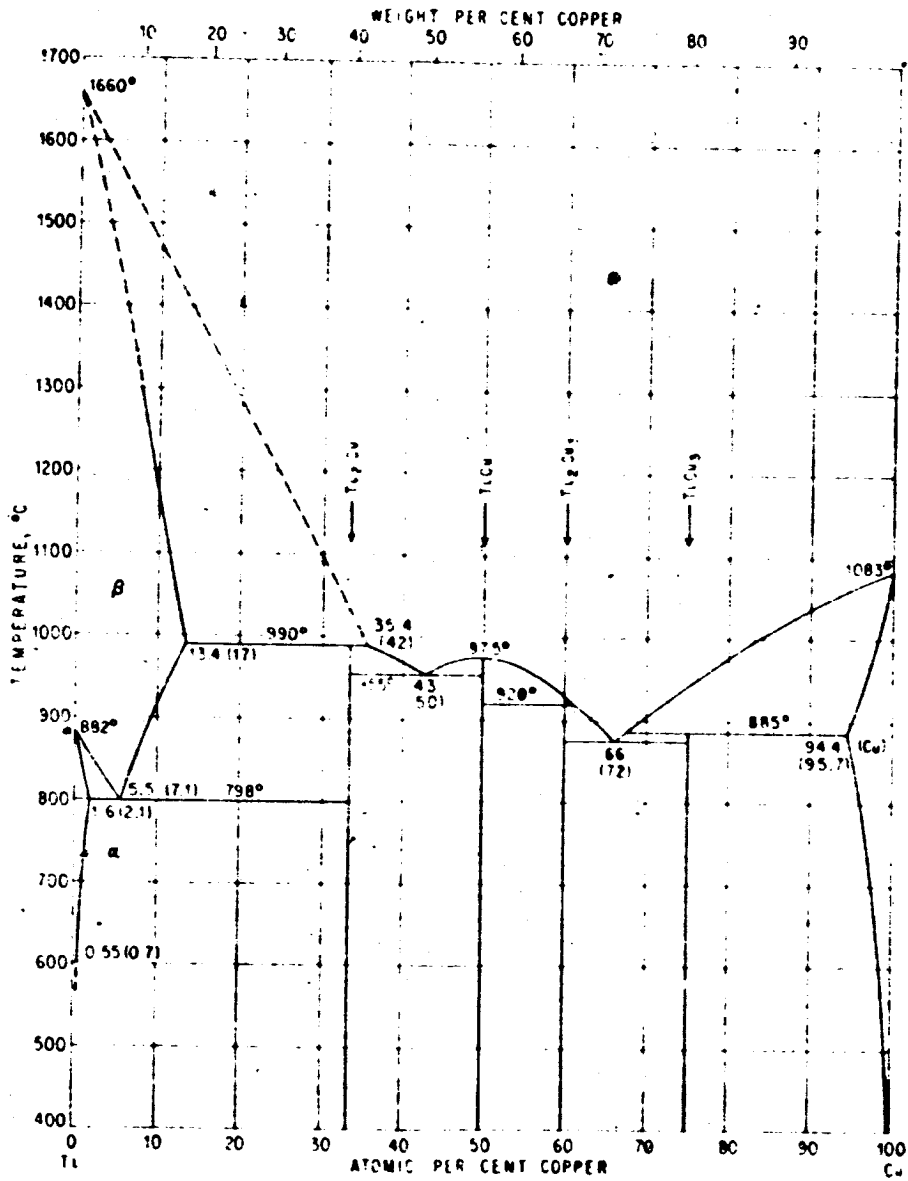
FIG. 2-105   N-Ti PHASE DIAGRAM

an unsound braze joint.

2.4.4 Vapor Depositions

2.4.4.1 Elements of the Technique

The technique of vapor deposition as a process for joining high temperature materials such as tungsten is only beginning to receive some limited attention. Essentially this method amounts to the decomposition of a gas, such as tungsten hexacarbonyl or tungsten hexafloride, on the materials to be joined. Extremely good vacuum backgrounds are not required, and the auxiliary equipment necessary for the vapor deposition is not extensive. The materials to be joined are placed on a heated mandrel, which raises the temperature of the joint to approximately 600°C to 800°C. A gas such as tungsten hexacarbonyl is forced over the heated joint. The tungsten hexacarbonyl decomposes on the hot surface, leaving pure tungsten on the surface with the remainder of the decomposition products being carried downstream and out of the region of concern. Other materials, such as tantalum hexafloride and rhenium hexafloride, may be used in much the same fashion.

2.4.4.2 Major Area of Application to Converter Fabrication

It would appear from the limited data available concerning this process that the major area of application of a vapor deposition joining technique would be to the emitter and emitter-support structure. For example, this technique may be very useful in joining a tungsten emitter slug to a tantalum envelope or emitter lead. Vapor deposition has been used by some experimenters to fabricate an entire emitter and emitter-support structure from tungsten. Emitter thickness and sidewall thickness up to 100 mils can easily be achieved with this technique. In general the method is still too new and untried to make sound recommendations concerning its applicability to converter fabrication.

2.4.4.3 Advantages and Disadvantages of Vapor Deposition

The major advantage of the vapor deposition joining technique is the possibility of forming extremely high temperature junctions at low processing temperatures. Another advantage is the relatively simple and inexpensive apparatus required to effect the joining.

The main disadvantage of this technique is in the area of porosity, or vacuum integrity, of the finished joint. It has generally been found that a minimum thickness of approximately 20 mils is required for a vapor deposited layer to insure vacuum tightness at high temperatures. Structures that have been fabricated by the vapor deposition technique are found to be leak-tight at room temperature but exhibit very large leaks at temperatures on the order of $1500^{\circ}C$ to $1700^{\circ}C$.

Another area of concern with this technique is the temperature control required in the region where vapor deposition is to take place. Since the material deposits most rapidly on the hottest area, a uniform temperature at the joint must be provided or uneven deposit thicknesses will result.

2.4.5 Recommendations

In general only two of the foregoing fabrication techniques, if highly developed, would be useful for metals joining in all areas of a thermionic converter. This includes the emitter structure, the collector structure, the radiator, and cesium reservoir structures. The methods referred to are electron beam welding, and as a secondary choice, tungsten inert gas welding. At the present time, perhaps only tungsten inert gas welding is really feasible as a single joining process from the standpoint of availability and cost. The electron beam welding technique is still in the infant stage of development, and at the present time is very costly and yields somewhat unreproducible results. The situation could, however, be substantially different in the event literally millions of converter

structures were to be fabricated. Specific recommendations for fabrication techniques to be used in the various converter structure areas follow.

2.4.5.1 Recommended Emitter Structure Fabrication Technique

As was previously mentioned there are two techniques that are generally superior for use in a high temperature zone. They are the electron beam welding method and the tungsten inert gas method. Both methods have previously been used by experimenters in the thermionic converter field for fabrication of emitter structures.

Except for very few brazing possibilities, such as the rhenium-tungsten eutectic system, the method of brazing is generally not recommended for use in the emitter area of a thermionic converter.

2.4.5.2 Recommended Collector Structure Fabrication Techniques

All the abovementioned methods of joining metals are applicable to the joining problems encountered in the collector structure in a thermionic converter. The cheapest and most highly developed methods for use in this area are the tungsten inert gas method and brazing. Again, one has to be extremely careful in using the brazing method to exclude all braze alloys or materials not compatible with cesium vapor and which may deteriorate at temperatures on the order of 900°C during the life of the converter. There are, however, a large number of potentially useful braze materials for this application. Among them are the nickel-zirconium, nickel-titanium, and nickel-niobium eutectic mixtures. Other possibilities which have been used successfully in ion engine fabrication are the moly-boron-carbon-ternery system and the moly-boron system. Those braze materials not containing noble metals are generally satisfactory as braze materials for the collector structure of a converter.

The tungsten inert gas welding method has been used for fabrication of collector structures and metal seal

flanges. Once developed for this specific application, this technique yields very reliable results. Jigging of the parts to be assembled by this technique can be somewhat tricky.

2.4.5.3 Recommended Fabrication Techniques for the Radiator and Cesium Reservoir Substructures

Joining of the cesium reservoir substructure to the collector structure of the thermionic converter can be effected most easily by brazing or tungsten inert gas welding techniques. This particular region of the converter operates at perhaps a maximum temperature of $800^{\circ}C$ during the life of a converter. Furthermore, the only part of the reservoir which operates at such a high temperature is that part which is in contact with the collector of the converter. Other areas in the reservoir structure usually operate at maximum temperatures near $400^{\circ}C$. In some cases low temperature braze materials could be used at the low temperature end of the cesium reservoir. From an overall consideration of life and reliability of a thermionic converter, however, it is generally not recommended that low temperature brazes be used on this structure. In general it might be stated that all components of a thermionic converter should have fabrication process temperatures in excess of $1200^{\circ}C$, except, perhaps, for the metal-to-ceramic seal.

The radiator of a thermionic converter can be assembled or joined to the collector most easily by brazing or tungsten inert gas welding. A diffusion bond technique, in which the radiator is bonded to the collector by subjecting the joint to high temperatures for long periods of time, may be used. The application of pressure to the high temperature joint promotes diffusion bonding. Since this joint does not usually have to be vacuum tight in a thermionic converter, the use of a diffusion bond here does not meet the same objections which are raised to this technique in the electron tube field. In the electron tube field it has been found that diffusion bond techniques are not reliable, particularly in high temperature

devices because difficulty is experienced with leaks.

In the realm of diffusion bonding in a practical converter device, a clean radiator may be bolted to a clean collector structure, and in the process of operating the converter for a number of hours at high temperatures, a diffusion bond will automatically be effected between these two elements. Such a technique has been used successfully in the fabrication of thermionic converters.

3. CERAMIC-METAL SEALS

3.1 Introduction

The metal-ceramic seal is composed of at least one metal unit in conjunction with one or more ceramic units, or of several ceramic units sharing metallic bonding interfaces. The ceramic, metal, and the bond areas must be impervious to the passage of liquids or gases. Obviously, the ceramic may function as a nonconductor, as a structural member, or as both. Likewise, the metal may be only a structural or bonding member, an electrical conductor, or both.

Thermionic converters presently under development consist of two primary device geometries - concentric and parallel plate. In each case the principal functions of the seals and insulators are the same:

1. To support in the structural sense the emitter with respect to the collector

2. To electrically insulate the emitter from the collector

3. To provide a hermetic seal between the inside of the device and the ambient environment

To perform these three basic functions certain physical and mechanical requirements are evident. These are defined and limited by operating temperatures, the requirement of compatibility with other optimum materials of construction of the device components, the possible presence of the radiation spectrum of a nuclear reactor or Van Allen radiation, the presence of cesium vapor, and mechanical requirements demanded by the design of the thermionic cell and the mission to be fulfilled.

The type of bond discussed in this text is formed by a brazing operation; the braze materials and techniques may vary according to specific thermionic diode design. Prior to discussion of the operational details, it is possible to establish several ground rules regarding the

braze which include:

1. The trend towards high emitter temperatures in order to raise diode efficiency will also raise the seal operational temperature. Seals should be designed to operate reliably at about 600° C.

2. None of the seal components should contain any of the noble metals such as Au, Ag, Pt, and Pl, as these metals are subject to extreme corrosion by the Cs vapor. The corrosion problem eliminates many of the commercial brazes used in electron tubes.

3. None of the seal components should contain materials that exhibit high vapor pressures at the temperatures encountered during final brazing or operation (nominally less than 10^{-6} mm Hg for brazing, 10^{-8} mm Hg for operation).

4. The combined yield point of the braze and metal components should be less than the tensile yield point of the ceramic, or the thermal expansion of the braze and metal component should match the ceramic closely enough so that the yield point of the ceramic is not exceeded.

The selection of materials for metal structural components and ceramics is discussed in other chapters; the following materials are of interest:

1. Metal structural components - Ta, Nb, Mo, W
2. Ceramics - Al_2O_3 (high purity), BeO_2

It should be noted that most workers in the high-temperature thermionic field favor the use of Ta and/or Nb in combination with Al_2O_3 due to the close thermal expansion match between metal and ceramic and the availability of high purity alumina.

The following paragraphs review the types of ceramic-metal seals that might find application to thermionic converters. The braze techniques of possible application are reviewed along with factors for consideration in seal design. The last subsection briefly summarizes

the avenues of approach recommended for metal-ceramic seals for thermionic converter application.

3.1.1 Types of Metal-Ceramic Bonds

Metal-to-ceramic bonds fall into three general categories, based in large part on the mechanism by which the required intimacy of contact at the ceramic-metal interface is obtained.

The first of these utilizes a molten ceramic wetting a relatively more refractory metal. Porcelain enamel on metal is of this type as are the glass bonded decorative metals applied to pottery and glass. Another application of this type of bond is found in the glass-to-metal seals commonly used in electronic work. Since this bond employs a molten or glassy ceramic phase the finished unit displays many of the brittle properties of glass. Fairly low melting ceramic composition are required, so the bond is generally restricted to low-temperature operations. Furthermore, the glass phases are unsuitable for operation in a cesium vapor.

A second type of bonding comes about in solid-state reactions. The intimacy of contact is provided mechanically by pressure, spraying, tipping, or painting, or gradual mixing techniques, and solid-state reactions occur during firing at a temperature slightly below the melting point of either metal or ceramic. This reaction is typical of refractory cermets.

The third type, pertinent to this discussion, occurs where the metal provides the fluid phase to wet a relatively more refractory ceramic. Examples of this sort may be found in certain classes of cermet, and in the "hard solder" metal-to-ceramic seals that are of particular interest in this discussion.

3.1.2 Geometrical Design of Brazed Joints

Brazed joints normally fall into one of three classes, which are shown in Part A of Fig. 3-1; lapp, butt, or scarf. The lapp joint has been used for many years in ceramic electron tubes and is illustrated by the radial-compression seals of part B. The lapp joint

A. BASIC JOINT
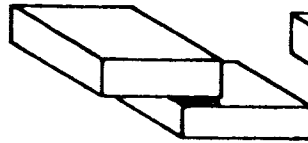
BUTT JOINT   LAP JOINT   SCARF JOINT
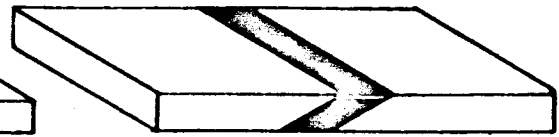
B. RADIAL COMPRESSION SEALS

CERAMIC

DUCTILE
PLATED
METAL
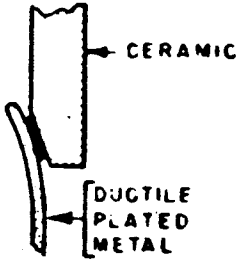
OUTSIDE SEAL   COAXIAL SEAL   OUTSIDE SEAL ON DISC

C. BUTT SEALS

UNCOMPENSATED
SEAL   COMPENSATED SEAL
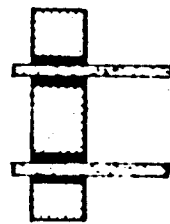
D. FLEXIBLE SEALS
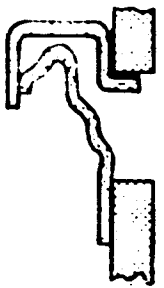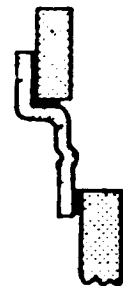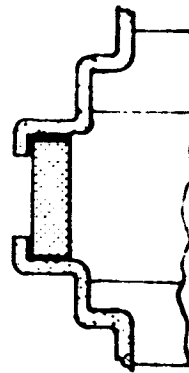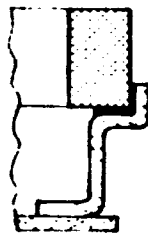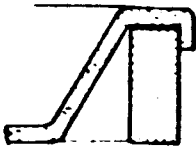
E. TERMINAL AND PIN SEALS
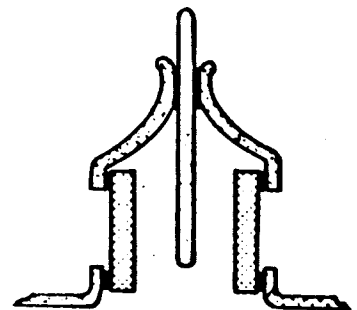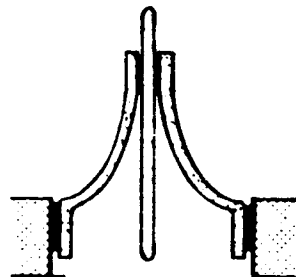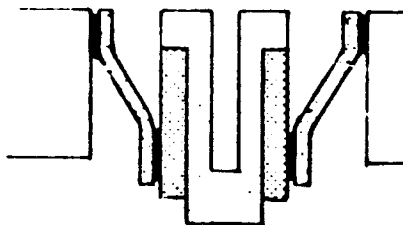
FIG.3-1 SEAL DESIGNS

is preferred for several reasons. First, the load is generally spread over a much larger braze area. Second, the problems associated with minor misalignment or with voids or bubbles are of lesser consequence.

Ceramic-metal butt seals are those in which the metal part is sealed or bonded directly to the end of the ceramic cylinder. The most reliable type is the compensated butt seal (also known as "disc" seal) illustrated in part C of Fig. 3-1, which has a ceramic cylinder bonded to each side of a flat metal member. In recent years there has been increasing use of butt seals in ceramic-metal electronic tubes and similar devices and butt seals are gradually replacing the more conventional concentric or compression types in which the metal is sealed around the outside circumference of the ceramic cylinder.

The scarf joint is actually an attempt to combine the neatness of a butt joint with the strength of the large area lap joint. Joint preparation and jigging are much more difficult than for the other two types and the scarf joint is therefore not commonly used.

Advantages of a butt joint over compression seals for electron tubes are:

1. Simple geometry - parts are easier and cheaper to make.
2. Tolerances on parts are less stringent.
3. Metalizing and braze can be more easily applied and thickness more easily controlled.
4. Structures are more adaptable to simple modular design, miniaturization and automative assembly.
5. Assembly procedures are simpler and metal parts need not be restricted by binding with refractory wire.
6. There is less tendency to form gaps and voids in the braze joint.
7. Butt joints are readily adaptable to active alloy sealing processes whereas lapp seals are generally restricted to the moly-manganese or similar processes.

Compression seals have some advantages over butt seals, as follows:

1. Much more is known about comparative strength and design parameters.

2. A better expansion match between metal and ceramic is required with butt seals compared to compression seals.

3. Stresses in a butt seal are concentrated in a small volume increment near the ceramic-metal interface and the whole load is put on a small braze area. Further, bubbles and voids in the braze area can serve as stress risers, putting as much as three times the normal stress on an immediately adjacent braze area.

4. Braze yield strength and brittleness complicate the alignment problem of butt seals. If there is misalignment, some area of the braze is usually stressed disproportionately and local rupture or local yielding is possible. Depending on the relative properties of braze and base materials, the rupture or tear may occur in one or the other or at the interface. Ruptures are usually catastrophic.

Parts D and E of Fig. 3-1 illustrate a number of flexible-type seals that are used when it is difficult to obtain adequate expansion and temperature match with available materials, or when outside forces may exert a force on the metal component. Stresses in the seal can be equalized by a slight movement of the metal members. Terminal and pin seals used in feedthroughs for vacuum systems are of this type. For a thermionic converter application, movement of the metal member is usually undesirable and flexible joints are restricted to laboratory models where a change in the position of the metal member may be wanted. Several forms that ceramic-metal seals and assemblies may take are illustrated in Fig. 3-2.

The dimensions of the metal and ceramic parts are generally dictated by the tensile stress limits of the ceramic, as
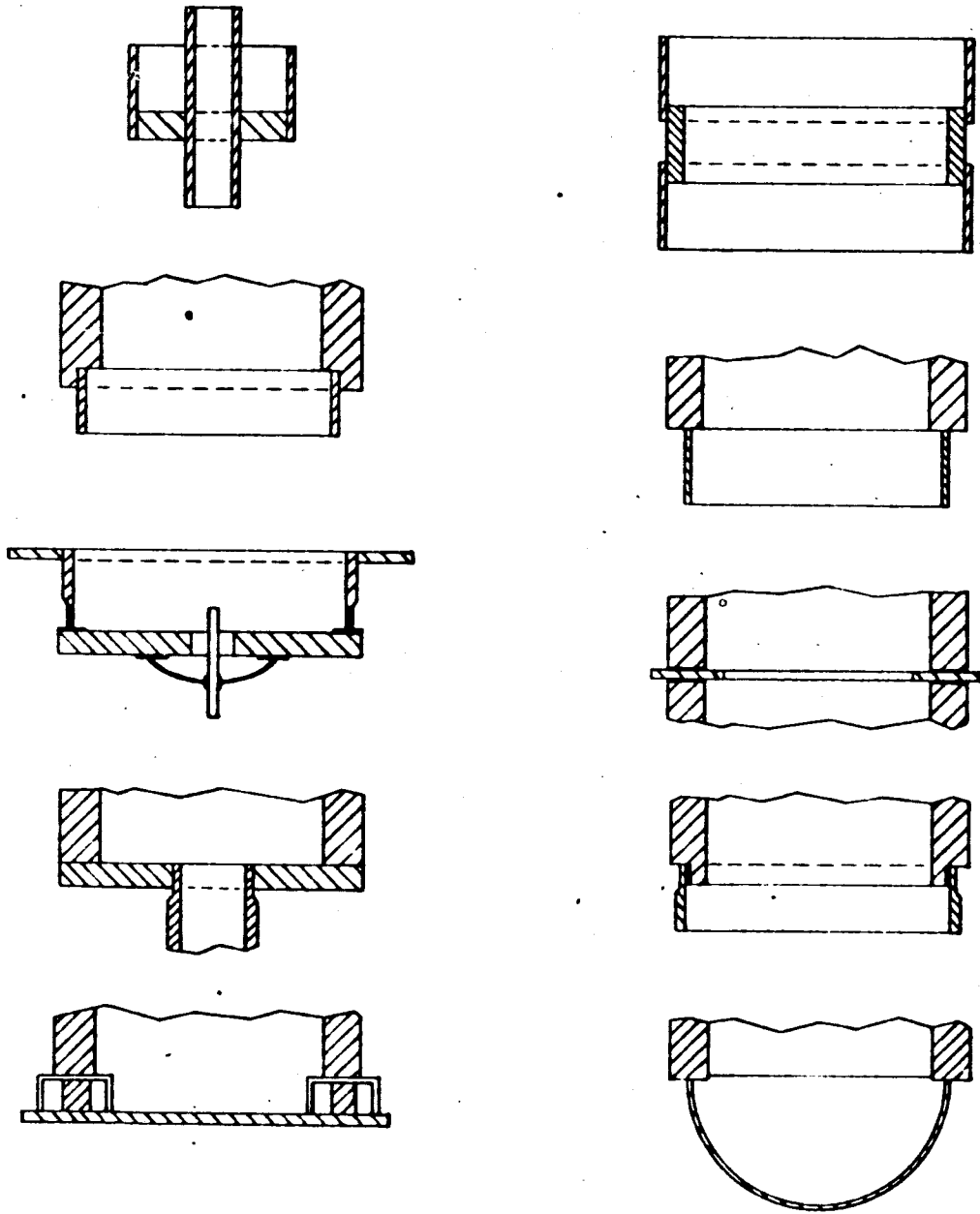
FIG. 3-2 SEVERAL OF THE FORMS THAT CERAMIC-METAL SEALS AND
ASSEMBLIES MAY TAKE

36488

discussed in subsection 3.2.4. Generally, the metal member should be much thinner than the ceramic to promote yielding. For successful butt seals the parts must be flat to within 0.001" or less, and successful lapp seals demand even closer tolerances.

3.1.3 Brazing Processes Applicable Towards Thermionic Converters

There are three basic techniques for developing metal-ceramic seals that are considered useful for thermionic converter applications. The techniques are similar in that each utilizes one or more of the metals which exhibit an affinity for ceramic bonding as the "active ingredient", and in the fact that a reducing or inert atmosphere is necessary before firing to prevent excessive oxidation of the metal before it can seal with a ceramic. The three techniques are known as the moly-manganese active metal and titanium hydride processes.

The moly-manganese process consists of the following basic steps:

1. The precleaned ceramic is painted, to a thickness of 0.001 to 0.002 inches, with a mixture of finely divided molybdenum and manganese powder held in a suitable organic binder.

2. This coating is air dried and then sintered in wet hydrogen for half an hour at a high temperature that is below the softening point of the ceramic being used. This treatment causes the powder mixture to bond firmly to the ceramic and provide a metalizing layer.

3. The bonded-metal layer is now electroplated with copper or nickel to improve wetting during the brazing operation.

4. The electroplated layers (or a nickel powder) are sintered in wet hydrogen to create a firm bond to the metalizing layer.

5. The body is now assembled with a shim of brazing metal or alloy in position and the braze is completed by heating the parts in a hydrogen atmosphere.

There are many other additives to the molybdenum powder other than manganese that can be used depending on the nature of the ceramic and many other factors. The moly-manganese process

will provide a strong bond, good reproducibility, and good dimensional control of metalized areas.

Furthermore, within the present state of the art, a moly-manganese (or sintered powder) seal is the only type applicable to reliable lapp or compression joints. Several disadvantages of the moly-manganese seal which result in their application being less favorable than active alloy or hydride seals in thermionic diode application. These include:

1. A multistep process that uses three firings at high temperature is required. The process controls on material preparation and time and temperature history are extremely stringent, and much of the success will depend on the individual skill of the operator.

2. The final braze or alloy is limited to a few materials such as Cu, which are not recommended for high temperature service in cesium vapor.

Seals of the sintered type have been made with the refractory metals in powder form in place of the molybdenum-manganese combination. Rhenium and tungsten have been used, generally with additions such as nickel, iron, or cobalt to improve seal properties. Burnside used a tungsten-iron seal, an important feature of which was that a rigid schedule was not required to produce successful seals, and considerably more variation in metal powder composition, firing rate, temperature and atmosphere could be tolerated.

It should be noted that premetalized ceramics are available from many sources, limiting the effort of the thermionic converter fabricator to the final braze operation.

Bondley in 1947 introduced the use of titanium hydride in conjunction with silver and copper solder and used the active metal hydride process. In this technique:

1. The precleaned ceramic is painted with a layer of titanium hydride powder in a suitable binder.

2. The coating is allowed to dry and the metal parts and alloying metal are located in position.

3. The fully assembled body is then heated in a vacuum (at least 10^{-4} mm Hg) or very dry hydrogen.

4. The hydride disassociates into hydrogen and active metal and the latter forms an alloy with the brazing metal already located in position. This alloy bonds to the ceramic and brazes to the metal member of the envelope in one operation.

Later work by Pearsall and Zingeser demonstrated the suitability of other hydrides, notably zirconium, and also showed that the active metals themselves produced comparable results. They found that active metals, particularly titanium and zironium, could be used to produce excellent seals in precut forms of an alloy with a brazing solder, or in powder form used much like the hydrides, or as a sandwiched thin layer between sheets of solder.

Active alloy and hydride techniques will provide strong bonds and excellent reproducibility. Only one firing operation is required in a vacuum or inert atmosphere rather than hydrogen, and firing temperatures are well below the softening point of the body. These low-firing temperatures enable outgassing of the seal components to occur well above brazing temperatures, thus reducing the danger of bubbles or voids. Braze materials that are recommended for high temperature service can be used. One disadvantage of the active alloy and hydride processes is the high fluidity of the solder at the brazing temperature, which may make dimensional control of the metalized area more difficult. Application of the hydride involves handwork of considerable skill to achieve product uniformity; however, precut shims of active alloy require relatively little skill. Design limitations may be necessary to control the flow of the superheated solder, e.g., enclosing the sealing zone between matching parts of the assembly where the length of the flow is relatively short and where the final brazed zone is quite thin.

Other methods of joining metals in ceramics have been investigated but possess inherent difficulties in processing that make them less attractive at the present time than the methods mentioned. These methods can be classified as pressed-diffusion seals, soldered seals, graded-powder seals, and electroformed seals.

Pressed-diffusion seals involve the simple procedure of pushing two surfaces against each other and letting the surface forces provide the permanent coupling. Commercial use is made of cold welding by interdiffusion in the construction of large power tubes with ceramic envelopes. High alumina ceramic cylinders as large as 20 inches in diameter are ground to a blunt bevel at the end and a copper plated tool steel cylinder of smaller i.d. than the o.d. of the ceramic cylinder is pushed onto the latter under considerable pressure to affect a seal. These seals have become known as crunch, or ram, seals. The formation of this type of bond is further promoted by making such pressure seals at an elevated temperature. A modified diffusion seal developed by workers at Eitel-McCullough, Inc. involves metalizing the ceramic ring by conventional methods prior to subjecting the ring to pressure at a moderate temperature. The apparently simple techniques for diffusion seals have so far been found to be practical only for relatively large components that can withstand the required pressure.

Solder seals are used even today for commercial tubes intended for low temperature applications and employ alloys of tin, lead, and indium. Knecht has investigated graded-powder seals consisting of layers of metal powder that are gradually enriched with ceramic powder until layers of pure ceramic are reached. This, in effect, produces a graded seal for metal to ceramic when such layers are pressed together. The electron tube laboratory of the Stanford University Electronics Research Laboratory has investigated electroformed seals that are made by stacking up premetaled copper plated ceramic cylinders in accurate alignment under slight pressure with disc electrodes inserted

between the abutting cylinder surfaces. The assembled stack is then placed in a copper plating bath for several days to build up the required thickness of copper at the joint.

3.2 Seal Design

The detailed structure of a metal-ceramic braze is complicated and in many instances not completely understood. This complexity is illustrated by the seal cross sections of Fig. 3-3, which illustrates the basic components of typical seals prior to assembly and the structure of the braze zones after final assembly. The following paragraphs will describe some of the details of these processes.

3.2.1 Brazing Metallurgy

Some principles of physical metallurgy are reviewed here in order to clearly understand the mechanisms of brazing. The formation of alloys is governed by the mutual solubility of the various metals used. In the case of binary alloys this behavior is best illustrated by constitutional diagrams, which are also called phase diagrams. For alloys containing three or more components a graphical representation becomes a little more involved but it is still possible for ternary systems.

Figure 3-4 shows the constitutional diagram for a binary alloy that represents a simple eutectic system. At composition F the liquid and solid phases are in equilibrium and an alloy of this composition will have a sharply defined melting point. The areas denoted by α and β are called terminal solid solutions and represent single phases. At room temperature, T_0, C percent of metal B can be dissolved in metal A as a solid solution, either substitutionally or interstitially. With increasing temperature, increasing amounts of metal B can be dissolved in metal A until temperature T_E is reached, above which the solid solubility, B in A, decreases. Similarly, a small amount of metal A is soluble in metal B at room temperature and this amount again increases with temperature up to T_E and then decreases with a further increase in temperature.

COMPONENTS   FINAL STRUCTURE

Metal structural component

Preformed shim of brazing alloy

Electroplated Ni or Cu layer

Metal powder held in organic binder

CERAMIC

— Metal structural component

Metallurgical bond formed by inter-diffusion between metal and braze alloy

Solidified braze alloy of eutectic composition

Metallurgical bond formed by inter-diffusion between braze alloy and Ni layer

Ni or Cu electroformed layer

Metalizing layer formed by firing metal powder layer

Chemical bond formed by reaction between metalizing layer and ceramic

CERAMIC

1) Metal structural component

✷
2) Preformed shim of brazing metal

3) Preformed shim of active metal or layer of active metal hydride powder

CERAMIC

— Metal structural component

Metallurgical bond formed by inter-diffusion between braze and component metals

Reactive alloy formed between active metal and brazing metal

Chemical bond formed by reaction between active metal and ceramic

CERAMIC

✷
2) and 3) Can usually be reversed

NOTE

SKETCHES ARE NOT DIMENSIONALLY CORRECT, IE,
THE ENTIRE BRAZE ZONE IS USUALLY ONLY
A FEW THOUSANDTHS OF AN INCH THICK

FIG. 3-3 TYPES OF BRAZES*

7364882
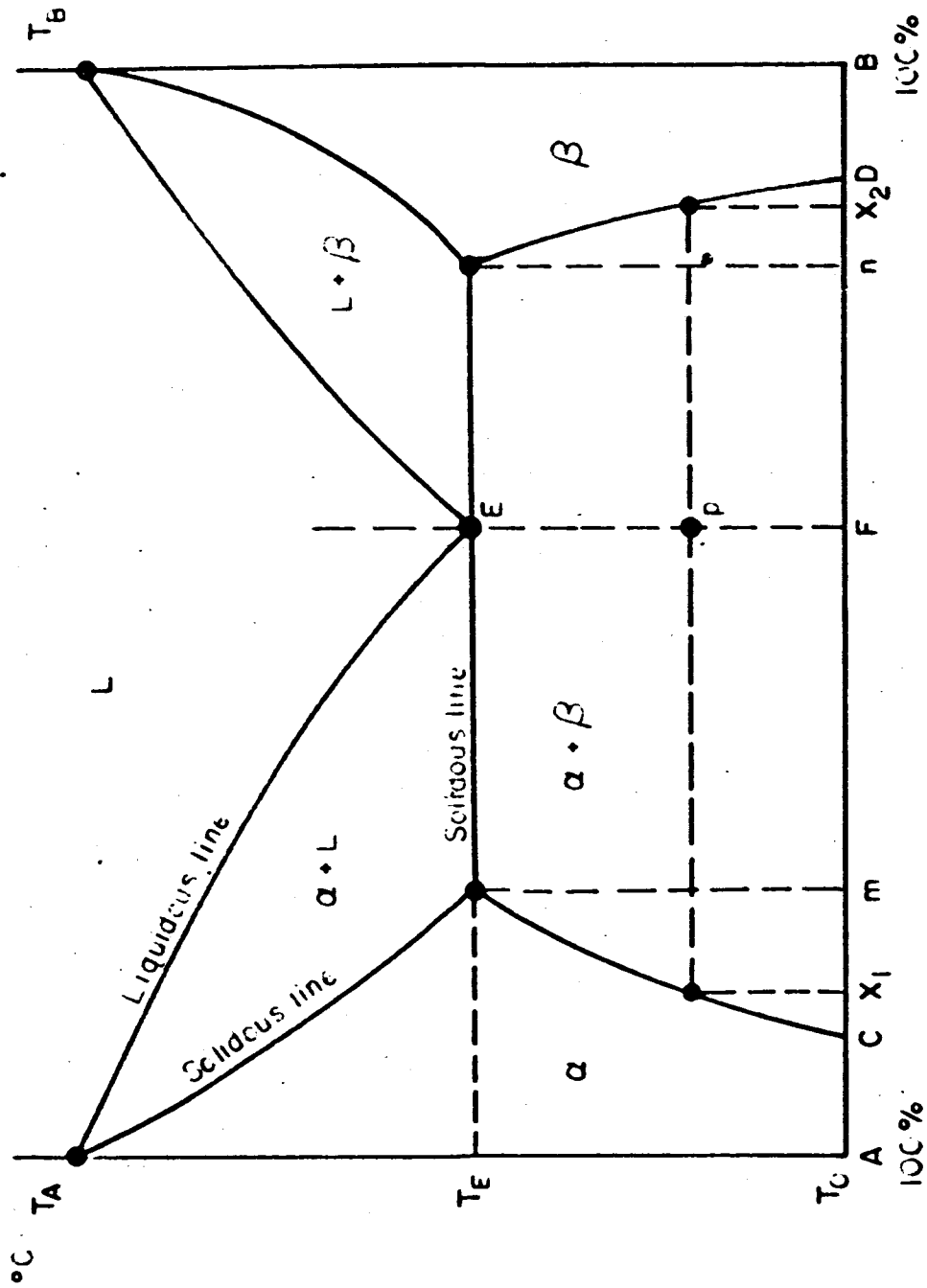
FIG.3-4   CONSTITUTIONAL DIAGRAM FOR SIMPLE EUTECTIC SYSTEM

7364003

When a melt of eutectic composition F is slowly cooled from the molten state to temperature T_E, the liquid phase solidifies to a eutectic mixture composed of solid solution α of composition m and solid solution β of composition n. The melting point of the eutectic composition is significantly lower than the melting point of other compositions on either side of F.

The melting range for any alloy composition is indicated by the vertical distance between the liquidus and solidus lines. All alloy compositions are solid in the area below the solidus line. An alloy of given composition is represented by a vertical line. The first solid crystals will appear when the temperature of the liquid melt is gradually lowered below the liquidus line, and very little of the liquid phase remains when the solidus line is reached; all the melt has solidified into a solid solution of $\alpha + \beta$. For example, on lowering the temperature of the alloy of the original composition F from the molten state, solidification will occur at temperature T_E; two separate solid phases appear that have a relative proportion, which can be expressed by the ratio $\alpha/\beta = px_1/px_2$.

Constitutional diagrams for most of the common alloys are compiled in the literature. Examples for specific brazing alloys appear in these pages. It should be emphasized that constitutional diagrams are equilibrium diagrams, i.e., sufficient times are allowed at any temperature to permit establishment of complete equilibrium between the various phases present in the system. At the eutectic point E in Fig. 3-4, for example, the liquid phase of composition F is in equilibrium with the α and β solid solutions explained above. On cooling below temperature T_E the liquid phase solidifies and must have time to change its composition to that of the terminal solids solutions. If temperature changes take place too rapidly in a practical process deviations from the idealized phase diagram will take place. Advantage is taken of this fact in processes such as precipitation hardening.

Brazing operations should, in general, be performed quickly after the joint assembly has reached a uniform temperature that is high enough to ensure melting of the filler metal, usually 20° to 50°C above the melting point. In most brazing operations there is a tendency for the brazing alloy to dissolve in the metal part and vice versa. As a consequence, the composition of the alloy tends to shift away from the eutectic and the liquidus temperature is raised. The erosion of the joint area is minimized by performing the braze quickly and staying at the brazing temperature not longer than necessary. Apart from the time factor, the relative amounts of filler metal and parent metal present at the joints will have a determining affect on the extent to which erosion can take place. Very thin members can be seriously damaged by erosion, especially when an excessive amount of filler metal is used.

3.2.2 The Moly-Manganese Process

The moly-manganese process requires several steps to produce a braze joint between ceramic and metal. First, finely divided powders of molybdenum, tungsten, tantalum, rhenium, or iron, plus suitable additives in a suspension of nitrocellulose lacquer are applied singly or in combination by brushing or spraying on the clean and smooth ceramic surface. This metal-powder coating is then sintered to the ceramic by firing in a hydrogen atmosphere at temperatures ranging from about 1300° to 1600°C, depending on the ceramic composition and that of the powder coating. After the first sintering operation at elevated temperature, a thin film of copper and nickel is applied by means of electroplating (or the reduction of oxide powders) and sintered in a hydrogen atmosphere at a temperature of about 1000°C. The metalized ceramic is then ready to be joined to the metal part by conventional methods of brazing in a controlled-atmosphere furnace.

The discussion below divides the seal process into three processes: metalizing of the ceramic, application of the copper or nickel films, and the final braze.

A cross section of a typical sintered metal powder seal was shown in Fig. 3-3 and illustrates the several types of bonds that are necessary for a leak tight seal.

3.2.2.1 Metalizing the Ceramic

3.2.2.1.1 Ceramic Composition

For thermionic diode application alumina and beryllia ceramics appear of most interest. Commercial alumina can be obtained in qualities ranging from 100 percent alumina (e.g., G. E. Lucalox) to ceramics containing large percentages of SiO_2, CaO, MgO and other oxides. Since cesium vapor will attack silica, magnesia, and other impurities at high temperatures, only those bodies with a high percentage of alumina are of interest.

A ceramic is generally a heterogeneous material, often not in an equilibrium state. The properties of a given product can vary widely. The constituents of the ceramic generally include the following:

1. Al_2O_3 or BeO Crystals
2. A glassy phase
3. Voids made of closed pores which are vacuum tight or interconnecting pores which are not vacuum tight.

One hundred percent pore-free sintered alumina consists of grains of α-alumina and has no glassy phase. It is less costly to sinter alumina with a little glassy phase, such as a 99% body with a remainder of SiO_2, CaO, and MgO, which will contain some pores.

A 94% alumina body is even easier to make. To reduce both the temperature and the time of firing, glass forming constitutes are added to the finely ground alumina. These consist of SiO_2, MgO, CaO, Fe_2O_3 and traces of other elements. These form a liquid phase at sintering temperatures and assist the sintering process. On cooling, the phase diagrams indicate that the primary phase is α-Al_2O_3 with secondary crystallization of Mullite ($3Al_2O_3 \cdot 2SiO_2$)

Anorthite (CaO $\cdot$ Al$_2$O$_3$ $\cdot$ 2SiO$_2$), plus smaller amounts of spinel and traces of other compounds which can lower the melting point to $\sim$1400°C. However, the cooling rate is too rapid to allow significant crystallization to proceed. This results in a glassy matrix surrounding the alumina crystals.

It is considerably easier to metalize to 94% alumina than to 100% alumina because of the glassy phase. Tensile test pieces of 99 or 100% alumina generally show low strength and the break occurs at the metalizing-ceramic interface.

Beryllia ceramics are useful and are available up to 99.6% BeO. The BeO-SiO$_2$ phase diagram indicates that liquids form at 1670°C and that 2BeO $\cdot$ SiO$_2$ crystallizes out as a secondary phase. The discussion that follows is about alumina, but most of the comments also apply to BeO.

3.2.2.1.2 Metalizing Paint Composition and Application

The conventional means of applying a metalizing layer of a refractory metal or its oxide to a ceramic surface is as a pigment (powder) suspended in a paint vehicle consisting of an organic binder, solvents and thinners. A large number of variables controls the effectiveness of the paint, including:

1. Method of application - brush, spray, or roller
2. Metal particle size
3. Metalizing paint thickness
4. Metalizing composition
5. Sintering temperature
6. Sintering time
7. Sintering rate
8. Impurities and additions to the metalizing composition
9. Furnace dew point
10. Hydrogen-nitrogen ratio
11. Type of electroplate coating

Each laboratory, while using sub-
stantially the same type of ingredients in the metalizing paint, has
slightly different procedures developed over a long period of trial
and error. Therefore, a process that has been successfully practiced
in one plant may not be successful in another unless care is taken to
duplicate the exact methods, equipment, materials, and in some instances,
personnel.

In considering a method of apply-
ing the metalizing composition, the primary objective is to obtain
both a uniform and reproducible thickness. This becomes difficult
with hand brushing, which tends to create low spots in the center of
coatings and high spots on the edges. Brush, roller, and spray coat-
ing techniques have been used.

The recommended thickness of the
metalizing coating varies between 0.5 and 2 mils, depending upon
specific composition. Recommended particle size for metal powders
varies between 1 and 2 microns. Uniform particle sizes are generally
achieved by ball milling the powder for as long as several days.

Consistency of a paint is an
important characteristic. After application it must flatten out under
the surface tension of its vehicle so as to eliminate irregularities;
it must not run down on inclined surfaces nor sag off the underside of
horizontal ones. The paint must act essentially as a non-newtonian
liquid. The yield point must be high enough to prevent running or
sagging. Viscosity, rate of particle settling, and rate of gel formation
are important characteristics for consideration.

The manufacture of a satisfactory
paint requires complete dispersion of the pigment in the vehicle.
This is accomplished by ball milling, a process that breaks up flocculent
pigment into the individual particles. There is an optimum vehicle-
pigment ratio for grinding, involving the presence of enough vehicle
to make complete particle dispersion possible, and sufficient pigment
to accentuate interparticle friction as the mass flows between the
grinding falls.

Large supplies of nitrocellulose are used rather extensively for binder purposes, and it has been available since World War I. The purpose of the binder is to hold the metalizing particles together during drying and firing until a sintered bond can be established.

The solvents are added to dissolve the binder and any grinding resins from the ball-milling process. They are adjusted to provide a good drying rate and viscosity compatible with the metalizing painting process. The installation of a clean, temperature and humidity controlled room and infrared drying for some parts greatly aids control of the process. Solvents used include ketones, alcohols, socals, ethers, pthalates, and esters.

In summary, many factors must be controlled in order to insure constant paint characteristics. These include:

1. The pigment - particle size, particle shape, particle size distribution, milling variations, initial particle characteristics, the form of paint, oxide, metal, or mixtures

2. The binders - purity and tolerance of variation, dissolved H_2O, burnout rate, chemical reaction with metalizing powders

3. Solvents - as above (2) plus evaporation rate for different applications

4. The paint - aging effects, gelling, settling, viscosity, density, the grind, surface tension, thixotropic behavior, dilatant behavior

5. Application - temperature, cleanliness, humidity, time for drying, thickness of layer, method of application

The metalizing compounds used almost universally are based on a molybdenum power base with additives that are selected depending on the ceramic used and individual experience. Manganese and titanium are commonly added in a ratio of about 20 percent and 3 percent by weight respectively. "Activated" mixtures, using small

percentages of alumina, silica, and titanium hydride are also used.

Table 3-I lists some of the metalizing compounds reported in the literature and indicates the percentage of additions, the type of ceramics used, and the sintering temperatures reported. Specific additives are used to provide strong adherence to the ceramic, as discussed in later paragraphs. The metalizing compound mixtures 1 through 6 in Table 3-I are reported by Kohl and are used commercially in electron tube applications. Mixtures 7 and 8 were used by Cole, et al. in an experimental study of adherence mechanisms. Mixtures 9 through 14 were selected by Cole, et al. from over 200 metalizing compositions as the mixtures that provided greatest seal strength. The tungsten-iron mixture was used successfully by Burnside at the Radio Corporation of America.

3.2.2.1.3 The Metalizing Process

The metalizing furnace generally contains three zones:

1. Preheat zone; room temperature to $1000^{o}C$
2. The sintering zone; 1000° to $1500^{o}C$
3. The cooling zone; $1000^{o}C$ to room temperature

The kiln atmosphere will vary according to the kinetics of the gas interactions and the thermodynamic requirements. Carbon boats are generally used in metalizing furnaces and react with the water vapor in the kiln atmosphere to form mostly CO_2 and H_2 below $1000^{o}C$. Above $1000^{o}C$ hydrogen will react with the CO_2 to form CO and water vapor.

Hydrogen and nitrogen are admitted to the furnace in each zone. The nitrogen will contain some oxygen and, in addition, oxygen and methane will enter an inefficient furnace. The several percent of oxygen will combine with hydrogen below $1000^{o}C$ to form water vapor. In each of the three zones, hydrogen, nitrogen, water vapor, and carbon monoxide are generally present.

In the pre-sintering stage the dried paint loses its binder in the range of 300° to $400^{o}C$. At this point the

TABLE 3-I

METALIZING COMPOUNDS FOR CERAMICS

Metalizing Compound	Ceramic	Sintering Temperature
1. 160g Mo (200 mesh) 40g Mn (150 mesh)	Forsterite	1250°C
2. 40g Mo fine 0.8g Fe fine	Steatite	1250°C - 20 min (72% N_2, 28% H_2)
3. 176g Mo (400 mesh) 44g Mn	Al-200 (Coors)	1525°C (2 coatings and firings)
4. 176g Mo (200 mesh) 44g Mn (200 mesh) 9g TiH	high-alumina	
5. 200g Mo (400 mesh) 40g Mn (400 Mesh) 10g hydrogen-reduced iron powder 2g silica 2g calcia	Al-300 (Wesgo)	
6. 200g Mo (400 mesh) 40g Mn (400 mesh) 10g hydrogen-reduced iron powder 8g alumina powder (Al-300) 90 mesh 2g silica powder 8g titanium hydride powder		
7. 80% Mo 20% Mn	AD-94,99 (Coors)	1500° to 1700°C
8. 97% Mo 3% Ti	AD-94,99 (Coors)	1500° to 1700°C

TABLE 3-I

METALIZING COMPOUNDS FOR CERAMICS (cont)

Metalizing Compound	Ceramic	Sintering Temperature
9. 292.5g Mo 7.5g Ti	AD-94 (Coors)	1500°C
10. 270g Mo 30g LiMnO$_3$	AD-94 (Coors)	1500°C
11. 291g Mo 9g Talc (MgO. SiO$_2$)	AD-94 (Coors)	1600°C
12. 240g Mo 73.6g CeO$_2$	AD-96 (Coors)	1500°C
13. 255g Mo 48g SiO$_2$ 22g Mn	AD-96 (Coors) Al-23 (Coors)	1300°C 1500°C
14. 255g Mo 48g SiO$_2$ 26g MnO$_2$	Al-23 (Coors)	1500°C
15. W (9 parts by wt.) (1 to 4) F (1 part by wt.)	high-alumina	1400°C (30 min) (15 to 30% H$_2$, and N$_2$)

layer is held together by mechanical interlocking of the particles. The nature of the reaction depends upon whether the metallic particles consist predominantly of the oxides or of pure metal. Starting with an all-metal paint, manganese and titanium react with water to form the oxides. The more water vapor present the quicker the oxide will be formed and gives reason for maintaining a high dew point in the furnace.

Starting with an all-oxide paint, the measured change that occurs is a conversion of the molybdenum-oxide to the metal. Depending on the time, temperature, and hydrogen flow rate, a resultant size of the moly particles ranges from 0.1 to 6 microns. Final size of the moly particles depends upon the source of moly-oxide powder and its firing treatment. Accompanying the reduction of molybdenum-oxide is a large contraction in volume, which may lead to the cracking of the pre-sintered paint layer.

3.2.2.1.4 <u>Adherence of the Metalizing Layer to the Ceramic</u>

Several arguments have been advanced regarding the adherence of the metalizing layer to the ceramic. These are:

1. The alumina-reaction theory, which depends upon a chemical reaction of the metalizing composition and the ceramic. This theory, as proposed by Pincus, predicts a compound formation between the alumina and one of the metals used in the metalizing mixtures. The presence of oxides of the metals can be predicted by thermodynamic calculations and can be enhanced by the presence of water vapor or hydrogen in the sintering furnace (e.g., MnO and TiO_2). It is possible to predict from phase diagrams the reactivity of aluminum oxides with other oxides.

2. The molybdenum-oxide theory, which depends upon the reaction of molybdenum oxide with ceramic to form a chemical bond.

3. The glass migration theory, which depends on glass migration from the ceramic into the metalizing coating. It has been proposed by Cole and Hynes that certain metals, such as titanium, after having oxidized in a wet hydrogen atmosphere enter the glassy phase of the ceramic and lower the viscosity of that glass. The glass is then free to flow out slightly and lock the ceramic to the somewhat porous molybdenum coating that remains.

4. The molybdenum-sintering mechanism postulates that the bond strength can be increased significantly by more thorough sintering of the molybdenum particles and cells. For sintering to occur, the sintering particles must be in intimate contact with each other so that bonding can take place at the point of contact. Theoretically, anything that would increase this contact area would enhance subsequent sintering by supplying more bonding points. An increase in temperature not above the melting point will enhance the sintering rate because of increased diffusion rate and plastic deformation. Additions to the metalizing mixture should be mutually soluble with the primary metalizing compound and should not oxidize in a wet hydrogen atmosphere (e.g., iron, nickel, and cobalt).

5. The glass-additive mechanism postulates that glassy or glass forming materials (e.g., SiO_2, CaO, MgO) can be added to a metalizing mixture composed basically of a refractory metal such as molybdenum. The glass that is added is then able to fuse to both the ceramic and the metal particles.

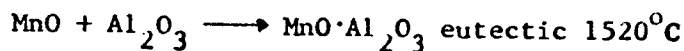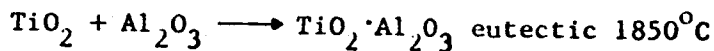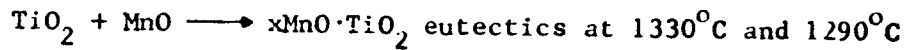The mechanisms which apply will depend on the percentage of glassy phase present in the ceramic. As an illustration, it is of interest to discuss possible reactions of a paint that contains MoO_3, MnO, and TiO_2.

TiO_2 melts at $1830^\circ C$ and MnO at $1785^\circ C$. These oxides react to form compounds $2MnO \cdot TiO_2$ and $MnO \cdot TiO_2$ at temperatures above $1000^\circ C$, and will sinter and shrink to a green-black

mass within the framework of the Mo structure.

The phase diagram of this system are shown in Fig. 3-5, and indicate a liquid eutectic at $1330^{o}C$. This eutectic point will occur within the ratio of MnO/TiO_2 used in the paint. TiO_2 is beneficial because it reduces the melting temperature of the active component of the paint phase from the $1785^{o}C$ of the straight MnO_3/MnO paint to $1330^{o}C$. This means that the reaction with the ceramic becomes a liquid-solid reaction rather than a solid-solid reaction.

At sintering temperatures many reactions are possible, including the following:

$TiO_2 + MnO \longrightarrow xMnO \cdot TiO_2$ eutectics at $1330^{o}C$ and $1290^{o}C$

$TiO_2 + Al_2O_3 \longrightarrow TiO_2 \cdot Al_2O_3$ eutectic $1850^{o}C$

$MnO + Al_2O_3 \longrightarrow MnO \cdot Al_2O_3$ eutectic $1520^{o}C$

These are indicated by the binary phase diagrams Figs. 3-6 and 3-7.

Unfortunately, no ternary phase diagram is available; a ternary eutectic point may occur below $1290^{o}C$. It is probable that there is a mixed Spinel ($2MnO \cdot TiO_2 - MnO \cdot Al_2O_3$) formed as the reaction between TiO_2, MnO, and Al_2O_3 proceeds. This would remove the liquid phase from the system. $MnO \cdot Al_2O_3$ decomposes at $1560^{o}C$; the mixed Spinel may melt between $1500^{o}C$ and $1600^{o}C$.

The system can be metalized if held at a sufficiently high temperature for sufficient time to allow reaction of the MnO and TiO_2 of the metalizing to proceed with the alumina phase. An interface layer of solid mixed Spinel crystals is laid down between the active $2MnO \cdot TiO_2 - MnO$ liquid phase and the alumina. Further reaction is thus substantially prevented by this solid crystal barrier. An addition to the metalizing mix which will prevent this Spinel precipitation is necessary if 100% alumina is to be metalized at low temperatures. Silica, with perhaps one percent of $MnO \cdot SiO_2$ in place of the MnO/TiO_2 combination, or the alumina-silicate glass might serve as an additive.
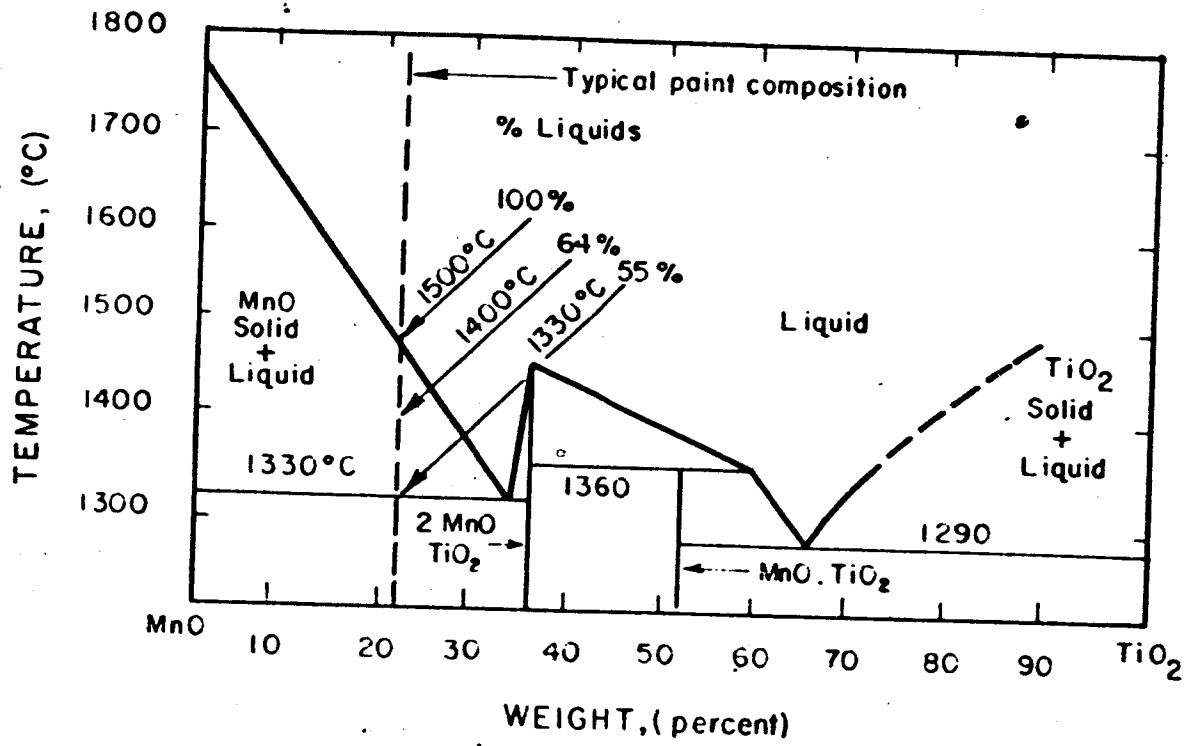
FIG.3-5 MnO-TiO$_2$ PHASE DIAGRAM

The introduction of a viscous glassy phase and porosity into the ceramic system alters the metalizing interactions drastically. Consider a 94% alumina ceramic. The composition of a typical alumina ceramic glassy phase is as follows:

SiO_2 — 30%

Al_2O_3 — 42%

CaO — 15.8%

MgO — 11.8%

FeO — 0.2%

The glass is essentially an alumina-silicate glass.

The viscous glassy phase will interact with the $MnO \cdot TiO_2$ liquid phase of the metalizing. This phase will be comparatively fluid. A new flow of the liquid metalizing phase will occur to fill the pores and cracks in the ceramic. The counter diffusion of the silicate liquid into the metalizing will involve initial movement of the Ca^{2+}, Mg^{2+}, Al^{3+}, Fe^{2+} ions into the metalizing and flow of the Mn^{2+}, Ti^{4+} ions into the ceramic, superimposed on which is the mass flow of the silicate network.

The driving force for the mixing of the liquid metalizing and the glassy ceramic phases will be diffusion gradients and "sucking effects," the surface tension forces tending to fill up the pores in the ceramic and the molybdenum layer.

If the reaction is allowed to proceed for sufficient time at a high enough temperature all MnO and TiO_2 will be drawn into the glassy phase which will, in turn, bond the sintered molybdenum metalizing to the ceramic. As equilibrium will not be completely obtained, a gradient from a rich MnO, TiO_2 glass at the metalizing to a glass devoid of MnO, TiO_2 at the ceramic will result.

There is no doubt that at conditions approaching equilibrium fluid low-melting liquids ($1100^{\circ}C$) exist at the interface between the molybdenum metalizing and 94 percent

alumina ceramics. These liquids result from reaction of the alumina phase and glassy phase with the MnO, TiO_2 metalizing components (see Figs. 3-6 and 3-7). The rate of formation of these liquids will be low at this temperature and in practice the reaction is allowed to proceed at 1400°C for one-half hour. The resultant seal structure is shown in Fig. 3-8.

3.2.2.2 The Intermediate Layer

The molybdenum (or tungsten) metalizing layer is not readily wetted by brazing materials; copper, for example does not wet molybdenum. Nielsen has carried out wetting studies of various systems in a helium atmosphere which verify this fact.

A nickel or copper coating electroplated and/or sintered onto the moly layer will remedy this deficiency. If the nickel plating is correctly processed, an adherent layer of nickel is deposited on the molybdenum. This layer may be firmly consolidated by a sintering operating. A further advantage of sintering the nickel layer on is that chance contaminants from the plating bath which have worked their way beneath the electroplated nickel will volatilize, their presence being denoted by blistering of the nickel layer.

The plating operation may be eliminated by silk screening the nickel or nickel oxide onto the metalizing by using a paint vehicle. The layer is subsequently sintered on.

The sintering time-temperature relationships are very important if the nickel layer on top of the metalizing is to be retained. This is evident from a study of the molybdenum-nickel phase diagram in Fig. 3-9.

The nickel-molybdenum interface from the metalizing side will start off with a phase having a very small solubility of Ni and Mo and end with a phase of 30 percent Mo and Ni; obviously the reaction must not be allowed to proceed too far or the molybdenum metalizing will be lost.

Copper plating onto the metalizing is also practiced. The solid solubility of copper in molybdenum at 900°C is almost zero. (The solubility of copper in tungsten is zero.) Copper

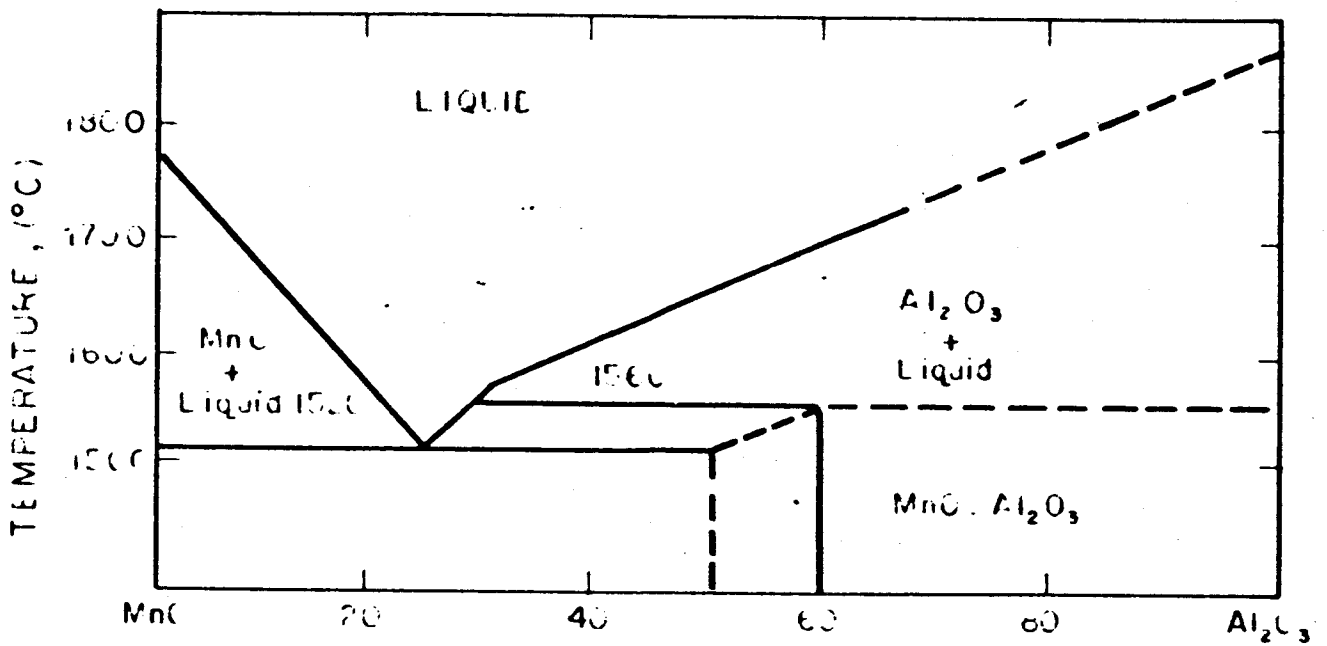FIG.3-6   THE MnO-Al$_2$O$_3$ SYSTEM   R. HAY, G. WHITE, A.B. McINTOSH, J. WEST SCOTT
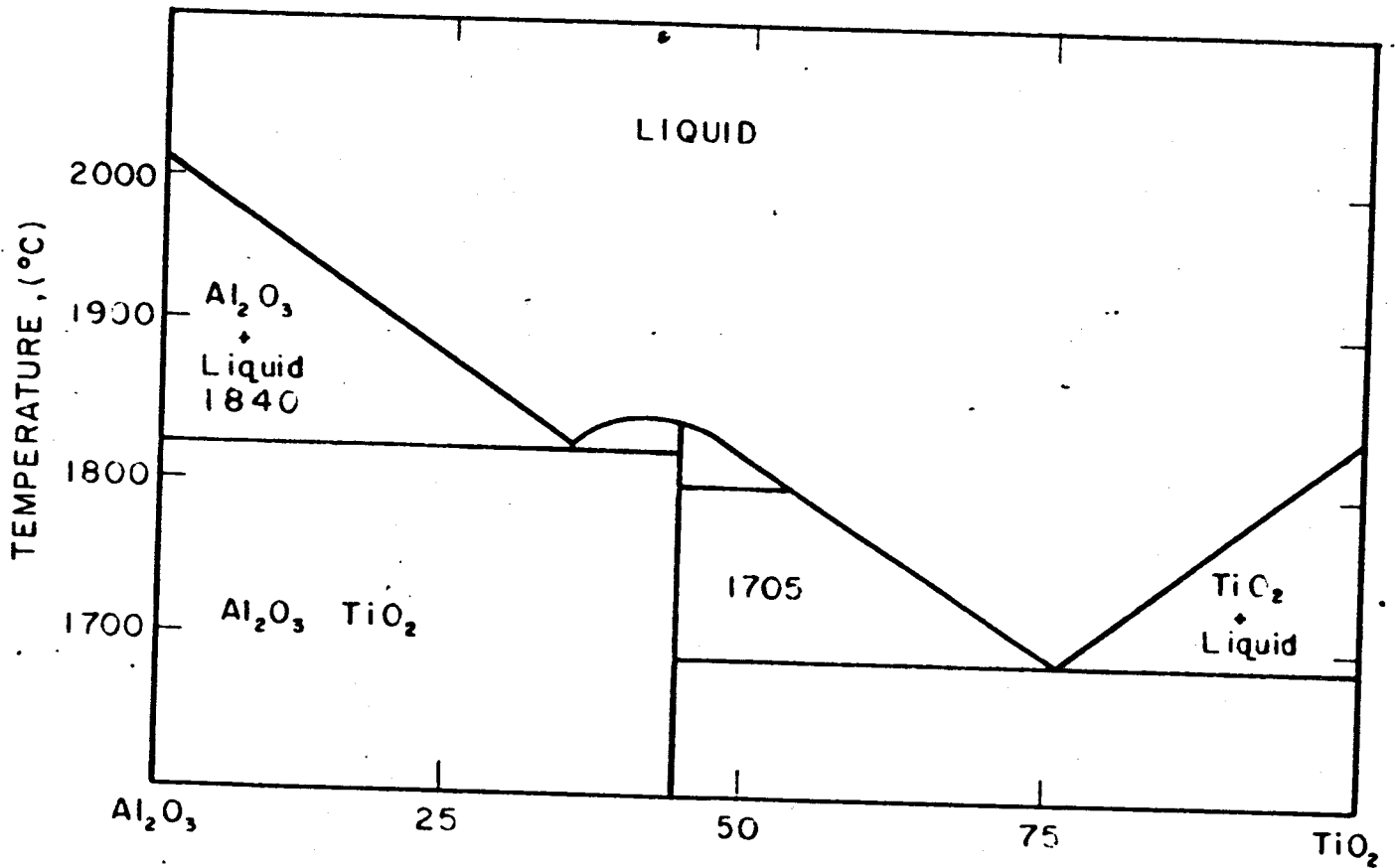IRON AND STEEL INSTITUTE. 42.99 , 1934-35

FIG. 3-7   THE TiO_2-Al_2O_3 SYSTEM   S.M. LANG, C.L. FILLMORE, L.H. MAXWELL,
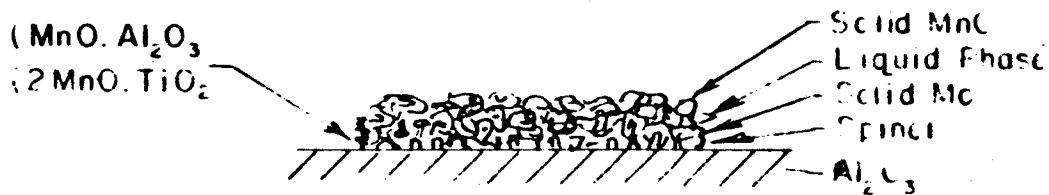J. NAT. BUR. STANDARDS, 48, (4) 301 (1952)

FIG.3-8a Mo, Mn, Ti PAINT SINTERED 100% ALUMINA CERAMIC
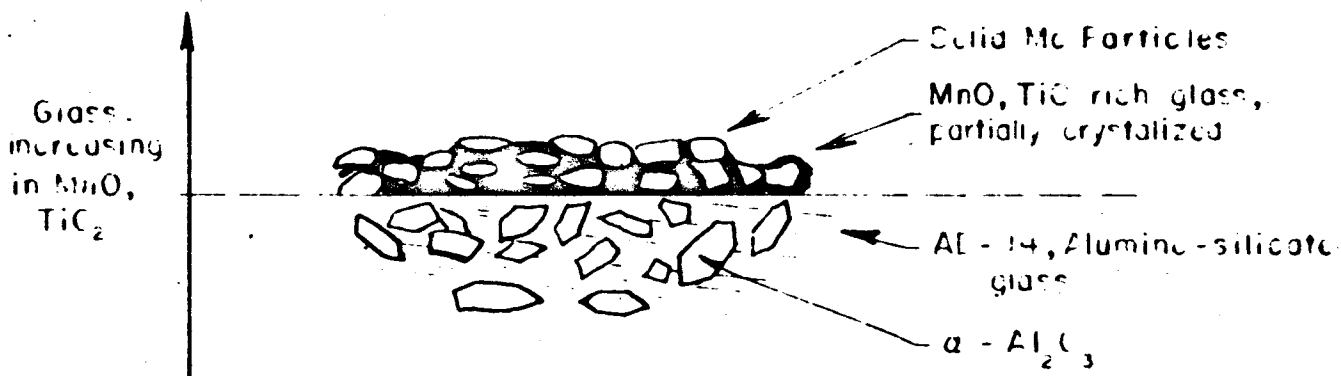
FIG.3-8b Mo, Mn, Ti PAINT SINTERED 94% ALUMINA CERAMIC
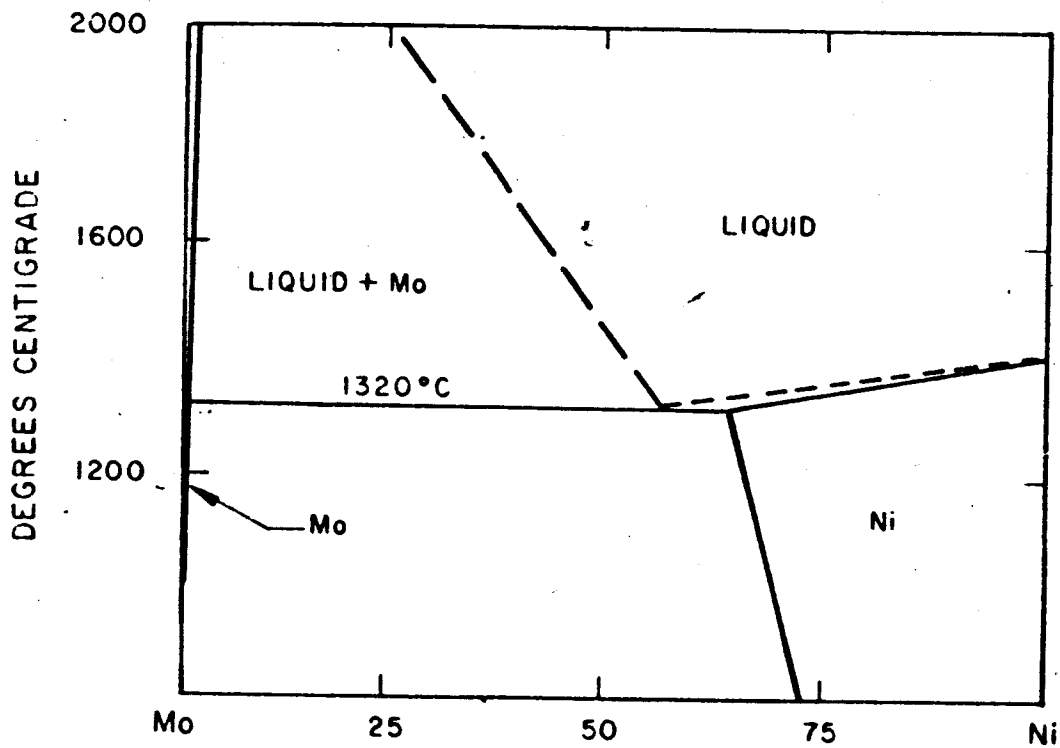
FIG. 3-9 THE Ni-Mo PHASE DIAGRAM (SIMPLIFIED)

does not wet molybdenum and tungsten well and is therefore a good intermediate layer material as it will not be absorbed by the molybdenum phase.

Some efforts have been directed at eliminating the intermediate layer but no successful process has been developed.

3.2.2.3 Brazing Operation

In commercial application the brazing of the metalized ceramic is typically accomplished by using the metal combinations given in Table 3-II, which all use a noble metal. In the presence of cesium vapor, the use of silver and gold is made undesirable by corrosion. Furthermore, the presence of silver is undesirable because of its tendency to migrate considerable distances across the ceramic.

Materials that do not dissolve the metalizing layer must be used in the intermediate plated layer and in the braze. Copper is one such material and is commonly used as a brazing layer between a nickel electroplate and a tantalum niobium, or tungsten structural component. The solid solubility of copper in the molybdenum at $900^{\circ}C$ is almost zero. Typically a braze will be made with a 0.004 inch copper solder washer at $1140^{\circ}C$ using a cycle which allows the copper to remain molten for 2 minutes. Another possibility is the use of a titanium-copper braze in which molybdenum structural part is used. A third possibility is the use of nickel-titanium.

A major problem with the use of copper at $500^{\circ}C$ or higher is the corrosion of the copper in cesium vapor (copper should be OFHC type or corrosion will take place at much lower temperatures).

The amount of brazing alloy applied and its location at or near the joint are also critical factors which frequently must be determined by experimentation on test samples. The furnace atmosphere has a critical influence on the seal quality, and it is generally recognized that moly-manganese seals require a slightly oxidizing atmosphere. A dew point of $25^{\circ}C$ is often chosen for the hydrogen.

TABLE 3-II

Metal	Composition	Liquidus °C	Solidus °C	Characteristics
Nicoro	Ni, Cu, Au	1020	990	Excellent wetting and flow on Kovar, copper, nickel and steel.
Wesgo 35% Au-65% Cu	Au, Cu	1005	970	For copper, Kovar, nickel brazes.
Nioro	Ni, Au	950	950	Will "wet" Tungsten and Moly as well as copper, Kovar, nickel, stainless steel. Excellent flow.
Wesgo 50% Au-50% Cu	Au, Cu	950	930	For copper, Kovar, nickel brazes where lower melting range dictates its use in place of more economical 35% Au-65% Cu alloy.
Nicoro 80	Au, Cu, Ni	910	900	Very low vapor presure, excellent wetting and flow. For secondary brazes on Kovar structures.
Cusil-Decarbonized	Ag, Cu	780	780	The eutectic alloy of silver and copper. Excellent flow, low melting, higher vapor pressure than gold alloys.

3.2.3 Active Alloy and Hydride Seals

Metal and ceramic parts are sealed in the active alloy process by inserting a thin sheet of metal that will form a reactive alloy with the ceramic and will also form an alloy with a brazing solder, as illustrated in Fig. 3-3. A wide choice of materials can be used, including many that seal at high temperature with little metallic evaporation. Materials can be used that can be predegassed at temperatures considerably above those used for final sealing.

Seals are made in a vacuum or inert gas. The parts can be stacked one on another so that several seals can be made at the same time. Seals have been made which can operate for many hours at temperatures as high as 800°C.

Figure 3-10 shows the seal components. Except for the usual cleaning and degassing, the metal and ceramic parts require no preparation prior to sealing. After being placed accurately into position, the parts are heated to a temperature high enough for the active metal and brazing solder to form a reactive alloy which can react with the ceramic and wet the structural metal part.

Titanium and copper can be used to form such a reactive alloy. If a shim of titanium is placed between copper and ceramic parts, an alloy will form at 875°C. That this should occur is evident from an inspection of the copper-titanium constitution diagram shown in Fig. 3-11. As soon as the temperature reaches 875°C, the titanium shim will alloy with the amount of copper needed to form a 28 percent titanium, 72 percent copper alloy. The thickness of the shim can be varied to control the amount of alloy formed. In the alloy, titanium is present in a liquid phase and can immediately come in contact with and react with the ceramic material and form the seal. Thus, the seal is completed and the heating can be stopped.

A typical seal is made by inserting a 0.0003-inch thick titanium shim between a copper shim and alumina parts. In this case, the amount of alloy that is formed causes the transition from metal to ceramic to occur over a region about two mils in width. The titanium
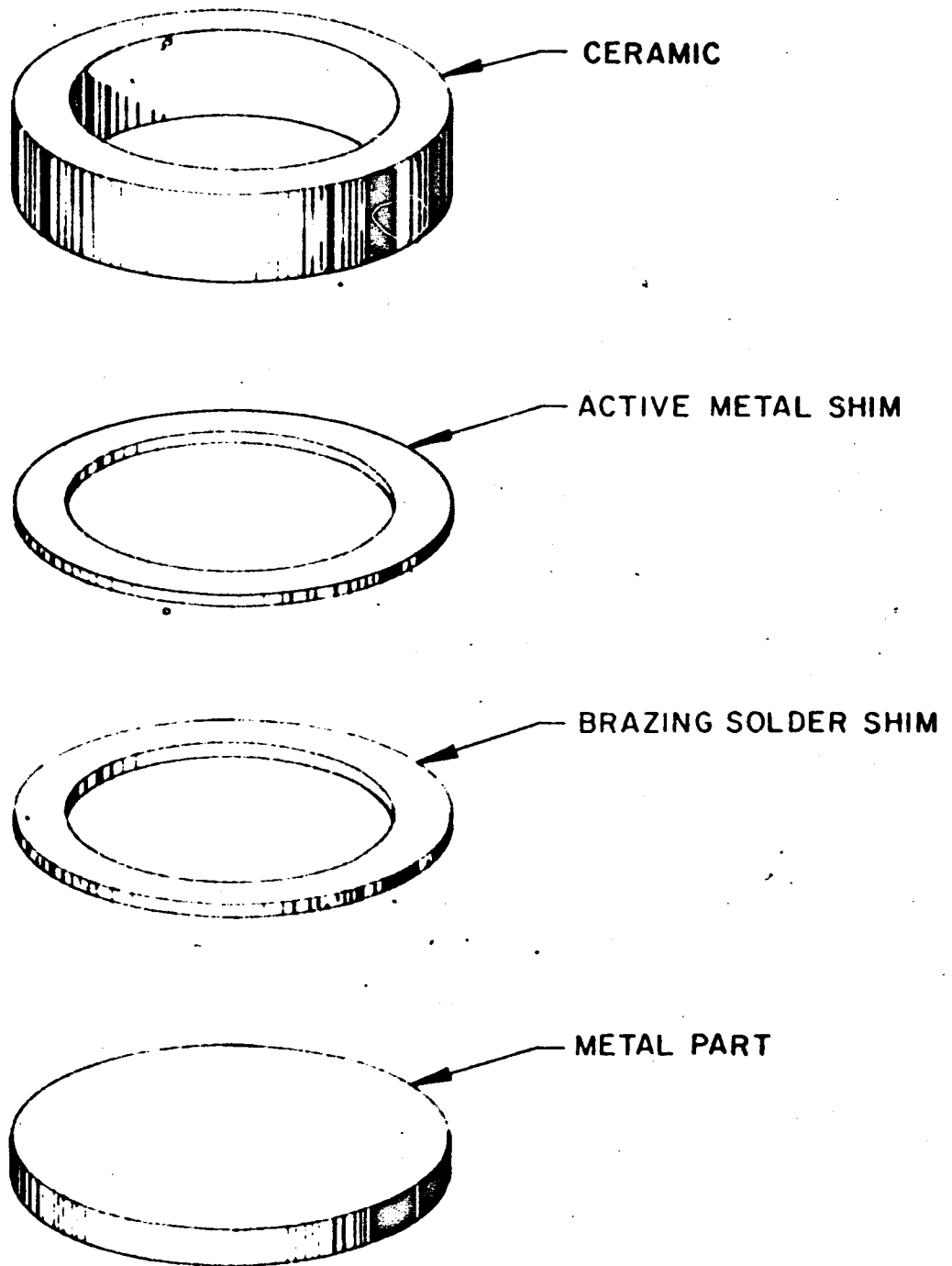
CERAMIC

ACTIVE METAL SHIM

BRAZING SOLDER SHIM

METAL PART

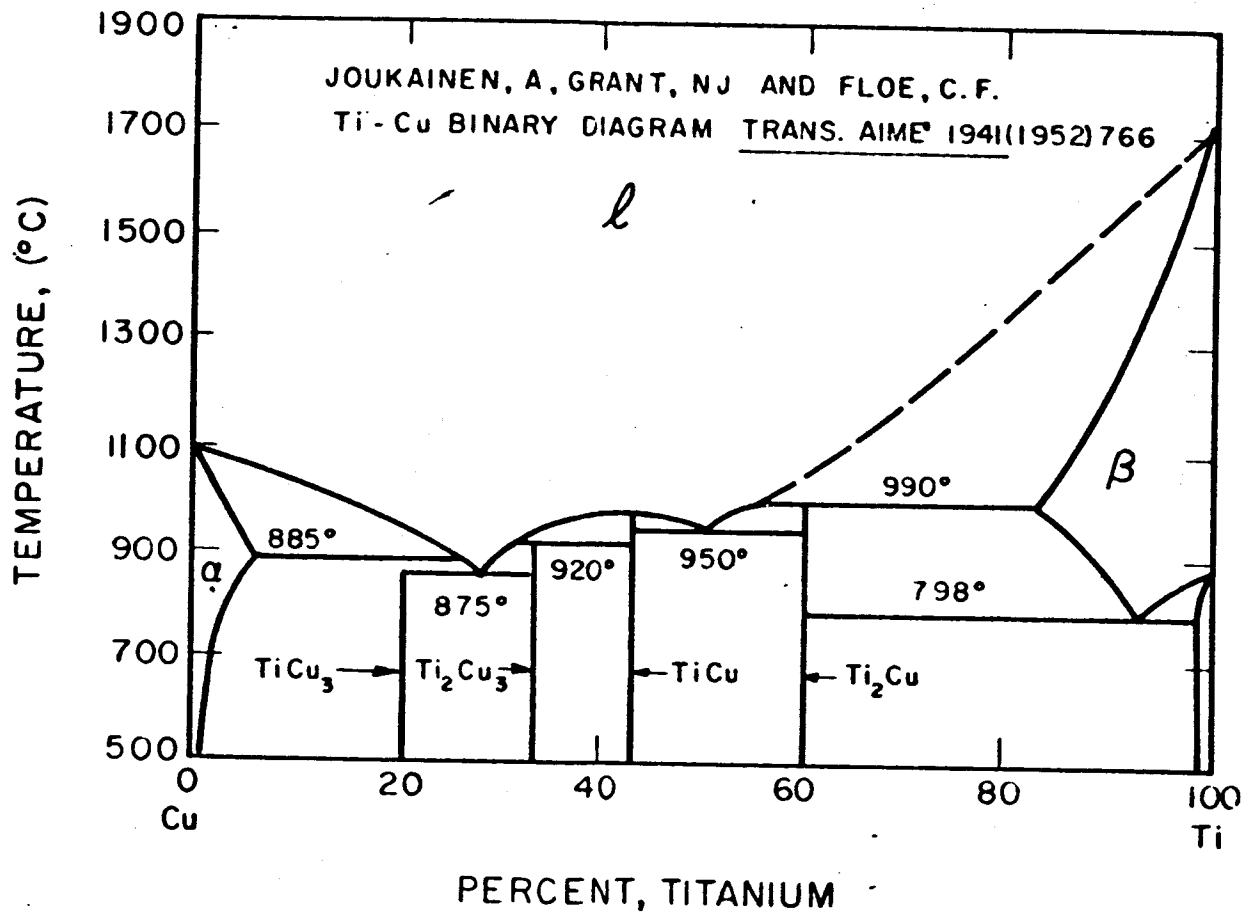FIG. 3-10   PARTS FOR AN ACTIVE ALLOY SEAL

54905

FIG. 3-11 COPPER - TITANIUM CONSTITUTION DIAGRAM

in the alloy reacts directly with the ceramic material to form an intimate bond.

Nickel is another metal that alloys readily with titanium. Figure 3-12 shows the Ni-Ti constitution diagram. It will be noted that about 11 percent nickel will reduce the melting point of titanium from approximately 1700°C to 955°C. Three eutectic points are present: 955°C, 1100°C, and 1285°C at 30, 66, and 84 percent nickel. Successful seals have been made in the range of temperatures from 955 C to 1300°C by using nickel parts with titanium shims, and from 955°C to 1100°C by using titanium parts with nickel shims.

A wide variety of materials can be sealed in this manner. Table 3-III shows a tabulation of a few of the materials that have been sealed and the temperatures at which the reactive alloys are formed. Also listed for each combination is the maximum temperature at which an enclosure can be sealed without formation of visible or conducting films. This is the temperature at which the most volatile component has a vapor pressure of 10^{-6} mm of Hg. Prolonged heating would require this maximum temperature to be somewhat lower, and rapid heating might permit it to be somewhat higher.

Molybdenum, tantalum, mobium, and tungsten do not form alloys with the active metals except at extremely high temperatures. They can be sealed to ceramic parts by using shims of two metals such as Ti and Ni, which will form a reactive alloy and wet the structural metal. In this case, it is usually desirable to use shim thicknesses that will give the eutectic proportions.

There are many combinations of metals that can be used to form reactive alloys. One of the metal shims must be an active metal such as titanium or zirconium. The other must be one that will form an alloy. It makes no difference which shim supplies the active metal. Nor does it make any difference whether or not the active metal is in contact with the ceramic. The sealing occurs as soon as the active metal is present in a liquid phase, when it can readily come in contact with and react with the ceramic material.
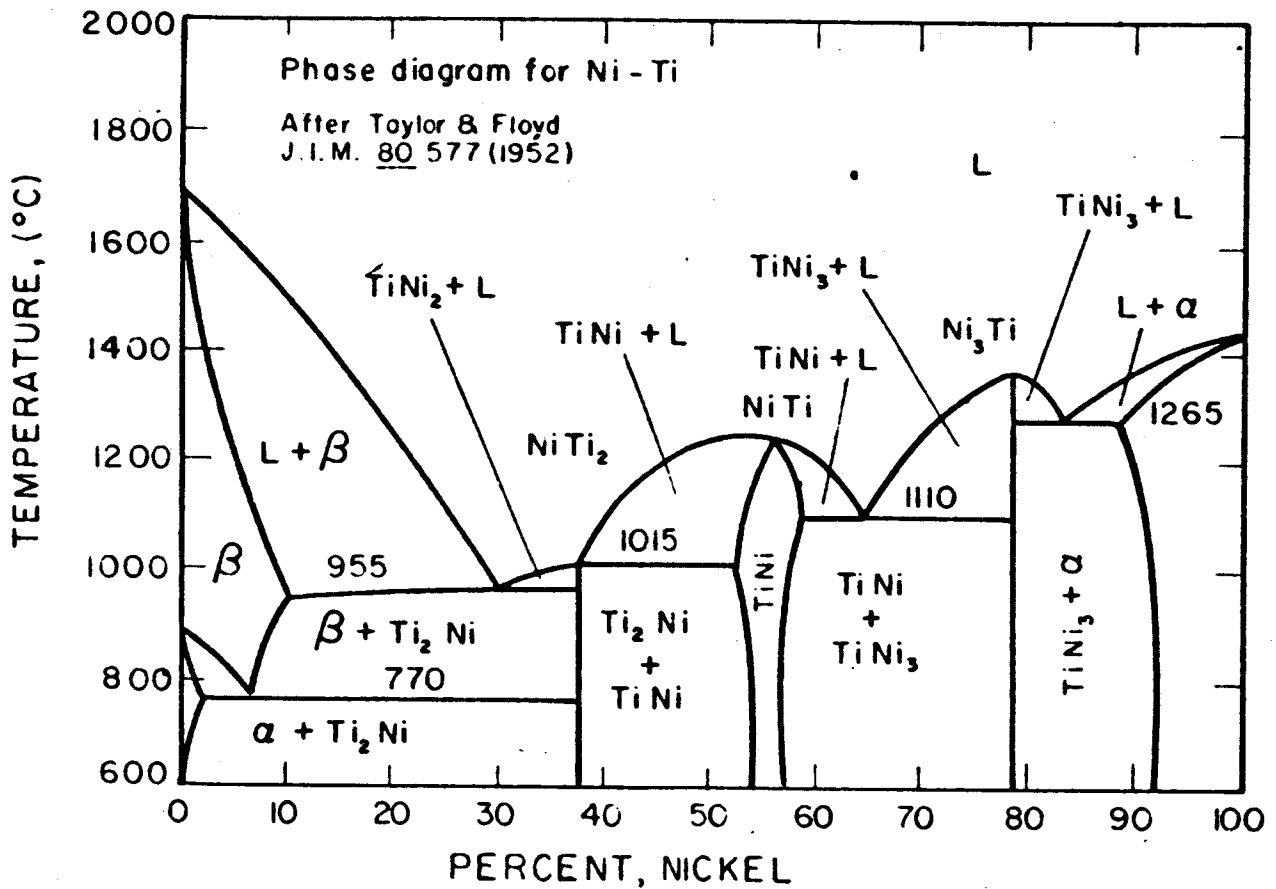
FIG. 3-12 NICKEL - TITANIUM CONSTITUTION DIAGRAM

164983

The amount of alloy that is formed depends largely on the particular metals chosen and the thicknesses of the shims that are used. In addition, it depends on the sealing temperature and the ceramic composition. Usually, the thickness of the shims necessary to provide a reasonable amount of reactive alloy might be in the range from 0.0003 to 0.0005 inch. However, they may be as thin as 0.0001 inch when the sealing is done at a temperature considerably above the eutectic temperature, or when ceramic bodies are used that have constituents that contribute to the amount of liquid formed. In fact, vacuum-tight seals can be made directly between titanium parts and some ceramic materials by heating to a temperature high enough for one of the ceramic ingredients to form an alloy with the titanium.

Satisfactory seals have been made to various alumina, forsterite, and zircon bodies. Usually, the strength of the seal is greater than 50 percent of the strength of the ceramic part. For large parts or where considerable heat shock might be encountered, it is desirable to use strong insulators and parts made of metals having now tensile strengths or materials having closely similar expansion-contraction characteristics. By proper choice of materials, it is possible to produce seals up to or even larger than 3 inches in diameter.

The seals are strongest when they are made in a vacuum of 10^{-4} mm of Hg or better, or in a pure, dry, inert gas. Impurities such as oxygen, nitrogen, carbon monoxide, and water vapor are detrimental because they reduce the ductility of the alloy, impair its reaction with the ceramic, and in general weaken the bond.

Prior to sealing, the parts must be flat to within a mil or less if successful butt seals are to be made with a minimum amount of alloy. Enough pressure must be applied during sealing to keep the parts intimately in contact. Formation of a minimum amount of sealing alloy is helpful in producing seals that are strong and is necessary when extremely small or thin insulators are being sealed. By stacking the parts one on the other, a large number of seals can be made at one time.

The ability of an alloy to bond with a ceramic body depends on the active metal used and the stability of the ceramic ingredients. For instance, an alloy containing titanium is more reactive than one containing tantalum, so that it will make a stronger bond to a stable oxide like alumina. On the other hand, if the ceramic body contains a material which is readily dissociated by the reactive alloy, porous seals can result.

TABLE 3-III

TYPICAL MATERIALS AND TEMPERATURES USED TO MAKE REACTIVE ALLOY SEALS WITH ALUMINA				
Active Metal Part	Braze Shim Material	Minimum Sealing Temperature $^{\circ}$C*	Maximum Sealing Temperature $^{\circ}$C**	Degassing Temperature $^{\circ}$C***
Cu	Ti	875	910	1000
CU	Zr	885	910	1000
Ti	Ni	955	1050	1200
Zr	Ni	960	1050	1200
Zr	Fe	934	1015	1200
Ni	Ti	955	1050	1200

* Temperature for formation of eutectic alloy.
** Limited by vapor pressure of most volatile material.
*** For the lowest melting material.

Powdered metals or metal hydrides can be used in lieu of foil shims. They can be painted on the ceramic surfaces in a manner similar to the molymanganese process using organic binders. The coated ceramics are placed in contact with the metal parts and, upon reaching an elevated temperature, a reactive alloy is formed and the seal is made as in the active alloy process.

Pearsall and Zingeser investigated the brazing of ceramics using the hydrides of titanium, zirconium, tantalum, and columbium. Zirconium hydrides showed somewhat superior wetting and bonding qualities of those of titanium hydride. Good results were also obtained with the hydrides of tantalum and columbium. It was

found possible to braze with alloys of these active metals as well as with their hydrides; silver, copper, and aluminum alloys were tried. For the case of zirconium, the brazing operation was successfully carried out in an atmosphere of dry nitrogen, while the titanium braze worked best in an inert atmosphere.

It was observed during the formation of alloys produced by heating brazing metals and metallic hydrides that most of the hydrogen was evolved at or near the melting point of the alloy, which was considerably below the values given for the dissociation of the hydride alone. After placing a piece of suitable solder in contact with the hydride-coated surface, the material is heated to approximately $1000^{\circ}C$ or to a temperature at which the solder flows freely in a vacuum or in an atmosphere of pure hydrogen or pure inert gas. When the proper temperature is reached, the brazing alloy will melt and flow over the hydride coated surfaces in a manner somewhat similar to that in the brazing of metals.

Titanium hydride, used by Bondley, exhibited considerable sensitivity to small amounts of oxygen and water and somewhat less sensitivity to nitrogen during the brazing operation. Large amounts of nitrogen will promote formation of titanium nitride and prevent bonding. Both titanium and zironium hydrides are very sensitive to small amounts of oxygen; conversion to their respective oxides will completely inhibit the brazing operation.

Zirconium hydride can be heated in vacuum at approximately 800° to $1000^{\circ}C$ to remove most of the hydrogen, leaving behind a relatively pure zirconium metal powder. This partially sintered metal powder may be exposed to air and then used in a manner similar to zirconium hydride to produce an equally good braze. In contrast to most zirconium metal powders, the sintered metal does not seem to be highly pyrophoric. The fact that the hydrogen may be removed prior to the brazing, and the reduced hydride exposed to the air, indicates that hydrogen is not essential to the process. Attempts to use titanium

hydride in a similar manner were not successful; this may be attributed to oxidation of the titanium metal and air. Apparently the function of the hydride is to yield a relatively pure active metal, free to alloy with a suitable solder. Pearsall and Zingser investigated a large number of brazing alloys, most of which are not particularly suitable for thermionic converter application because they contained a noble metal such as silver and gold.

3.2.4 Seal Strength

There are two primary factors to consider when evaluating the strength of a ceramic-metal seal.

1. The adherance of the braze to the ceramic and metal parts.
2. The relative thermal expansion coefficients of the ceramic, the metal, and the braze material.

Braze adherance can be measured by several methods, the most common of which is a tensile test where the ceramic and metal specimens are pulled apart with a force parallel to the axis of symmetry. Compression and peel tests are also used for evaluation. Cole presents a description of each test and shows an empirical equivalence between the tensile, peel, and compression tests.

A good braze will have tensile strength on the order of or greater than the safe limit on ceramic tensile stress. Although alumina tensile strengths of over 30,000 psi have been demonstrated, a limit of 10,000 to 15,000 psi is regarded as maximum for consistently leak-tight seals.

Cole presents the results of tensile tests of several samples using alumina ceramics with a moly-manganese type of braze using copper solder. As shown in Tables 3-IV and 3-V, the results illustrate the wide variation in adherance strengths which can occur with minor variations in braze composition and time and temperature history.

It has been shown previously that the sealing zone between a metal and ceramic is complex, and displays fairly extensive cation diffusion and the formation of intermediate oxide or glassy layers.

TABLE 3-IV

Composition and Weight (gm)	Sintering Temperature	Body	Tensile Test Values
295.5 Mo 7.5 Ti	1500°C	AD-94[2]	28,400 19,350 16,400
270 Mo 30 LiMnO$_3$	1500	AD-94	15,500 15,700 14,500
291 Mo 9 (MgO, SiO$_2$)	1600	AD-94	12,300 17,900 16,100
240 Mo 73.6 CeO$_2$	1500	AD-96[3]	9,430 22,000 16,050
255 Mo 48 SiO$_2$ 22 Mn	1300	AD-96	15,700 13,200 10,700
255 Mo 48 SiO$_2$ 22 Mn	1500	AL-23[4]	14,000 16,100 15,200
255 Mo 48 SiO$_2$ 26 MnO	1500	AL-23	11,300 11,600 16,100

TENSILE STRENGTH OF SEVERAL SEALS[1]

1 Copper brazing solder was used

2 Coors 94 percent alumina

3 Coors 96 percent alumina

4 Materials for Electronics, Inc. 99.6 percent alumina

TABLE 3-V				
RESULTS OF TENSILE TESTS				
Ceramic type*	Metallizing sintering temperature (°C)	Tensile strength of seals (lb/sq in.)		
		80% Mo 20% Mn	97% Mo 3% Ti	100% Mo
AD-99	1700	2900	6600	1700
	1600	750	2700	600
	1500	3100	2900	220
AD-94	1700	9400	12000	9600
	1600	9700	12000**	13000
	1500	8000**	10100	10600

* Designation of the Coors Porcelain Company, Golden, Colorado
** Average values based on several hundred production control tests

It might be expected that this area should be weaker than either the ceramic or metal, and that its strength should be strongly affected by the development of the bonding layer. It is a rather surprising fact, therefore, that seals commonly fail in the ceramic adjacent to, but not directly at, the metal-ceramic interface. This might result from the following factors:

1. The surrounding ceramic is weakened during the sealing process. Mechanisms for such a deterioration are certainly available; for example, infiltration of Ti and other impurity ions, as well as liquids, can catalyze harmful grain growth in the ceramic. Furthermore, if these liquids solidify to glasses, strength will be much reduced in the permeated areas. However, these processes also occur in the seal zone itself-- and probably to a greater extent than in the neighboring ceramic; consequently, there is no reason for the deterioration to be greater outside the bonding layers than at the seal interface.

2. The bonding layer can undergo limited plastic deformation above its elastic limit whereas the adjacent ceramic fails by cracking. In the case of active metal or hydride seals on a pure oxide, the plasticity argument is supported by observations on alumina and zirconia ceramics containing very thin films of titanium. Such composites show a ductile type of indentation and have even been bent through an angle of about 3-1/2 degrees at 660°F.

   Ductility at the seal interface is a desirable condition since this area is normally a zone of weakness. However, if plastic deformation is a possibility, the strength of the joint is set by that of the ceramic itself (minus residual stresses caused by expansion discrepancies) and it is in the ceramic that failure occurs. This limited ductility probably has its highest development in active metal or hydride seals on pure oxides. Where bonding occurs through

a glassy phase rather than through suboxide layers, it might be predicted that plastic deformation at low temperature will be at a minimum and that the seal will fail right at the interface. In this case, the strength of the seal will probably depend on the amount of glassy phase present and on such other factors as the extent of penetration of the glass into the ceramic, the development and characteristics of the oxide layer on the metal, and its solution in the glass.

Few metals have coefficients of expansion similar to the ceramics of interest to thermionic converters. For a reliable seal, careful consideration must be given to the individual component expansion curves, the thermal cycle, the section size and strength of the ceramic, the strength and dimensions of the metallic body, the expansion coefficient and ductility of the filler alloy, and the geometry of the component being joined. A rough analysis of the stresses developed during bonding can be made if these factors are understood.

The thermal expansion curves for several materials of interest are shown in Fig. 3-13, based on manufacturer's data and several literature references. The refractory metals tungsten, molybdenum, niobium and tantalum exhibit expansion coefficients which are less than the coefficients for alumina bodies. Niobium is closest to matching alumina, particularly the 100 percent pure alumina; tantalum also appears usable. An increase in the glassy constituents of an alumina body increases the expansion coefficient, a desirable feature of pure alumina.

For thermionic converter application, the combination of high purity alumina in combination with either niobium or tantalum is used almost exclusively where high seal temperatures will occur. This selection is made because of the thermal expansion match and the relatively low yield strength of the metals (about 10,000 psi for tantalum at 1000°C and about 30,000 psi for niobium at 1000°C).
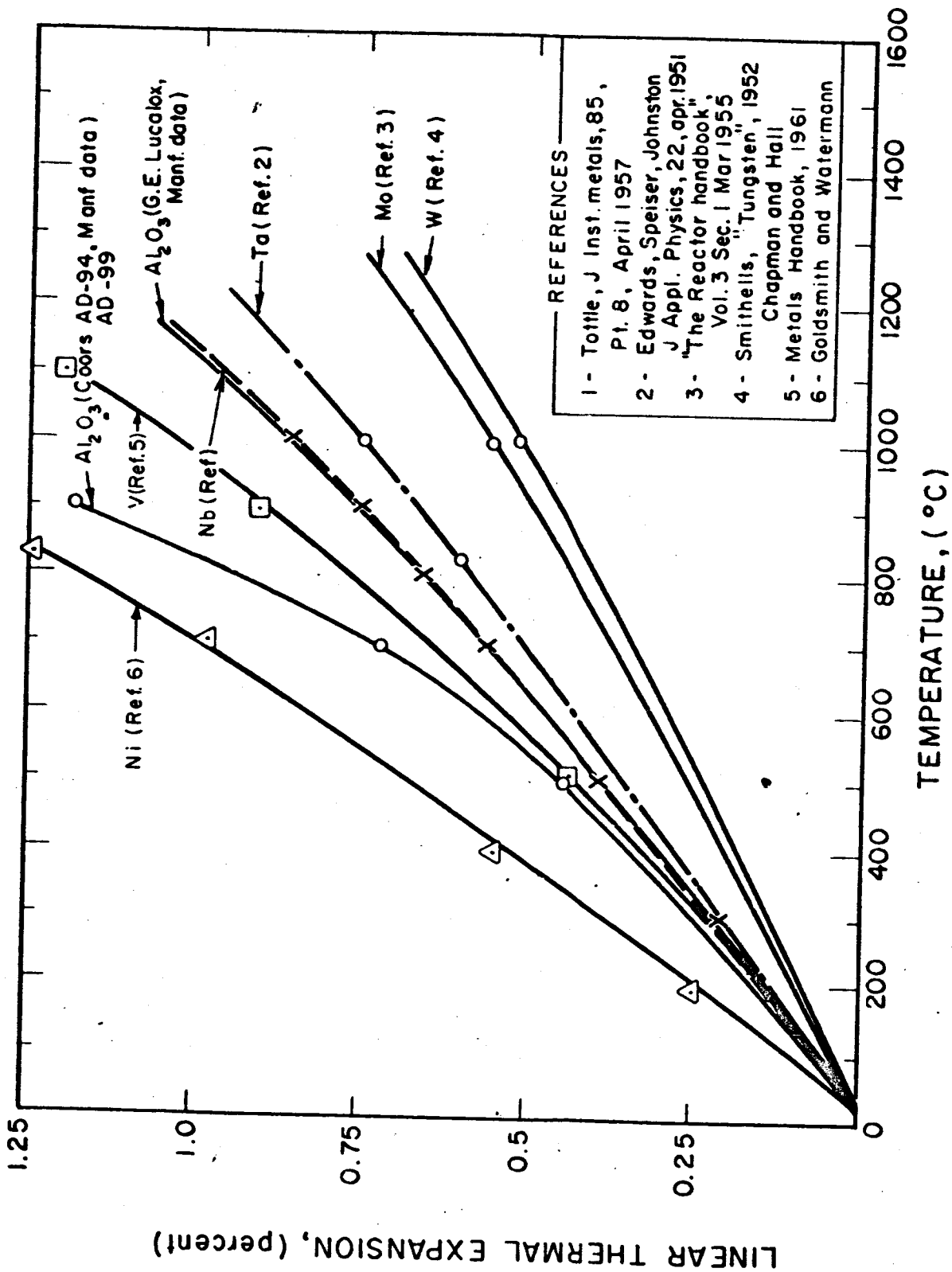
FIGURE 3-13   LINEAR THERMAL EXPANSION OF SELECTED ENVELOPE AND SHIM MATERIALS
W, Ta, Mo, Nb, Al₂O₃ , V and Ni

Consider a compensated butt seal such as is shown in Fig. 3-14, made of tantalum and AD-94 alumina ceramic. Differences in thermal contraction between metal and ceramic cause stresses to be set up in the ceramic (and metal) during cooling of the seal from the temperature at which the brazing alloy freezes. These stresses may be diminished by the yielding or plastic flow of the metal or brazing alloy during cooling.

Residual stresses produced in the ceramic by the differential contraction are the result of radial shear forces, V_o, which act around the circumference on the end of the ceramic cylinder (Fig. 3-14). Associated with these shear forces is a bending moment, M_o, which tends to cause the walls of the cylinder near the seal end to bend outward toward its axis. Figure 3-14 and the discussion in this section are based on the situation in which the ceramic has a higher thermal expansion coefficient than the metal. For the opposite case, the direction of forces and sign of stresses will be reversed. The bending moment creates axial tension on the inner surface of the cylinder and axial compression on the outer surface with maxima for each occurring a short distance from the seal interface. A tensile circumferential or hoop stress is also produced in the ceramic cylinder as a result of the radial shear forces.

The forces cause a radial displacement of the ceramic cylinder walls away from its axis and, if unrestrained, a change of slope, θ, of the ceramic wall. Because the ceramic cylinder is rigidly held at the interface, the effect of a change in slope can be considered to be counteracted by a second bending moment which acts as shown in Fig. 3-14 to make θ zero.

For well-matching combinations of ceramic and metal, residual stresses which result from sealing the two materials together will be low. Most ceramic-metal seals employed today, however, rely on yielding of the metal part to limit the stresses on the ceramic. This condition exists, for example, for alumina or forsterite ceramics
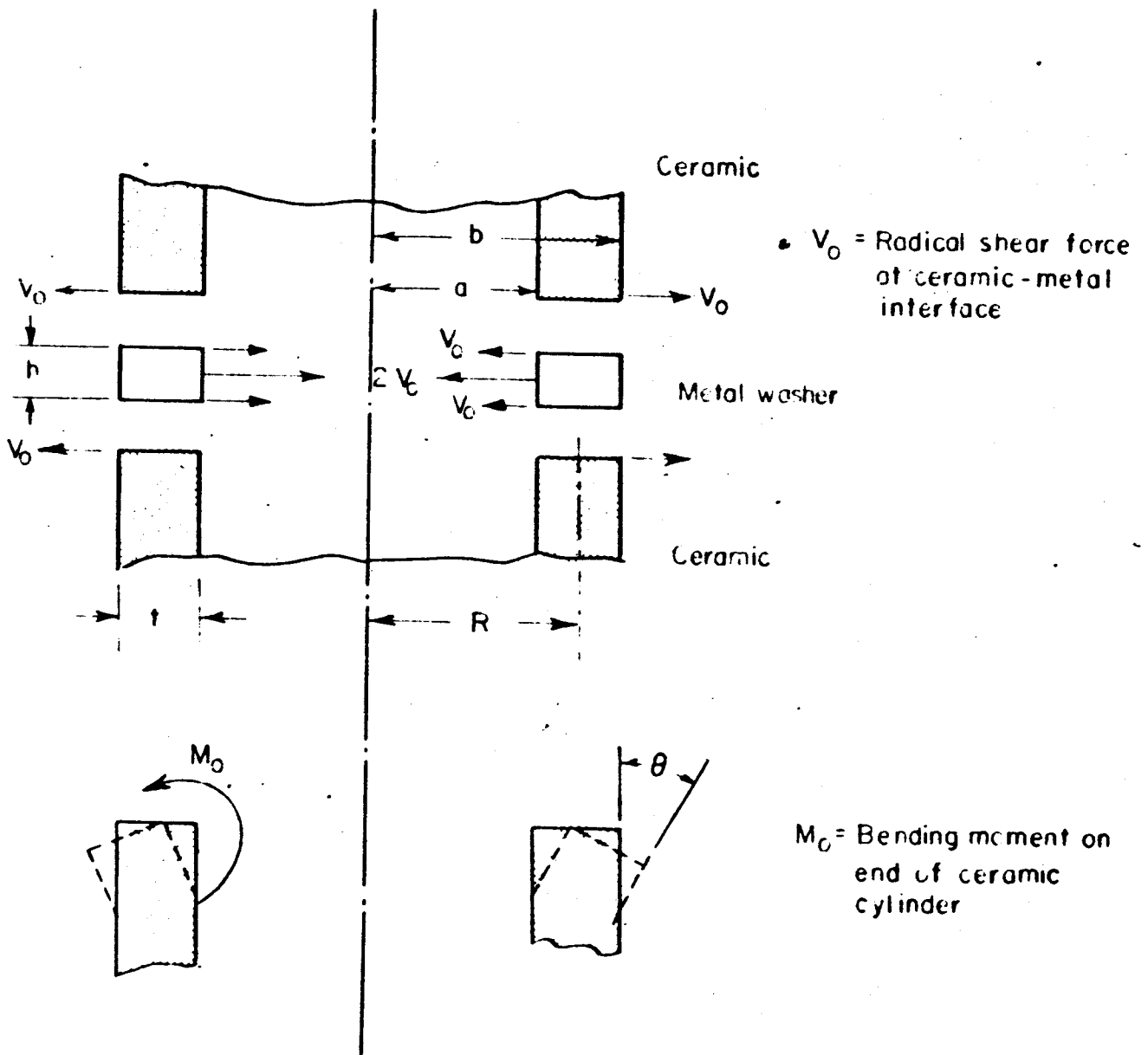
FIG. 3-14   FORCES ON COMPENSATED BUTT SEAL

Labels within figure:

Ceramic

V_0 = Radical shear force at ceramic-metal interface

Metal washer

Ceramic

M_0 = Bending moment on end of ceramic cylinder

sealed to copper, nickel, copper-clad stainless steel, tantalum and niobium. Under these conditions, therefore, it can be assumed that the maximum residual stress on the ceramic will be determined by complete yielding of the metal to which it is bonded so as to limit the radial shearing force V_o. A metal washer with a ceramic cylinder sealed to each face will have a radial shearing force V_o per unit length of circumference acting on each face as shown in Fig. 3-14. For thin metal washers, this force can be represented, as shown, by a radial shearing force equal to $V = 2V_o$ acting on the mean radius R in the plane through the center of the disk parallel to its surfaces. This force will exert a radial pressure inward equal to:

$$P_r = \frac{2V_o}{h}$$

where he is the thickness of the metal disk in inches.

A washer may be considered as a short cylinder under internal pressure. According to Timoshenko, the internal pressure required to bring the entire wall of a cylinder into a state os plastic flow is:

$$P = -2T_{yp} \ln\left(\frac{a}{b}\right) = 2T_{yp} \ln\left(\frac{b}{a}\right)$$

Where T_{yp} is the yield point of the metal in shear, P is the internal pressure in psi and a and b are the internal and external radii of the cylinder, respectively.

Expressing the pressure on the mean radius R as a function of the internal pressure

$$P_r = \frac{aP}{R} = \frac{2aT_{yp}}{R} \cdot \ln\left(\frac{b}{a}\right)$$

Substituting the value for P_r gives for V_o, the radial shearing force per unit length of circumference of the ceramic

$$V_o = \frac{ahT_{yp}}{R} \cdot \ln\left(\frac{b}{a}\right)$$

The equation above represents the maximum radial shearing force resulting from complete yielding of the metal washer.

Using the expression for V_o obtained above, the maximum hoop and axial stresses on the ceramic cylinder can be calculated as a function of the axial distance from the seal interface.

Substituting equations from Roark, the following formulas can be derived (see Fig. 3-14 for nomenclature).

Maximum Hoop Stress

$$\left(S_h\right)_{max} = \frac{V_o \lambda R}{t} = \frac{ah\lambda T_{yp}}{t} \ln\left(\frac{b}{a}\right)$$

where

$$\lambda = \left[\frac{3\left(1-\upsilon^2\right)}{R^2 t^2}\right]^{1/4}$$

and

υ = Poisson's ratio for the ceramic (about 0.3)

Maximum Axial Stress

$$\left(S_a\right)_{max} = \frac{2.22\, V_a}{\lambda t^2} = \frac{2.22\, ahT_{yp}}{\lambda R t^2} \ln\left(\frac{b}{a}\right)$$

$$\approx \left(S_h\right)_{max} (1.335)$$

The maximum axial stress occurs at a distance X from the interface where

$$X = \frac{1.095}{\lambda}$$

For the case under consideration where the ceramic has a higher coefficient of expansion than the metal, both $\left(S_h\right)_{max}$ and $\left(S_a\right)_{max}$ are tensile stresses. For the case where the expansion coefficient of the metal is lower, $\left(S_h\right)_{max}$ is compressive.

Using the equation above, calculations can be made to determine the effect of seal dimensions on the maximum residual stress on the ceramic which could be produced by sealing together mismatching combinations of metal and ceramic. Actual stresses may be below this level if the elastic stresses are insufficient to cause complete

yielding of the metal. In Fig. 3-15, the maximum axial stress, $(S_a)_{max}$, divided by the thickness of the metal, h, and its yield point in shear, T_{yp}, has been plotted against the wall thickness of the ceramic cylinder for cylinders of 1/2, 1, 2, and 4 inches in outside diameter. The curves are applicable to any ceramic inasmuch as the only distinctive factor involved in these calculations is Poisson's ratio, υ, which does not vary greatly for ceramics.

The curves in Fig. 3-15 show that the maximum residual axial stress diminishes rapidly with increasing wall thickness of the ceramic. The maximum axial stress also decreases with increasing diameter of ceramic cylinders of constant wall thickness. These relationships apply to the effect of variables cited on stress limits, not to stresses themselves.

The effects indicated in the figure and in the equation apply only to maximum stresses which can result from differences in thermal expansion between the metal and ceramic as limited by yielding of the metal. Other important factors also contribute to actual stresses developed in seals. Among these are thermal stresses arising from temperature gradients. It is well known that large thick-walled ceramics will fail from thermal shock alone if heated or cooled too quickly, whereas small thin-walled pieces may often be taken in and out of very hot furnaces without failure. Large pieces are also statistically subject to a greater number of flaws, which lower strength and produce localized stresses. These factors make the design of brazing fixtures and the rate of heating or cooling extremely important.

The maximum hoop or axial stress as limited by yielding of the metal in the butt seal is directly proportional to the thickness of the metal. Below these stress limits in the elastic behavior region, this proportionality may not apply. For metal thicknesses of from about 10 to 30 mils, the relationship between thickness and strength does not differ greatly from a linear one.
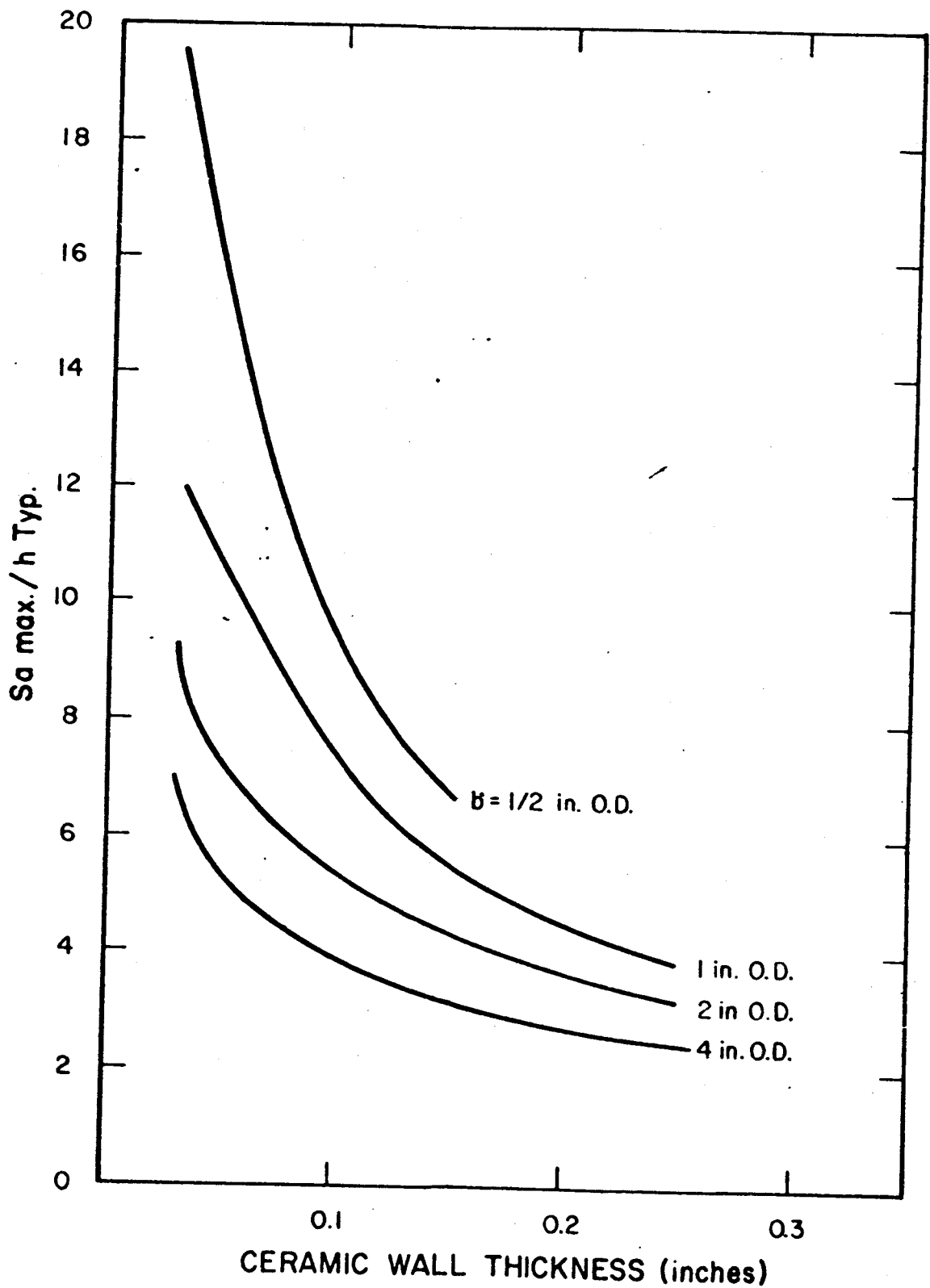
FIG. 3-15 EFFECT OF WALL THICKNESS AND DIAMETER ON CALCULATED MAXIMUM
AXIAL STRESS IN CERAMIC MEMBER

To summarize, residual stresses in ceramic-metal butt seals of the type shown in Fig. 3-14 may be reduced by one or more of the following methods:

1. Using of materials having comparable thermal expansions.
2. Keeping metal thickness at the minimum consistent with strength requirements.
3. Increasing wall thickness of the ceramic and the width of seal area for a constant outside diameter.
4. Using sandwich-type seals, i.e., ceramic cylinders on both sides of the metal.
5. Using ductile metals or brazing alloys, alloys clad with a ductile metal, or buffer washers of a ductile metal placed between the nonmatching metal part and the ceramics.
6. Heat treating seals.

The case for cylindrical seals is well explored in the literature and formulas can be found for maximum stress in Roark. Timenskiko and other standard texts. If the ceramic has a higher expansion coefficient than the metal, the metal should be sealed inside the ceramic to maintain the ceramic in compression. At. the seal the metal wall should be very thin to provide a yielding member.

REFERENCES

Section 3

1. H. Pulfrich: "Ceramic-to-Metal Seal," U. S. Patent 2, 163, 407 (June 20, 1939); Ceram. Abstr. 18, (8), (1939), p. 226.

2. H. Pulfrich and R. Magner: "Ceramic-to-Metal Seal," U. S. Patent 2, 163, 410 (June 20, 1939); Ceram. Abstr. 18, (8), (1939), p. 226.

3. H. Pulfrich; U. S. Patents, 2,163,408 (1939); 2,163,409 (1939); 2,174,390 (1940); German Patent 659,427 (1938).

4. M. J. Gross: "New Vacuum-Tube Techniques of Telefunken Rohrenwerke; Berlin, "FIAT Final Report, No. 560, PB 17, 553 (Dec. 2, 1945).

5. H. Bender: "High Temperature Metal-Ceramic Seals," Ceramic Age, 63 (Apr. 1954), pp. 15-24.

6. H. J. Nolte and R. F. Spurck: "Metal-Ceramic Sealing with Manganese," Television Eng., _ (Nov. 1950), pp. 14-18.

7. W. E. Coykendall: "Annular Ceramic Tube," Ceramic Age, 63 (Mar. 1954), pp. 33-36, disc. p. 36.

8. D. G. Burnside: "Ceramic-Metal Seals of the Tungsten-Iron Type," RCA Review, 15 (March, 1954), pp. 46-61.

9. R. J. Bondley: "High Temperature Metal-Ceramic Brazed Seals," Electronics, 20 (7), (1947) pp. 97-99.

10. C. S. Pearsall, P. K. Zingeser: "Metal to Non-Metallic Brazing," Tech. Rep. No. 104, Res. Lab. of Electronics, MIT (Apr. 5, 1949).

11. R. J. Bondley: "Low-Melting-Temperature Solders in Metal-Ceramic Seals," Ceramic Age, 58 (1), (1951), pp. 15-18.

12. G. W. Hume, "New Aluminum-Ceramic Bond Produces Hermetic Seal," Materials and Methods, 41 (Apr. 1955), pp. 110-111.

13. H. Bender: "New Developments in Metal-Ceramic Seals," Sylvania Technologist, 8, (Jan. 1955), pp. 22-26.

14. E. Ryshkewitch, Oxide Ceramics, Physical Chemistry and Technology Chap. 9, pp. 437-451, Academic Press, (1960).

15. V. F. Zackay, D. W. Mitchell, S. P. Mitoff, J. A. Pask: "Funda- mentals of Glass-to-Metal Bonding: Pt. I. Wettability of Some Group I and Group VIII Metals by Sodium Silicate Glass," Amer. Ceramic Soc. Jnl., 36 (March 1953), pp. 84-89.

16. S. P. Mitoff: "Fundamental of Glass-to-Metal Bonding: Pt. II. Reactions of Tantalum and Sodium Silicate Glass," Amer. Ceramic Soc. Jnl., 40 (Apr. 1957), pp. 118-120.

17. W. D. Kingery: "Role of Surface Energies and Wetting in Metal-Ceramic Sealing," Amer. Ceramic Soc. Bull., 35 (March 1956,), pp. 108-112.

18. B. C. Allen and W. D. Kingery: "Surface Tension and Contact Angles in Some Liquid Metal-Solid Ceramic Systems at Elevated-Temperatures," Trans. AIME, 215, (1959), pp. 30-37.

19. W. D. Kingery and F. H. Norton: "Study of Metal-Ceramic Interactions at Elevated Temperatures," MIT Progress Report Submitted to AEC, Oak Ridge, Tennessee, Contract No. AT(30-1)-1192.

20. A. E. Williams: "Bonding Ceramics to Metals," Industrial Finishing (London) 10 (Jan. 1958), pp. 22-26.

21. A. E. Williams: "Bonding Ceramics to Metals, Pt. 2," Ceramics, 9 (Dec. 1957) pp. 26-30.

22. H. Adam: "Compressed Glass-to-Metal Seals," Soc. of Glass Tech., Jnl., 38, No. 182 (June 1954), pp. 285T-296T.

23. B. G. Bender: "How to Seal Glass to Metal in Mass Output," Ceramic Industry 57, (Dec. 1951), pp. 76-78, 113, 115.

24. P. Whibley: "Glass Tube Technology, I. Glass to Metal Seals," Eng. Exp. Station News (Ohio State Univ.) 23 (Dec. 1951), pp. 48-51, 55-56.

25. H. Schwartzbart: "Fiber Metal Shim Brazing." Armour Research Foundation, Document No. 60-156 BX.

26. J. E. Beggs: "Sealing Metal and Ceramic Parts by Forming Reactive Alloys," Inst. of Radio Engineers, Professional Group on Component Parts, Trans. 4 (Mar. 1957), pp. 28-31 (ema).

27. H. Rawson and E. P. Denton: "The Glass Sealing Properties of Titanium and Zirconium," British Jnl. of App. Phys., 5 (Oct. 1954) pp. 352-353.

28. W. Knecht: "Application of Pressed Powder Technique for Production of Metal-to-Ceramic Seals," Ceramic Age, 63 (Feb. 1954), pp. 12-13, disc. p. 13.

29. W. Knecht: Air Force Tech. Rep. No. 6101 (Feb. 1950).

30. H. Palmer: "Review of High Temperature Metal-Ceramic Seals." Electrochemical Society Jnl., 102 (July 1955), pp. 160e-164c.

31. N. Anton: "Fused Vacuum Tight, Metal-to-Ceramic, Ceramic-to-Glass, Metal-to-Glass, and Metal-to-Mica Sealing by Powdered Glass Technique," Ceramic Age, 63 Sec. I (June 1954), pp. 15-16, 18-19, disc. p. 19.

32. "Development of High Altitude Waveguides," Work in Progress, WADC Contract No. AF(33) (600)-32202, Armour Research Foundation Project No. E 066.

33. L. J. Cronin: "Trends in Design of Ceramic to Metal Seals for Magnetrons," Amer. Ceramic Soc. Bull., 35 (Mar. 1956) pp. 113-116.

34. H. Hermann: "Optical Stress Measurements on Glass-Metal Bonds at Higher Temperature," Zeitschrift fur Angewandte Physik, 7, No. 4, (Apr. 1955), pp. 174-176 (In German).

35. H. Hermann: "Modern Testing Method for Glass-Metal Joints by Use of Polarized Light," Metall, 9, Nos. 17-18 (Sept. 1955), pp. 744-747 (In German).

36. T. L. Evans: "Ceramic-to-Metal Seals for Vacuum Tubes," Ceramic Age, 64, sec. 1 (Aug. 1954), pp. 9-13, disc. pp. 13-14.

37. M. Kuhner: "Metal-Ceramic Seals," Vide 2 (7), (1947), pp. 194-204; Ceram. Abstr. (Sept. 1947) p. 180.

38. A. G. Pincus: "Metallographic Examination of Ceramic-Metal Seals," Amer. Ceram. Soc. Jnl., 36 (May 1953), pp. 152-158.

39. S. S. Cole, Jr. and J. E. Inge, "Calculation and Measurement of Stress in a Ceramic-to-Metal Seal," Ceramic Bulletin, 40, No. 12, pp. 738-743, (Dec. 1961).

40. S. Timoshenko and J. N. Goodier: "Theory of Elasticity," McGraw-Hill Book Co., New York (1951).

41. S. Timoshenko: "Strength of Materials, Pt. II, Advanced Theory and Problems," D. Van Nostrand Co., Inc., New York (1956).

42. RADC-TR-60-236, Final Technical Report, "Metal-to-Ceramic Seal Technology Study," Contract No. AF 30(602)2047, prepared by Cole, et al, October 1960, AD 248 535 -- also RADC-TN-59-370, RADC-TN-60-53, RADC-TN-60-108, RADC-TN-60-192, first through fourth technical notes.

43. R. J. Roark: "Formulas for Stress and Strain," 2nd Ed. McGraw-Hill, (1943), p. 261.

44. "Seal and Insulator Problems in Thermionic Converters," Summary Report Contract NONR-33(00), Armour Research Foundation Report ARF 2215-6, (Mar. 1962).

45. W. Kohl: "Electron Tubes for Critical Environments," WADC-TR 57-434, (Mar. 1958).

46. W. Kohl: "Materials and Techniques for Electron Tubes," Reinhold, (1960).

47. G. Van Houten: "A Survey of Ceramic-to-Metal Bonding," Amer. Ceram. Soc. Bull. 40 (June 1959), pp. 305-307.

48. D. Jenkins: "Ceramic-to-Metal Sealing; Its Development and Use in the American Valve Industry," Electronic Engineering, London, 27 (July, 1944) pp. 390-394.

49. H. Vatter: "On the History of Ceramic-to-Metal Sealing Techniques," 4 (Feb. 1956).

50. H. Vatter: German Patents 645,871 (1935); 682,962 (1939); 689,504 (1938); 706,045 (1938); 720,064 (1938).

51. F. C. Kelley: "Metalizing and Bonding Nonmetallic Bodies," U. S. Patent 2, 570, 248, (Oct. 9, 1951).

52. A. Pincus: "Metallographic Examination of Ceramic-to-Metal Seals," J. Amer. Ceram. Soc. 36 (May 1953), pp. 152-158.

53. A. Pincus: "Mechanism of Ceramic-to-Metal Adherence," Ceramic Age, (Mar. 1954), pp. 16-20, 30-32.

54. Armour Research Foundation, Illinois Institute of Technology, "Literature Review and Industrial Survey of Brazing," Final Report, Project No. 90-1060B for Frankford Arsenal.

55. Gulbransen and Sysong: "Thin Oxide Films on Molybdenum," A.I.M.M.E. (Metals Tech.) 14 T.P. No. 2226, 1-17 (Sept. 1947).

56. S. Dushman: "Scientific Foundations of Vacuum Technique," New York, John Wiley & Sons, (1949).

57. Kubaschewski and Evans: "Metallurgical Thermochemistry," Pergamon Press (1958) Table E.

58. J. Coughlin: "Contributions to the Data on Theoretical Metallurgy," (XII Heats and Free Energies of Formation of Inorganic Oxides), Bulletin 542, Bureau of Mines, pp. 23, 31.

59. E. P. Denton and H. Rawson: "The Metallizing of High Alumina Ceramics," Brit. Ceram. Soc. Trans., (1960), pp. 25-37.

60. S. S. Cole and F. J. Hynes: "Some Parameters Affecting Ceramic-to-Metal Seal Strength of a High Alumina Body," Bull. Amer. Ceram. Soc. 37, No. 3, (1958), pp. 135-138.

61. "Symposium on Metal to Ceramic Seals," Rutgers University (1953).

62. "Alumina Radome Attachment," 2nd Quarterly Report on Contract No. AF 33(616)-8157 by NARM Co., (Oct. 20, 1961), AD 266073.

63. F. H. Norton, W. D. Kingery, G. Economos, and M. Humenik, Jr.: "Study of Metal-Ceramic Interactions at Elevated Temperatures," U. S. Atomic Energy Comm., Natl. Sci. Foundation, Washington, D.C., NYO-3144, 83pp. (1953).

64. H. W. Barr, L. E. Marchi, H. H. Rice and J. A. Stavrolakis: "Application of Fundamental Concepts of Bonding Metals and Ceramics," Armour Research Foundation, Chicago, Ill., (Oct. 1953), Office of Technical Services, Washington, D. C., PB-117936, AD 10554, Ceram. Abstr., (Aug. 1954), p. 142f.

65. W. D. Kingery: "Metal-Ceramic Interactions: I, Factors Affecting Fabrication and Properties of Cermet Bodies," J. Amer. Ceram. Soc., 36 (11)362-65 (1953).

66. G. Economos and W. D. Kingery: "Metal-Ceramic Interactions: II, Metal-Oxide Interfacial Reactions at Elevated Temperatures," ibid., (12)403-400.

67. S. S. Cole, Jr., and G. Sommer: "Glass-Migration Mechanism of Ceramic-to-Metal Seal Adherance," J. Amer. Ceram. Soc. 44, No. 6, (June, 1961) pp. 265-271.

68. RADC-TN-61-217, First Technical Note, "Ceramic-Metal Seals for High-Power Tubes," Contract No. AF 31(002)-2371, prepared by Cole, et al., (July 1961).

69. J. A. Zollman and M. Berg: "Evaluation of Ceramics for Ceramic-to-Metal Seals," presented at 63rd annual meeting for the American Ceramic Society, April 23-26, 1951.

70. G. Lewin and R. Mark: "Theory of Dissimilar Tubular Seals of Glass, Ceramics and Metals for Critical Applications," American Vacuum Society Transactions, 1958 Vacuum Symposium.

71.   J. A. Zollman, I. E. Martin and J. A. Powell: "Ceramic, Sapphire and Glass Seals for the Model C-Stellarator," American Vacuum Society Symposium Transactions, (1959).

72.   M. D. Hare, R. F. Keller and H. A. Menesis: "Electroformed Ceramic-toMetal Seal for Vacuum Tubes," prepared under Signal Corps. Contract DA 36(039)SC-73178, Technical Report No. 453-3, (Nov. 1958), AD-210323.

4. HEAT TRANSFER IN A THERMIONIC CONVERTER

4.1 Electron Cooling in a Converter

4.1.1 Electron Cooling of an Emitter in Vacuum

The evaporation of electrons from the surface of a hot conductor, similar to the evaporation of molecules from a liquid, causes a cooling of that surface. If a steady state is to be maintained, heat must be supplied to the emitter surface from external sources such as a power supply. The entropy per electron of the electron gas near the emitter depends on its density and, hence, the work function of the surface. To compute this entropy, note that in any process the change in the Helmholtz free energy $F \equiv U - TS$ of the electron gas is:

$$dF = -SdT - pdv + \bar{\mu}\,dn$$

where $\bar{\mu}$ is the electrochemical potential defined as

$$\bar{\mu} \equiv (\partial F/\partial n)_{T,\,v}$$

The work function of a surface is defined as the difference between $\bar{\mu}$ inside the conductor and $\bar{\mu}$ just outside it. One may view the electrochemical potential as equivalent to the Fermi level.

Since the Gebbs function, G, is defined as F + pv,

$$dG = -SdT + vdp + \bar{\mu}dn$$

and

$$\bar{\mu} = \left(\frac{\partial G}{\partial n}\right)_{T,p}$$

The number of electrons outside of the emitter in the interelectrode spacing is changed but the tempeature and pressure of the space are

constant. If electrons are removed from the emitter by an accelerating field or a distribution of positive charges such that a constant potential exists between collecting electrode and emitter, then,

$$\left(\frac{\partial U}{\partial n} \right)_{T,P} = 3/2 \ kT - e\phi$$

$$\left(\frac{\partial (pv)}{\partial n} \right)_{T,P} = kT$$

$$\therefore \ \bar{\mu} = (5/2) \ kT - e\phi - T \ (\partial S/\partial n)_{T,P}$$

where ϕ is the potential of the region outside the emitter. From the relation of work function to electrochemical potential

$$entropy/electron = (\partial S/\partial n)_{T,P} = e\phi/T + (5/2)k$$

hence, the heat removed per electron is

$$p = e\phi + 5/2 \ kT$$

or in terms of practical units

$$P_{ec} \ (watts) = J\phi + 5/2 \ kT$$

where J is current flow in amps/cm^2.

This is strictly a classical derivation involving the thermodynamic potentials and assuming the ideal gas laws. A more sophisticated argument employing the Maxwell-Boltzmann statistics yield,

$$P_{ec} = J\phi + 2 \ kT$$

Additionally, the assumption of a constant potential region between emitter and collector is not usually realized. A space charge minimum of some magnitude generally exists and a more useful expression

for electron cooling in a vacuum operated or space charge limited
device is:

$$P_{ec} = JV_m + 2 \, kT$$

Even this expression does not account for the possibility of back-
scattered electrons from V_m which in turn may reduce the cooling
expression.

4.1.2 Electron Cooling in a Plasma

An exact analysis of electron cooling in a practical converter does not exist for lack of sufficient data concerning the emitter sheath and density of excited states in the plasma. A general expression for electron cooling with plasma present may be written as follows:

$$P_{ec} = JV_m + 2kT - fJ\Delta V$$

The first two terms are repeated from the classical derivation in the preceding section. It may be noted that if a Langmuir double sheath exists at the emitter then V_m is the potential height of the sheath maximum. The term of interest is the last term which identifies a population of excited states derived by any process and returning to the emitter. A certain fraction, f, of these excited atoms arrives at the emitter and (1-f) arrives at the collector. For lack of better information f may be assumed to equal one-half, reasoning that the velocity distribution of states is Maxwellian. f may well be more than 1/2 considering the origin of excited atoms.

From data based on practical and some experimental devices, electron cooling of an emitter may vary from 10 - 20 watts/cm^2. The return of excited states to an emitting surface is capable of reducing this amount by 10 to 20 percent. These estimates are based on devices operating in the discharge mode. Devices or vehicles that operate in the space charge mode evaporate electrons from the emitter by consideration in the preceding section. Electron cooling in this mode is an order of magnitude less than in the discharge mode.

4.2 Radiation Heat Transfer

4.2.1 Radiation Heat Transfer in Vacuum

The problem of heat transmission between two parallel
surfaces in a vacuum is most simply treated by the Stephan Boltzmann
Radiation Law. The effective emissivity for the system, as described,
is given by:

$$\epsilon_{eff} = \frac{1}{\frac{1}{\epsilon_{coll}} + \frac{1}{\epsilon_{emitt}} - 1}$$

hence the equation of heat transfer is:

$$P_{Rad.} = \epsilon_{eff} \; \sigma \; (T_{emitt}^4 - T_{coll}^4)$$

One must excercise some caution in the calculation since the emissivity
of both electrodes is a function of temperature. Figures 4-1, 4-2,
and 4-3, are representative examples of materials and temperature pertinent
to converter technology. For a given emitter temperature the heat trans-
fer follows a pattern as expected; i.e., at low collector temperatures
the collector emissivity is quite low ($\sim.05$) and, therefore, the effective
emissivity is low, allowing only a small amount of heat transfer. At high
collector temperatures as the temperature difference between electrodes
becomes less, the heat transfered is less and is null when the two
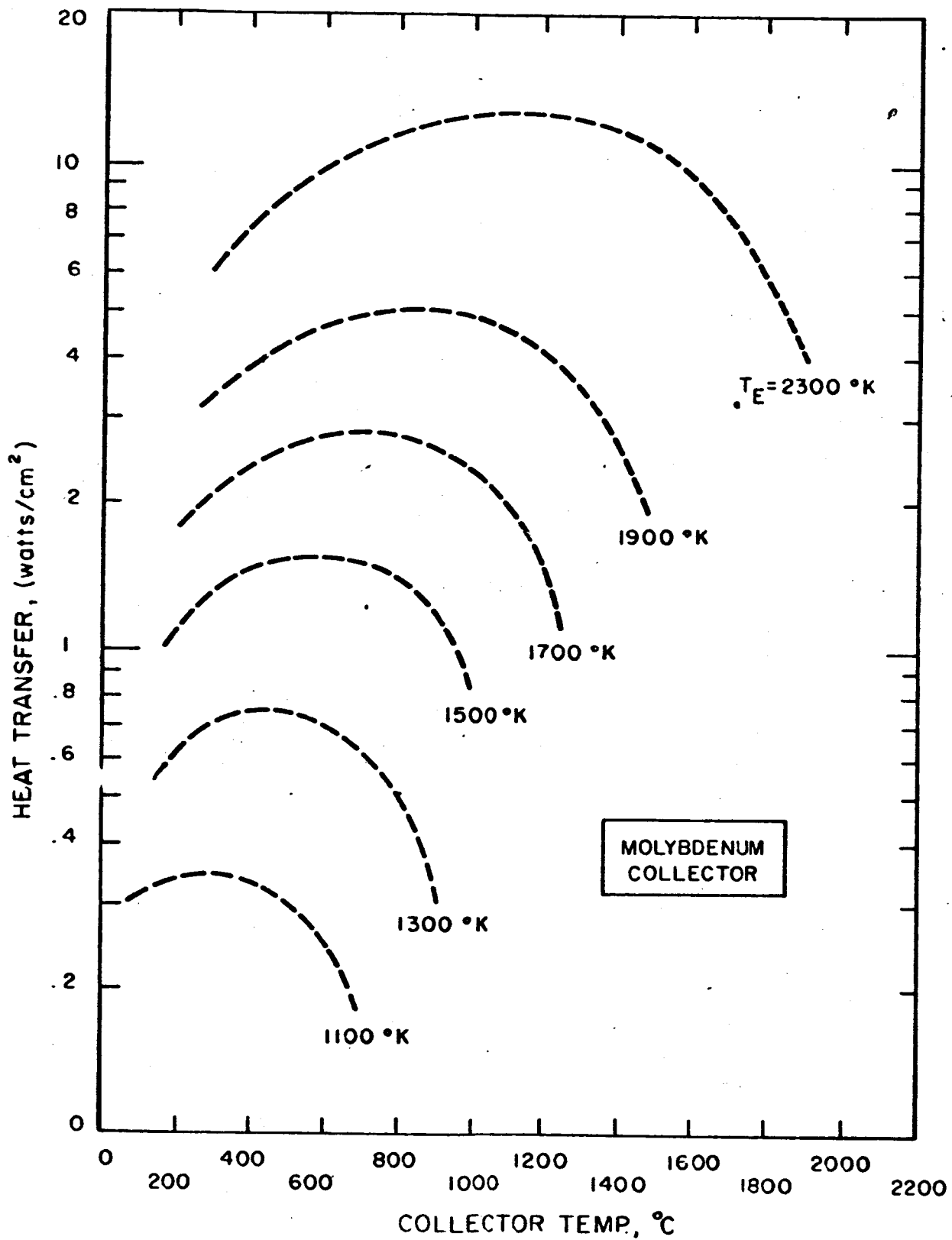temperatures are equal.

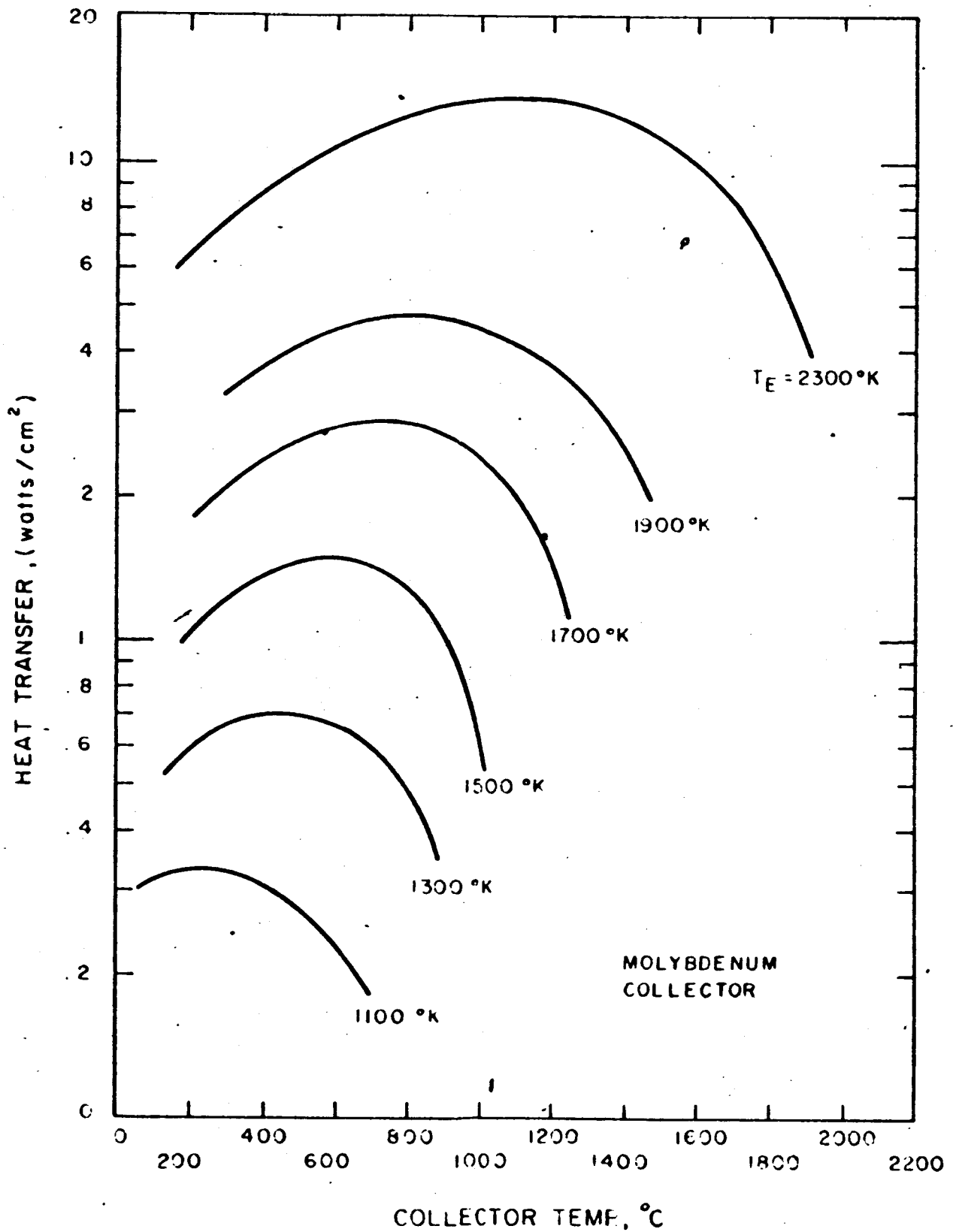FIG. 4-1   RADIATION HEAT TRANSFER FOR PARALLEL ELECTRODES OF Ta-Mo

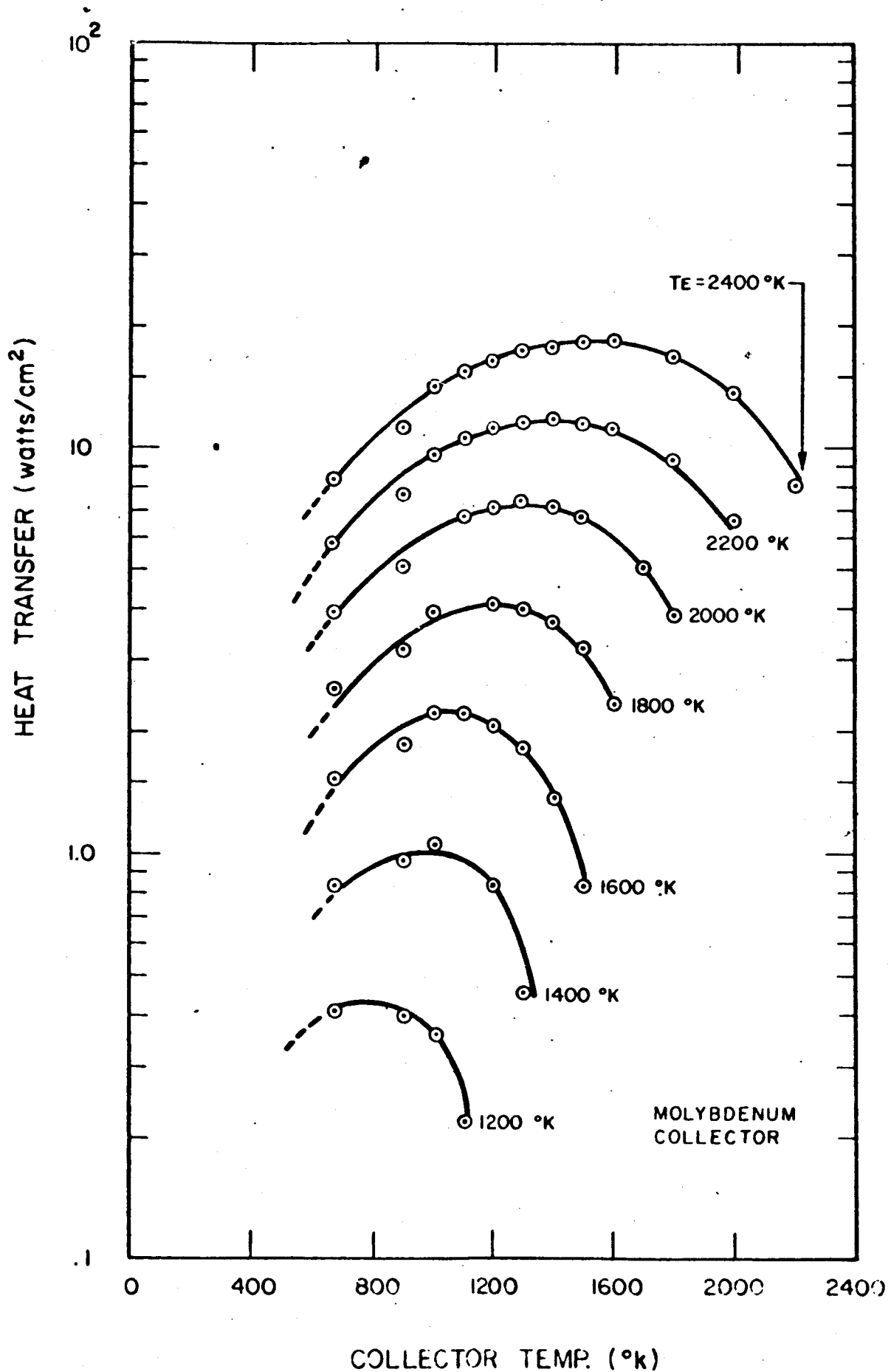FIG. 4-2   RADIATION HEAT TRANSFER FOR PARALLEL ELECTRODES OF Mo-Mo

FIG. 4-3   RADIATION HEAT TRANSFER FOR PARALLEL ELECTRODES OF W-Mo

4.2.2 Radiation Heat Transfer in the Presence of a Plasma Medium

The problem of examining radiation heat transfer between two flat parallel plane electrodes is somewhat more complicated when an absorbing medium such as cesium vapor exists between these electrodes. This is the case in a cesium vapor thermionic converter. When the cesium vapor pressure is low (in the range of 1 micron to 100 microns) and the spacing between emitter and collector is small (10 mils) one might expect that the radiation heat transfer would be little different than that observed when the electrodes are separated by vacuum. For most cases of interest in practical cesium vapor thermionic converters, the cesium vapor pressures are substantially higher (in the millimeter mercury range) with spacings of approximately 10 mils and below. In this instance, one might expect a very large percentage of the radiation from the emitter to be a absorbed in the cesium vapor medium. One would qualitatively expect a minimum of approximately 1/2 of this absorbed radiation to be returned to the emitter, with the net result that the radiation loss would be reduced in a practical converter structure. This is due to the fact that if the cesium vapor medium between the electrodes is uniformly excited one could logically expect at least 50 percent of this energy ultimately to be transferred to the emitter and 50 percent of said energy to the collector. In a more quantitative vein, it is impossible, at this time, to calculate the exact radiation losses in a cesium converter vapor thermionic since the absorption in cesium vapor as a function of wavelength is not known for the major spectrum of interest to converter technology. Data is not available in the infrared region where most of the radiation occurs. At this time, about all that can be said about the radiation losses between emitter and collector in the presence of cesium vapor is that these losses might be expected to be the same as or less than the radiation heat transfer between the same two surfaces in vacuum. In order to make an exact calculation of the radiation heat transfer between two parallel electrodes immersed in cesium vapor, one must know both the absorption characteristics of cesium vapor over the entire wavelength spectrum of

interest and the spectral emissivity characteristics of both the emitter and collector over the wavelength region of interest.

Generally speaking, this wavelength spectrum of interest for thermionic conversion would extend from approximately 0.7 microns through about 6 microns. In the wavelength region from 0.9 to about 6 microns one would find approximately 90 percent of the emitted radiation from the emitter for emitter temperatures near 1600°K. For emitter temperatures near 2000°K the wavelength band from approximately .72 microns to 4.8 microns would include approximately 90 percent of the emitted radiation. The spectral emissivity of the collector should be known over a much greater wavelength region since it operates at a considerably lower temperature than the emitter. The collector spectral emissivity characteristics would not appear to be as critical, however, as those of the emitter.

4.3 Conduction Losses in a Vapor Converter

4.3.1 Cesium Vapor Thermal Conductivity

One of the mechanisms through which heat is lost from the emitter is that of conduction by cesium vapor. A paucity of data and the spread of existing data precludes an accurate estimate of the amount of heat lost by this mechanism.

Fig. 7-8 (chapter 7: cesium properties) displays data recently obtained for cesium conditions vs cesium pressure. In the region of interesting pressure, i.e. 1-10mm.Hg., the spread in data gives a condition value of $2 \pm 2 \frac{watts}{cm \, ^oK}$

In spite of recent information released at the 1962 Thermionic Power Conference, definitive data from carefully controlled experimental conditions is lacking. Theoretical predictions of vapor conductivity depends upon cross-section estimates which vary widely. The conclusion is a requirement for more basic data.

4.3.2 Converter Lead Design

The electrical leads of a thermionic converter have received previous attention (Ref. 1) in more generalized papers concerned with overall converter efficiency. This section discusses the specific problem of proportioning converter leads relative to the balance between thermal and electrical losses. The analysis and accompanying assumptions are as follows: Let α be defined as the ratio of electrical loss to thermal loss, ΔT is the temperature difference across the lead, I is the current through the lead in amperes, ρ is the electrical resistivity in ohm-cm, K is the thermal conductivity in watt cm^{-1} $°C^{-1}$. The electrical loss may be written immediately as $I^2 (\rho L/A)$. The thermal loss may be written as $K \Delta T (A/L)$ when no current is flowing in the lead. When current flows it is assumed that half the Joule loss will flow in either direction. Hence, $1/2 \left[I^2 \rho (L/A) \right]$ is conducted in the wrong direction (i.e., to the hottest end) and must be subtracted from the thermal loss without current.

$$\therefore \quad \alpha = \frac{I^2 \rho (L/A)}{K \Delta T (A/L) - 1/2 (I^2 \rho (L/A))}$$
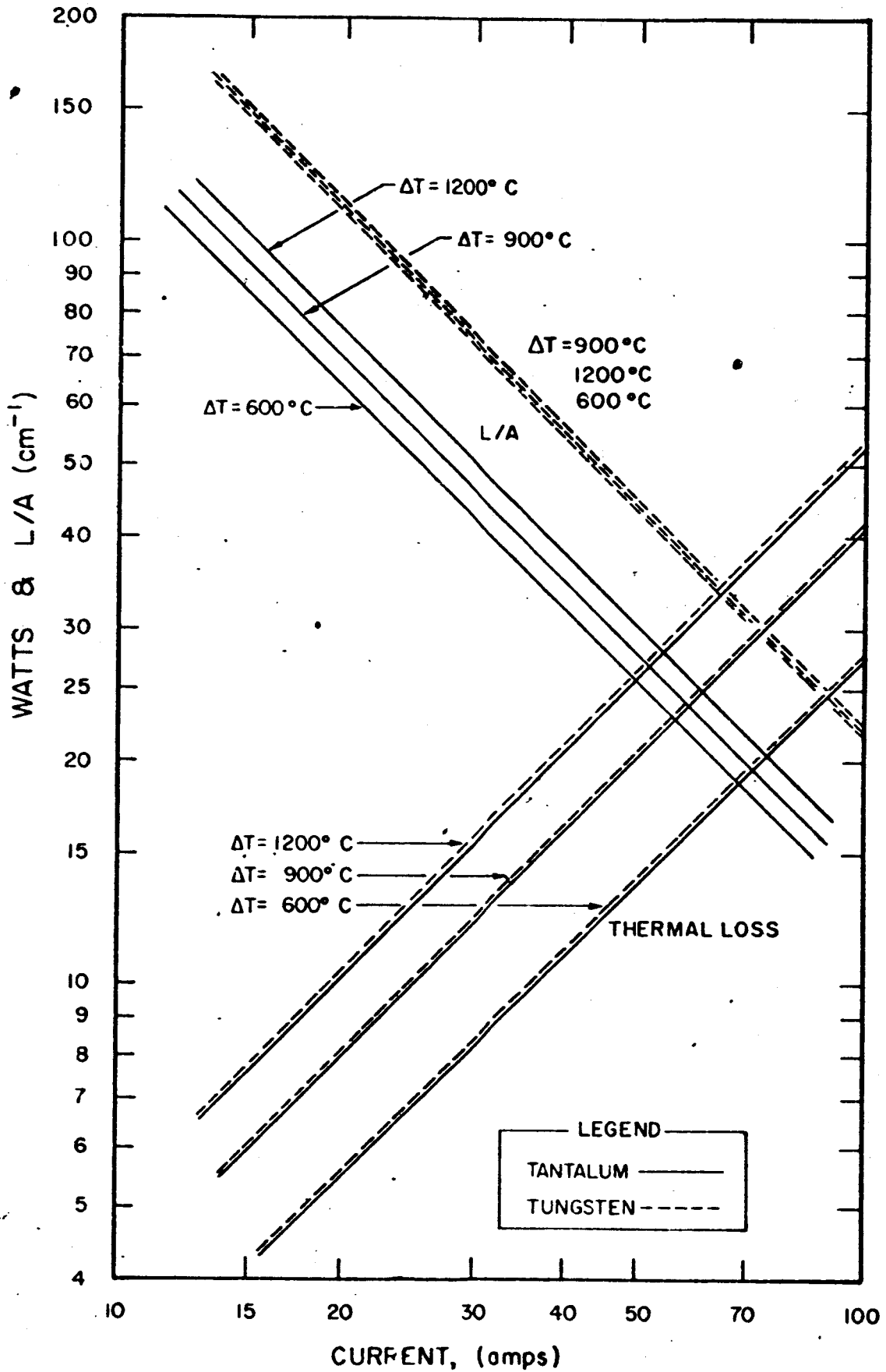
It is assumed in this analysis that there is no radiant heat loss, which is a reasonable assumption for $\alpha < 0.2$. Additionally, a more exact treatment of the problem would account for the resistance varying along the lead due to a non-uniform temperature distribution.

Figures 4-4, 4-5, and 4-6, are thermal loss and L/A lead ratios calculated from the above expression for α. Values for electrical resistivity and thermal conductivity were taken from Malter and Langmuir, Phys. Rev. 55, 743-747, 1939 and The American Institute of Physics Handbook, McGraw-Hill Book Co., Inc., New York, 1957. The temperatures assumed in these illustrations are:
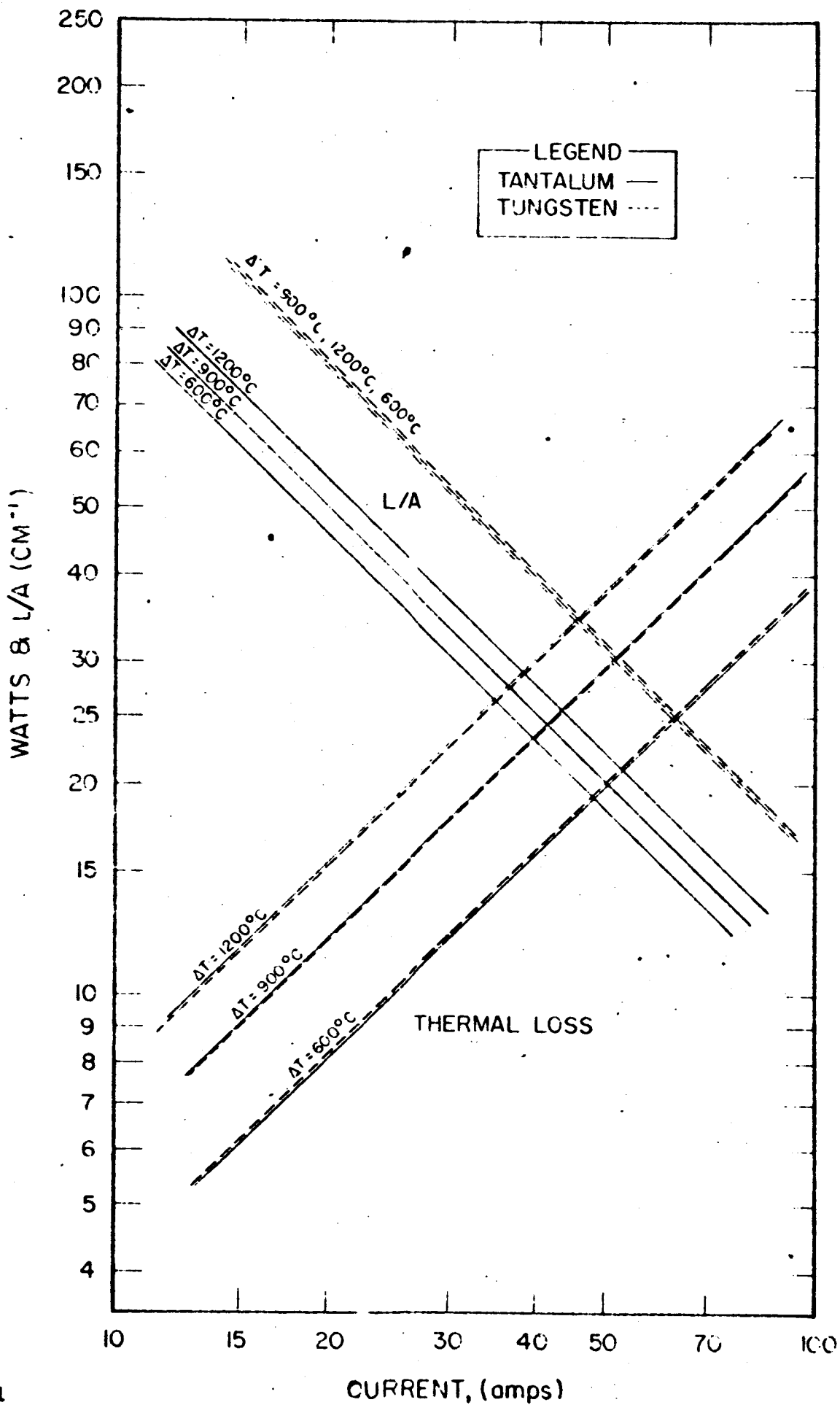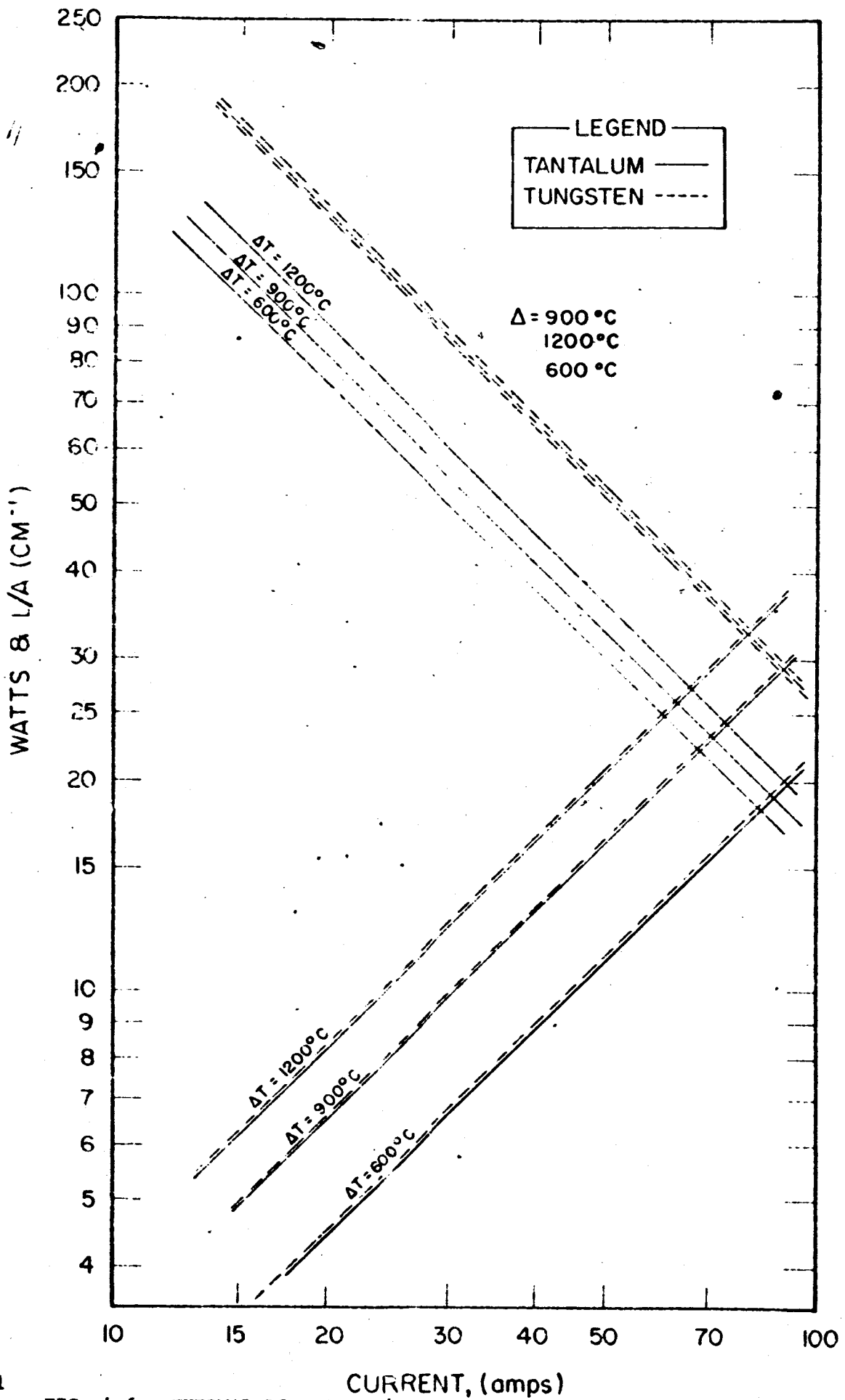
FIG. 4-4   THERMAL LOSS AND L/A LEAD RATIO VS CURRENT FOR $\alpha = 0.1$

FIG. 4-6   THERMAL LOSS AND L/A LEAD RATIO VS CURRENT FOR α = 0.3

$T_{emitter}$ (^{o}C)	T_{seal} (^{o}C)	ΔT(^{o}C)	Average Temperature
2000	800	1200	1400
1550	650	900	1100
1100	500	600	800

4.3.3 Ceramic Conduction Losses

The requirement for positive spacing in a close-spaced thermionic converter will result in some sort of conduction loss across the spacer. Resorting to elementrary heat transfer methods, a calculation may be made as follows:

Assume that two sapphire rods (10 mils in diameter and 3/4" long) are employed between converter electrodes to preserve spacing for prolonged, reliable operation.

$$Q = - KA \frac{\Delta T}{\Delta X}.$$

where,

$$K \simeq .08 \text{ watts/cm}^{o}\text{C}$$

$$A \sim 10^{-3} \text{ cm}^2$$

ΔT is difficult to ascertain since intimate contact is not achieved. Hence, there is obviously heat transfer by radiation and the calculation suffers considerably.

If ΔT is of the order of 700°C and the transfer is only 10 percent efficient due to the aforementioned reasons, then

$$Q \simeq 2 \text{ watts.}$$

Thus it is seen that the conduction mechanism is small and positive spacing is certainly justified from a heat loss mechanism.

REFERENCE

1. J. M. Houston, J. Appl. Phys. 30, p. 48 (1959)

5. SPACING TECHNIQUES

A variety of techniques has been employed for separating the emitter and collector of experimental and prototype thermionic diodes. Many of these techniques are borrowed from the previous experience of the electron tube industry.

The required spacing may vary from 0.00025 inches up to 0.25 inches, depending upon specific diode design. It is known that power output and efficiency will increase when a vacuum converter spacing decreases. However, insufficient data are available to tell whether extremely close spacing, (less than 2 to 5 mils) is desirable, particularly at emitter temperatures below about 1500°C.

Whatever the selected spacing distance, the spacing technique must accurately maintain relative collector-emitter spacing over long periods of time at the temperatures of operation. Problem areas include the effects of long term creep of materials, recrystallization phenomena, corrosion by cesium vapor and incompatible materials, and gradual changes in the temperature distribution throughout the diode.

The following paragraphs comprise the first draft of a chapter that will be included in the final report of this contract. A variety of spacing techniques described in the technical literature are reviewed. The material in this first draft will be augmented for the final report by inclusion of additional spacing techniques and an analysis of their relative merit.

5.1 Use of Positive Spacers for Close Emitter-Collector Positioning

Small spacers inserted between the collector-emitter structure have been used at G.E., Thermo Electron Engineering Corporation, and other companies to maintain close spacing. The spacing is maintained by positive pressure upon the spacers resulting from the thermal expansion characteristics of the structural materials. Figures 5-1, 5-2, and 5-3 illustrate several positive spacing techniques used and/or designed by G.E. (Ref. 5-1).

METAL
SPACER

CATHODE
ELECTRODE

CERAMIC
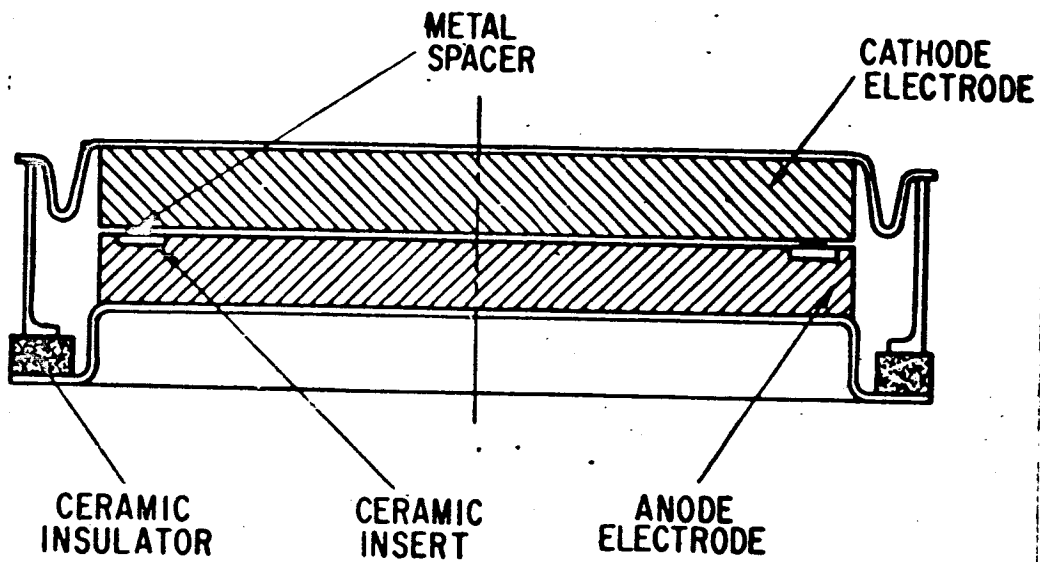INSULATOR

CERAMIC
INSERT

ANODE
ELECTRODE

FIG. 5-1   CROSS SECTIONAL VIEW OF PLANAR TYPE VACUUM THERMIONIC
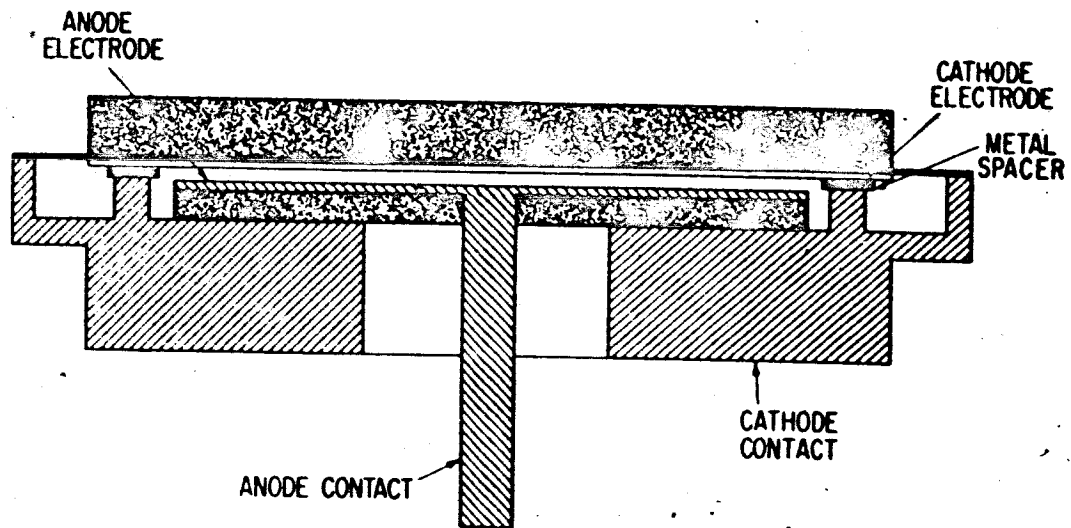ENERGY CONVERTER (REF. 1)

FIG. 5-2 CROSS SECTIONAL VIEW OF A VACUUM THERMIONIC ENERGY
CONVERTER HAVING THE ANODE ELECTRODE RIGIDLY SPACED
FROM THE CATHODE SO THAT THE SPACING WILL BE CONSTANT
WHEN OPERATED IN EITHER AN ATMOSPHERIC OR VACUUM
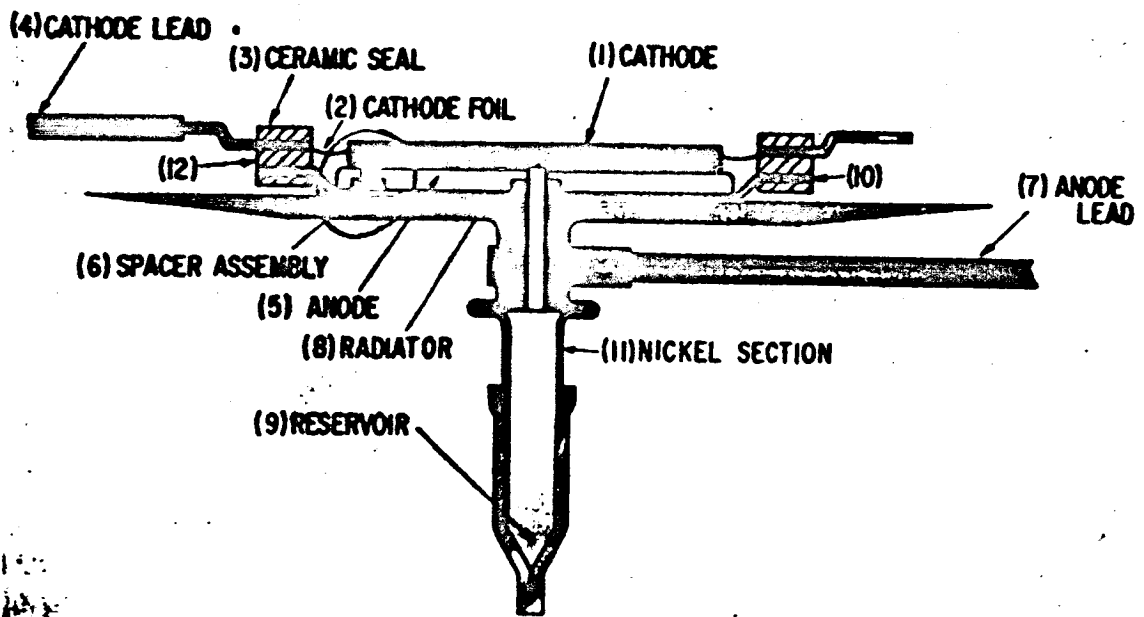ENVIRONMENT

FIG. 5-3   CROSS SECTION OF THERMIONIC CONVERTER AND RADIATOR

(4) CATHODE LEAD
(3) CERAMIC SEAL
(2) CATHODE FOIL
(1) CATHODE
(12)
(10)
(7) ANODE LEAD
(6) SPACER ASSEMBLY
(5) ANODE
(8) RADIATOR
(11) NICKEL SECTION
(9) RESERVOIR

For any positive spacing technique, the collector and emitter structures must be made of materials that are strong and rigid at high temperatures at which they operate and must be capable of being ground flat and smooth so they can be spaced very close to each other. The spacing technique would preferably aid in preventing warpage and eventual shorting of the two electrodes.

Figure 5-1 illustrates the use of ceramic inserts in the electrode structure. These inserts are usually placed in the collector to avoid the problems associated with high emitter temperatures. In Figure 5-1, the collector electrode is made of tungsten and is provided with three inserts of ceramic material. Hafnia is used for these inserts because of its low thermal conductivity and its excellent insulation properties. The surfaces of the collector and emitter electrodes are ground smooth and flat by conventional surface grinding techniques. Three small pieces of molybdenum foil are placed on the ceramic inserts to space the electrodes from each other.

In order to ensure that a reasonably uniform gap exists between the electrodes, it has been customary to use spacers for test purposes that are thinner than the ones to be used in the final assembly. For example, if a converter is to be placed at 0.003 in., it is assembled and tested prior to exhaust with spacers half that thickness. The actual spacing is determined by a capacitance test.

Figure 5-1 is a cross sectional view of a planar type of vacuum thermionic converter that has been placed on a semi-production basis at the G.E. Power Tube Laboratory. Spacings ranging from 0.0022 inches up to 0.005 inches have been achieved reproducibly. The uncertainty in spacing is about $\pm$ 0.005 inches. The spacing will change during the life of the converter due to warpage, gradual "sinking" of the inserts into the emitter and other effects.

Figure 5-2 shows a converter design in which the spacing pins are anchored to a part of the collector structure that is electrically part of the emitter structure. The spacers can be brazed into position

to hold the emitter and collector structure rigid and in correct relationship to each other regardless of whether or not external pressure is applied.

Figure 5-3 illustrates a third method of positive spacing, and shows the cross section of a thermionic converter and radiator designed for solar thermionic application. The collector-emitter spacing was maintained by permitting the emitter to rest upon three 0.020-inch diameter tungsten pins brazed with nickel-titanium into alumina cups, in turn nickel-titanium brazed to a small nickel disc. A tantalum spinning piece was used as part of the enclosure and to hold the spacer pin assemblies in place. The radiator was copper brazed to the tantalum piece. The emitter assembly and the three spacer assemblies were first brazed, and then the entire tube was assembled and vacuum brazed in one operation.

5.2 Thermal Expansion Spacing

It is theoretically possible to control the emitter-collector spacing by differential thermal expansion of the structural members. The accuracy of the spacing depends upon the degree of knowledge concerning the temperature distribution in the diode structure and the thermal expansion characteristics of the diode structure.

Figure 5-4 illustrates a cross section of a thermionic diode, which uses differential thermal expansion as a means for spacing, that was built for the SET program by Thermo Electron Engineering Corporation. The emitter structure is held by means of a thin cylindrical tantalum spacer. How large a spacing is dependent on the accuracy of thermal expansion calculations. Unless the collector and emitter expansion characteristics are properly matched, upon cooling the diode, an interference fit would result at the interface of the emitter and collector. This would produce a rather high compressive stress at the interface and an undesirable balancing tensile stress in the spacer ring and diode support structure. The condition chosen for achieving the smallest interelectrode spacing at operating

2 Emitter, Ta
4 Spacer, Ta
7 Insulator, Al$_2$O$_3$
8 Upper insulator support, Nb
9 Center insulator support, Nb
10 Lower insulator support, Nb
11 Lead ring, Cu
12 Exhaust tube, Ni
18 Radiator, Cu
23 Lead straps, Cu

25 Cesium reservoir, Mo
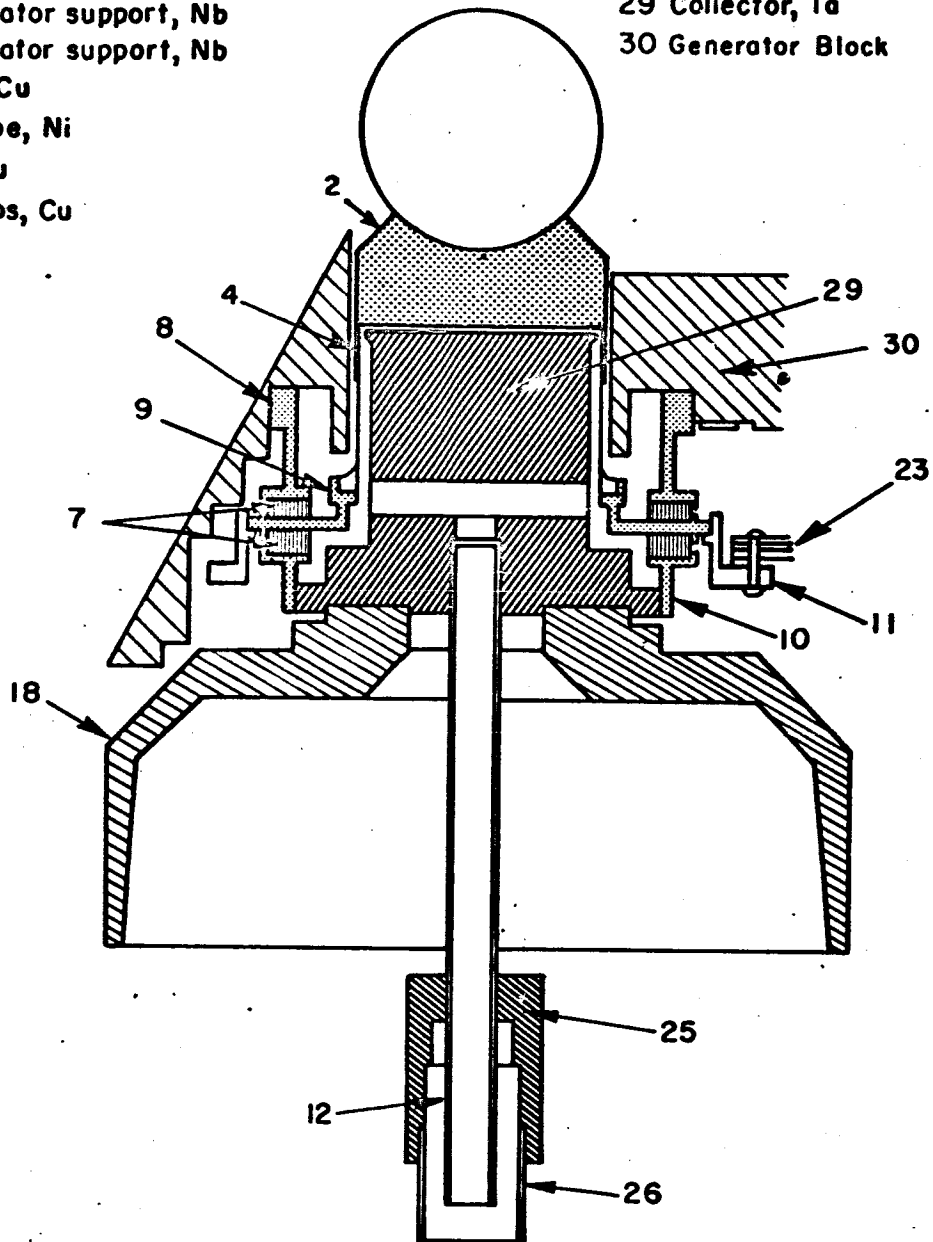26 Crimp-off tube, Cu
29 Collector, Ta
30 Generator Block

FIG. 5-4 CROSS SECTION OF SET DIODE

temperature, but at the same time obtaining a practical design in terms of fabricability, was to design the diodes so that the electrode surfaces just come into contact when the diode is cooled to room temperature.

For this particular diode the thermal expansion calculation assumed a linear temperature gradient and that the tantalum spacer, niobium ring, and molybdenum collector are the only affected parts. The resultant spacing at an emitter temperature of $1700^{\circ}C$ and an estimated collector temperature of $900^{\circ}C$ was about 0.0015 inches.

The use of thermal expansion of the primary method of regulating spacing incurs many difficulties. There is no positive spacer to prevent warpage and creep effects from shorting or increasing the diode spacing. The exact thermal expansion of a structural member is often not known to the required degree of accuracy; also, the real temperature distribution can vary radically from the assumed distribution and can change during the course of the diode life.

5.3 External Spacing

If the seal structure of the thermionic diode is designed to be flexible, and it is possible to control the emitter-collector spacing by means of external adjustments such as set screws, micrometer measurements and other means. Figure 5-5 illustrates this arrangement, and shows a cesium converter proposed by TRW and TEC (Ref. 5-3).

Figure 5-6 illustrates a tapering cylindrical diode wherein the emitter structure is guided into place by means of guide insulators and the spacing is controlled by the vertical adjustment set by the adjusting screw.

The problems encountered by this type of spacing adjustment are similar to those encountered when using thermal expansion as a means of spacing. Warpage and long term creep effects are not prevented by positive spacers, and knowledge of final spacing is much dependent on the thermal expansion characteristics of materials used.
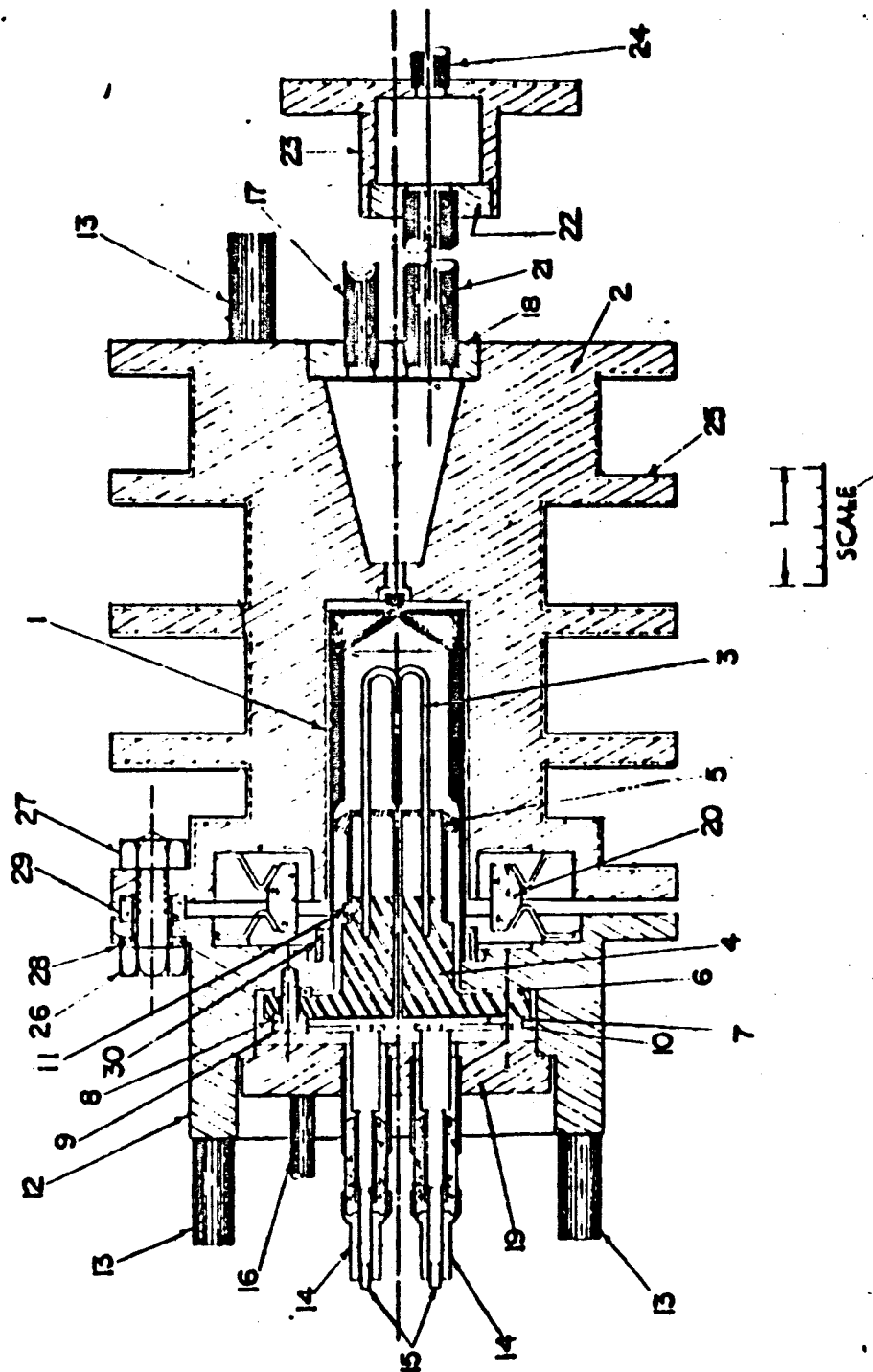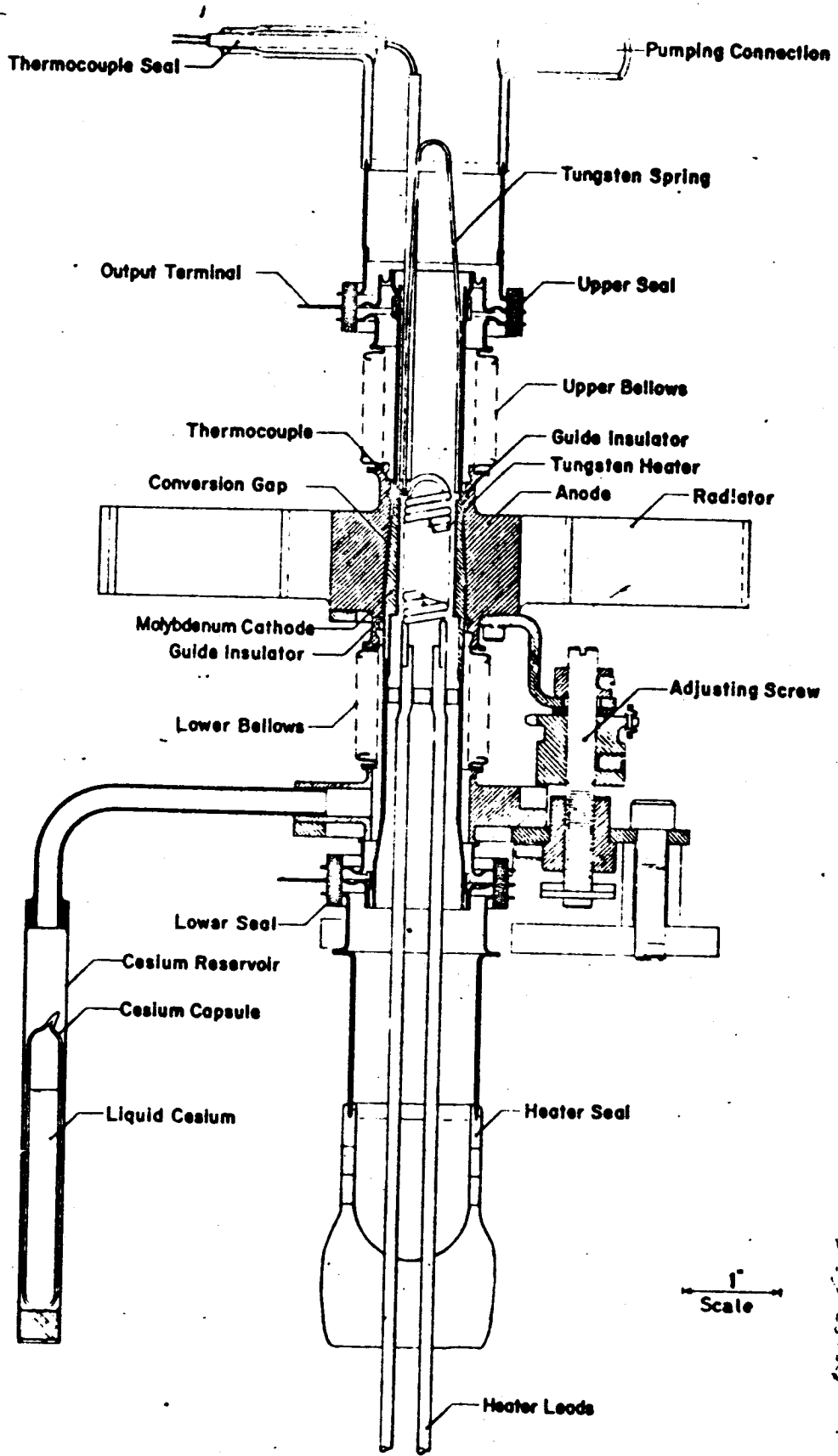
FIG. 5-5 CESIUM CONVERTER ASSEMBLY

Thermocouple Seal

Pumping Connection

Tungsten Spring

Output Terminal

Upper Seal

Upper Bellows

Thermocouple

Guide Insulator

Conversion Gap

Tungsten Heater

Anode

Radiator

Molybdenum Cathode

Guide Insulator

Adjusting Screw

Lower Bellows

Lower Seal

Cesium Reservoir

Cesium Capsule

Liquid Cesium

Heater Seal

Heater Leads

1"
Scale

FIG. 5-6 THERMIONIC CONVERTER

5.4 Electrode Support by the Ceramic Seal

Ceramic-metal electron tubes often utilize a simple support mechanism for the collector-emitter and grid wherein these members are simply brazed to the ceramic spacer that is also used as the insulator between these electrodes. This configuration is illustrated in Fig. 5-7 (Ref. 5-4), which shows a low temperature arc mode converter being developed by Ford Instrument Company. For this particular converter the emitter-collector spacing is quite large and bending, warping and long term creep effects are likely to be small. The cup design of the converter in Fig. 5-7 provides a high thermal impedance $(1200^{\circ}C)$ between the emitter and the ceramic spacer, thus enabling the ceramic to operate at relatively low temperatures and minimizing the effects of cesium attack.

Ceramic-metal tubes made by General Electric (Ref. 5-5) and other companies use cathode-to-grid and grid-to-anode spacings as small as 0.003 inches. To maintain these close spacings, it has been found necessary to provide schemes for stretching and tensioning the grid during the sealing process. An illustration of one of these schemes shown in Fig. 5-8 has been used in the experimental development of ceramic-metal tubes. Techniques of a similar nature could be applied towards thermionic diode development.

5.5 Variable Spacing Techniques

Difficulties in realizing very small spacings, such as uneven thermal expansion and warping, have led to feasibility studies of variable anode surfaces that automatically adapt themselves to the contour of the cathode. This work has been conducted at ITT Federal Laboratories, G.E. Research Lab., G.E. Power Tube Lab., Thermo Electron Engineering Corporation, and other places and has been confined thus far to analytical study and preliminary experiments.

One method, studied by ITT, employs a subliming anode surface that automatically adapts itself to the cathode surface. ITT explains the physical mechanism in the following manner:

EVACUATION TUBE

CESIUM TUBE

ANODE FLANGE

CERAMIC SPACER

ANODE CUP

KOVAR
ELECTRON-GUN
CUP

CATHODE CUP

INTER-
ELECTRODE
SPACE

PHILIPS
IMPREGNATED
CATHODE

BOROSILICATE
GLASS FOR
ELECTRON-GUN

1/2   0   1/2   1
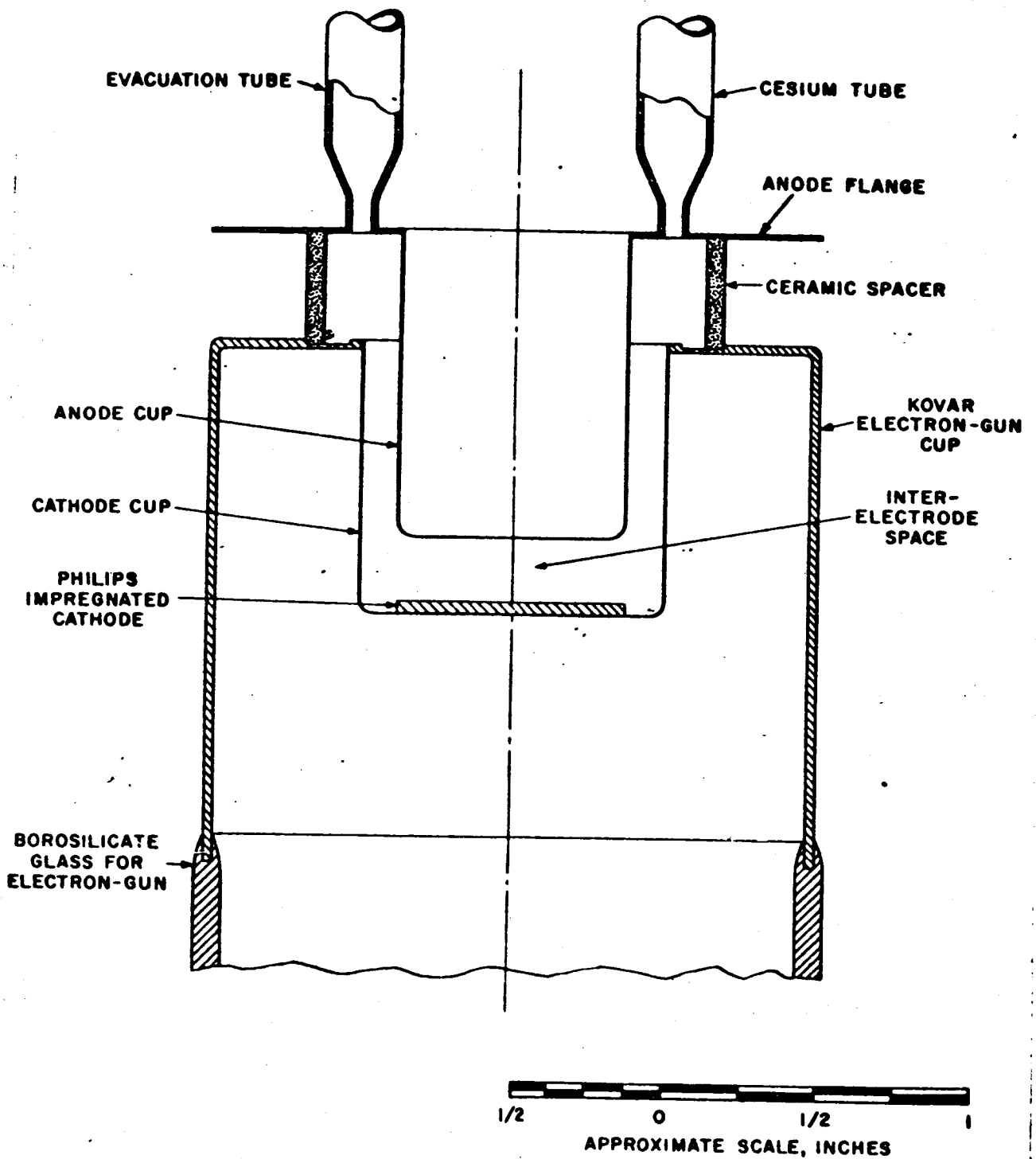APPROXIMATE SCALE, INCHES
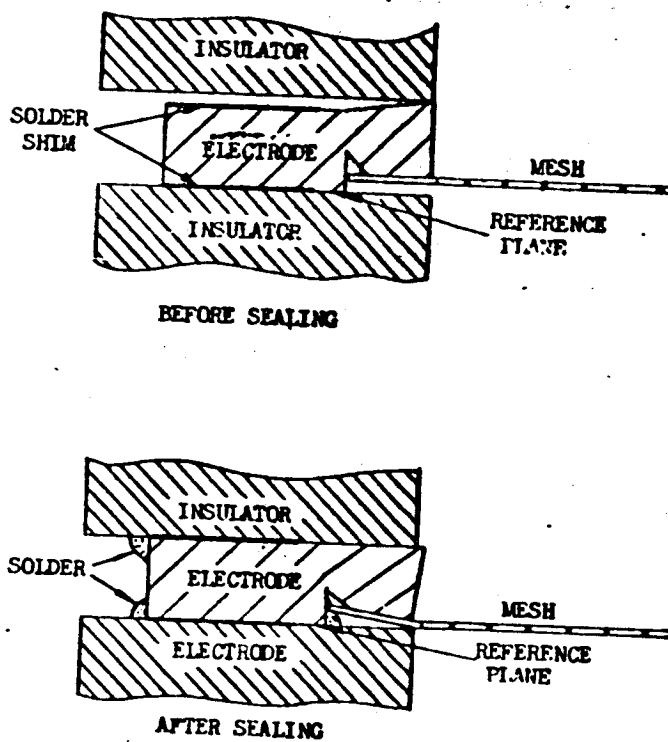
FIG. 5-7   DESIGN OF THE METAL-CERAMIC THERMIONIC CONVERTER

FIG. 5-8 CROSS SECTION OF TENSIONING GRID ELECTRODE

The heat required to control sublimation of the anode is derived from the electron stream as it enters the anode and converts potential energy (corresponding to the anode work function) into heat. This mechanism tends to maintain a uniform spacing over the anode surface, provided that the current distribution is at least partially controlled by the local space charge.

In the temperature saturation region, where a space charge no longer regulates the current, the anode surface can be expected to approach very close to the cathode, until a second regulatory mechanism comes into play, which may be explained as a reduction of work function of the cathode. In this region, the cathode current again increases until its eating effect on the anode stops further deposition of subliming metal at that location.

If the cathode and anode were both perfectly uniform, then the anode-cathode spacing required to affect the work function would be only a few angstrom units. However, actual cathodes and anodes are probably rather patchy in this respect, so that an effective change in work function is expected at considerably greater distances. No experimental data are reported from the ITT work thus far.

A second method of variable spacing is the employment of liquid anode consisting of cesium liquid that also acts as the reservoir. The cesium is separated from the emitter by the pressure of the cesium vapor. TEC reports (Ref. 5-7) that a controlled experiment has been conducted and has shown it is possible to achieve a stable cesium vapor balance in the liquid collector that will not collapse.

Several advantages of the liquid collector are the independence of the emitter shape, the ability of the cesium bath to absorb impurities, and the low work function of the cesium surface. However, the liquid collector is extremely limited in terms of the heat transfer capabilities of the cesium bath and the inability to independently adjust cesium vapor and collector temperature in an optimum fashion.

REFERENCES

5-1. Final Report AFCRL430, "Research on Thermionic Converters", Contract No. AF 19 (604)-5472, performed by G.E. Research Lab., for. Cambridge Research Lab., AFOAR, June 1961.

5-2. Final Report on "Solar Energy Thermionic Conversion Systems", Contract JPL-950109, November 1961.

5-3. Interim Summary Technical Report, WADD TR 60-698, on "Design Study for Advanced Solar Thermionic Power Systems", Item II, Part 1, Vapor Type Thermionic Generator, September 1960.

5-4. Haring, L. L., "Summary of the Ford Instrument Company Presentation", contained in the Proceedings of the Third Government-Industry Thermionic Roundtable Discussions, Vol. II.

5-5. Interim Engineering Report No. 2, AF 33 (616)-8096, "Research and Investigation on Radiator Resistant, High Temperature Thermionic Circuitry", Receiving Tube Department, G. E., Owensboro, Kentucky.

5-6. Coles, D. K., "Study of a Close Spaced Thermionic Converter" contained in Proceedings of the Third Government-Industry Thermionic Roundtable Discussions, Vol. II.

5-7. "Cs Vapor Item Produces 30W", p. 120, Electronic News, March 26, 1962.

6. CONVERTER PHYSICS

6.1 Ionization Processes

Much confusion exists in the literature as to the exact ion-
ization and space charge neutralization processes which are dominant
in cesium vapor thermionic converters. One school of thought ascribes
space charge neutralization in cesium vapor converters to ions formed
by surface ionization processes at the emitter (or collector) surface
which then drift out into the interelectrode region and there become
effective in neutralizing space charge. This particular concept is
not in agreement with findings in the alkali vapor discharge literature.
An extended study on low voltage rubidium vapor diode discharges (Ref. 1)
reports an experiment wherein surface ionization at the collector was
supposed to produce ions which would drift into the interelectrode
space and neutralize space charge, thus lowering the arc drop to
approximately zero. The experimental findings were essentially negative
in that only a gain of approximately two in space charge limited current
from the emitter could be observed experimentally. This was in agree-
ment with the predictions of Langmuir in a paper on ion and electron
sheaths in gas discharges (Ref. 2). It might be observed that the
potential distribution in the experimental rubidium vapor diode favored
extraction of ions from the surface whereas the same situation does not
hold in the case of ions generated at the surface of the emitter in a
cesium vapor thermionic converter operating in the discharge mode. In
fact, the field is probably retarding for ions at the emitter surface
in a converter.

A trivial calculation based on reasonable data from operating
converters indicates that insufficient ions are produced by surface
mechanisms to neutralize random electron currents in the plasma.
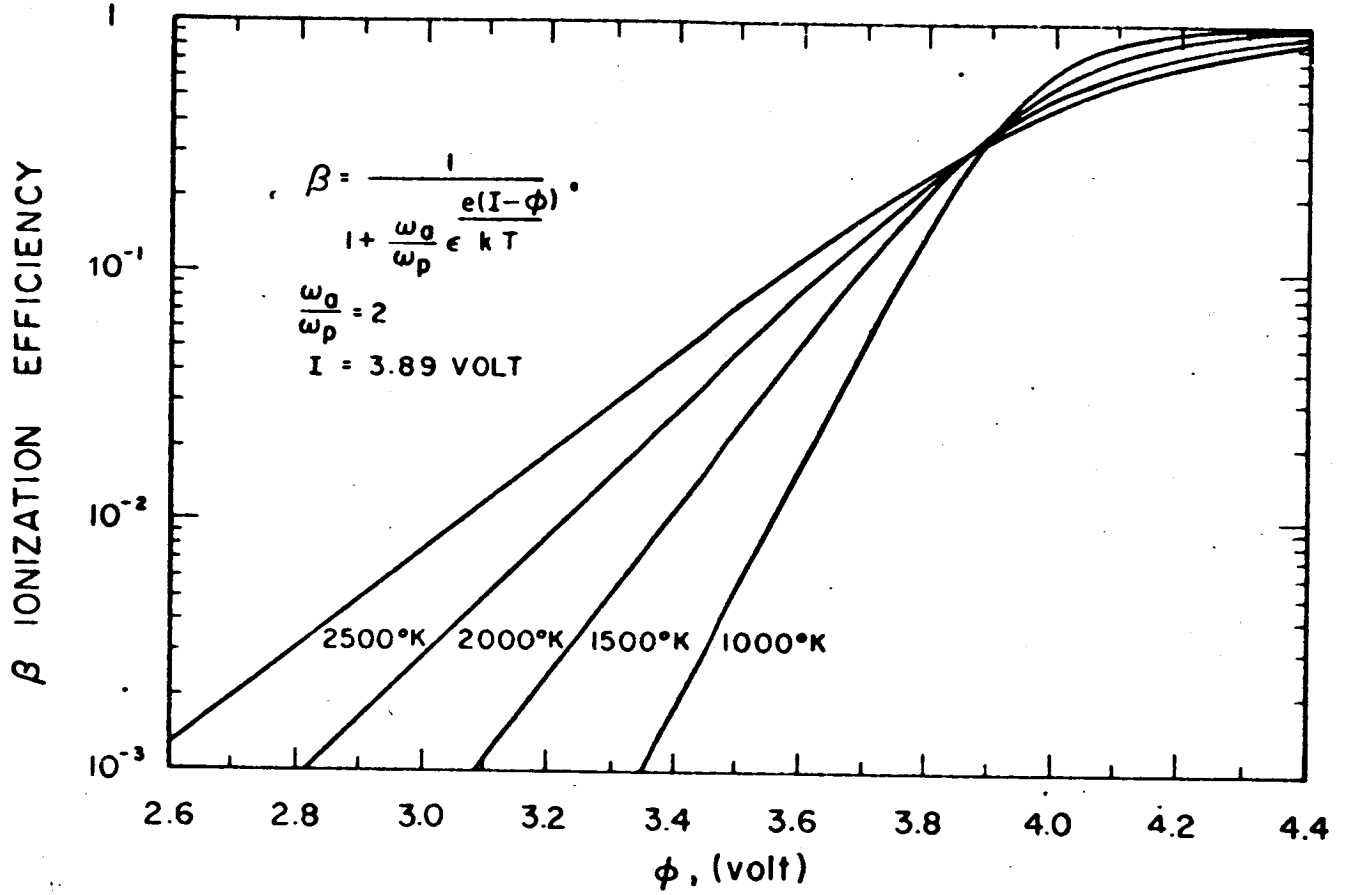Figure 6-1 is a plot of the ionization efficiency, β, the probability that

FIGURE 6-1 SURFACE IONIZATION PROBABILITY FOR CESIUM
FROM THE LANGMUIR-SAHA EQUATION

an arriving ion or neutral atom will leave the emitter as an ion, versus emitter work function. The ion current available is found by combining the arrival rate expression with Auer's derivation of ion emission from an emitter. The result is:

$$J^+ = 488\beta P T^{-1/2}$$

For a converter operating at $2033°K$ and a cesium reservoir temperature of $401°C$ an effective work function of 3.1 volts is obtained from the Langmuir-Taylor curves. From the β plot, $\beta = 6 \times 10^{-3}$ and from vapor pressure curves, $P = 18$ mm Hg.

$$\therefore \quad J^+ = 488 \times 6 \times 10^{-3} \times 18 \times (2033)^{-1/2}$$

$$J^+ = 1.04 \text{ amp/cm}^2$$

This value of ion current may be compared to the random electron current density in a plasma of electron temperature $4000°K$.

$$\bar{c} = 6.22 \times 10^3 \sqrt{Te}$$

$$\bar{c} \simeq 40 \times 10^4 \text{ meters/sec}$$

and

$$j_{rand} = 1/4 \, ne\bar{c} \simeq 1/4 \times 10^{19} \times 1.6 \times 10^{-19} \times 4.0 \times 10^5$$

$$j_{rand} \simeq 16 \text{ amp/cm}^2$$

but values up to 100 amp/cm^2 are possible since the electron density can vary by a factor of 10. At any rate, it is established that the ion current is at least low by an order of magnitude.

The other major school of thought maintains that in essence the cesium vapor thermionic converter in its interesting range of operation is little more than a gas discharge diode or plasma diode with high work function emitter and low work function collector. Jensen demonstrated in 1960 (Ref. 3) the gas discharge nature of the cesium vapor thermionic converter by means of breakdown measurements on an operating converter in the low emitter temperature region (1200°C). More detailed breakdown curves were presented in (Ref. 5) in the spring of 1961 at the thermionic converter contractors meeting at Cambridge, Massachusetts. Other investigators have since corroborated these results. The significant difference in interpretation deals with the nature of production of ions in the interelectrode space for purposes of neutralization. It has long been known that volume ionization in a gas discharge diode occurs when electrons are accelerated across the cathode sheath gaining a kinetic energy equivalent to a loss in potential energy of $e\Delta V$. In the case of noble gas hot cathode discharges this "cathode fall" ΔV is of the order of the ionization potential in the gas or of the excitation level of certain long life metastable states of the gas. Once the interelectrode space has been broken down (a plasma has been established) the drift current density in the discharge is given by:

$$j_{sc} = \alpha \frac{4}{9} E_o \left(\frac{2e}{m} \right)^{1/2} \frac{(\Delta V)^{3/2}}{d^2} \leq j_{sat}$$
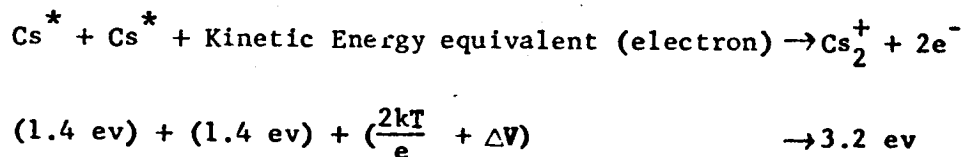
where

α is a factor of 1.86 under certain conditions given by Langmuir, ΔV is the cathode fall, and d is the cathode sheath thickness, E_o is the permittivity of free space, e electron charge, m the electron mass, and j_{sat} the saturation current possible from the emitter.

When the space charge current approaches the saturation current, the sheath voltage increases and an increase in current due to Schottky effect is observed. In cases of interest to vapor thermionic

converters the current may increase by a factor of two or so (Figure 6-2) as the converter approaches the short circuit condition. This increase in current over the zero field saturation emission is generally not of much importance due to the fact that the output voltage of the converter is approaching zero in order to realize the increase in current and hence no gain in useful power output of the converter is realized. Measurements made by this investigator (Ref. 4) on operating vapor thermionic converters give values of the emitter sheath voltage (or cathode fall) on the order of 0.6 volts to 0.8 volts in the low emitter temperature region. Measurements of arc drop in rubidium vapor hot cathode discharges (Ref. 1) give values of the tube drop less than approximately 2 volts. Similar measurements in hot cathode discharge in cesium vapor (Ref. 5) also show tube drops of less than 2.0 volts. Probe measurements on the devices of References 1 and 5 give electron temperatures in the neighborhood of 4000°K, (characteristic of cathode falls of approximately 0.5 volts) with no major potential maxima in the interelectrode space.

These measurements can be interpreted to mean that ionization is taking place by stepwise processes involving the capture of resonance radiation. This latter process almost certainly involves one (or two) cesium resonance levels near 1.4 ev. One such stepwise ionization process may be represented by the following equation:

$$Cs^{*} + Cs^{*} + \text{Kinetic Energy equivalent (electron)} \rightarrow Cs_{2}^{+} + 2e^{-}$$

$$(1.4 \text{ ev}) + (1.4 \text{ ev}) + (\frac{2kT}{e} + \Delta V) \qquad\qquad \rightarrow 3.2 \text{ ev}$$

The formation of the cesium molecular ion at an energy of roughly 3.2 ev has been given in the literature. This would require a cathode fall on the order of only a few tenths of an electron volt in order to complete the ionization process if the cesium vapor existed in a state of high percentage excitation at the resonance level. In the case of low temperature emitters only a small percentage of the energy radiated from the emitter exists in the 0.83 micron band and the excitation
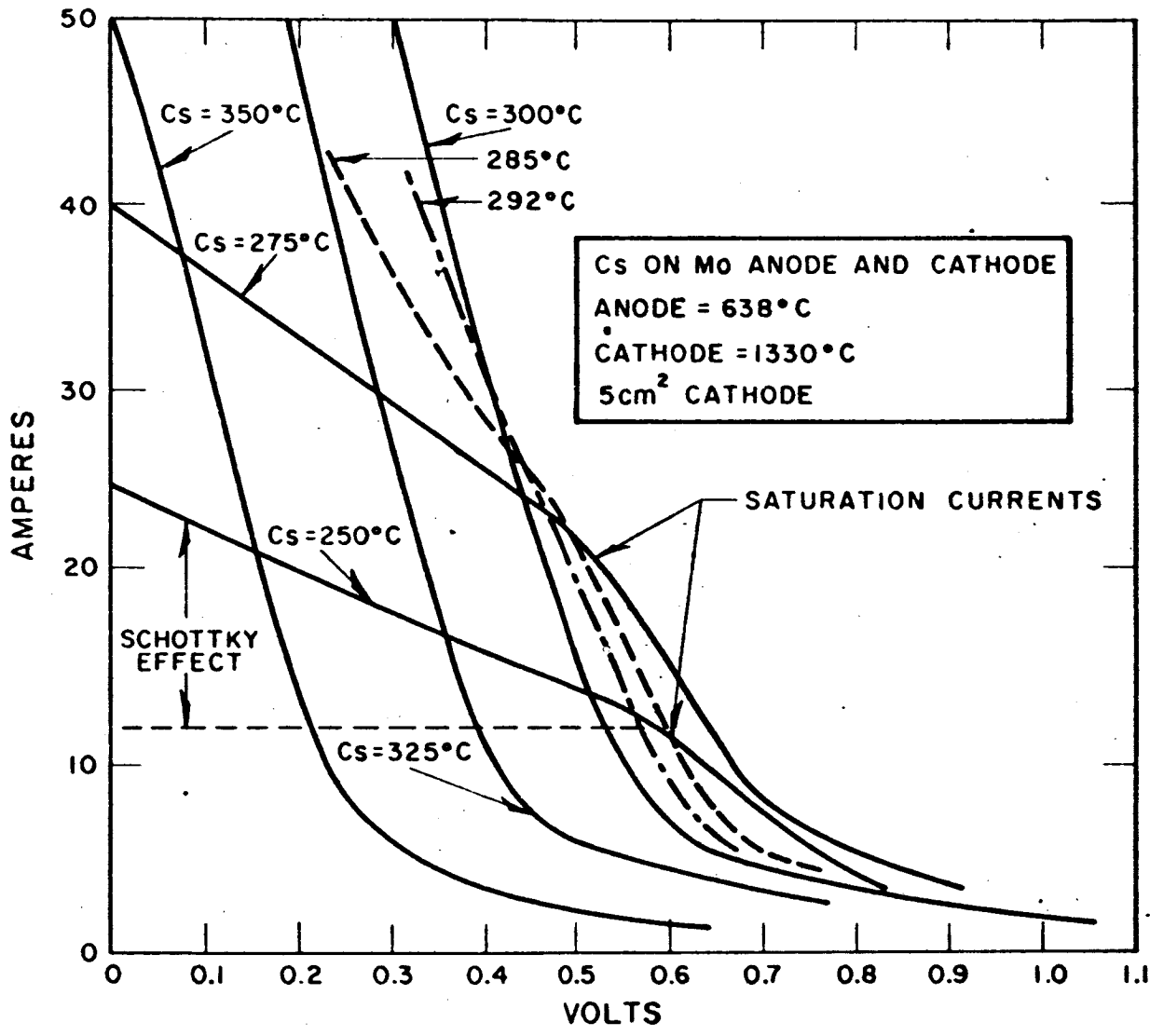
FIGURE 6-2. VOLT-AMPERE CURVES FOR VARIOUS CESIUM TEMPERATURES
ILLUSTRATING THE SHOTTKY EFFECT

energy would have to come from electron impact (and a resultant cathode fall of approximately 1.4 volt). As an emitter temperature increases, the peak of the radiation from the emitter shifts to shorter wavelengths according to the Wein displacement law ($\lambda_m = \frac{a}{T}$) and substantially more energy is available near the cesium resonance wavelength. In a limiting case at high emitter temperatue (2000°K) one might expect all excitation in a cesium diode converter to be due to radiation from the emitter and a small cathode fall of only a few tenths of a volt.

6.2 Plasma and Electrode Consideration

In the last section it was advanced that the practical cesium vapor converter functions as a gas discharge device. There are converters which have operated and are still operating in the space charge mode. This space charge mode can be broken down into a plasma region by applying voltage. The breakdown phenomenon of a space charge region in a thermionic converter may be pictured as follows: the device may be considered to be a "double diode" wherein both electrodes are a source of electron emission. The double diode has received preliminary treatment from Ivey (Ref. 6) and Dugan (Ref. 7) but complete analytic solutions are not available. Complete probe measurements of the space charge distribution in the double diode are also lacking. However, one may visualize the potential minimum V_m (see Figure 6-3) as a virtual electrode wherein high energy electrons are emitted and accelerated to the other electrode. It is the product of this distance and the pressure within the electrode gap that determine the condition for breakdown. It may well be that the population of excited states in the interspace (see Section 6.1: Ionization Processes) must reach a certain critical level before the impact of electrons accelerated from this virtual electrode produce ions.

Additional evidence of "breakdown" in a vapor thermionic converter has been recently submitted in detail by investigators at TEECO (Ref. 8). The existence of such a breakdown phenomenon wherein the interelectrode region undergoes a transition from essentially a "vacuum" region to a highly conducting plasma region is the strongest possible evidence of the plasma or gas discharge nature of the vapor converter. The fact that a breakdown "spike" is not noticable for high emitter temperatures is only an indication of the greater contact potential difference between emitter and collector which is available for initiating the breakdown process (see Figure 6-4).

Langmuir and Mott-Smith (Ref. 9) in a series of papers concerning electrical discharges in gases at low pressure, experimentally
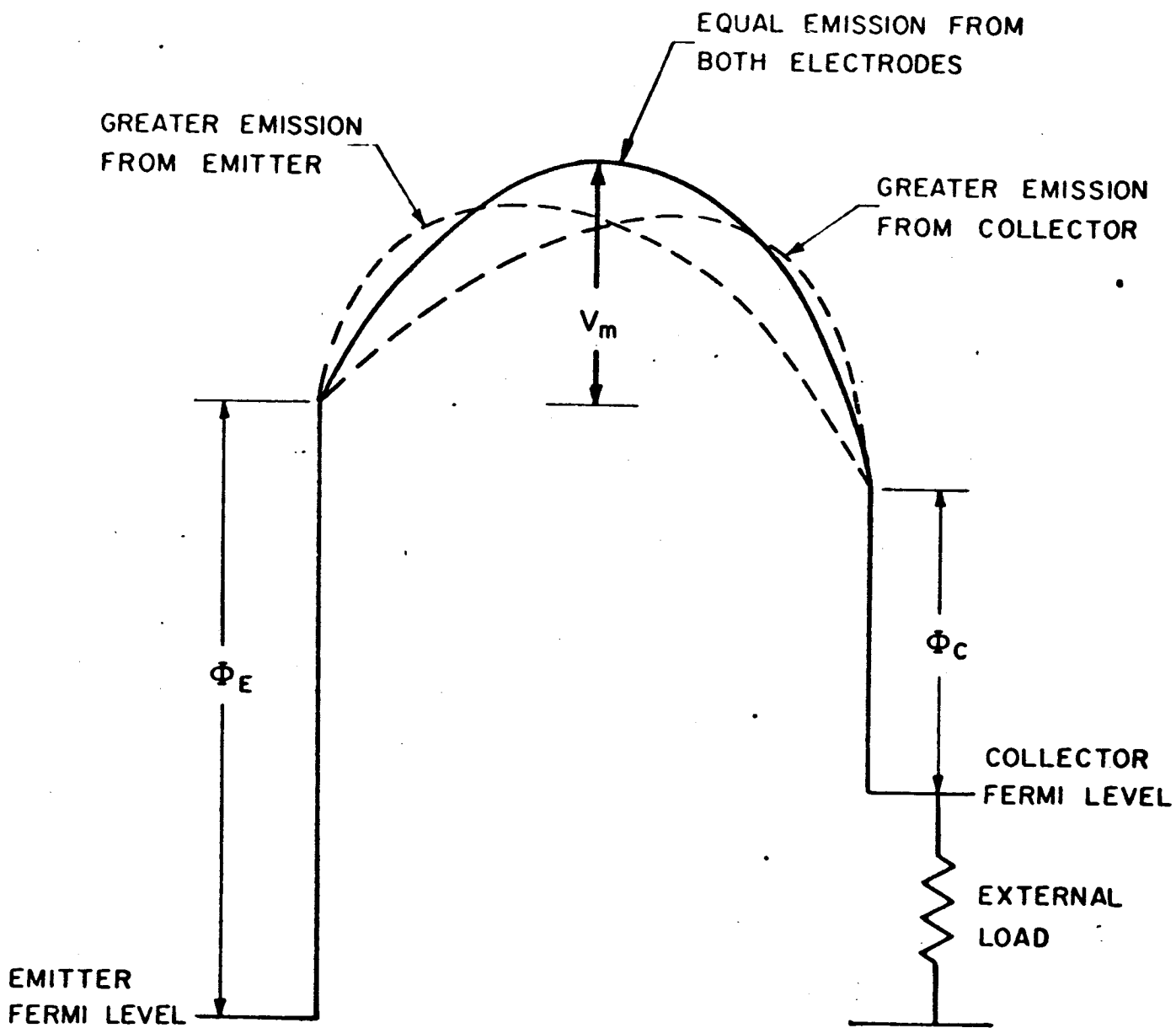
FIGURE 6-3   SPACE CHARGE DISTRIBUTION FOR EMITTER AND
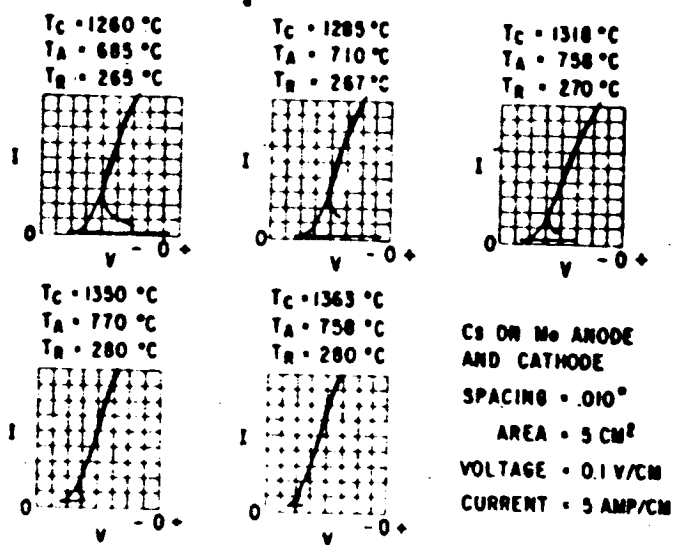COLLECTOR EMITTING ELECTRONS BEFORE BREAKDOWN

FIG. 6-4   BREAKDOWN CHARACTERISTICS OF CESIUM VAPOR
THERMIONIC CONVERTER

established the existence and extent of the cathode fall (or emitter sheath) region. The essence of these and other similar investigations (Ref. 10) is that the sheath thickness may be calculated very closely from the modified space charge equation given by Langmuir.

In some cases (Ref. 10) the sheath voltage and current and the sheath thickness have been measured directly in low voltage arcs with excellent agreement between experiment and theory resulting. The conclusion to be drawn from the sheath experiments is that in order to extract the electrons which an emitter is capable of emitting a sheath with an accelerating potential must be present. As pointed out in the last section, the value of the sheath voltage need only be as great as the resonance potential of the vapor in a well designed discharge device (1.4 volts in cesium) where cumulative ionization is taking place, and may be less than such a resonance potential by an amount equal to the electron kinetic energy ($\frac{2kt}{e}$). In the event that the vapor is excited by external means (radiation or contract excitation, for example) the sheath voltage only need be large enough to draw saturation emission from the emitter across a space equal approximately to the Debye shield distance. Typically, this voltage would be 0.5 volts for a sheath thickness of 0.15 mils for a current density of 10 amps/cm^2 (n_e 10^{12} $\frac{electrons}{cm^3}$).

The effect of such an emitter sheath on the output of a vapor thermionic is that it reduces the available output voltage from that which would be ideally expected by simply calculating the contact potential difference between emitter and collector.

The emitter sheath has further ramifications which bear on the achievement of an optimum spacing in a vapor thermionic converter. When impact ionization is necessary for establishing an adequate ion population in the interelectrode space, it has been found in numerous gas discharge investigations that ionization never takes place right at the emitter sheath edge but occurs throughout a region in the plasma which may extend to 100 times the sheath thickness. This, of course, is a direct consequence of the electron-atom collison probability and

the probability of ionization on impact. As the emitter to collector spacing is reduced in a practical vapor thermionic converter one would expect at first a very small increase in output voltage at constant current. As the spacing becomes too close (too few collision distances between emitter and collector) the output voltage should drop since the electron energy must rise in order to perform the same specific ionization in the gap. The increase in electron energy is brought about by an increase in the sheath drop at the expense of the output voltage. Such a state of affairs is clearly depicted in Figure 6-5. These data were taken by Jensen under carefully controlled experimental conditions and are felt to be representative of the phenomenon. The measurements were not extended to the higher emitter temperature range. This should be done in order to present a complete picture.

On the basis of the data shown in Figure 6-1, further calculations have been made concerning the optimum spacing to be anticipated at higher emitter temperatures. Such an optimum spacing curve is shown in Figure 6. The difference in the curves at various emitter temperatures is due to the correction in vapor density which must be made when the region of interest has a different average temperature than the cesium reservoir. Figure 6 is based on the similarity relationships which, with regard to the present discussion, state that where single stage impact ionization alone is the cause of ionization, two plasma regions are similar if E/p in volts/cm/mm Hg and p x d in mm Hg-cm are the same. It should be pointed out that in general a cumulative ionization process does <u>not</u> obey the similarity relations. The same general considerations of pressure and distance, however, should hold for cumulative ionization and Figure 6-6 should give a reasonably accurate prediction of the state of affairs at least in the 1 to 20 mm Hg region. The optimum spacing for a high efficiency vapor converter should thus be close to 4 mils for cesium pressures in the 5 to 10 mm Hg region with emitter temperature near 2000°K. Spacings closer than this (i.e., 1 mil) should tend to decrease the power output of the converter. It is only when the spacing approaches the sheath thickness (0.1 mil) that the power output again
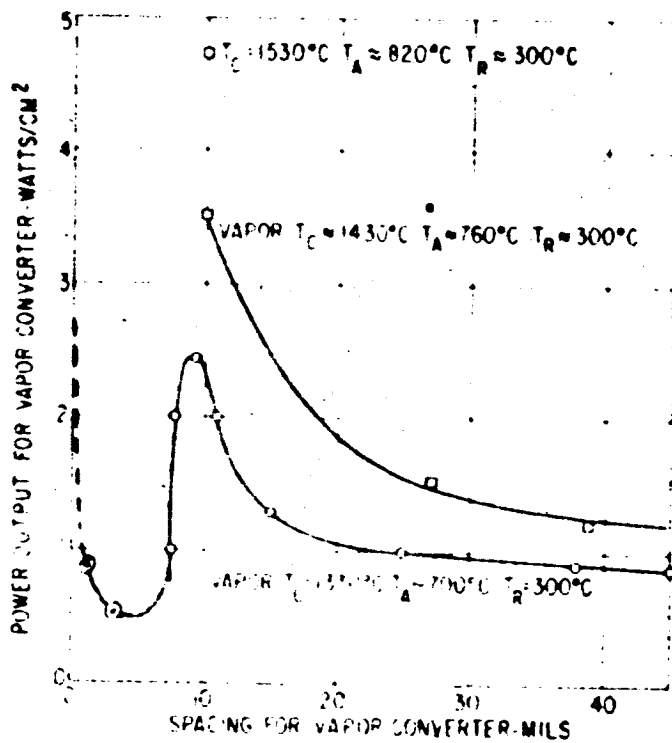
FIG. 6-5   Variation in Output Power Density as a Function of
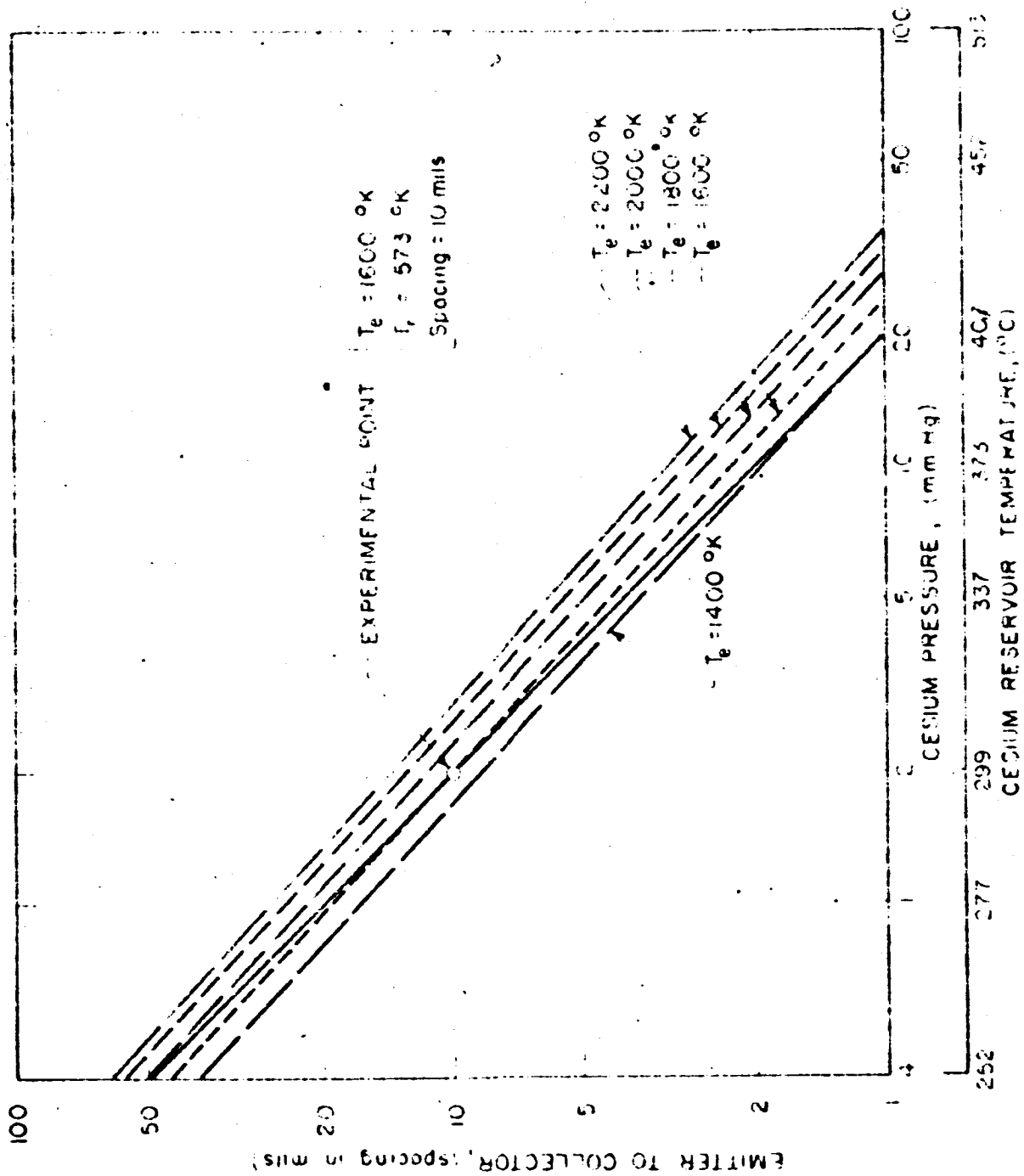Electrode Spacing for Sealed off Vapor Thermionic Converter

FIG. 6-6 CALCULATED OPTIMUM VAPOR THERMIONIC CONVERTER EMITTER TO COLLECTOR SPACING VERSUS CESIUM PRESSURE

rises and we approach a vacuum converter type of operation. Spacings of 0.1 mil are totally unrealistic for high temperature vapor converters.

In Figure 6-7 are shown vapor converters power output versus collector temperature curves (Ref. 11) for various emitter temperatures. If we extrapolate this curve to higher emitter temperatures (see Figure 6-8) we see that near emitter temperatures of $2000^\circ K$, a collector temperature of approximately $1200^\circ K$ is called for.

An important, but often overlooked, fact about the Langmuir curves is that they apply equally to emitter and collector. At lower temperatures where the collector assumes a work function appropriate to cesium, the theory (Ref. 11) predicts an optimum work function of 1.69 volts instead of 1.88 volts. For systems other than Cs-W, optimum collector work functions of 1.4 - 1.5 volts have been experimentally observed (Refs. 12 and 13) for Cs-Ta. Figure 6-9 illustrates the necessity of adjusting the collector temperature to maintain an optimum work function for varying arrival rates. Since the voltage output of a converter is directly dependent upon the contact potential difference, a loss of .3 or .4 or .4 volts at the collector would seriously impair a practical converter. A simple consideration of optimum collector work function (1.5 ev for Cs on molybdenum) and collector temperature ($1200^\circ K$) would lead one to predict a "back emission" of approximately 100 amps/cm^2 from the Langmuir "S" curves. If the same simple considerations were applied to calculating converter power output, the results would indicate converter current in the reverse direction since the emitter is only capable of supplying approximately 20 amps/cm^2 for a temperature of $2000^\circ K$ and an arrival rate of about 10^{21} atoms/cm^2/sec. What has not been taken into consideration is the condition for matching a current collecting probe to the plasma. One can advance a good argument to the effect that if the collector is not to disturb the plasma it must be capable of emitting a current equal to the random electron current in the plasma (see Figure 6-10). One can calculate, as in the previous section, random plasma current densities of 50 to 100 amps/cm^2 using reasonable assumptions. The sheath condition at the collector is thus seen to require more than a simple treatment and should be investigated in more detail.
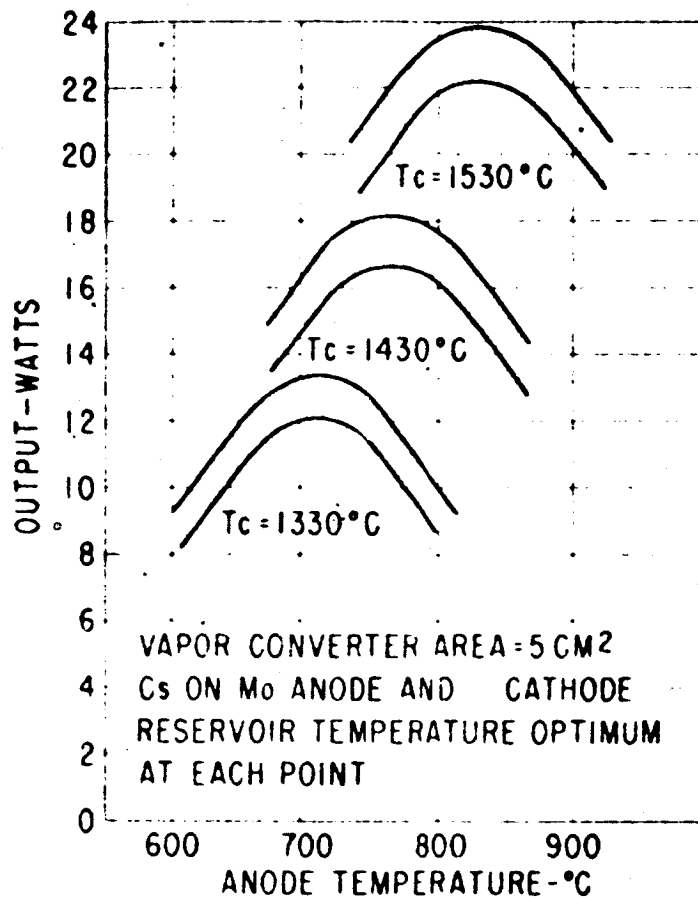
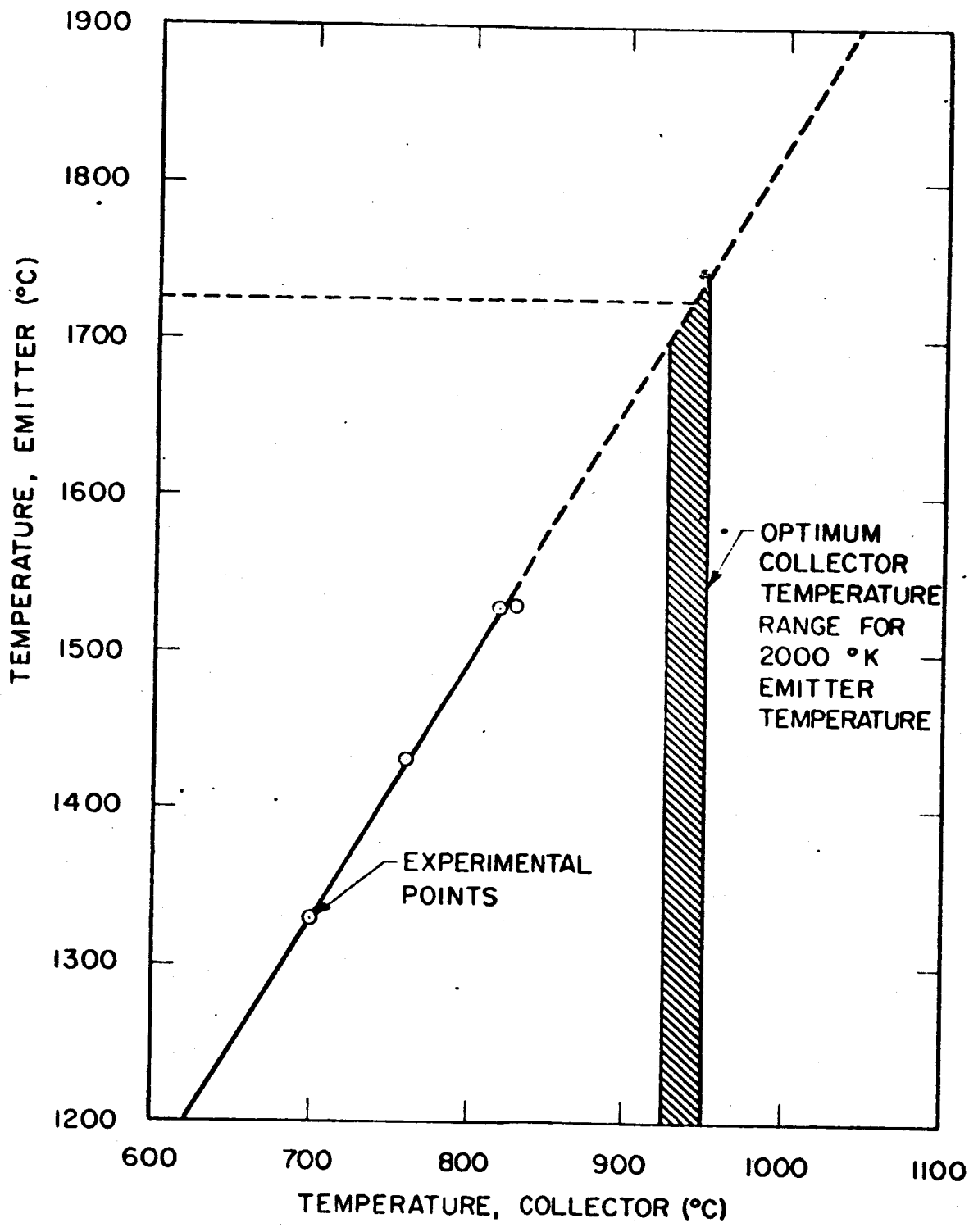FIG. 6-7   Power Output vs Anode Temperature for Sealed-off Vapor Thermionic Converter

FIGURE 6-8 OPTIMUM COLLECTOR TEMPERATURE FOR VARIOUS EMITTER TEMPERATURES IN AN OPTIMIZED VAPOR THERMIONIC CONVERTER
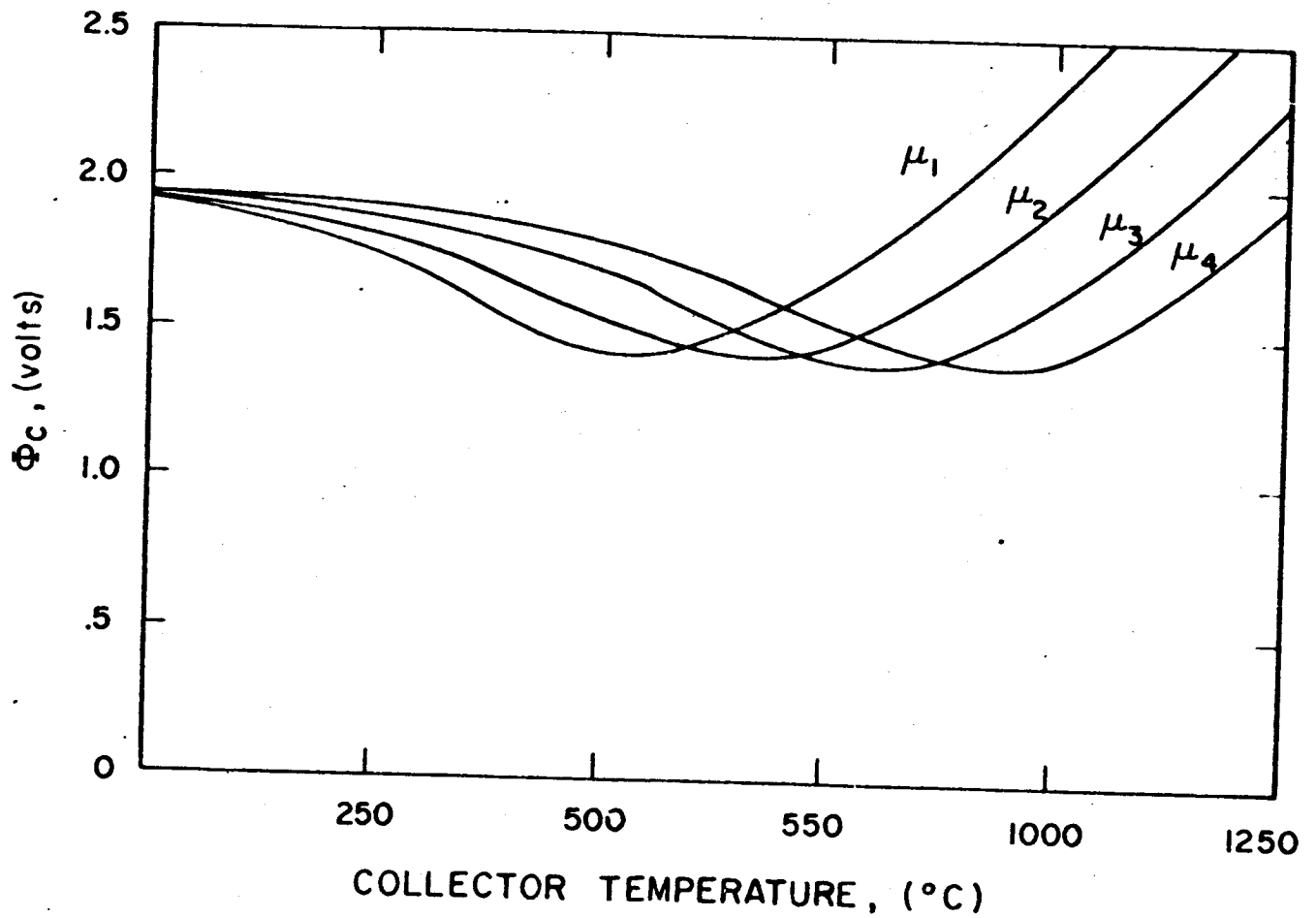
FIGURE 6-9 COLLECTOR WORK FUNCTION VS. COLLECTOR TEMPERATURE
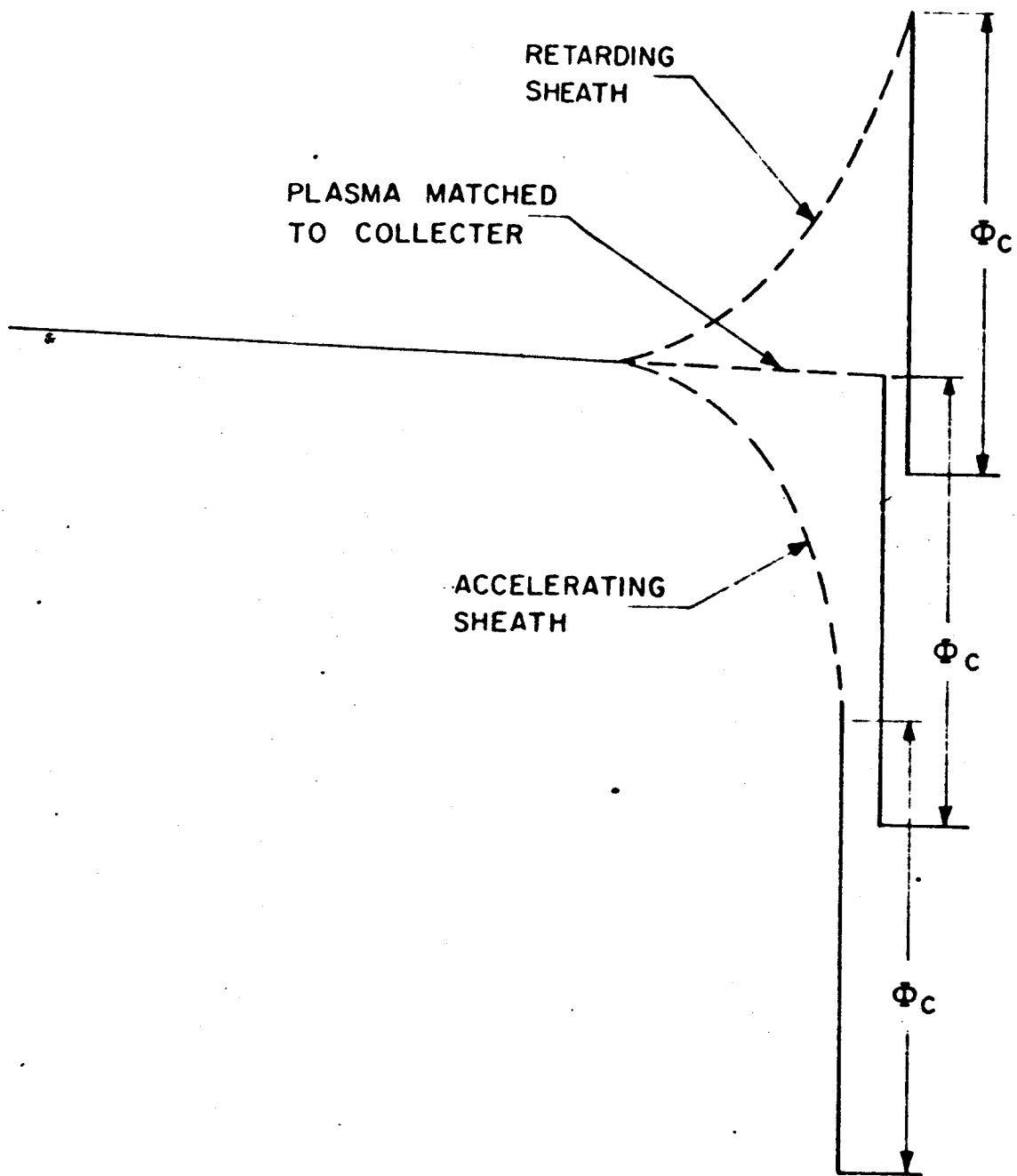WITH CESIUM ARRIVAL RATE AS THE PARAMETER

FIGURE 6-10 POTENTIAL DIAGRAM AT COLLECTOR

165693

6.3 Interpretation of Cesium Vapor Thermionic Diode Volt-Ampere Characteristics

Volt-ampere characteristics for operating cesium vapor thermionic converters are shown in Figures 6-4, 6-11, 6-12, and 6-13. To a large extent these curves contain practically all of the information which is necessary for interpretation of vapor filled thermionic converter phenomena. The two major pieces of information which are needed to supplement these curves for interpretational purposes are the curves of Figure 6-5, concerning converter power output versus spacing and the Langmuir-Taylor "S" curves for the particular emitter and collector materials used (these may be found in Chapter 2). As we have already pointed out earlier in this chapter, there appears to be no reasonable doubt that all practical vapor thermionic converters operate as gas devices. At low emitter temperatures a breakdown phenomena is definitely in evidence, power output varies with spacing as would be predicted from elementary gas discharge considerations, the output voltage of the converter at maximum power is dictated not only by the contact potential difference between emitter and collector but also by the magnitude of the emitter and collector sheath drops and the plasma resisitivity losses. We are in essence saying that the interpretation of the characteristics of the practical cesium vapor thermionic converter resolves into an understanding of the Langmuir-Taylor "S" system for the applicable emitter and collector, an understanding of the importance of the breakdown phenomena at low emitter temperatures, and an understanding of the pre-breakdown currents in the device. With these thoughts in mind, we will proceed to an interpretation of some typical cesium vapor volt ampere characteristics.

In Figure 6-4 are shown a series of volt ampere chracteristics which were observed on an operating thermionic converter with varying emitter temperatures but for nearly constant collector and cesium reservoir temperatures. The major point of interest is the manner in which the
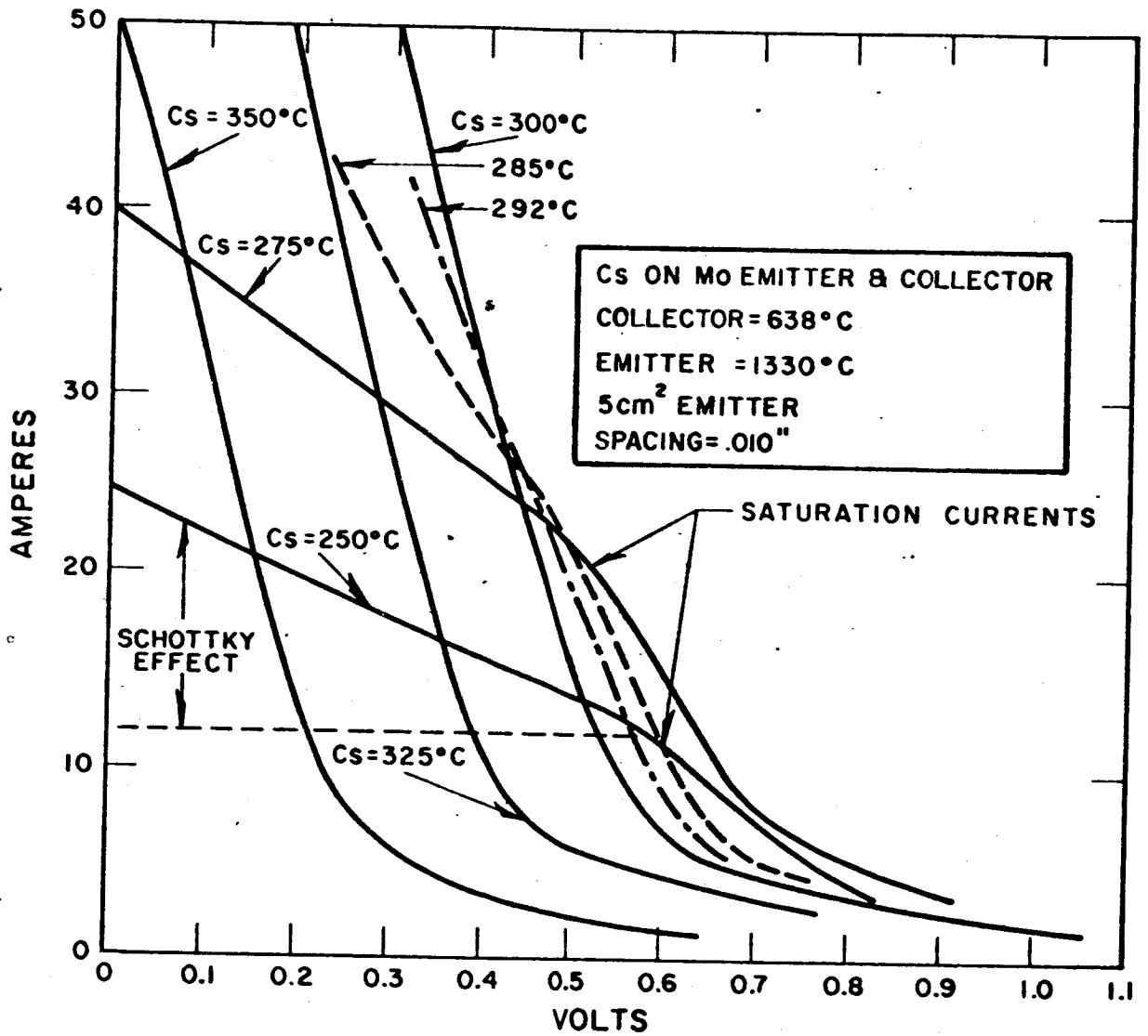
FIG. 6-11 VOLT-AMPERE CHARACTERISTICS OF A CESIUM VAPOR
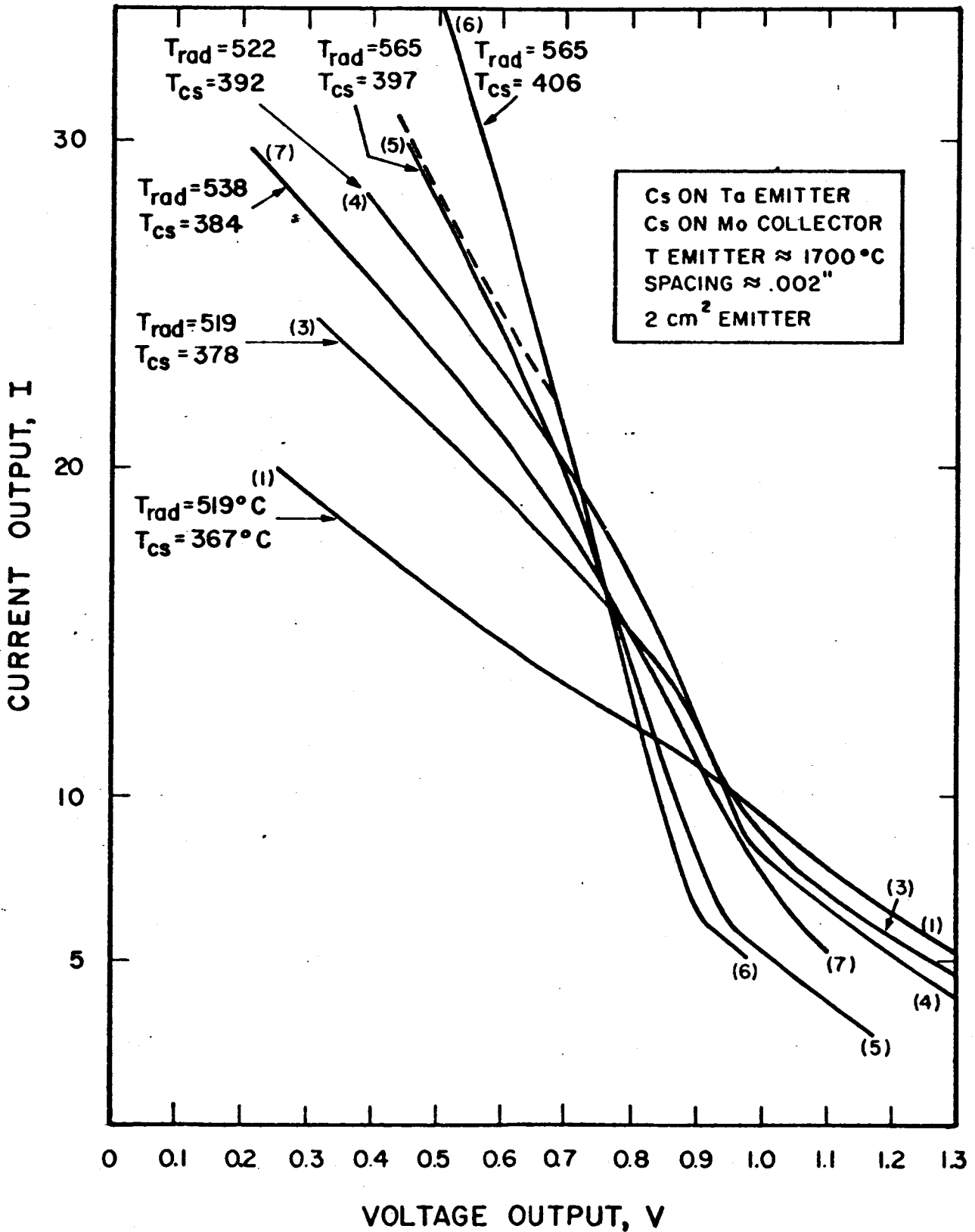THERMIONIC CONVERTER FOR VARIOUS CESIUM TEMPERATURES

FIG. 6-12 VOLT-AMPERE CHARACTERISTIC OF CESIUM VAPOR THERMIONIC CONVERTER

magnitude of the breakdown "spike" changes with varying cesium reservoir temperature or with p x d (the cesium pressure x electrode spacing) relationship in the gap between the emitter and the collector. As may be seen in Figure 6-4, a positive voltage must be applied to the converter in order to breakdown the gap between emitter and collector for emitter temperatures of the order of $1260^{\circ}C$. Were it not for this positive applied voltage, one would not observe the high current branch of the characteristic. In fact, most of the misinterpretation of cesium vapor diode phenomena probably resolves around this single point. Many investigators being unaware of the discharge nature of this type of device, by not applying a positive applied voltage have never observed the high current branch of the volt-ampere characteristic and have, therefore, assumed the low current branch corresponded to the saturation emission density from the cesium on refractory metal emitter. As the emitter temperature is raised one can follow the reduction in breakdown voltage required until at temperatures in the neighborhood of $1300^{\circ}C$ the breakdown spike almost completely disappears. The disappearance of the breakdown spike is only evidence of the fact that at the higher emitter temperatures sufficient voltage exists between the space charge potential minimum in the gap and the surface of the collector to initiate a breakdown by electron-atom impact processes without going closer to a short circuit condition than the steeply rising portion of the volt ampere characteristics.

To phrase the situation in another manner, the breakdown condition is still present but not observable on the volt ampere characteristics due to an increase in contact potential difference within the device at the higher emitter temperature.

Proceeding to Figure 6-11, one readily observes the condition just mentioned wherein the presence of the breakdown spike is no longer observed. In evidence in Figure 6-11 is the parametric optimization of a practical vapor converter for fixed collector and emitter temperatures. A further series of similar curves at various collector and emitter temperatures is required in order to achieve complete

parametric optimization of the converter. Points of interest to note about this set of characteristics are: (1) the rather linear low current branch which, in essence, corresponds to a slightly enhanced space charge limited current flow in the device, (2) the point of breakdown, (3) the rapid rise of current at nearly constant voltage (as observed in any gas discharge diode), (4) the saturation current level, and finally, (5) a Schottky increase in current as the diode approaches short circuit condition.

As is evident from the curves, at the higher cesium reservoir temperatures the available current density from the emitter exceed 10 amps/cm^2 in agreement with values predicted by the Langmuir-Taylor "S" curves. As one increases the cesium reservoir temperature beyond the optimum, which for the present case is approximately 300°C, one observes a steady shift of the volt-ampere characteristics towards the zero voltage axis. This is primarily due to two things: (1) the decrease in contact potential difference due to the fact that the collector is now operating at greater than optimum cesium coverage and, (2) the increasing pressure which ultimately dictates increasing elastic collison loss as in the plasma which also subtracts from the available output voltage of the converter. The situation appears to be more or less obvious when measurements are taken in a carefully controlled converter wherein the spacings and element temperatures are very carefully measured and controlled.

In many respects the curves of Figure 6-11, which were obtained at EOS on an entirely different diode than those of Figure 6-11, reflect the identical situation just discussed with respect to the curves of Figure 6-11. The major difference is that the whole pattern of curves is now shifted to higher voltages and saturation currents indicative of the higher emitter and reservoir temperatures which increases the available contact potential difference and saturation current density. The only major difference between these two diodes is possibly in the fact that the diode of Figure 6-11 did not

contain a positive spacing and thus the spacing of the diode may
have been varying with the current through the diode, which would
tend to obscure some of the behavior observed in Figure 6-11.

The curves of Figures 6-13 indicate the type of volt ampere
characteristics which may be observed from a cesium vapor thermionic
converter when the cesium pressure, the spacing, and the collector
temperature conditions are not optimized. In particular, attention
is drawn to the curve for an emitter temperature of $1822^{\circ}K$, which
may be compared with those curves of Figure 6-11. From these curves
it may be seen that at approximately 1/2 volt output, proper selection
of the spacing and collector temperature accounts for approximately an
increase in power density output by a factor of 5. It is obvious
that the converter whose characteristics are shown in Figure 6-13
was operated with either much too close a spacing, much too low a
collector temperature, cr a combination of both. The publication of
such characteristics in the past has accounted for a great deal of
confusion prevelant in the interpretation of thermionic converter
characteristics.

Observation of the characteristics which have just been
shown clearly indicates that in order to achieve maximum efficiency from
a cesium vapor thermionic converter, the converter should be operated
in the arc mode near the saturation current density point. Consider
for example the curves of Figure 6-11 at a cesium reservoir temperature
of $300^{\circ}C$; one may achieve approximately a maximum of 3 watts from the
device when operating the device in the space charge limited mode
(the lower branch of the volt-ampere characteristic). When this same
device at identical temperatures is operated in the arc mode near the
knee or saturation part of the current characteristics, a power output
of 12-1/2 watts is achieved, or essentially a factor of 4 increase in
power density output. Since the efficiency of these devices will
normally increase in approximately a linear fasion with power density
output, a great increase in efficiency has been achieved by operating
the device in the most appropriate part of its characteristic. The
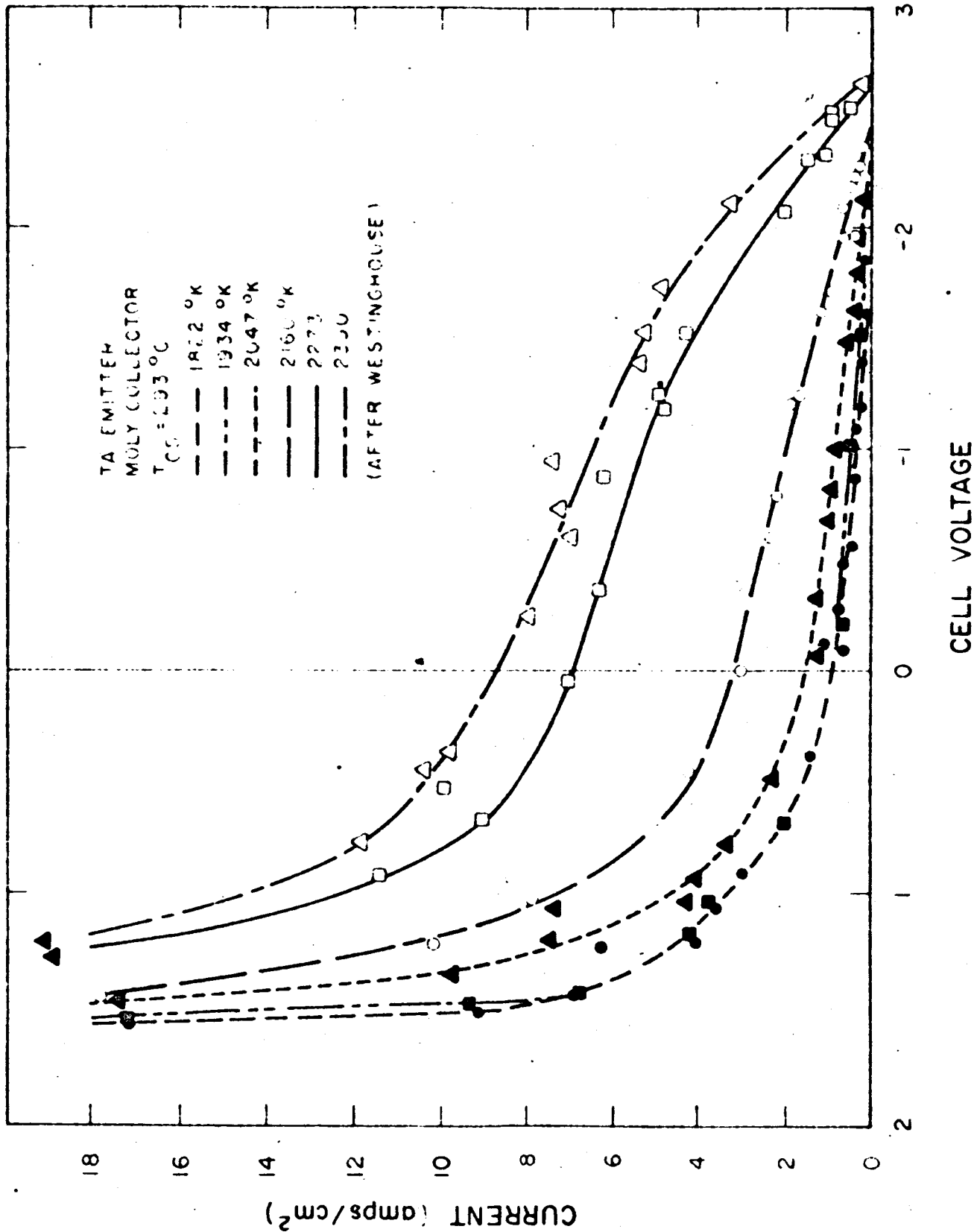same considerations may be seen to hold at higher emitter temperatures

FIG. 6-13   VOLTAGE-AMPERE CHARACTERISTIC AFTER WESTINGHOUSE

564730

as borne out by the curves of Figure 6-12 for emitter temperatures of 1700°C.

Perhaps the major reason why the present interpretation has not been considered obvious by all investigators is that the inexperience and poor measurement technique exhibited in most experimental studies of record has resulted in a bewildering array of data which is almost impossible to correctly interpret.

REFERENCES

1. W. J. Kearns and J. O. Pehek: Low Anode Voltage Thyratron, WADC Technical Report 57-422, March 1958

2. I. Langmuir: The Interaction of Electron and Positive Ion Space Charges in Cathode Sheaths, Phys. Rev., Vol. 33, No. 6, pp 954-989, June 1929

3. E. A. Baum and A. O. Jensen: Thermionic Converters - Design Status and Forecast, Proceedings of 15th Annual Power Sources Conference, May 1961

4. A. O. Jensen: Arc Mode Vapor Thermionic Converter, Proceedings of the Round Table Discussion on Thermionic Materials and Processes, June 1, 1961

5. R. K. Steinberg: Hot Cathode Arcs in Cesium Vapor, M.I.T., Res. Lab of Electronics, Technical Report No. 128, June 1949

6. H. F. Ivey: Space Charge Limited Currents, Advances in Electronics and Electron Physics, Vol. VI, 1954

7. A. F. Dugan: J. of Applied Physics, Vol. 31, No. 8, pp 1397-1400, August 1960

8. S. Kitrilakis and E. N. Carabatess: Experimental Study of the Ignited Mode in Cesium Vapor Thermionic Converters, to be presented at A.I.E.E. winter meeting, January 30, 1962

9. I. Langmuir and H. Mott-Smith: General Electric Review, Vol. 27, p. 449, 1924

10. M. J. Druyvesteyn and F. M. Penning: Rev. Mod. Phys., 12, 146, 1960

11. Final Report, 22 May - 22 November 1961, Solar Energy Thermionic Conversion System, Contract No. JPL-950109, Electro-Optical Systems, Inc., Report 1850-Final, 20 December 1961

12. M. D. Gibbons: Experimental Studies of the Emission and Discharge Characteristics of the Ta-Cs System Thermionic Power Sources Conference, Colorado Springs, May 1962

13. A. E. Campbell: Thesis (San Diego State College), unpublished, 1962

7. PROPERTIES OF CESIUM

TABLE 7-I

TYPICAL ANALYSES OF COMMERCIAL CESIUM AS GIVEN BY THE SUPPLIERS
FOR CESIUM AVAILABLE - FEBRUARY 1962

Impurities in ppm.

	American Potash	Dow Chemical	U.S. Ind. Chemical	Kawecki	
Cesium, percent	99.92	99.9	99. +	99.5	99.9
Rubidium, ppm	450	270	900	max 1000	max 100
Potassium "	150	45		max 100	max 100
Sodium "	<10	24		max 1100	max 100
Lithium "	5			ND	ND
Alkali Metals "	1000(approx)	max 400			
Calcium "	20	10		max 1000	max 100
Iron "	6	6			
Aluminum "	5	5			
Magnesium "	2	2			
Other Metals	10	max 200	(Fe and Al)	max 100	max 10
Heavy Metals (Pb,etc.)	22				
Silicon	2		(Fe and Al)	max 100	max 10
Oxygen	20		1-100		
Nitrogen	28				
Carbon					
Hydrogen					
Non Metal	48	max 100			
Highest minimum purity of Cs guaranteed upon special request		99.97	99.0	99.9	

TABLE 7-II

Resistance to Corrosion in Cs Vapor

Refractory Metals	hrs °C	200 247	100 302	200 497	450 1002	Non-Metals	100 hrs. 207°C
W		G	G	G	G	Alumina	G
Ta						Pyrex	G
Mo		G		G		Vycor	G
Cb						W Glass	G
Ti						Soft Glass	G
Ir						Teflon	C
Pt		G		G		Nylon	C
Ferrous Fe						Asbestos	C
Mild Steel			S			Duroid	C
18/8 SS			G			Rubber - 18007	G
308 SS						66-018	C
410 SS		G		S		Natural	G
Non-Ferrous						Zirconia	G
Au			L				
Al							
Cu		S	S	L	P		
Brass			S			G - Good	
Ni		G	G	S	G	S - Surface Pitting	
Nichrome			G			C - Color change from	
Inconel X					G	white to dark	

TABLE 7-III

Suggested Limits for Structural Materials for Cesium Systems

	Resistance	^{o}C	Usual Application
Structural Metals			
Refractory Metals	excellent	2000	High temperature emitters and walls
Steels	good	600	Walls
Stainless Steels	excellent	1000	Walls
Ni and its alloys	excellent	1000	Resistance wire
Aluminum	unusable	200	Light weight wall, electrical cond.
Copper	unusable	200	Electrical and thermal cond., gaskets
Brass	poor	200	Walls
Silver	unusable	100	Braze, electrical conductor
Gold	unusable	100	"O" rings
Cadmium	unusable	100	In Easy-Flo
Zinc	unusable	100	In Easy-Flo
Tin	unusable	100	Soft solder
Lead	unusable	100	Soft Solder
Insulators			
Alumina	good	800	
BN	poor		
Glass	limited	200	
Fused quartz	limited	500	
Teflon	unusable	100	Gaskets
Kel-F	unusable	100	
Other			
Rubber	poor	100	"O" rings
Graphite	poor		

TABLE 7-IV

Corrosion by Liquid and Gaseous Cesium
(from Fig. 7-1 and Fig. 7-2)

Material in vial	352°C 240 hrs.	Material in vial	T °C	Result
SS 304	Good	Uranium and borosilicate glasses.	384	No attack except when strained like at glass-to-metal seal.
SS 316	Good			
SS 321	Good			
SS 347	Good			
17-7PH Steel	Best	Al_2O_3	200-400	Surface attack
Ni-Cr Braze	No Transport	Fiber	260	100 hrs., poor.

Resistance Heated Wire	T °C	Time hrs.	Cs press. mm Hg	Result
Mo .008	1023	Below 100	0.5	Broke due to recrystallization.
.010	1023	Below 100	0.5	
.015	1023	65	0.5	Recrystallized and reduced to .013 - .014".
W	1002	6 mo.	0.1	In progress, very small change in resistance.
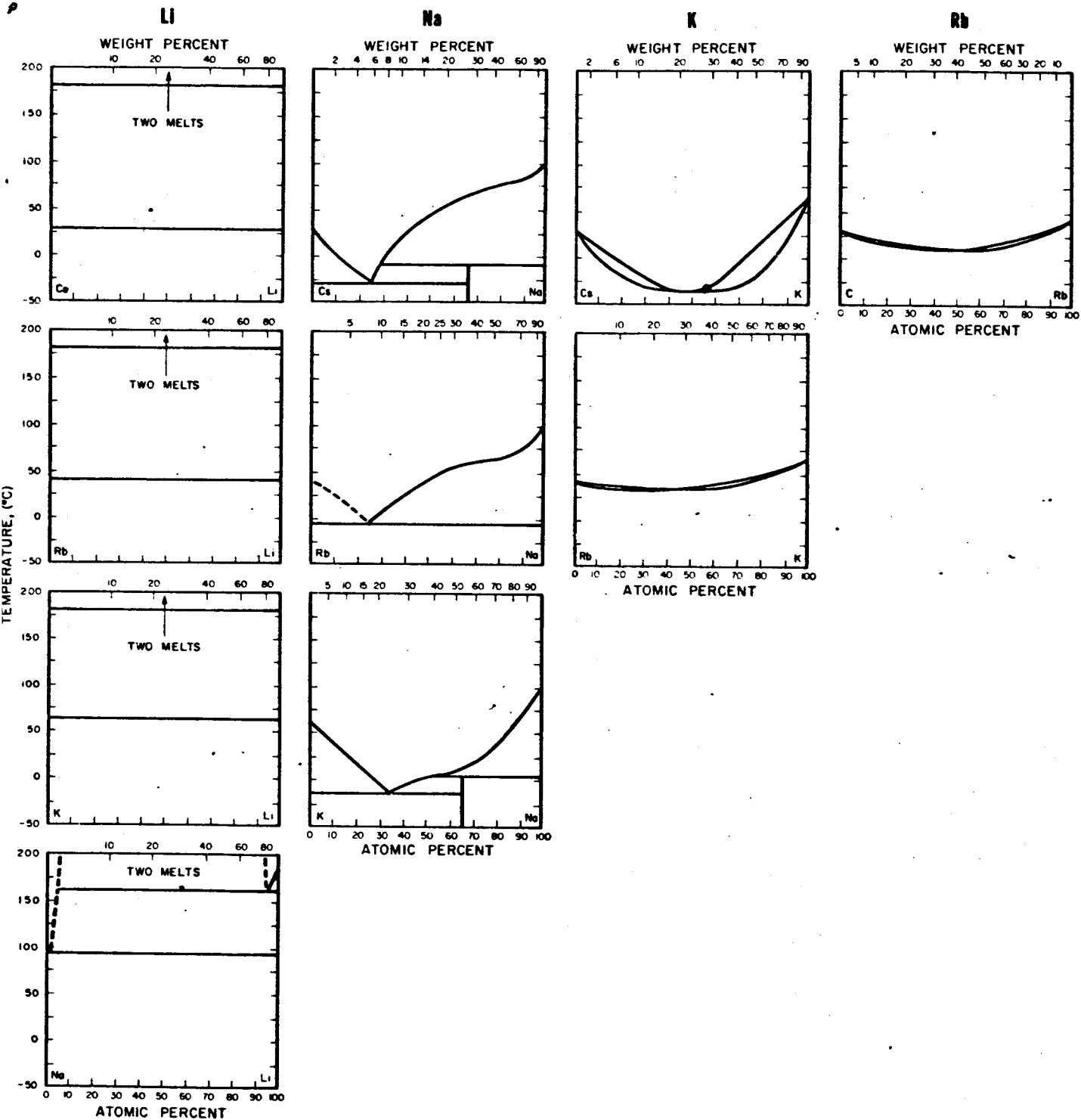
FIG. 7-1   PHASE DIAGRAMS FOR BINARY MIXTURES FOR ALKALI METALS
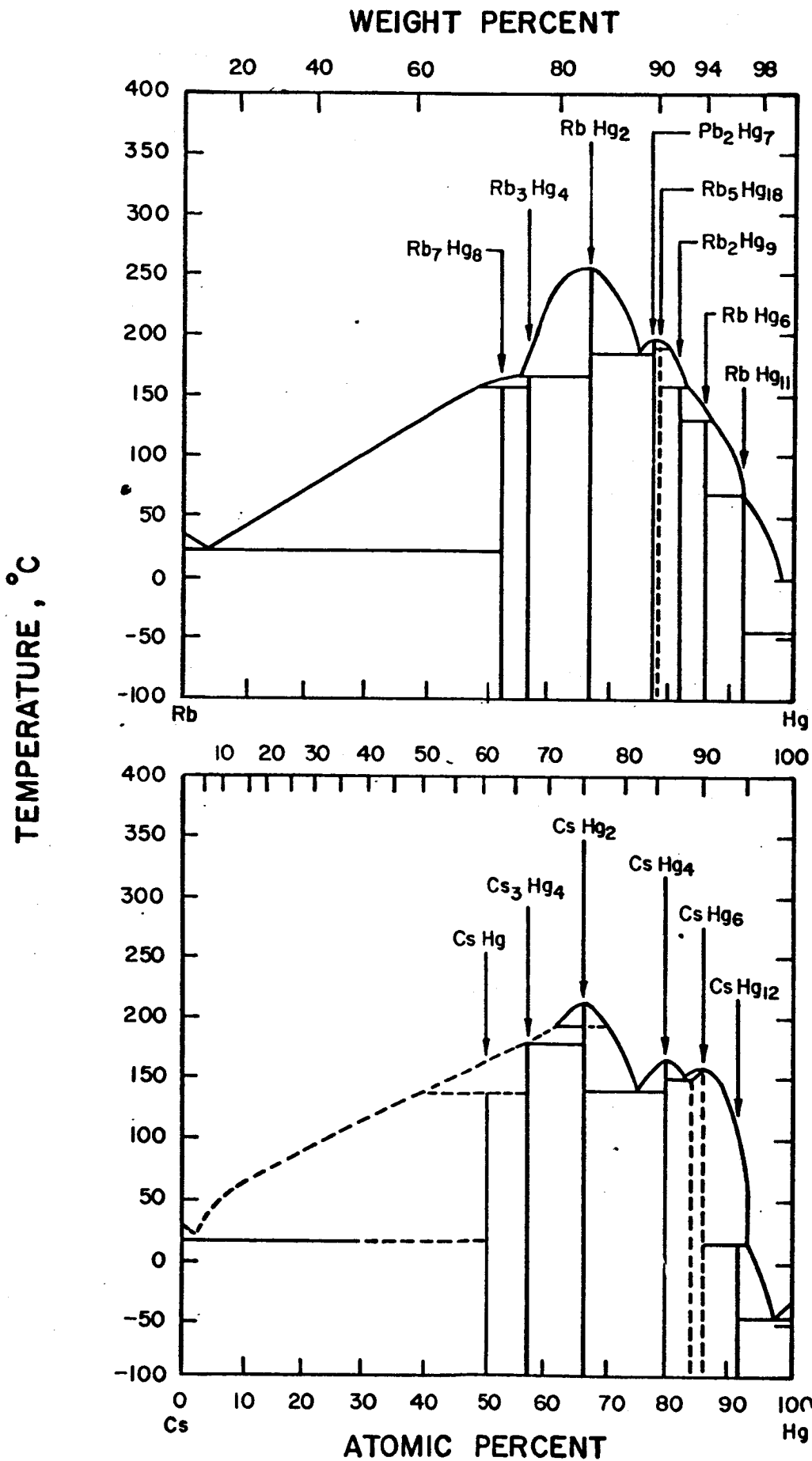
FIG. 7-2   PHASE DIAGRAMS FOR Rb-Hg, Cs-Hg
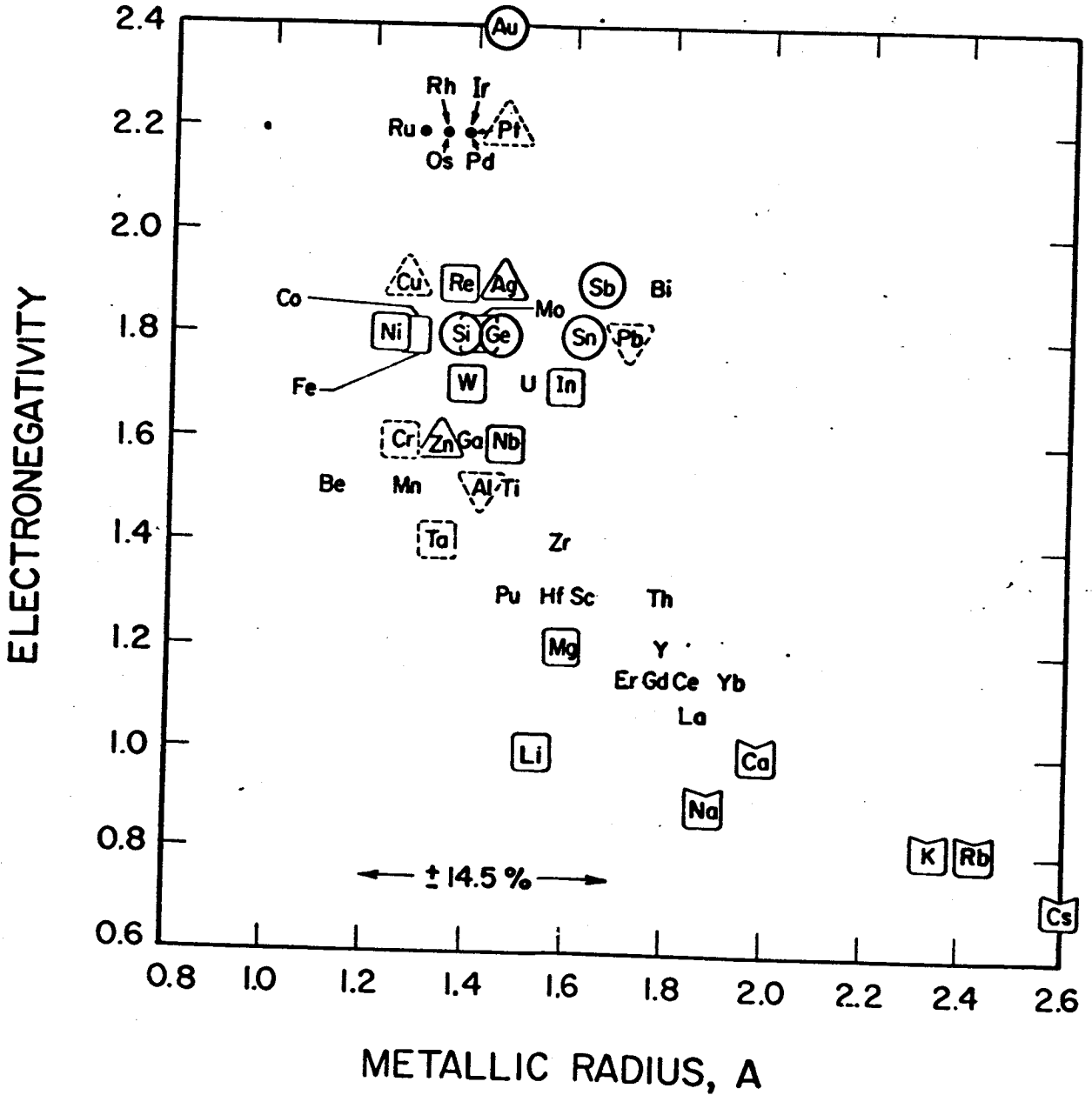
FIG. 7-3   HUME-ROTHERY PLOT FOR CESIUM ALLOYS
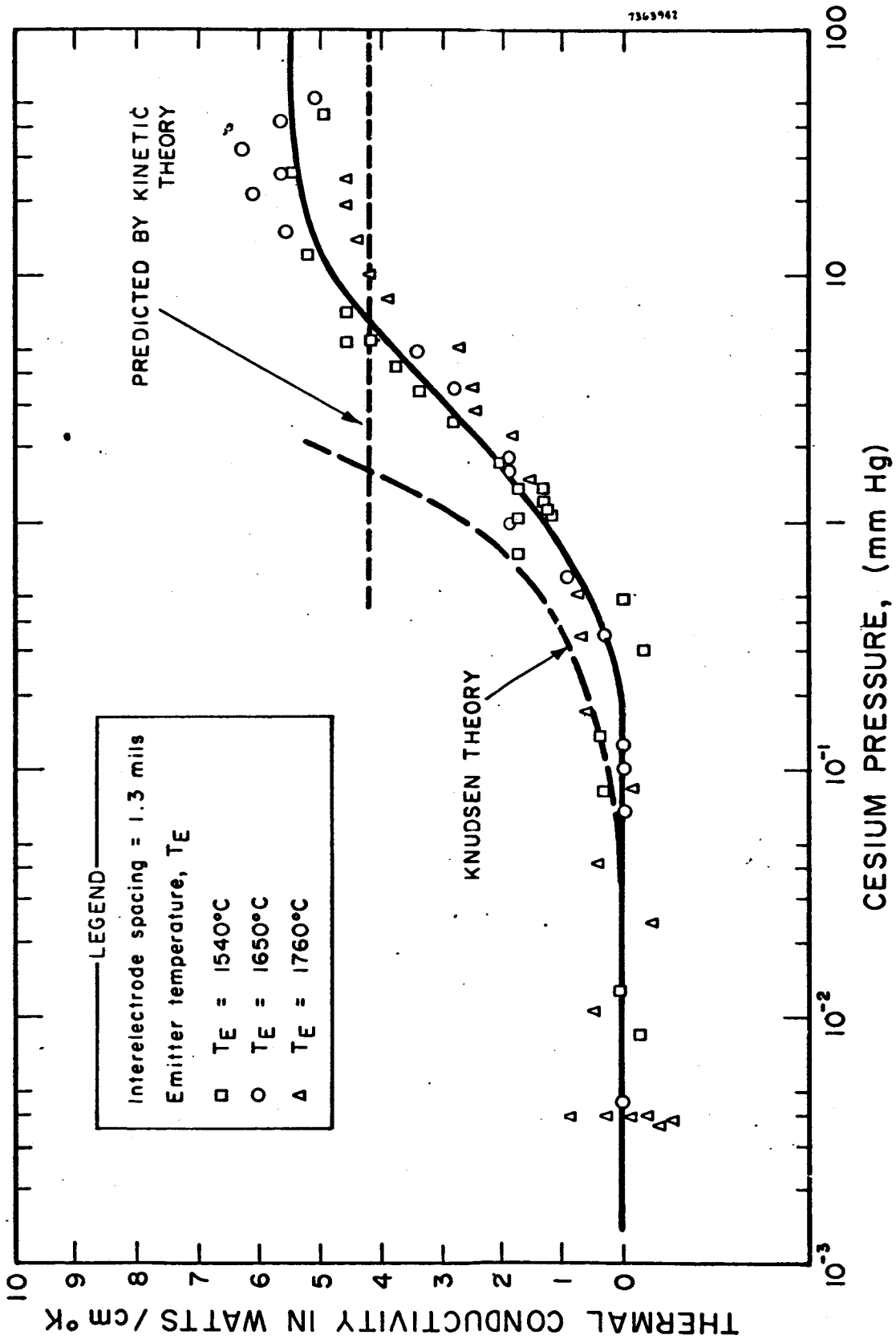
FIG. 7 -4   CESIUM CONDUCTION VS CESIUM PRESSURE

7363942
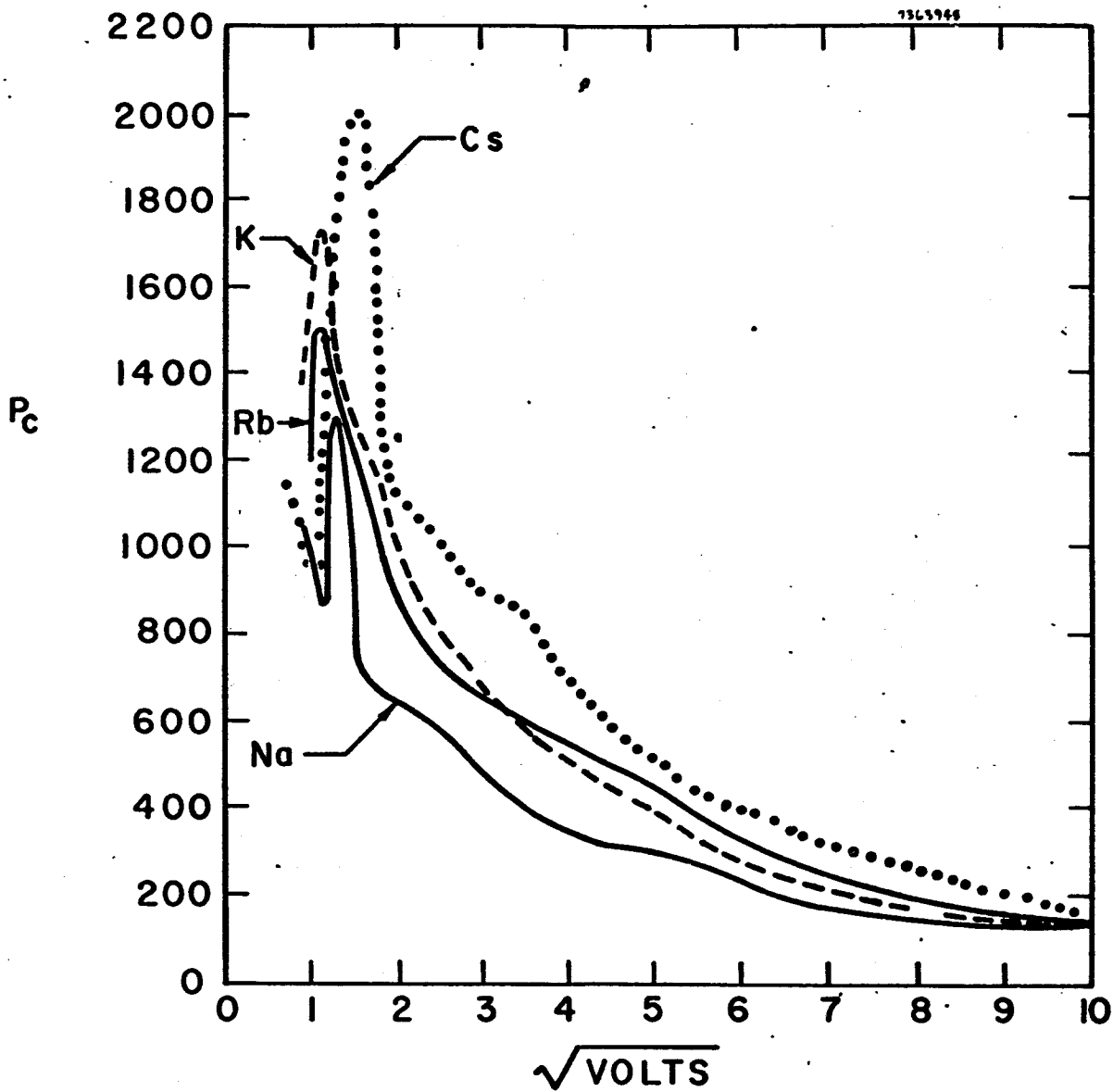
FIG. 7-5   PROBABILITY OF COLLISION IN THE ALKALI METALS
(REF. R.B. BRODE, REUS. MODERN PHYS. 5, 257 (1933))
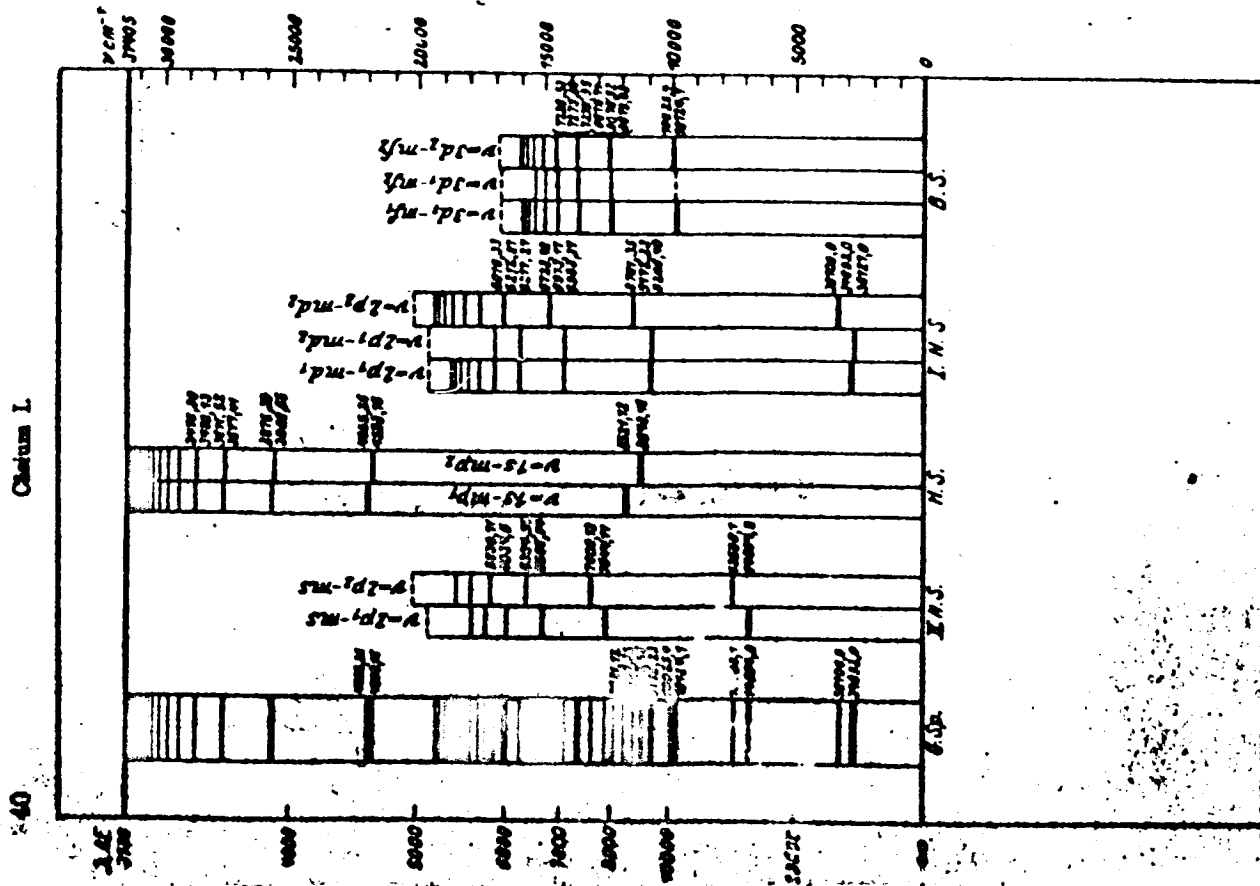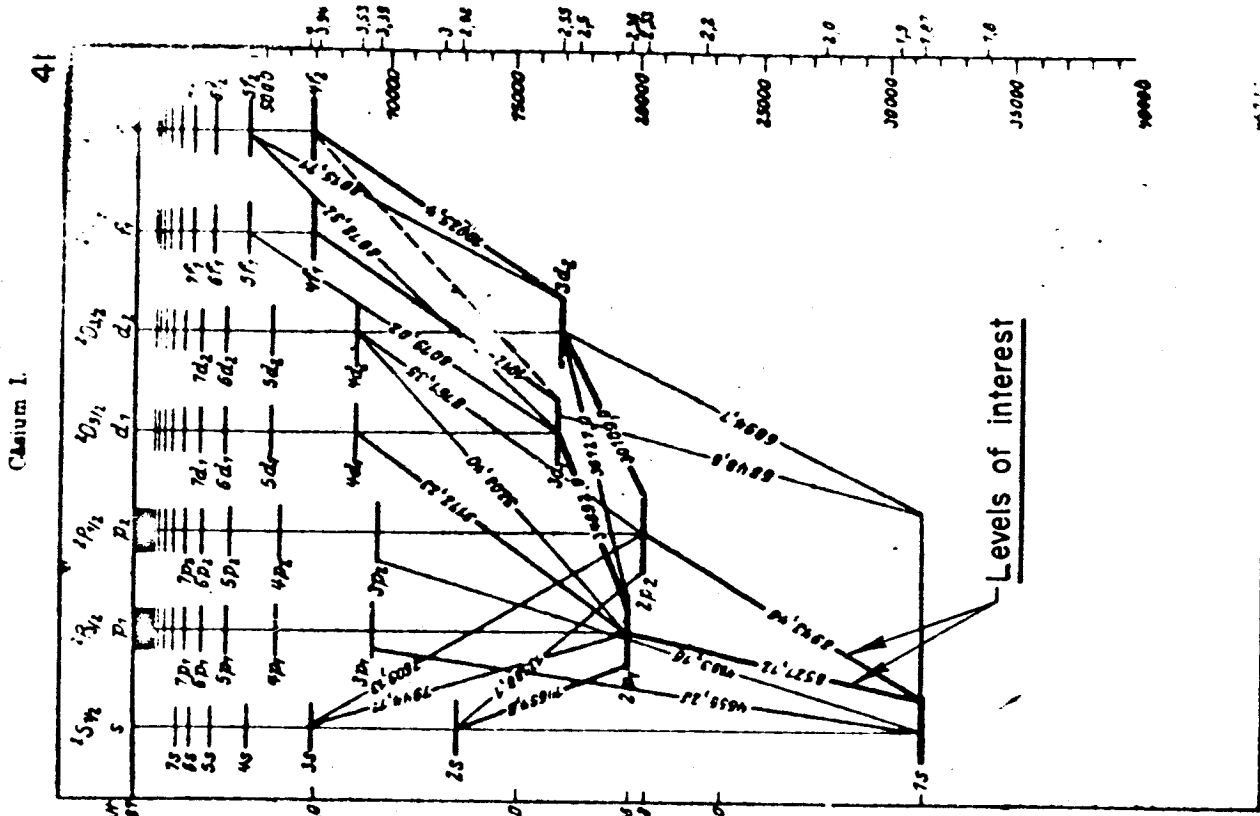
FIG. 7-6 CESIUM I
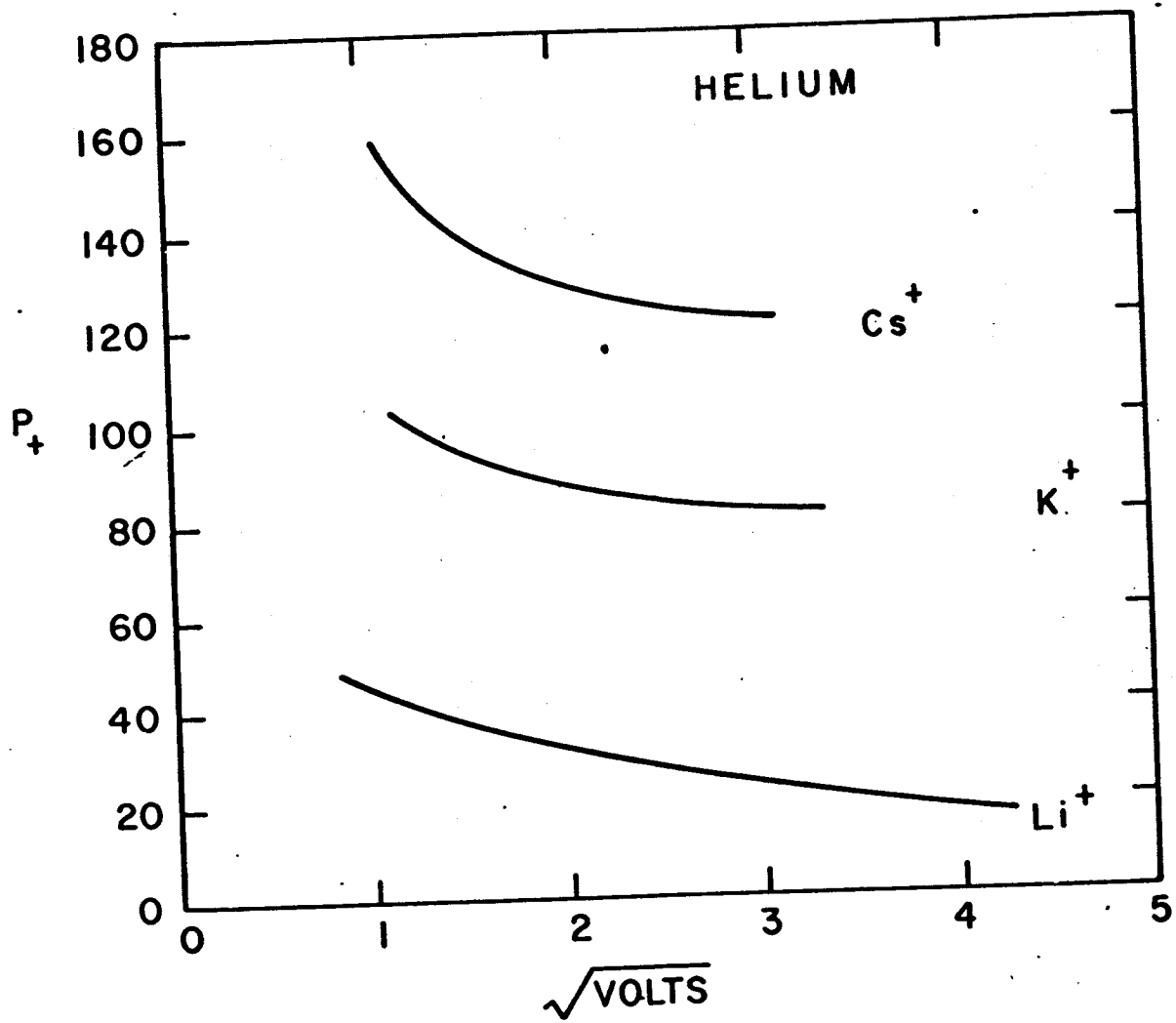
FIG. 7-7   PROBABILITY OF COLLISION FOR POSITIVE IONS OF Li, K, AND Cs
IN HELIUM

2210-Final
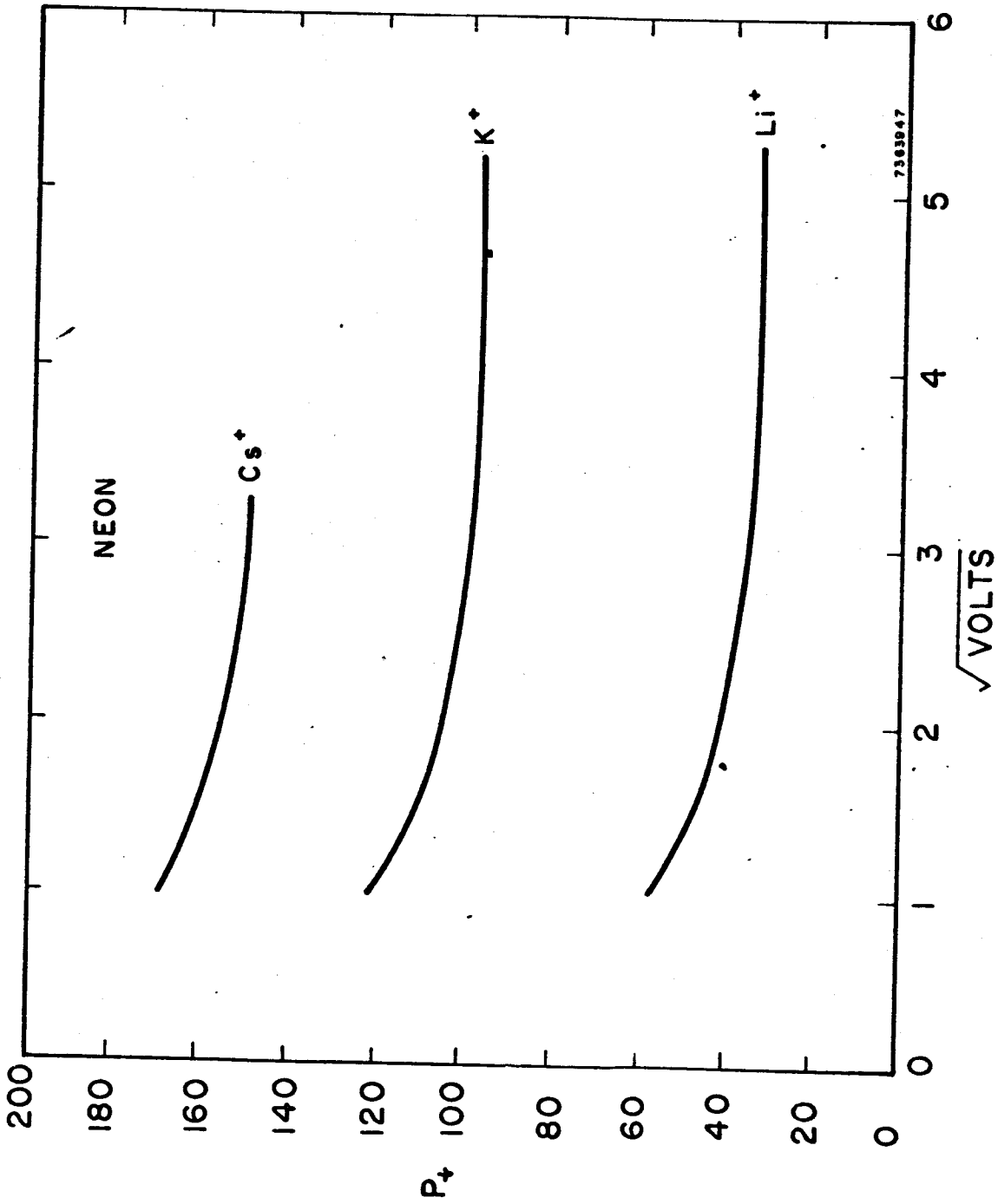
FIG. 7-8   PROBABILITY OF COLLISION FOR POSITIVE IONS OF Li, K, AND Cs IN NEON
(REF. C. RAMSAUER AND O. BEECK, ANN. PHYSIK 87, 1 (1928))
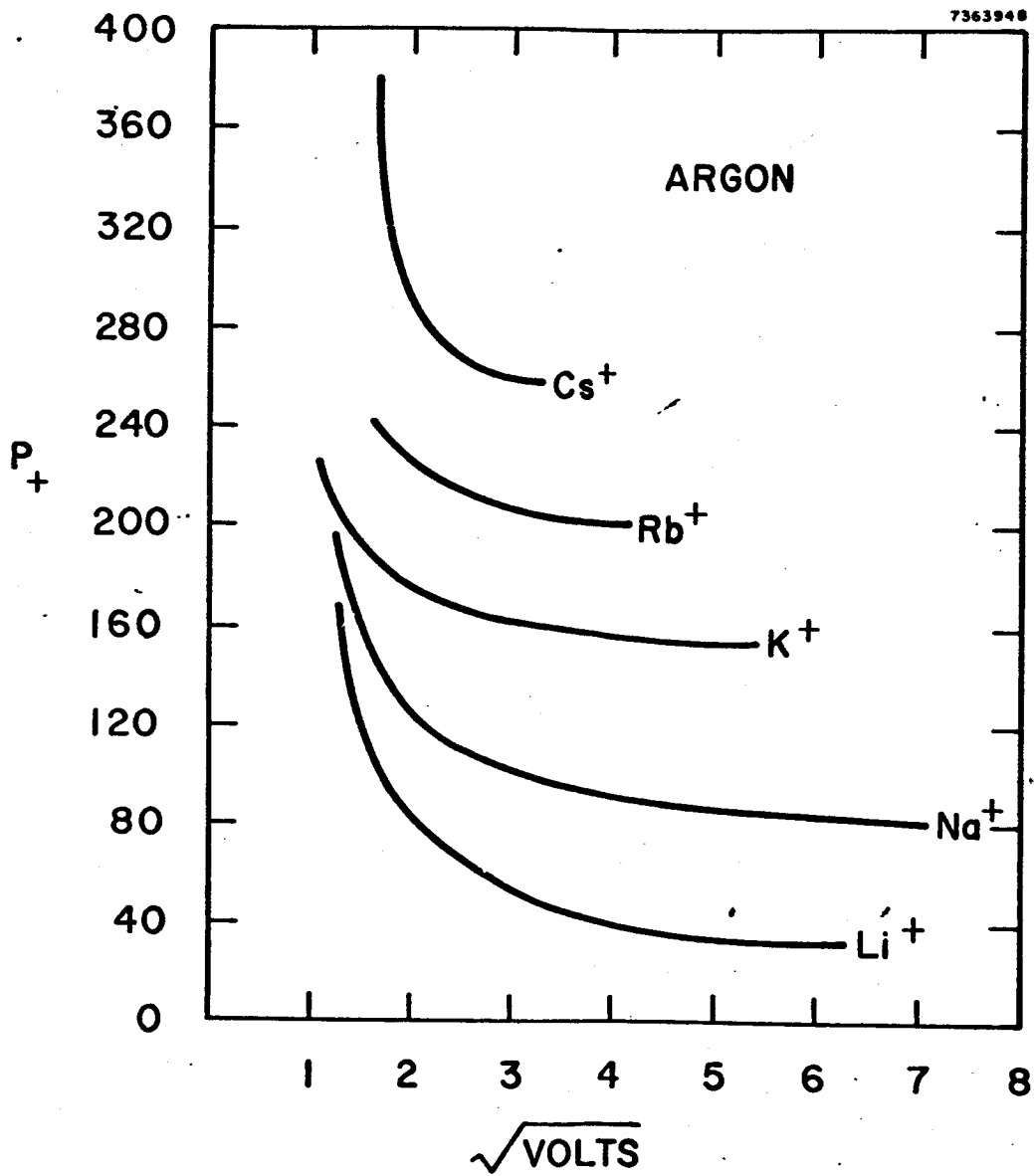
FIG. 7 -9   PROBABILITY OF COLLISION FOR POSITIVE IONS OF
Li, Na, K, Rb, AND Cs IN ARGON
(REF. RAMSAUER AND O. BEECK, ANN. PHYSIK 87, 1 (1928))
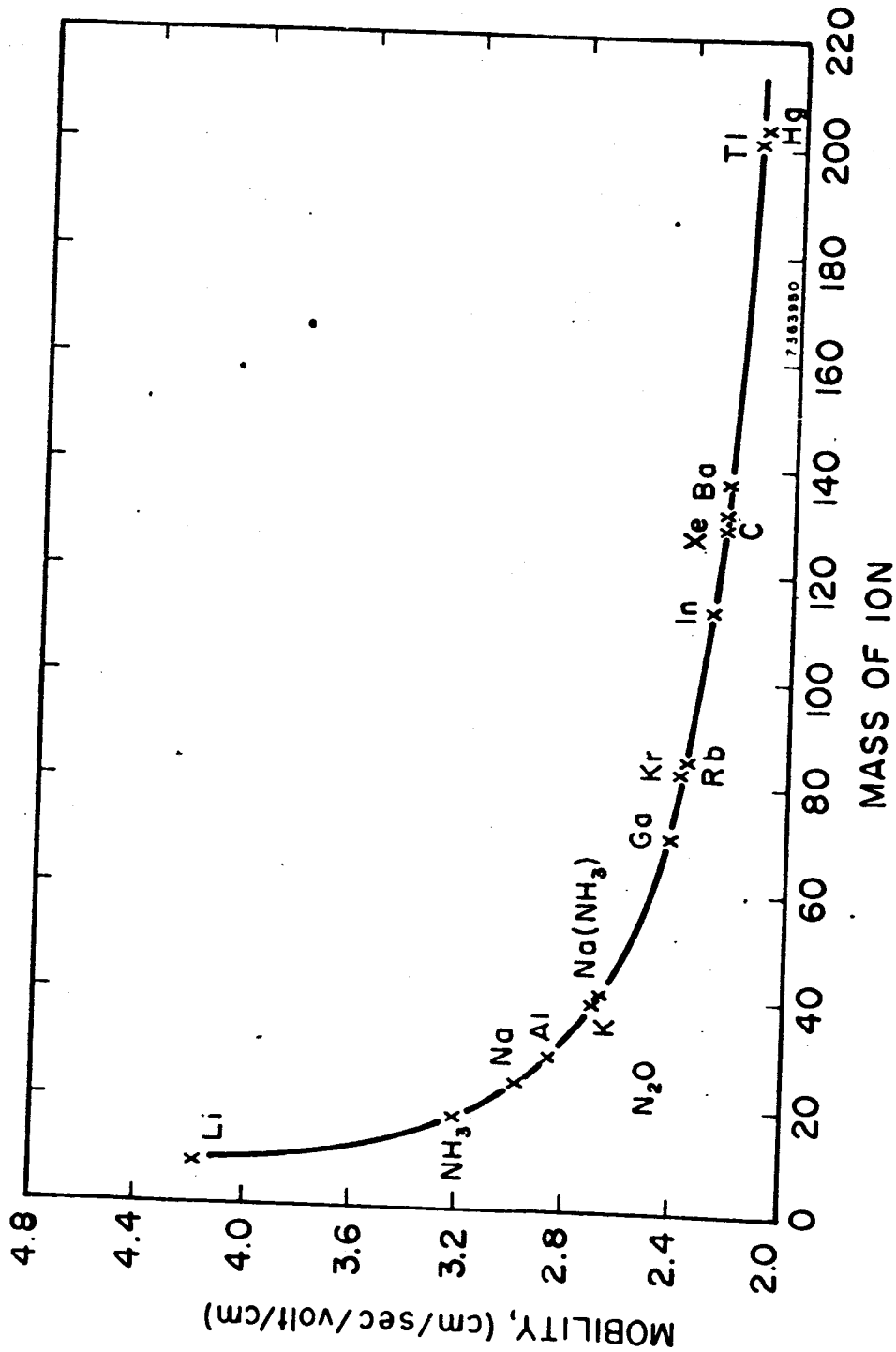
FIG. 7-10 MOBILITY IN NITROGEN OF VARIOUS IONS AS A FUNCTION OF MASS AT 1 ATMOSPHERE PRESSURE
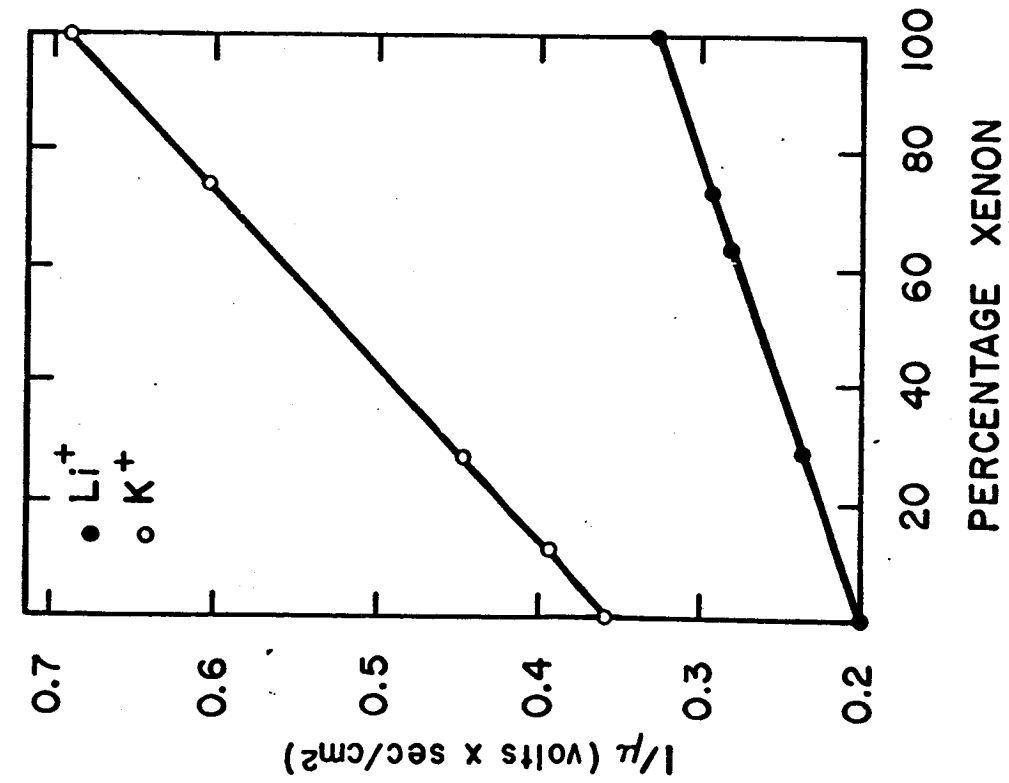(REF. J. H. MITCHELL AND K. E. W. RIDLER, PROC. ROY. SOC. (LONDON) A146 911 (1934))
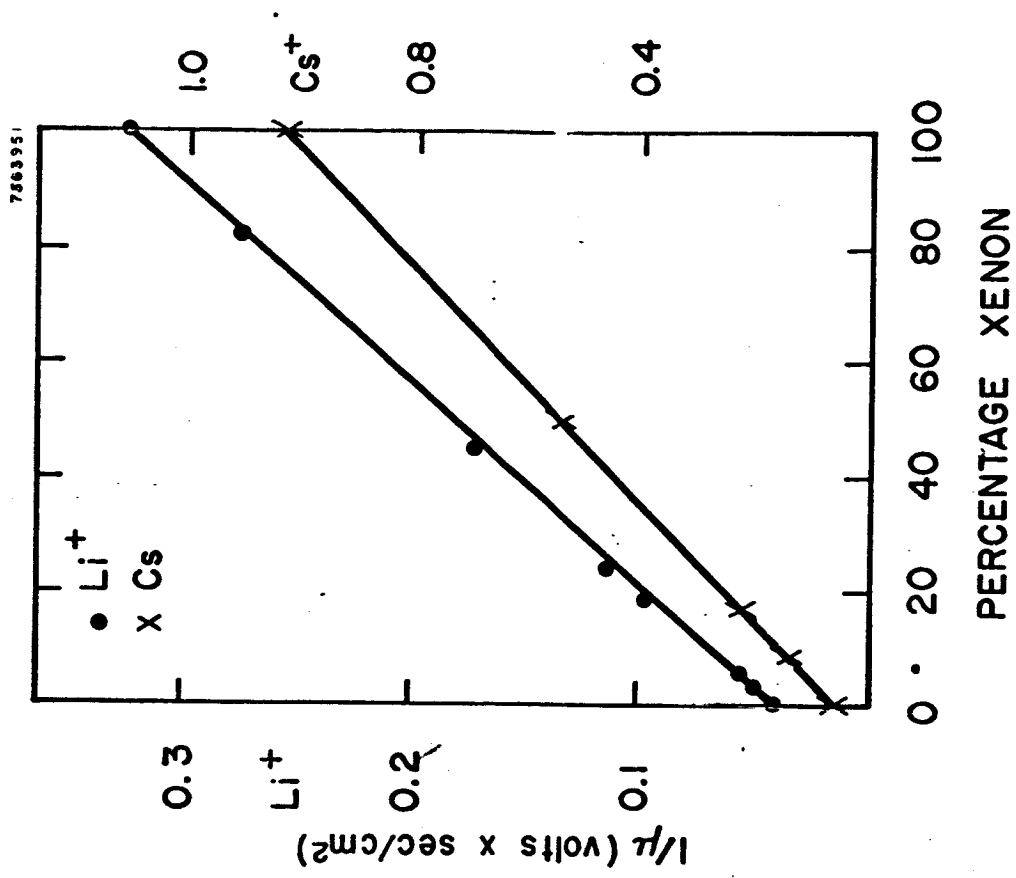
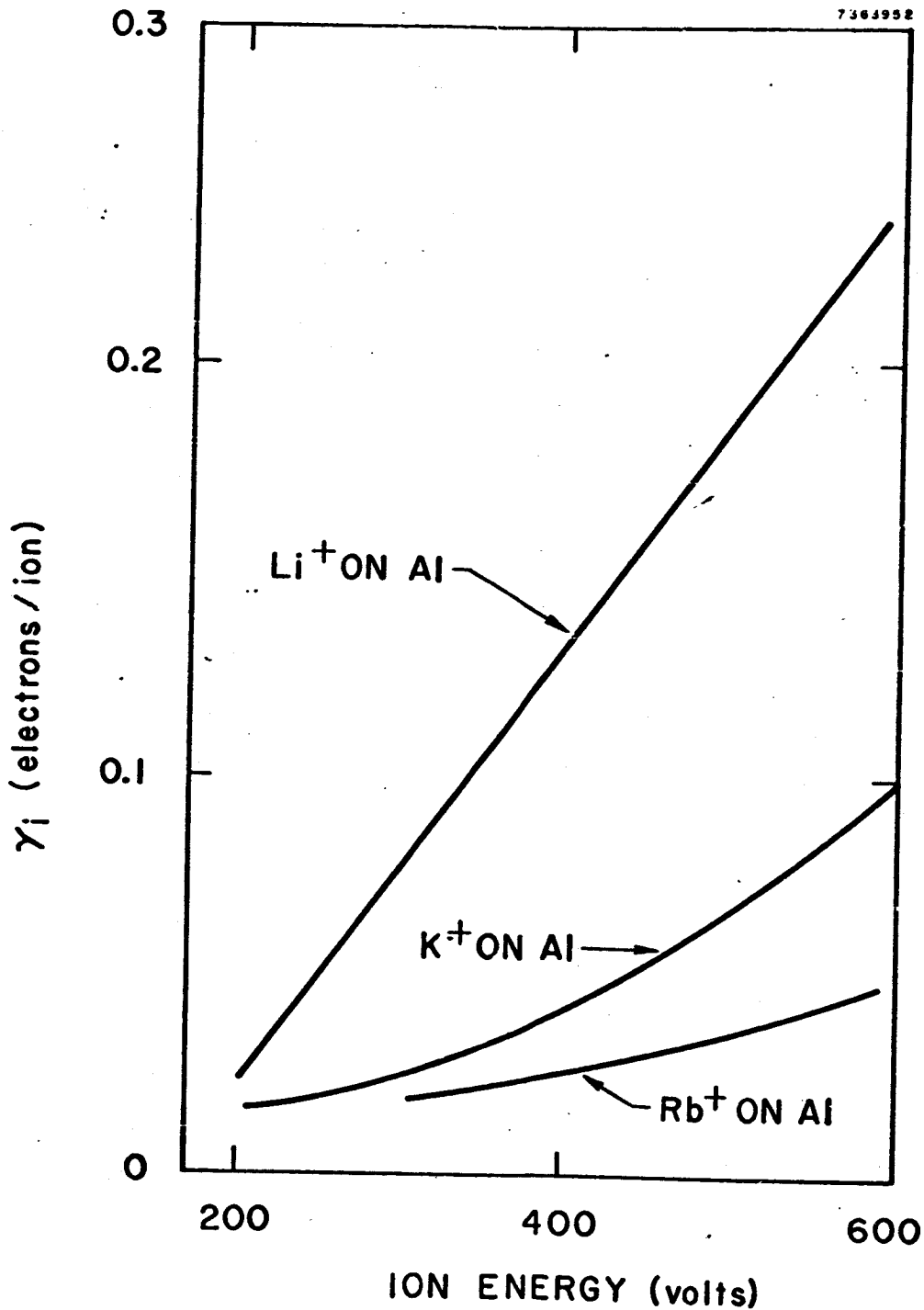FIG. 7 -11   MOBILITY OF ALKALI IONS IN He-Xe MIXTURES

FIG. 7-12   EJECTED ELECTRO YIELD OF Li$^+$, K$^+$, AND Rb$^+$ ON ALUMINUM
(REF. H. S. W. MASSEY AND E. H. S. BURHCP, ELECTRONIC
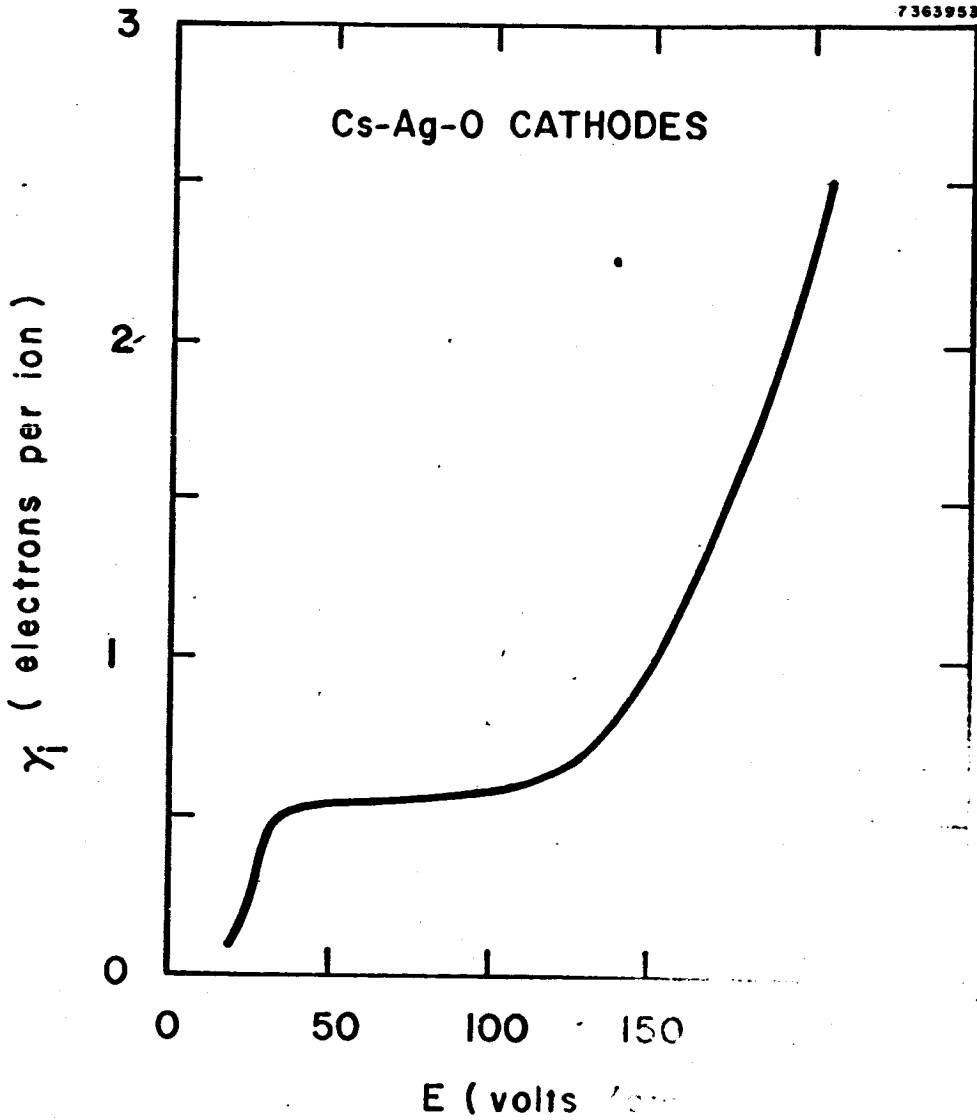AND IONIC IMPACT PHENOMENA, CLARENDON PRESS, OXFORD
(1952), p. 549.)

FIG. 7 -13 SECOND TOWNSEND COEFFICIENT OF ARGON IONS ON Cs-Ag-O SURFACE
(REF. W. S. HUXFORD, PHYS. REV. 55, 754 (1939))